CONTENTS

Part I

PREFACE . . . . iii 1/A5

WELCOME 1 1/A10
R. R. Heldenfels

SESSION I - OVERVIEWS
Chairman: A. J. Henderson

1. HYPERSONIC STRUCTURES: AN AERODYNAMICIST'S PERSPECTIVE (OR ONE MAN'S DREAM IS ANOTHER MAN'S NIGHTMARE) 5 1/B1
J. D. Watts, L. R. Jackson, and J. L. Hunt

2. STRUCTURAL REQUIREMENTS FOR MILITARY HYPERSONIC SYSTEMS (Paper not available for publication)
P. Lane

3. AIRFRAME-INTEGRATED PROPULSION SYSTEM FOR HYPERSONIC CRUISE VEHICLES 39 1/F13
Robert A. Jones and Paul W. Huber

4. RECENT ADVANCES IN CONVECTIVELY COOLED ENGINE AND AIRFRAME STRUCTURES FOR HYPERSONIC FLIGHT 47 1/G7
H. Neale Kelly, Allan R. Wieting, Charles P. Shore, and Robert J. Nowak

SESSION II - ENGINE STRUCTURES
Chairman: H. N. Kelly

5. DESIGN AND ANALYSIS OF A SCRAMJET ENGINE 65 2/A13
O. A. Buchmann

6. THERMOSTRUCTURAL ANALYSIS OF A SCRAMJET FUEL-INJECTION STRUT 119 3/B11
Allan R. Wieting and Earl A. Thornton

7. ADVANCED FABRICATION TECHNIQUES FOR COOLED ENGINE STRUCTURES 145 3/F7
O. A. Buchmann

8. HYDROGEN EMBRITTLEMENT AND ITS CONTROL IN HYDROGEN-FUELED ENGINE SYSTEMS 195 4/F11
W. T. Chandler

9. CARBON-CARBON COMPOSITE APPLICATION FOR INTEGRAL ROCKET RAMJET COMBUSTORS (Paper not available for publication)
H. A. Holman

SESSION III - COOLED AIRFRAME STRUCTURES
Chairman: C. P. Shore

10. DESIGN AND FABRICATION OF A SKIN STRINGER DISCRETE TUBE ACTIVELY COOLED STRUCTURAL PANEL 253 6/A5
Frank M. Anthony

11. DESIGN AND ANALYSIS OF A PLATE-FIN SANDWICH ACTIVELY COOLED STRUCTURAL PANEL 319 7/C13
L. M. Smith

12. FLUXLESS BRAZING AND HEAT TREATMENT OF A PLATE-FIN SANDWICH ACTIVELY COOLED PANEL 375 8/E1
Charles S. Beuyukian

13. DESIGN AND FABRICATION OF A RADIATIVE ACTIVELY COOLED HONEYCOMB SANDWICH PANEL 449 10/A13
Leland C. Koch

14. RADIATIVE, ACTIVELY COOLED PANEL TESTS RESULTS 493 11/A5
Charles P. Shore, Robert J. Nowak, and Ellsworth L. Sharpe

JUN 5 1979
JUN 5 1979

ITEM- 830-H-10

NAS 1.55: 2065/pt.1

COMPLETED

NASA Conference Publication 2065
Part I

Recent Advances in Structures for Hypersonic Flight

Proceedings of
a symposium held at
Langley Research Center
Hampton, Virginia
September 6-8, 1978

5 44

NASA

Microfilmed From
Best Available Copy

NASA Conference Publication 2065
Part I

Recent Advances in Structures for Hypersonic Flight

Proceedings of
a symposium held at
Langley Research Center
Hampton, Virginia
September 6-8, 1978

NASA
National Aeronautics
and Space Administration

**Scientific and Technical
Information Office**

1978

PREFACE

The proceedings of the NASA Symposium - Recent Advances in Structures for Hypersonic Flight held at Langley Research Center on September 6-8, 1978, are reported in this NASA Conference Proceedings. The papers at this Symposium were presented by 24 speakers representing airframe, missile, and engine manufacturers, the U.S. Air Force, and two NASA Research Centers.

The Symposium was organized in six sessions as follows:

I. Overviews
II. Engine Structures
III. Cooled Airframe Structures
IV. Hot Structures and TPS
V. Tankage and Insulation
VI. Analysis Methods

Papers and the authors thereof are grouped by session and identified in the CONTENTS. The order of papers is the actual order of speaker appearance at the Symposium.

The papers contained in this compilation were submitted as camera-ready copy and have been edited only for clarity and format. Technical contents and views expressed are the responsibility and opinions of the individual authors. The size of the compilation necessitated publication in two parts (Parts I and II). A list of attendees, by organizational affiliation, is included at the back of Part II.

We would like to express appreciation to session chairmen and speakers whose efforts contributed to the technical excellence of the Symposium.

Certain commercial materials are identified in this paper in order to specify adequately which materials were investigated in the research effort. In no case does such identification imply recommendation or endorsement of the product by NASA, nor does it imply that the materials are necessarily the only ones or the best ones available for the purpose. In many cases equivalent materials are available and would probably produce equivalent results.

S. C. Dixon
Symposium Chairman

C. P. Shore
Symposium Coordinator

BLANK PAGE

CONTENTS

Part I

PREFACE iii

WELCOME 1
R. R. Heldenfels

SESSION I - OVERVIEWS
Chairman: A. J. Henderson

1. HYPERSONIC STRUCTURES: AN AERODYNAMICIST'S PERSPECTIVE (OR ONE MAN'S DREAM IS ANOTHER MAN'S NIGHTMARE) 5
J. D. Watts, L. R. Jackson, and J. L. Hunt

2. STRUCTURAL REQUIREMENTS FOR MILITARY HYPERSONIC SYSTEMS (Paper not available for publication)
P. Lane

3. AIRFRAME-INTEGRATED PROPULSION SYSTEM FOR HYPERSONIC CRUISE VEHICLES 39
Robert A. Jones and Paul W. Huber

4. RECENT ADVANCES IN CONVECTIVELY COOLED ENGINE AND AIRFRAME STRUCTURES FOR HYPERSONIC FLIGHT 47
H. Neale Kelly, Allan R. Wieting, Charles P. Shore, and Robert J. Nowak

SESSION II - ENGINE STRUCTURES
Chairman: H. N. Kelly

5. DESIGN AND ANALYSIS OF A SCRAMJET ENGINE 65
O. A. Buchmann

6. THERMOSTRUCTURAL ANALYSIS OF A SCRAMJET FUEL-INJECTION STRUT 119
Allan R. Wieting and Earl A. Thornton

7. ADVANCED FABRICATION TECHNIQUES FOR COOLED ENGINE STRUCTURES 145
O. A. Buchmann

8. HYDROGEN EMBRITTLEMENT AND ITS CONTROL IN HYDROGEN-FUELED ENGINE SYSTEMS 195
W. T. Chandler

9. CARBON-CARBON COMPOSITE APPLICATION FOR INTEGRAL ROCKET RAMJET COMBUSTORS (Paper not available for publication)
H. A. Holman

SESSION III - COOLED AIRFRAME STRUCTURES
Chairman: C. P. Shore

10. DESIGN AND FABRICATION OF A SKIN STRINGER DISCRETE TUBE ACTIVELY COOLED STRUCTURAL PANEL 253
Frank M. Anthony

11. DESIGN AND ANALYSIS OF A PLATE-FIN SANDWICH ACTIVELY COOLED STRUCTURAL PANEL 319
L. M. Smith

12. FLUXLESS BRAZING AND HEAT TREATMENT OF A PLATE-FIN SANDWICH ACTIVELY COOLED PANEL 375
Charles S. Beuyukian

13. DESIGN AND FABRICATION OF A RADIATIVE ACTIVELY COOLED HONEYCOMB SANDWICH PANEL 449
Leland C. Koch

14. RADIATIVE, ACTIVELY COOLED PANEL TESTS RESULTS 493
Charles P. Shore, Robert J. Nowak, and Ellsworth L. Sharpe

Part II*

SESSION IV - HOT STRUCTURES AND TPS
Chairman: H. L. Bohon

15. TESTS OF BEADED AND TUBULAR STRUCTURAL PANELS 539
John L. Shideler, Roger A. Fields, and Lawrence F. Reardon

16. STRUCTURES FOR HYPERSONIC AIRBREATHING TACTICAL MISSILES 577
William C. Caywood and Robert M. Rivello

17. STRUCTURES AND TPS FOR THE NHFRF/HYTID 601
Harvey J. Hoge

18. DESIGN AND FABRICATION OF A SUPER ALLOY THERMAL PROTECTION SYSTEM 629
A. Varisco, W. Wolter, and P. Bell

19. MULTIWALL TPS 671
L. Robert Jackson

*Papers 15 to 24 are presented under separate cover.

20. DRYDEN FLIGHT RESEARCH CENTER HOT STRUCTURES RESEARCH 707
Roger A. Fields

SESSION V - TANKAGE AND INSULATION
Chairman: R. D. Witcofski

21. LIQUID HYDROGEN TANKAGE DESIGN 759
George W. Davis

22. EXTERNAL INSULATION FOR LIQUID HYDROGEN TANKS 807
Ellsworth L. Sharpe

SESSION VI - ANALYSIS METHODS
Chairman: W. C. Walton, Jr.

23. RECENT ADVANCES IN THERMOSTRUCTURAL FINITE ELEMENT ANALYSIS 851
Earl A. Thornton and Allan R. Wieting

24. RECENT ADVANCES IN THERMAL-STRUCTURAL ANALYSIS AND DESIGN 897
Howard M. Adelman and James C. Robinson

ATTENDEES 943

WELCOME

R. R. Heldenfels
NASA Langley Research Center

Welcome to the Langley Research Center and the NASA Symposium on Recent Advances in Structures for Hypersonic Flight. We are pleased that you are here and hope that you find this a productive exchange of information on a frontier area of structures technology.

In NASA, the research program in aeronautics is funded and reported separately from research in space technology, but some activities are very similar. For example, hypersonic aircraft are in aeronautics whereas launch vehicles and space transportation systems are in space. This symposium on hypersonic flight is part of the aeronautics program concerned with vehicles that cruise at high speed in the atmosphere. The structures technology required for hypersonic cruise vehicles has much in common with that required for many missiles and space vehicles. Consequently a few papers from such programs have been included on the agenda of this symposium.

Interest in hypersonic vehicles has a long history with much activity dating from the late 50's when, for example, the USAF studied a vehicle called Aerospaceplane. NASA has been conducting hypersonic research for more than 20 years. I began to work on hypersonic structures in 1955 and have seen the level of activity go up and down as potential applications were born and died. Space vehicle programs have usually increased as aeronautical programs have gone down so that our high temperature structures programs for aircraft and space vehicles here at Langley have maintained a reasonable pace. Hypersonic aircraft research and development seems to be at a low point now, but hopefully it will pick up again with identification of useful military and civil applications.

NASA held a Conference on Hypersonic Aircraft Technology in May 1967 (NASA SP-148) to review NASA hypersonics research when that work was at one of its high points. The Hypersonic Research Engine (HRE) project was in the hardware phase and plans were being developed for a modified X-15 research airplane. The conference included mission studies of cruise and launch vehicles, aerodynamics, and propulsion, and a one-half day session on structures and materials. That Structures and Materials Session contained 8 papers by 15 Langley authors. All but two of those authors are still at Langley, many still working in hypersonics, and seven of them are authors, speakers, or session chairmen at this symposium.

I was chairman of the Structures and Materials Session at that hypersonic conference and my introductory remarks then (11 years ago) are equally applicable today. I quote: "The structural designer of a long-range, hypersonic cruise airplane will face one of the great challenges of aeronautics. He will be expected to provide a lightweight structure, with an efficiency approaching that of the best subsonic aircraft, for a very large, low-density vehicle subjected to severe aerodynamic heating." I went on to say that the structural problems of hypersonic cruise vehicles were then just beginning to be studied in depth with substantial contributions being made by USAF and NASA.

Subsequent progress has not been as great as expected; much of our effort here has been devoted to providing technology for the space shuttle, but hypersonic aircraft work has continued and several NASA in-house and contractual activities have been completed recently. Therefore, we considered it appropriate to present these NASA results and other related work to interested individuals. We want you to be well informed and ready to participate in the next expansion of hypersonic research. We are very glad that you are here and hope that your attendance proves to be worthwhile.

SESSION I - OVERVIEWS

BLANK PAGE

BLANK PAGE

HYPERSONIC STRUCTURES: AN AERODYNAMICIST'S PERSPECTIVE

or

(ONE MAN'S DREAM IS ANOTHER MAN'S NIGHTMARE)

J. D. Watts, L. R. Jackson, and J. L. Hunt
NASA Langley Research Center

INTRODUCTION

From the title of this paper, one might infer that the age-old tradition of compromise between aerodynamicists and structural designers was going to be treated with some degree of levity. We hope you have not been misled, as the relationship between aerodynamicists and structures research and design engineers is indeed a very serious matter. And, the faster our aircraft become, the more serious the relationship becomes.

I think it is a well-established fact that hypersonic aerodynamicists can generate more structural problems in five minutes than the structural designer can solve in five years. However, the cooperation of engineers in the aerodynamics, propulsion, and structures fields is the only way aircraft get built. Hypersonic aircraft are going to require closer cooperation and more extensive trades and compromises than any other aeronautical task we've had to face.

X-15 RESEARCH AIRPLANE

(Figure 1)

In the 1960's, when hypersonics was still a highly active discipline in the aeronautical engineering field, the X-15 research airplane shown in Figure 1 was successfully probing the "thermal thicket" and proving beyond a shadow of doubt that we could indeed build a metal airplane structure which would withstand the rigors of Mach 6 flight and temperatures of 1000 K (1340°F). The designers may not have been able to predict thermal stresses extremely well with the primitive tools they had then, but they did have a high respect for thermal loads. Their design held up under those thermal stresses, even if there were a few wrinkles and buckles here and there on the airframe after the 200-flight program. I would venture to say that if we had had today's powerful finite element analysis tools to check the X-15's thermal stresses in 1962, we would probably have been too scared to make another flight.

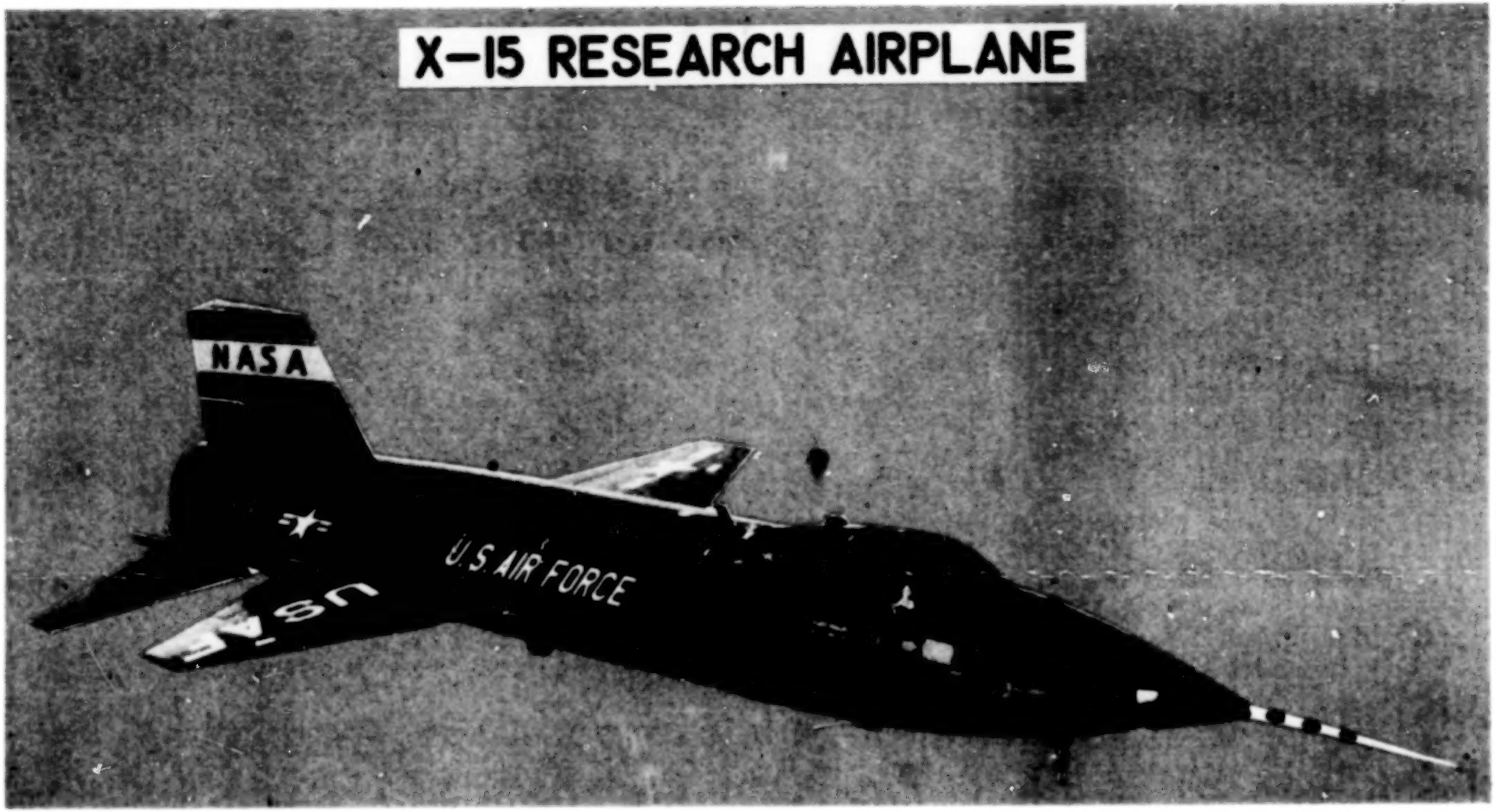
X-15 RESEARCH AIRPLANE
NASA
U.S. AIR FORCE
US AF

Figure 1

HYPERSONIC VEHICLE DESIGN STUDIES OF THE 1960's

(Figure 2)

You may recall that during the same period of time that the X-15 airplane was flying, a number of advanced hypersonic vehicle systems studies were going on and the mission planners, the aerodynamicists, and the propulsion engineers were able to generate a mountain of problems for the structures engineers to solve. Figure 2 shows two vehicle concepts studied during the 1960's. The vehicle on the left is the Air Force's DynaSoar, a small manned boost-glide craft which was to have attained suborbital speeds prior to making a gliding reentry. The large vehicle on the right was the Air Force's Aerospaceplane, a horizontal take-off single-stage-to-orbit airplane which used multimode propulsion and separated its own oxygen out of the atmosphere while flying at hypersonic speeds. The stored LOX was then used with liquid hydrogen fuel to power a rocket which boosted the vehicle into orbit.

HYPERSONIC VEHICLE DESIGN STUDIES OF THE SIXTIES

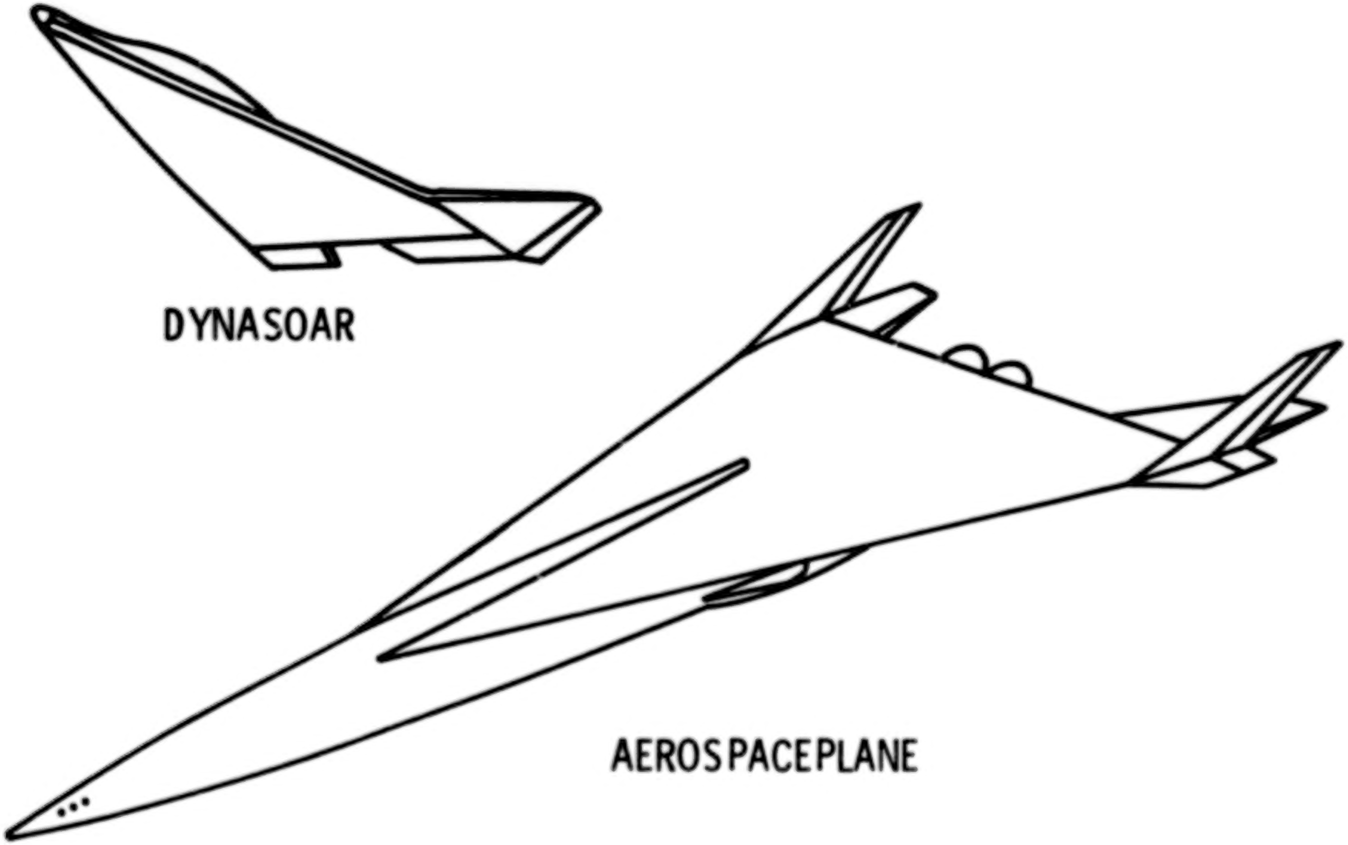
DYNASOAR
AEROSPACEPLANE

Figure 2

HYPERSONIC VEHICLE STRUCTURES

(Figure 3)

The basic structural approaches used with the two vehicles in the previous figure are shown in Figure 3. The DynaSoar wing structure was composed of Rene'41 panels on both surfaces supported by the load-bearing structure, which was a pin-jointed truss. The lower surface heat shields were coated refractory metal, which covered a fibrous insulation. The Aerospaceplane fuselage structure was a titanium integral liquid hydrogen tank. The tank was covered with an evacuated multilayer insulation and the whole system was protected by a stand-off refractory metal or nickel alloy heat shield, depending on the local surface temperature.

Through the process of attacking extremely difficult missions with out-of-reach technology, the aircraft industry was able to thoroughly convince the military sponsors of hypersonic technology development that hypersonic systems were impractical and far too costly. This was, as you will remember, the beginning of a long dry spell in hypersonics. Except for a few lingering groups of researchers here and there, hypersonic aeronautics ceased to exist for over 10 years. It is good to know that one of the research areas that has survived has been structures.

HYPERSONIC VEHICLE STRUCTURES

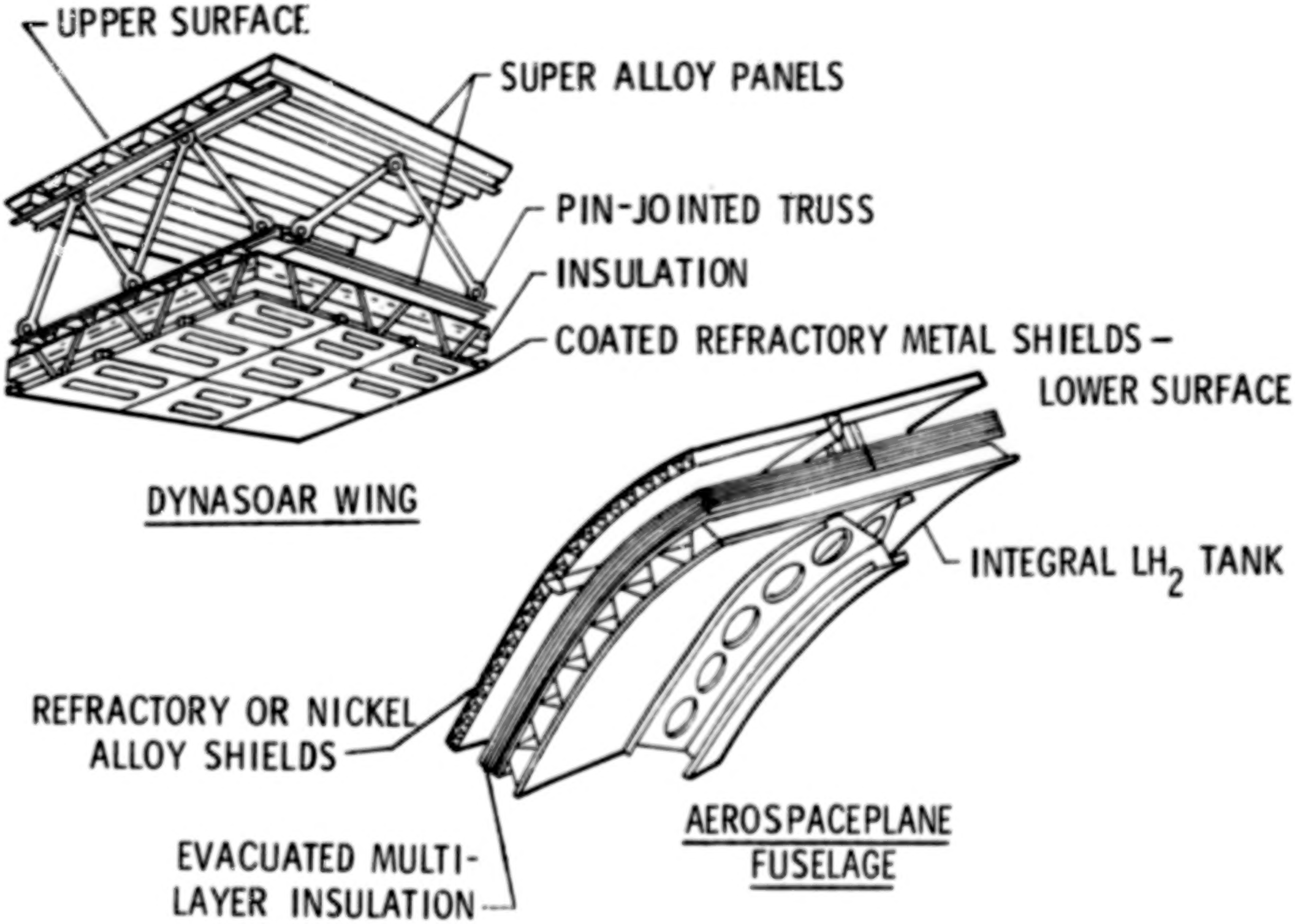
UPPER SURFACE
SUPER ALLOY PANELS
PIN-JOINTED TRUSS
INSULATION
COATED REFRACTORY METAL SHIELDS - LOWER SURFACE
DYNASOAR WING
INTEGRAL LH_2 TANK
REFRACTORY OR NICKEL ALLOY SHIELDS
EVACUATED MULTI-LAYER INSULATION
AEROSPACEPLANE FUSELAGE

Figure 3

THERMAL PROTECTION SYSTEMS OF THE MANNED SPACE PROGRAM

(Figure 4)

When hypersonic aeronautics received the coup de grace in the late 1960's, the national aerospace focus was on the manned space program. One might have assumed that the structural problems associated with reentry would be considerably more difficult than those addressed earlier in aeronautics. However, an interesting thing happened. A means of coping with reentry heating was developed which drastically reduced the temperature environment of the structure. The next figure shows the two basic types of space reentry vehicles developed in the manned space program over the past 20 years. The first was the capsule-type vehicle with an ablative heat shield. This type represents Mercury, Gemini, and Apollo. For these vehicles, the structural problems previously identified with high-speed flight were essentially sidestepped through the application of ablatives. This approach effectively kept the pressure off the structural designers for some time. Then came the Space Shuttle which puts together the nonmetallic heat shield technology with an aircraft-type reentry vehicle. Again, the structural designer's task was relieved of the high-temperature problems by a liberal application of external insulation.

I certainly hope that the remaining experts in the advanced structural technology arena have not been lulled to sleep by past trends in reentry vehicle design because the airplane people are once again getting busy in the wind tunnels with some far-out and some not-so-far-out ideas, all of which will undoubtedly have serious structural implications. Most of these structural problems are not likely to be solved through the use of ablatives or available external insulators.

THERMAL PROTECTION SYSTEMS OF THE MANNED SPACE PROGRAM

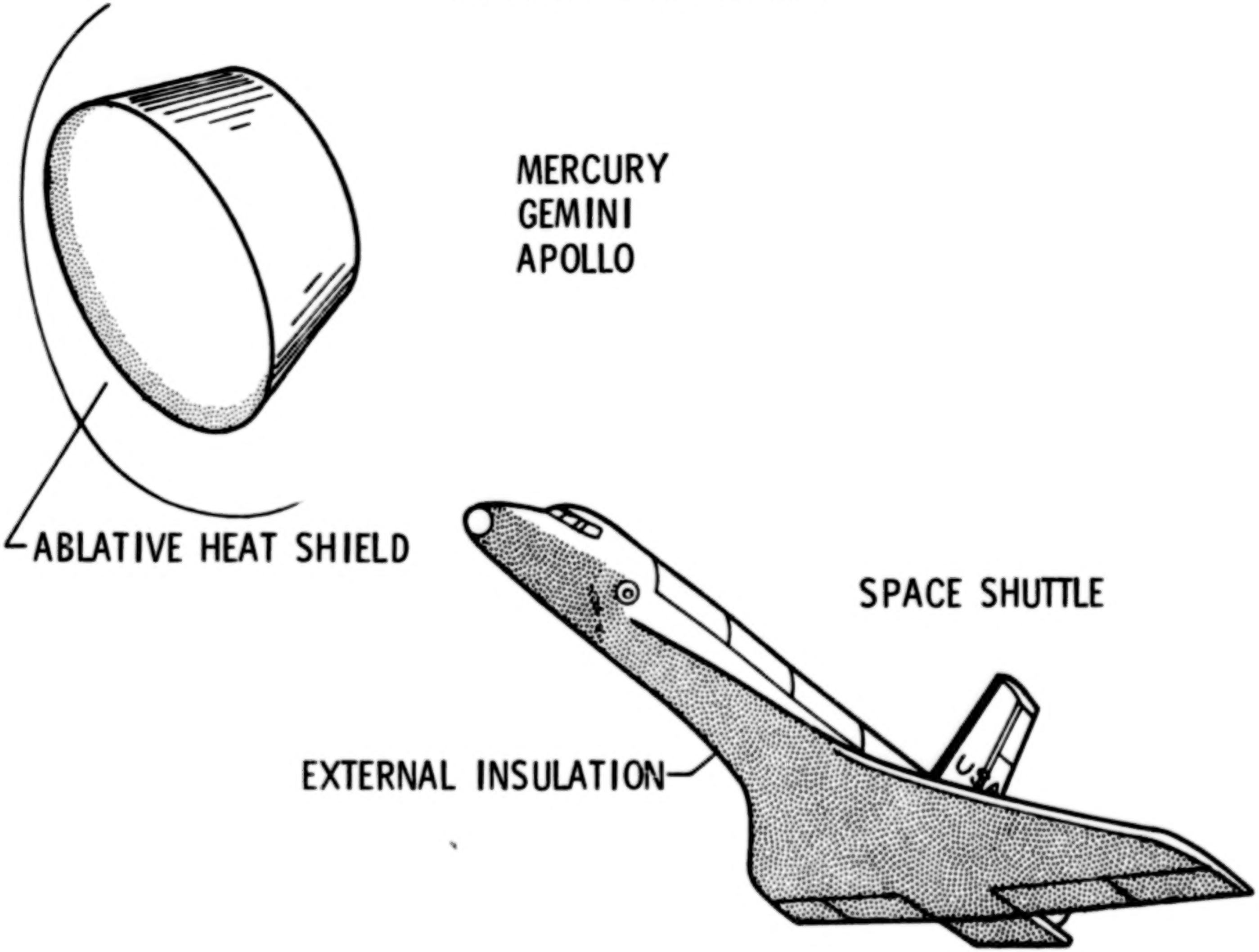
MERCURY
GEMINI
APOLLO
ABLATIVE HEAT SHIELD
SPACE SHUTTLE
EXTERNAL INSULATION
USA

Figure 4

VEHICLE CATEGORIES NOW UNDER STUDY IN HYPERSONIC AERODYNAMICS

(Figure 5)

The primary objective in our current hypersonic aerodynamics program is to develop a broad experimental data base for three classes of vehicles. These three categories of hypersonic vehicles are shown in Figure 5. First, we are currently studying the airbreathing space launch system shown on the left. The vehicle shown is a two-stage system which utilizes turbojet propulsion in twin boosters up to the staging Mach number of about 3.0. The middle vehicle in the figure represents the second class under study, hypersonic cruise missiles. We're working in the Mach 4 to Mach 8 speed range with these missile configurations. The third category, shown on the right, is the cruise aircraft which may someday find applications in both military and civilian missions. The speed range we're emphasizing is Mach 4 to 6 and the fuels being considered include JP, LH_2, and a combination of both.

We are in the early stages of our aerodynamics research program now but already we are seeing several challenging structural problems starting to precipitate out.

VEHICLE CATEGORIES NOW UNDER STUDY IN HYPERSONIC AERODYNAMICS

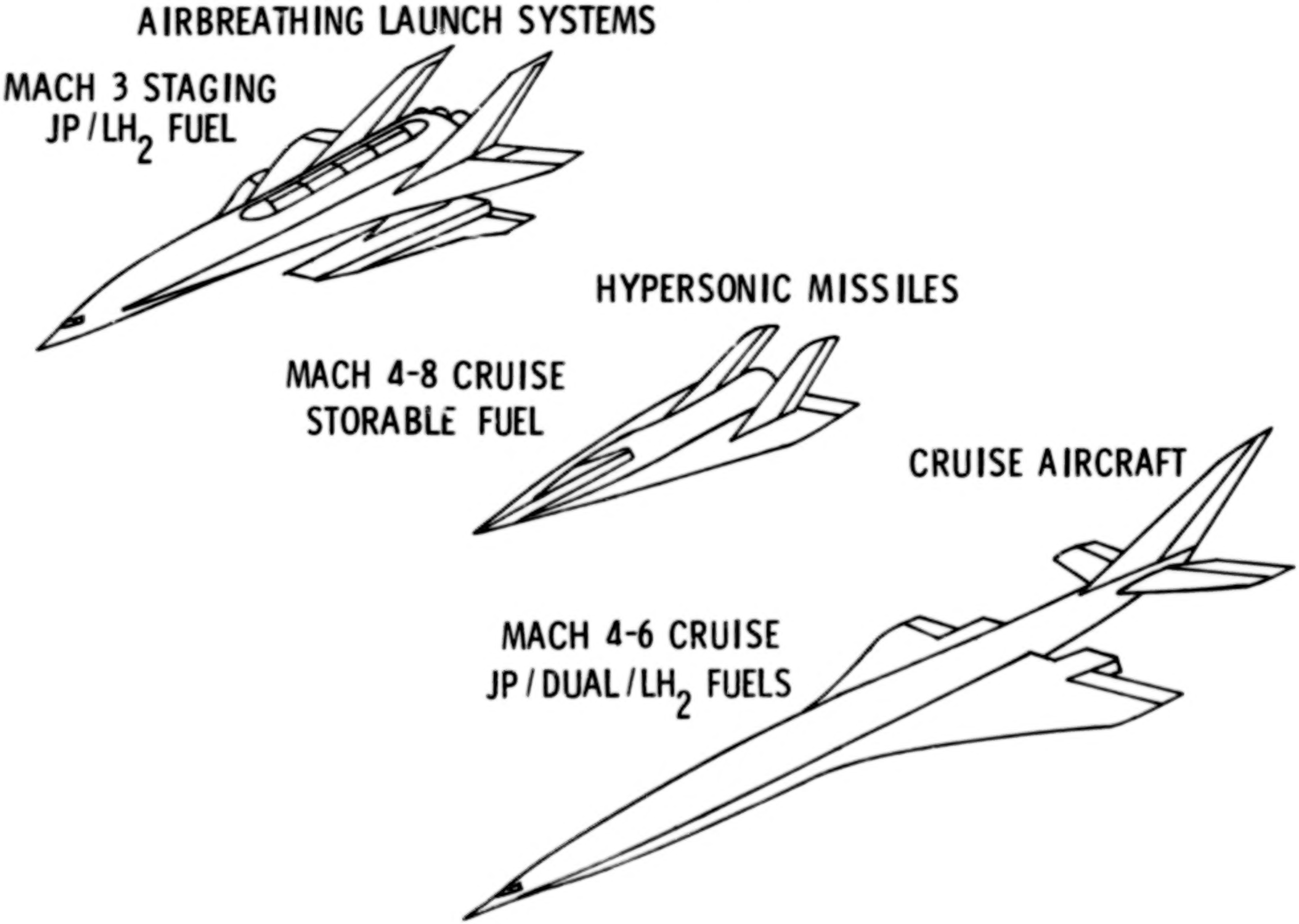
AIRBREATHING LAUNCH SYSTEMS
MACH 3 STAGING
JP/LH$_2$ FUEL
HYPERSONIC MISSILES
MACH 4-8 CRUISE
STORABLE FUEL
CRUISE AIRCRAFT
MACH 4-6 CRUISE
JP/DUAL/LH$_2$ FUELS

11

Figure 5

TURBOJET-BOOSTED LAUNCH SYSTEM

(Figure 6)

Figure 6 is a sketch of a turbojet-boosted spacecraft which utilizes near-term aerodynamic and propulsion technology to boost a rocket-powered orbiter to the staging Mach number of about 3. A study of this concept indicated that, for a 29,400 kg (65,000 lbm) payload (east launch), the gross lift-off weight was about 1,200,000 kg (2,700,000 lbm). It required eight to nine turbojet engines per booster (16 to 18 total) each in the 445,000 N (100,000 lbf) sea level thrust class. The concept could potentially provide a totally reusable space launch system with extremely flexible operations. Many of the problems associated with this system are aerodynamic and a wind tunnel test program addressing the major questions will be underway very shortly. The structural questions that one might anticipate with it will probably fall into two major categories: the structural dynamics of the mated vehicles, and the thermal-structural aspects of the orbiter. Without going into great detail on a spacecraft at an aeronautical symposium, I will simply say that this low-wing-loading orbiter concept, which is similar to others studied in the past by NASA, Boeing, and others, utilizes advanced structures technology. It assumes a significant improvement over space shuttle structure/TPS technology with either nickel alloy hot structure or insulated metal heat shields. The booster vehicles could take advantage of either aluminum heat-sink structure or titanium since their structural temperatures would be within the range of today's Mach 3 aircraft.

TURBOJET–BOOSTED LAUNCH SYSTEM

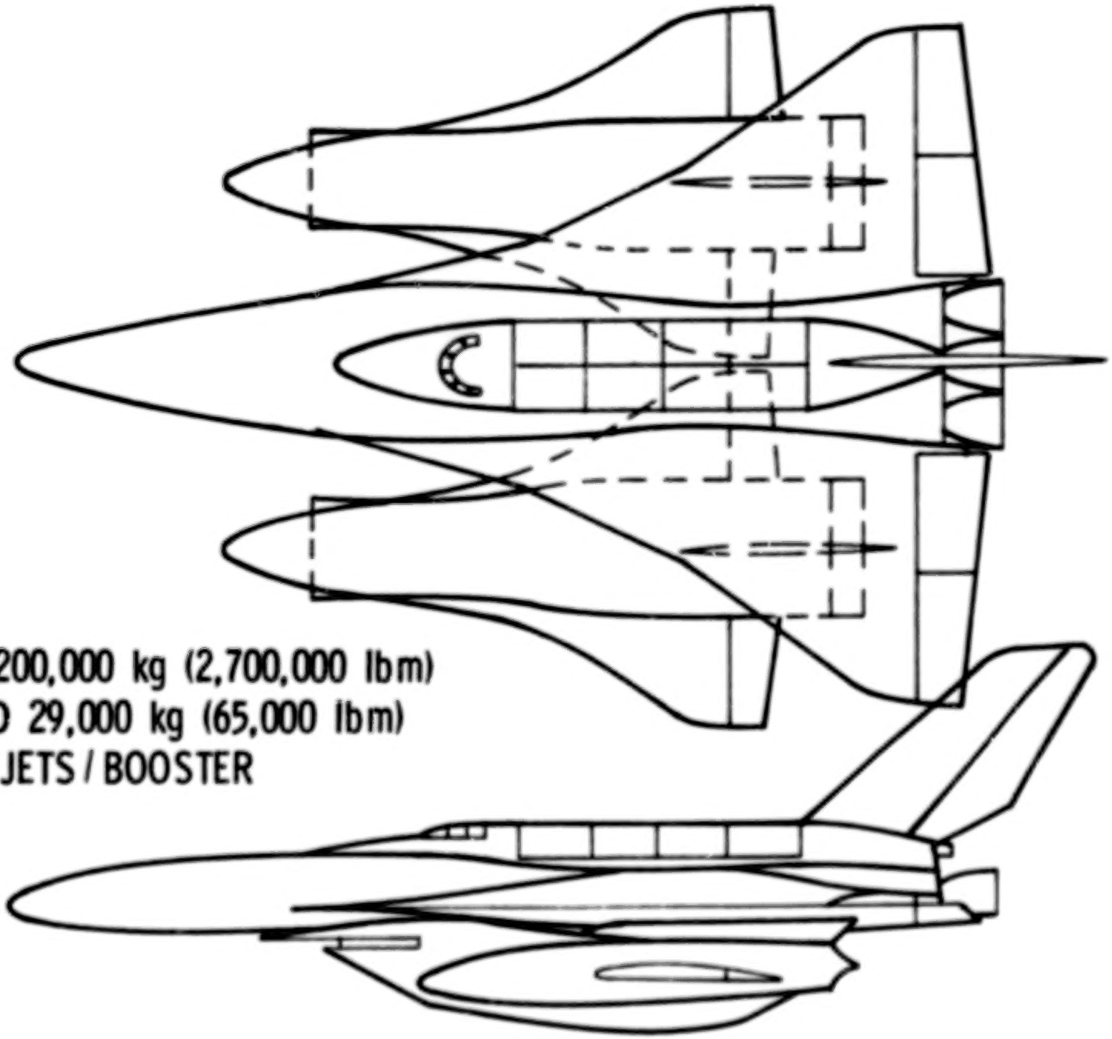

GLOW 1,200,000 kg (2,700,000 lbm)
PAYLOAD 29,000 kg (65,000 lbm)
8 TURBOJETS / BOOSTER

Figure 6

THE MISSILE DESIGN TASK

(Figure 7)

Compared to the other types of hypersonic vehicles, the hypersonic missile has some unique characteristics and limitations which make it a very different design problem. Missiles fly for short periods in a severe flight environment which combines the problems of high dynamic pressure, high heating rates and high maneuver load factors. They are usually geometrically constrained by the launcher which puts a severe limitation on fuel volume and dictates high-density storable fuel. The need for range brings in the high desirability for airbreathing propulsion and its attendant increment in specific impulse over rocket power. In assessing the technology needs of a hypersonic missile, we had to consider all these factors and others, as shown in Figure 7, and try to determine where it might lead us in the airframe and engine structural design. The airframe requirements which seemed to surface were stiffness, heat-sink capacity, strength, and thermal conductivity, all at minimum weight. This combination of properties led us to consider the use of Lockalloy and beryllium for primary airframe structure, as had been proposed earlier for hypersonic research aircraft. The high-temperature combustor in the ramjet/scramjet engine requires a material with strength at very high temperatures. The development of a structural material which can survive the engine combustor environment without cooling is a key to the success of this class of missile. Some progress in the "hot" combustor materials area will be presented by Mr. Holman of McDonnell-Douglas later in the symposium. The only missile characteristic which is less severe than other hypersonic vehicles is its short service life, since the missile is a one-shot vehicle.

THE MISSILE DESIGN TASK

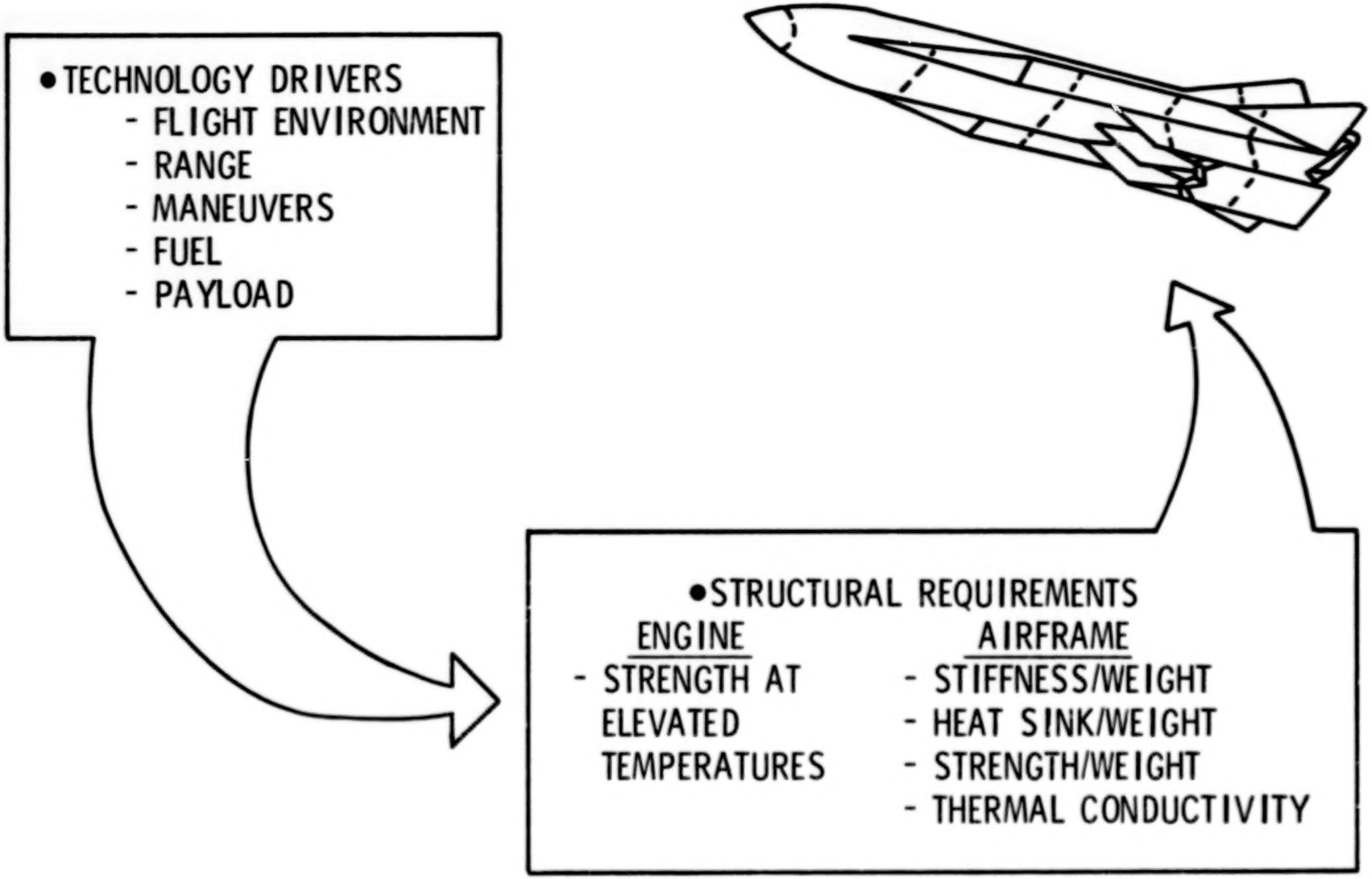

- TECHNOLOGY DRIVERS
  - FLIGHT ENVIRONMENT
  - RANGE
  - MANEUVERS
  - FUEL
  - PAYLOAD

- STRUCTURAL REQUIREMENTS

ENGINE	AIRFRAME
- STRENGTH AT ELEVATED TEMPERATURES	- STIFFNESS/WEIGHT - HEAT SINK/WEIGHT - STRENGTH/WEIGHT - THERMAL CONDUCTIVITY

Figure 7

HYPERSONIC MISSILE STRUCTURAL CONCEPT

(Figure 8)

Adhering to the characteristics shown in the last figure, some of our aerodynamicists have concocted the structural approach illustrated in Figure 8 for a hypersonic missile. This configuration is designed to cruise at a lift/drag ratio of 3.5 at Mach 6 at a 30,500 m (100,000 ft) altitude. The small-span wings are structurally efficient and have relatively low heat loads. The body incorporates an ogive nose shape attached to a constant-cross-section shell structure fuselage with a fineness ratio of 9.5. The flat lower fuselage surface is designed to provide a precompressed inlet flow to the propulsion system. The low wing placement also contributes to the precompression and uniformity of the inlet flow as well as to provide more space for engine installation.

For short flight times, the situation was analogous to the hypersonic research airplane structural problem and led to the examination of heat-sink systems. The main fuselage structure was designed with 0.76 cm (0.3 in.) thick Lockalloy material to provide a heat-sink range of about 370 km (200 n mi.) at Mach 6 (30,500 m (100,000 ft) altitude). The fuselage structure was not allowed to exceed 530 K (494°F) in order to keep the internal insulation requirements manageable. This heat-sink shell can withstand an ultimate boost acceleration of 600g axially at 295 K (70°F) and 100g normal acceleration at 530 K (494°F). The wings are designed with beryllium plate. Beryllium is also used for the control surfaces because of potentially high interference heating rates.

HYPERSONIC MISSILE STRUCTURAL CONCEPT

HEAT SINK

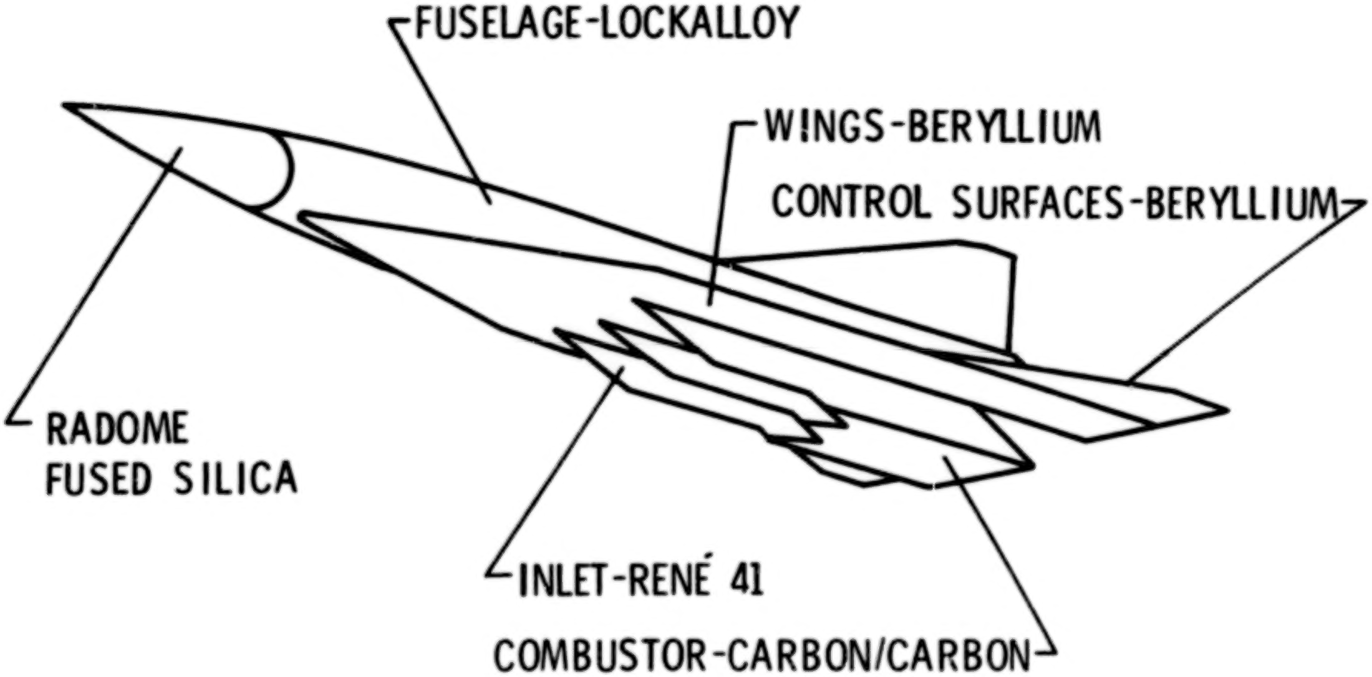
FUSELAGE-LOCKALLOY
WINGS-BERYLLIUM
CONTROL SURFACES-BERYLLIUM
RADOME
FUSED SILICA
INLET-RENÉ 41
COMBUSTOR-CARBON/CARBON

Figure 8

MISSILE WINDWARD SURFACE TPS

(Figure 9)

For ranges exceeding the Lockalloy fuselage structure heat-sink limit, a radiation TPS was added which kept the underlying structure from exceeding 530 K (494°F). This multiwall radiation shield will be discussed by Mr. Jackson in a later paper. Figure 9 shows some temperature-time histories and the associated Mach 6 ranges for a bare Lockalloy airframe and the same airframe protected by a multiwall TPS as illustrated in the figure. Calculations indicate that a straight heat-sink structure is applicable for short-range defensive or stand-off missiles and a heat sink structure which incorporates metallic TPS might well do the job for long-range cruise missiles.

I would like to point out that our conceptual studies of hypersonic missiles and the related airframe and engine structures has been very limited in scope. We have attempted to derive some basic concepts on which to base our aerodynamics research. Obviously, there are many other ways to build missiles.

MISSILE WINDWARD SURFACE TPS

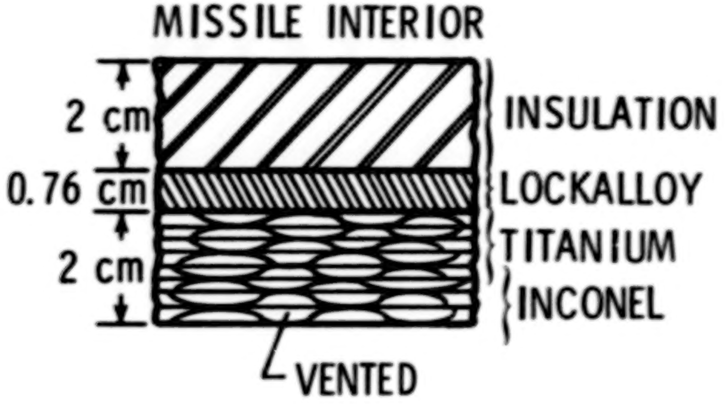

MISSILE INTERIOR
2 cm
INSULATION
0.76 cm
LOCKALLOY
TITANIUM
2 cm
INCONEL
VENTED

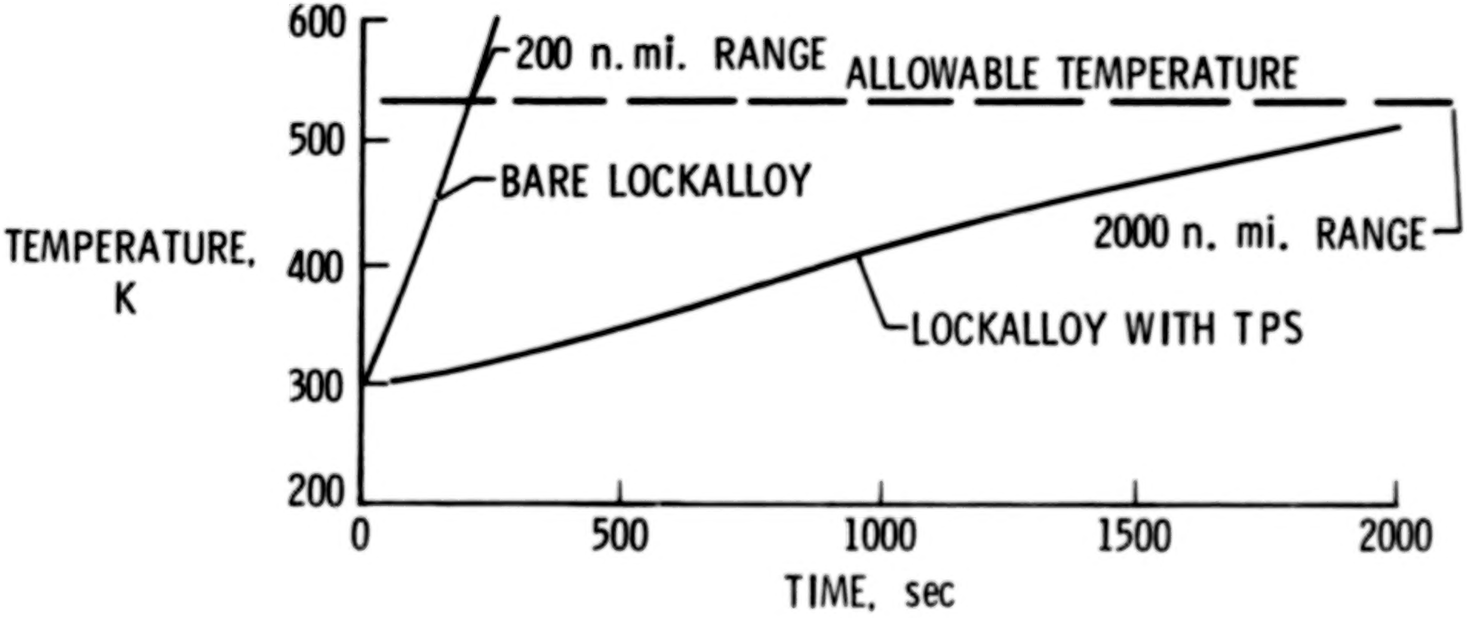

Figure 9

2

11

EXAMPLE ADVANCED RESEARCH CONFIGURATIONS

(Figure 10)

The need for better aerodynamic efficiency, improved propulsion integration, and lower radar cross-section has given impetus to our current missile aerodynamics research program. We're trying to increase aerodynamic performance without greatly compromising needed compactness while experimenting with engine placement and inlet and nozzle design.

Figure 10 shows two advanced aerodynamic configurations for missiles which we are presently studying. The one on the left is aimed at high volumetric efficiency. The primary objective with the one on the right is high precompression. As you can see, we do not intend to limit our parametric data base development to circular cylinders with a variation of stabilizers.

EXAMPLE ADVANCED RESEARCH CONFIGURATIONS

UPPER SURFACE ENGINES

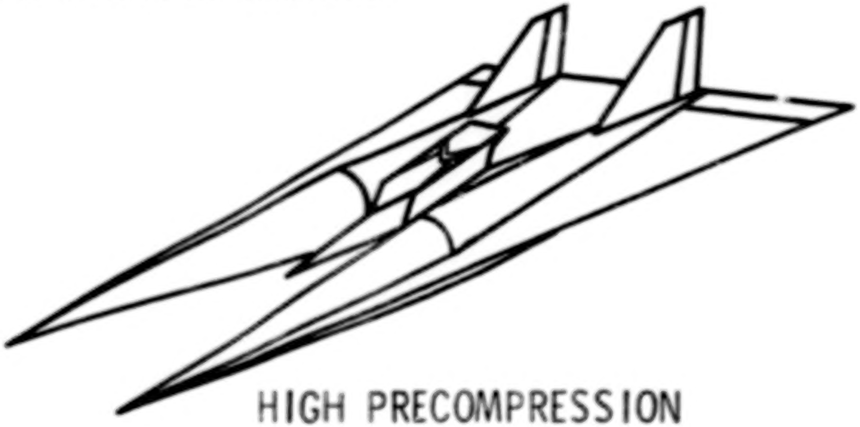

HIGH PRECOMPRESSION

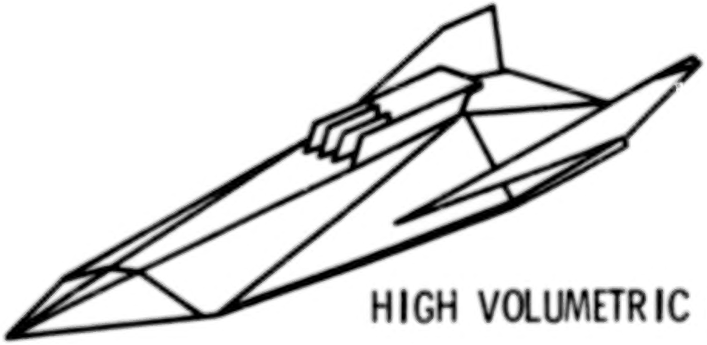

HIGH VOLUMETRIC EFFICIENCY

Figure 10

HYPERSONIC AIRCRAFT TECHNOLOGY —— CURRENT AREAS OF INTEREST

(Figure 11)

In contrast to the hypersonic aircraft studies of the 1960's which tended to emphasize the upper end of the hypersonic speed regime, our current effort is emphasizing the long-neglected technology "gap" between Mach 4 and Mach 6. Also, we are addressing the total problem of how to get a hypersonic aircraft to take off like any other aircraft, accelerate to its cruise speed, perform whatever mission it has, and decelerate and land like any other aircraft. By taking the approach of "walking before we run" we tend to emphasize such menial problems as reducing transonic drag, inventing ways of integrating turbojet and ramjet/scramjet propulsion systems, and at the same time, trying to maintain satisfactory hypersonic performance.

Figure 11 describes the three areas of emphasis in our current aerodynamic research program for cruise aircraft. Each of these areas has its own unique structural requirements defined by fuel selection, material limits, and propulsion modes. By addressing these specific areas in a parametric manner, we hope to provide an aerodynamic data base which spans the entire region. Structurally, of course, this probably implies three separate and extensive research programs.

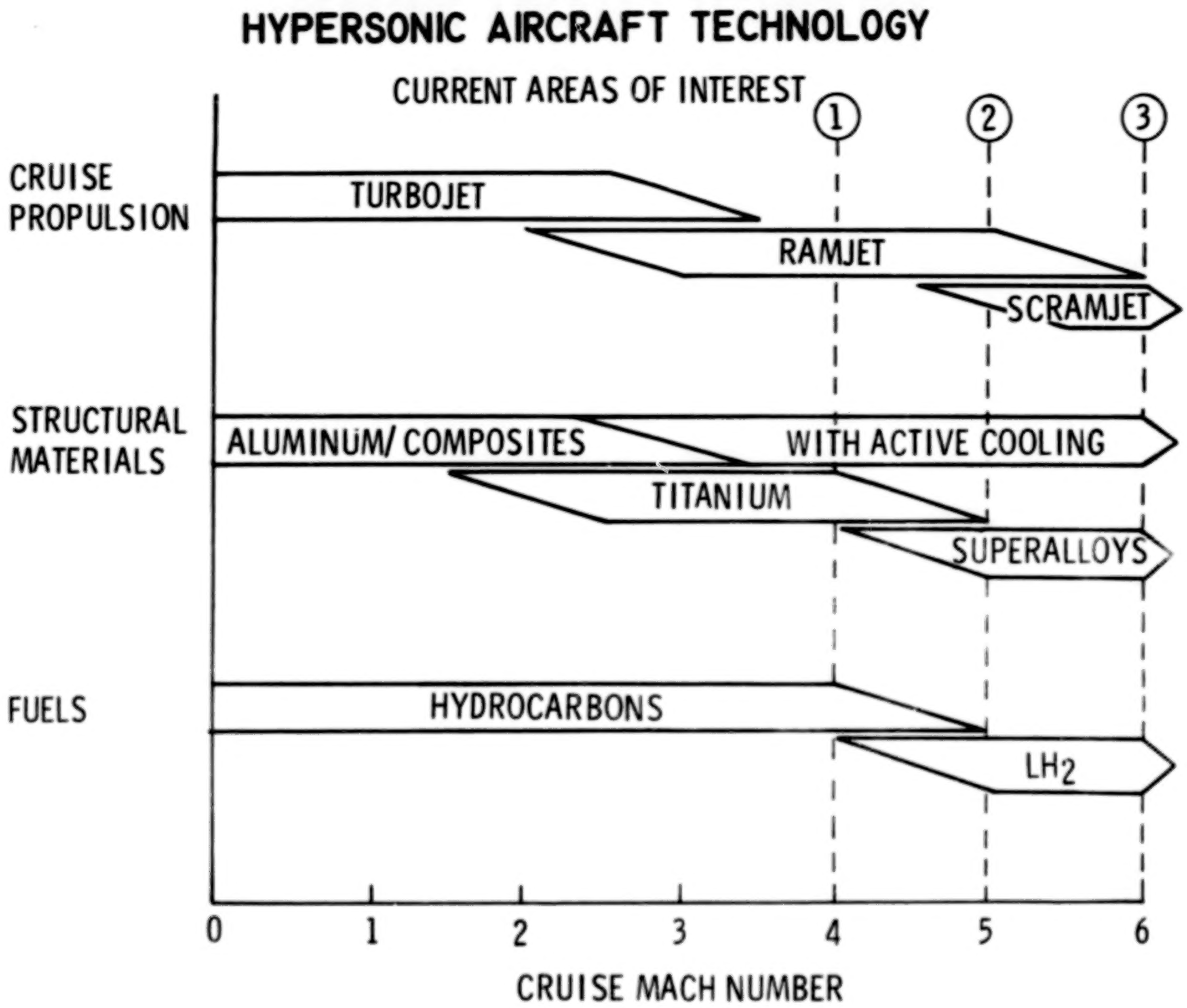
HYPERSONIC AIRCRAFT TECHNOLOGY
CURRENT AREAS OF INTEREST
①
②
③
CRUISE PROPULSION
TURBOJET
RAMJET
SCRAMJET
STRUCTURAL MATERIALS
ALUMINUM/ COMPOSITES
WITH ACTIVE COOLING
TITANIUM
SUPERALLOYS
FUELS
HYDROCARBONS
LH2
0
1
2
3
4
5
6
CRUISE MACH NUMBER

Figure 11

HYPERSONIC TRANSPORT CONFIGURATION

(Figure 12)

Figure 12 is a hypersonic transport configuration currently being studied for us under contract. The airplane concept is sized for a 200-passenger payload and a range of 9,260 km (5,000 n. mi.) It cruises at Mach 6 and uses all hydrogen fuel with its separate turbojet and dual-mode scramjet engines. The structural design of this aircraft has not been addressed except for attempting to keep the structural mass fraction in a reasonable range. Several structural approaches could be applied to this vehicle including hot structure, metal heat shield TPS, and/or actively-cooled structure.

One of the very difficult aspects of a hypersonic transport airframe structure is the need for long life. This is difficult to get at elevated temperatures, and this fact has led to extensive studies of active structural cooling. Several papers on active cooling will be presented at this symposium.

HYPERSONIC TRANSPORT CONFIGURATION

LH_2 FUEL, WING-MOUNTED PROPULSION

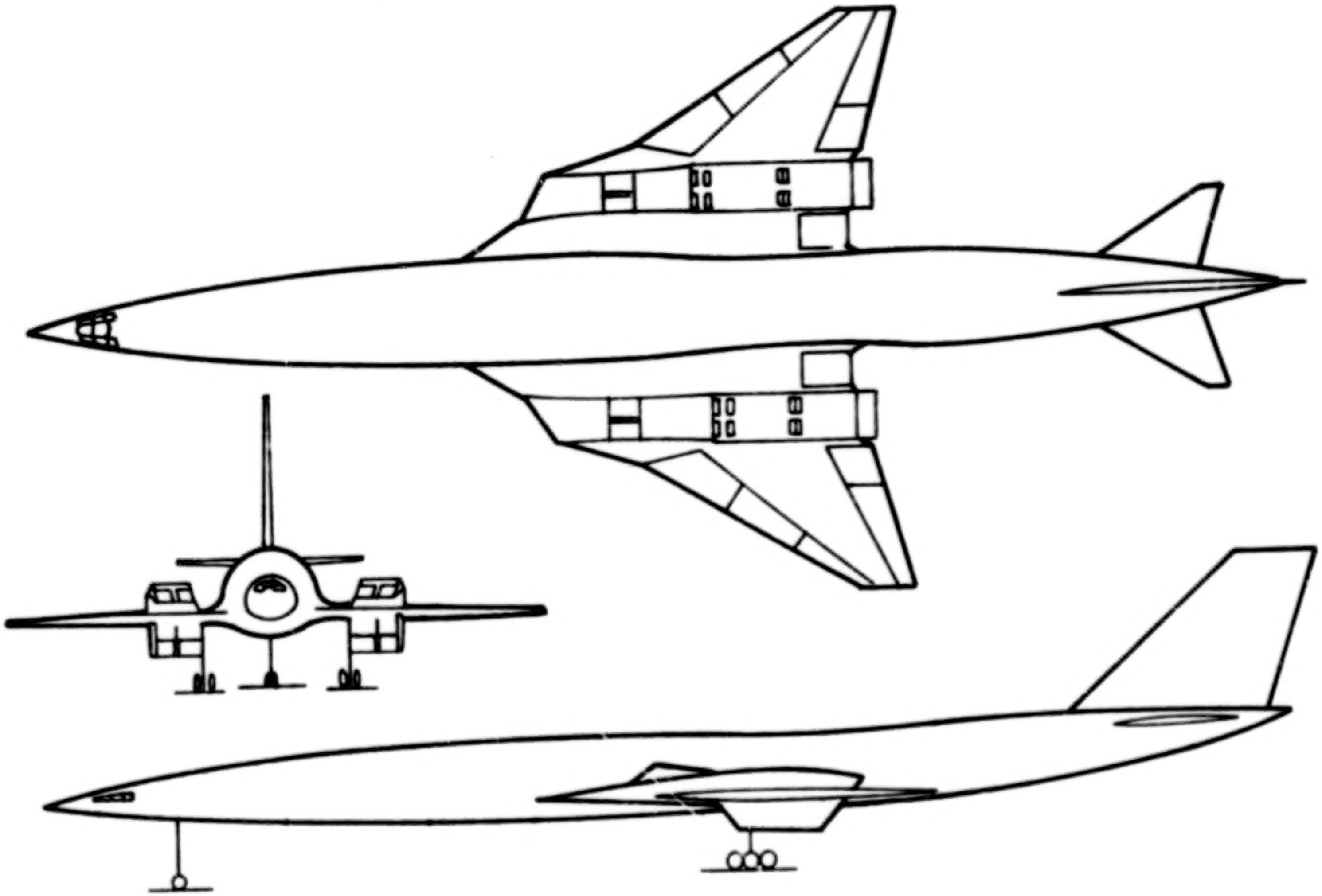

Figure 12

CONCEPTUAL TURBOJET-SCRAMJET SYSTEM

(Figure 13)

Figure 13 shows a chordwise section view of the wing-mounted turbojet-scramjet propulsion system used with the hypersonic transport of the previous figure. The turbojets are buried in the wing with a retractable inlet. The dual-mode scramjet engines are of the same external arrangement as the Langley fixed-geometry scramjet but they require sufficient variable geometry to allow operation from transonic speed up to the Mach 6 cruise speed. The turbojets operate from take-off to about Mach 3, where they are shut down for the cruise portion of the flight. The general idea of a two-dimensional, variable geometry nozzle is shown to indicate that the turbojet and scramjet nozzles may be compatible in their operation but the design problem will be complex indeed. The inlet temperatures for this Mach 6 arrangement will be in the 1370 K (2000°F) range.

CONCEPTUAL TURBOJET-SCRAMJET SYSTEM

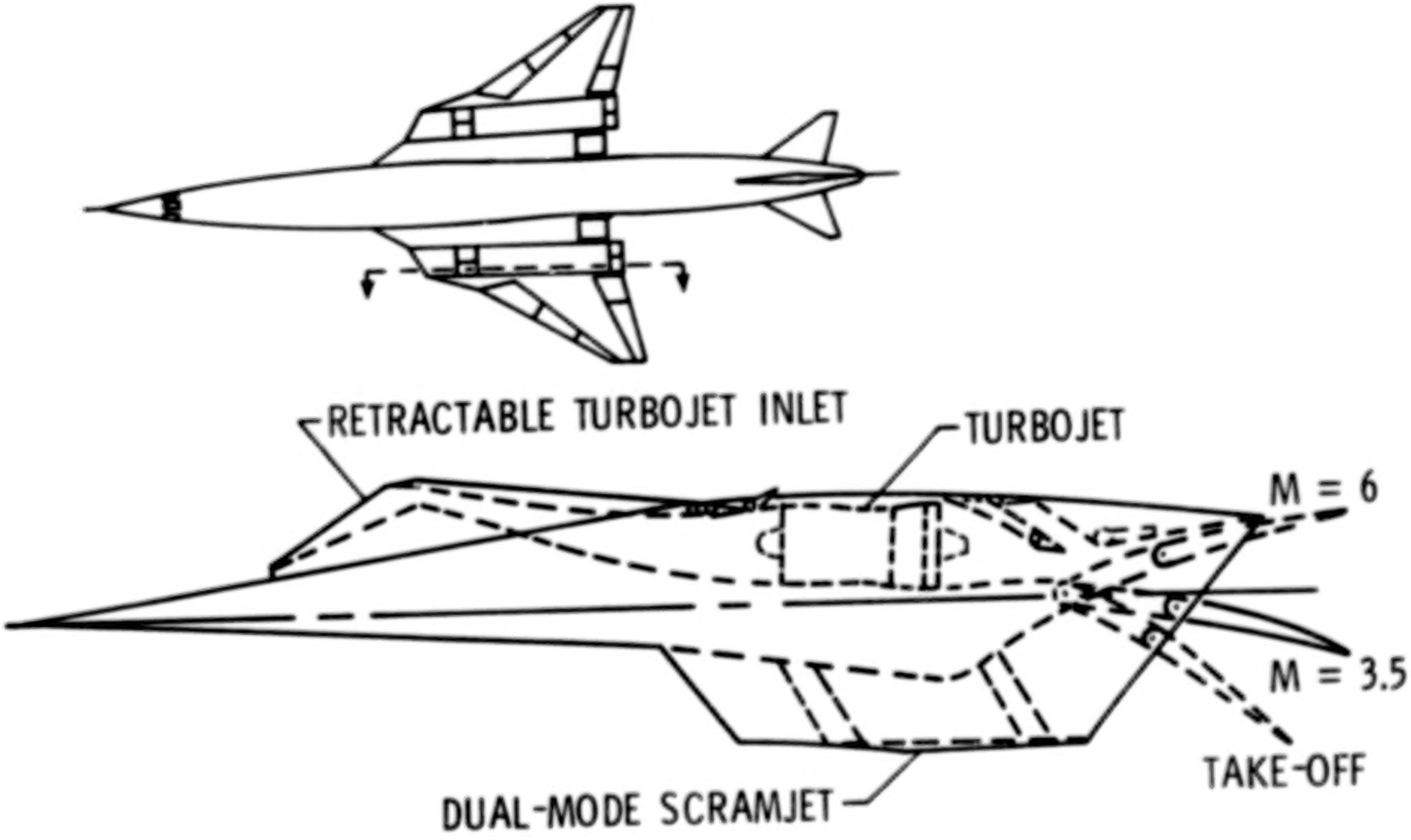
RETRACTABLE TURBOJET INLET
TURBOJET
M = 6
M = 3.5
TAKE-OFF
DUAL-MODE SCRAMJET

Figure 13

ADVANCED MACH 5 MILITARY CONFIGURATION

(Figure 14)

Figure 14 is a sketch of an advanced configuration, now in the analysis stage, for application to future military missions which may require extremely high altitude performance and extended ranges in conjunction with reduced radar cross section. This concept used JP fuel for turbojet operation and hydrogen for ramjet cruise. This configuration may undergo extensive modifications by the time it reaches the wind tunnel stage.

There are various types of military applications of hypersonic aircraft which would not require the long life of a transport airframe. Hot structure or metal heat shield TPS could do the job in these cases.

ADVANCED MACH 5 MILITARY CONFIGURATION

DUAL JP / LH_2 FUEL

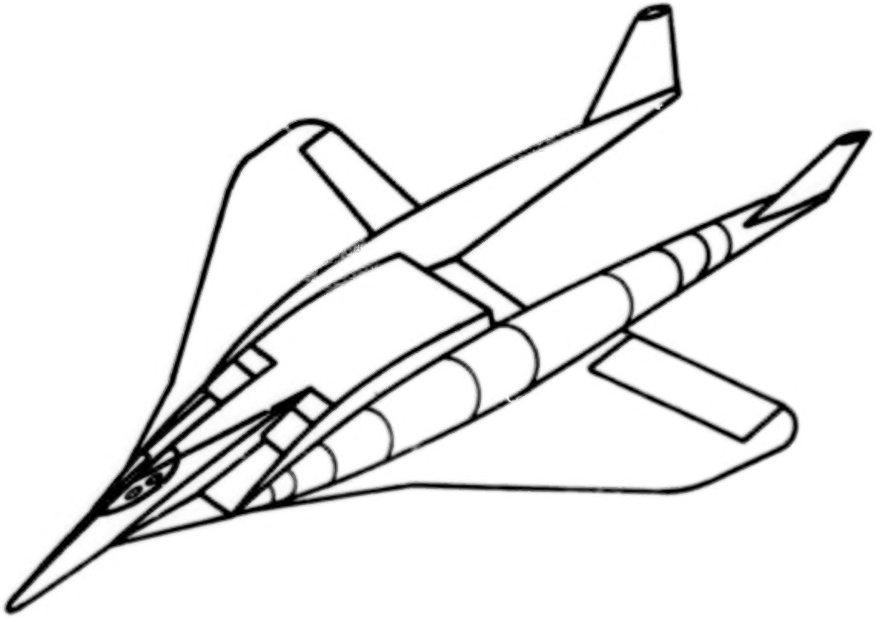

Figure 14

CONCEPTUAL TURBOJET-RAMJET SYSTEM

(Figure 15)

Figure 15 shows a section view of the centrally-located turbojet-ramjet propulsion system from the military configuration of the previous figure. The inlet is inverted on top of the aircraft in an effort to keep the system out of the line of sight of radar in front of and below the aircraft. The system design allows for turbojet propulsion from take-off to Mach 3 and ramjet propulsion from transonic speed to the Mach 5 cruise. Note that both engines are in operation during the supersonic acceleration. Inlet temperatures in the 1100 K (1500°F) range would be expected on this Mach 5 design. We will be in the process of better defining the environment for such a propulsion system structure during the next year. Again, a two-dimensional variable-geometry nozzle is shown.

CONCEPTUAL TURBOJET—RAMJET SYSTEM

TURBOJET - MACH 0 - 3.0

RAMJET - MACH 0.8 - 5.0

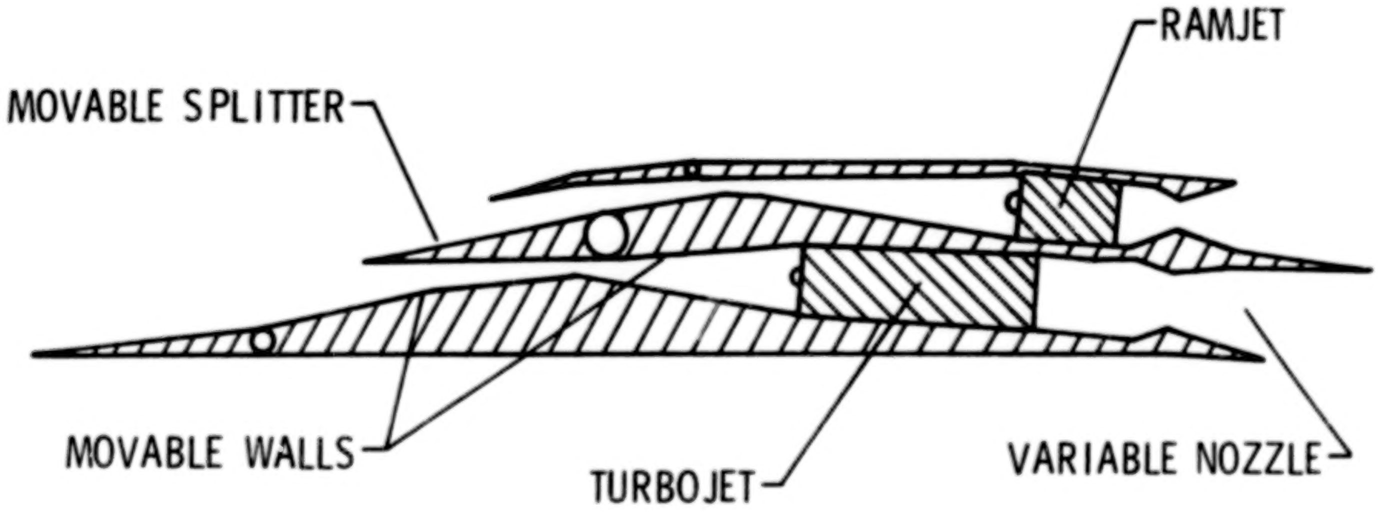
RAMJET
MOVABLE SPLITTER
MOVABLE WALLS
TURBOJET
VARIABLE NOZZLE

Figure 15

"COMMON DENOMINATOR" HYPERSONIC STRUCTURES TECHNOLOGY

(Figure 16)

With the current severe limitations on the research and development resources in hypersonics, it is almost ludicrous to carry on and on, identifying endless high-potential areas of research which we will be unable to address. In my opinion, it is also a waste of time to continually seek the ultimate mission panacea toward which we can direct all our resources. We might do well to ask ourselves if there are any common denominators in hypersonic structures technology which stand out among the others as being generally useful. I think there are a few and I've listed them on Figure 16. By addressing areas like these, or portions of them, we tend to advance technology which can be applied to any number of mission vehicles.

The first is the area of propulsion system structures. As you will see later in this symposium, progress is already being made at the upper end of the hypersonic regime with regeneratively-cooled scramjet engine structures. If we can solve the problems of a Mach 4-5 turbojet/ramjet propulsion system, we will also have in hand the means of solving most of the airframe problems for the entire Mach 4-6 speed range.

Another "common denominator" technology is that of liquid hydrogen fuel tank structure, insulation, and thermal protection. I would like to thank our subsonic friends for the work they have recently done in studying the use of liquid hydrogen as aircraft fuel and experimentally evaluating several candidate insulation materials, which you will hear more about later. Although we high-speed people complicate the liquid hydrogen system design problem by going to higher temperatures and requiring thermal protection, many of the LH_2 fuel structural problems are the same.

The development of efficient and practical internally-insulated metal heat shield systems and active cooling would provide needed alternatives to hot structure at the higher Mach numbers. The weight and cost trades among these options may very well dictate that most hypersonic aircraft will employ all three approaches in varying degrees, depending on the mission.

Last, but not least, in the list of "common denominators" is thermo-structural design capability. There are few, if any, established design methods, procedures, and criteria which apply directly to hypersonic aircraft. In addition, designers will have to develop a clearer understanding of thermal stress — its sources and the means of alleviating or minimizing it. So many new concepts become involved in the design of a hypersonic aircraft that current design practices simply are not adequate. The designer will have to be prepared to deal with such complex problems as design optimization where thermal stress, creep, cooling system performance, and thermal protection systems are involved.

These separate components cannot be completely separated by discipline and dealt with individually. They should be considered as integral with the basic airframe structure. Perhaps we're talking about a new "super discipline" of thermo-structural design which might combine several of the current disciplines. This is, of course, a very difficult problem to deal with and it probably will not be dealt with until the various aerospace companies can see some profit in making the required investment. But it does represent a deficiency in our present capability which we should recognize and be prepared to overcome when required.

We in the research and development sector of aerospace should keep in mind that, as the speed of hypersonic aircraft and missiles increases, the disciplines of aerodynamics, aero-heating, propulsion, thermal protection, and structures become more and more closely related and even interdependent. Therefore, the research that is done in these areas needs to be focused on similar objectives with a lot of communication between disciplines. Breakthroughs in one discipline may very well allow breakthroughs in the others, but only if they are communicated in a timely manner.

COMMON DENOMINATOR
HYPERSONIC STRUCTURES TECHNOLOGY

- PROPULSION SYSTEM STRUCTURES
  - VARIABLE-GEOMETRY COMMON INLETS FOR TJ/RJ
  - VARIABLE-GEOMETRY NOZZLES
  - HIGH-TEMPERATURE AND REGENERATIVELY-COOLED COMBUSTORS
  - FIXED-GEOMETRY SCRAMJET ENGINES
- LIQUID HYDROGEN FUEL SYSTEM - TANK - INSULATION - TPS
- METALLIC HEAT SHIELD TPS
- ACTIVE STRUCTURAL COOLING
- THERMO-STRUCTURAL DESIGN CAPABILITY

Figure 16

CONCLUDING REMARKS

One of the questions which will undoubtedly be asked toward the end of this symposium is, "Where shall we go with our hypersonic structures effort in the future?" Rather than attempting to answer the question, we from the aerodynamics side of the street have added significantly to your list of options. We do feel, however, that there are several fertile areas for future research which support most of the vehicle concepts discussed here. We in aerodynamics have decided not to wait until the starting gun sounds in the race toward an advanced hypersonic vehicle. We think that by applying our best judgment and setting out on a deliberate, broad research program, we will provide future options to the decision-makers that they wouldn't have otherwise. We know of no reason why the same general line of reasoning doesn't apply in structures.

When the time finally arrives when useful hypersonic vehicles are designed and built, it will be as a result of breakthroughs in hypersonic technology. These breakthroughs, as you know quite well, happen as natural products of a strong research and development program and a sustained high level of activity in the wind tunnels and structures test facilities. With a little cooperation and communication, we may even be able to come up with a hypersonic structural concept that will fly, or an aerodynamic configuration that can be built.

AIRFRAME-INTEGRATED PROPULSION SYSTEM FOR HYPERSONIC CRUISE VEHICLES*

Robert A. Jones and Paul W. Huber
NASA Langley Research Center

ABSTRACT

Research is underway on a new, hydrogen burning, airbreathing engine concept which offers good potential for efficient hypersonic cruise vehicles. Features of the engine which lead to good performance include; extensive engine-airframe integration, fixed geometry, low cooling, and the control of heat release in the supersonic combustor by mixed-modes of fuel injection from the combustor entrance. The engine concept is described along with results from inlet tests, direct-connect combustor tests, and tests of two subscale boilerplate research engines presently underway at conditions which simulate flight at Mach 6 and 7.

I. INTRODUCTION

It now appears certain that vehicles capable of repetitive long range flights in the atmosphere at hypersonic speeds can become a reality. How soon depends on the timing of the perfection and application of several areas of advanced technology - most especially those concerned with airbreathing propulsion and long-life, low-weight (actively-cooled) airframe structures and systems. This paper describes recent research on a totally airframe-integrated supersonic combustion ramjet (scramjet) which offers potential for efficient cruise propulsion at speeds from Mach 5 to 8. Regeneratively-cooled engine and actively-cooled airframe structure for hypersonic aircraft using the present propulsion concept are discussed in another paper in these same proceedings by Kelly, Wieting, Shore, and Nowak.

Most of the previous scramjet concepts that have been considered were of the "pod" type, capable of providing good internal performance but incapable of high installed thrust, due to the excessive cowl drag associated with the large nozzle expansions needed at high speeds. At speeds above Mach 4, practical considerations reduce the attractiveness of the pod approach. (See Fig 1). In addition to high external drag from the pressure force on the expanding cowl surface (necessary to obtain a suitable nozzle exit to inlet capture area ratio), the "pod" type engine installation suffers from insufficient capture area due to the inefficient use of cross section area of the flow within the vehicle shock layer. It also has drag increases and locally high heating rates due to flow interference between pods and vehicle. Variable geometry adds mechanical complexity and introduces significant weight penalties. The high internal contraction ratios and narrow annular passages typical of previous podded engines having good internal performance substantially increase cooling requirements to the point that more fuel might be needed to cool the engine than for combustion. This is particularly serious at the high Mach numbers where the fuel is required to cool certain parts of the airframe structure in addition to the engine. The design concept that has emerged from research at Langley emphasizes all three major areas of concern: internal thrust minus total external drag, cooling requirements for the combined airframe and engine, and the total weight of airframe and engine. This airframe-integrated scramjet concept blends aircraft forebody and afterbody functions in combination with fixed geometry propulsion units utilizing a mixed mode of fuel injection.

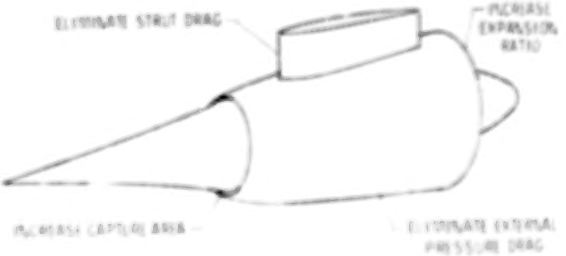

Figure 1. Improving "pod" Type Engine Performance

As illustrated in Figure 2, in order to obtain the required thrust at higher Mach numbers, the inlet area must be large enough to capture nearly all the airflow processed by the vehicle's undersurface bow shock. This suggests an annular inlet contiguous with the vehicle undersurface. Dividing the annular area into smaller rectangular units produces in effect a number of identical engine modules of a size and shape more nearly suited for ground tests.

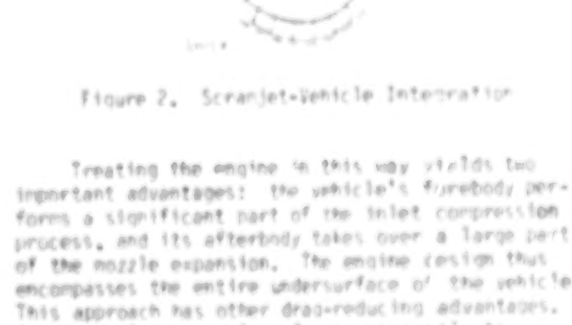

Figure 2. Scramjet-Vehicle Integration

Treating the engine in this way yields two important advantages: the vehicle's forebody performs a significant part of the inlet compression process, and its afterbody takes over a large part of the nozzle expansion. The engine design thus encompasses the entire undersurface of the vehicle. This approach has other drag-reducing advantages. The engine's external surfaces can easily be shaped to minimize installation losses by making them parallel to the local flow, and the vehicle's base region can be used to continue the nozzle expansion process to the large exit to inlet area ratios required for efficient propulsion without incurring an excessive drag penalty.

---

*Presented at The 11th Congress of the International Council of the Aeronautical Sciences, Lisbon, Portugal, Sept. 10-16, 1978.

This airframe-integrated scramjet concept has behind it extensive research on basic combustion and turbulent reaction flow processes, engine component configurations, and lightweight regeneratively-cooled structures. Two complete, subscale, research engines of heat sink structure are presently undergoing performance tests at conditions which simulate flight at Mach 4 and 7.

II. AIRFRAME-INTEGRATED MODULE

Inlet

Subscale models of the fixed-geometry inlet have been tested under conditions simulating a flight Mach number range from 3 to 7 in conventional wind tunnels. This inlet has a rectangular capture area. (See Fig 3). The vehicle bow shock compresses flow in the vertical direction while the wedge-shaped inlet sidewalls compress the flow horizontally. This two-plane compression reduces the degree of change in the inlet flow field that occurs with changing flight speed or angle-of-attack and makes fixed geometry feasible. Sweep of the compression wedges and a cutback cowl provide spillage. This allows the inlet to start at low flight speeds. It also reduces the pressure gradient on the top surface to permit ingestion of the forebody boundary layer. Swept wedge-shaped struts at the throat complete the inlet compression process. These block about 60 percent of the flow cross section in the swept plane. In addition to making the inlet shorter, lighter, and lessening its cooling requirements, these struts also provide multiple planes for fuel injection; and therefore the mixing distance and the combustor are also shortened.

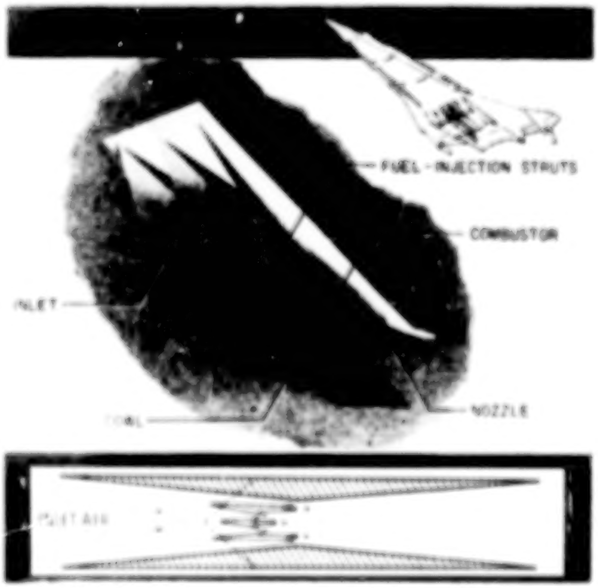

Figure 3. Airframe-Integrated Supersonic Combustion Ramjet

Experimentally determined schedules for mass capture ratio, contraction ratio, and total pressure recovery (Fig 4) have shown this to be a practical, high-performance inlet concept.[1] The inlet starts easily for flight Mach numbers above 3, has a variable mass capture ratio with low loss spillage at the lower Mach numbers, and an aerodynamic contraction ratio that varies with Mach number in a desirable way. In addition to its low drag, cooling, and weight, it rivals variable-geometry inlets in aerodynamic performance. In fact, it has demonstrated a higher pressure recovery than previous variable-geometry inlets such as the NASA Hypersonic Research Engine (HRE).[2]

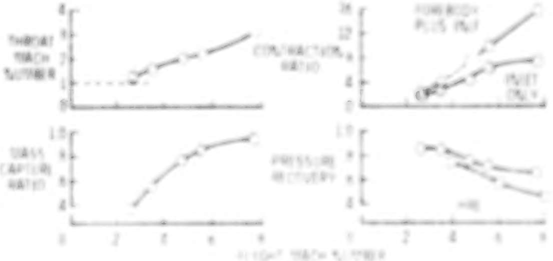

Figure 4. Inlet Aerodynamics

Combustor

Over a period of several years, both analytical and experimental research has been conducted on the physics, thermodynamics, and physical means for injection, mixing, ignition, and combustion of hydrogen/air mixtures at locally supersonic speed and high enthalpy. From this effort has emerged a fuel injector-combustor concept which direct-connect tests have shown to provide a good combustion efficiency over a range of flight Mach numbers, and at the same time have low cooling and low structural-weight requirements.[3]

From this work has also come a unique mixed-fuel injection mode that allows effective control of the streamwise heat-release distribution over the Mach-number range (Fig. 5).

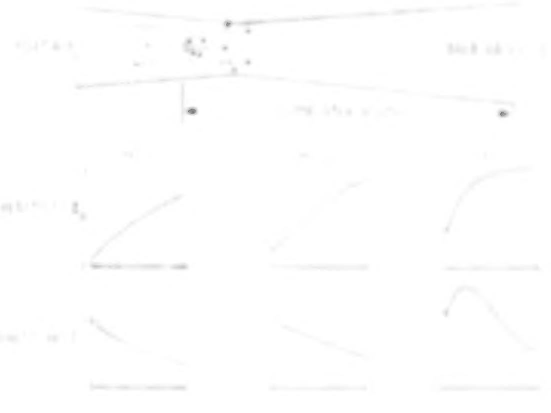

Figure 5. Combustor Operation

Dual-mode (subsonic/supersonic) combustion and minimum combustor length are obtained without necessity for additional fuel-injection stages (as required by previous concepts), which increase weight and cooling requirements. This is important because supersonic-combustion devices are sensitive to the distribution of heat release along the combustor flow length and its change with Mach number. For high propulsive efficiency, heat should be released as early in the combustor as possible (i.e.; higher pressure). At high flight speeds, fuel injected normal to the stream mixes, reacts, and releases its heat rapidly. At lower speeds, the large pressure rise associated with the rapid heat release can thermally choke the engine. At these lower speeds part of the fuel is injected parallel to the flow in the wake of the struts where it mixes and reacts much more slowly.

By proper apportionment of the fuel injected in the two modes, heat release can be tailored as desired. This combustor design also uses the struts to provide multiple in-stream planes for fuel injection. This in-stream fuel injection shortens the combustor length and lowers heat and skin friction losses compared to wall type fuel injectors. Combining these features, along with divergence of the combustor walls, yields efficient combustion performance over a wide Mach number range.

Nozzle

The flow into the nozzle is supersonic as there is no sonic throat. The after undersurface of the vehicle acts as the largest portion of the contoured nozzle wall. Essentially it is a half-nozzle, with only part of the dividing wall (partial cowl extension). The short cowl extension intercepts only a portion of the expansions from the contoured wall. At a Mach number of 6, about half the net thrust is generated by the large vehicle undersurface portion of the nozzle.

As a result of these factors, along with interactions between adjacent module wakes, spillage from the inlet, and nonuniform nozzle-entrance conditions, the nozzle plume has a highly 3-dimensional structure which changes with engine operating conditions, altitude, flight speed, vehicle attitude, etc. Furthermore, the nozzle flow analysis must account for multicomponent reacting species, shock, and viscous effects.

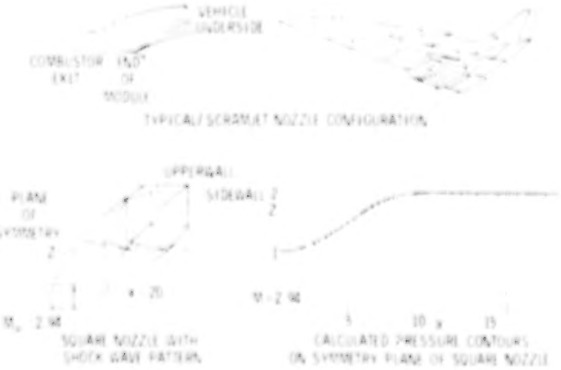

Figure 6. Integrated Scramjet Nozzle

Because of this great complexity, it is necessary to employ a combination of lengthy computational methods(4) and experimental simulations(5) to approximate the nozzle flow structure. Figure 6 shows results of a nozzle computation.

III. SUBSCALE MODULE TESTS

The modular nature of the integrated scramjet engine provides certain inherent advantages for ground testing. For example, testing a single module can yield performance data representative of a wide range of engine sizes and thrust levels. The effects of the vehicle-forebody boundary layer on the ingested engine flow are readily simulated as to scale (the actual profiles depend on the particular forebody shape) by placing the engine so that it swallows the test facility nozzle boundary layer flow. Precompression by the vehicle's forebody bow shock can be simulated by testing at the flight enthalpy but at a Mach number reduced to account for the change in flow Mach number across the bow shock. In tests such as these it is not possible to include the large external nozzle of the vehicle afterbody (which provides about 50 percent of the net thrust at Mach numbers of 6 and above), but the installed performance (thrust minus drag) of the inlet-combustor module can be measured directly by supporting the model on a thrust balance.

To adequately verify engine performance over the design Mach number range, test data are needed at the higher Mach numbers where the fuel is injected primarily normal to the flow as well as the lower Mach numbers where the fuel is injected primarily parallel to the flow. To obtain such data, two subscale heat sink, research engine modules have been built. One is being tested at conditions simulating Mach 7 flight in an arc heated facility at Langley. The other is undergoing test at conditions simulating Mach 4 flight at the General Applied Sciences Laboratory (GASL) in New York. These engines are the same size, 20.3 cm by 16.3 cm (8 inch by 6.4 inch) inlet capture area and about 1.5 m (5 ft) in length and very similar in design. Both are heat sink designs intended for short duration tests of up to 20 seconds. Figure 7 shows the engine which is being used for Mach 7 tests prior to installation in the facility. It is made of copper with water-cooled leading edges for the sidewalls, the cowl, and the struts.

Figure 7. Instrumented Subscale Scramjet Module

The Mach 4 engine is made of nickel. Both models are well instrumented internally with pressure orifices and heat transfer gauges. These research engines are designed for easy interchangeability of the fuel injection struts. The combustor area distribution near the fuel injectors can be varied by changing the struts or attaching pieces of different shape to downstream edges. Changes in downstream combustor area distribution can be simulated by air injection from the combustor sidewalls.

A schematic of the test setup in the Mach 7 facility is shown in figure 8 and a photograph of the facility with the research engine mounted in the test section is shown in figure 9. Note that the top wall of the engine model is positioned directly in line with the facility nozzle wall to swallow the facility boundary layer and thus simulate ingestion of the vehicle forebody boundary layer. A complete description of this arc-heated facility is given in Reference 6. It duplicates the Mach number, enthalpy and forebody boundary-layer conditions expected at the inlet for a vehicle at a flight Mach number of 7, but at dynamic pressure corresponding to only the very lowest values expected in flight, 16.8 kPa ($q_\infty = 350$ lb/ft^2).

AIR HEATER
THRUST BALANCE

Figure 8. Schematic of Mach 7 Scramjet Test Facility

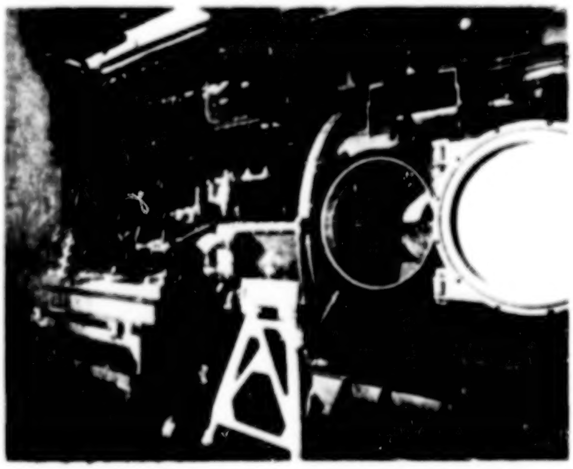

Figure 9. Mach 7 Scramjet Test Facility

The Mach 4 test setup at GASL is similar in that it duplicates the Mach number and enthalpy and forebody boundary-layer conditions expected at the inlet for a vehicle at a flight Mach number of 4. However, the facility heater is of the combustion type. Hydrogen and air are burned in the stagnation chamber and oxygen is added to replace that used for burning so that the test gas stream contains water-vapor as well as nitrogen and oxygen.

Preliminary tests in both facilities have been made in which hydrogen was burned in the engine. In these preliminary tests the modes of fuel injection and the split between parallel and perpendicular injection were varied, different strut geometries were tested, and various amounts of air were injected from the combustor sidewalls to change effective area distribution. No ignitors were used - spontaneous ignition was relied upon. As might be expected in the first tests of a new scramjet concept, these initial parametric tests uncovered a whole range of problems. These included facility-model interactions in which fuel injection caused test cabin pressure to increase, with subsequent inlet unstart (this problem has now been solved), cases where ignition did not occur at all in the engine, and cases where combustion heat release caused the inlet to unstart. There were also cases where combustion was achieved in the engine with no apparent interaction in the inlet, and measured internal thrust levels close to the predicted values were obtained.

Some of the results from one of the more successful of these preliminary tests in the Mach 7 facility are shown in Figure 10. For this test the total enthalpy of the flow approaching the inlet was 2.6 MJ/kg (1128 Btu/lb) with a total pressure of 30 atmospheres simulating a flight condition of Mach 7 at an altitude of 35 km (115,000 ft). Estimates using the method of Reference 7 with the reaction rate correlation of Reference 8 indicate that for stoichiometric fuel-air ratios at the low pressure of these preliminary Mach 7 tests only 20 percent of the fuel reacts. Therefore air equal to about 7 percent of that captured by the inlet was injected from the sidewalls to decrease the effective cross sectional area further downstream in the combustor, raise static pressure, and thus increase the reaction efficiency. Hydrogen fuel was injected from the struts normal to the flow at a fuel equivalence ratio of 0.5 and the drag and internal pressures measured (solid symbols in Figure 10). Note the large increase in pressure due to combustion which begins just downstream of the fuel injection location. The internal thrust obtained from the difference in balance readings with and without fuel was 225 N (50.6 lb). An estimate of the change in force due to internal pressures was made by interpolating for pressure between orifice locations and integrating over the entire internal surface of the engine. This integration gave a value of approximately 351 N (79 lb) but, of course, internal shear forces which act in the drag direction were not included.

From the change in measured heating rate in the combustor with and without fuel and the use of a correlation method of Orth and Billig,(9) the overall reaction efficiency (percentage of available fuel actually reacted) was estimated to be

59 percent; since the injected equivalence ratio was 0.5, this gave a reacted fuel equivalence ratio of 0.34.

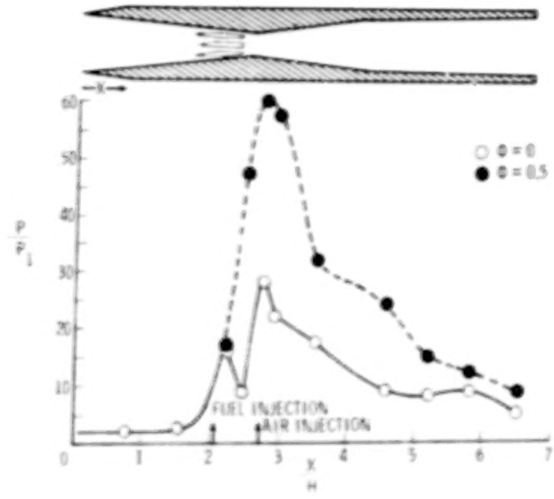

Figure 10. Internal Sidewall Pressure Distribution (Mach 7 Flight Simulation)

A comparison of the measured internal thrust with predictions based on simple one-dimensional theory(7,8) as a function of reaction efficiency is given in Figure 11. The solid line represents a real gas calculation assuming zero chemical reaction time (equilibrium) and no air injection from the combustor sidewalls. The fuel is assumed to react completely as soon as it is mixed (mixing controlled combustion) and an empirical relation for mixing as a function of flow length is used. The assumption of instantaneous reaction becomes inappropriate for low pressure levels. Because of the present low dynamic pressure conditions of the Mach 7 facility, 16.8 kPa (350 lb/ft^2) or about one-third of the design operating condition of the engine), the combustion process appears to be significantly affected by the finite time required for chemical reactions as well as the mixing rate. The use of air injection from the combustor sidewalls was employed to increase the pressure in the initial combustion region. The method of Reference 7 was modified to account for sidewall air injection and finite chemical reaction rates using the correlation for non-equilibrium hydrogen-air reactions of Pergament.(8) These results are shown as open symbols in Figure 11 for various ratios of injected air mass flow to inlet capture mass flow.

The results of the preliminary parametric tests made to date indicate that the inlet-combustor interactions experienced at large fuel-air ratios can be solved with minor geometric changes in the region of the fuel injector struts and that the reaction-rate limited combustion can be solved by increasing the operating pressure of the facility. Furthermore, the agreement between experimental results obtained so far and the theoretical performance predictions lends credence to the predictions of overall performance (thrust, specific impulse, and cooling requirement) of this airframe-integrated scramjet concept.

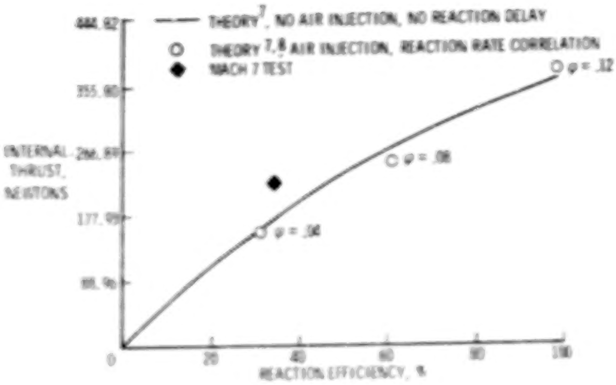

Figure 11. Predicted Internal Thrust

IV. PREDICTED PERFORMANCE CHARACTERISTICS

As a result of the large background of research compiled on components of the airframe-integrated scramjet, reasonable estimates can be made of the installed module performance (C_T and I_{sp}), module and system weights, module cooling requirements, and flight characteristics of an airframe-integrated scramjet vehicle.

It is interesting to compare the predicted specific impulse of the integrated scramjet with other high-speed propulsion systems. Figure 12 shows the fuel specific impulse for turbojets, ramjets, scramjets, and rockets as a function of the flight Mach number for hydrocarbon (JP) and hydrogen (H_2) fuel. The H_2-fueled scramjet at Mach 6 has a higher specific impulse than the JP-fueled turbojet at Mach 2. No real competitor to the scramjet exists at Mach numbers greater than about 6, even for an on-design cruise application.

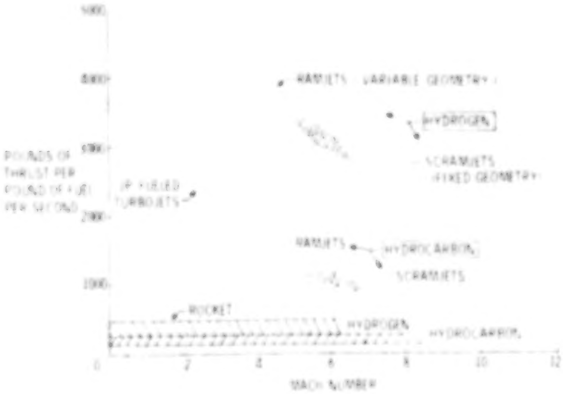

Figure 12. Propulsion Options

Installed Thrust

It is obviously not possible to define installed engine performance independent of vehicle characteristics. The vehicles forebody length, shape, and surface have a marked influence on the boundary layer and flow distribution entering the engine inlet, while the afterbody geometry strongly influences nozzle expansion, as previously discussed. Here for simplicity, we treat scramjet performance of a "nominal" forebody and afterbody, along with suggested means to estimate effects on performance due to departures from the "nominal." We distinguish installed from internal performance by accounting for several external effects chargeable to the engine. These include additive (or spillage) drag forces, cowl drag forces, effects of ingested forebody boundary layer on entering mass, energy and momentum, frictional and heat-transfer losses, and effects in the flight direction of normal forces on the capture flow and exhaust plume (since the coordinate system for thrust calculation goes in the forebody, or engine-flow, direction). Pinckney(10) has given a description of the complete performance calculation method, along with numerical results as functions of the various dependent parameters. Figure 13 shows thrust coefficient (C_T) and specific impulse (I_{sp}) as functions of fuel-air equilivance ratio (ϕ) and flight Mach number (M_∞) for the "nominal" vehicle underbody. The values of C_T and I_{sp} are for a dynamic pressure of 23.9 kPa (500 lb/ft^2) but are applicable to other altitudes as long as the reactions are controlled by mixing. The crossing of the curves is a result of different splits between parallel and normal fuel injection used to avoid thermal choking below Mach 6 and to reduce combustor heat load at Mach 8.

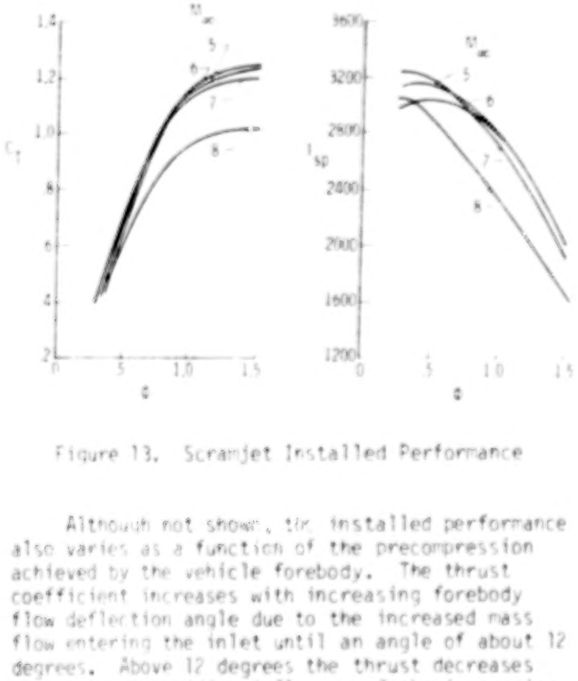

Figure 13. Scramjet Installed Performance

Although not shown, the installed performance also varies as a function of the precompression achieved by the vehicle forebody. The thrust coefficient increases with increasing forebody flow deflection angle due to the increased mass flow entering the inlet until an angle of about 12 degrees. Above 12 degrees the thrust decreases due to the overriding influence of the increasing normal-force component in the flight direction. While the installed engine performance includes external effects chargeable to the engine such as spillage, cowl drag, and effects of ingesting the forebody boundary layer, it does not include the aircraft drag. When vehicle drag is included, the peak thrust minus drag of the total system occurs at forebody flow deflection angles near 7 1/2 degrees for configurations optimized to cruise at Mach 6.

Forebody boundary-layer ingestion by the inlet represents one of the more important non-ideal flow effects on installed scramjet performance. Defects in entering mass flow due to the boundary-layer displacement show up directly as thrust decrements, while defects in entering momentum also degrade the performance. However, the loss in performance associated with ingesting the forebody boundary layer is less than the drag increase associated with diverting this flow or mounting the engine on a pylon. To account approximately for forebody boundary layers different from the "nominal" case cited, the thrust should be changed in proportion to the change in mass flow entering the inlet (due to change in boundary-layer-displacement thickness).

The forebody-boundary-layer characteristics used in determining the scramjet performance in Figure 13 are based on flat-plate flow of 12.2 m (40 ft) length and 667 K (1200°R) surface temperature. Transition was assumed to occur at $R_\theta = 10^3$ (momentum thickness Reynolds number). It is interesting that the ingested boundary-layer thickness, and hence thrust decrement, can be reduced by cooling the forebody. The energy loss to the cold wall can be recovered in the regenerative heating process (higher fuel T). The nozzle area ratio (engine nozzle exit to cowl) used in the calculations was about 3.6, and the external surface of the cowl lip was inclined 3 degrees to the forebody surface. The cowl drag forces amounted to about 5 percent of the thrust.

The influence of afterbody geometry (nozzle expansion) on the thrust coefficient is illustrated in Figure 14. Values of C_T as functions of nozzle expansion angle (θ) and length (L_N/H_C) for Mach 6 and a fuel equivalence ratio of 1.0 are shown. For expansion angles in the range of 16 to 24 degrees, thrust coefficient is primarily sensitive to the nozzle length (area ratio) up to values of about 4 H_C (module cowl height).

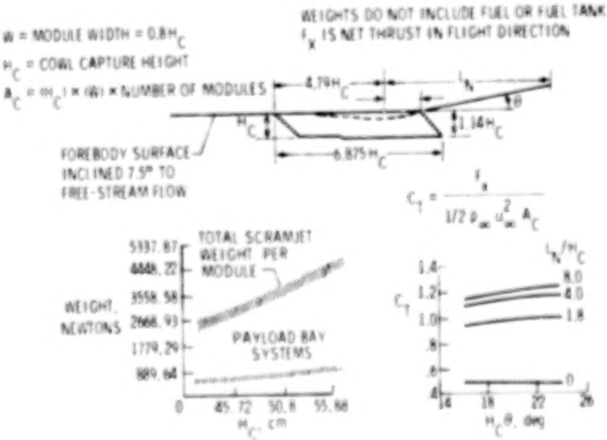

Figure 14. Scramjet Weight and Nozzle Geometry

Engine Weight

Detailed estimates of scramjet engine module weights and weights of the associated subsystems have been made based on both in-house and contractual structural(11) and system studies, including results from the HRE flight-weight regeneratively-cooled engine program. Figure 14 shows variation of module and systems weight as a function of the module cowl height, H_C. This case assumes a six-module scramjet engine of 4.1 kg/sec (9 lb/sec) hydrogen flow (maximum fuel flow rate for this study) which corresponds to ϕ = 1.5 operation at q_∞ = 71.3 kPa (1500 lb/ft^2) and M_∞ = 6.

For illustration, the weight breakdown for the case of six 45.7 cm (18 in.) high modules would be as follows: in-board engine modules, 236 kg (520 lb) each; outboard engine modules, 259 kg (570 lb) each, where both numbers include the engine subsystems (controls, valves, plumbing, and instrumentation); other subsystems, total 279 kg (615 lb). These weights average out, per module, to 290 kg (639 lb) total (engine and subsystems) and 47 kg (103 lb) for the other subsystems. The weight of hydrogen fuel and tankage would be additional.

Engine Cooling Requirements

Detailed computations of the heat-transfer rates and resulting cooling requirements for the component sections of the scramjet module have been made and compared with the available heat sink in the hydrogen fuel (also used as a coolant). The results depend strongly, of course, upon the assumptions of allowable wall and fuel temperature, type of material, coolant flow path, etc

Figure 15 shows the heat load for various engine module components as a percentage of the available heat sink in the hydrogen fuel as it flows to the combustor at an equivalence ratio of 1.0 for flight at Mach 6 and q_∞ = 23.9 kPa (500 lb/ft^2). For this condition, the total cooling required by the engine is about 50 percent of the available fuel heat sink.(11) The excess cooling available could be used to cool portions of airframe structure.

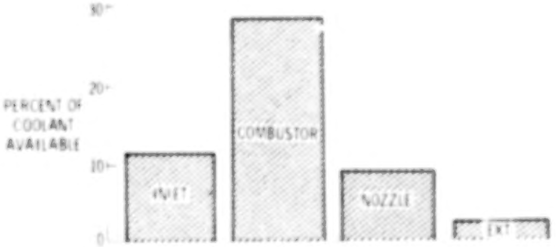

Figure 15. Engine Heat Load; M_∞ = 6, q_∞ = 23.9 kPa (500 lb/ft^2).

V. CONCLUDING REMARKS

Based on the concept of total engine-vehicle integration, the present scramjet concept appears to be capable of providing efficient airbreathing propulsion at Mach number of 5 and higher. We conclude this airframe-integrated scramjet concept has the potential for high thrust and efficiency, low drag and weight, low cooling requirement with excess cooling available to cool airframe components, and application to a wide range of vehicle sizes.

VI. REFERENCES

1. Trexler, C. A.: Inlet Performance of the Integrated Langley Scramjet Module. AIAA Preprint No. 751212, Sept. 1975.

2. Staff, AiResearch: Hypersonic Research Engine Project Phase II Aerothermodynamics Integration Model Development. Final Technical Data Report. NASA CR-132654, May 1975.

3. Henry, J. R.; and Anderson, G. Y.: Design Considerations for the Airframe-Integrated Scramjet, NASA TM X-2895, Dec. 1973.

4. Dash, S. M.; and Del Guidice, P. D.: Numerical Methods for the Calculation of Three-Dimensional Nozzle Exhaust Flow Fields. NASA SP-347, Part I, Mar. 1974.

5. Cubbage, J. M.; Talcott, N. A., Jr.; and Hunt, J. L.: Scramjet Exhaust Simulation for Hypersonic Aircraft Nozzle Design and Aero Model Tests. AIAA Preprint No. 77-82, Jan. 1977.

6. Boatright, W. B.; Sabol, A. P.; Sebacher, D. J.; Pinckney, S. Z.; and Guy, R. W.: Langley Facility for Tests at Mach 7 of Subscale, Hydrogen Burning, Airframe-Integrated, Scramjet Models. AIAA Preprint No. 76-11, Jan. 1976.

7. Anderson, G. Y.: An Examination of Injector/Combustor Design Effects on Scramjet Performance. 2nd International Symposium on Air-Breathing Engines, Sheffield, England, Mar. 25-29, 1974.

8. Pergament, H. S.: A Theoretical Analysis of Non-equilibrium Hydrogen-Air Reactions in Flow Systems. AIAA-ASME Paper No. 63-113, Apr. 1963.

9. Orth, R. C.; Billig, F. S.; and Grenleski, S. E.: Measurement Techniques for Supersonic Combustion Testing. Instrumentation for Airbreathing Propulsion Progress in Astronautics and Aeronautics, vol. 34, 1973.

10. Pinckney, S. Z.: Internal Performance Predictions for the Langley Scramjet Engine Module. NASA TM X-74038, Jan. 1978.

11. Killackey, J. J.; Katinszky, E. A.; Tepper, S.; and Vuigner, A. A.: Thermal-Structural Design Study of an Airframe-Integrated Scramjet. NASA CR-145368, June 1978.

BLANK PAGE

RECENT ADVANCES IN CONVECTIVELY COOLED ENGINE AND AIRFRAME STRUCTURES FOR HYPERSONIC FLIGHT*

H. Neale Kelly, Allan R. Wieting, Charles P. Shore, and Robert J. Nowak
NASA Langley Research Center

Abstract

The paper reviews Langley Research Center sponsored research on convectively cooled engine and airframe structures. The first section focuses on a hydrogen-cooled structure for a fixed-geometry, airframe-integrated scramjet; however, the thermal/structural problems, concepts, design features, and technological advances are applicable to a broad range of engines. The second section describes the most attractive convectively cooled airframe structural concepts that have evolved from an extensive series of investigations, the technology developments that have led to these concepts, and the benefits that accrue from their use.

Introduction

For hypersonic aircraft to become a practical reality, techniques must be developed for the design and fabrication of low-mass, airframe and engine structures that can withstand repeated and prolonged exposure to the severe aerodynamic heating encountered in hypersonic flight. The advancement of structural technology for this hostile flight regime has been the objective of continuing coordinated research at the NASA Langley Research Center.

At the 5th Congress of the International Council of the Aeronautical Sciences, September 1966, Heldenfels(1) reviewed the structural prospects for hypersonic vehicles. Emphasis then was on hydrogen-fuel-cooled structures for engines and passive hot structures of high temperature materials for airframes. Predicated on prospects of hydrogen-fueled scramjets with low cooling requirements(2), Becker, at the 7th ICAS Congress(3) proposed convectively cooled airframe structures of conventional low-temperature, low-mass materials (e.g., aluminum) that used the hydrogen fuel as the ultimate heat sink for all cooling requirements. Subsequently, status reports on convectively cooled structures technology were presented by Wieting and Guy(4) for scramjet structures and Nowak and Kelly(5) for airframe structures.

The present paper reviews recent advances in convectively cooled structures for both engine and airframe applications. The paper is divided into two main sections. The engine section is somewhat narrowly focused on a hydrogen-cooled structure for the Langley airframe-integrated scramjet described in detail by Jones and Huber(6). However, the baseline thermal structural configuration, design features, technology advances, and fundamental problems investigated are applicable to a broader range of engine structures. The airframe section describes the most attractive convectively cooled airframe structural concepts that have evolved from a series of investigations, the technology developments that have led to these concepts, and the benefits that accrue from their use. In addition, experience gained in fabrication of several airframe panel concepts is documented.

Engine Structures

Work on hydrogen-cooled engine structures at the Langley Research Center began with the Hypersonic Research Engine (HRE) Program of the 1960's and culminated, from a thermal/structural standpoint, in tests of a complete flight-weight hydrogen-cooled engine assembly in the Langley 8-foot high-temperature structures tunnel (fig. 1). These tests(7) and others(8) confirmed the suitability of the basic approach for research purposes. However, two major thermal/structural problems were uncovered that must be solved before a hydrogen-cooled scramjet can become a practical reality: (1) the coolant requirements must be reduced (the HRE required almost three times as much hydrogen for coolant as for fuel) and (2) the thermal fatigue life must be increased (HRE had an anticipated fatigue life of only 135 operational cycles). Both these problems stemmed, at least in part, from the annular design and high compression ratio of the engine which resulted in large areas being exposed to an intense heating environment. A fundamental goal of the continuing research program was to develop an engine concept which required only a fraction of the total fuel heat sink for engine cooling.

Airframe-Integrated Scramjet

Studies of airframe-integrated scramjets with high potential performance led to the sweptback, fixed-geometry, hydrogen-fueled, rectangular scramjet module shown in figure 2. Two inner scramjet modules are shown; the sidewall of one module is removed to reveal the internal engine surfaces. The scramjet modules are integrated with the airframe and use the entire undersurface of the aircraft to process engine airflow. The aircraft forebody serves as an extension of the engine inlet, and the afterbody serves as an extension of the engine nozzle. A number of aerodynamic/propulsion advantages are obtained with this concept.(6) Structural advantages include the fixed geometry and reduced wetted surface area and heating rates. Surface area is reduced by the nonannular configuration and by the multiple fuel injection planes which promote fuel mixing and combustion and thereby reduce the combustor length. Heat transfer rates are reduced by the lower inlet compression ratio and by the large combustor exit-to-entrance area ratio which reduce pressures.

By 1971 propulsion technology for the airframe-integrated scramjet had advanced sufficiently to warrant development of the thermal/structural technology. A preliminary thermal/structural design analysis study(4) based on HRE technology indicated viability from both an engine structural mass and coolant requirement standpoint. This study revealed a number of critical areas (e.g., panel-to-panel seals, fuel injection struts) and reemphasized the need for advances in fabrication and materials technology to obtain reasonable structural life.

---

*Presented at The 11th Congress of the International Council of the Aeronautical Sciences, Lisbon, Portugal, Sept. 10-16, 1978.

Recently, a more detailed study(9) of this scramjet concept was undertaken by a major engine manufacturer while the effort at Langley concentrated on the fuel-injection strut. As a focal point, the scramjets for these studies were sized for a conceptual hypersonic research aircraft and each module is approximately 46 cm high, 37 cm wide, and 315 cm long. Salient features from the thermal/structural design and analysis studies are presented in this paper.

Aerothermal Environment

The scramjet is designed to operate over a flight Mach number range of 4 to 10, and a dynamic pressure range of 24 kPa to 72 kPa. The maximum loading conditions occur during 2g maneuvers at a dynamic pressure of 72 kPa. The maximum thermal loading (heating rates up to 6 MW/m^2 on plane surfaces) occurs at Mach 10. The maximum pressure loading occurs at Mach 5.2.

The loading is characterized by the heat flux and pressure distribution along the longitudinal centerline of the sidewall component shown in figure 3. The heating is highly nonuniform because of boundary-layer transition, shock-boundary-layer interactions, and combustion. The critical pressure loads occur during an engine unstart (i.e., transition from supersonic to subsonic flow) which results if thermal choking occurs in the combustor. When the initial design study(4) was undertaken, the operational flow system was well understood; however, the unstarting process was not. Consequently, the basic unstart phenomena and loading were characterized experimentally(10).

The unstarting process is highly transient as indicated by the shaded area on the typical pressure history shown in the insert on figure 3. The peak pressure occurs during the unstart and is an order of magnitude higher than the normal operating pressure (p_o) and may be 2 to 7 times higher than the steady state unstarted pressure levels, which have typically been used in prior engine designs such as the HRE. These peak levels are conservatively predicted by normal shock wave theory. Since the complete dynamic characteristics of the transient pulse are not known, the envelope of the peaks along the engine (p_x on figure 3) currently serves as the basis for the engine structural design. The transient loading is particularly critical for the slender airfoil-like struts.

Shell Structure

To provide in-service accessibility and replaceability of parts, each scramjet module has detachable major structural components (see figs. 2, 4, and 5): a top wall, cowl, and two sidewalls, which form the basic shell structure, and the three fuel-injection struts.

Coolant System. All engine surfaces wetted by the airstream are regeneratively cooled by circulating the hydrogen fuel through a cooling jacket before injecting the fuel into the combustor. The cooling jacket, which is brazed to the primary structure, consists of the aerodynamic skin and multiple straight-fin or pin-fin coolant passages; straight-fin passages are shown as part of figure 4.

Although a fundamental design goal was the minimization of coolant requirements, the coolant routing scheme, depicted in figure 5, results primarily from requirements to minimize thermal stresses and deflections to yield the least complex thermal/structural and seal concepts. In general, the coolant enters each component leading and trailing edge (low heat load areas) and flows longitudinally toward the component center (highest heat load area), where it is collected in manifolds and routed to a fuel plenum. (Leading edge stagnation heating is intense but the heat load is low because of the small area). From there it is dispersed to the fuel manifolds in each strut and injected into the airstream. This routing scheme reduces the temperature variation transverse to the flow direction, the temperature differential through the cooling jacket, and to a lesser extent the total aerodynamic heat load thereby reducing the cooling requirements. Two coolant circuits per component were necessitated by the fuel pressure requirements, as frictional pressure losses with only one circuit would be excessive. The aerodynamic skin temperature distribution for each of the basic shell components is given in figure 6. A common outlet manifold location was selected to minimize thermal mismatch and simplify seals between components; although minimization of coolant flow rate and pressure drop would dictate different locations for the outlet manifold of each component.

All leading edges exposed to stagnation heating from the airflow are impingement cooled. The coolant is injected through a slot in the coolant inlet manifold and impinges on the inside surface of the leading edge, which then turns the coolant around to flow along the component surface (section A-A of fig. 7). This technique permits the use of the total sidewall coolant flow for impingement cooling. Even though the impingement cooling technique augments the coolant heat transfer characteristics along the stagnation line by a factor of two to three, the total circuit flow is required because of the high stagnation line heating.

A unique feature of the coolant routing scheme is the commonality of the cooling circuits for the sidewalls of adjoining modules. This scheme minimizes temperature gradients across the sidewall component and thus reduces thermal stresses and warpage in the sidewall. However, the primary structure is not common to the adjoining module sidewalls in that the frames are split as shown in section B-B of figure 7 to relieve top wall and cowl thermal stress by allowing the sidewalls to translate laterally relative to each other. The seal design is also simplified as the lateral expansion of only one module need be accommodated. In addition, module cowls are independent and allowed to slip relative to one another. The leading- and trailing-edge sections of the sidewall remain integral between adjoining scramjet modules; however, since these sections are near ambient temperature, the thermal stresses are acceptable(4,9). The design features expansion joints and seals at the top and bottom of the sidewall and a sliding seal between the cowls. This overall freedom to expand precludes any thermal stress due to the absolute temperature change from ambient; however, thermal stresses caused by the nonlinear temperature profiles can be relieved only by minimizing the thermal gradients.

Primary Structure. Three basic engine shell concepts were investigated: two frame-stiffened honeycomb-core sandwich panels and a deep-core honeycomb sandwich panel. One of the stiffened concepts had sidewall frames swept 48 degrees (parallel to isotherms to minimize thermal stresses) and the other had vertical sidewall frames (parallel to isobars to minimize unstart pressure stress); the latter is shown in figure 4. Both stiffened configurations use a 10-mm-thick honeycomb-core sandwich and seven frames; the deep-core honeycomb concept has a core thickness which varies from 6 to 50 mm and has two vertical frames. Analytical results$^{(9)}$ indicate relative displacements between adjoining components are generally small for all three configurations at steady state conditions. The small relative displacements, which are a direct result of matching temperature distributions at the component interfaces (fig. 6), permit the panel corners to be rigidly joined allowing the use of a simple static seal or even a welded corner. All three concepts have approximately the same mass per unit capture area of 1260 kg/m^2. As a comparison, the HRE with a mass per unit capture area of 1500 kg/m^2 was heavier in spite of the more structurally efficient circular shell construction. The deep-core honeycomb concept was selected as the baseline design primarily because it exhibits the least deflection in the sidewall and nozzle areas and is the least complex structure.

Preliminary results$^{(9)}$ indicate that the basic shell concepts have a significant temperature gradient through the thickness during thermal transients (e.g., maneuvers, combustion shutdown) which may significantly impact the final design of both the seals and basic shell structure.

Fuel-Injection Struts

The fuel-injection struts (see figs. 2, 4, and 8) presented the most formidable cooling and structural problems. The struts must simultaneously support a large side load, contain high-pressure hydrogen at two temperature extremes, and withstand the high thermal stresses resulting from complex aerodynamic heating as well as convective heating from the hot hydrogen in the internal manifolds. To compound these problems, the cross-sectional area and contour cannot be altered without significantly changing the engine propulsion performance.

The struts, shown in figure 8, have a maximum thickness of 2.5 cm and chords of 25 cm (center strut) and 38 cm (side struts), span 46 cm, and are swept back 48°. As shown in figure 9, each strut is subdivided internally into four longitudinal compartments. The fore and aft compartments serve as coolant inlet and outlet manifolds respectively and the central compartments serve as fuel manifolds for the strut trailing edge (parallel to airflow) and wall (perpendicular to airflow) fuel injectors. Coolant in the inlet manifold is injected through a slot, impinges on the leading edge, and splits (unequally) to flow along each wall to the trailing edge, where it is collected in the outlet manifold. This quadrilateral manifold configuration was selected over a more structurally efficient (high pressure containment) tubular configuration because the former has a greater volumetric efficiency which results in larger fuel and coolant flow areas and thus lower pressure losses.

Thermal Loading. Overall thermal expansions of the strut are accommodated by the mounting system. The strut top wall and cowl mounts are basically at midchord. At the top the strut has rotational freedom about the transverse axis and translational freedom in longitudinal and transverse directions. At the cowl the strut has rotational freedom about all axes and translational freedom along the 48° sweep line.

Analytical results$^{(4)}$ revealed temperature differences of up to 470 K through the primary structure wall and attendant thermal stresses up to 80 percent of the allowable stress. These large temperature differences and stresses were caused by internal convective heating from the hot hydrogen in the manifolds. The internal heating, which is normally negligible compared to the aerodynamic heating, is increased significantly by the higher velocities caused by the restricted flow area. Attempts to reduce these stresses by rearranging the fuel and cooling manifolds as well as the coolant circuitry proved fruitless. However, the addition of a metallic plate-fin thermal buffer (fig. 10a) in the hot manifolds reduced primary structure thermal stresses by approximately 64 percent, as indicated in figure 10b. The thermal buffer fins are oriented transverse to the fuel flow direction to restrict flow and provide essentially stagnant hydrogen in the passages between the shield and the strut wall, thereby eliminating direct convective heating to the strut wall.

External Pressure Loading. The maximum external pressure loading occurs at the Mach 5.2 thermal choke condition when the aerodynamic flow in the passage between the sidewall and a side strut unstarts and the flow in the other three passages remains started. The net side loading due to pressure on the strut is approximately 0.7 MPa.

Analytical results$^{(4,9)}$ indicate that the combined thermal and pressure stresses exceed the allowable stress (σ_a). The thermal stress (0.8 σ_a) is caused by the nonlinear chordwise temperature gradient and wall in-depth temperature gradient shown in figure 11a for a coolant outlet temperature equivalent to the superalloy temperature limit of 890 K. The temperature gradients are significantly reduced, as shown in figure 11a, by increasing the coolant flow to obtain an outlet temperature equal to the fuel temperature (430 K). Attendant thermal stresses are reduced to 0.3 σ_a and the combined stresses are reduced approximately 50 percent to acceptable levels as shown in figure 11b. This technique adds no complexity to design or fabrication and even though the strut coolant flow rate is doubled, the overall cooling requirement is increased only 5 percent. As discussed later, excess coolant is available at this flight condition. An alternate technique, identified in reference 4, ties the three struts together at midspan; however, the tie greatly complicates cooling design and fabrication.

Vibration analysis of the strut indicates a first mode (bending) frequency of 170 Hz. This frequency is within the range of engine time varying loads (e.g., combustion, shocks, transient unstart). A cursory look at the flutter potential indicated a factor of safety of nine on dynamic pressure. However, the dynamic response of the strut to the time varying pressure loads may be critical, consequently a detailed analysis is planned.

Low-Cycle Fatigue Life

A program is in progress to develop and experimentally validate the fabrication and materi technology required to obtain reasonable thermal fatigue life for the cooling jacket. The goal for the airframe-integrated scramjet is 1000 hours and 10 000 cycles of hot operation which represents an improvement of two orders of magnitude over the HRE. Analytical predictions of the fatigue life as a function of the temperature difference between the hot aerodynamic skin and the back surface are presented in figure 12. The life goal appears attainable through a number of factors such as engine design, fabrication, and material selection. The improvements attributable to these factors are graphically illustrated in the figure. The bottom curve indicates the anticipated life of the Hastelloy X coolant jacket for the HRE. The solid symbol at the right denotes the HRE design point and the open symbols indicate experimental data. A fundamental change in engine design to decrease the heat flux intensity and thus the temperature difference, as indicated by the horizontal arrow, is the first factor to increase the life of the airframe-integrated scramjet. An additional increase, as indicated by the vertical arrow, is obtained through an advanced fabrication technique. In this technique the fin coolant passages are photochemically etched into the aerodynamic skin which eliminates the strain concentration caused by local thickening of the skin by the fin and eliminates the hot skin-to-fin braze joint present in the HRE configuration. (The braze joint to the cooler primary structure remains, however.) The two candidate configurations fabricated by this process are shown in the figure. Finally, another increment in life is attained through the selection of a material with high thermal conductivity, which decreases the temperature difference, and with high ductility, which increases the fatigue life directly. To date Nickel 201 and Inconel 617 appear to be the most attractive materials. However, since these materials are not suited for primary structure application because of low strength, a new problem arises because high strength materials required for the primary structure generally have different coefficients of thermal expansion than the Nickel 201 and Inconel 617. Thus residual stresses may occur at ambient conditions because of thermal growth during the braze cycle. This problem is currently being investigated.

Cooling Requirements

The fraction of the stoichiometric fuel flow required to cool the scramjet engine at two dynamic pressures is shown in figure 13 as a function of Mach number. (A value of 1.0 indicates that all of the fuel flowing to the engine is required for cooling). Preliminary, and somewhat more optimistic, estimates of the cooling requirements have been presented in other papers (2,3,11); however, the present results are based on more detailed analyses and are more realistic. The results are presented inversely to the normal manner - with cooling requirements increasing from top to bottom - to highlight the impact of hydrogen temperature indicated by the secondary scale on the right. The curves are based on a hydrogen supply temperature of 56 K and the assumption that all cooling routes are balanced so that the hydrogen exits from each at a temperature of 890 K, a limit set by the superalloy material used in the primary structure. Any reduction in the average exit temperature, such as proposed for the struts, would increase the coolant flow required for cooling the engine. The fuel provides an adequate heat sink for cooling the engine at Mach numbers up to approximately 9 at a dynamic pressure of 24 kPa and to even higher Mach numbers at a dynamic pressure of 72 kPa. The cooling requirements are less severe at the higher dynamic pressure because the heat load increases as the 0.8 power of the dynamic pressure while the fuel requirement increases linearly. At lower Mach numbers there is surplus hydrogen fuel heat sink for airframe and/or additional engine cooling.

The curves presented in the figure can also be interpreted as a good approximation of the maximum hydrogen coolant supply temperature that the engine could tolerate without exceeding the prescribed outlet temperature if all of the fuel passed through the engine cooling circuits. When viewed from this perspective, it is more readily apparent that all of the surplus fuel heat sink is not available for airframe cooling. For example, at Mach 6 and a dynamic pressure of 24 kPa the engines require approximately 50 percent of the fuel heat sink for cooling and the coolant supply temperature could be approximately 450 K. However, that is too hot for cooling an aluminum airframe and, although 50 percent of the fuel heat sink is not required for engine cooling, only about 32 percent is available for airframe cooling. The other 18 percent would most likely be used to reduce the engine operating temperature levels and thereby increase the material strength and life, provided the reduced operating temperature is not detrimental to the engine propulsion performance. As shown by the figure, the engine requirements begin to reduce the fraction of heat sink available for airframe cooling above a Mach number of approximately 7.5.

Airframe Structures

Since Becker proposed the use of convectively cooled airframe structures of conventional low temperature materials (e.g., aluminum) at the 7th ICAS Congress,(3) a major portion of structures research for high-speed cruise flight sponsored by the Langley Research Center has involved such structures. The basic concept, suggested by Becker, (fig. 14) uses a closed-loop secondary cooling circuit with liquid coolant flowing through passages in the surface structure to transport the absorbed aerodynamic heating to a heat exchanger where the heat is rejected to the cryogenic hydrogen fuel flowing to the engine. The concept which uses a high-level cooling system (i.e., one that absorbs virtually all of the incident heat load) with the fuel as the ultimate heat sink evoked visions of largely unshielded hypersonic cruise vehicles with long-life, low-mass structures of conventional low-temperature materials.

Although early studies recognized problems in matching the instantaneous aerodynamic heat load with the heat sink capacity of the hydrogen fuel flowing to the engines and proposed partial heat shielding to reduce the absorbed heat load, both system studies(12-17) and hardware studies(5,18,19), following the lead of Becker, concentrated on bare cooled structures with high-level cooling. Recent studies(20-22) have yielded a better understanding of the significance of heat sink matching and the mass penalties associated with high-level cooling. From these studies a coherent and consistent definition of the most attractive convectively cooled structural approach is emerging, an approach that combines both passive and active thermal protection.

Recommended Application Regions

Recommended application regions for airframe concepts that combine passive and convective cooling are indicated in figure 15. The limits shown are approximate, and precise definition depends on the intended application. At the lower incident heat fluxes an overcoated convectively cooled structure is the favored concept. The overcoat, which is a moderate-temperature elastomeric material applied to the outer surface of the structure, is an outgrowth of the fail-safe abort studies by Jones(23). At higher heat fluxes the overcoat is replaced by high temperature insulation and metallic heat shields. This approach represents a marriage of convective active cooling with the mature radiative heat shield technology developed for entry vehicles(24). Only at the highest heat flux levels where heat shields reach excessive temperatures would bare convectively cooled structures be used. Fortunately, high heat flux areas represent only a small fraction of the surface of vehicles operating at Mach numbers up to approximately 10. As discussed in subsequent sections the use of hot surface thermal protection (overcoats or heat shields) with convectively cooled structures reduces total mass and provides other benefits including improved heat-load/heat-sink compatibility, increased safety and reliability, tolerance to off-design conditions, and ease of fabrication.

Hot-Surface Thermal Protection

Before discussing the benefits of integrating passive and convective cooling it is appropriate to review the status of hot surface thermal protection (heat shields and overcoats).

Heat Shields. Various radiative metallic heat shields have been considered for use with convectively cooled structures (22). The corrugation-stiffened shield shown in figure 15 has been extensively investigated analytically and experimentally as part of the NASA space transportation system effort(24). Corrugated superalloy heat shields have been shown to be suitable for reentry applications up to 1260 K which corresponds to a heat flux that is approximately 40 kW/m^2 higher than the upper use limit suggested in figure 15. TD nickel chrome shields to 1480 K which corresponds to an incident heat flux in excess of 400 kW/m^2, and refractory alloys to even more severe conditions. As concluded in reference 24, the basic technology for metallic heat shields is "in hand." Increasing service life of heat shields from the hundreds of mission cycles required for space transportation systems to the thousands required for hypersonic aircraft remains a significant but hardly insurmountable task since the heating environment for aircraft is less severe.

Overcoats. The low-density silicone, elastomeric material recommended as an overcoat is representative of a class of materials that also has been extensively investigated as part of the space effort - originally as an ablator(25) and more recently as a surface insulator.(26) When maintained at temperatures below about 600 K, as in the intended application, the material provides a resiliant insulation surface; if inadvertently overheated the material becomes a tenacious charring ablator providing an additional margin of safety. The overcoat concept in contrast to metallic shields is not limited by minimum gage restraints and can be sized to provide the optimum insulation thickness. Typically the thickness, which would vary with heat flux and overcoat material properties, would be less than 1.0 cm. The life and durability of overcoats have not been directly addressed and therefore remain unproven. However, a coating of silicone rubber (a probable base material for overcoats) applied to an area on the bottom of a high speed research aircraft (YF-12) to prevent impingement damage from jettisoned covers for a heat-transfer experiment showed no evidence of damage after over two years of service. During the two years, the material was exposed to temperatures up to 560 K and foreign object damage from the experiment and debris from landings including one on a dry lake bed.

Safety and Reliability

Safety and reliability are critical concerns for convectively cooled structures because such structures depend on mechanical equipment and contain liquid coolant under pressure. These concerns have prompted studies of means of permitting hypersonic aircraft to decelerate to a less hostile flight environment without exceeding the temperature limitations of the structure if the cooling system malfunctions(20,23). These studies involved methods of detecting malfunctions, configuration modifications to extend or augment the heat sink capacity of the structure, and minimum total heat-load flight maneuvers. The most recent of these "fail-safe abort" studies(23) presents highly convincing evidence that fail-safe abort systems are completely feasible throughout the Mach 3-6 speed range (the limits of the study). Additionally, results of the study indicate that hypersonic cruise aircraft capable of safely aborting flight from the cruise condition [illegible] lighter than a bare convectively cooled configuration without abort capability! Table I, which contains information extracted from reference 20, summarizes the structural mass and cooling characteristics of three pairs of convectively cooled aircraft designed for 200 passengers and a range of 9.26 Mm at Mach numbers of 3.0, 4.5, and 6.0. At each Mach number one of the two aircraft is a bare configuration with no abort capability, the other is the configuration with the best abort performance, as defined by the study, for that Mach number. At Mach 3.0 the total mass of the structural system for the configuration with abort capability is only 57 percent of the mass for the bare configuration; at Mach 4.5, 84 percent; and at Mach 6.0, 66 percent. The key to the abort capability and lower mass is the hot surface insulation (overcoat or heat shield). Insulation provides a thermal response delay that enables the aircraft to decelerate to a less hostile flight environment if the system fails. Insulation also reduces the instantaneous heat load to the cooling system during normal flight to or below the heat sink capability of the hydrogen fuel flow thereby eliminating the need for extra hydrogen solely for cooling.

The results of table I highlight the importance of matching heat load with available heat sink. The penalty for not matching the heat sink, as indicated by the additional hydrogen required for cooling, is most pronounced at the lowest Mach number. The severity of the penalty is the consequence of the higher lift-to-drag ratio and lower specific fuel consumption postulated for the Mach 3 vehicle and the duct burning turbo fan engine. The trend is consistent with early analytical work$^{(3)}$ which indicated increased heat sink matching difficulty with higher aircraft and engine performance.

Durability of the coolant passages is also an important consideration; however, preliminary ambient temperature fatigue tests of convectively cooled surface structural elements$^{(5,18)}$ indicate that coolant passages can be designed and fabricated with adequate life and noncatastrophic failure characteristics. Test results showed that even with surface flaws intentionally placed in the external skins of the structure a design life of 20 000 fully reversed cycles at limit load was exceeded before leakage occurred, and failure was always gradual rather than catastrophic with leakage increasing slowly until final failure occurred. In fact, tests of a honeycomb configuration with discrete cooling tubes$^{(18)}$ indicated that cracks in the structural skin would propagate past the tubes without penetrating them; furthermore the tubes retarded crack growth at tube-skin intersections.

Off Design

In a study$^{(21)}$, which assumed an adequate fuel heat sink was always available, shielded convectively cooled structures were recommended for uniform heat fluxes greater than about 85 kW/m^2 and nonuniform heat fluxes as low as 35 kW/m^2. This recommendation was based on a merit parameter which included mass, fabricability, inspectability, and reliability. The study recommended bare configurations with either plain tubes or tubes with internal fins at low heating rates; however, overcoated configurations were not considered.

Unit masses for bare and shielded panels from reference 21 and recently calculated unit masses for overcoated panels are presented in figure 16 for two different heating distributions. The results are shown as a function of the uniform heat flux that would be absorbed by a bare cooled structure with a surface temperature of 394 K. For the nonuniformly heated panels an additional heat load with a half cycle sine wave distribution and a peak intensity five times the uniform intensity was assumed to exist over 15 percent of the panel surface; thus, the average heat flux to the panel was 1.4 times the uniform flux. Both the bare and overcoated configurations employed coolant passages with internal fins since experimental heat transfer data upon which the study was based indicated that at Prandtl numbers encountered with convective cooling systems, fins augment heat transfer without significantly increasing pressure losses and thus yield the lowest mass configurations. Unit masses for the overcoated configuration were calculated by the authors using structure and system masses from reference 21 and overcoat material properties from reference 27. The overcoat had a maximum thickness of about 1.0 cm at a heat flux of about 10 kW/m^2. At higher fluxes the thickness was reduced to avoid exceeding the material maximum use temperature and at lower fluxes the thickness was reduced to decrease mass. As shown in figure 16, overcoated configurations exhibit a clear mass advantage over bare configurations for both uniform and nonuniform heating. Figure 16 also illustrates the low sensitivity of the heat-shielded configurations to heat flux level and nonuniformity. Slopes of the curves for heat shielded panels are less than 10 percent of the minimum slopes for bare configurations. Similarly, a change from uniform to nonuniform heating which increases the average heat flux by a factor of 1.4, increases shielded panel mass by less than 8 percent and bare configuration mass by 16 to 50 percent.

Besides facilitating accommodation of heating nonuniformities, insulation (both overcoats and heat shields) decreases the sensitivity of convectively cooled structures to transients as indicated by figure 17. The figure shows the structural temperature response to the transient heat pulse for a 90° - 2g turn of bare and heat-shielded convectively cooled panels designed for an aerodynamic heating environment that would produce a heat flux of 136 kW/m^2 to a 422 K surface. For the factor of two step increase in aerodynamic heat transfer coefficient the temperature of the structure protected by the shield slowly increases by an insignificant 10 K and the shield temperature increases about 149 K to 1232 K. (A temperature within the use range of superalloy shields). In contrast, the bare structure responds rapidly and increases about 57 K to 479 K which is unacceptable for aluminum. The lower sensitivity of shielded structures will certainly simplify cooling system controls and may make it possible to size insulated convectively cooled structures for steady-state heat loads, whereas bare configurations must be sized for the most severe maneuver heat load.

Fabrication

Reference 5, which surveys several design and fabrication studies, indicates the feasibility of designing, optimizing, and fabricating bare convectively cooled structures for a heat flux of 136 kW/m^2. However, the report cites several problems that were encountered during the fabrication of small fatigue specimens and larger (0.61 by 1.22 m) convectively cooled structural panels for experimental verification and performance testing. These problems are more tractable for shielded configurations.

For example, the conductance of the bond-line between cooling tubes and the structural skin is a critical concern for bare convectively cooled structures which absorb virtually all of the incident heat flux, but is a minor concern for shielded configurations which absorb only a small fraction of the incident flux. The importance of conductance is illustrated in figure 18 which presents maximum skin temperatures for bare and shielded convectively cooled configurations. Both configurations were designed for the same aerodynamic heating environment and employed similar construction with discrete cooling tubes spaced 2.54 cm. As shown, skin temperatures for the bare structure are excessive at conductances representative of available adhesives. Thus, bond-line conductance was the controlling factor which dictated soldering as the joining process for the bare structure and ultimately was the achilles heel of the bare panel design. Fabrication of this concept was abandoned after two unsuccessful attempts to solder a large panel(19). At the lower heat flux adhesive bonding yields acceptable temperatures and was used successfully to attach cooling tubes to the structure of a shielded configuration(22).

Another problem that was more difficult for bare than shielded structures was the bolted joints at the end of a structural panel. As shown in figure 19, for a bare panel (heat flux = 136.2 kW/m^2) a single row of fasteners was used to avoid excessive temperature at the joints which were cooled by conduction to the manifold. However, this type of joint permitted excessive motion and fretting in tests of small fatigue specimens(5,18) and was redesigned for the shielded structure(22) (heat flux = 9.1 kW/m^2). The redesign took advantage of the lower temperature rise at the end of the panel associated with the lower absorbed heat flux to add an additional row of fasteners which alleviated the motion problem.

System Trades

Collectively, previous studies have indicated the inadequacies of bare convectively cooled aluminum structures for hypersonic cruise aircraft and identified the numerous benefits attainable by combining passive thermal protection with convective cooling. Once it is accepted that some type of hot surface insulation is inevitable, and in fact desirable, it is possible to consider trades to establish the optimal use of convectively cooled structures and the potential use of mixed thermal/structural concepts.

Lowest total unit mass, which has been the primary criterion for selecting a concept in the preceding discussion, may not be the proper criterion in an overall trade study. The composition of the masses and perhaps more importantly the cooling requirements of different configurations vary radically even when the unit masses are the same because surface temperatures and hence absorbed heat fluxes vary widely. For example, at a uniform heat flux of 131 kW/m^2 both the overcoated and heat-shielded configurations (previously presented in figure 16) have a unit mass of 18.5 kW/m^2; however, as shown in figure 20, the cooling system comprises approximately 43 percent of the mass of the overcoated configuration and less than 13 percent of the mass of the shielded configuration. Furthermore, the cooling requirement of the shielded configuration, which absorbs only 7 percent of the incident heat flux, is less than 10 percent of the requirement of the overcoated configuration. For comparison, a bare configuration, which must absorb the total incident heat load, can accommodate less than three-fourths the heat load (91 vs 131 kW/m^2) of protected configuration with the same total mass. In fact, if cooling capacity is critical, it may be advantageous even at low heat fluxes to select shielded configurations, despite attendant mass penalties (fig. 16), because of greatly reduced cooling requirements.

There may be areas for which convectively cooled structures are not desirable. For example, a study of actively cooled structures(17) which used overall vehicle performance as a merit parameter and assumed an unlimited fuel heat sink concluded that improved performance could be obtained by replacing the cooled engine nacelle structure with a hot structure because the reduction in cooling system mass more than offset the mass increase of the hot structure. In fact, the fuselage tankage area, which was the focal point of the study, may not be a desirable application for convectively cooled structures. Preliminary calculations by the authors based on the insulation system of reference 28, heat shields of reference 20, and structure of the fuselage/tankage study(17) indicate a simple insulated and shielded configuration is lighter than a convectively cooled configuration. Results of these calculations, summarized in figure 21, indicate that in addition to being 21 percent lighter, the insulated configuration is 30 percent thinner thereby increasing the volumetric efficiency; even though the insulation was actually sized for a Mach 8 airframe whereas the cooled configuration was designed for Mach 6. The shielded and insulated configuration is less complex and avoids the ironic situation of requiring thermal protection to prevent freezing of the coolant in the feeder lines(29).

Finally, it appears desirable to consider cooled structure temperature from a total system standpoint. Generally, in system studies, the temperature has been arbitrarily set near the limit for the structural material to conserve the limited heat sink. With the increased design flexibility provided by insulated convectively cooled structures it may be desirable to operate the structure in some areas, such as the passenger compartment, at temperatures nearer the desired interior environment. Additionally, thermal/structural optimization studies of insulated structures(30,31) have shown that minimum mass designs do not necessarily coincide with the maximum use temperature for the structural material. In fact, reference 30 states that the structural operating temperature should be included as a design variable.

Experimental Program

To complement the system studies a series of design and fabrication studies has produced three 0.61 m by 1.22 m structural panels for thermal structural testing. The test structures, shown in figure 22, include a shielded panel and two bare panels of different construction. All panels were designed for the same environment: a uniaxial inplane limit load of ± 210 kN/m, a uniform normal pressure of ± 6.89 kPa, and a thermal environment that would produce a uniform heat flux of 136 kW/m^2 to a 0.61 by 6.1 m full scale panel with a surface temperature of 422 K. Additionally, each panel was designed for a life of 10 000 hours and 20 000 fully reversed limit load cycles. The panels differed in both structural and cooling concepts but each used aluminum as the structural material and a 60/40 glycol-water mixture as a coolant. The heat-shielded configuration features a corrugation stiffened René 41 heat shield and an adhesively bonded honeycomb sandwich structure with half round coolant tubes. One of the bare configurations uses an adhesively bonded stiffened-skin structure with redundant, counter-flow, quarter-ellipse coolant tubes; the other uses a brazed plate-fin sandwich with adhesively bonded stiffeners for both the structure and cooling passages. Additional characteristics and features of the concepts are presented in reference 5 and complete details of the shielded panel design and fabrication are presented in reference 22.

A breakdown of the unit masses and absorbed heat fluxes (i.e. cooling requirements) for the three test panels and a fourth bare honeycomb concept that was abandoned because of fabrication difficulties(19) are presented in table II. As indicated the cooling requirement (absorbed heat flux) for the shielded configuration is over an order of magnitude less than that for the bare configurations. As a result, the mass of the auxiliary active-cooling system (pumps, heat exchangers, distribution system, etc.) is reduced sufficiently so that the total configuration mass for the shielded configuration is 7 percent lighter than the corresponding bare configuration even though the mass of the shielded structure alone is approximately 11 percent higher than the mass of the bare panel. The bare stiffened sandwich and stiffened-skin structures are lighter than the honeycomb sandwich; therefore, since the mass savings afforded by shielding is primarily in the cooling system mass, it is apparent that shielding could be applied to the other structural concepts in table II to obtain configurations that are even lighter.

To date the design and fabrication studies have provided insight into some of the practical problems of designing and fabricating low mass convectively cooled structures(5,19,22) and a preliminary appraisal of the fatigue characteristics using small ambient temperature specimens(5,18). Currently, the large (0.61 by 1.22 m) specimens are being tested at the Langley Research Center. All three of the convectively cooled panels will be tested in a special test apparatus shown in figure 23. The structure will be simultaneously heated with the radiant lamp array, cooled with a chilled glycol-water solution, and cyclically loaded by the servo-controlled testing machine. The shielded configuration will also be tested at a Mach number of 7 in the Langley 8-foot high-temperature structures tunnel to detect possible aerothermal problems and investigate possible hot gas ingress problems which would seriously degrade overall performance. In addition, durability and thermal cycle tests of hot surface insulations are planned. Data from the experimental program will permit a quantitative assessment of the thermal and structural performance and structural integrity of both shielded and bare convectively cooled structures.

Concluding Remarks

Closely coordinated research over the past decade has identified critical thermal/structural design problems and has produced viable design concepts for a second generation experimental scramjet. The design concepts for the hydrogen-fuel-cooled engine structure involve a variety of innovative features to accommodate the harsh aerothermal environment encountered within the engine. The baseline concept that has evolved has reasonable mass characteristics, and cooling requirements that permit engine operation to Mach numbers of 9-10 without additional hydrogen for engine cooling. At lower Mach numbers significant excess heat sink capacity is available for airframe cooling or reduced engine structural temperatures. Studies have identified fabrication techniques and coolant passage configurations that increase fatigue life of the structure an order of magnitude over previous configurations. Future research will involve experimental verification of the selected concepts.

Extensive studies of hypersonic airframe structures provide a coherent and consistent definition of the most attractive convectively cooled structural approach. The studies indicate that at the lower incident heat fluxes (lower Mach numbers) an overcoated convectively cooled structure is the favored concept. (The overcoat is a moderate temperature elastomeric insulation applied to the exterior surface of the structure.) At higher heat fluxes the overcoat is replaced by high temperature insulation and metallic heat shields, and only at the highest heat fluxes in areas where the heat shield temperatures are excessive would bare convectively cooled structures be used. Overcoats or heat shields provide numerous benefits including: improved heat-load/heat-sink compatibility, increased safety and reliability, tolerance to off-design conditions, lower mass, and ease of fabrication. An experimental program is presently underway to verify the performance and life of bare and shielded convectively cooled airframe structures in a realistic heating, loading, and cooling environment. The program includes heating and loading in a special test apparatus and aerothermal testing at a Mach 7 in the Langley 8-foot high-temperature structures tunnel.

References

[1] Heldenfels, R. R., "Structural Prospects for Hypersonic Air Vehicles," Paper No. 66-31, Presented at the Fifth Congress of the International Council of the Aeronautical Sciences (ICAS), London, England, Sept. 12-16, 1966.

[2] Henry, John R., and Anderson, Griffin Y., "Design Considerations for the Airframe-Integrated Scramjet," Presented at the 1st International Symposium on Air Breathing Engines, Marseille, France, June 19-23, 1972 (Also NASA TMX-2895, Dec. 1973).

CONTENTS

Part I

PREFACE . . . . iii 1/A5

WELCOME 1 1/A10
R. R. Heldenfels

SESSION I - OVERVIEWS
Chairman: A. J. Henderson

1. HYPERSONIC STRUCTURES: AN AERODYNAMICIST'S PERSPECTIVE (OR ONE MAN'S DREAM IS ANOTHER MAN'S NIGHTMARE) 5 1/B1
J. D. Watts, L. R. Jackson, and J. L. Hunt

2. STRUCTURAL REQUIREMENTS FOR MILITARY HYPERSONIC SYSTEMS (Paper not available for publication)
P. Lane

3. AIRFRAME-INTEGRATED PROPULSION SYSTEM FOR HYPERSONIC CRUISE VEHICLES 39 1/F13
Robert A. Jones and Paul W. Huber

4. RECENT ADVANCES IN CONVECTIVELY COOLED ENGINE AND AIRFRAME STRUCTURES FOR HYPERSONIC FLIGHT 47 1/G7
H. Neale Kelly, Allan R. Wieting, Charles P. Shore, and Robert J. Nowak

SESSION II - ENGINE STRUCTURES
Chairman: H. N. Kelly

5. DESIGN AND ANALYSIS OF A SCRAMJET ENGINE 65 2/A13
O. A. Buchmann

6. THERMOSTRUCTURAL ANALYSIS OF A SCRAMJET FUEL-INJECTION STRUT 119 3/B11
Allan R. Wieting and Earl A. Thornton

7. ADVANCED FABRICATION TECHNIQUES FOR COOLED ENGINE STRUCTURES 145 3/F7
O. A. Buchmann

8. HYDROGEN EMBRITTLEMENT AND ITS CONTROL IN HYDROGEN-FUELED ENGINE SYSTEMS 195 4/F11
W. T. Chandler

9. CARBON-CARBON COMPOSITE APPLICATION FOR INTEGRAL ROCKET RAMJET COMBUSTORS (Paper not available for publication)
H. A. Holman

SESSION III - COOLED AIRFRAME STRUCTURES
Chairman: C. P. Shore

10. DESIGN AND FABRICATION OF A SKIN STRINGER DISCRETE TUBE ACTIVELY COOLED STRUCTURAL PANEL 253 6/A5
Frank M. Anthony

11. DESIGN AND ANALYSIS OF A PLATE-FIN SANDWICH ACTIVELY COOLED STRUCTURAL PANEL 319 7/C13
L. M. Smith

12. FLUXLESS BRAZING AND HEAT TREATMENT OF A PLATE-FIN SANDWICH ACTIVELY COOLED PANEL 375 8/E1
Charles S. Beuyukian

13. DESIGN AND FABRICATION OF A RADIATIVE ACTIVELY COOLED HONEYCOMB SANDWICH PANEL 449 10/A13
Leland C. Koch

14. RADIATIVE, ACTIVELY COOLED PANEL TESTS RESULTS 493 11/A5
Charles P. Shore, Robert J. Nowak, and Ellsworth L. Sharpe

[3] Becker, J. V., "New Approaches to Hypersonic Aircraft," Presented at the Seventh Congress of the International Council of the Aeronautical Sciences (ICAS), Rome, Italy, Sept. 1970.

[4] Wieting, Allan R., and Guy, Robert W., "Preliminary Thermal-Structural Design and Analysis of an Airframe-Integrated Hydrogen-Cooled Scramjet," AIAA Paper 75-137, Pasadena, Calif., 1975 (Also J. of Aircraft, Vol. 13, March 1976, pp. 192-197.)

[5] Nowak, Robert J., and Kelly, H. Neale, "Actively Cooled Airframe Structures for High-Speed Flight," Presented at the AIAA/ASME/SAE 17th Structures, Structural Dynamics and Materials Conference, King of Prussia, PA, May 5-7, 1976. (Also J. Aircraft, Vol. 14, No. 3, March 1977, pp. 244-250

[6] Jones, Robert A., and Huber, Paul W., "Airframe Integrated Propulsion System for Hypersonic Vehicles," Recent Advances in Structures for Hypersonic Flight, NASA CP-2065, 1978. (Paper no. 3 in this compilation.)

[7] Wieting, Allan R., "Aerodynamic and Thermal Analysis of Results of Tests of a Hydrogen-Cooled Scramjet Engine (HRE-SAM) at Mach 6.3," NASA TMX-2767, May 1973.

[8] Staff of Langley Research Center and AiResearch Manufacturing Co., The Garrett Corp., "Hypersonic Research Engine Project Technological Status 1971," NASA TM X-2572, 1972.

[9] Killackey, J. J., Katinsky, E. A., Tepper, S., and Vuigner, A. A., "Thermal-Structural Design Study of an Airframe-Integrated Scramjet," Interim Summary Report, NASA CR-145368, 1978.

[10] Wieting, Allan R., "Exploratory Study of Transient Unstart Phenomena in a Three-Dimensional Fixed-Geometry Scramjet Engine," NASA TN D-8156, March 1976.

[11] Jones, Robert A., and Huber, Paul W., "Toward Scramjet Aircraft," Astronautics & Aeronautics, Vol. 16, No. 2, February, 1978, pp. 38-48.

[12] McConarty, W. A., and Anthony, F. M., "Design and Evaluation of Active Cooling Systems for Mach 6 Cruise Vehicle Wings," NASA CR-1916, 1971.

[13] Helenbrook, R. G., McConarty, W. A., and Anthony, F. M., "Evaluation of Active Cooling Systems for a Mach 6 Hypersonic Transport Airframe," NASA CR-1917, 1971.

[14] Helenbrook, R. G., and Anthony, F. M., "Design of a Convective Cooling System for a Mach 6 Hypersonic Transport Airframe," NASA CR-1918, 1971.

[15] Anthony, F. M., Dukes, W. H., and Helenbrook, R. G., "Internal Convective Cooling Systems for Hypersonic Aircraft," NASA CR-2480, 1974.

[16] Brewer, G. D., and Morris, R. E., "Study of Active Cooling for Supersonic Transports," NASA CR-132573, 1975.

[17] Pirrello, C. J., Baker, A. H., and Stone, J. E., "A Fuselage/Tank Structure Study for Actively Cooled Hypersonic Cruise Vehicles-Summary," NASA CR-2651, 1976.

[18] Sharpe, Ellsworth L., and Elber, Wolf, "Ambient Temperature Fatigue Tests of Elements of An Actively Cooled Honeycomb Sandwich Structural Panel," NASA TM X-3557, Sept. 1977.

[19] Koch, L. C., and Pagel, L. L., "High Heat Flux Actively Cooled Honeycomb Sandwich Structural Panel for a Hypersonic Aircraft," NASA CR-2959, 1978.

[20] Pirrello, C. J., and Herring, R. L., "Study of a Fail-Safe Abort System for an Actively Cooled Hypersonic Aircraft-Volume I, Technical Summary," NASA CR-2652, Jan. 1976.

[21] Herring, R. L., and Stone, J. E., "Thermal Design for Areas of Interference Heating on Actively Cooled Hypersonic Aircraft," NASA CR 2828, December, 1976.

[22] Ellis, D. A., Pagel, L. L., and Schaeffer, D. M., "Design and Fabrication of a Radiative Actively Cooled Honeycomb Sandwich Structural Panel for a Hypersonic Aircraft," NASA CR 2957, March, 1978.

[23] Jones, R. A., Braswell, D. O., and Richie, C. B., "Fail-Safe System for Actively Cooled Supersonic and Hypersonic Aircraft," NASA TM X-3125, 1975.

[24] Bohon, Herman L., Shideler, John L., and Rummler, Donald R., "Radiative Metallic Thermal Protection Systems - A Status Report," Presented at the ASME/AIAA/SAE 18th Structures, Structural Dynamics, and Materials Conference, San Diego, CA, March 21-23, 1977.

[25] Howell, William E., "Ablative Performance of Various Low-Density Elastomeric Composites," NASA TN D-6130, Feb. 1971.

[26] Lane, Paul Jr., and Kirlin, Ronald, "Development of Bond-On Thermal Protection Systems for Hypersonic Research Vehicle," AIAA Paper No. 78-478. Presented at the AIAA/ASME 19th Structures, Structural Dynamics, and Materials Conference, Bethesda, Maryland, April 3-5, 1978.

[27] Peeples, M. E., and Herring, R. L., "Study of a Fail-Safe Abort System for an Actively Cooled Hypersonic Aircraft- Volume II, Technical Report," NASA CR-144920, Jan, 1976.

[28] Helenbrook, R. G., and Colt, J. Z., "Development and Validation of Purged Thermal Protection Systems for Liquid Hydrogen Fuel Tanks of Hypersonic Vehicles," NASA CR-2829, June, 1977.

[29] Stone, James E., "A Fuselage/Tank Structure Study for Actively Cooled Hypersonic Cruise Vehicles-Active Cooling System Analysis, NASA CR-132669, 1975.

[30] Adelman, Howard M., Sawyer, Patricia L., and Shore, Charles P., "Development of Methodology for Optimum Design of Structures at Elevated Temperatures," Presented at the AIAA/ASME 19th Structures, Structural Dynamics and Materials Conference, Bethesda, Maryland, April 3-5, 1978.

[31] Thornton, William A., and Schmit, Lucien A. Jr., "The Structural Synthesis of An Ablating Thermostructural Panel," NASA CR-1215, December 1968.

TABLE I. FAIL-SAFE ABORT ACTIVELY COOLED AIRCRAFT
[200 PASSENGER, 9.26-Mm RANGE (REF. 20)]

MACH NUMBER		3.0		4.5		6.0	
ENGINE		DUCT BURNING TURBO FAN		TURBO RAMJET		TURBO RAMJET	
FAIL SAFE ABORT		NO	YES	NO	YES	NO	YES
THERMAL PROTECTION	UPPER SURFACE	BARE	SILICONE OVERCOAT	BARE	SILICONE OVERCOAT	BARE	SILICONE OVERCOAT
	LOWER SURFACE	BARE	SILICONE OVERCOAT	BARE	TITANIUM HEAT SHIELD	BARE	RENÉ 41 HEAT SHIELD
MASS SUMMARY, Mg							
Actively Cooled Structure		38.2	37.7	38.7	37.7	38.9	37.7
Thermal Protection System		0	1.5	0	5.2	0	8.4
Active Cooling System		3.3	2.3	5.6	2.6	7.7	3.2
Failure Detection System		0	0.5	0	0.5	0	0.6
SUBTOTAL		41.5	42.0	44.3	46.0	46.6	49.9
Additional Hydrogen for Cooling		32.1	0	10.7	0	29.4	0
TOTAL		73.6	42.0	55.0	46.0	76.0	49.9
HEAT LOAD TO HEAT SINK RATIO							
		1.62	1.0	1.23	0.41	1.67	0.46

TABLE II. UNIT MASSES OF FOUR CONVECTIVELY COOLED STRUCTURAL CONCEPTS

THERMAL CONCEPT	SHIELDED DISCRETE TUBES	UNSHIELDED DISCRETE TUBES	UNSHIELDED PLATE-FIN SAND.	UNSHIELDED REDUNDANT TUBES
STRUCTURAL CONCEPT	HONEYCOMB SANDWICH	HONEYCOMB SANDWICH	STIFFENED SANDWICH	STIFFENED SKIN
*ABSORBED HEAT FLUX, kW/m^2	9.1	136.2		
COMPONENT	UNIT MASS, kg/m^2			
Optimized Mass				
Dry				
Skins	5.86	3.76	3.95	3.66
Cooling Passages	0.78	2.73	0.64	0.93
Stiffening	1.42	1.32	1.71	3.91
SUBTOTAL	8.06	7.81	6.30	8.50
Wet				
Cooling Inventory	0.59	1.86	2.49	1.46
Pumping Penalty	0.01	0.34	0.53	0.29
SUBTOTAL	0.60	2.20	3.02	1.75
Non Optimums				
Manifolds	0.78	0.64	0.44	0.53
Closeouts	0.63	1.76	1.71	0.93
Adhesives	1.95	2.10	0.29	0.10
Fasteners, etc.	1.02	0.49	0.64	0.34
SUBTOTAL	4.38	4.99	3.08	1.90
Radiation System	7.27	-	-	-
Total Panel Mass	20.31	15.00	12.40	12.15
Distribution System	1.76	** 8.64	** 9.40	** 8.6
Total Concept Mass	22.07	23.64	21.80	20.75

* All concepts designed for an incident heat flux of 136.2 kW/m^2

** Approximate values based on results from reference 22; distribution system mass was not included in the original design of these concepts.

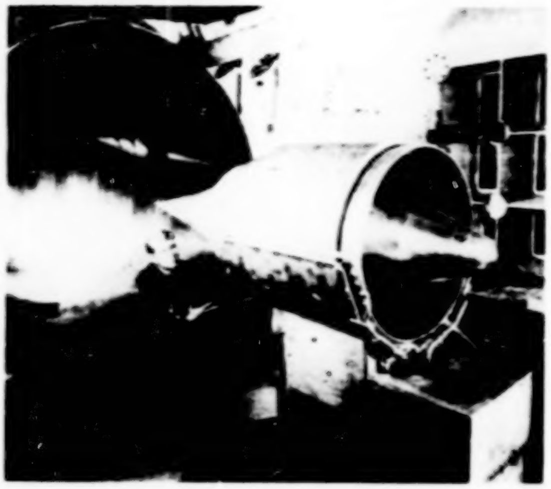

Figure 1. Hypersonic Research Engine (rear view) installed in the Langley 8-foot high-temperature structures tunnel.

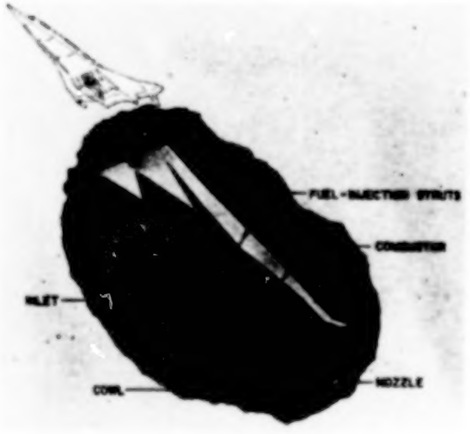
FUEL-INJECTION STRUTS
COMBUSTOR
INLET
COWL
NOZZLE

Figure 2. Airframe-integrated supersonic combustion ramjet.

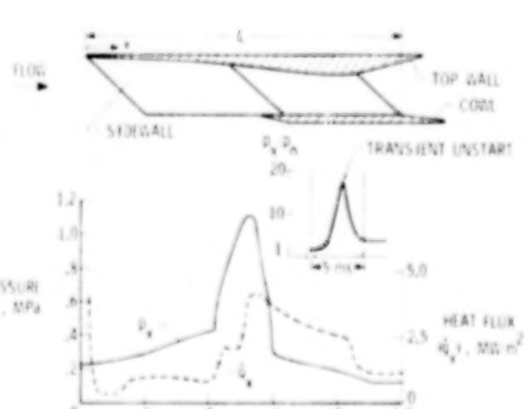

Figure 3. Typical design loads - sidewall.

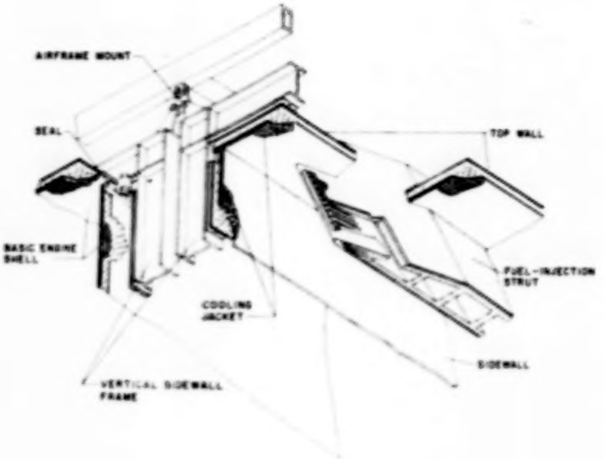
AIRFRAME MOUNT
SEAL
TOP WALL
BASIC ENGINE SHELL
FUEL-INJECTION STRUT
COOLING JACKET
SIDEWALL
VERTICAL SIDEWALL FRAME

Figure 4. Typical construction of engine shell and fuel-injection strut.

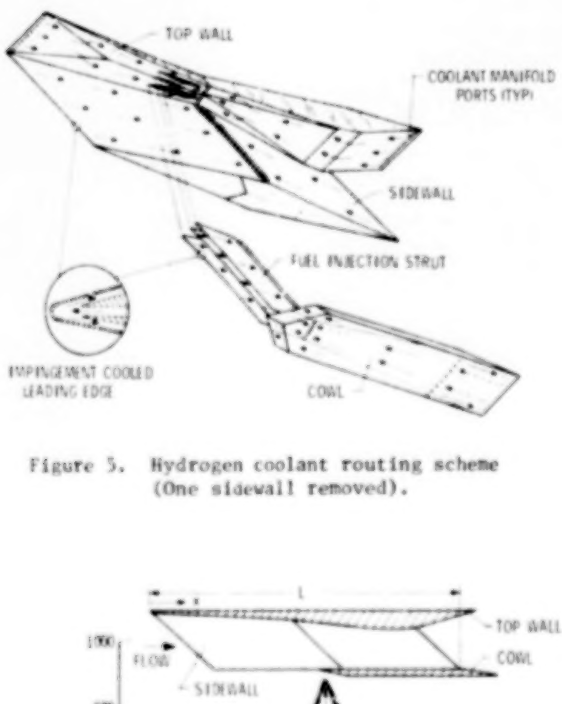
TOP WALL
COOLANT MANIFOLD PORTS (TYP)
SIDEWALL
FUEL INJECTION STRUT
IMPINGEMENT COOLED LEADING EDGE
COWL

Figure 5. Hydrogen coolant routing scheme (One sidewall removed).

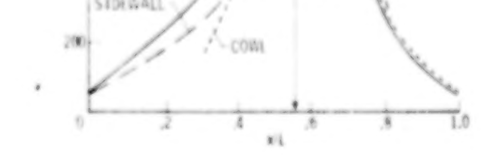

Figure 6. Engine component temperature distributions.

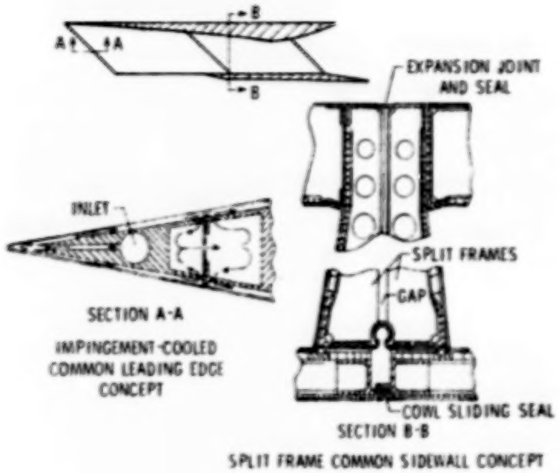
B
A
A
B
EXPANSION JOINT AND SEAL
INLET
SPLIT FRAMES
GAP
SECTION A-A
IMPINGEMENT-COOLED COMMON LEADING EDGE CONCEPT
COWL SLIDING SEAL
SECTION B-B
SPLIT FRAME COMMON SIDEWALL CONCEPT

Figure 7. Leading edge and sidewall concept.

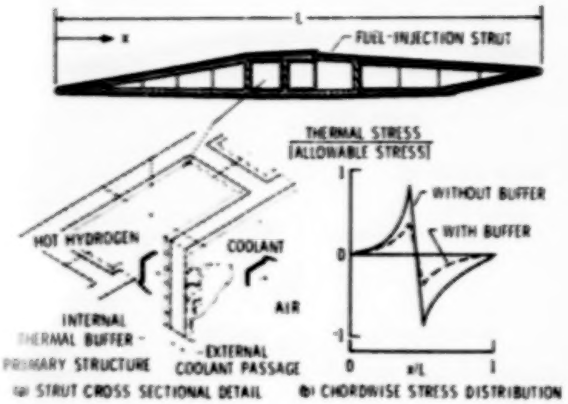
L
x
FUEL-INJECTION STRUT
THERMAL STRESS / (ALLOWABLE STRESS)
1
0
-1
WITHOUT BUFFER
WITH BUFFER
HOT HYDROGEN
COOLANT
AIR
INTERNAL THERMAL BUFFER
PRIMARY STRUCTURE
EXTERNAL COOLANT PASSAGE
0
x/L
1
(a) STRUT CROSS SECTIONAL DETAIL
(b) CHORDWISE STRESS DISTRIBUTION

Figure 10. Internal thermal-buffer concept.

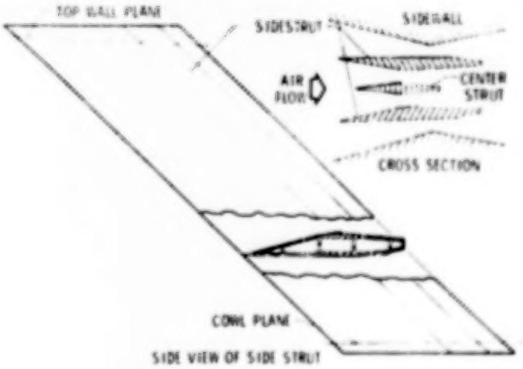
TOP WALL PLANE
SIDESTRUT
SIDEWALL
AIR FLOW
CENTER STRUT
CROSS SECTION
COWL PLANE
SIDE VIEW OF SIDE STRUT

Figure 8. Fuel-injection struts.

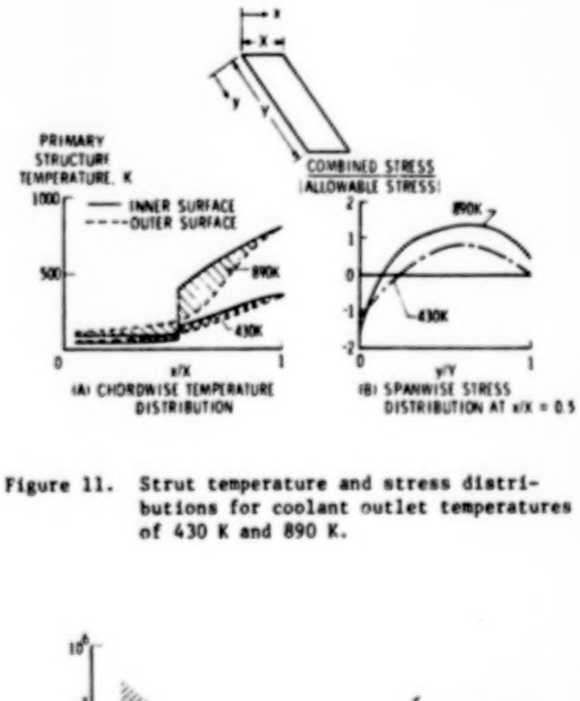

Figure 11. Strut temperature and stress distributions for coolant outlet temperatures of 430 K and 890 K.

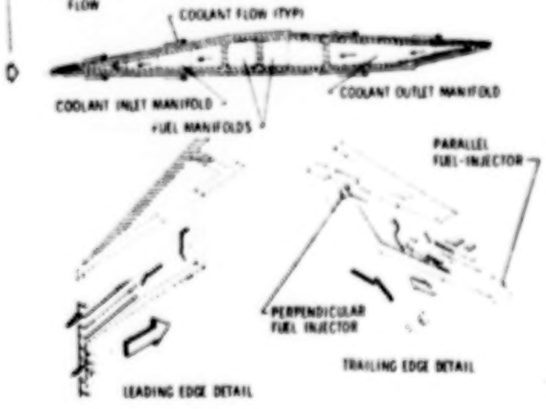
AERODYNAMIC FLOW
COOLANT FLOW (TYP)
COOLANT INLET MANIFOLD
FUEL MANIFOLDS
COOLANT OUTLET MANIFOLD
PARALLEL FUEL-INJECTOR
PERPENDICULAR FUEL INJECTOR
TRAILING EDGE DETAIL
LEADING EDGE DETAIL

Figure 9. Fuel-inje.tion strut detail.

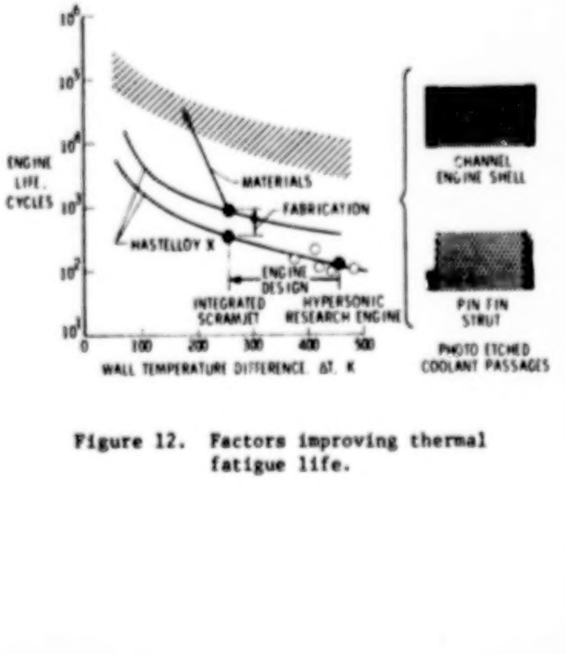

Figure 12. Factors improving thermal fatigue life.

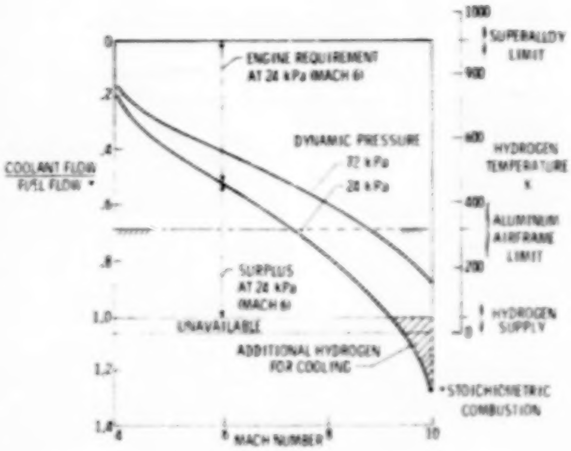

Figure 13. Engine cooling requirements.

Figure 14. Convective cooling system for hypersonic aircraft.

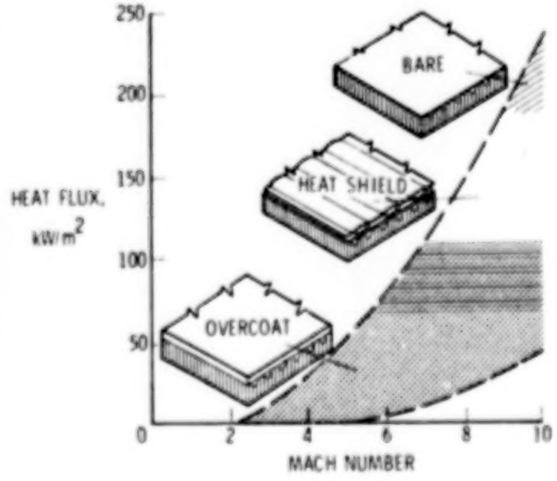

Figure 15. Recommended application regions for convectively cooled airframe structures.

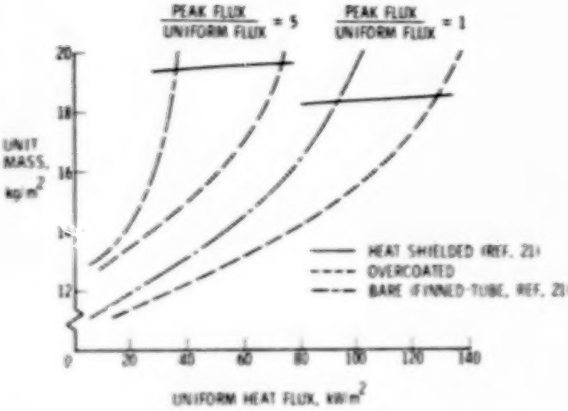

Figure 16. Convectively cooled panel masses.

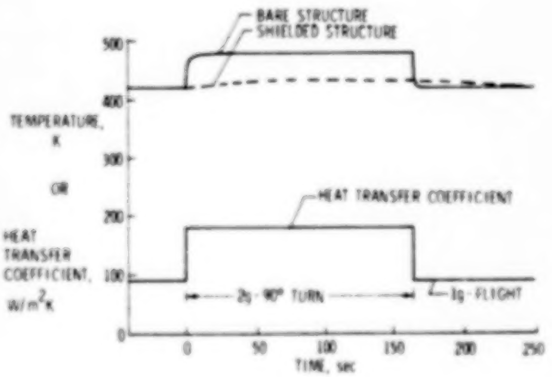

Figure 17. Sensitivity of convectively cooled structures to transient heat loads.

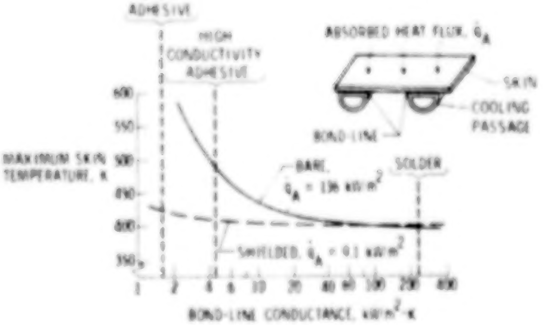

Figure 18. Effect of bond-line conductance on maximum skin temperature for bare and shielded configurations.

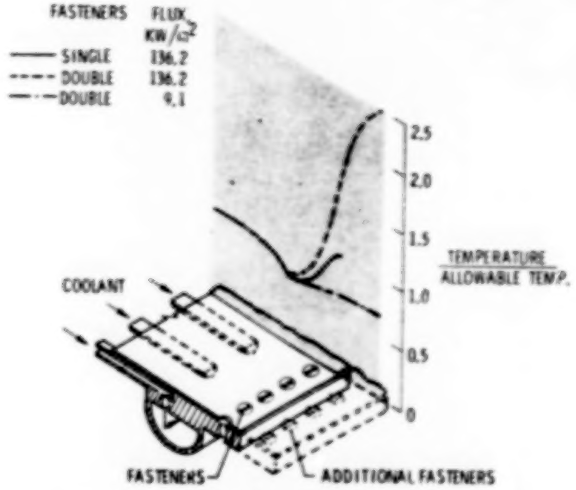

Figure 19. Effect of absorbed heat flux on joint design.

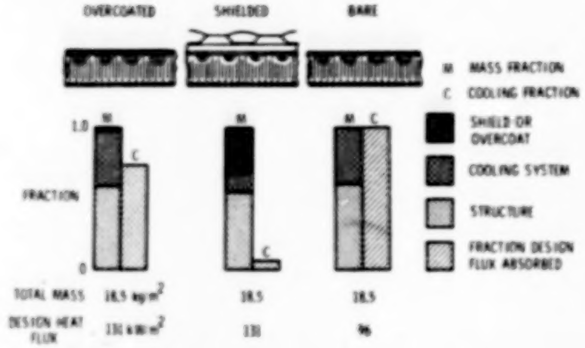

Figure 20. Mass and cooling characteristics of convectively cooled structures.

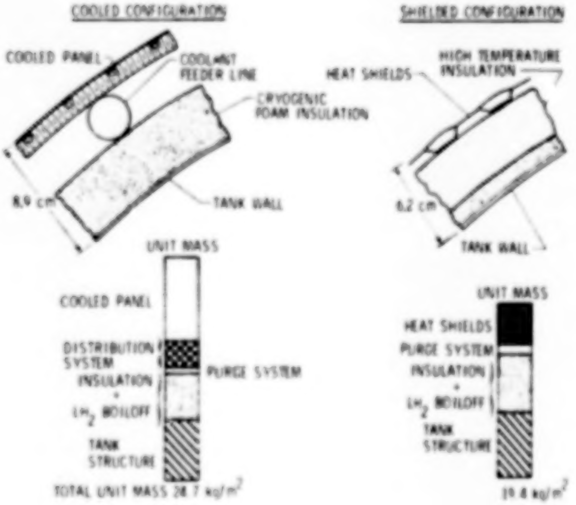
COOLED CONFIGURATION
COOLED PANEL
COOLANT FEEDER LINE
CRYOGENIC FOAM INSULATION
TANK WALL
8.9 cm
UNIT MASS
COOLED PANEL
DISTRIBUTION SYSTEM
PURGE SYSTEM
INSULATION + LH₂ BOILOFF
TANK STRUCTURE
TOTAL UNIT MASS 28.7 kg/m²
SHIELDED CONFIGURATION
HEAT SHIELDS
HIGH TEMPERATURE INSULATION
6.2 cm
TANK WALL
UNIT MASS
HEAT SHIELDS
PURGE SYSTEM
INSULATION + LH₂ BOILOFF
TANK STRUCTURE
19.4 kg/m²

Figure 21. Comparison of convectively cooled and shielded tank structures.

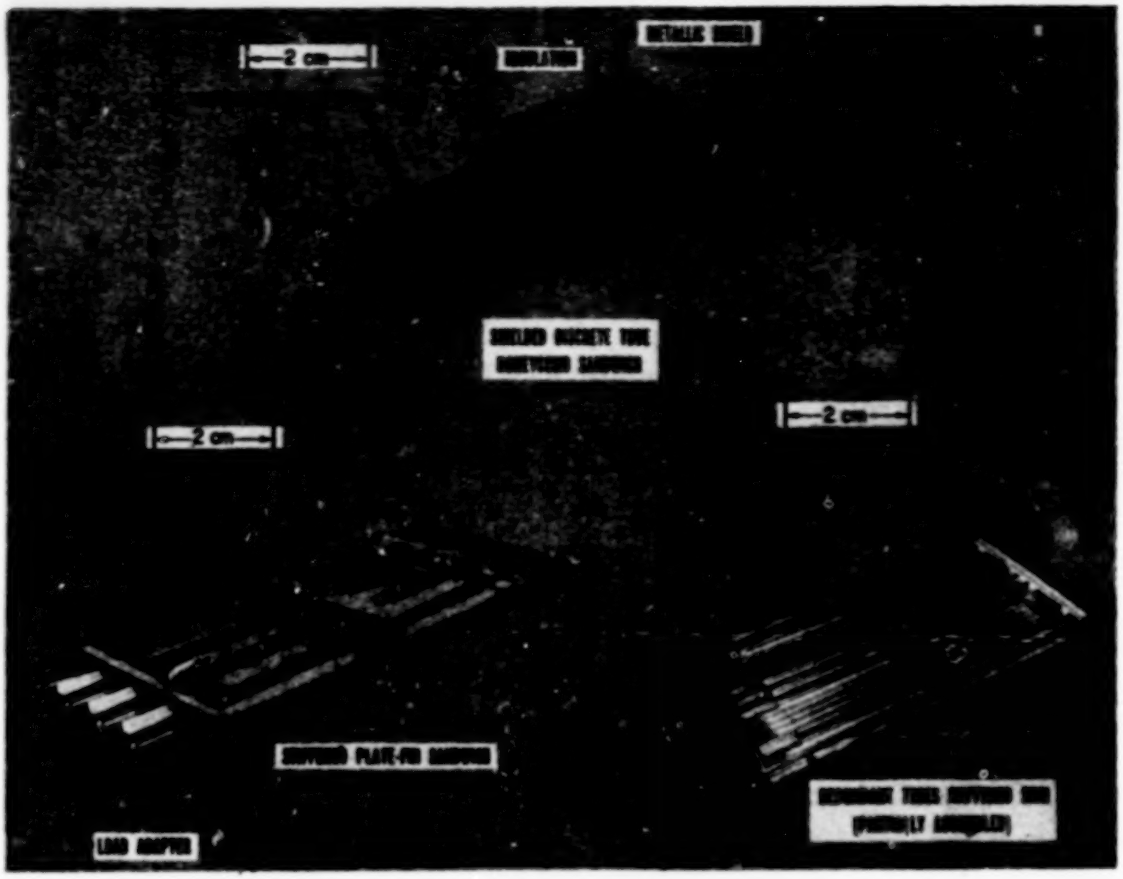
2 cm
2 cm
2 cm
LOAD ADAPTER

Figure 22. Large (0.61 by 1.22 m) convectively cooled test panels with cooling passage details.

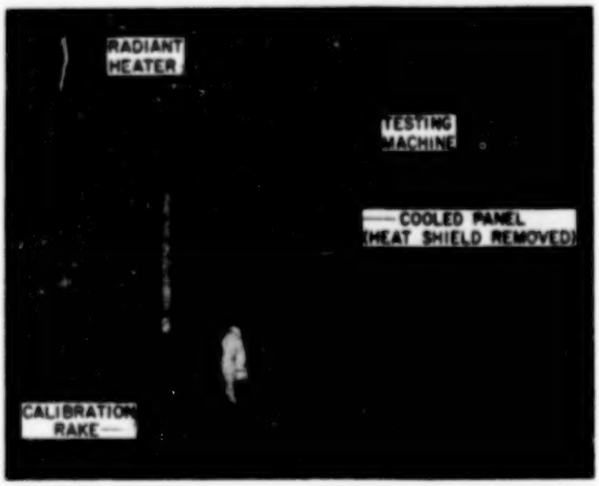
RADIANT HEATER
TESTING MACHINE
COOLED PANEL (HEAT SHIELD REMOVED)
CALIBRATION RAKE

Figure 23. Test apparatus for convectively cooled structures.

BLANK PAGE

SESSION II - ENGINE STRUCTURES

BLANK PAGE

BLANK PAGE

DESIGN AND ANALYSIS OF A SCRAMJET ENGINE*

By O. A. Buchmann
AiResearch Manufacturing Company, Los Angeles, California

INTRODUCTION

A preliminary design of a hydrogen-fueled, regeneratively cooled, airframe-integrated Scramjet was accomplished at NASA Langley Research Center. The three-dimensional, fixed-geometry Scramjet concept is designed to operate over a flight Mach number range of 4 to 10. The concept was found to be viable from the standpoints of both engine structural mass and coolant requirements. The overall objectives of this program were to extend these studies and to define a practical engine concept.

The work falls into four broad areas: (1) to develop and evaluate a design concept for the cooled-structures assembly of the engine; (2) to develop concepts for engine subsystems in sufficient detail to show feasibility and to estimate mass, volume, and operating requirements; (3) to establish design concepts for the aircraft/engine interface; and (4) to identify problem areas requiring further R&D.

Conclusions from study are that: (1) excess-fuel heat sink is available at all flight conditions; (2) a service life of 1000 cycles and 100 hr is feasible at steady state temperatures and with temperature differences; (3) structure and thermal protection system (TPS) masses are reasonable; (4) a modularized concept can provide accessibility and replaceability of components; and (5) thermal transients during ascent and descent along typical mission trajectories will govern design and operating procedures for the TPS and the engine. The resulting cooled-structure design is feasible and can utilize current materials and manufacturing technology.

The presentation will show the design configurations evolved during the study and the results of various analyses performed in support of the design. The discussion emphasizes the engine structure and TPS, including the fuel injection struts. These represent the main study areas during the program and the main issues with respect to feasibility.

---

*This work is being performed under Contract NAS1-13984 with the NASA Langley Research Center. The Project Manager for NASA is Mr. A. R. Wieting, Thermal Structures Branch, Structures and Dynamics Division.

PROGRAM OBJECTIVES

The program objectives were to define a cooled-structures assembly given the engine geometry and engine operating conditions. Consideration was also given to engine subsystems, in particular, the fuel subsystem associated with the operating engine. The engine mounting and the interfacing with the airplane were evaluated, and conceptual designs were defined. This presentation, however, emphasizes the cooled-structures assembly. Most of the work was done in this area, and the basic technology issues are in this area.

SCRAMJET CONCEPT

(Figure 1)

The concept of the three-dimensional Scramjet is a modular one. It uses a rectangular configuration. Several of these modules are mounted to the compression surface of the airplane. The reference configuration for the study used six modules for design purposes. Installation and removal of the engines are based on an assembly of modules rather than single modules.

This shows the main components of the engine. The inlet is defined by the sidewalls and has a 48 deg sweep. It has fixed geometry. The three struts are mechanically inserted and mounted between the topwall and the cowl. The combustion area and nozzle are defined by the topwall, sidewalls, and cowl. All surfaces exposed to the engine internal and external gas flows are regeneratively cooled using the hydrogen fuel.

SCRAMJET CONCEPT

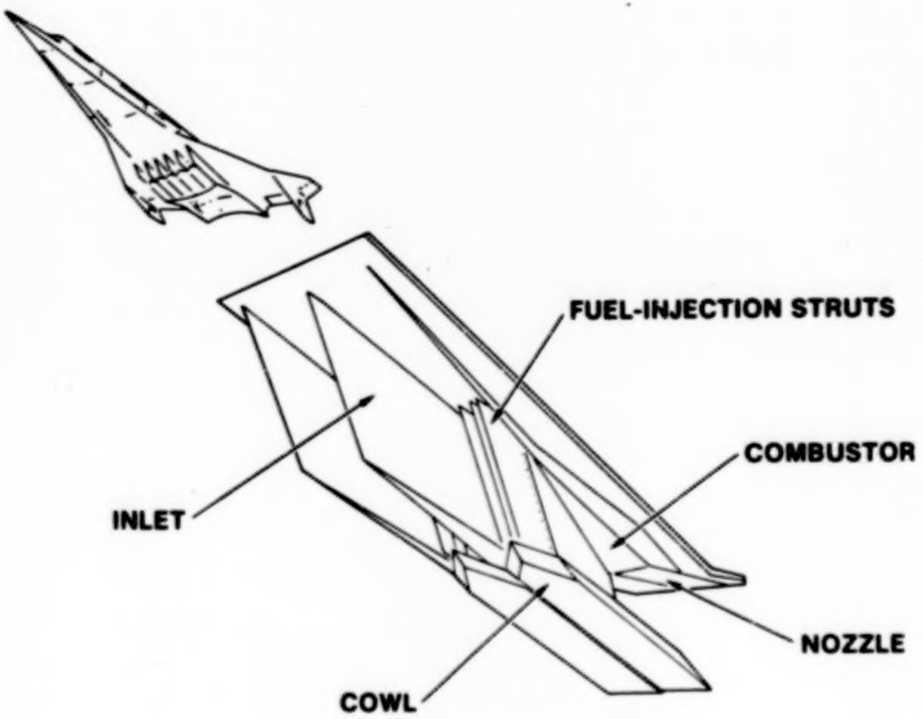
FUEL-INJECTION STRUTS
COMBUSTOR
INLET
NOZZLE
COWL

Figure 1

COOLED SCRAMJET STRUCTURE

(Figure 2)

The selected configuration consists of the thermal protection system (TPS), which is a regeneratively cooled hydrogen heat exchanger, mounted to the primary support structure. The primary support structure is all honeycomb. Beam-stiffened configurations were studied and honeycomb was selected as the most desirable. Results of the analysis leading to this selection will be shown.

Beams are used in two locations, at the forward and aft mounts, to distribute the loads. The assembly of the panels is by a bolted connection. Brazed or welded assemblies were also considered. Bolted assembly, although heavier and potentially with more design and manufacturing difficulty, is the only practical one if disassembly and reassembly of components is a design requirement. The outside of the cowl is removable to permit access for engine assembly and installation.

The fuel injection struts represent one of the most critical design areas of the engine. Design of the load carrying structure, the TPS, the fuel and coolant manifolding, and the mounting in the topwall and cowl are all constrained by the envelope imposed by aerodynamic requirements.

COOLED SCRAMJET STRUCTURE

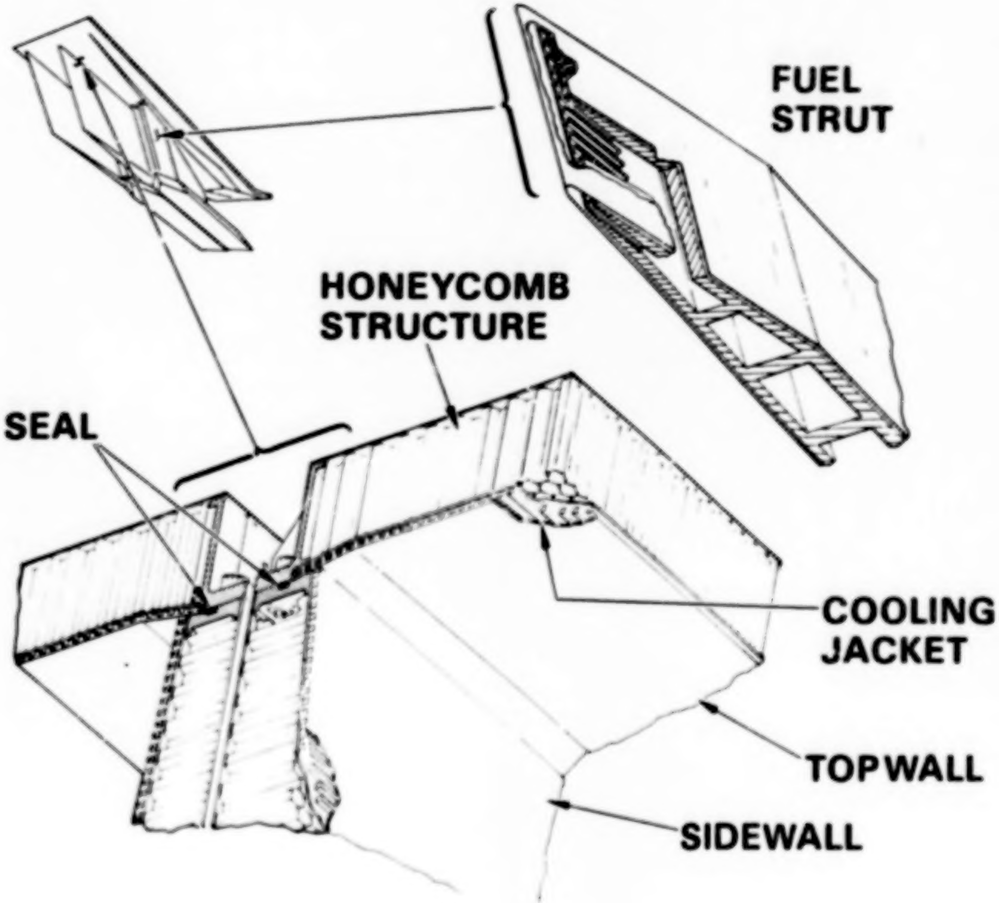
FUEL
STRUT
HONEYCOMB
STRUCTURE
SEAL
COOLING
JACKET
TOPWALL
SIDEWALL

Figure 2

DESIGN CONDITIONS

(Figure 3)

The most important constraint on design is the need to achieve a 100-hour life with 1,000 cycles of operation for any operating condition. The design approach was to evaluate and define the structure and the materials combinations at steady state conditions, that is, at ΔT's corresponding to steady state. The resulting design was then evaluated under conditions of transient thermal and pressure loads.

The metal temperature limit for the TPS was set at 1140 K (1600°F). This was deemed the maximum practicable temperature for the nickel-base superalloys which are available for use in the engine. Specifically, Hastelloy X and Nickel 200 are the TPS face sheet materials.

The hydrogen outlet pressure was set at 5.3 MPa (750 psia), which is the fuel injection pressure; the inlet pressure is consistent with hydrogen pump technology. The 890 K (1600°R) maximum coolant temperature was selected to avoid creep in the primary structure. Coolant equivalence ratio was to be less than one in all cases to avoid dumping of hydrogen. In addition, the desirability of having hydrogen cooling capacity available for aircraft cooling provides further incentive for limiting coolant equivalence ratio.

DESIGN CONDITIONS

LIFE	**100 HRS AND 1000 CYCLES**
DEFLECTIONS	**<5% AREA AND 0.4 DEGREES**
METAL TEMP	**<1140 K (1600°F)**
HYDROGEN	
INLET	**6.9 MPa, 55 K (1000 PSIA, 100°R)**
OUTLET	**5.3 MPa, 890 K (750 PSIA, 1600°R)**
COOLANT ϕ	**<1.0**

Figure 3

CANDIDATE CONFIGURATIONS

(Figure 4)

The candidate configurations for the TPS heat exchangers are summarized here. A plate-fin configuration was used on the hypersonic research engine (HRE). In this application, it will not have the required cycle life and creep life. The reason it does not is the braze joints next to the hot face sheet. These result in stress concentrations and degraded material at the hottest point in the heat exchanger.

All of the machined configurations shown have the braze joint at the cold side of the heat exchanger. They also provide an opportunity to reduce the stress concentration at the hot face sheet by appropriate contouring, with a minimum obtained for the circular configuration. In fact, when a photochemically milled channel is used, the geometry tends to a full radius at the hot face sheet.

The pin-fin configuration has high heat transfer coefficients and high pressure drop. It is used in localized areas which require high heat transfer for short flow lengths.

Of these, the plate-fin configuration has the best heat transfer performance. As noted, it will not satisfy the structural criteria. The pin fins are used in the struts to get the necessary heat transfer coefficients. The pressure drop is available to use there, since the flow lengths are short. In all other areas, plain channel configurations are used.

CANDIDATE CONFIGURATIONS

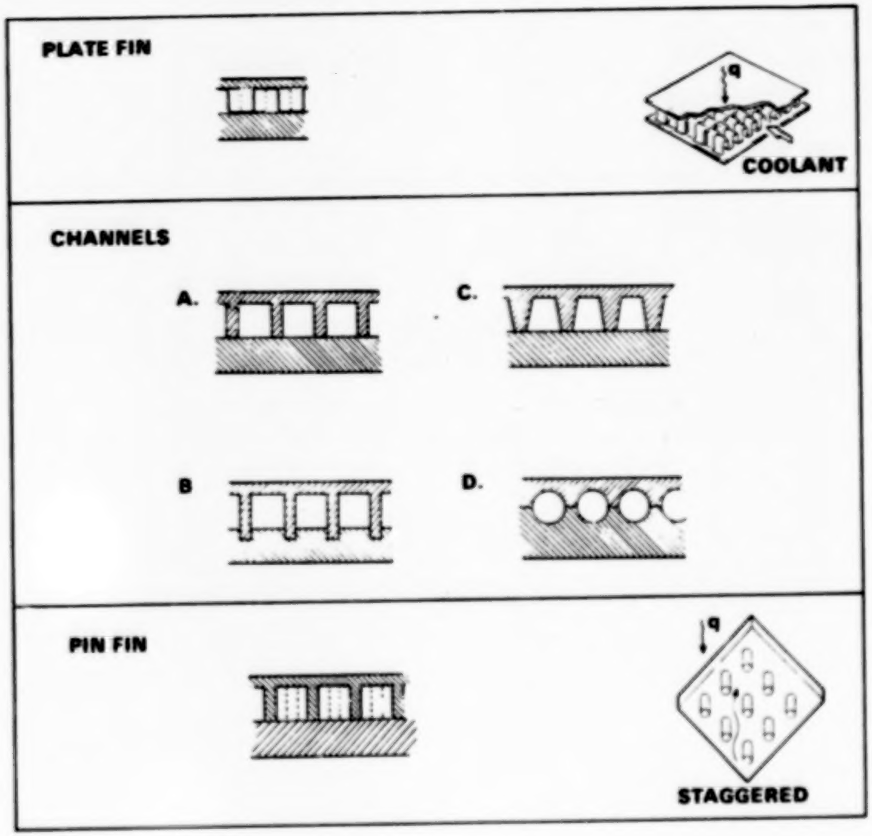
PLATE FIN
q
COOLANT
CHANNELS
A.
C.
B
D.
PIN FIN
q
STAGGERED

Figure 4

TPS PASSAGE SELECTION

(Figure 5)

The height of the channels is indicated. It ranges from 0.63 to 1.27 mm (0.025 to 0.050 in.). At the leading edges of the sidewalls and cowl, pure nickel is used - Nickel 200 or Nickel 201. Pure nickel is also used as the hot face sheet of the strut TPS. All other areas in the engine use Hastelloy X as the face sheet material.

TPS PASSAGE SELECTION

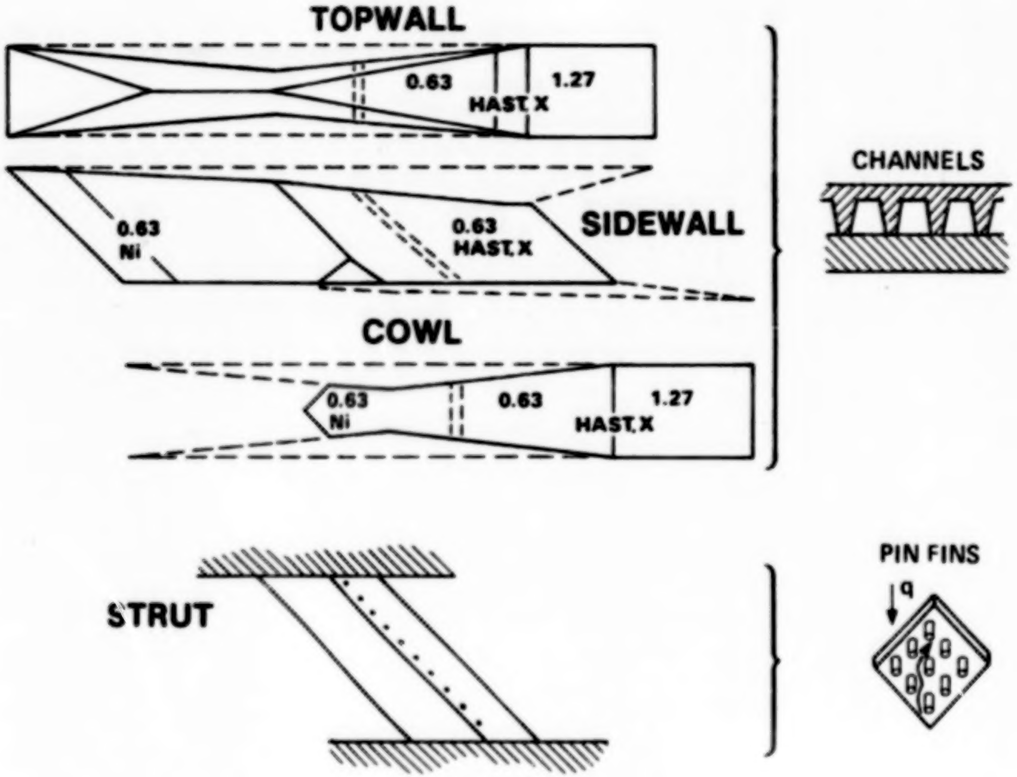
TOPWALL
0.63
HAST. X
1.27
SIDEWALL
0.63
Ni
0.63
HAST. X
COWL
0.63
Ni
0.63
HAST. X
1.27
CHANNELS
STRUT
PIN FINS
q

(DIMENSIONS IN mm)

Figure 5

ENGINE COOLING PERFORMANCE

(Figure 6)

Using the selected heat exchangers, the engine cooling performance was derived in terms of the coolant equivalence ratio for each of the operating conditions. (Coolant equivalence ratio is the ratio of the required coolant flow to engine fuel flow.) In all cases, the ratio is below the design limit of 1.0.

The design condition has a high fuel equivalence ratio. Consequently, the coolant equivalence ratio appears to be low. The adverse effect here is that a high coolant flow must be accommodated within the allowable pressure drop limits. This represents an area for trade-off with respect to other operating conditions. Generally, the high fuel equivalence ratios are associated with off-design operation and, as such, need not govern the design.

ENGINE COOLING PERFORMANCE

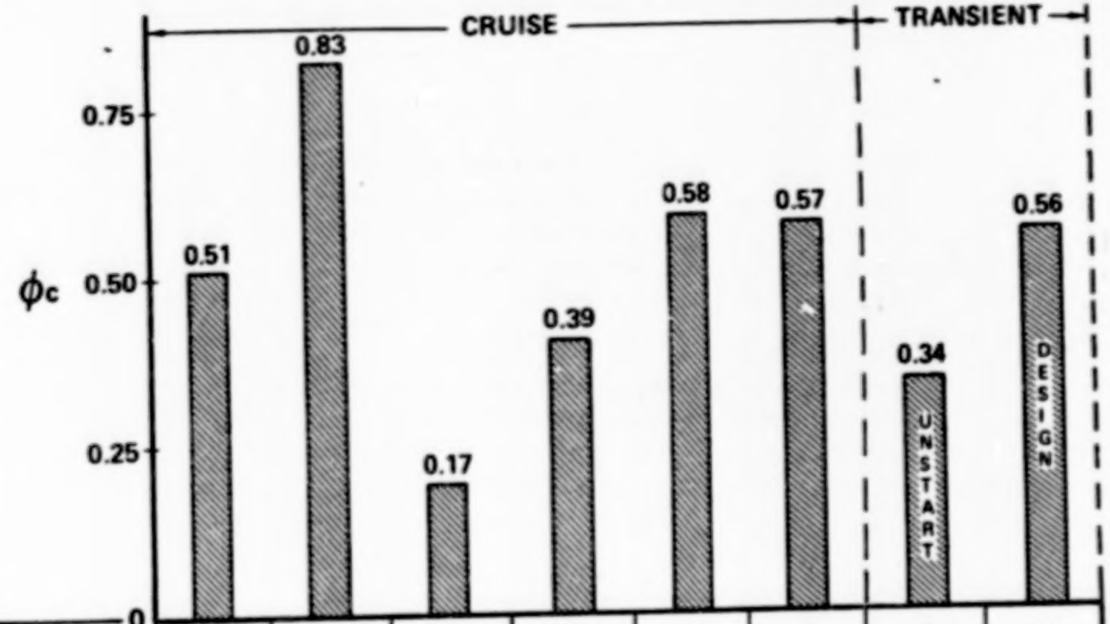

CONDITION	A	B	C	D	E	F	G	H
MACH NO.	6	10	4	6	8	10	5.1	10
ϕ_f	1.0	1.5	1.0	1.0	1.0	1.5	1.0	1.5

Figure 6

TPS CYCLE LIFE--STEADY STATE

(Figure 7)

Published data for parent metals (Hastelloy X for the panels and nickel for the struts) was used to assess the cycle life at ΔT's corresponding to steady state operation. Maximum steady state ΔT is about 220 K (400°F) for any of the operating conditions, including design condition H. Results for both the forward and aft flow routes of the cowl and sidewall are shown; the top panel has a single flow route; the center struts were individually considered. Based on the published data, the 1,000-cycle design requirement is achievable for all components at steady state conditions. The design is, therefore, governed by engine transient operations, as shown subsequently.

TPS CYCLE LIFE – STEADY STATE

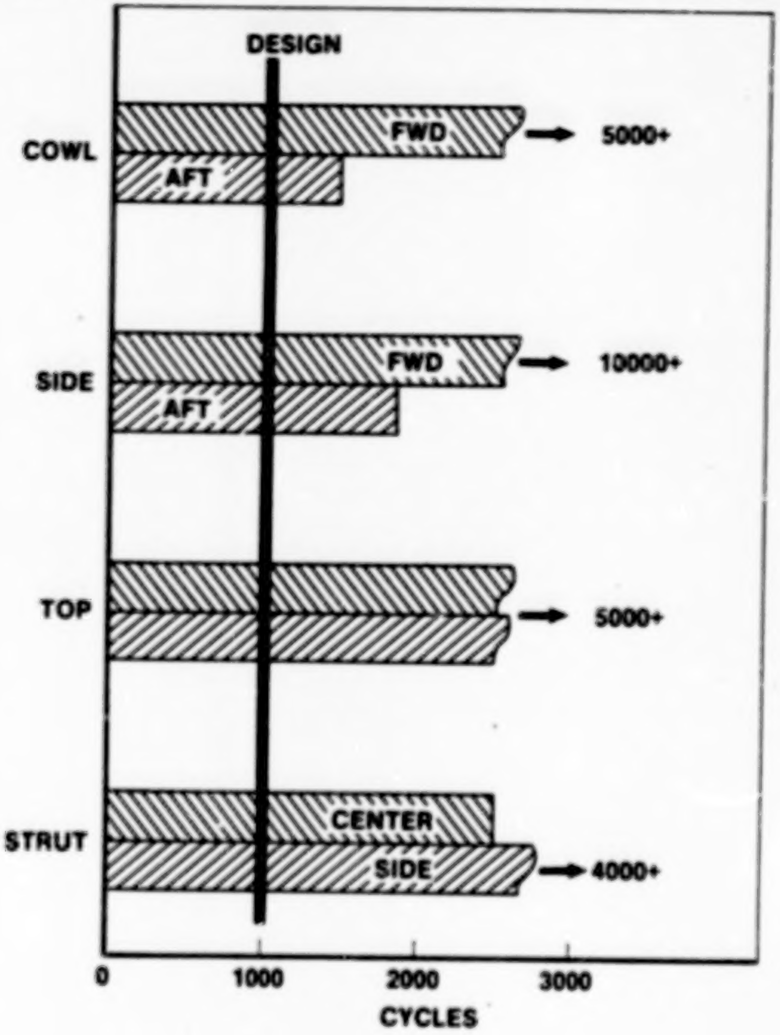

Figure 7

LEADING EDGE CYCLE LIFE

(Figure 8)

Leading edge cycle life was separately considered. In each case, the leading edges are nickel. Hastelloy X meets the requirements of the sidewall, but offers no particular advantage. Nickel is required to achieve a 1,000-cycle life in all other locations.

The strut and panel leading edges use direct impingement cooling. The cowl apex is a hemispherical point on the cowl and is also cooled by impingement. Its heat flux is the highest of any of the leading edge areas, 4600 W/cm^2 (4040 Btu/sec-ft^2) vs 2030 W/cm^2 (1790 Btu/sec-ft^2) for the center strut and 1060 W/cm^2 (935 Btu/sec-ft^2) for the sidewall. A leading edge radius of 1.27 mm is used in all areas.

LEADING EDGE CYCLE LIFE

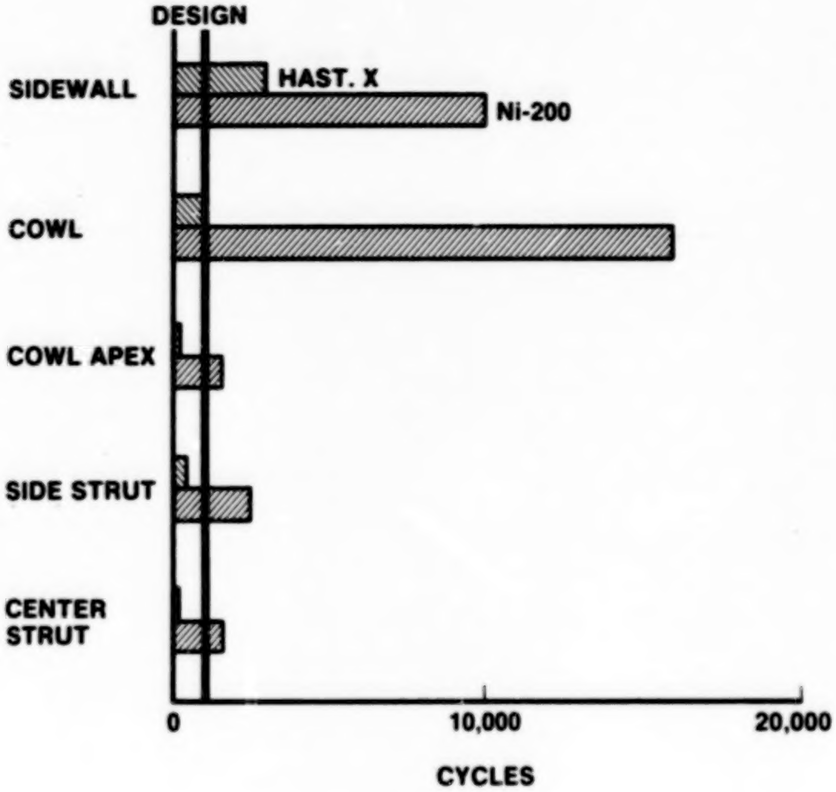

Figure 8

81

FINITE ELEMENT MODELS

(Figure 9)

Three basic engine structural concepts were studied: swept frame, in which a set of 7 beams was used to support a relativley shallow-depth, honeycomb panel structure; vertical frame, which used the same 7 beams, but ran these beams normal to the engine axis; and all honeycomb, in which only 2 beams were used at the mount points. The models were symmetrical about the centerline and were evaluated using the ANSYS computer program.

FINITE ELEMENT MODELS

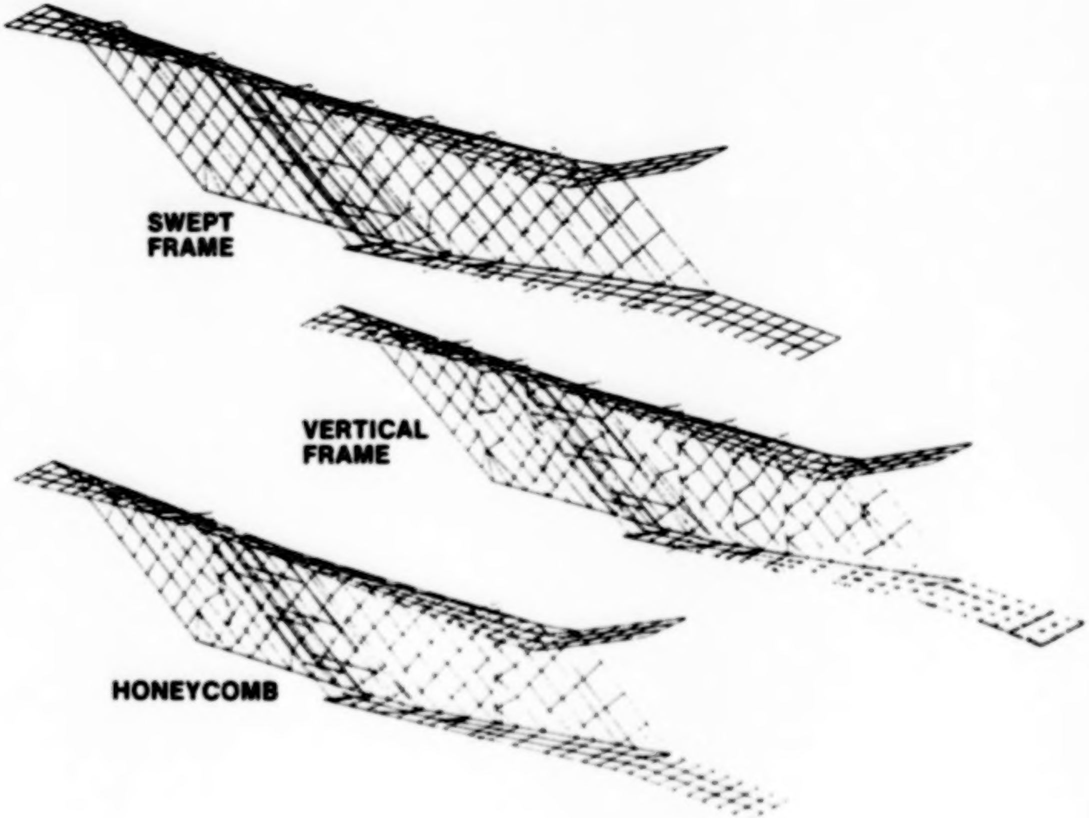
SWEPT
FRAME
VERTICAL
FRAME
HONEYCOMB

Figure 9

83

SIDEWALL DISPLACEMENTS

(Figure 10)

This shows the performance of the sidewall as obtained from the finite element models for each of the configurations. Its design is critical at the maximum pressure load, which occurs during the Mach 5.1 unstart condition. Maximum displacement occurs at the bottom corner of the leading edge. The maximum stress for all of the structures occurs in an area near the nozzle, in the relative position shown here. The honeycomb shows both the lowest displacement and lowest comparative stress. These comparative stresses are not absolute values. A separate analysis of the topwall was run to assess the quantitative validity of these stress. The conclusion drawn was that they do permit a general evaluation of structural performance. Since these results are for a transient, nonoperating condition, limitation of stress is the primary concern.

The results shown here were the main reasons for selecting the all-honeycomb configuration as the most desirable. Other components similarly favored the all-honeycomb structure, although not as strongly as in the case of the sidewall.

SIDEWALL DISPLACEMENTS

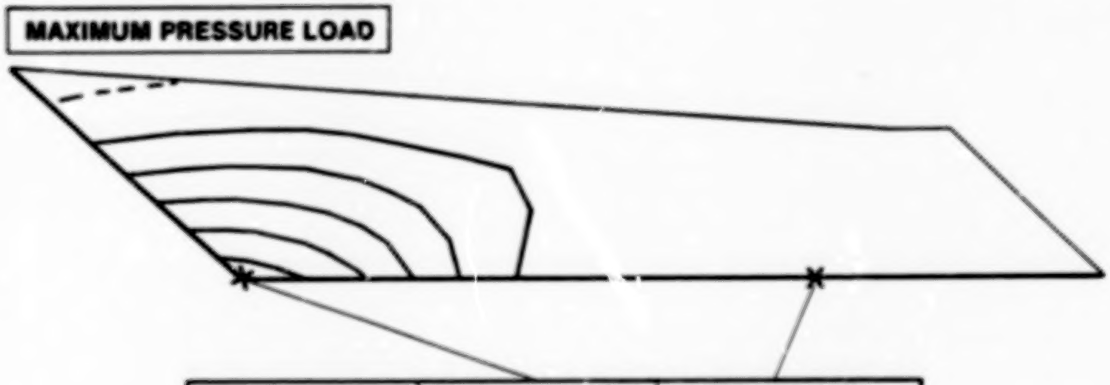
MAXIMUM PRESSURE LOAD

STRUCTURE	DISPLACEMENT, cm (IN.)	COMPARATIVE STRESS, MPa (KSI)
SWEPT BEAM	5.81 (2.29)	469 (68)
VERTICAL BEAM	2.74 (1.08)	594 (86)
HONEYCOMB (SHOWN)	0.58 (0.23)	400 (58)

Figure 10

SIDEWALL DISTORTED GEOMETRY

(Figure 11)

The vertical displacement of the sidewall, plus and minus, is shown for each of the three configurations. The honeycomb shows the maximum displacement at the top of the leading edge of the sidewall. In other areas, it is equivalent to or better than any of the other configurations.

The distorted geometry shown here is indicative of conditions at the panel corner joints. Initial engine design concepts used sliding seals at all of the corners. These are difficult to achieve in the thermal environment of a Scramjet. The distortion results obtained suggested the use of rigid connections at the corners. Results from finite element models showed that the stresses associated with rigid connections are acceptable.

SIDEWALL DISTORTED GEOMETRY

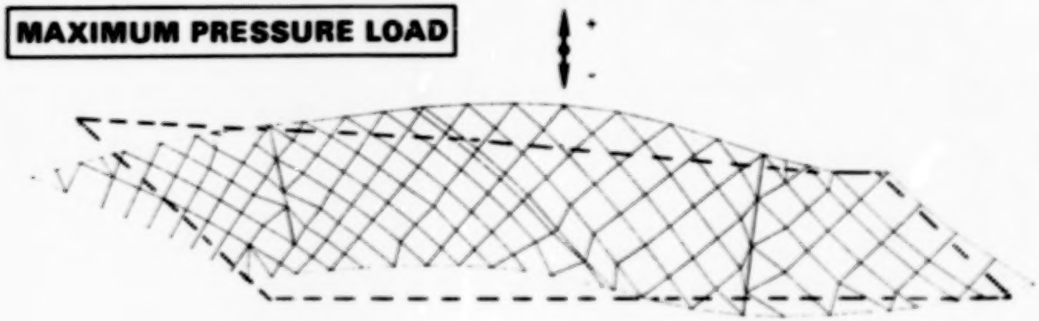

STRUCTURE	VERTICAL DISPLACEMENT, mm					
	LE TOP	LE BOTTOM	MID TOPWALL	MID COWL	TE TOP	TE BOTTOM
SWEPT BEAM	+ 0.127	+ 7.61	+ 2.79	0	- 2.34	- 2.74
VERTICAL BEAM	- 3.91	+ 3.70	+ 3.81	+ 4.16	0	+ 0.127
HONEYCOMB (SHOWN)	- 4.36	+1.29	+ 3.21	+ 2.31	0	+ 0.913

Figure 11

88

STRUT LOADS-kN (LB)

(Figure 12)

The Mach 5.1 unstart condition that is critical for design of the engine panels is also the most severe loading condition for the struts. The most severe assumption that can be made is that it is possible for the engine to remain started on one side of a strut and be unstarted on the other side. There is not sufficient experimental data to say whether or not this is in fact possible.

These are the net loads that go with the conditions shown. They are quite substantial in relation to the strut geometry, which is that of a long, slender body. Both the deformations and stresses produced by these loads make strut structural design one of the most critical areas of the engine.

STRUT LOADS-kN (LB)

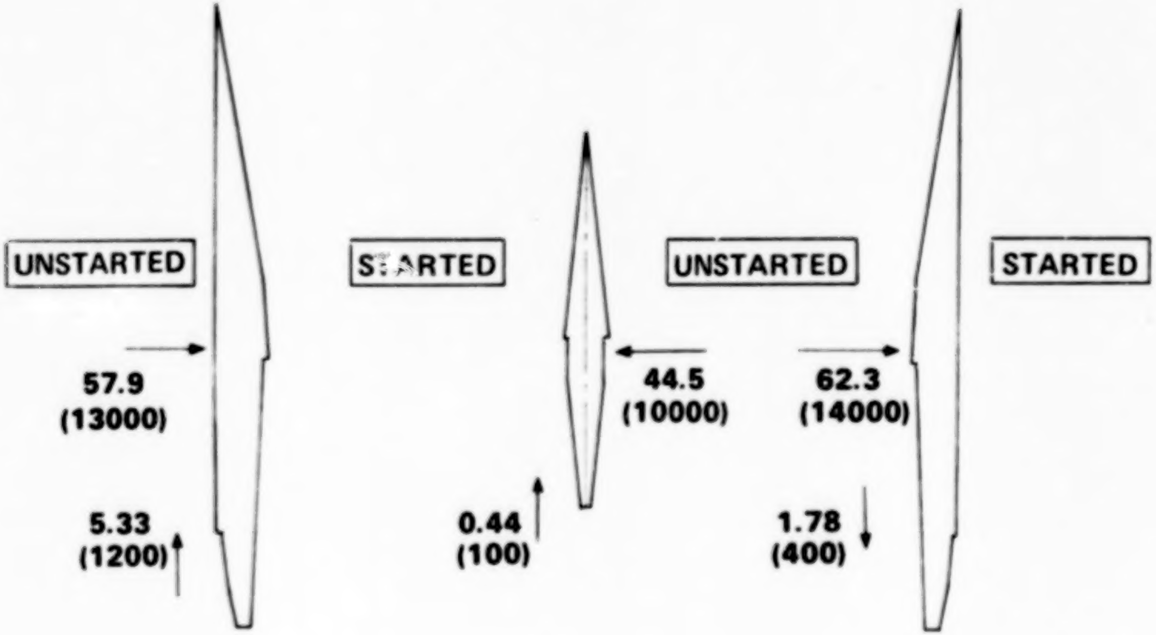
UNSTARTED
57.9
(13000)
5.33
(1200)
STARTED
0.44
(100)
UNSTARTED
44.5
(10000)
62.3
(14000)
1.78
(400)
STARTED

Figure 12

STRUT STRUCTURAL DESIGN

(Figure 13)

The materials used in the strut are Inconel 718 for the primary structure and Nickel-200 for the face sheet of the TPS. A 3-D model was used at the Mach 5.1 unstart condition to evaluate stress and deformation. The design that evolved used 2.03-mm (0.080-in.) walls with 3.17-mm (0.125-in.) ribs and webs. The goal was to keep all the stresses elastic. In fact, localized stresses, for the model used, exceed the elastic limit and deformations exceed 3.81 mm (0.150 in.). These result from the assumptions made with respect to mounting the strut in the top panel. Imposition of constraints representative of the actual design is expected to reduce both stresses and deformations to the desired levels.

STRUT STRUCTURAL DESIGN

- METHOD:
    - 3-D MODEL
- DESIGN:
    - 2.03mm (0.080-IN) WALLS
    - 3.17mm (0.125-IN.) RIBS AND WEBS
- GOALS:
    - STRESSES ELASTIC
    - 3.81mm (0.15-IN.) DEFORMATION
- MATERIALS:
    - INCONEL 718
    - NICKEL-200 TPS

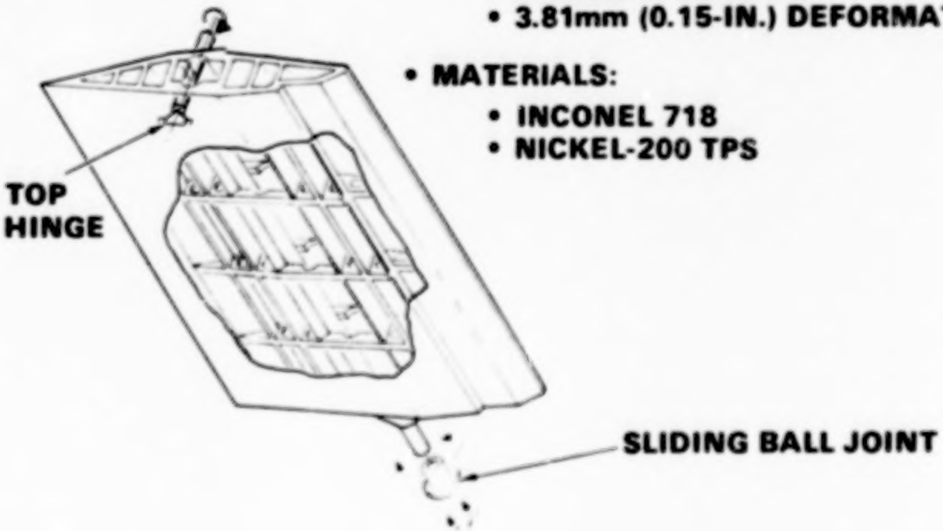
TOP HINGE
SLIDING BALL JOINT

Figure 13

STRUT DISPLACEMENTS

(Figure 14)

The calculated displacements range to 7.6 mm (0.3 in.), twice the value set as a goal. The stresses near the top center of the strut, in the shaded region, exceed the elastic limit. The model used, however, allows for no constraint by the strut mounts in the topwall. In fact, these mounts restrict the motion of the strut to essentially zero. As a result, deflections are expected to decrease by 50 percent. Stresses would be similarly reduced. Preparation of an extensive new model will be required for a more precise, quantitative assessment of the mount effects. Based on qualitative estimates, successful operation of the strut without a midspan support tie appears feasible.

STRUT DISPLACEMENTS

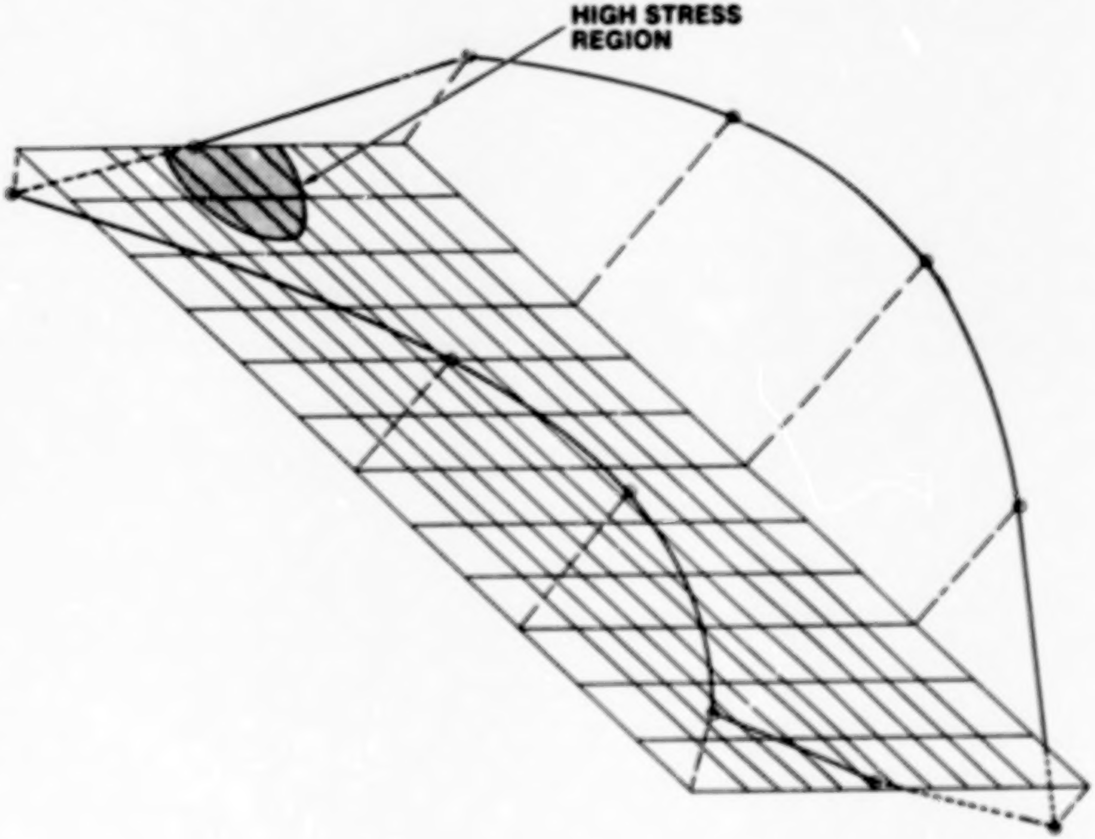
HIGH STRESS
REGION

Figure 14

SIDE STRUT

(Figure 15)

This is a wet-wall strut. Configurations in which the coolant flowed in separate tubes were also studied. There is not enough cross-sectional area in the strut to use this type of configuration within the pressure drop design limits.

The main features of the strut thermal design appear in the enlarged view. The strut manifolds incorporate a plate-fin heat shield around the wall. This heat shield isolates the strut structure during transients and limits the temperature differences to acceptable values. The thermal protection system heat exchanger is a pin-fin configuration throughout. Pin fins can be used in the strut because the flow lengths are relatively short and the relatively high pressure drops become acceptable. The high heat transfer performance of pin fins is required, in turn, because of the high heat flux loadings on the strut.

SIDE STRUT

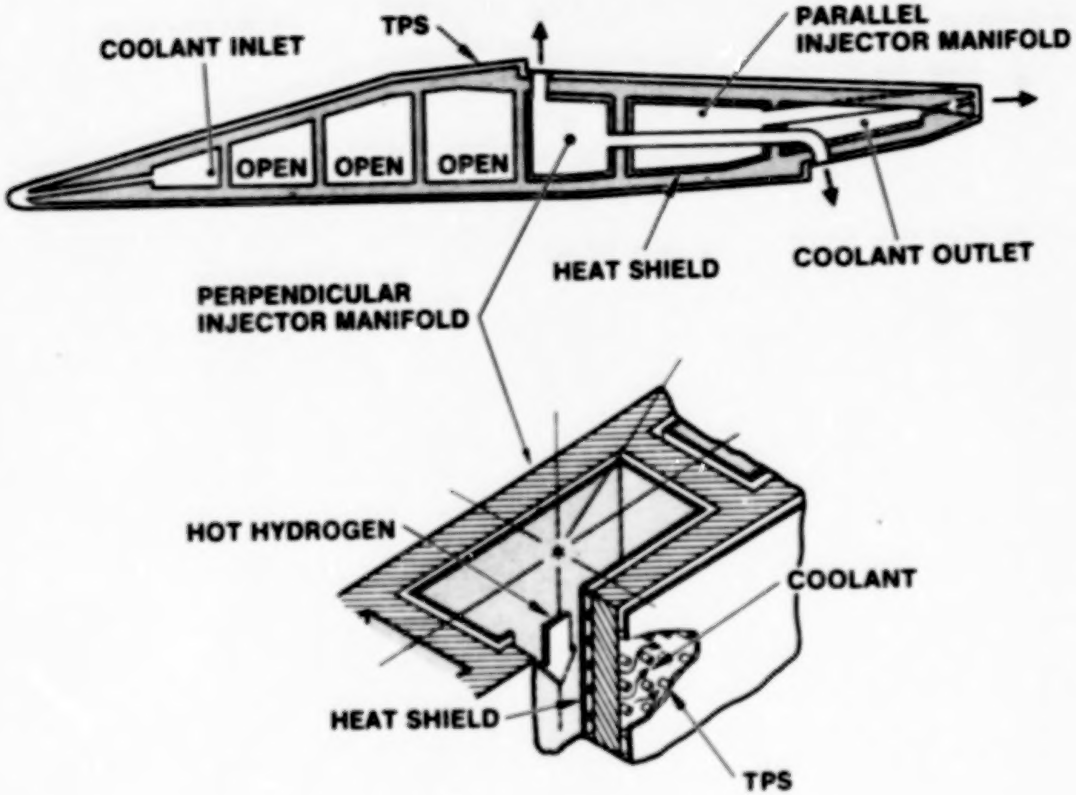
TPS
COOLANT INLET
PARALLEL INJECTOR MANIFOLD
OPEN
OPEN
OPEN
HEAT SHIELD
COOLANT OUTLET
PERPENDICULAR INJECTOR MANIFOLD
HOT HYDROGEN
COOLANT
HEAT SHIELD
TPS

Figure 15

STRUT COOLANT MANIFOLDS

(Figure 16)

Coolant inlet and outlet occurs from the same (top) end of the strut. This results in a relatively long manifold flow length. Because of the relatively limited space available in the struts, Mach numbers are also fairly high. Flow distribution in the coolant manifolds was therefore investigated. The conclusions, however, were the same for all of the manfiolds, i.e. that acceptable design solutions are available within the existing constraints.

The chart shows the static pressure distribution in the inlet and outlet coolant manifolds. The coolant temperature in the inlet manifold is 55 K (100°R) and the Mach number fairly low. As a result, the pressure in the inlet manifold is essentially constant.

The temperature in the outlet manifold is about 550 K (1,000°R), the density is much reduced, and the Mach number considerably higher. Nevertheless, the static pressure variation in the manifold is fairly small. The resulting maldistribution, therefore, was smaller than anticipated, ranging from 11 percent in a side strut to 6 percent in the center strut. These values are associated with condition H (Mach 10, 2g turn, fuel equivalence ratio 1.5). Since this is an off-design operating point, these maldistributions appear acceptable. At other conditions, the flow maldistributions would be even less.

Because of the pressure gradient in the outlet manifold, there is a tendency for the flow in the strut sides to skew. To control this skewing and assure controlled flow in the strut sides, flow dividers are incorporated in the pin-fin surface.

STRUT COOLANT MANIFOLDS

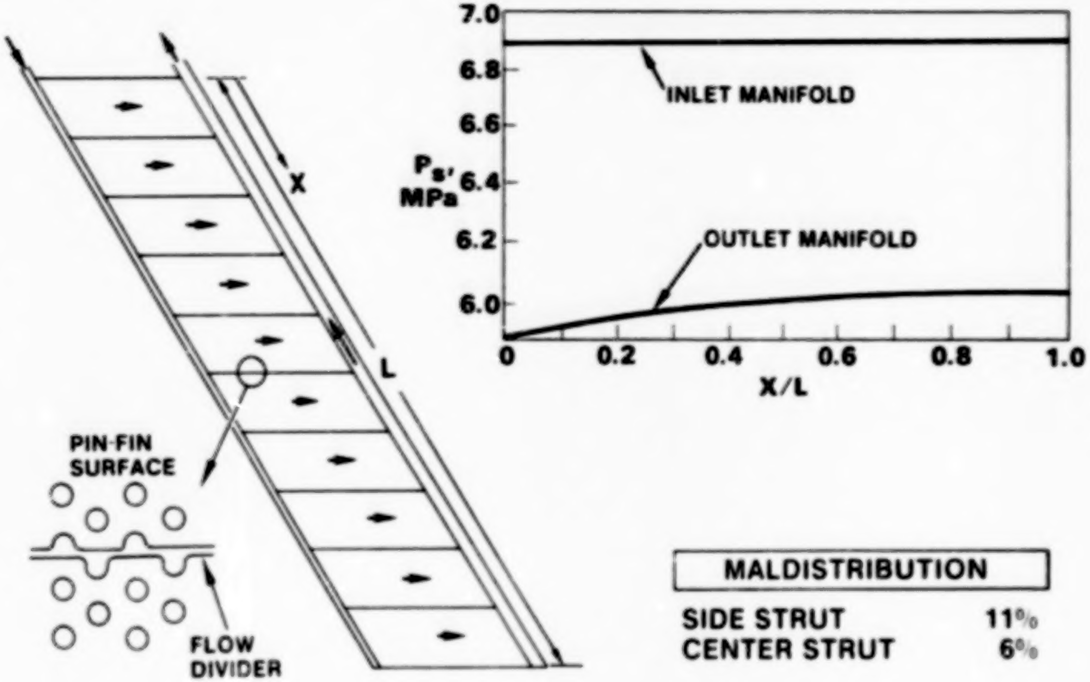

MALDISTRIBUTION	
SIDE STRUT	11%
CENTER STRUT	6%

Figure 16

HONEYCOMB TRANSIENT ANALYSIS CASES

(Figure 17)

After the various steady state analyses and designs were completed, the selected all-honeycomb structure was modeled on a thermal analyzer program. Sections of the structure that were analyzed are identified by the numbered paths. Since the corner of a module was expected to be critical, all cross-sections analyzed were taken in this area.

HONEYCOMB
TRANSIENT ANALYSIS CASES

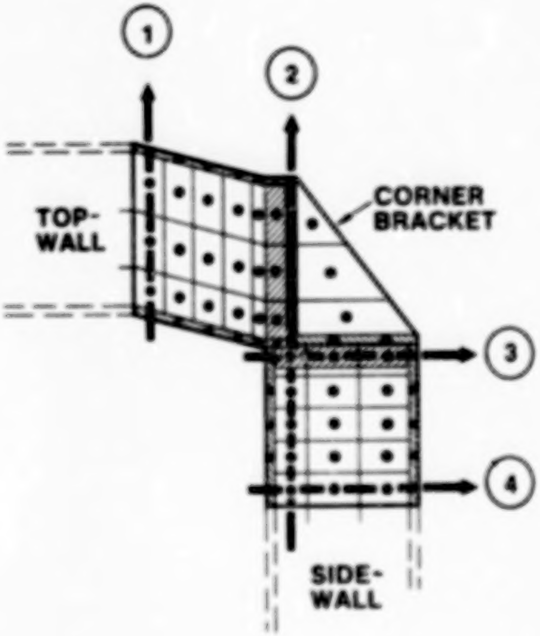
1
2
TOP-
WALL
CORNER
BRACKET
3
4
SIDE-
WALL

Figure 17

COOLANT OUTLET TRANSIENT

(Figure 18)

The coolant transient response was evaluated in the area of the outlet manifold for a trajectory that combines acceleration by rocket (typical of a research airplane) with extended cruise at Mach 6. In addition, it was assumed that fuel and coolant flow control was on a step basis. This is an unusually severe combination and represents an extreme condition.

The first 80 seconds involve acceleration to Mach 3. At Mach 3, the coolant is turned on, on a step basis. Acceleration continues to Mach 6, at which point the fuel is turned on and combustion starts. Following deceleration to Mach 3, coolant is turned off, again on a step basis. Alternative coolant and fuel scheduling is certainly possible and even likely, but was not analyzed. Most trajectories considered for cruise applications have used slow acceleration (0.2g), with durations of around fifteen minutes to attain Mach 6.

COOLANT OUTLET TRANSIENT

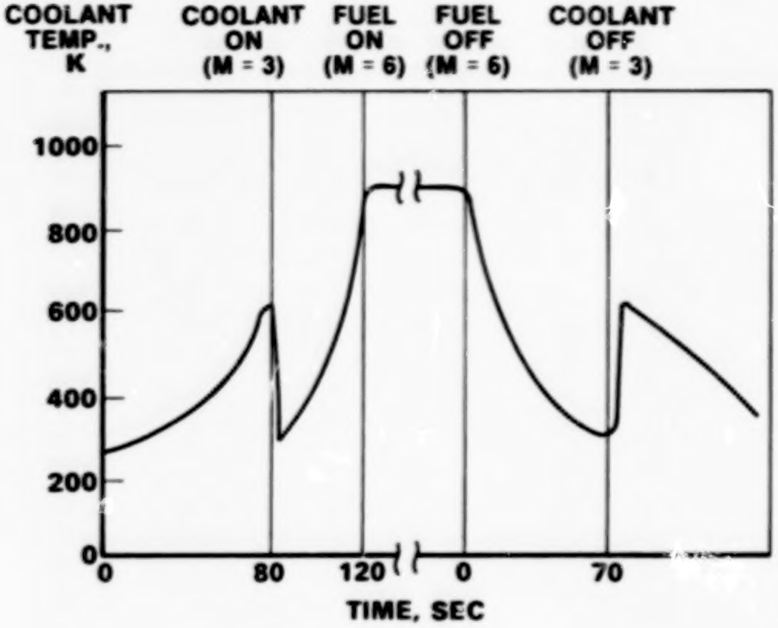

Figure 18

4

TPS/HONEYCOMB TEMPERATURE HISTORY ④

(Figure 19)

This temperature history goes with the trajectory, fuel schedule assumptions, and coolant response discussed above. It was obtained with the thermal analyzer model. The 'front' is the hot face sheet of the TPS; the 'back' is the unheated face sheet of the honeycomb, as much as 5 cm (2 in.) from the hot face sheet. Hastelloy X and nickel were investigated for the honeycomb core. For the face sheet, whether the core be nickel or Hastelloy, the response is extremely fast. At the startup, the front sheet very quickly goes to 890 K (1600°R) resulting in a ΔT of 670 K (1200°R). The resulting low-cycle fatigue life is too short. At shutdown, the temperature relationships of the front of the TPS and the back of the honeycomb are reversed. The ΔT developed is somewhat less than at startup, on the order of 550 K (1,000°R), but still higher than desired.

These results point up the need to find a way to limit ΔT. It cannot be done with change of materials. A combination of a material change combined with changes in the mission trajectory and with coolant and fuel scheduling, however, can reduce temperature differences to acceptable values. Design solutions that produce such reduced ΔT's are also available, but add complexity to the engine.

TPS/HONEYCOMB TEMPERATURE HISTORY ④

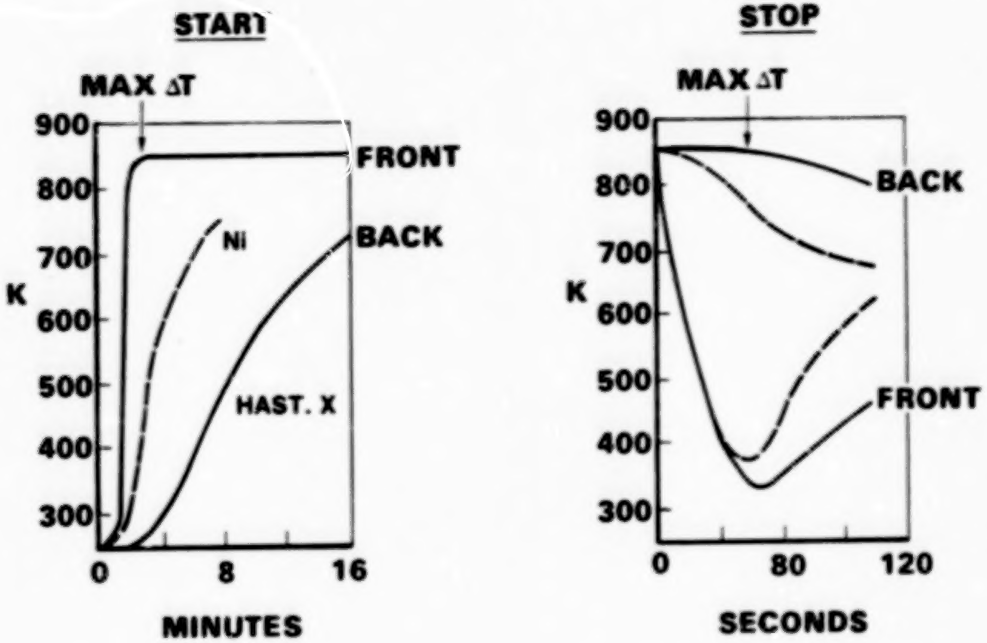

Figure 19

104

TRANSIENT STRESS ANALYSIS MODEL

(Figure 20)

A short axial section of the engine was structurally modeled to permit evaluation of the transient stresses at selected times along the trajectory. This shows how the various elements of the structure were modeled and what elements were modeled. The temperatures used in the analysis were obtained from the thermal analyzer program.

TRANSIENT STRESS ANALYSIS MODEL

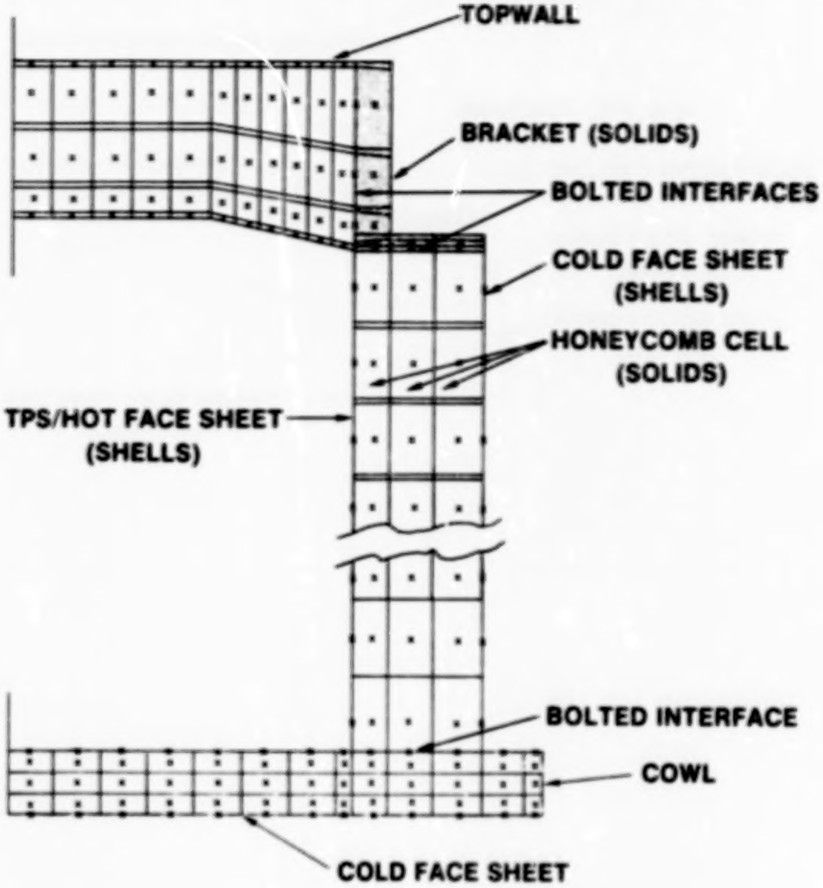
TOPWALL
BRACKET (SOLIDS)
BOLTED INTERFACES
COLD FACE SHEET (SHELLS)
HONEYCOMB CELL (SOLIDS)
TPS/HOT FACE SHEET (SHELLS)
BOLTED INTERFACE
COWL
COLD FACE SHEET

Figure 20

PEAK THERMAL STRESSES (ELASTIC)

(Figure 21)

These are the peak thermal stresses that result from the transient ΔT's discussed above. They were calculated as elastic stresses and are of magnitudes that will result in plastic flow of the material. At start-up, 1520 MPa (220 KSI), the yield for the material, 900 MPa (130 KSI), is greatly exceeded. At shutdown, the calculated stress is lower because of the somewhat reduced ΔT, but still well above the yield. As indicated previously, these high stresses must be reduced (to about half the values shown) by reduction of the ΔT's, by changes in engine operation, mission trajectory, or by TPS design.

PEAK THERMAL STRESSES
(ELASTIC)

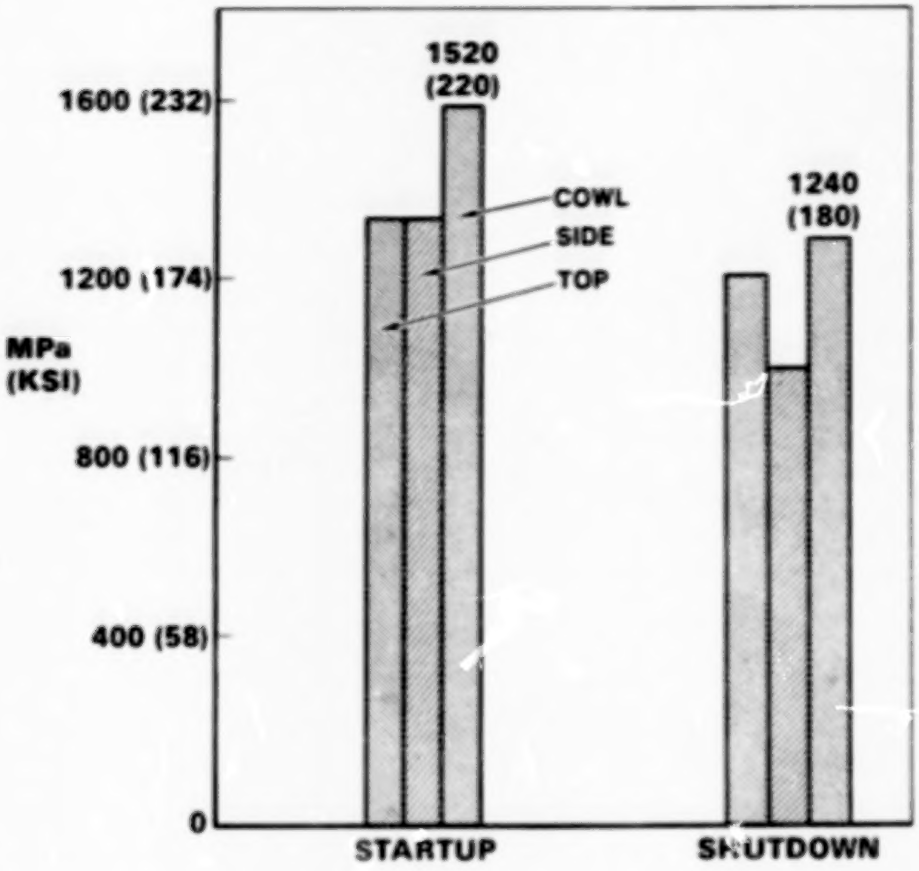

Figure 21

CONTENTS

Part I

PREFACE . . . . iii 1/A5

WELCOME 1 1/A10
R. R. Heldenfels

SESSION I - OVERVIEWS
Chairman: A. J. Henderson

1. HYPERSONIC STRUCTURES: AN AERODYNAMICIST'S PERSPECTIVE (OR ONE MAN'S DREAM IS ANOTHER MAN'S NIGHTMARE) 5 1/B1
J. D. Watts, L. R. Jackson, and J. L. Hunt

2. STRUCTURAL REQUIREMENTS FOR MILITARY HYPERSONIC SYSTEMS (Paper not available for publication)
P. Lane

3. AIRFRAME-INTEGRATED PROPULSION SYSTEM FOR HYPERSONIC CRUISE VEHICLES 39 1/F13
Robert A. Jones and Paul W. Huber

4. RECENT ADVANCES IN CONVECTIVELY COOLED ENGINE AND AIRFRAME STRUCTURES FOR HYPERSONIC FLIGHT 47 1/G7
H. Neale Kelly, Allan R. Wieting, Charles P. Shore, and Robert J. Nowak

SESSION II - ENGINE STRUCTURES
Chairman: H. N. Kelly

5. DESIGN AND ANALYSIS OF A SCRAMJET ENGINE 65 2/A13
O. A. Buchmann

6. THERMOSTRUCTURAL ANALYSIS OF A SCRAMJET FUEL-INJECTION STRUT 119 3/B11
Allan R. Wieting and Earl A. Thornton

7. ADVANCED FABRICATION TECHNIQUES FOR COOLED ENGINE STRUCTURES 145 3/F7
O. A. Buchmann

8. HYDROGEN EMBRITTLEMENT AND ITS CONTROL IN HYDROGEN-FUELED ENGINE SYSTEMS 195 4/F11
W. T. Chandler

9. CARBON-CARBON COMPOSITE APPLICATION FOR INTEGRAL ROCKET RAMJET COMBUSTORS (Paper not available for publication)
H. A. Holman

SESSION III - COOLED AIRFRAME STRUCTURES
Chairman: C. P. Shore

10. DESIGN AND FABRICATION OF A SKIN STRINGER DISCRETE TUBE ACTIVELY COOLED STRUCTURAL PANEL 253 6/A5
Frank M. Anthony

11. DESIGN AND ANALYSIS OF A PLATE-FIN SANDWICH ACTIVELY COOLED STRUCTURAL PANEL 319 7/C13
L. M. Smith

12. FLUXLESS BRAZING AND HEAT TREATMENT OF A PLATE-FIN SANDWICH ACTIVELY COOLED PANEL 375 8/E1
Charles S. Beuyukian

13. DESIGN AND FABRICATION OF A RADIATIVE ACTIVELY COOLED HONEYCOMB SANDWICH PANEL 449 10/A13
Leland C. Koch

14. RADIATIVE, ACTIVELY COOLED PANEL TESTS RESULTS 493 11/A5
Charles P. Shore, Robert J. Nowak, and Ellsworth L. Sharpe

TYPICAL HONEYCOMB TEMPERATURES

(Figure 22)

This chart considers the structural transient response along the engine axis. (The assumptions were slightly different than thore used for the previous analysis, resulting in somewhat different values.) At 125 sec into startup, the ΔT is 500 K (900°F). It falls off fairly sharply with distance from the outlet manifold. At about 46 cm (18 in.) from the outlet manifold, ΔT's are at steady state values and acceptable. Design solutions aimed at reducing ΔT are only required over an approximately one meter length. The rest of the engine will be controlled by steady state ΔT's, which have been found compatible with the design goals.

TYPICAL HONEYCOMB TEMPERATURES

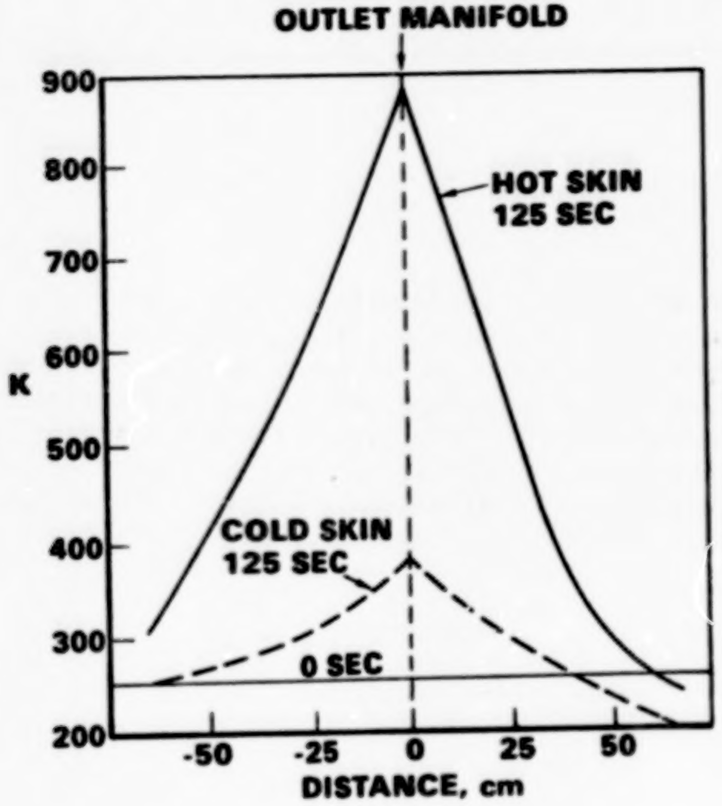

Figure 22

ENGINE WEIGHT--6 MODULES @ 37 X 46 cm

(Figure 23)

Looking at the swept-beam, vertical-beam, and all-honeycomb structures, the conclusion is that there is really not much to choose between them. Other considerations than weight will select the configuration. Some of these considerations have been discussed. Deflection, ease of fabrication, and ease of assembly favor the all-honeycomb configuration. The transient ΔT's and the associated problems would have to be accommodated in each one of the designs. In addition, the beams in the beam-supported configurations have a very slow thermal response. So in those configurations, means are needed to accommodate the ΔT between the beams and the panels, an additional complexity. Given the transient problem, the honeycomb therefore remains the favored configuration. The core of the honeycomb used here has a quarter-inch cell size.

The weight for the mounting is based on an Inconel 718 mounting frame accommodating the six modules. The weight of a fuel system was estimated based on controlling two groups of three modules each. Plumbing and instrumentation weight were based on a typical Scramjet installation.

ENGINE WEIGHT
6 MODULES @ 37 x 46 cm

	N (LB)		
ITEM	SWEPT BEAM	VERT BEAM	HONEY-COMB
STRUCTURE	13570(3050)	13430(3020)	13080 (2940)
TPS & MANIFOLDS	6230(1400)	6230(1400)	6230 (1400)
HONEYCOMB	2850 (640)	2850 (640)	3700 (830)
BEAMS & CLIPS	1690 (380)	1510 (340)	310 (70)
L.E.,T.E.,STRUTS	2850 (640)	2850 (640)	2850 (640)
MOUNTING	620 (140)		
FUEL SYSTEM	2410 (540)		
PLUMBING INSTRUMENTATION	1330 (300)		
	4360 (980)		
TOTAL	17930 (4030)	17800 (4000)	17440 (3920)

Figure 23

SUMMARY—THERMAL-STRUCTURAL DESIGN

(Figure 24)

A thermal-structural design has been defined in terms of the required flow routing. That flow routing is based on minimizing temperature discontinuities in the axial direction. Specific configurations have been defined both as regards the heat exchanger passage geometry and the layout of the heat exchanger, and material selections have been made. Hastelloy X, nickel, and Inconel 718 are the three materials used in the engine. Fabrication of the TPS/structure is considered to be within current technology.

In case of the structure, beam-supported and all-honeycomb configurations were considered, the latter using beams at the mounts only. The all-honeycomb configuration has been selected because of its good deflection and stress performance and its favorable manufacturing aspects.

In the case of the strut, various structural and manifolding arrangements were considered. The configuration that has been evolved is believed to satisfy deflection and stress limits. Verification of this will require additional, fairly extensive computer remodeling. The manifold design has been analytically verified for the wet-wall configuration, with the pressure loads carried by the strut structural shell.

SUMMARY
THERMAL-STRUCTURAL DESIGN

- TPS
  - FLOW ROUTING
  - CONFIGURATION
  - MATERIALS
- STRUCTURE
  - BEAMS
  - ALL-HONEYCOMB
- STRUTS
  - STRUCTURE
  - MANIFOLDS

Figure 24

DESIGN DATA REQUIREMENTS

(Figure 25)

Design of the engine will benefit from additional data in critical areas. Better definition of the engine unstart pressures is of particular interest because of their effect on the structure and controls requirements. The unstart loads that are being used are generally considered unrealistically severe. The vertical and horizontal pressure distributions are unknown. The possibility of an unsymmetrical unstart within a module (strut to strut) was assumed, but needs evaluation.

No data exists on aerodynamic interaction of one module with the next module. Is a single module unstart equivalent to unstarting the whole group of six modules? How does the unstart propagate, if at all. The dynamics associated with propagation of the unstart through a module and from module to module are similarly unknown, as is the possible existence of a buzz problem with the inlet. These data will be needed to support a final detailed design for the engine.

In the case of the thermal-structural design, a better definition of the distribution of heat flux in the combustor is needed. The shock pattern needs to be defined. Corner heating is a problem peculiar to a 3-D engine. The data used predict no problem in the corners from the heating point of view. That needs to be verified, because test configurations from which the data were derived were not the same as the 3-D Scramjet configurations.

The basic aerodynamic data used in the study assumed sharp leading edges. Instead, blunting to 1.27 mm (0.05 in.) was required for pressure drop, heat transfer, and structural reasons. The aerodynamic interaction of the aircraft and the engine is clearly important to thermal-structural design of the engine itself and of the interfaces with an airplane.

DESIGN DATA REQUIREMENTS

- ENGINE UNSTART
  - PRESSURES
    VERTICAL
    HORIZONTAL
    SYMMETRY
  - MODULE-MODULE
    INTERACTION
    PROPAGATION
  - DYNAMICS
    PROPAGATION
    BUZZ
- HEAT FLUX DISTRIBUTION
  - COMBUSTION
  - SHOCKS
  - CORNERS
  - BLUNTING
  - AIRCRAFT INTEGRATION

Figure 25

CONCLUSIONS

(Figure 26)

The transient performance of the TPS/structure during engine start-up and shutdown governs the design. For the most severe assumptions concerning mission trajectory and engine operating procedures, ΔT's can range to 670 K (1200°R). Reduction of ΔT's to acceptable levels is possible by changes in operating procedures and, if required, in design of the TPS.

Specific structural design solutions have been identified for the engine. These have been incorporated in layout drawings of the engine. Analyses have verified that there are no basic structural problems once the transient operation is accommodated.

The design objectives for the engine, given control of the temperatures during transients, are feasible: 1000 cycles and 100 hours of engine operation. TPS temperatures are being limited to 1140 K (1600°F) on the surface and 890 K (1600°R) at the prime structure. Deflections during normal engine operation can be limited to the specified values and remain acceptable during the severe loadings assumed for engine unstart.

CONCLUSIONS

- TRANSIENTS GOVERN DESIGN
- DESIGN SOLUTIONS IDENTIFIED
- DESIGN OBJECTIVES FEASIBLE

Figure 26

118

BLANK PAGE

THERMOSTRUCTURAL ANALYSIS OF A SCRAMJET FUEL-INJECTION STRUT

Allan R. Wieting
NASA Langley Research Center

and

Earl A. Thornton
Old Dominion University

120

THERMOSTRUCTURAL ANALYSIS OF A SCRAMJET FUEL-INJECTION STRUT

Allan R. Wieting
NASA Langley Research Center

and

Earl A. Thornton
Old Dominion University

INTRODUCTION

AIRFRAME-INTEGRATED SCRAMJET

(Figure 1)

Studies of airframe-integrated scramjets with high potential performance led to the sweptback, fixed-geometry, hydrogen-fueled, rectangular scramjet module shown in figure 1. Two inner scramjet modules are shown; the sidewall of one module is removed to reveal the internal engine surfaces. The scramjet modules are integrated with the airframe and use the entire undersurface of the aircraft to process engine airflow. The aircraft forebody serves as an extension of the engine inlet, and the afterbody serves as an extension of the engine nozzle. Discussion of the propulsion aspects of this scramjet concept can be found in the paper by Jones (ref. 1).

A preliminary thermal/structural design analysis study (ref. 2) based on Hypersonic Research Engine (HRE) technology (ref. 3) indicated viability from both an engine structural mass and coolant requirement standpoint. This study revealed a number of critical areas (e.g., panel-to-panel seals, fuel injection struts) and reemphasized the need for advances in fabrication and materials technology to obtain reasonable structural life.

Recently, a more detailed study (ref. 4) of this scramjet concept was undertaken by a major engine manufacturer while the effort at Langley concentrated on the fuel-injection struts. The primary function of the three fuel-injection struts is to provide the mechanism for multiplanar fuel injection into the supersonic airstream. Salient features from the thermal/structural design and analysis of the struts are presented in this paper.

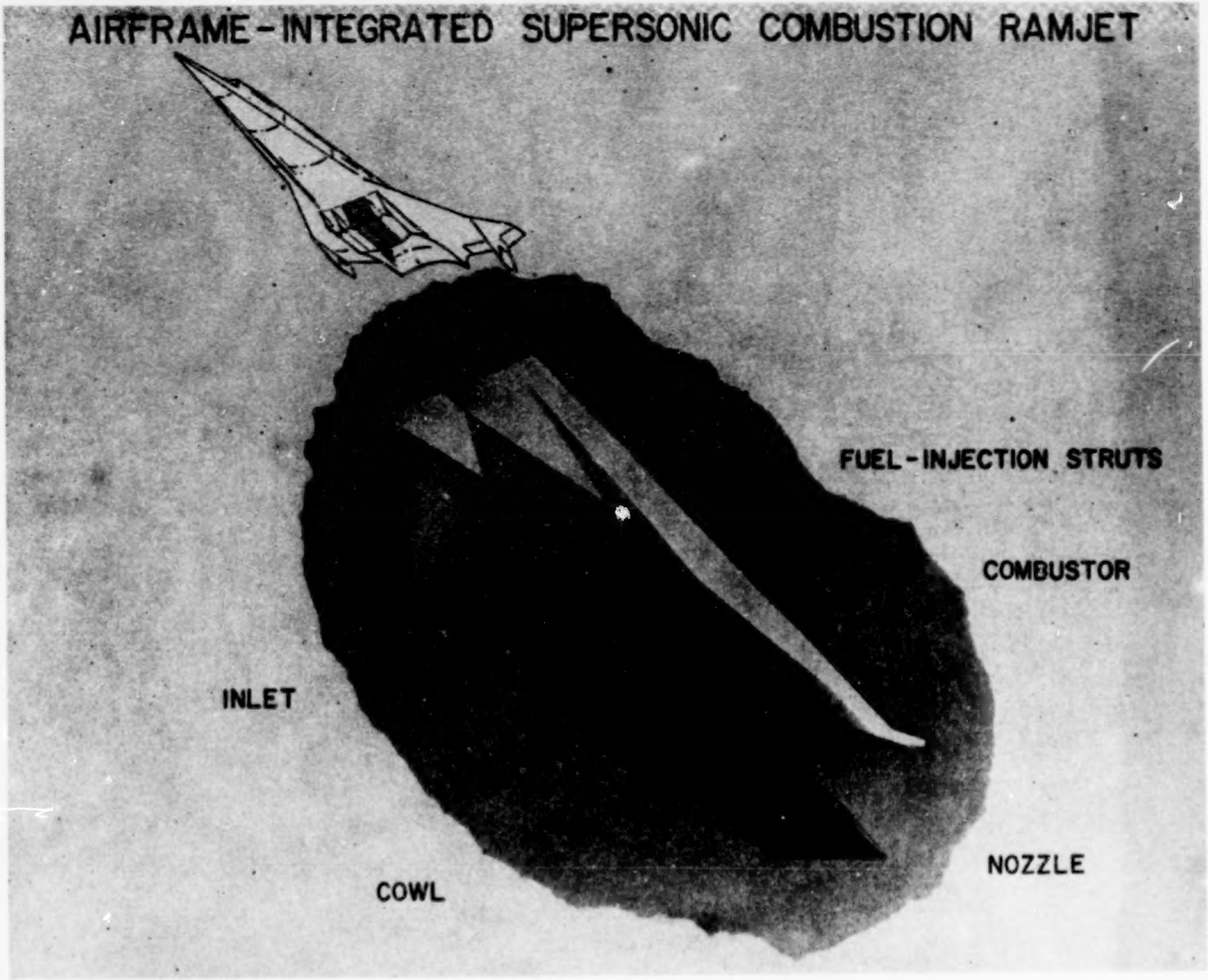
AIRFRAME-INTEGRATED SUPERSONIC COMBUSTION RAMJET
FUEL-INJECTION STRUTS
COMBUSTOR
INLET
NOZZLE
COWL

7

Figure 1

STRUT GEOMETRY AND AEROTHERMAL ENVIRONMENT

(Figure 2)

The struts, which are shown in figure 2, have a slender wing-like configuration. The struts are swept back 48° and span the distance between the engine top wall and cowl. An axial cross section at any spanwise location along the sweep line is shown in the upper right figure. The center strut is symmetric and the two side struts are asymmetric. The side strut thickness is approximately 7 percent of the chord; the chord is approximately 45 percent of the span. The struts are immersed in the supersonic flow, partially in the inlet and partially in the combustor and therefore are exposed to a hostile environment.

The thermal environment is characterized by the chordwise heat flux $\dot{q}$ distribution along both sides of the strut shown in the lower left figure. The heating is highly nonuniform because of stagnation, shock boundary-layer interaction, and combustion. The heat flux which varies by an order of magnitude is also asymmetric.

STRUT GEOMETRY AND THERMAL ENVIRONMENT

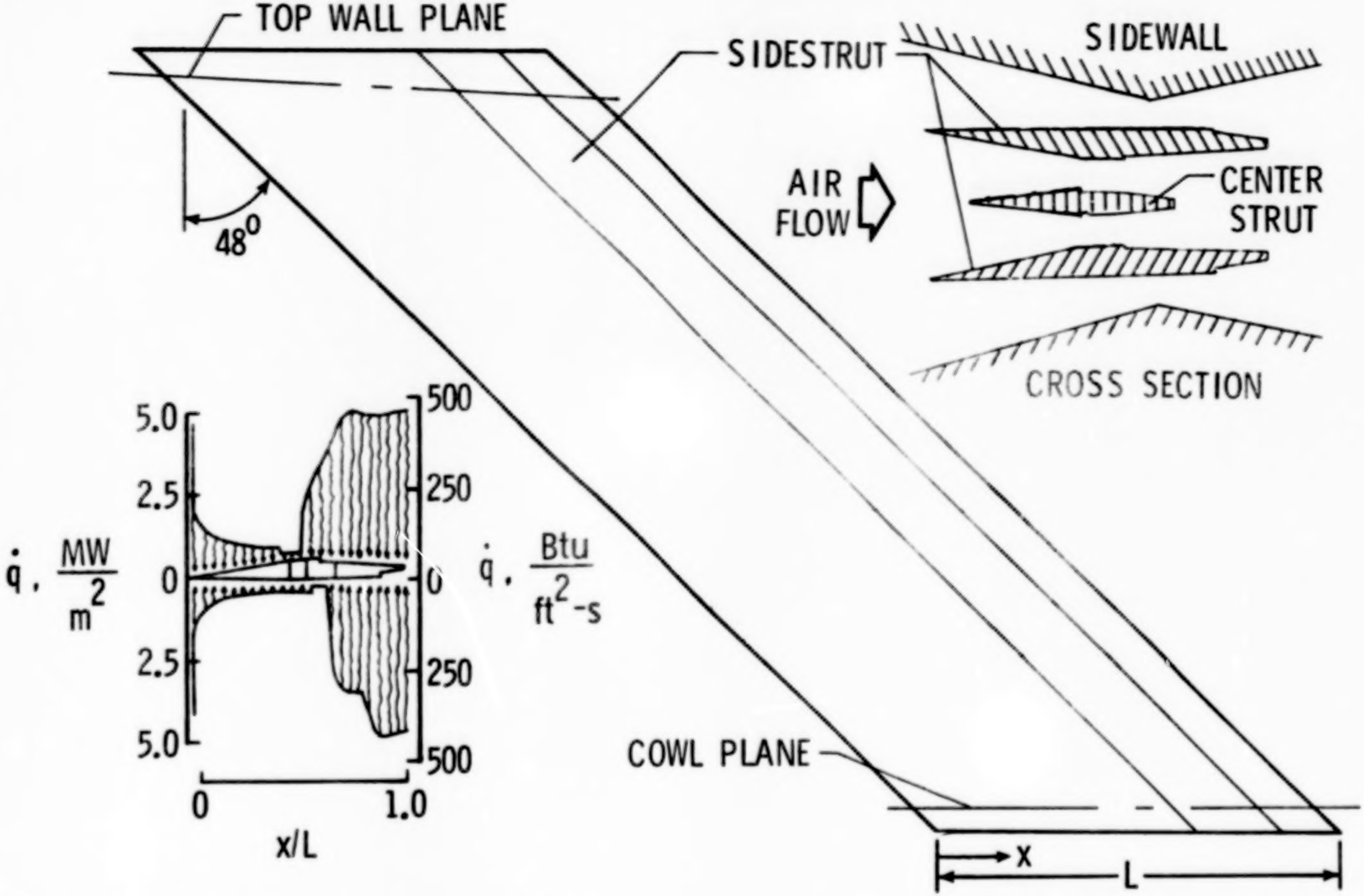
TOP WALL PLANE
48°
SIDESTRUT
SIDEWALL
AIR FLOW
CENTER STRUT
CROSS SECTION
5.0
2.5
0
2.5
5.0
500
250
0
250
500
$\dot{q}$, $\frac{MW}{m^2}$
$\dot{q}$, $\frac{Btu}{ft^2\text{-}s}$
0
1.0
x/L
COWL PLANE
x
L

CHORDWISE HEAT FLUX DISTRIBUTION

STRUT CONFIGURATION

Figure 2

STRUT CONSTRUCTION

(Figure 3)

The struts must simultaneously support a large side load, contain high-pressure hydrogen at two temperature extremes, and withstand high thermal stresses resulting from complex aerodynamic heating as well as convective heating from the hot hydrogen in the internal manifolds. To compound the design problem, the cross-sectional area and contour cannot be altered without significantly changing the engine propulsion performance.

Each strut is subdivided internally into four longitudinal compartments by three major bulkheads as shown in the figure. The fore and aft compartments serve as coolant inlet and outlet manifolds, respectively, and the central compartments serve as fuel manifolds for the strut trailing edge (parallel to airflow) and wall (perpendicular to airflow) fuel injectors. Coolant in the inlet manifold is injected through a slot, impinges on the leading edge, and splits (unequally) to flow along each wall to the trailing edge, where it is collected in the outlet manifold. This quadrilateral manifold configuration was selected over a more structurally efficient (high pressure containment) tubular configuration because the former has a greater volumetric efficiency which results in larger fuel and coolant flow areas and thus lower pressure losses. Structural details are shown in the lower figure. The primary structure is basically a 2.5 mm (.1 in.) thick wall. Normally, internal convective heating from the hot hydrogen in the manifolds would be negligible compared to the aerodynamic heating. However, because of the higher velocities caused by the still restricted flow area, internal convective heating is significant. A metallic plate-fin thermal buffer, with the fins oriented transverse to the fuel flow direction to restrict flow and provide essentially stagnant hydrogen in the passages between the shield and the strut wall, eliminates direct convective heating to the strut wall. A pin fin coolant passage is used on the external surfaces. Hydrogen coolant routed through the passage absorbs the aerodynamic heat load.

STRUT CONSTRUCTION

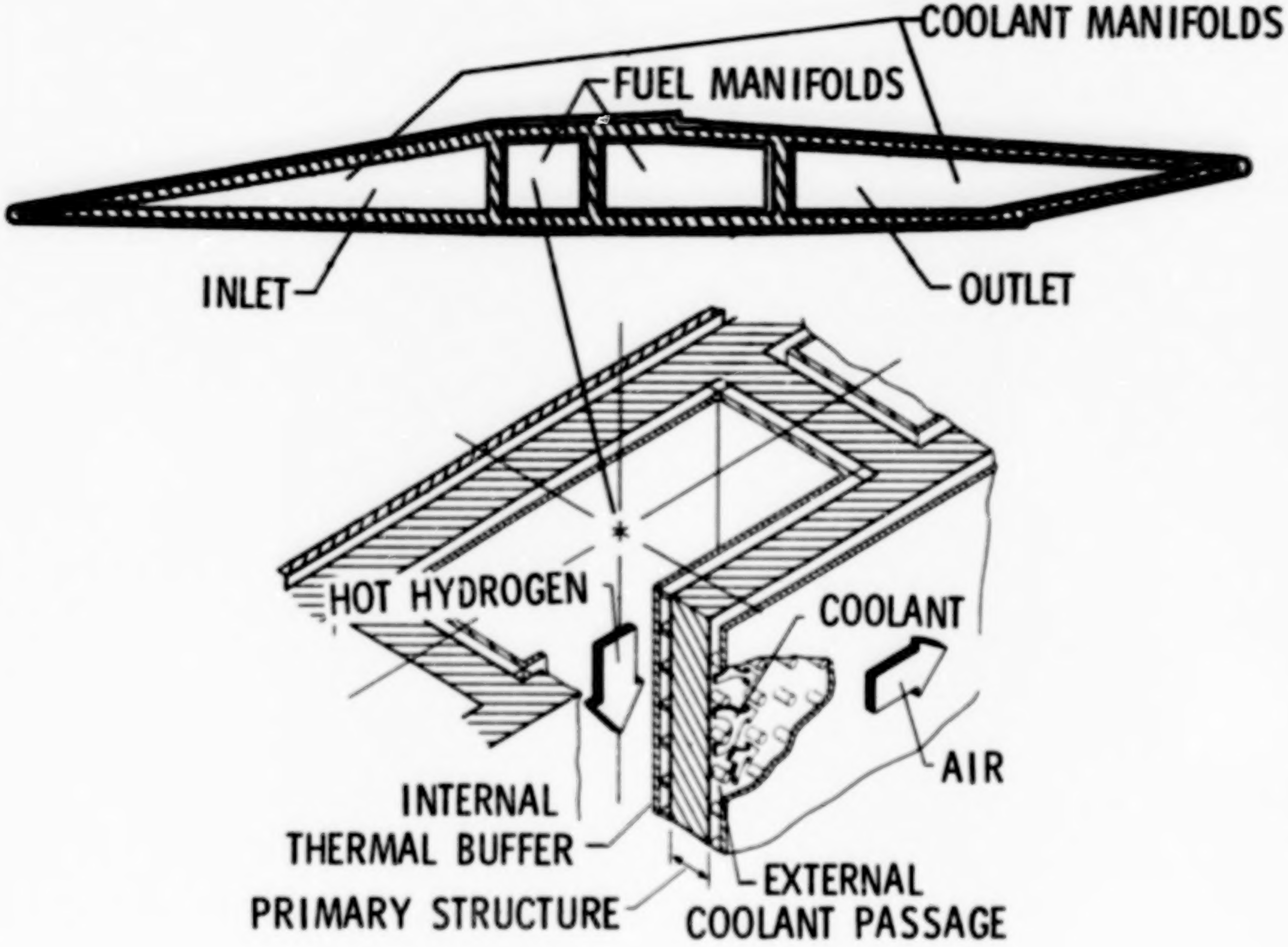
COOLANT MANIFOLDS
FUEL MANIFOLDS
INLET
OUTLET
HOT HYDROGEN
COOLANT
AIR
INTERNAL THERMAL BUFFER
PRIMARY STRUCTURE
EXTERNAL COOLANT PASSAGE

Figure 3

DESIGN TEMPERATURE LOADS

(Figure 4)

The design temperatures are characterized by the chordwise temperature (T) distributions shown in the figure for the starboard structural wall of the strut. The temperature distributions along the port wall are similar. The solid line indicates the wall temperature adjacent to the coolant passage, and the dashed line indicates the wall temperature adjacent to the manifold. The solid symbols denote the average temperature of the major bulkheads. During operation the forward section is below ambient, and the aft section is above ambient. Significant thermostructural loads result from the nonlinear chordwise temperature gradient and the transverse temperature gradients through the walls and bulkheads. The chordwise temperature gradient is caused by the highly non-uniform aerothermal heating (fig. 2), and the transverse gradients by the internal convective heating.

DESIGN TEMPERATURE LOADS

STARBOARD SIDE

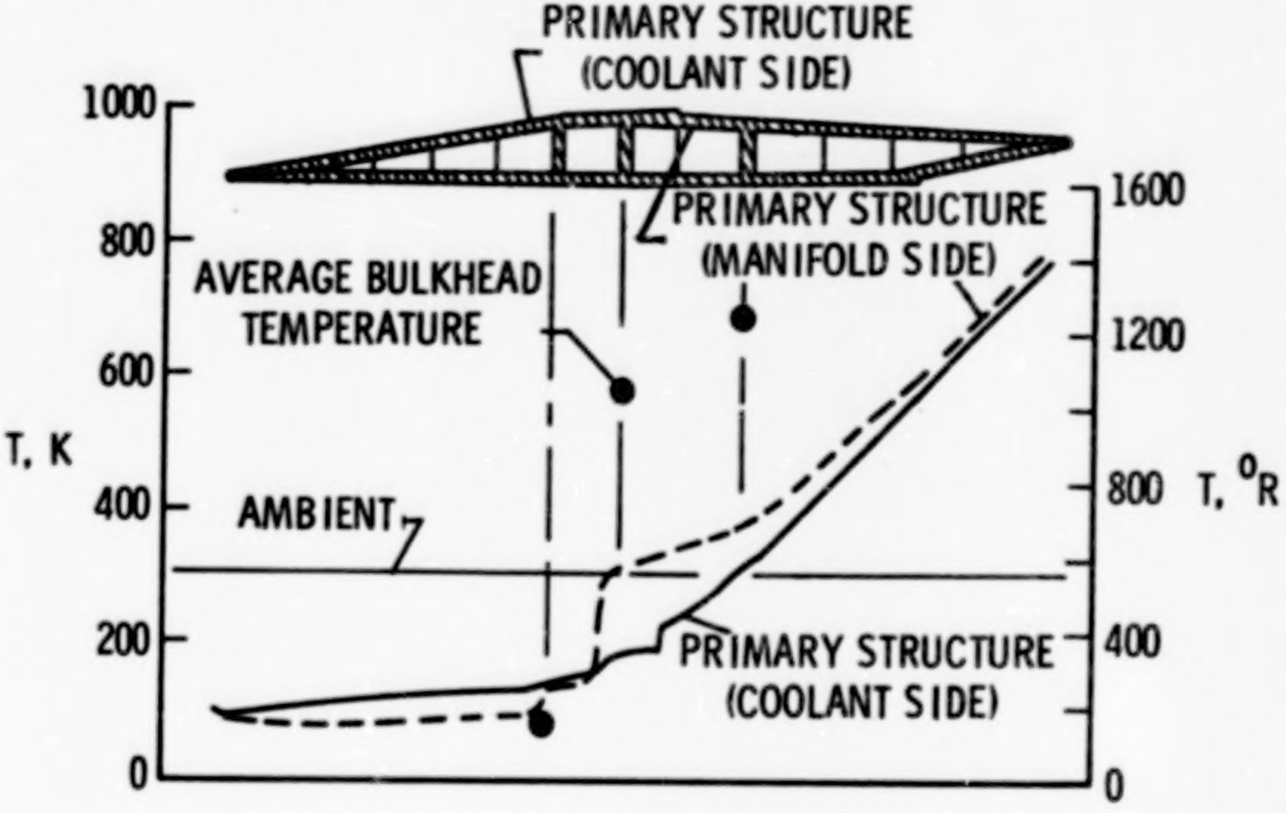

Figure 4

ATTACHMENT SCHEME AND DEFORMATIONS DUE TO CHORDWISE TEMPERATURE GRADIENT

(Figure 5)

Overall thermal expansions of the strut are accommodated by the mounting system shown schematically in the left figure. The strut top wall and cowl mounts are approximately at mid-chord. At the top the strut has rotational freedom about the pin axis and translational freedom fore and aft from the pin. At the cowl the strut has rotational freedom about all axes and translational freedom along the 48° sweep line.

The deformations due to the nonlinear chordwise temperature gradient are primarily in the spanwise plane as shown schematically in the right figure. The leading edge shrinks and the trailing edge expands, causing bending about the spanwise axes. The maximum deflection in the chordwise direction is 3.0 mm (0.12 in.) and is the result of bending caused primarily by the chordwise temperature gradient. The bending of the strut causes local changes in the sweep angle. The local sweep angle change along the leading and trailing edge is between 1 to -2 degrees. The radius of curvature which defines the local angle change, can be approximately by $r = w/\alpha\Delta T$ where w is the perpendicular distance between leading and trailing edge, α is the coefficient of thermal expansion, and ΔT is the chordwise temperature difference. The maximum deflection in the spanwise direction (4.3 mm (0.17 in.)) is at the trailing edge at the cowl plane and is caused primarily by the increase in the trailing edge temperature above ambient (ΔT = 550 K (ΔT = 1000°F)). These deformations are critical to the seal design at the top wall and the cowl. The cowl seal is particularly critical because the strut leading edge overhangs the cowl leading edge and the aft section of the strut penetrates the cowl.

ATTACHMENT SCHEME AND DEFORMATIONS DUE TO CHORDWISE TEMPERATURE GRADIENT

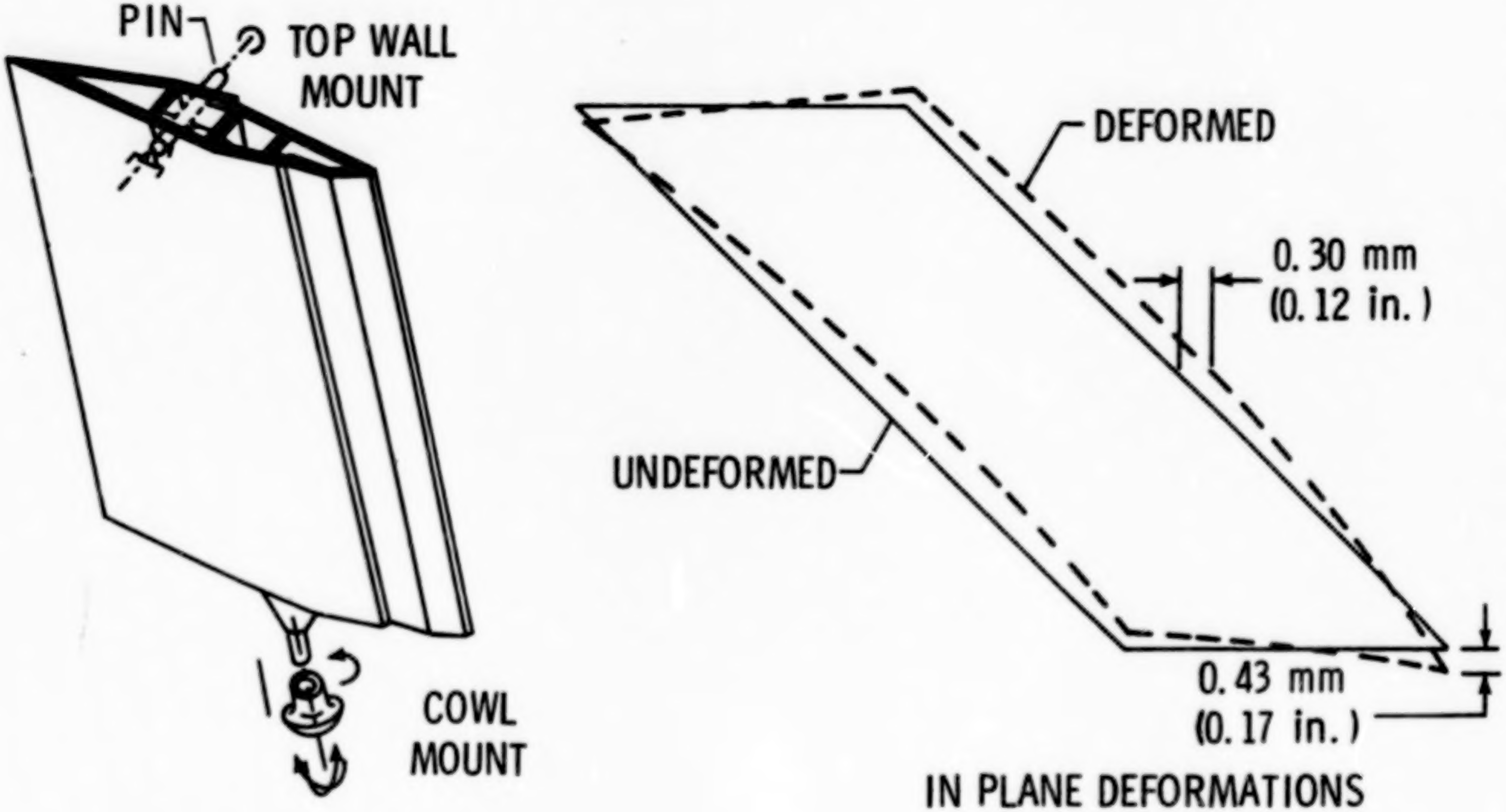
PIN
TOP WALL MOUNT
COWL MOUNT
DEFORMED
0.30 mm (0.12 in.)
UNDEFORMED
0.43 mm (0.17 in.)

ATTACHMENT SCHEME

IN PLANE DEFORMATIONS (NOT TO SCALE)

Figure 5

STRESSES DUE TO CHORDWISE TEMPERATURE GRADIENT

(Figure 6)

As shown in the left figure, the stresses due to the nonlinear chordwise temperature gradient concentrate primarily in the rectangular midsection of the strut, leaving the ends relatively lowly stressed, which simplifies the attachment design. The principal stresses are basically aligned with the sweep which is indicative of the overall bending action in the spanwise plane. A chordwise distribution of the principal stress in the spanwise direction normalized by the allowable stress is shown in the right figure. As expected, the leading and trailing edges are in compression - with a maximum stress approximately 50 percent of the allowable - and the midsection is in tension - with a maximum stress of approximately 30 percent of the allowable. The results are typical for both walls.

STRESS DUE TO CHORDWISE TEMPERATURE GRADIENT

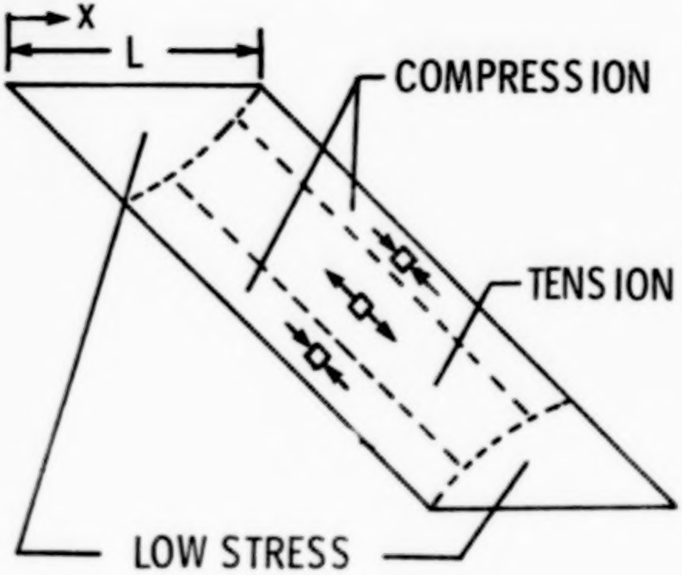
X
L
COMPRESSION
TENSION
LOW STRESS

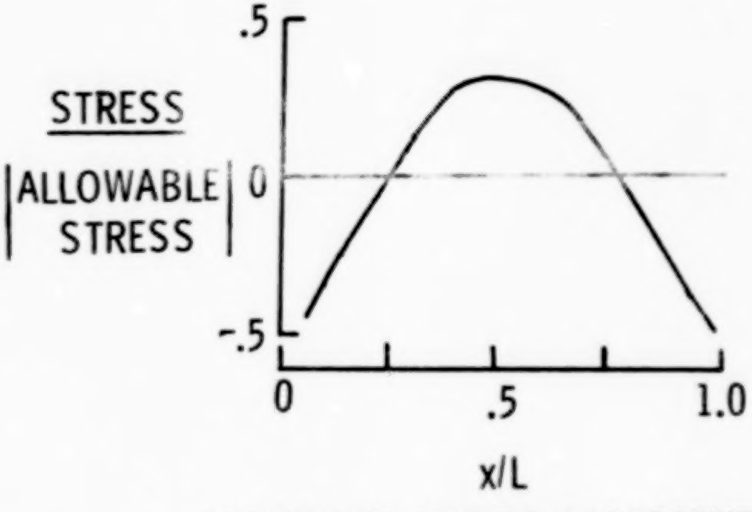

CHORDWISE STRESS DISTRIBUTION

- o STRESSES UNIAXIAL
- o STRESSES LOW IN MOUNT AREA

II

Figure 6

DEFORMATIONS AND STRESSES DUE TO TRANSVERSE TEMPERATURE GRADIENTS

(Figure 7)

The transverse temperature gradients primarily result from the internal convective heat transfer from the hydrogen in the manifolds although the asymmetric aerodynamic heating is also a contributor. The result of these heat loads is a wall gradient ΔT_W and a bulkhead gradient ΔT_B. These gradients result in local wall bending and the out of plane deformation illustrated in the left figure. The two solid lines are nodal lines (zero deflection) and the two shaded areas indicate the areas of maximum positive and negative deflection which are negligible at approximately 0.0076 mm (0.0003 in.).

The chordwise stress distribution (in extreme fiber) resulting from the transverse gradients is shown normalized to the allowable stress in the figure on the right. The solid line illustrates the stress distribution due to the overall transverse gradient ($\Delta T_B + \Delta T_W$). The maximum stress is about 50 percent of the allowable. The bulkhead gradient (ΔT_B) primarily causes local bending in the wall in the vicinity of the bulkhead. The dashed line illustrates the stress distribution due to the wall gradient (ΔT_W) only. The maximum stress due to ΔT_W occurs near midchord and is approximately 30 percent of the allowable. This gradient (ΔT_W) results in a biaxial stress through the wall and therefore the spanwise component will add to the stress from the chordwise temperature gradient.

The combined thermal stresses (not shown), which dominate the design, are approximately 60 to 80 percent of the allowable. The stresses due to the pressure load for normal engine operating conditions are approximately 20 percent of the allowable, yielding a combined stress of 80 to 100 percent of the allowable and therefore a thermal/structural concept that is feasible under normal operating loads. However, the maximum external pressure loads do not occur during normal engine operation.

DEFORMATIONS AND STRESSES DUE TO TRANSVERSE TEMPERATURE GRADIENTS

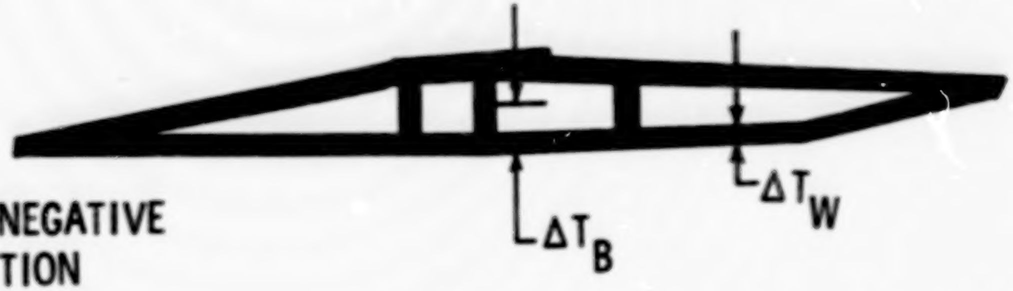
ΔT_W
ΔT_B

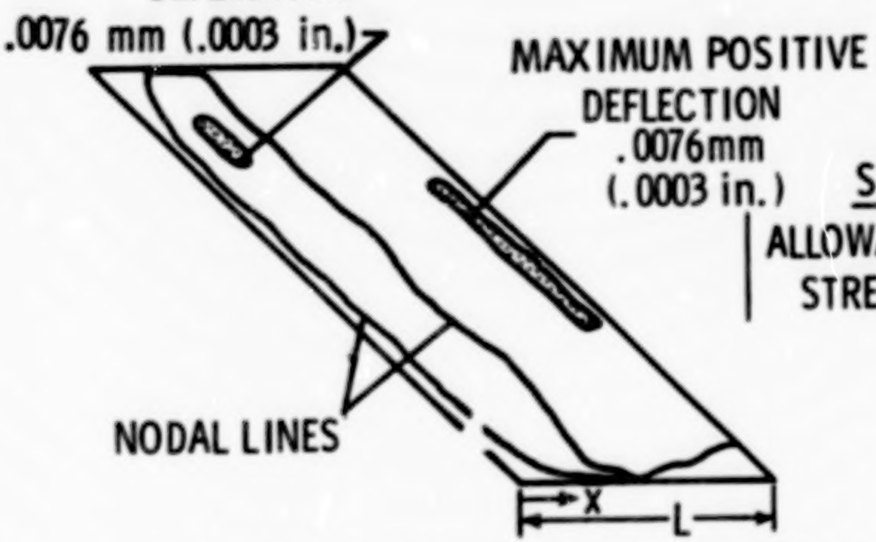
MAXIMUM NEGATIVE DEFLECTION .0076 mm (.0003 in.)
MAXIMUM POSITIVE DEFLECTION .0076mm (.0003 in.)
NODAL LINES
X
L

OUT OF PLANE DEFORMATION CONTOURS

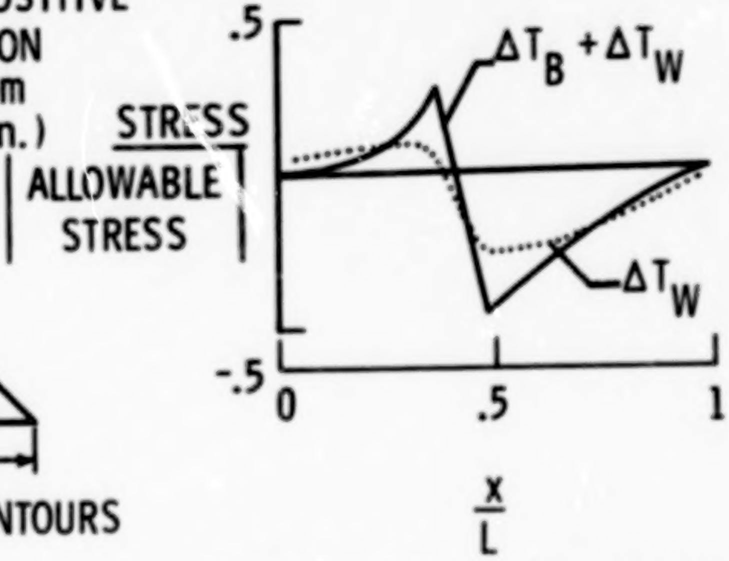

CHORDWISE STRESS DISTRIBUTION

Figure 7

CRITICAL PRESSURE LOADS

(Figure 8)

The maximum external pressure loads occur during an engine unstart (i.e., transition from supersonic to subsonic flow) which results if thermal choking occurs in the combustor. When the initial design study (ref. 2) was undertaken, the operational flow system was well understood; however, the unstarting process was not. Consequently, the basic unstart phenomena and loading were characterized experimentally (ref. 5). The maximum external pressure loading occurs at approximately Mach 5, when the aerodynamic flow in the passage between the sidewall and the side strut unstarts and the flow in the other three passages remains started as depicted in the upper left figure.

The unstarting process is highly transient as indicated by the shaded area on the typical pressure history shown in the right figure. The pressure is normalized to the steady state started pressure. The peak pressure occurs during the unstart and is an order of magnitude higher than the normal operating pressure and may be 2 to 7 times higher than the steady state unstarted pressure levels, which have typically been used in prior engine designs such as the HRE. These peak levels are conservatively predicted by normal shock wave theory. Since the complete dynamic characteristics of the transient pulse are not known, the envelope of the peaks along the strut currently serves as the basis for the structural design. The design pressure load isobars are shown schematically in the lower figure. Peak pressures are between 4.8 and 5.7 kPa (100 and 120 psi) over the majority of the strut.

CRITICAL PRESSURE LOADS

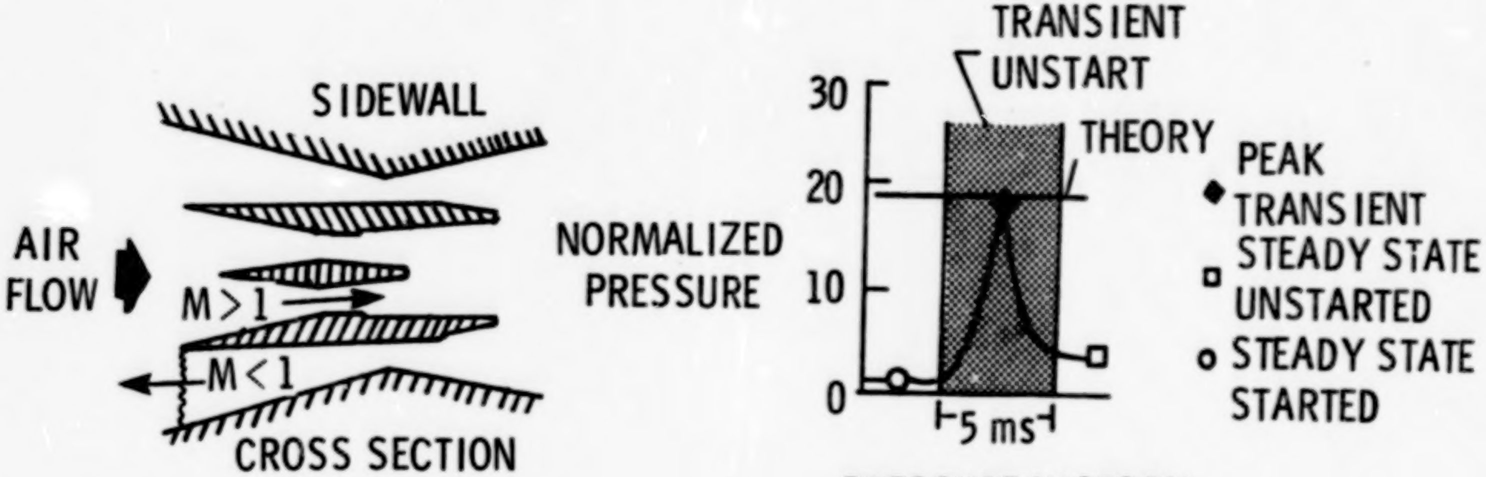
SIDEWALL
AIR FLOW
M > 1
M < 1
NORMALIZED PRESSURE
30
20
10
0
TRANSIENT UNSTART
THEORY
5 ms
◆ PEAK TRANSIENT
☐ STEADY STATE UNSTARTED
○ STEADY STATE STARTED

CROSS SECTION
ASYMMETRIC UNSTART

PRESSURE HISTORY

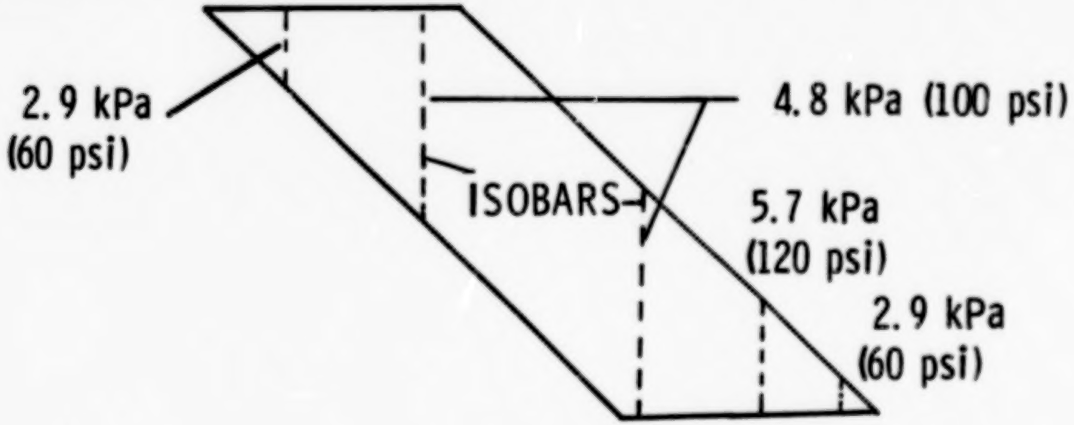
2.9 kPa (60 psi)
4.8 kPa (100 psi)
ISOBARS
5.7 kPa (120 psi)
2.9 kPa (60 psi)

DESIGN PRESSURE LOADS

Figure 8

COMBINED STRESSES

UNSTART

(Figure 9)

Analytical results (refs. 2 and 4) indicate that the combined thermal and unstart pressure stresses exceed the allowable stress. As stated earlier the thermal stresses (60 to 80 percent of the allowable) are caused by the nonlinear chordwise temperature gradient and transverse temperature gradient shown in the left figure for a coolant outlet temperature (T_o) equivalent to the superalloy temperature limit of 890 K (1600°R). The temperature gradients are significantly reduced, as shown in the figure, by increasing the coolant flow to obtain an outlet temperature of 430 K (770°R). Attendant thermal stresses are reduced to approximately 30 percent of the allowable and the combined stresses are reduced approximately 50 percent to acceptable levels as shown in the right figure. Reducing the coolant outlet temperature yields a feasible strut concept and adds no complexity to the design or fabrication, and even though the strut coolant flow rate is doubled, the overall engine cooling requirement is increased only 5 percent. As discussed in reference 6, excess coolant is available at this flight condition. An alternate technique, identified in references 2 and 4, ties the three struts together at mid span; however, the tie greatly complicates cooling design and fabrication.

COMBINED STRESSES

UNSTART

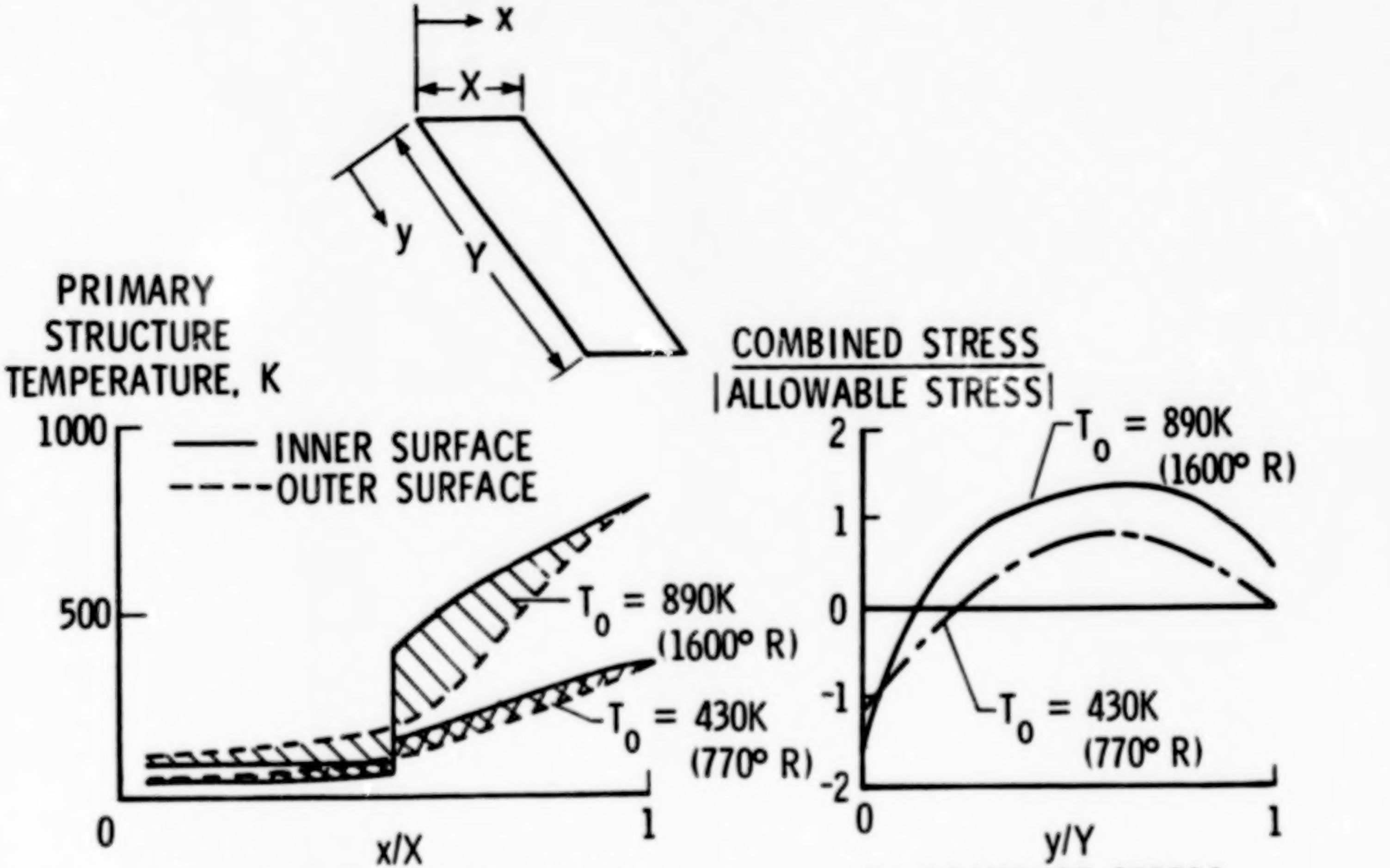

(A) CHORDWISE TEMPERATURE DISTRIBUTION

(B) SPANWISE STRESS DISTRIBUTION AT x/X = 0.5

Figure 9

DEFORMATIONS DUE TO THE UNSTART PRESSURE

(Figure 10)

The out of plane deformations due to the unstart pressure load only are indicated by the contour plot shown in the figure. Overall deformation indicates a twisting action with the maximum chordwise deformations at mid span and a maximum deflection of approximately 1.5 cm (0.6 in.) at the trailing edge. Maximum displacements at the top wall and cowl planes are between 0.5 and 0.8 cm (0.2 and 0.3 in.) These deformations are considered a maximum as no constraint at the top wall and cowl planes was assumed in the analysis. A schematic of the side strut displacement at midspan is shown in the right hand figure. The large deflection of the side strut greatly constricts the flow passage between the struts. The constriction will alter the aerodynamic flow characteristics, most likely resulting in coupled-interaction between the flow and the strut.

DEFORMATIONS DUE TO UNSTART PRESSURE

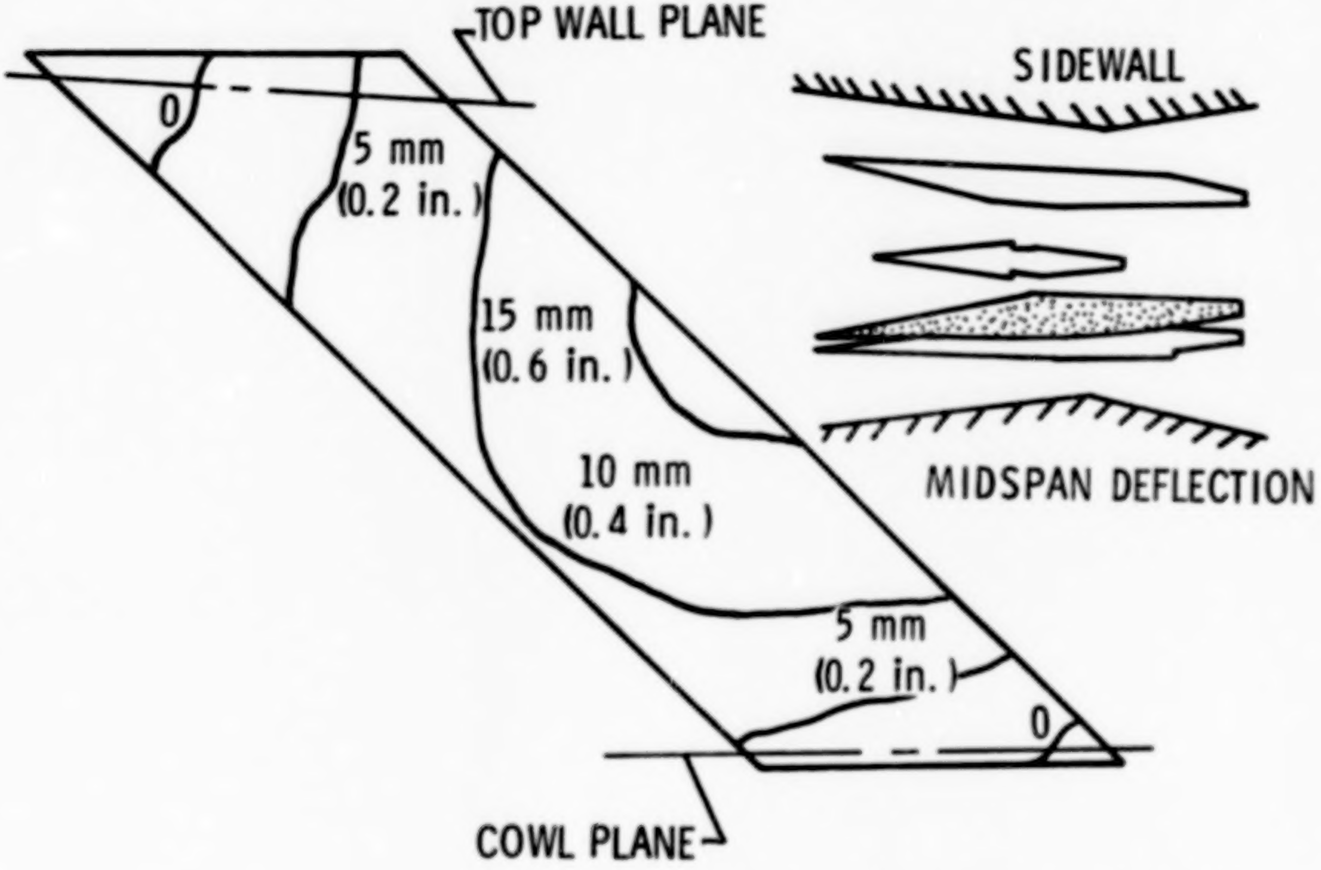
TOP WALL PLANE
0
5 mm
(0.2 in.)
15 mm
(0.6 in.)
10 mm
(0.4 in.)
5 mm
(0.2 in.)
0
COWL PLANE
SIDEWALL
MIDSPAN DEFLECTION

OUT OF PLANE DISPLACEMENT CONTOURS

Figure 10

DYNAMICS

(Figure 11)

A feasible thermal/structural strut concept has been identified based on static loads; however, the response of this concept to potential dynamic loads has not been investigated. A cursory look at flutter indicated a factor of safety of three on flutter speed. The dynamic response of the strut to time varying pressure loads such as inlet/combustor instabilities, shock boundary-layer interactions, and the unstart transients needs to be determined; however, the dynamic characteristics of these loads have not been sufficiently defined. A preliminary vibration analysis of the strut indicates a first mode (bending) frequency of 170 Hz which is potentially within the range of engine time varying loads and indicates the possibility of large dynamic deformations and stresses.

DYNAMICS

- FLUTTER - FACTOR OF SAFETY OF 3 ON FLUTTER SPEED
- TIME VARYING LOAD CHARACTERISTICS UNDEFINED
  - INLET/COMBUSTOR INSTABILITIES
  - SHOCK BOUNDARY-LAYER INTERACTIONS
  - UNSTART TRANSIENT
- VIBRATION ANALYSIS SHOWS FUNDAMENTAL FREQUENCY OF 170 Hz
- KNOWLEDGE OF DYNAMIC RESPONSE REQUIRED

Figure 11

11

142

CONCLUDING REMARKS

(Figure 12)

Results of a thermal-structural design analysis study of a fuel-injection strut for a NASA concept of an airframe integrated hydrogen-cooled scramjet indicate a feasible thermal/structural concept has been identified for the static load conditions. Thermal stresses dominate the static response. Potentially critical dynamic loads exist and consequently a knowledge of the dynamic response is required to finalize the design. However, the basic design has progressed sufficiently to warrant development of fabrication processes and testing of flight hardware to verify the thermal/structural performance.

CONCLUDING REMARKS

- FEASIBLE THERMAL/STRUCTURAL CONCEPT IDENTIFIED FOR STATIC LOADS
- THERMAL STRESS DOMINATES STATIC RESPONSE
- KNOWLEDGE OF DYNAMIC RESPONSE REQUIRED
- NEED HARDWARE AND TESTS TO VERIFY FABRICATION AND PERFORMANCE

Figure 12

REFERENCES

1. Jones, Robert A.; and Huber, Paul W.: Airframe-Integrated Propulsion System for Hypersonic Cruise Vehicles. Recent Advances in Structures for Hypersonic Flight, NASA CP-2065, 1978. (Paper no. 3 of this compilation.)
2. Wieting, Allan R.; and Guy, Robert W.: Thermal-Structural Design/Analysis of an Airframe-Integrated Hydrogen-Cooled Scramjet. AIAA Journal of Aircraft, vol. 13, no. 3, Mar. 1976, pp. 192-197.
3. Staff of Langley Research Center and AiResearch Manufacturing Co., The Garrett Corp.: Hypersonic Research Engine Project Technological Status 1971. NASA TM X-2572, 1972.
4. Buchmann, O. A.: Design and Analysis of a Scramjet Engine. Recent Advances in Structures for Hypersonic Flight, NASA CP-2065, 1978. (Paper no. 5 of this compilation.)
5. Wieting, Allan R.: Exploratory Study of Transient Unstart Phenomena in a Three-Dimensional Fixed-Geometry Scramjet Engine. NASA TN D-8156, 1976.
6. Kelly, H. Neale; Wieting, Allan R.; Shore, Charles P.; and Nowak, Robert J.: Recent Advances in Convectively Cooled Engine and Airframe Structures for Hypersonic Flight. Recent Advances in Structures for Hypersonic Flight, NASA CP-2065, 1978. (Paper no. 4 of this compilation.)

ADVANCED FABRICATION TECHNIQUES FOR COOLED ENGINE STRUCTURES*

O. A. Buchmann
AiResearch Manufacturing Company

INTRODUCTION

Past studies of hydrogen-cooled hypersonic propulsion systems led to the use of rectangular-offset-fin, plate-fin coolant passages, culminating in the successful design, fabrication, and test of the structural assembly model of the hypersonic research engine (HRE). The design life of the HRE cooled structures was 100 cycles and 10 hr and was limited by creep and low-cycle fatigue.

The purpose of this program is to develop coolant passage geometries, material systems, and joining processes that will produce long-life hydrogen-cooled structures. The goal is to produce structures with a fatigue life that is one order of magnitude greater than that of the HRE. The selected panel must yield adequate heat transfer with an acceptable pressure drop, and suitable structural properties with reasonable weight and fabrication complexity.

During the initial phase of the contract, studies have been conducted to finalize the configuration design, material selection, and fabrication process. Tensile and fatigue tests were performed to establish basic material properties. Small samples were constructed to substantiate the fabrication process and inspection techniques. Development tests, including burst and creep rupture, were performed to validate structural performance.

The program has produced configuration, design, and materials selections for the application. Panel fatigue tests are required to determine the capability of these selections to meet the goal set for the program. The presentation will show the configuration and materials that were studied and summarize the test data, as well as present preliminary conclusions regarding the potential of the selections.

---

*The work was performed under Contract NAS1-14180 with the NASA Langley Research Center. The Project Manager for NASA is Mr. H. N. Kelly, Thermal Structures Branch, Structures and Dynamics Division.

PROGRAM APPROACH

(Figure 1)

Following concept selection, the performance of different configurations and materials was evaluated at the operating conditions. The program then proceeded along two branches. One was aimed at evaluating the material properties from a structural and environmental point of view. The tests were tensile and low-cycle fatigue. The tensile tests were run on sheet specimens. Low-cycle fatigue testing was done on hollow bar specimens to simulate the sheet properties. Evaluation of fabrication processes considered different configurations and different materials for face sheet, back panel, and the braze filler alloy. Butt-braze tensile tests were run on bars and panel creep-rupture tests were run using the selected configurations and materials. All panels were non-destructively evaluated using holography prior to tests. That was an important part of the program.

PROGRAM APPROACH

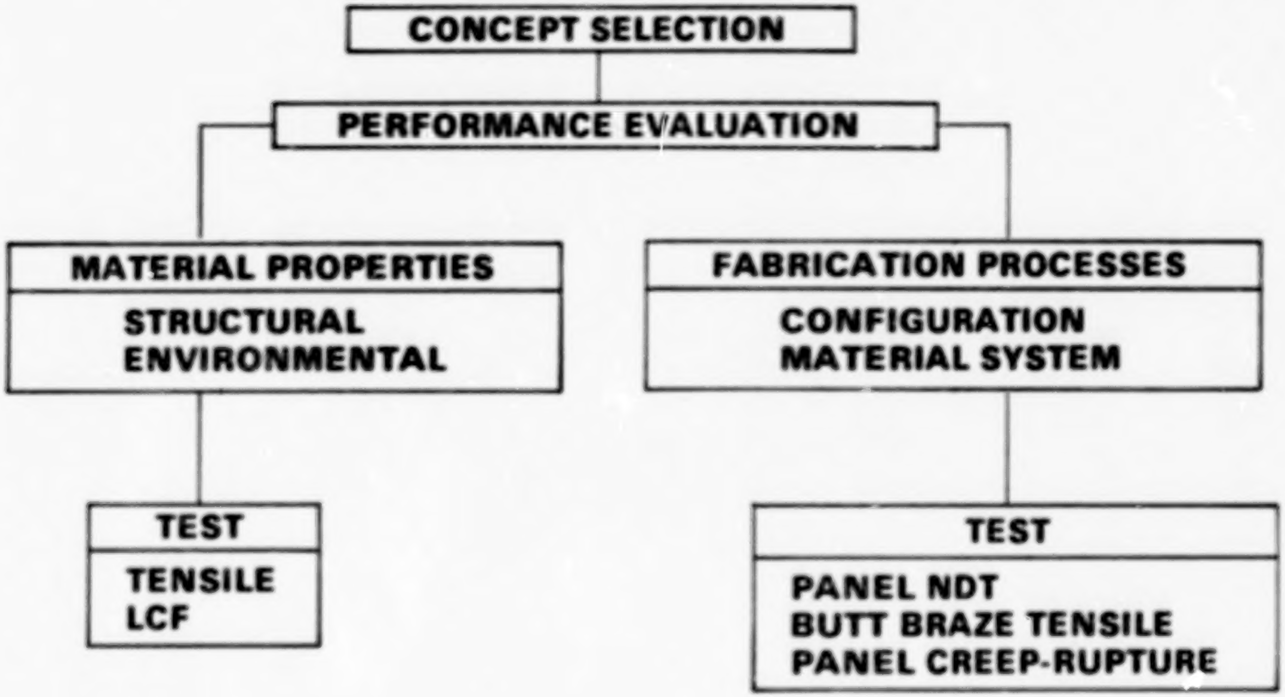

CONCEPT SELECTION

PERFORMANCE EVALUATION

MATERIAL PROPERTIES
- STRUCTURAL
- ENVIRONMENTAL

TEST
- TENSILE
- LCF

FABRICATION PROCESSES
- CONFIGURATION
- MATERIAL SYSTEM

TEST
- PANEL NDT
- BUTT BRAZE TENSILE
- PANEL CREEP-RUPTURE

Figure 1

PROGRAM GOAL

(Figure 2)

The goal is a design with a life of 10,000 cycles and 1,000 hours at Scramjet operating conditions. The delta-T plotted here is the delta-T through the thermal protection system of the structure. Parent metal performance is predicted from published literature properties. The design condition used and the data obtained on the HRE Program are shown, along with an extrapolation to lower delta-T's. The NASA 3-D Scramjet study operates near 200°K delta-T, approximately half the delta-T of the HRE. It has a design goal of 1,000 cycles for 100 hours. The reduction in severity of the operating condition was achieved by aerodynamic design. The improvement in life being sought on this program is based on a change in materials or fabrication techniques rather than a reduction in operating parameters.

PROGRAM GOAL

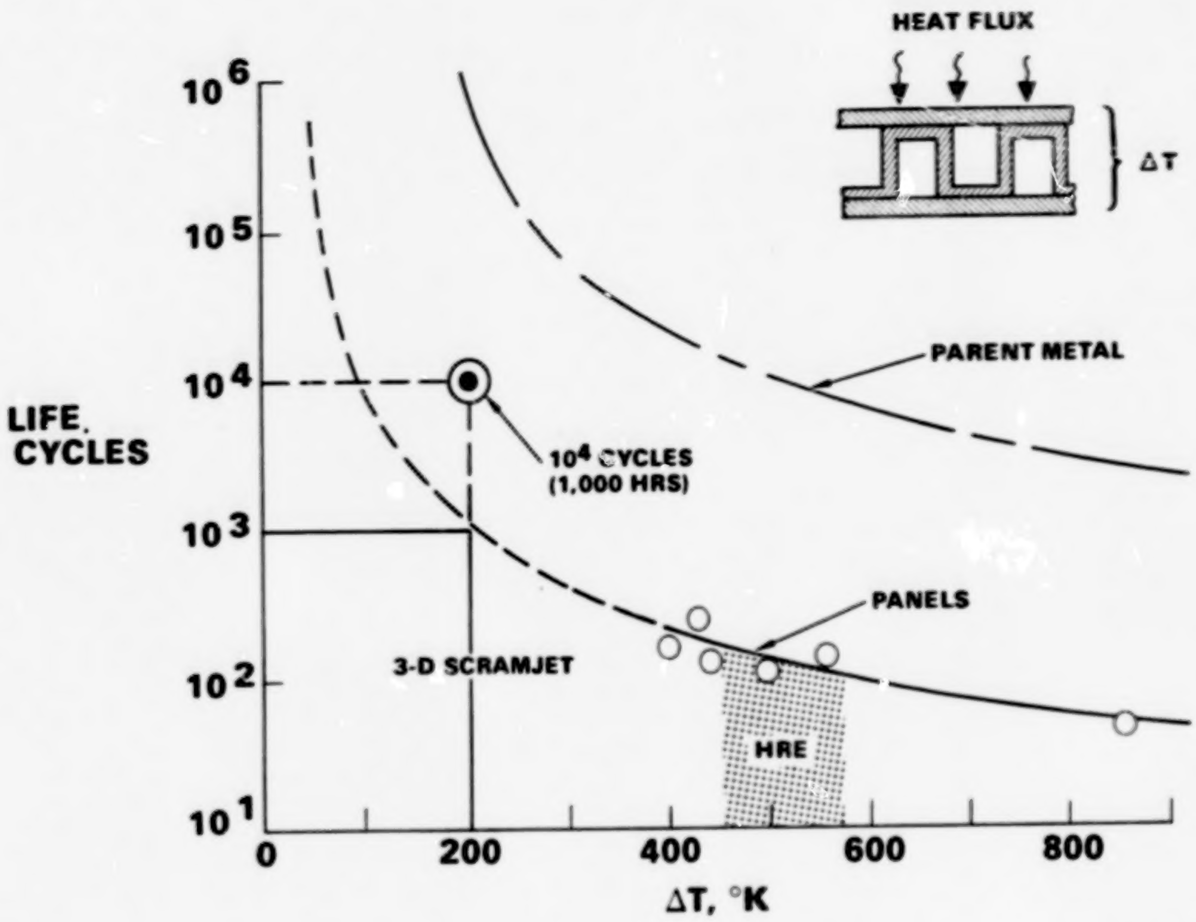

Figure 2

PANEL THERMAL DESIGN

(Figure 3)

The heat fluxes imposed are typical of the maximums and averages encountered in the 3-D Scramjet design. The inlet temperatures are consistent with the use of liquid hydrogen as a fuel; the outlet temperature is consistent with elastic operation in the primary structure of the engine. Outlet pressure is set to be compatible with the required fuel injection pressure; inlet pressure is compatible with high-pressure, liquid hydrogen pumps.

PANEL THERMAL DESIGN

- **PANEL LENGTH** — — — — — — 0.6m (2 FT)
- **HEAT FLUX** - MAXIMUM - 565 X 10^4 W/m^2 (500 BTU/SEC-FT^2)
  AVERAGE - 340 X 10^4 W/m^2 (300 BTU/SEC-FT^2)
- **TEMPERATURE** - INLET — — 55-280°K (100 - 500 °R)
  OUTLET — — 900 °K (1600°R)
- **PRESSURE** - INLET — — 6.9 MPa (1000 PSIA)
  OUTLET — — 5.2 MPa (750 PSIA)

Figure 3

CANDIDATE CONFIGURATIONS

(Figure 4)

These configurations are the ones that were considered as candidates on the program. The plate-fin configuration was used on the Hypersonic Research Engine (HRE). It uses a thin, formed sheet metal fin and has a braze joint next to the hot face sheet. This results in relatively high stress concentrations and in high joint temperatures. Consequently, low-cycle fatigue and creep-rupture life are too limited at the selected operating conditions.

The other configurations shown use machined coolant passages and have their braze joints remote from the face sheet. This is an important feature. They also have a certain amount of flexibility in shaping of the coolant passage. This allows stress concentrations near the hot face sheet to be minimized. On the other hand, the applicable machining processes tend to limit the proportions that can be achieved in terms of passage height and width and of land thickness.

CANDIDATE CONFIGURATIONS

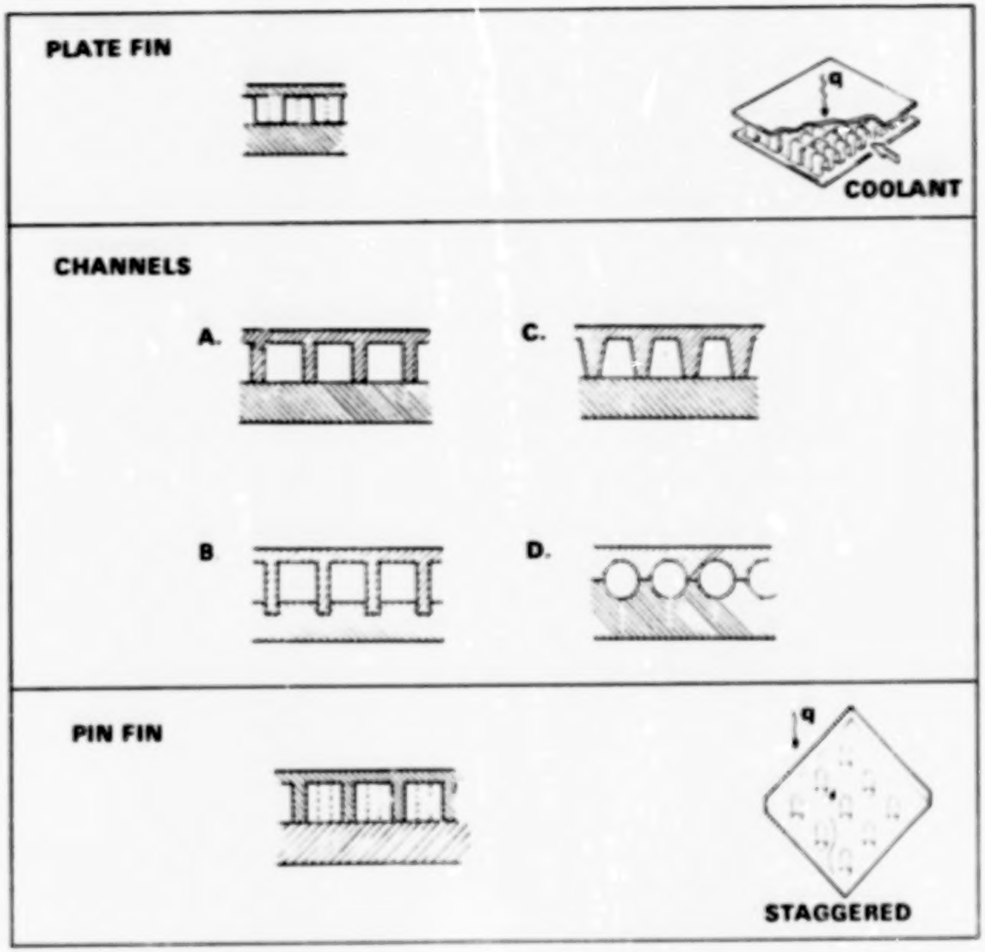
PLATE FIN
q
COOLANT
CHANNELS
A.
B
C.
D.
PIN FIN
q
STAGGERED

Figure 4

LOW CYCLE FATIGUE LIFE--CONFIGURATION EFFECTS

(Figure 5)

This comparison of the candidate configurations is based on published properties. The objective here was to select configuration rather than material. Hastelloy X was used for all configurations. The best of these is the one having a circular passage. It shows 60 percent longer life than any of the other machined configurations and four times longer life than plate-fin. The trapezoidal configuration is nominally a rectangular passage. It was selected as the baseline for the program because of its simplicity. Data obtained with it can be used to predict the performance of the other machined passages. In addition, a staggered pin-fin configuration was selected for evaluation because of its applicability in engine design to localized regions of high flux.

To summarize, the remote (cool) braze joint and the low stress concentrations are desirable features of the machined coolant passages. The two configurations that were selected for evaluation evolved from the Scramjet design studies. The plain channel is the most generally applicable. It has low pressure drop, but it also is limited as to the heat transfer coefficients that are obtainable. The pin-fin is used where high heat transfer coefficients are needed and the higher pressure drop can be tolerated.

LOW CYCLE FATIGUE LIFE
CONFIGURATION EFFECTS

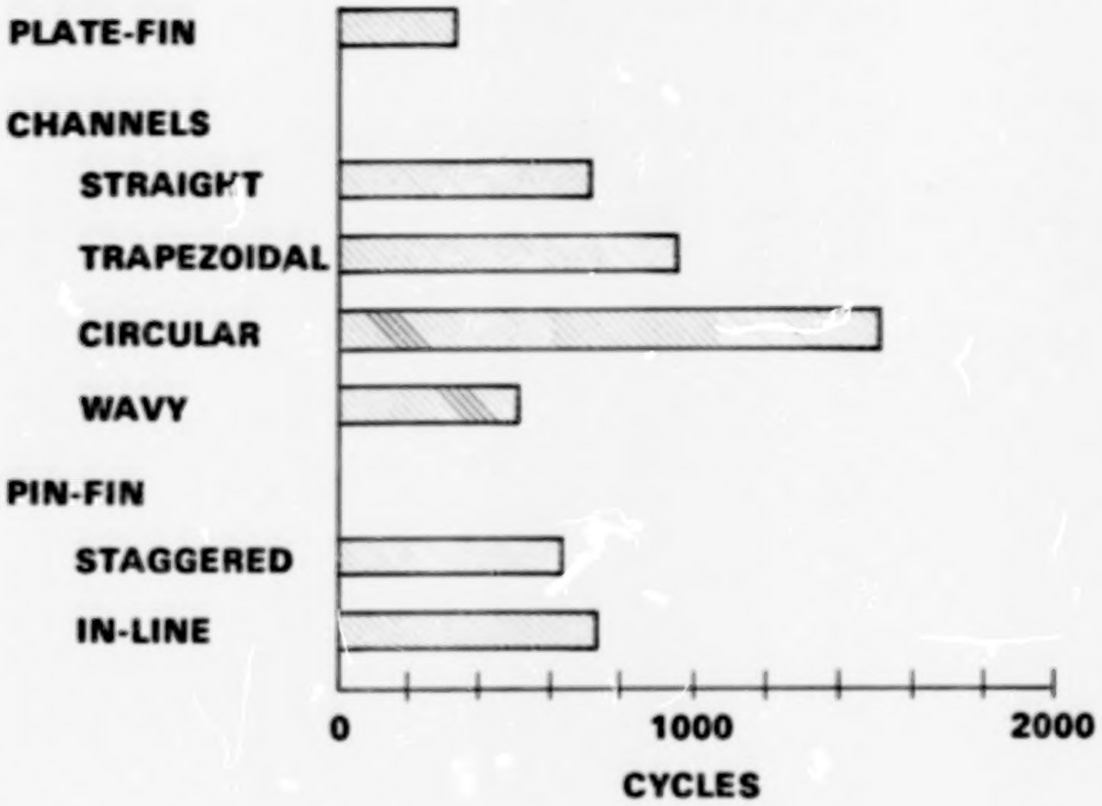

Figure 5

CONTENTS

Part I

PREFACE . . . . iii 1/A5

WELCOME 1 1/A10
R. R. Heldenfels

SESSION I - OVERVIEWS
Chairman: A. J. Henderson

1. HYPERSONIC STRUCTURES: AN AERODYNAMICIST'S PERSPECTIVE (OR ONE MAN'S DREAM IS ANOTHER MAN'S NIGHTMARE) 5 1/B1
J. D. Watts, L. R. Jackson, and J. L. Hunt

2. STRUCTURAL REQUIREMENTS FOR MILITARY HYPERSONIC SYSTEMS (Paper not available for publication)
P. Lane

3. AIRFRAME-INTEGRATED PROPULSION SYSTEM FOR HYPERSONIC CRUISE VEHICLES 39 1/F13
Robert A. Jones and Paul W. Huber

4. RECENT ADVANCES IN CONVECTIVELY COOLED ENGINE AND AIRFRAME STRUCTURES FOR HYPERSONIC FLIGHT 47 1/G7
H. Neale Kelly, Allan R. Wieting, Charles P. Shore, and Robert J. Nowak

SESSION II - ENGINE STRUCTURES
Chairman: H. N. Kelly

5. DESIGN AND ANALYSIS OF A SCRAMJET ENGINE 65 2/A13
O. A. Buchmann

6. THERMOSTRUCTURAL ANALYSIS OF A SCRAMJET FUEL-INJECTION STRUT 119 3/B11
Allan R. Wieting and Earl A. Thornton

7. ADVANCED FABRICATION TECHNIQUES FOR COOLED ENGINE STRUCTURES 145 3/F7
O. A. Buchmann

8. HYDROGEN EMBRITTLEMENT AND ITS CONTROL IN HYDROGEN-FUELED ENGINE SYSTEMS 195 4/F11
W. T. Chandler

9. CARBON-CARBON COMPOSITE APPLICATION FOR INTEGRAL ROCKET RAMJET COMBUSTORS (Paper not available for publication)
H. A. Holman

SESSION III - COOLED AIRFRAME STRUCTURES
Chairman: C. P. Shore

10. DESIGN AND FABRICATION OF A SKIN STRINGER DISCRETE TUBE ACTIVELY COOLED STRUCTURAL PANEL 253 6/A5
Frank M. Anthony

11. DESIGN AND ANALYSIS OF A PLATE-FIN SANDWICH ACTIVELY COOLED STRUCTURAL PANEL 319 7/C13
L. M. Smith

12. FLUXLESS BRAZING AND HEAT TREATMENT OF A PLATE-FIN SANDWICH ACTIVELY COOLED PANEL 375 8/E1
Charles S. Beuyukian

13. DESIGN AND FABRICATION OF A RADIATIVE ACTIVELY COOLED HONEYCOMB SANDWICH PANEL 449 10/A13
Leland C. Koch

14. RADIATIVE, ACTIVELY COOLED PANEL TESTS RESULTS 493 11/A5
Charles P. Shore, Robert J. Nowak, and Ellsworth L. Sharpe

LOW CYCLE FATIGUE LIFE--MATERIAL EFFECTS

(Figure 6)

Nickel 201 and Inconel 617 were selected for the program, based on this comparison. Published properties were used, with emphasis on sheet properties where available. The effects of aging, which have been determined to be important for many of the nickel-base superalloys, were not included because they were not generally available. Inconel 617 is limited by low-cycle fatigue; its creep-rupture properties are excellent and are not expected to pose a constraint. Nickel 201 is creep-rupture and oxidation limited.

Narloy-Z, although it looks excellent from the standpoint of low-cycle fatigue, overages during extended exposure (time greater than 100 hours) above 920°K (1200°F). The properties then revert to those of annealed material.

TZM was rejected because of the lack of an oxidation-protection coating and because of its relatively high ductile-to-brittle transition temperature (in the range of 200°K).

LOW CYCLE FATIGUE LIFE
MATERIAL EFFECTS

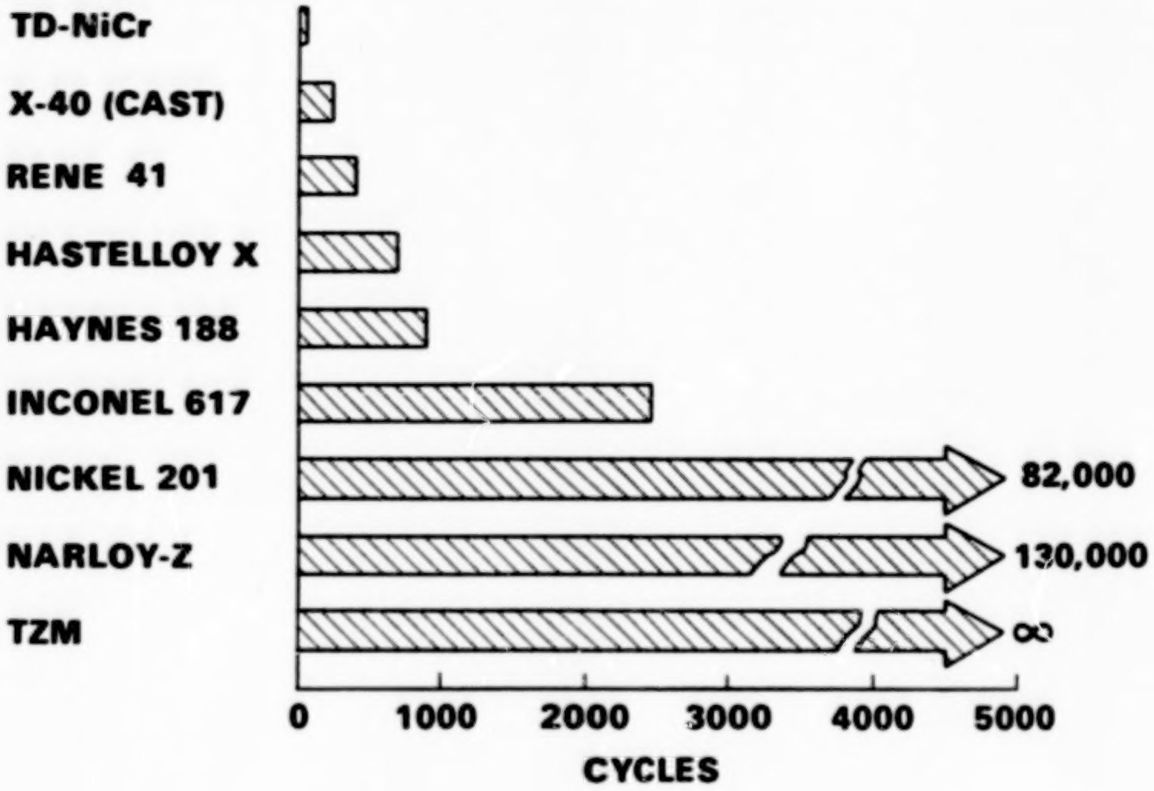

Figure 6

FABRICATION DEVELOPMENT

(Figure 7)

Given a configuration and a material, selection of the method of fabrication becomes the next consideration. The Scramjet engine is 2.4 m (8 ft) long and has large, multiplanar surfaces. Any fabrication process has to lend itself to that kind of configuration. When various processes are considered, photochemical machining (PCM) appears most applicable and was selected.

At program start, limited data was available on PCM of Nickel 201 in the required configurations. There was no data on PCM of Inconel 617 and, again, only limited data for Hastelloy X. Hastelloy X was tested to establish general applicability. It is the material about which most is known at the program conditions. For brazing, there is a good deal of data on Hastelloy X that can be used as a reference. For Inconel 617, no data was available, while for Nickel 201, there was a limited amount of data applicable to the selected configurations.

FABRICATION DEVELOPMENT

- PHOTOCHEMICAL MACHINING
  - NICKEL 201
  - INCONEL 617
  - HASTELLOY X
- BRAZING
  - NICKEL 201
  - INCONEL 617
  - HASTELLOY X

Figure 7

PCM FACE SHEETS--CREEP-RUPTURE PANELS

(Figure 8)

These face sheets were made to evaluate the photochemical milling and for use in creep-rupture test panels. The plain channels are approximately 0.5 mm (0.02 in.) deep, the lands are 0.5 mm (0.02 in.) wide with grooves that are 1.5 mm (0.06 in.) wide. Pin-fin panels have a pin height of 0.65 to 1.55 mm (0.025 to 0.06 in.) and 0.75 mm (0.03 in.) diameter pins on 2.0 mm (0.08 in.) centers. The spaced channel specimen eliminated a channel and replaced it with solid material. This was done to provide a large braze surface area and to be able to apply high pressures, as a test of the face sheet in creep-rupture.

PCM FACE SHEETS
CREEP-RUPTURE PANELS

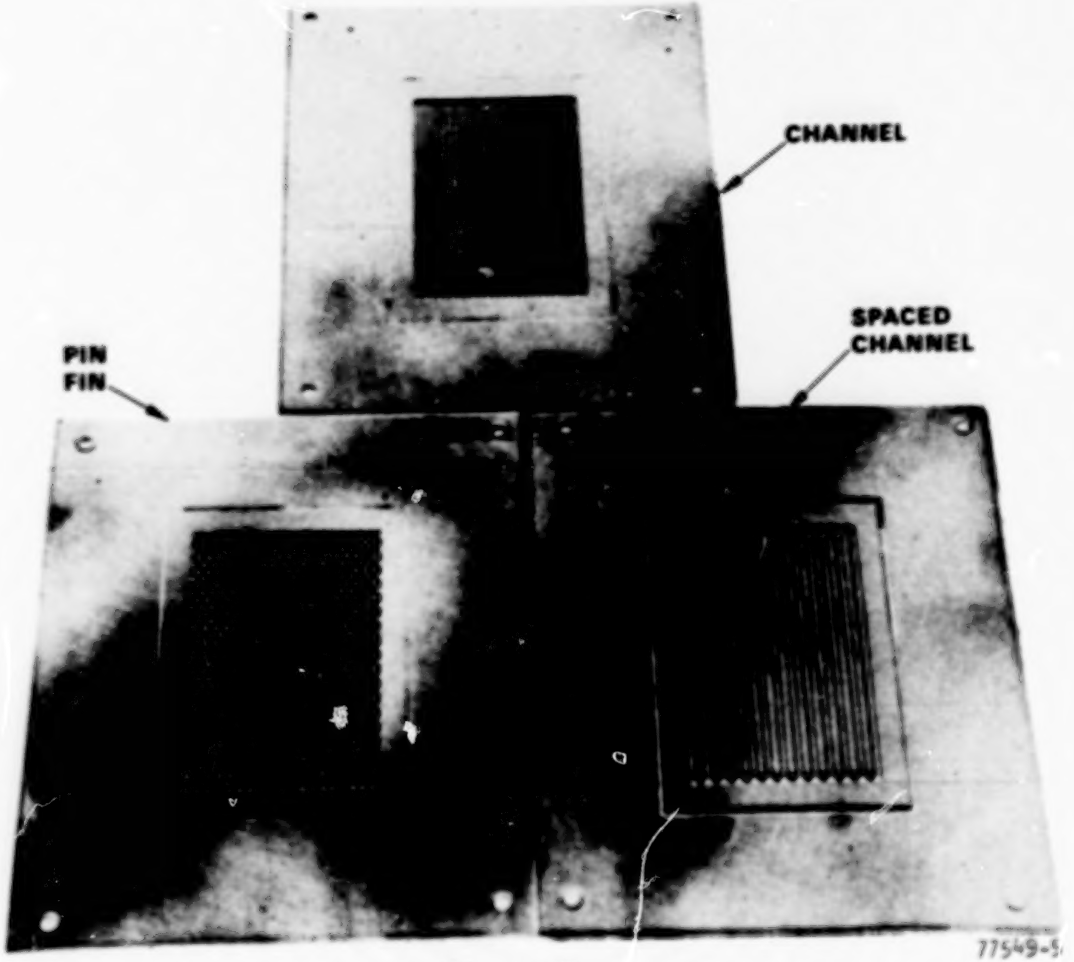
CHANNEL
SPACED CHANNEL
PIN FIN
77549-5

Figure 8

PANEL HOLOGRAPHY

(Figure 9)

As mentioned previously, non-destructive testing was important on this program for establishing the quality of the test panels. It also would certainly be important on an engine development program. This shows Inconel 617 pin-fin and channel specimens tested at 13.8 MPa (2,000 psig). At 13.8 MPa, the quality of the braze is such that the channel looks like a solid piece of material. There is no print-through. In the case of the pin-fins, a slight print-through appears at 13.8 MPa. The Nickel 201 panels show print-through in all cases. For both materials, it was possible to detect a void of a single pin.

PANEL HOLOGRAPHY

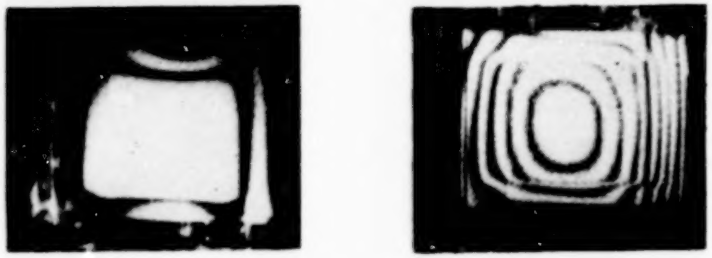

INCONEL 617

CHANNEL
13.8 MPa

PIN-FIN
13.8 MPa

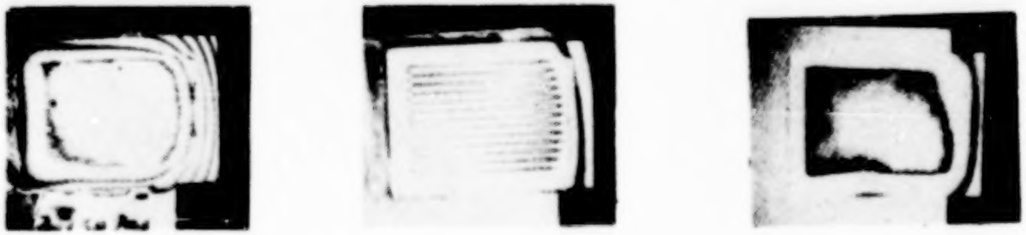

NICKEL 201

CHANNEL
13.8 MPa

SPACED
CHANNEL
13.8 MPa

PIN-FIN
2.8 MPa

Figure 9

164

CREEP-RUPTURE LIFE--NICKEL 201 PANELS

(Figure 10)

In the case of the Nickel 201 panels, the concern is more with the face sheet than with the braze joint. The braze joint in this case is operating at 920 to 950°K (1200 to 1250°F), while the face sheet is operating at 1030°K (1400°F), a high temperature for pure nickel. The required creep-rupture life is shown for three cases with relation to the published properties. The test life that was obtained for the different panels is also shown. In each case, the tests show the capability for meeting the design requirements.

CREEP-RUPTURE LIFE
NICKEL 201 PANELS

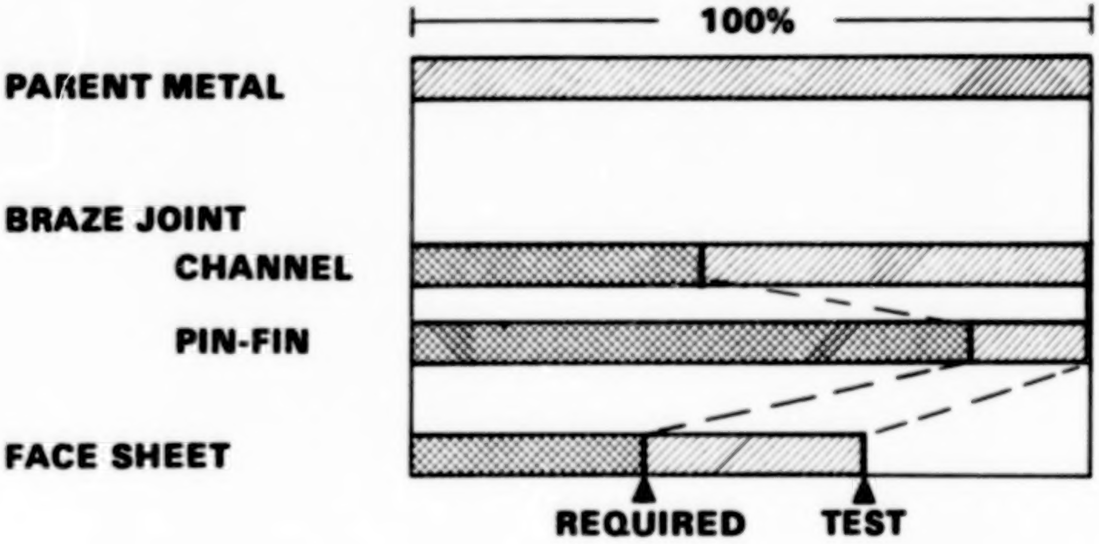

Figure 10

166

PANEL CREEP-RUPTURE--NICKEL 201

(Figure 11)

The braze joint looks quite sound using Palniro 1 as the filler alloy. The breaks are ductile and are through the pins and the lands of the channels. In each case, the high stress occurs not at the joint, but above the joint. A finite element analysis of the configuration confirmed this.

PANEL CREEP-RUPTURE
NICKEL 201

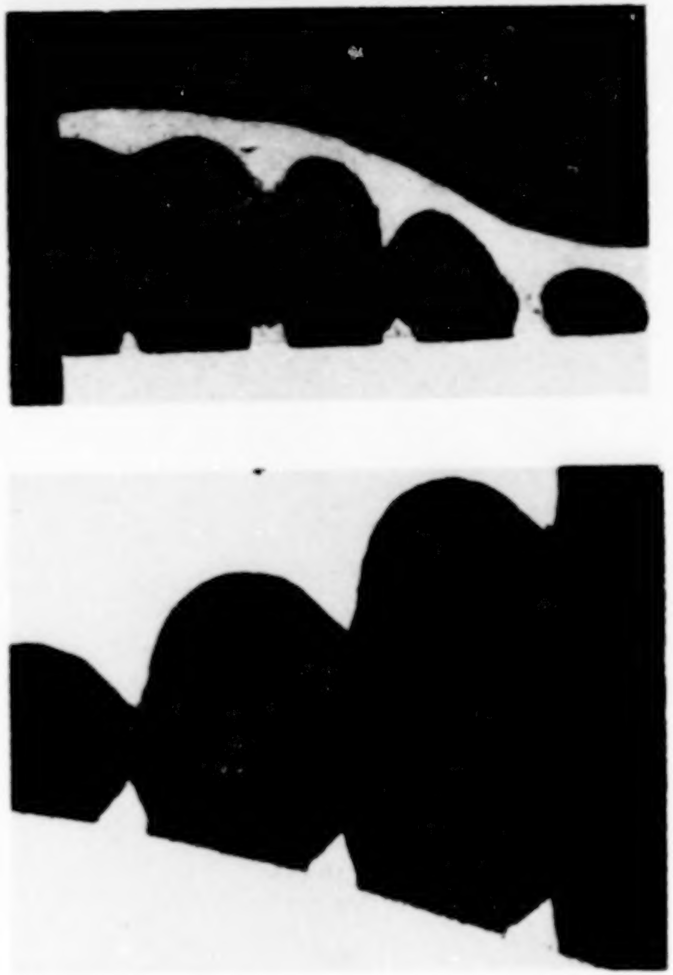

PIN FIN

CHANNEL

Figure 11

168

CREEP-RUPTURE LIFE--INCONEL 617 PANELS

(Figure 12)

These panels were tested at 920°K (1200°F) to evaluate the strength of the braze joint rather than of the face sheet. The configuration is not creep-rupture limited in the parent metal.

With the Palniro 1 joint, rupture was considered to be premature, even though the test life exceeds the required life. Metallography showed that the brazing was erratic and somewhat unpredictable. As a result, alternative braze materials and techniques were investigated. The method selected used boronized nickel-chrome in an isothermal solidification process. The test results for this process were equivalent to 100 percent of parent metal. Test times ranged to over 2000 hours with these joints.

CREEP-RUPTURE LIFE
INCONEL 617 PANELS

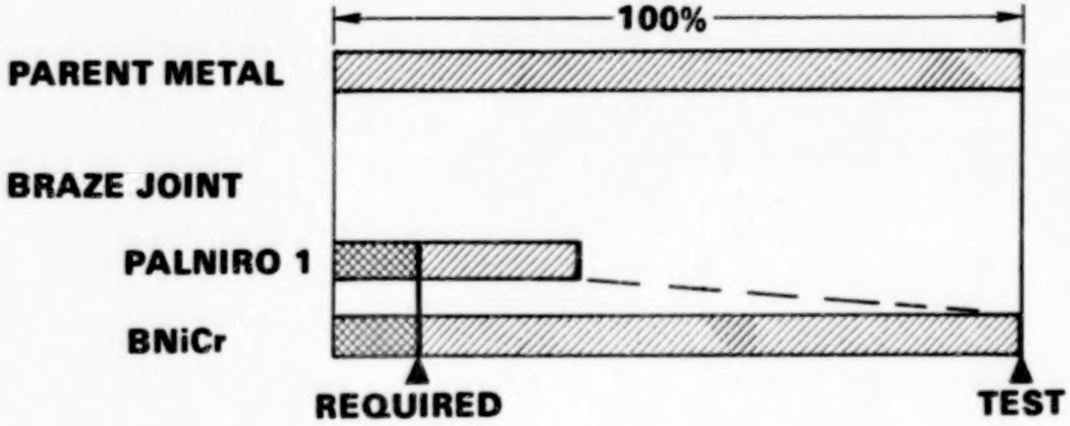

Figure 12

BRAZE ALLOY SEGREGATION--INCONEL 617

(Figure 13)

A joint in Inconel 617 made with Palniro 1 braze alloy is shown in the upper photograph. This cross-section has been metallographically polished and etched to show the light-colored, gold-rich phase as well as the darker reaction product. The reaction product is actually a mixture of gold-rich and nickel-rich phases. The separated joint shown in the lower photograph shows that rupture of this joint occurred through the gold-rich phase, which is expected to be considerably softer than the reaction product. Experiments with Palniro 1 using various plating techniques, surface preparation techniques, and brazing cycles produced similar structures. Such discrete phases of relatively large size can generally be expected to result in low strength and relatively short life. As a result, a number of alternate braze alloys for Inconel 617 were investigated in an attempt to obtain a braze joint that would be more uniform in structure. The alloys and processes that were investigated included: (1) NB30, a nickel-boron braze alloy in powder form, brazed conventionally; (2) boron-nickel-chrome foil brazed by isothermal solidification; and (3) other gold-base braze alloys (Palniro 7, Palniro RE, and Nioro).

BRAZE ALLOY SEGREGATION
INCONEL 617

GOLD-RICH PHASE
REACTION PRODUCT

CONTINUOUS JOINT

SEPARATED JOINT

Figure 13

INCONEL 617--BRAZING ALLOY EFFECTS

(Figure 14)

The boron-nickel-chrome brazed sample prepared by isothermal solidification is shown in cross-section in the upper left hand corner. It shows a number of favorable characteristics. (1) There is only moderate grain growth in the parent metal away from the braze joint and grains have grown across the joint. This indicates that the strength, ductility and elastic properties of the joint can approach those of the parent metal. (2) There is not a discrete layer of a soft braze alloy of a brittle phase. (3) There are essentially no voids visible in this picture, and likewise, there is no segregation of phases present within the braze joint.

In the case of the gold-base braze alloys that were investigated, the appearance of all three was quite similar. There was good filleting, but there were also voids.

In joints made with NB30 alloy, there was a notable lack of filleting, and indications of poor flow, of lumpiness in the alloy, and voids. The voids and lumpiness are shown more clearly in the right hand lower photograph. There is no segregation, however; rather, a single phase was observed in the braze joint.

INCONEL 617
BRAZING ALLOY EFFECTS

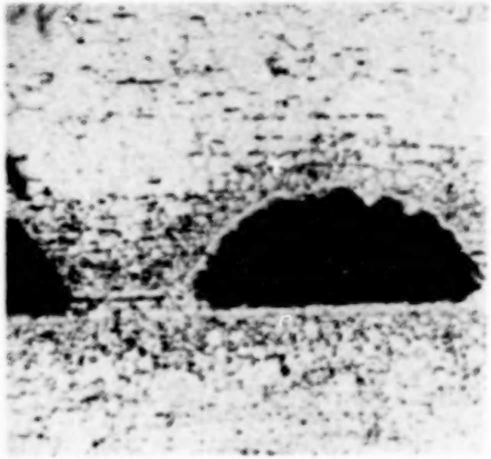

BNI Cr

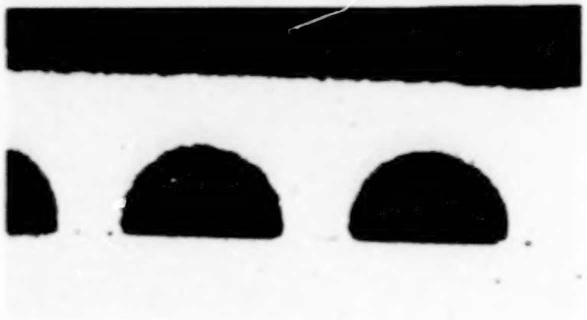

GOLD-BASE

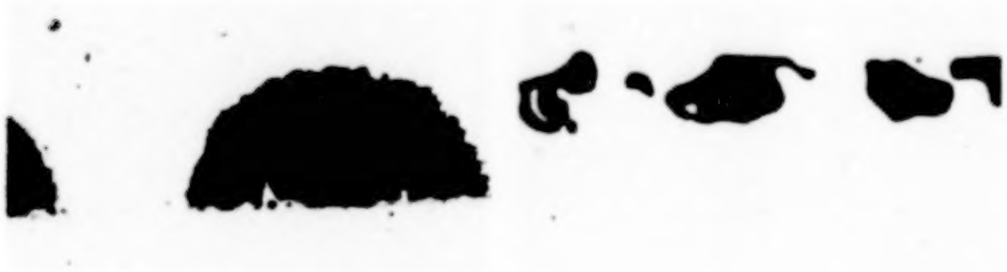

NICKEL BORON (NB30)

Figure 14

BNiCr BRAZE ALLOY--ISOTHERMAL SOLIDIFICATION TIME EFFECT

(Figure 15)

These two photographs show the effect of increasing time at the 1420°K (2100°F) brazing temperature with the boron-nickel-chrome braze alloy. For a one-hour brazing cycle, there is a ten-point variation in hardness between the adjacent parent metal and the center of the joint. This variation indicates incomplete boron diffusion. There is an excess amount of boron immediately next to the joint and a hardness variation of this magnitude would be expected to result in different mechanical properties in the two regions. This would localize any plastic flow and probably result in low strength. By extending the time to ten hours, the hardness variation has been reduced to a mere three points. This indicates that the boron has diffused much more completly into the parent metal. Much more uniform mechanical properties at the joint can be expected at this condition.

BNiCr BRAZE ALLOY
ISOTHERMAL SOLIDIFICATION
TIME EFFECT

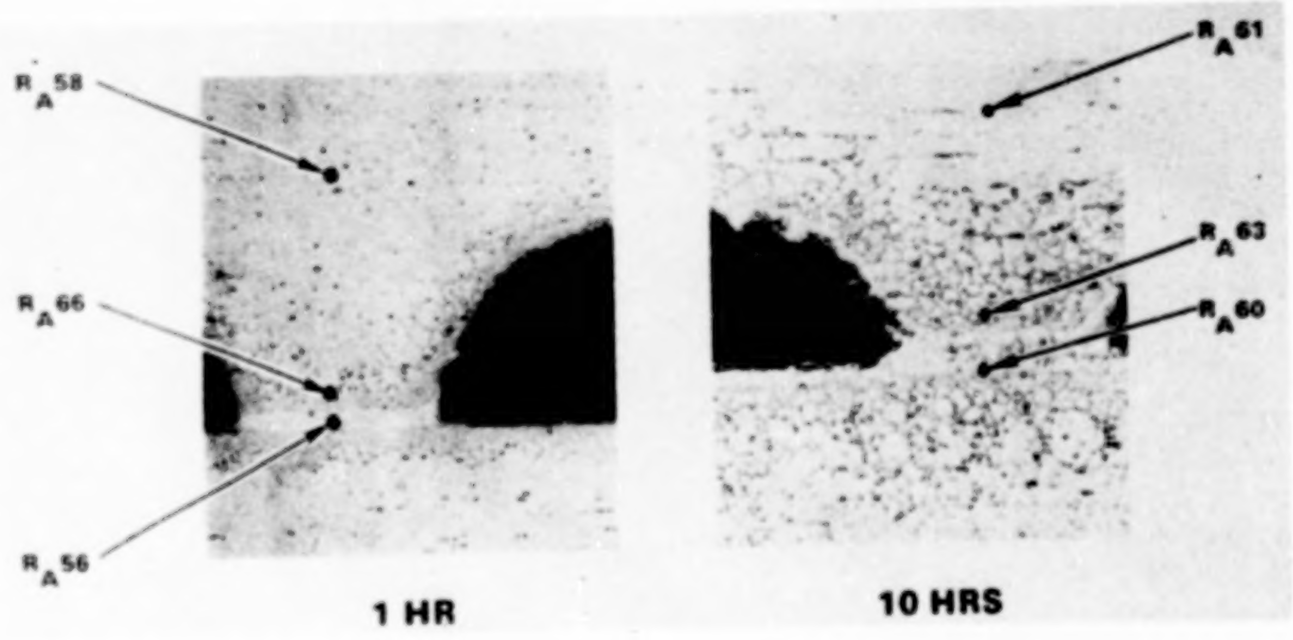

$R_A 58$
$R_A 66$
$R_A 56$
$R_A 61$
$R_A 63$
$R_A 60$
1 HR
10 HRS

Figure 15

MATERIAL TEST SPECIMENS

(Figure 16)

Photochemically machined (PCM) Nickel 201 and Inconel 617 specimens were made to determine the tensile properties of sheet material having the same surface condition as a PCM panel would have. These specimens were made in two configurations as shown in the upper picture. The lower specimens were used for room temperature tensile tests with friction grips. The upper specimens were used for elevated temperature tensile tests, where pin-loading was used.

The lower picture on the left shows the standard Inconel 617 tensile test bar. This is a solid bar that was used to determine Inconel 617 properties at elevated temperature and room temperature.

To more closely simulate the behavior of sheet material, hollow specimens, such as that shown on the lower right, were made. This tubular specimen simulated the sheet material in that the tube wall thickness was of the same order as the sheet material that would be used. An elliptical hole was machined in the center of the gage length as a strain concentrator, to further simulate the effect of the geometry of the PCM panel.

MATERIAL TEST SPECIMENS

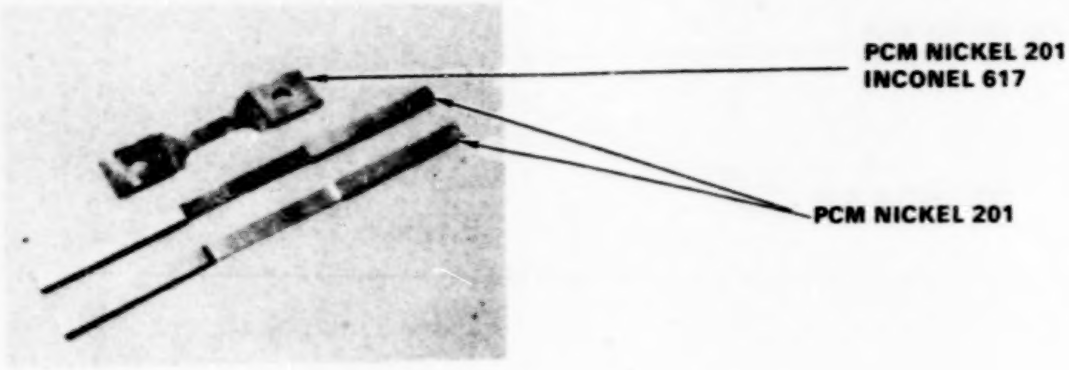
PCM NICKEL 201
INCONEL 617
PCM NICKEL 201

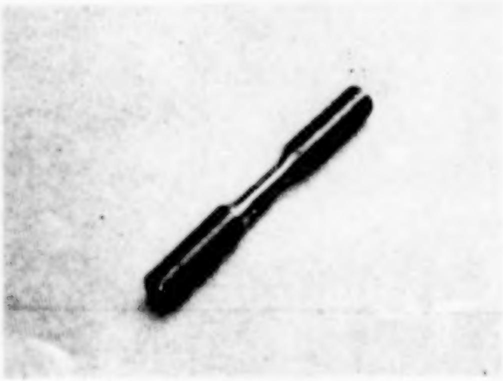

INCONEL 617
TENSILE BAR

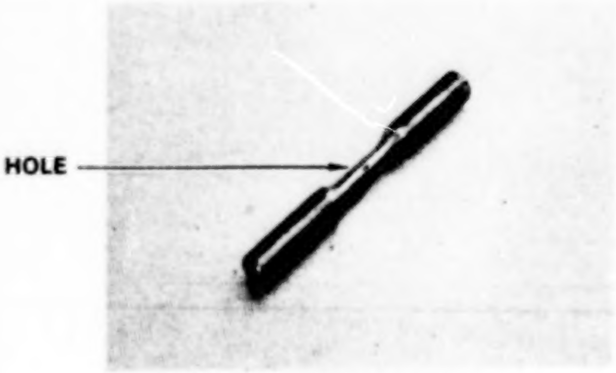

INCONEL 617
FATIGUE BAR

Figure 16

MATERIAL TESTS--INCONEL 617

(Figure 17)

Tests were conducted at room temperature, 900°K (1150°F) and 1150°K (1600°F), on sheet and bar tensile specimens and on bar fatigue specimens. Specimens were tested in the as-received condition, solution-treated after receipt, braze-coated and air aged for 1000 hours, braze-cycled and air aged, and only air aged. The tests of the braze-coated and air aged samples were expected to have the lowest properties and were, therefore, emphasized in the high temperature tests.

MATERIAL TESTS
NICKEL 201

	°K		
	290	1030	1060
AS-RECEIVED SHEET	X		
ANNEALED SHEET	X		X
PCM + BRAZE-COATED + AIR AGED	X		X
PCM + BRAZE-CYCLED	X		X
PCM + BRAZE-CYCLED + AIR AGED	X		X
PCM + AIR AGED	X	X	
PCM + BRAZE-CYCLED + ARGON AGED	X	X	
PCM + ARGON AGED	X	X	

Figure 17

INCONEL 617 TENSILE TESTS--LCF PARAMETER (1150°K)

(Figure 18)

The low-cycle fatigue (LCF) parameter is the yield strength multiplied by the reduction of area. It provides an indication of the LCF life of a material. The LCF parameter for solution-treated sheet was taken to be 100 percent as the baseline. Braze coating and aging reduced the LCF parameter to approximately 25 percent of the value for solution-treated sheet material value. Solid bar samples experienced a reduction of about 50 percent of the original value; i.e., they compared very well with the braze-coated and aged sheet material. The butt-brazed joints made with nickel-chrome-boron foil showed a relatively high LCF parameter though not equal to that for the parent material. Thus, some braze cycle degradation in the material did occur.

INCONEL 6[illegible] TENSILE TESTS
LCF PARAMETER (1150 °K)

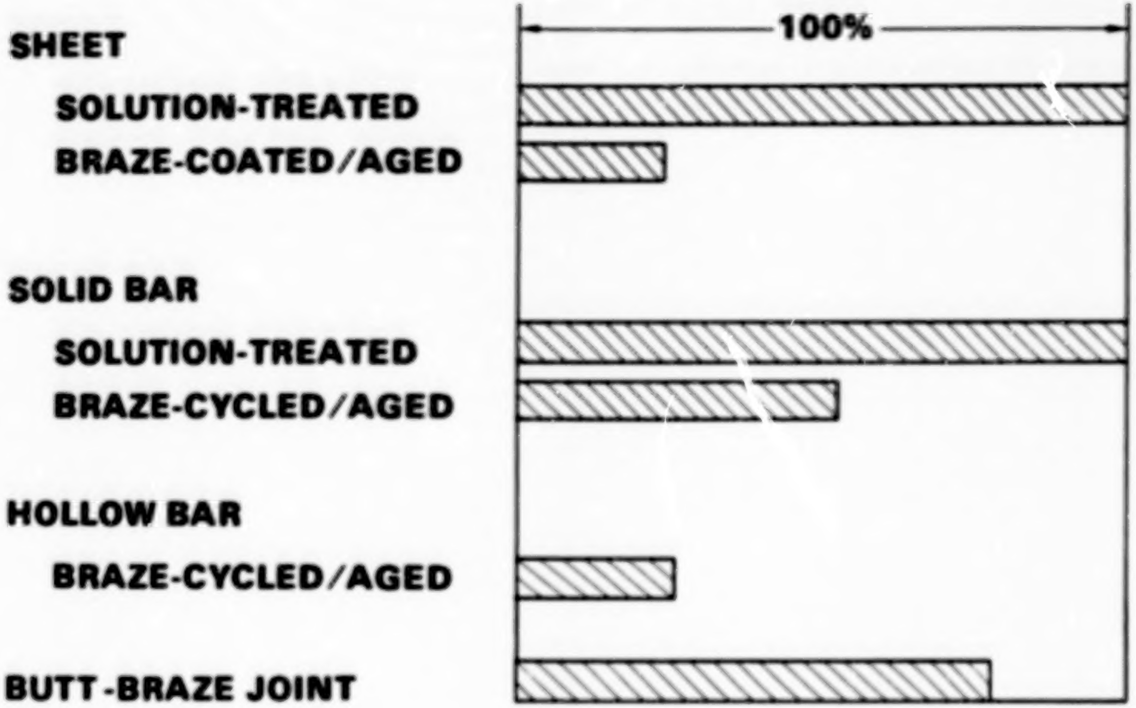

Figure 18

182

INCONEL 617 BUTT-BRAZE TENSILE BARS

(Figure 19)

Bars of Inconel 617 were machined with flat ends. These were then brazed in the center of the gage section. From these brazed bars (shown at the top) tensile specimens were machined. The third specimen from the top was tested at 950°K (1250°F). It fractured at the braze joint with an elongation of 36 percent. A test at 1150°K (1600°F) resulted in an elongation of 52 percent. This specimen fractured in the parent metal, remote from the braze joint, indicating that the braze joint was stronger than the parent metal at this temperature.

INCONEL 617
BUTT-BRAZE TENSILE BARS

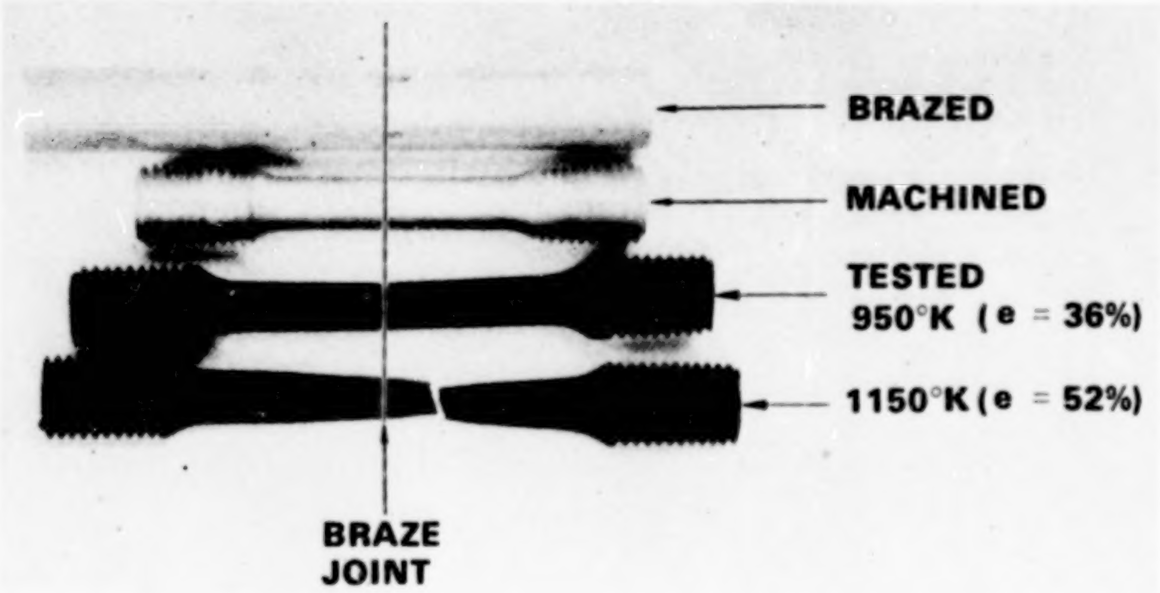
BRAZED
MACHINED
TESTED
950°K (e = 36%)
1150°K (e = 52%)
BRAZE
JOINT

Figure 19

11

184

MATERIAL TESTS--NICKEL 201

(Figure 20)

Nickel 201 tests were conducted on as-received and annealed sheet material; on photochemically machined sheet; and on sheet material exposed to braze coating, braze cycling, air aging, and argon aging. Tests were run at room temperature as well as elevated temperatures. The highest temperature used for Nickel 201 was 1060°K (1450°F). This reflects the expected surface temperature in the Nickel 201 panel and is lower than for Inconel 617 due to its higher conductivity compared to Inconel 617. Tests at the elevated temperature are particularly significant for Nickel 201 because of oxidation effects.

MATERIAL TESTS
NICKEL 201

	°K		
	290	1030	1060
AS-RECEIVED SHEET	X		
ANNEALED SHEET	X		X
PCM + BRAZE-COATED + AIR AGED	X		X
PCM + BRAZE-CYCLED	X		X
PCM + BRAZE-CYCLED + AIR AGED	X		X
PCM + AIR AGED	X	X	
PCM + BRAZE-CYCLED + ARGON AGED	X	X	
PCM + ARGON AGED	X	X	

Figure 20

NICKEL 201 TENSILE TESTS--LCF PARAMETER (1030°K)

(Figure 21)

Published data on Nickel 201 was used to calculate the LCF parameter at 1030°K (1400°F), which was taken to be 100 percent. The results of the tests are shown as a percentage of that computed value. Annealed sheet material tested at AiResearch showed a yield strength and reduction of area that resulted in approximately one-third of the value computed from published data. Air aging for 1,000 hours at 1060°K (1450°F) reduced that initial value to approximately one half. Braze cycling and aging had about the same effect. Argon aging for 1,000 hours at 1060°K (1450°F) gave a somewhat lower LCF parameter than that obtained from air aging of specimens. Braze-cycled samples aged in argon also showed a lower LCF parameter.

NICKEL 201 TENSILE TESTS
LCF PARAMETER (1030 °K)

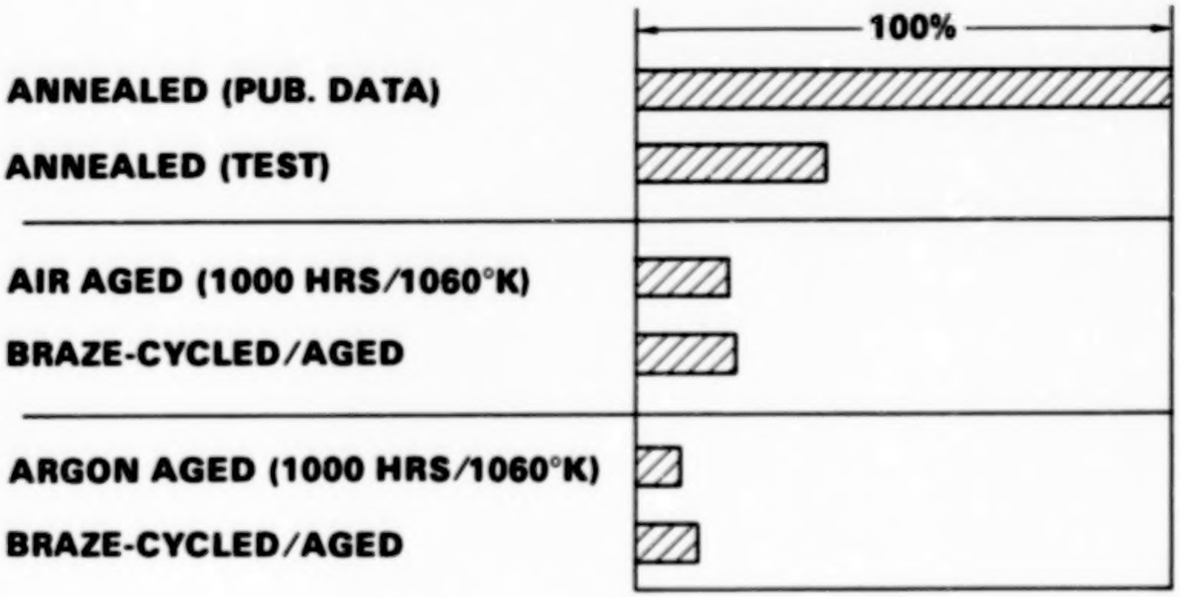

Figure 21

188

OXIDATION OF NICKEL 201

(Figure 22)

On the left is a braze-cycled specimen: it was not braze coated or exposed to oxidation, but only vacuum brazed-cycled. The original surface roughness is due to etching. During exposure, the oxide grows in both directions, into the material and outward. This reflects an increase in mass due to the formation of nickel oxide. After aging for 1,000 hours at 1060°K (1450°F), specimens had approximately 0.05 mm (0.002 in.) oxide coating, which is significant compared with the design material thicknesses.

OXIDATION OF NICKEL 201

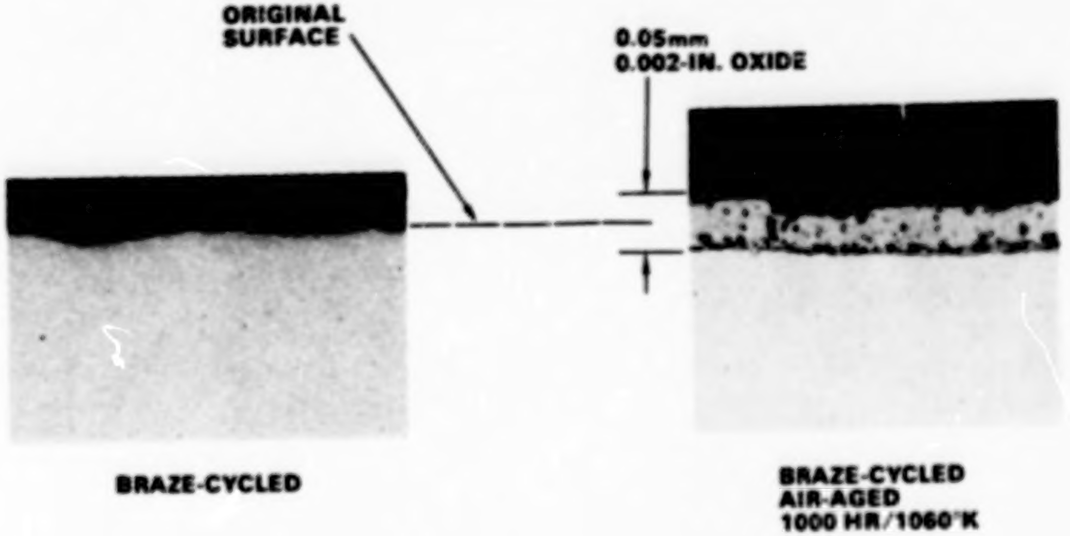
ORIGINAL SURFACE
0.05mm
0.002-IN. OXIDE
BRAZE-CYCLED
BRAZE-CYCLED
AIR-AGED
1000 HR/1060°K

Figure 22

PREDICTED LCF LIFE

(Figure 23)

Given the test data, an assessment of Inconel 617 performance is of interest, i.e., the capability of the Inconel 617 to meet the desired life requirements and its capability relative to Hastelloy X. As noted previously, Nickel 201 is predicted to meet the specified cycle life.

This chart compares the predicted lives of Inconel 617 and Hastelloy X based on published data. Then, using the results of tensile and low cycle fatigue tests, the performance of Inconel 617 and Hastelloy X is again shown. There is a significant reduction in Inconel 617 life predicted under actual operating conditions based on sheet metal properties and performance. This performance, however, still appears superior to that predicted for Hastelloy X. The Hastelloy X predictions, it should be noted, are extrapolations. No data was available for Hastelloy X aged in a manner comparable to what was done with Inconel 617.

Based on these predictions, therefore, Inconel 617 remains the choice with respect to Hastelloy X. The actual performance of Inconel 617 under realistic plastic loading must be experimentally explored. Until that data becomes available, final conclusions cannot be drawn.

PREDICTED LCF LIFE

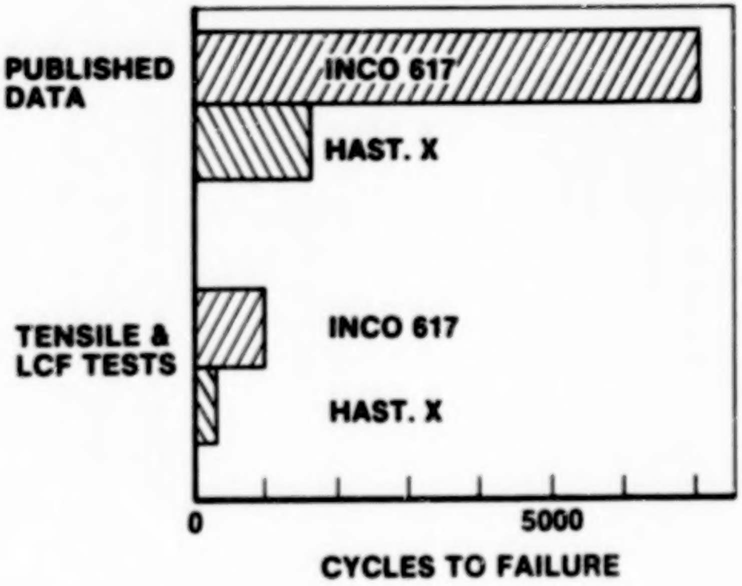

Figure 23

SUMMARY

(Figure 24)

The program has identified an improved design for regeneratively cooled engine structures. This design uses photochemically machined (PCM) coolant passages. It permits the braze joint to be placed in a relatively cool area, remote from the critical hot face sheet. The geometry of the passages at the face sheet also minimizes stress concentration and, therefore, enhances the low-cycle fatigue performance.

The two most promising alloys identified for this application are Inconel 617 and Nickel 201. Inconel 617 was selected because it has excellent creep-rupture properties, while Nickel 201 was selected because of its predicted good performance under low-cycle fatigue loading. The actual capability of both alloys needs to be verified in actual low-cycle fatigue tests using panels before final conclusions can be drawn as to the ultimate capabilities of these alloys.

The fabrication of the PCM coolant passages in both Inconel 617 and Nickel 201 was successfully developed. During fabrication of Inconel 617, undesirable characteristics were observed in the braze joints. A development program to resolve this condition was undertaken and led to definition of an isothermal solidification process for joining Inconel 617 panels. This process produced joints which approach parent metal strength and homogeneity.

SUMMARY

- IMPROVED DESIGN IDENTIFIED
  - PCM COOLANT PASSAGES
  - INCO 617 AND Ni-201
  - ISOTHERMAL SOLIDIFICATION

- FURTHER WORK
  - LCF TESTS
  - H2 EMBRITTLEMENT TESTS
  - ALTERNATE CONFIGURATIONS
  - FABRICATION TECHNIQUE SCALING

Figure 24

194

BLANK PAGE

HYDROGEN EMBRITTLEMENT AND ITS CONTROL IN HYDROGEN-FUELED ENGINE SYSTEMS*

W. T. Chandler
Rockwell International/Rocketdyne Division

INTRODUCTION

It has been found that hydrogen environments, particularly high-pressure hydrogen environments, seriously degrade the mechanical properties of many metals, including several of those considered for use in advanced propulsion systems (ref. 1). Thus, the design, fabrication, and operation of such systems require a thorough understanding and consideration of all aspects of hydrogen embrittlement.

---

*The work performed at Rocketdyne reported on herein was sponsored by the National Aeronautics and Space Administration, Marshall Space Flight Center, Alabama, under Contract NAS8-27980 (SSME Program) and other contracts.

SSME PROPELLANT FLOW SCHEMATIC

(Figure 1)

An example of an advanced, hydrogen-fueled engine is the Space Shuttle Main Engine (SSME), the rocket engine that will be used for the propulsion of the Space Shuttle vehicle. These engines, currently under construction at Rocketdyne Division/Rockwell International, are high-performance rocket engines that use oxygen and hydrogen propellants, and the hydrogen pressures in the SSME are higher than encountered in previous production engines. As shown in the flow schematic in the figure, liquid hydrogen is pumped first through a low-pressure turbopump and then a high-pressure turbopump to a pressure above 41.4 MN/m^2 (6000 psi). The high-pressure hydrogen is used to cool various structures such as the rocket nozzle and the hot-gas manifold and to drive the low-pressure pump turbine and, when reacted with oxygen, the high-pressure pump turbine before it is further reacted with oxygen and exhausted out the rocket nozzle to provide the thrust. Thus, in the SSME, metals are in contact with hydrogen at pressures from 0.21 MN/m^2 (30 psi) to over 41.4 MN/m^2 (6000 psi) and at temperatures from 20 K (-423 F) to over 922 K (1200 F).

In this paper, the nature of hydrogen embrittlement by high-pressure gaseous hydrogen will be described and methods of designing the SSME gaseous hydrogen systems, including techniques of hydrogen embrittlement prevention, will be discussed. Other than the possible effects of the cryogenic temperature, a liquid hydrogen environment does not have a deleterious effect on the properties of metals. Thus, the paper will be limited to discussing the effects of gaseous hydrogen environments. Extensive investigations of the effects of gaseous hydrogen environments on metals have been conducted at Rocketdyne under the SSME program and other NASA programs, all monitored by Marshall Space Flight Center. Results from these programs will be presented.

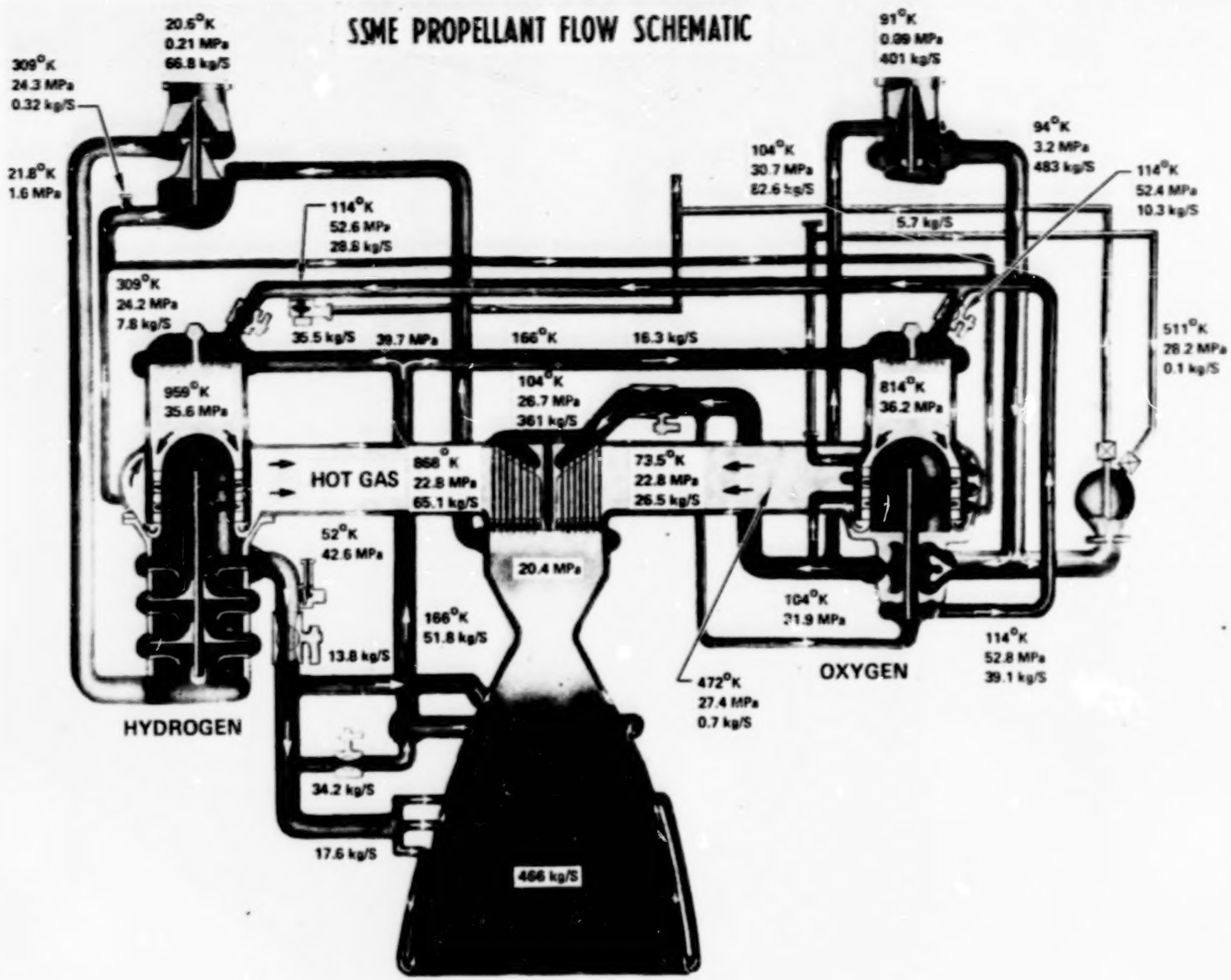
SSME PROPELLANT FLOW SCHEMATIC
20.6°K
0.21 MPa
66.8 kg/S
309°K
24.3 MPa
0.32 kg/S
21.8°K
1.6 MPa
91°K
0.99 MPa
401 kg/S
104°K
30.7 MPa
82.6 kg/S
94°K
3.2 MPa
483 kg/S
114°K
52.4 MPa
10.3 kg/S
5.7 kg/S
114°K
52.6 MPa
28.8 kg/S
309°K
24.2 MPa
7.8 kg/S
35.5 kg/S
39.7 MPa
166°K
16.3 kg/S
511°K
28.2 MPa
0.1 kg/S
104°K
26.7 MPa
361 kg/S
959°K
35.6 MPa
814°K
36.2 MPa
HOT GAS
868°K
22.8 MPa
65.1 kg/S
73.5°K
22.8 MPa
26.5 kg/S
52°K
42.6 MPa
20.4 MPa
104°K
31.9 MPa
166°K
51.8 kg/S
13.8 kg/S
114°K
52.8 MPa
39.1 kg/S
472°K
27.4 MPa
0.7 kg/S
OXYGEN
HYDROGEN
34.2 kg/S
17.6 kg/S
466 kg/S

Figure 1

TYPES OF HYDROGEN EMBRITTLEMENT

(Figure 2)

It is important to recognize that there are different types of hydrogen embrittlement that may be interrelated but have different embrittlement characteristics.

Hydrogen embrittlement may be classified into: (1) hydrogen reaction embrittlement, (2) internal-hydrogen embrittlement, and (3) hydrogen-environment embrittlement (ref. 1). Hydrogen-reaction embrittlement results when a chemical reaction occurs between hydrogen and the metal or some constituent in the metal to form an embrittling phase. For example, metals such as titanium, zirconium, columbium, and tantalum (present either as the base metal or as an alloying element) can react with hydrogen to form embrittling hydrides. Other long recognized examples of hydrogen-reaction embrittlement are the reaction of hydrogen with oxygen in copper to form water vapor or with carbon in steels to form methane. In either case, the resultant gas settles into voids or cracks at very high pressures, thus embrittling the metal by tending to force the crack apart and extending it. Also, the decarburization of a steel will reduce its strength. Hydrogen-reaction embrittlement is essentially a permanent, non-reversible embrittlement and increased temperatures and hydrogen pressures increase the rates of reaction and thus increase the tendency toward this type of embrittlement.

Internal-hydrogen embrittlement is that due to hydrogen which has been absorbed and permeated into the metal. The most widely recognized example of this embrittlement is the delayed failure of hydrogen-charged, high-strength steels. The absorption of hydrogen from a gas will be increased by increased temperature and gas pressure; however, for a given concentration of absorbed hydrogen, internal-hydrogen embrittlement is most severe in the vicinity of room temperature. Internal-hydrogen embrittlement is reversible in that, if cracks have not been formed, and if the hydrogen is removed from the metal, there is no embrittlement.

The term hydrogen-environment embrittlement (HEE) is used to signify the degradation of mechanical properties of a metal that occurs while the metal is exposed to a hydrogen environment as compared to an inert environment.

TYPES OF H_2 EMBRITTLEMENT

- HYDRIDE FORMATION - Ti, Zr, Cb, Ta
- HYDROGEN REACTION - C IN STEEL → CH_4

  O_2 IN Cu → H_2O
- INTERNAL HYDROGEN EMBRITTLEMENT - STEELS
- HYDROGEN-ENVIRONMENT EMBRITTLEMENT

Figure 2

200

CHARACTERISTICS OF HEE

(Figure 3)

Susceptible metals are embrittled by hydrogen environments in the sense that: (1) the ductility of the metal is lower in hydrogen than in other environments, (2) tensile plastic deformation in hydrogen results in surface cracking, (3) subcritical crack growth occurs in hydrogen, and (4) crack growth rates for given cyclic or sustained stress intensities are faster in hydrogen than in inert environments (ref. 1).

CHARACTERISTICS OF HEE

- NOTCH STRENGTH IS LOWER IN GH_2
- DUCTILITY IS LOWER IN GH_2
- TENSILE PLASTIC DEFORMATION IN GH_2 RESULTS IN SURFACE CRACKING
- THRESHOLD STRESS INTENSITIES FOR CRACK GROWTH ARE LOWER IN GH_2
- CRACK GROWTH RATES ARE FASTER IN GH_2

Figure 3

TENSILE TEST

(Figure 4)

The elastic properties and tensile yield strengths of metals are the same in hydrogen as in air or inert environments, as shown in the idealized stress/strain curve for a tensile test in hydrogen in the figure. The most significant effects of high-pressure hydrogen environments are on tensile ductility, notch tensile strength, and crack behavior. More precisely, the effect of the hydrogen environment is to embrittle the surface. The embrittled "surface" may be the immediate surface or a surface layer of some finite but limited thickness. The metal surface cannot undergo plastic deformation in tension to the same degree in hydrogen as it can in air or inert environments. When a susceptible metal is stressed in tension in hydrogen to some critical amount of plastic deformation, the surface fractures (i.e., a surface crack forms).

From the time that surface cracking begins, the test is no longer a normal tensile test but is a rather complex test of a crack specimen; this must be considered in assessing the meaning and usefulness of the strength and ductility data obtained from these tests.

TENSILE TEST

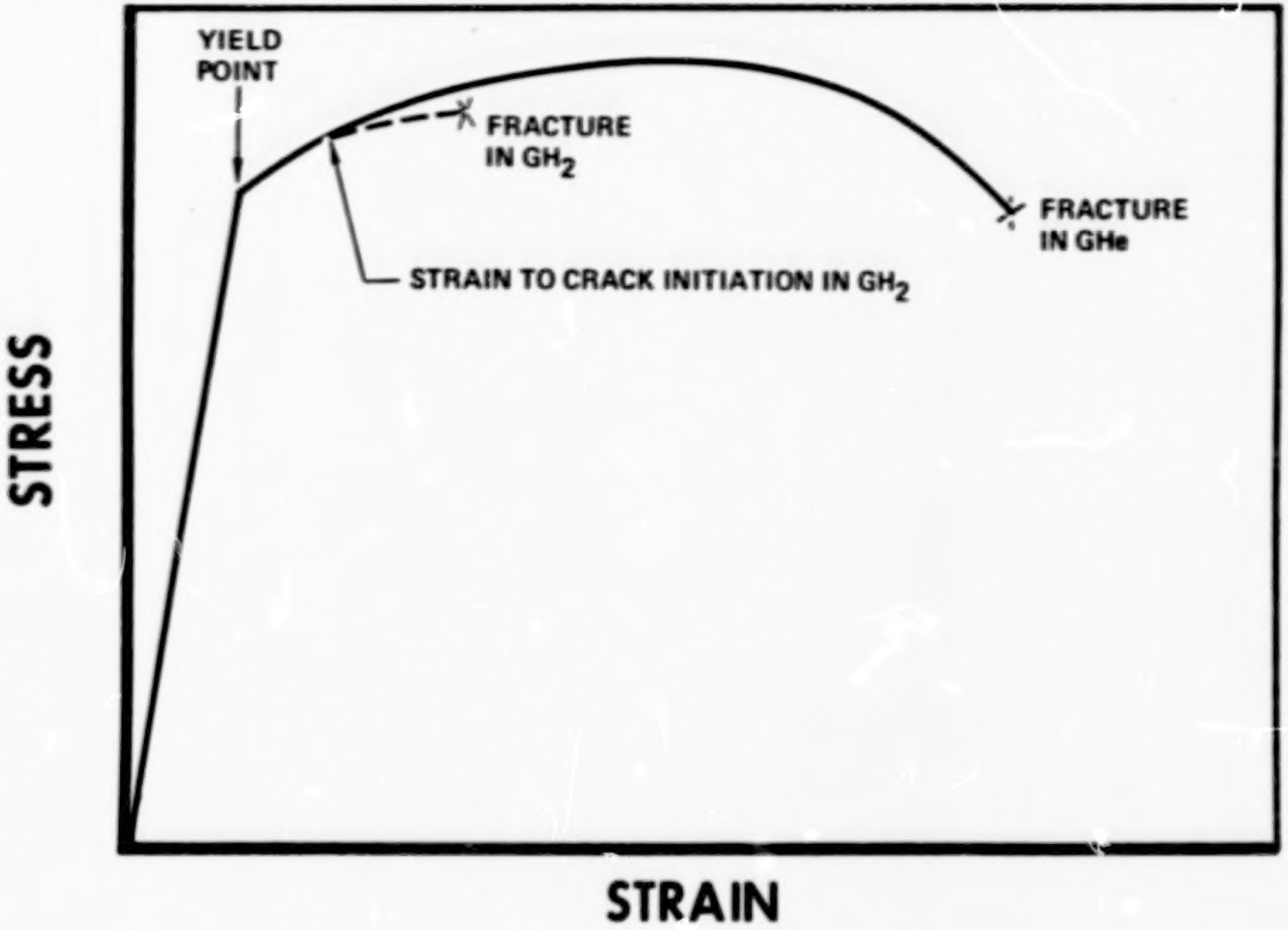

Figure 4

CONTENTS

Part I

PREFACE . . . . iii 1/A5

WELCOME 1 1/A10
R. R. Heldenfels

SESSION I - OVERVIEWS
Chairman: A. J. Henderson

1. HYPERSONIC STRUCTURES: AN AERODYNAMICIST'S PERSPECTIVE (OR ONE MAN'S DREAM IS ANOTHER MAN'S NIGHTMARE) 5 1/B1
J. D. Watts, L. R. Jackson, and J. L. Hunt

2. STRUCTURAL REQUIREMENTS FOR MILITARY HYPERSONIC SYSTEMS (Paper not available for publication)
P. Lane

3. AIRFRAME-INTEGRATED PROPULSION SYSTEM FOR HYPERSONIC CRUISE VEHICLES 39 1/F13
Robert A. Jones and Paul W. Huber

4. RECENT ADVANCES IN CONVECTIVELY COOLED ENGINE AND AIRFRAME STRUCTURES FOR HYPERSONIC FLIGHT 47 1/G7
H. Neale Kelly, Allan R. Wieting, Charles P. Shore, and Robert J. Nowak

SESSION II - ENGINE STRUCTURES
Chairman: H. N. Kelly

5. DESIGN AND ANALYSIS OF A SCRAMJET ENGINE 65 2/A13
O. A. Buchmann

6. THERMOSTRUCTURAL ANALYSIS OF A SCRAMJET FUEL-INJECTION STRUT 119 3/B11
Allan R. Wieting and Earl A. Thornton

7. ADVANCED FABRICATION TECHNIQUES FOR COOLED ENGINE STRUCTURES 145 3/F7
O. A. Buchmann

8. HYDROGEN EMBRITTLEMENT AND ITS CONTROL IN HYDROGEN-FUELED ENGINE SYSTEMS 195 4/F11
W. T. Chandler

9. CARBON-CARBON COMPOSITE APPLICATION FOR INTEGRAL ROCKET RAMJET COMBUSTORS (Paper not available for publication)
H. A. Holman

SESSION III - COOLED AIRFRAME STRUCTURES
Chairman: C. P. Shore

10. DESIGN AND FABRICATION OF A SKIN STRINGER DISCRETE TUBE ACTIVELY COOLED STRUCTURAL PANEL 253 6/A5
Frank M. Anthony

11. DESIGN AND ANALYSIS OF A PLATE-FIN SANDWICH ACTIVELY COOLED STRUCTURAL PANEL 319 7/C13
L. M. Smith

12. FLUXLESS BRAZING AND HEAT TREATMENT OF A PLATE-FIN SANDWICH ACTIVELY COOLED PANEL 375 8/E1
Charles S. Beuyukian

13. DESIGN AND FABRICATION OF A RADIATIVE ACTIVELY COOLED HONEYCOMB SANDWICH PANEL 449 10/A13
Leland C. Koch

14. RADIATIVE, ACTIVELY COOLED PANEL TESTS RESULTS 493 11/A5
Charles P. Shore, Robert J. Nowak, and Ellsworth L. Sharpe

204

SURFACE CRACKING IN ASTM A-533-B STEEL IN H_2 AT RT

(Figure 5)

Surface cracks, examples of which are shown in the figure, provide some of the most dramatic visual evidence of hydrogen-environment embrittlement. The figure presents photomacrographs (10X) of ASTM A-533-B steel specimens that have been tensile tested in helium and in hydrogen at two pressures, all at room temperature (RT). The ASTM A-533-B steel is a low alloy steel that has been used extensively in large vessels for the storage of gases, including hydrogen, at high pressures.

For a susceptible metal, an existing crack or one formed in the hydrogen environment will propagate at a lower stress intensity and at a more rapid rate for a given stress intensity in hydrogen than in air or inert environments.

SURFACE CRACKING IN ASTM A-533-B STEEL IN H_2 AT RT

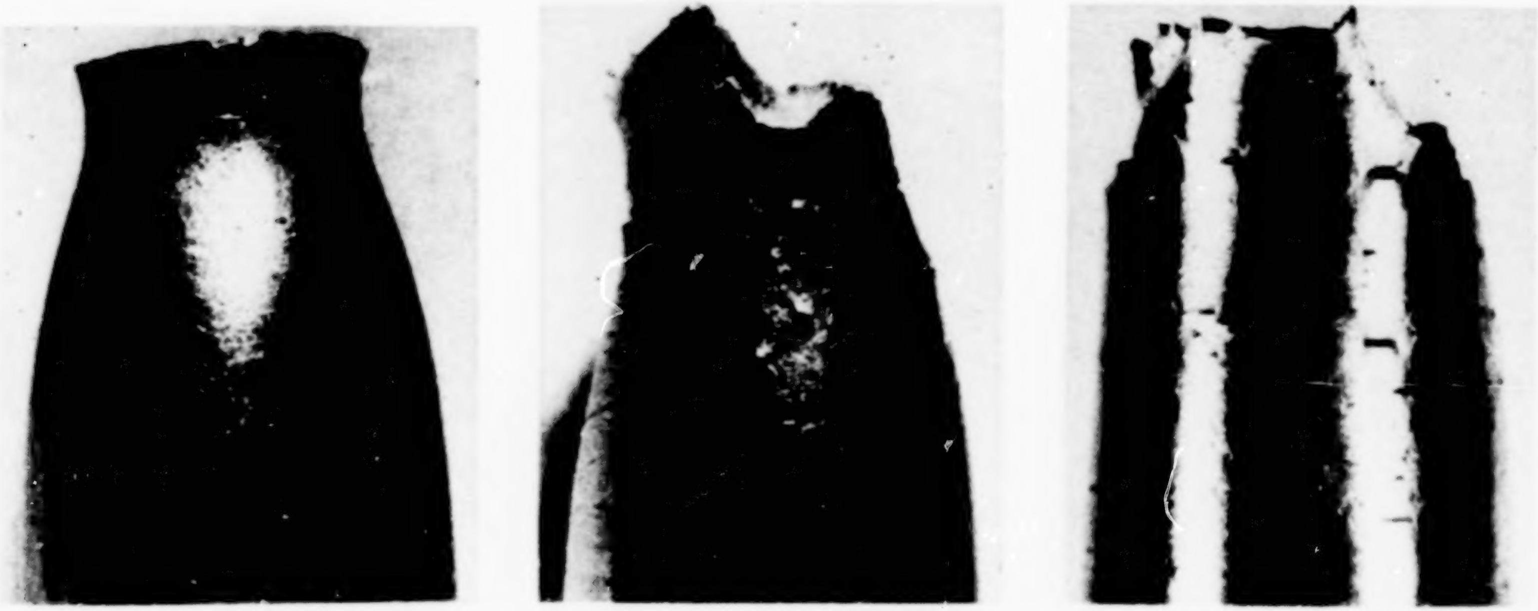

HELIUM
68.9 MN/m^2 (10,000 PSI)

HYDROGEN
6.89 MN/m^2 (1000 PSI)

HYDROGEN
68.9 MN/m^2 (10,000 PSI)

Figure 5

HEE OF EDNi VERSUS HYDROGEN PRESSURE H_{P_2}

(Figure 6)

Hydrogen-environment embrittlement is an environmental effect and no hold time in the hydrogen environment is required to establish the embrittlement. However, hydrogen-environment embrittlement is very sensitive to test rate, that is, strain rate or crack propagation rate. At high strain or crack propagation rates, the effect of the hydrogen environment will be reduced or eliminated. This is evidenced by the fact that the final failure in a tensile specimen pulled in hydrogen is a ductile, overload failure that is unaffected by the hydrogen environment. The effect of test rate is related to the rates of the processes by which hydrogen moves from the environment onto or into the metal. Thus, environmental parameters are of great importance.

For example, the degradation of tensile properties by hydrogen environments increases with increasing hydrogen pressure as shown in the figure for electrodeposited nickel, EDNi (N_{H2} and N_{air} are the tensile strengths of notched specimens in hydrogen and air, respectively). It should be noted that significant effects of hydrogen environments on properties can occur at pressures of 1 atmosphere or lower.

The effect of hydrogen pressure on the degree of hydrogen-environment embrittlement probably pertains to any property involving a test rate, for example, strain rate or crack growth rate, and is related to the effect of hydrogen pressure on the rate of transfer of hydrogen from the environment onto or into the metal as noted above.

HEE OF EDNi
vs
P_{H_2}

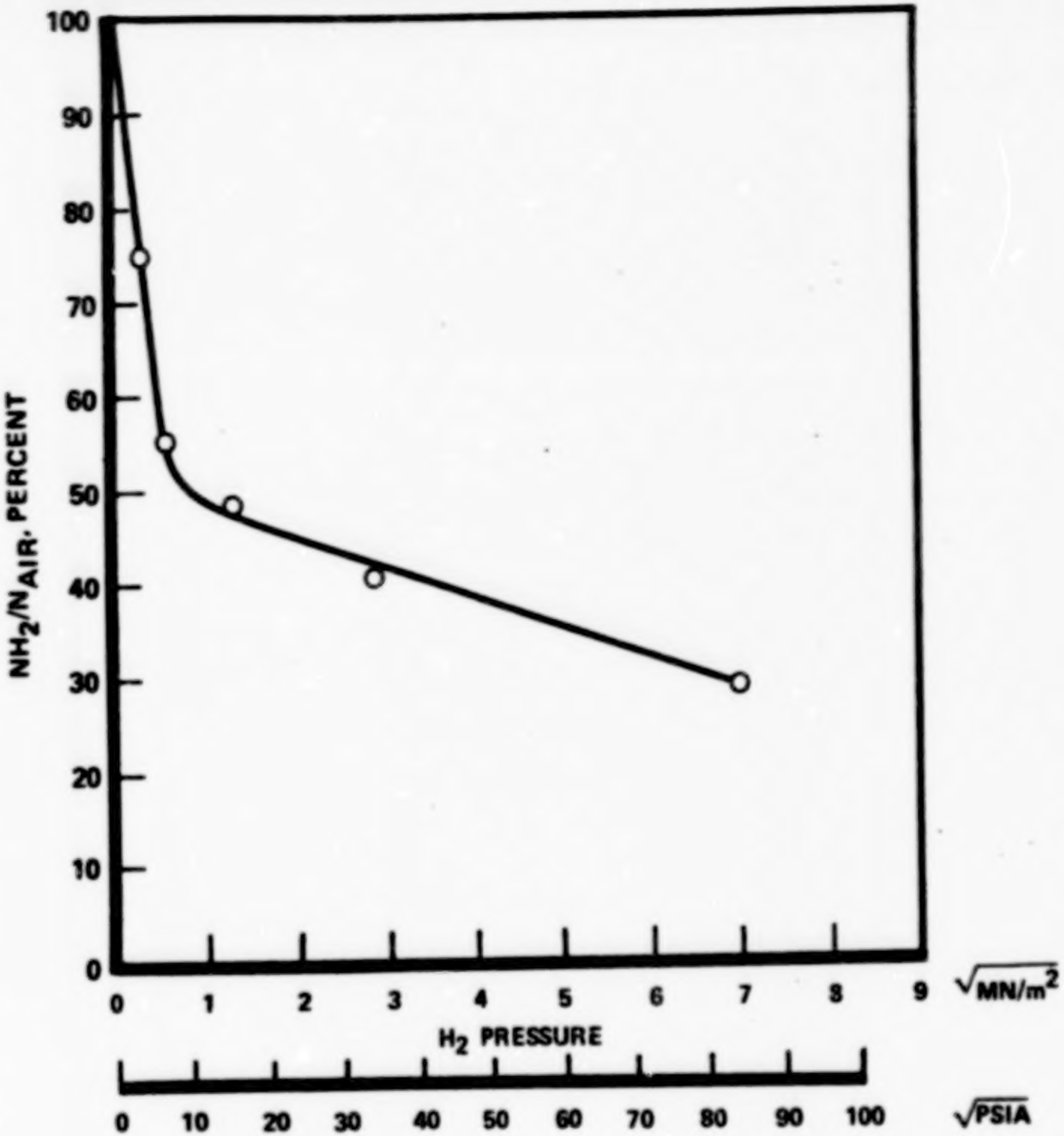

Figure 6

207

EFFECT OF TEMPERATURE ON HEE OF EDNi IN 8.3 MN/m^2 (1200 PSI) H_2

(Figure 7)

Hydrogen-environment embrittlement occurs over a wide range of temperatures from cryogenic (ref. 2) to at least 1144 K (1600 F), reference 3, but is most severe in the vicinity of (but not necessarily exactly at) room temperature. The variation in embrittlement with temperature may be quite rapid in the vicinity of room temperature as is shown in the figure for EDNi.

It should be remembered that at the higher temperatures there is the potential for hydrogen-reaction embrittlement or for the absorption of sufficient hydrogen to result in internal hydrogen embrittlement, particularly on subsequent cool down.

The interest at Rocketdyne in the hydrogen-environment embrittlement of electrodeposited nickel (EDNi) stems from the fact that the regeneratively cooled SSME combustion chamber is constructed of a copper-alloy liner in which slots are machined and closed out with EDNi to form the channels for the coolant hydrogen.

EFFECT OF TEMPERATURE ON HEE OF EDNi IN $8.3 MN/m^2$ (1200psi)H_2

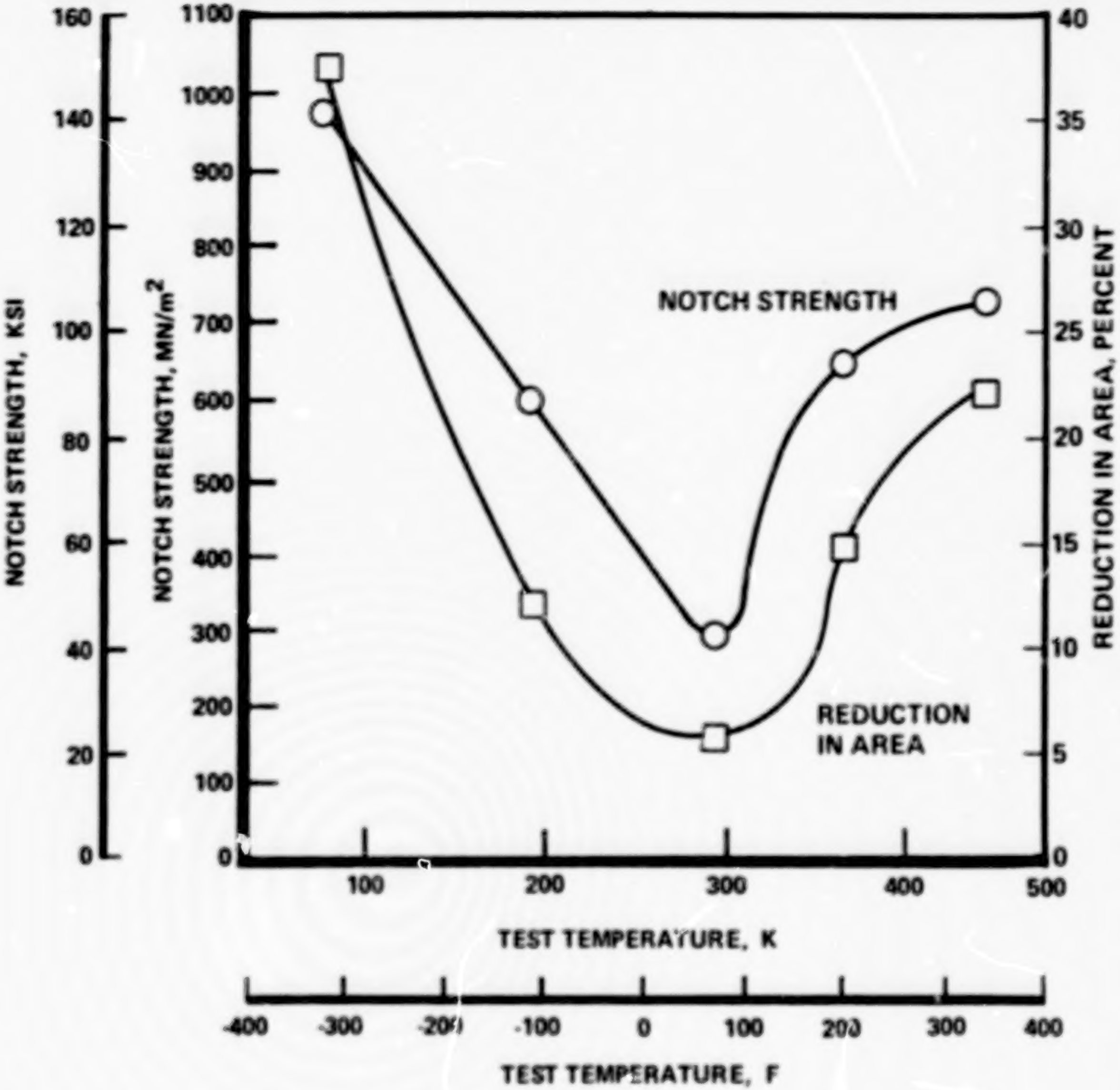

Figure 7

209

EFFECT OF O_2 IN GH_2 ON HEE AT RT

(Figure 8)

The purity of the hydrogen is important. For example, it has been found that even small amounts of oxygen in hydrogen inhibits hydrogen-environment embrittlement, as shown in the figure for a plain carbon (approximatley 0.20 percent carbon) steel (ref. 4). The embrittlement inhibiting effect of oxygen in 10.1 MN/m^2 (1500 psi) hydrogen becomes noticeable above 0.1 ppm oxygen.

The hydrogen gas to which the metals are exposed in the SSME is of very high purity. Thus, considerable effort has been expended at Rocketdyne in developing hydrogen purification and test system purging techniques to give a high purity hydrogen for property testing (ref. 5). Analyses of hydrogen samples taken at test location have yielded the following: < 0.2 ppm O_2, < 0.5 ppm Argon, 0.6 to 0.9 ppm N_2, < 0.5 ppm CH_4, < 0.5 ppm CO, < 0.5 ppm CO_2, and 208 K (-85°F) dewpoint (~1 ppm H_2O).

EFFECT OF O_2 IN GH_2 ON HEE AT RT

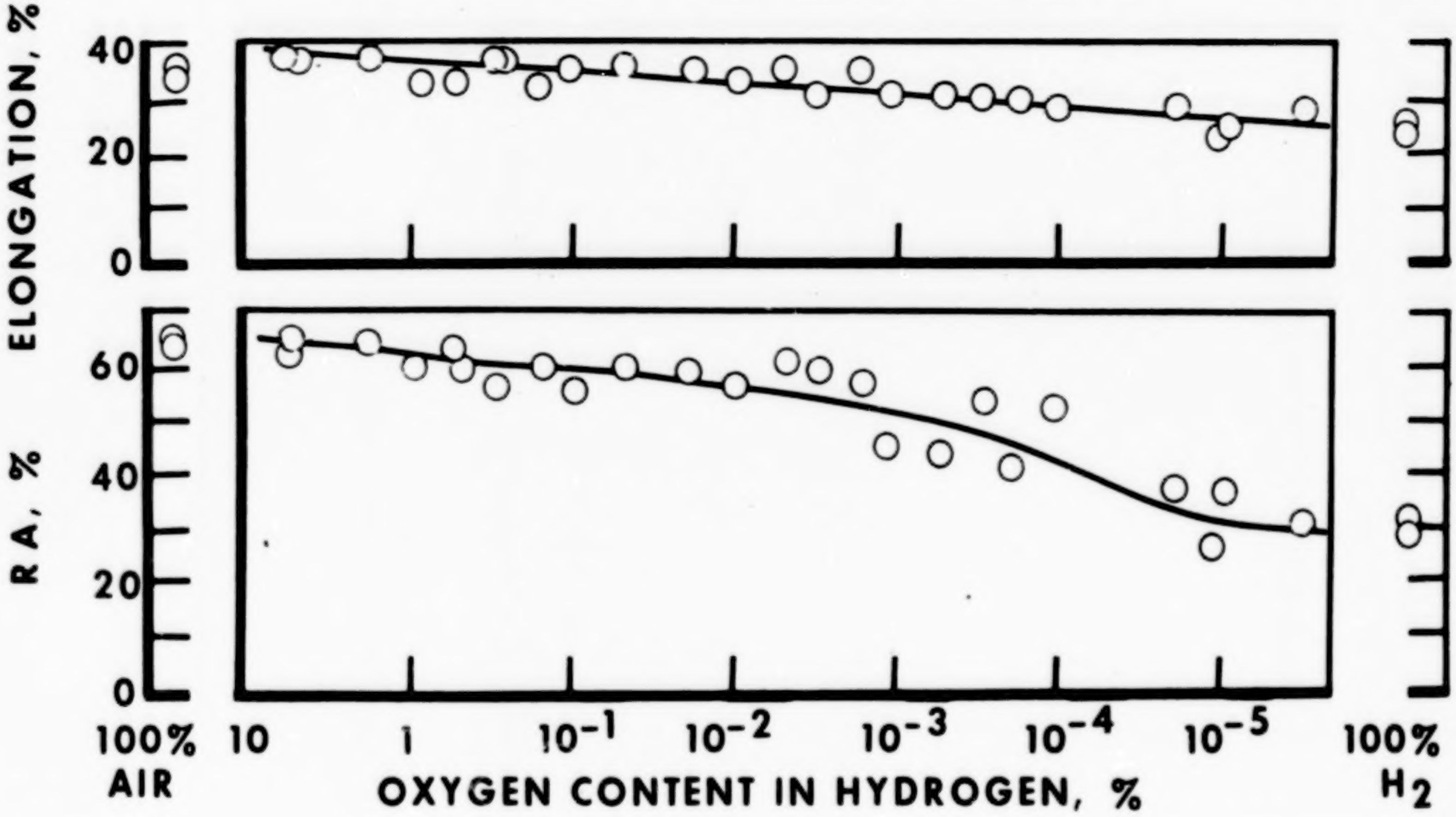

Figure 8

2 11

DESIGNING FOR GH$_2$ SERVICE

(Figure 9)

The preceding summary of the characteristics of hydrogen-environment embrittlement suggests a number of approaches that can be employed in the design of hydrogen systems. The accompanying figure shows a simplified logic diagram for designing for hydrogen service. The remainder of the paper will be devoted to working through this diagram particularly as it has been applied to the SSME and with the presentation of supporting data.

First, of course, the service conditions should be carefully reviewed (considering all transient conditions) to determine if hydrogen-environment embrittlement is a potential problem.

DESIGNING FOR GH_2 SERVICE

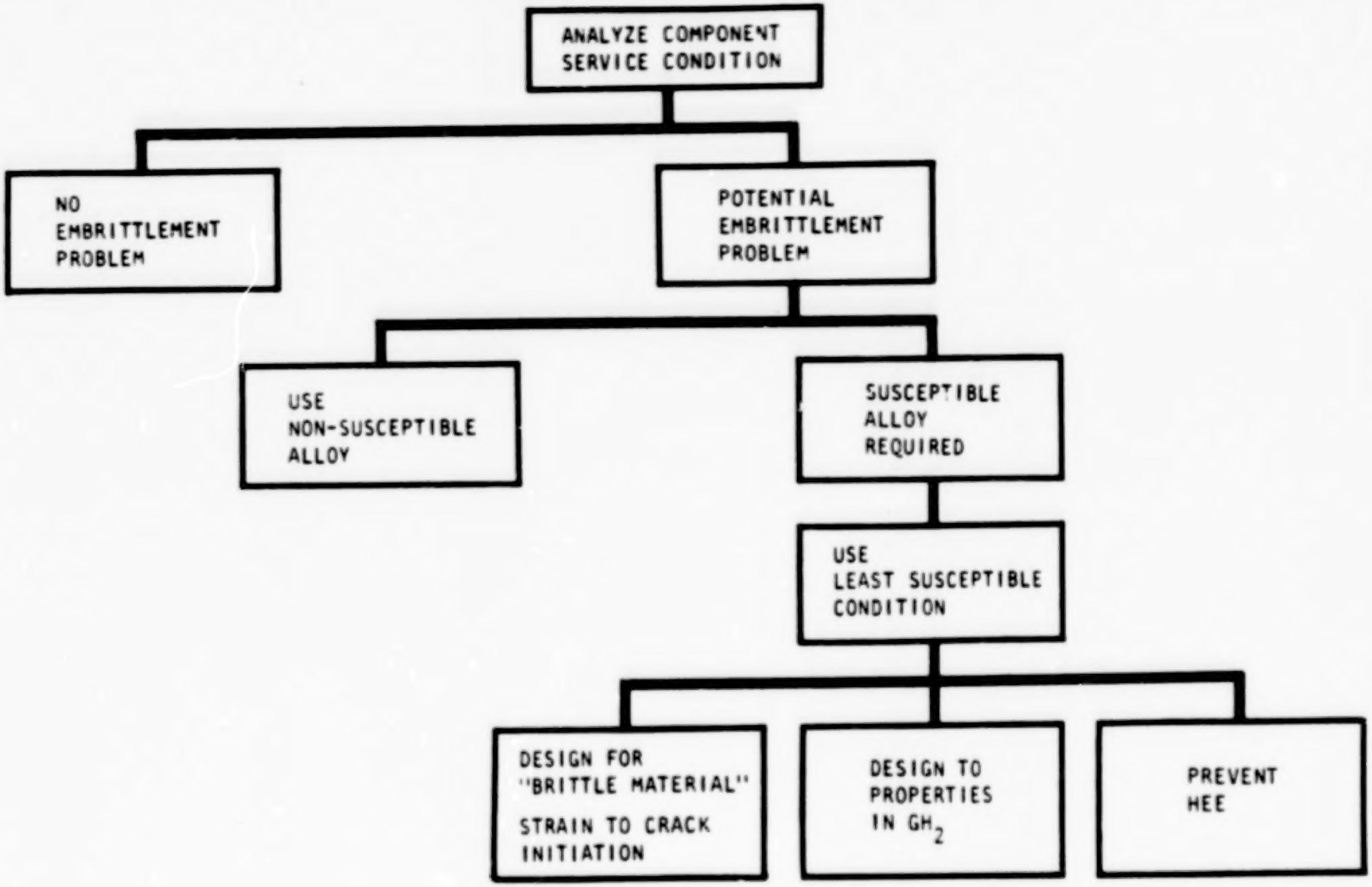

ANALYZE COMPONENT SERVICE CONDITION

NO EMBRITTLEMENT PROBLEM

POTENTIAL EMBRITTLEMENT PROBLEM

USE NON-SUSCEPTIBLE ALLOY

SUSCEPTIBLE ALLOY REQUIRED

USE LEAST SUSCEPTIBLE CONDITION

DESIGN FOR "BRITTLE MATERIAL" STRAIN TO CRACK INITIATION

DESIGN TO PROPERTIES IN GH_2

PREVENT HEE

Figure 9

K_{IC} AND K_{TH} OF INCONEL 718 IN 34.5 MN/m^2 (5000 PSI) H_2 AND He

(Figure 10)

If the temperature of the metal part always remains well below room temperature, there may be no embrittlement caused by the hydrogen environment. For example, the figure presents low-temperature fracture mechanics data, K_{IC}, for Inconel 718, which is used extensively in the SSME. It can be seen from the sustained-load crack growth threshold stress intensity (K_{TH}) that there is a large effect of hydrogen at room temperature but a negligible effect at 144 K (-200 F).

K_{IC} AND K_{TH} OF INCONEL 718

IN 34.5 MN/m^2(5000 psi) H_2 AND He

HEAT TREATMENT	TEMPERATURE		HELIUM				HYDROGEN	
			K_{IC}		K_{TH}		K_{TH}	
	K	F	MN/m$^{3/2}$	KSI$\sqrt{\text{IN.}}$	MN/m$^{3/2}$	KSI $\sqrt{\text{IN.}}$	MN/m$^{3/2}$	KSI $\sqrt{\text{IN.}}$
1214, 991-894K (1725, 1325-1150F)	294	70	78	71	58	53	14	13
	144	-200	98	89	81	74	73	66
1325, 1033-922K (1925, 1400-1200F)	294	70	119	108*	112	102	42	38
	200	-100	160	146*	160	146*	< 46	< 42
	144	-200	122	111	138	126	123	112

*NOT VALID PLANE STRAIN FRACTURE TOUGHNESS

Figure 10

216

MATERIALS EXTREMELY EMBRITTLED

(Figure 11)

If it is established that the conditions of hydrogen exposure are conducive to hydrogen-environment embrittlement, then, obviously, the first approach is to select metals not susceptible to hydrogen-environment embrittlement.

A large number of alloys have been investigated at Rocketdyne, and on the basis of tensile tests on unnotched and notched (stress intensity factor, K_t, = 8.4) specimens in 68.9 MN/m^2 (10,000 psi) hydrogen at room temperature, the alloys have been classified into four categories, viz., extreme, severe, slight, and negligible embrittlement. Unfortunately, as can be seen from this figure, most of the high-strength iron- and nickel-base alloys are extremely embrittled.

Embrittlement of alloys in this category is characterized by a large decrease of notch strength and ductility and some decrease of unnotched strength. Large reductions of ductility are found for all three common measures of ductility (elongation and reduction of area of unnotched specimens and reduction of area of notched specimens). Surface cracks are not usually found in failed specimens because the first crack to form quickly proceeds to failure before another crack can form.

MATERIALS EXTREMELY EMBRITTLED

68.9 MN/m^2 (10,000 psi) GH$_2$, RT

MATERIAL	STRENGTH RATIO, H_2/He		UNNOTCHED DUCTILITY			
			ELONGATION, PERCENT		RA, ** PERCENT	
	NOTCHED (K_t = 8.4)	UNNOTCHED	He	H_2	He	H_2
18 Ni-250 MAR	0.12	0.68	8.2	0.2	55	2.5
410 SS	0.22	0.79	15	1.3	60	12
1042 QT	0.22	--	--	--	--	--
17-7 PH SS	0.23	0.92	17	1.7	45	2.5
Fe-9Ni-4Co-0.20C	0.24	0.86	15	0.5	67	15
H-11	0.25	0.57	8.8	0	30	0
RENE 41	0.27	0.84	21	4.3	29	11
ELECTROFORMED Ni*	0.31	--	--	--	--	--
4140	0.40	0.96	14	2.6	48	9
INCONEL 718	0.46	0.93	17	1.5	26	1
440 C	0.50	0.40	--	--	3.2	0

*TESTED IN 48.3 MN/m^2 (7000-PSI) H_2

**RA = REDUCTION IN AREA

Figure 11

MATERIALS SEVERELY EMBRITTLED

(Figure 12)

Metals that are severely embrittled by high-pressure hydrogen include ductile, lower strength steels, Armco iron, pure wrought nickel, and the titanium-base alloys. Embrittlement is characterized by a considerable reduction of notch strength and ductility, but no reduction of unnotched strength. The measure of ductility most affected by the high-pressure hydrogen environment is the reduction of area of notched specimens. A large number of deep surface cracks are found in failed specimens.

MATERIALS SEVERELY EMBRITTLED

68.9MN/m^2(10,000psi)GH_2,RT

MATERIAL	NOTCH STRENGTH RATIO, H_2/He (K_t = 8.4)	UNNOTCHED DUCTILITY			
		ELONGATION, PERCENT		RA*, PERCENT	
		He	H_2	He	H_2
Ti-6Al-4V (STA)	0.58	--	--	--	--
430 F	0.68	22	14	64	37
NICKEL 270	0.70	56	52	89	67
A-515	0.73	42	29	67	35
HY-100	0.73	20	18	76	63
A-372 CLASS IV	0.74	20	10	53	18
1042 NORMALIZED	0.75			59	27
A-533-B	0.78			66	33
Ti-6Al-4V (ANNEALED)	0.79	--	--	--	--
AISI 1020	0.79			68	45
HY-80	0.80			70	60
Ti-5Al-2.5Sn ELI	0.81			45	39
ARMCO IRON	0.86			83	50

*RA = REDUCTION IN AREA

Figure 12

MATERIALS SLIGHTLY EMBRITTLED

(Figure 13)

The alloys shown in this figure were found to be only slightly embrittled by high pressure hydrogen with the embrittlement characterized by some decrease of strength of notched specimens, a negligible decrease in ductility of unnotched specimens, and the formation of only a few shallow surface cracks.

It should be noted that others have found 304 stainless steel to be more severely embrittled than is indicated in the figure. A more extensive discussion of the effects of high-pressure hydrogen on stainless steels can be found in reference 6.

Also, although pure titanium was found to be relatively unembrittled under these conditions of tensile testing in high-pressure hydrogen at room temperature, titanium and titanium alloys are subject to serious embrittlement by hydride formation at higher temperatures.

MATERIALS SLIGHTLY EMBRITTLED

$68.9 MN/m^2$(10,000psi)GH_2,RT

MATERIAL	NOTCH STRENGTH RATIO, H_2/He (K_t= 8.4)	UNNOTCHED DUCTILITY (R A , PERCENT) *	
		He	H_2
304 ELC SS	0.87	78	71
305 SS	0.89	78	75
Be-Cu ALLOY 25	0.93	72	71
TITANIUM	0.95	61	61

*R A = REDUCTION IN AREA

Figure 13

MATERIALS NEGLIGIBLY EMBRITTLED

(Figure 14)

The alloys essentially unaffected by high-pressure hydrogen in tensile tests at room temperature are shown in this figure. Thus, if one were to select a metal not susceptible to hydrogen-environment embrittlement for use in a hydrogen system, it would come from this group. It is immediately apparent that the range of properties available from this group of alloys is limited and, in many instances, will not meet other requirements.

Before one of these alloys could be considered for incorporation in a system on the basis of non-susceptibility to hydrogen-environment embrittlement, it would be necessary to confirm that the alloy is not embrittled by hydrogen under the particular hydrogen exposure and part stressing conditions pertinent to the system. Alloys found not to be embrittled by hydrogen in tensile tests have been found to be embrittled by hydrogen in other tests, as will be discussed.

MATERIALS NEGLIGIBLY EMBRITTLED

68.9 MN/m^2(10,000)GH_2, RT

MATERIAL	NOTCH STRENGTH RATIO H_2/He (K_t =8.4)	UNNOTCHED DUCTILITY (R A, PERCENT)**	
		He	H_2
310 SS	0.93	64	62
A-286	0.97	44	43
7075-T73 Al ALLOY	0.98	37	35
INCOLOY 903***	1.00	50	47
316 SS	1.00	72	75
OFHC COPPER	1.00	94	94
NARloy-Z*	1.10	24	22
6061-T6 Al ALLOY	1.10	61	66
1100-0 Al	1.40	93	93

*ROCKWELL INTERNATIONAL CORPORATION TRADEMARK; TESTED IN 40 MN/m^2 (5800-psi) H_2

**RA = REDUCTION IN AREA

***TESTED IN 48.3 MN/m^2 (7000-psi) H_2

Figure 14

9

HEE OF INCO 718 IN VARIOUS CONDITIONS

(Figure 15)

In many cases, metals susceptible in some degree to hydrogen-environment embrittlement will have to be used in a hydrogen system. In such cases, the selected metal should be used in the condition least embrittled by the hydrogen environment.

It has been found that the condition of an alloy can have a profound effect on the degree of hydrogen-environment embrittlement of the alloy. Inconel 718 is an example. The first Inconel 718 to be tested in high-pressure hydrogen was that listed in Figure 11, which had been given a 1214, 991-894 K (1725, 1325-1150 F) heat treatment. Subsequently, much less embrittlement was found for Inconel 718 specimens that had been given a 1325, 1033-922 K (1925, 1400-1200 F) heat treatment. This led to a more comprehensive investigation (ref. 7) in which tensile tests were performed on notched specimens in 34.5 MN/m^2 (5000 psi) hydrogen at ambient temperature on Inconel 718 in three forms and three heat treatment conditions.

The results are given in the accompanying figure. The microstructures resulting from the different forming operation/heat treatment conditions could be related to the degree of hydrogen-environment embrittlement. Unfortunately, identification of the condition least embrittled by hydrogen environments is, as yet, limited to a very few metals, examples are Udimet 700/Astroloy (ref. 5) and electrodeposited nickel (ref. 8), for which the effects of deposition current density and post-deposition annealing temperatures on hydrogen-environment embrittlement have been investigated.

HEE OF INCO 718 IN VARIOUS CONDITIONS

34.5 MN/m^2 (5,000 psi), RT

HEAT TREATMENT	MATERIAL	ENVIRONMENT	NOTCHED PROPERTIES		
			STRENGTH, MN/m^2	NH_2/NHe	RA, PERCENT
1214, 991-894 K (1725, 1325-1150 F) (A)	ROLLED BAR	HELIUM	1950	--	2.9
		HYDROGEN	1050	0.54	0.9
	FORGING	HELIUM	2000	--	3.0
		HYDROGEN	1170	0.59	1.1
	PLATE	HELIUM	1980	--	3.0
		HYDROGEN	1700	0.86	2.0
1214, 1089-922 K (1725, 1500-1200 F) (B)	ROLLED BAR	HELIUM	1650	--	2.9
		HYDROGEN	1160	0.70	1.8
	FORGING	HELIUM	1740	--	2.2
		HYDROGEN	990	0.57	1.2
	PLATE	HELIUM	1730	--	2.7
		HYDROGEN	1500	0.86	2.1
1325, 1033-922 K (1925, 1400-1200 F) (C)	ROLLED BAR	HELIUM	2220	--	5.0
		HYDROGEN	1590	0.71	1.7
	FORGING	HELIUM	2340	--	4.6
		HYDROGEN	1780	0.76	1.8
	PLATE	HELIUM	2210	--	3.7
		HYDROGEN	1700	0.77	2.3

Figure 15

STRAIN AT CRACK INITIATION OF INCONEL 718 EXPOSED TO 48.3 MN/m^2 (7000 PSI) H_2 AT RT

(Figure 16)

In some instances, when the design permits, a susceptible metal may be designed into a hydrogen system by utilizing a "brittle material" design approach. Generally, such an approach would be limited to nonwelded structures. The conditions under which a brittle material design approach is appropriate are difficult to define precisely and must be based on engineering judgment; however, the following characteristics are essential. The structure must not contain sharp notches and the finish and accessibility to inspection of the surface in contact with hydrogen must be such that the absence of surface cracks can be ensured. The stress and strains must be predictable with a high degree of confidence based on accurately known loads and configuration simplicity. Most importantly, the peak or localized stresses and strains must be less than the "available" stress and strain for the material in hydrogen, i.e., the stress and strain at crack initiation in hydrogen under the appropriate conditions.

Results of tensile tests to determine strain at crack initiation for Inconel 718 are presented in the figure. Although the two heat treatment conditions listed in the figure experienced very different degrees of degradation of notch strength as shown in Figure 15, the strain at crack initiation was essentially the same. However, the strain at failure was quite different, indicating that the major effect of hydrogen environments on tensile specimens is on crack growth rates.

STRAIN AT CRACK INITIATION OF INCONEL 718

EXPOSED TO 48.3 MN/m^2(7,000psi) H_2 AT RT

HEAT TREATMENT	PERCENT ELONGATION	
	AT CRACK INITIATION	AT FAILURE
1214, 991-894K (1725, 1325-1150F)	3	3 TO 5
1325, 1033-922K (1925, 1400-1200F)	3 TO 5	21

Figure 16

INCONEL 718 LOW-CYCLE FATIGUE DATA

(Figure 17)

When metals that are susceptible to hydrogen embrittlement are to be used in hydrogen systems, the design must be based on properties of the metal determined in the hydrogen environment under conditions simulating service conditions.

Notch tensile strength is one of the properties most sensitive to hydrogen environments because of the large plastic strains that occur at the tip of the notch. When designs of hydrogen components are based on tensile properties, it appears feasible to use the reduction of notch tensile strength in hydrogen under appropriate conditions combined with good engineering judgment to set additional safety factors to compensate for the effect of the hydrogen environment.

In many cases, properties other than tensile properties must be considered in designing components of hydrogen systems. Then, the appropriate property determined in hydrogen under appropriate conditions must be used in designing the part.

The most severe property degradation in high-pressure hydrogen of specimens that do not initially contain cracks occurs in tests involving plastic strain. Thus, considerable reductions of stress-rupture strengths and cycles to failure in low-cycle fatigue (strain cycling) tests in hydrogen are to be expected. The figure shows the decrease of low-cycle fatigue life of Inconel 718 (Heat Treatment C, Fig. 15) during exposure to 41.4 MN/m^2 (6000 psi) hydrogen at ambient temperature. A substantial portion of low-cycle fatigue life occurs after crack initiation. The cyclic-crack growth rate in aggressive environments is strongly dependent upon the cyclic rate. Thus, low-cycle fatigue testing should be performed at strain cycling rates which simulate the hardware application.

INCONEL 718 LOW CYCLE FATIGUE DATA

41.4 MN/m^2 (6000 PSI), RT, Hz = 0.5

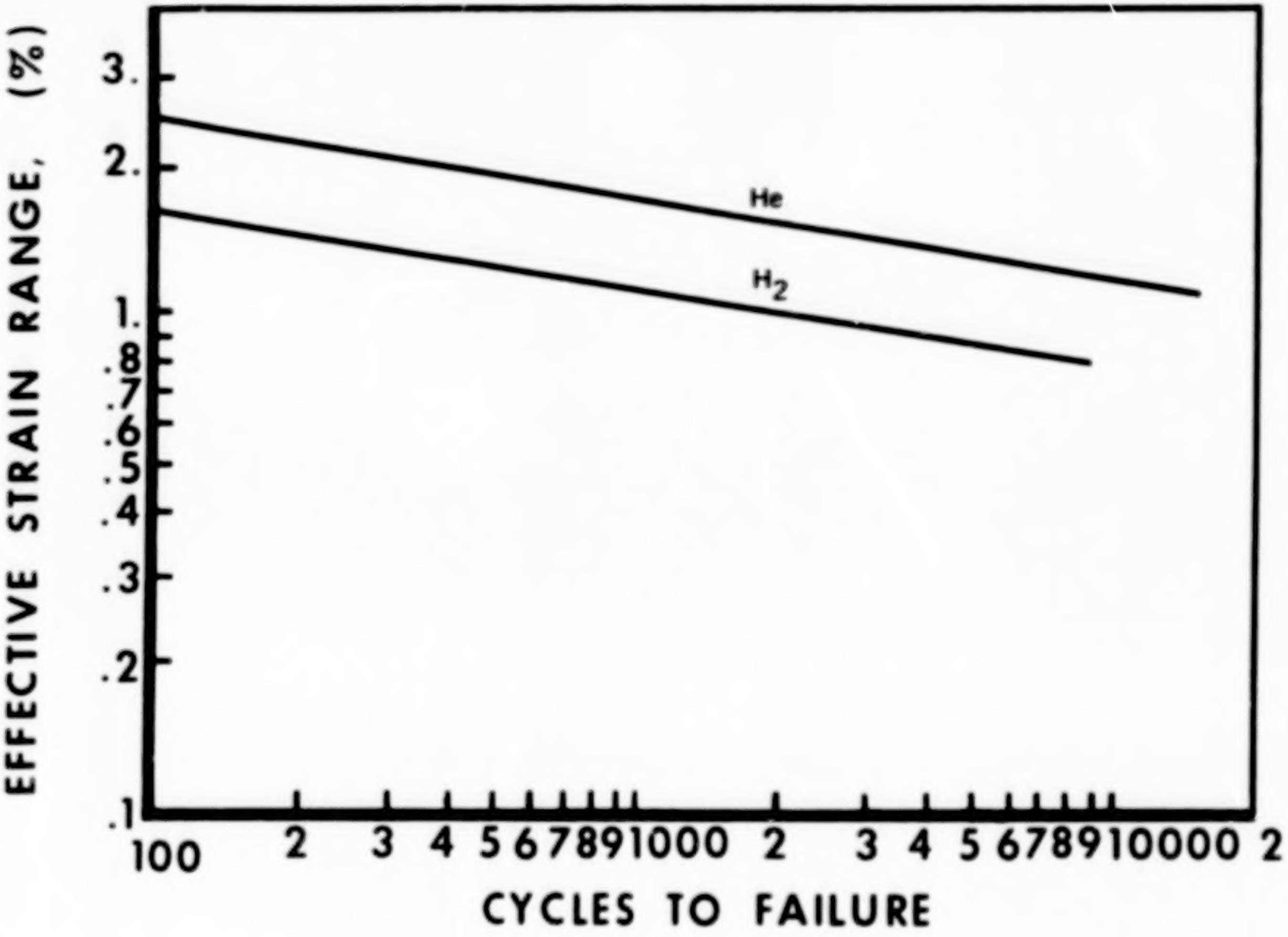

Figure 17

CREEP OF A-286

(Figure 18)

Harris and Van Wanderham (ref. 3) found degradation of the stress-rupture life by hydrogen environments for a number of nickel- and iron-base alloys. Their test results for A-286 stainless steel tested in 34.5 MN/m^2 (5000 psi) hydrogen and helium environments at 950 K (1250 F) are shown in the figure and the large effect of the hydrogen environment on the creep rate and stress-rupture life is very evident. It is interesting to note that the ambient temperature tensile properties of A-286 stainless steel are not reduced by exposure to high-pressure hydrogen environments (Fig. 14). This shows the importance of performing the test (or tests) appropriate to a given application in hydrogen and that it is not possible to draw conclusions as to the effect of hydrogen on one property from the effect of hydrogen on different properties.

CREEP OF A-286

34.5MN/m_2 (5,000 psi), 950K(1250F)

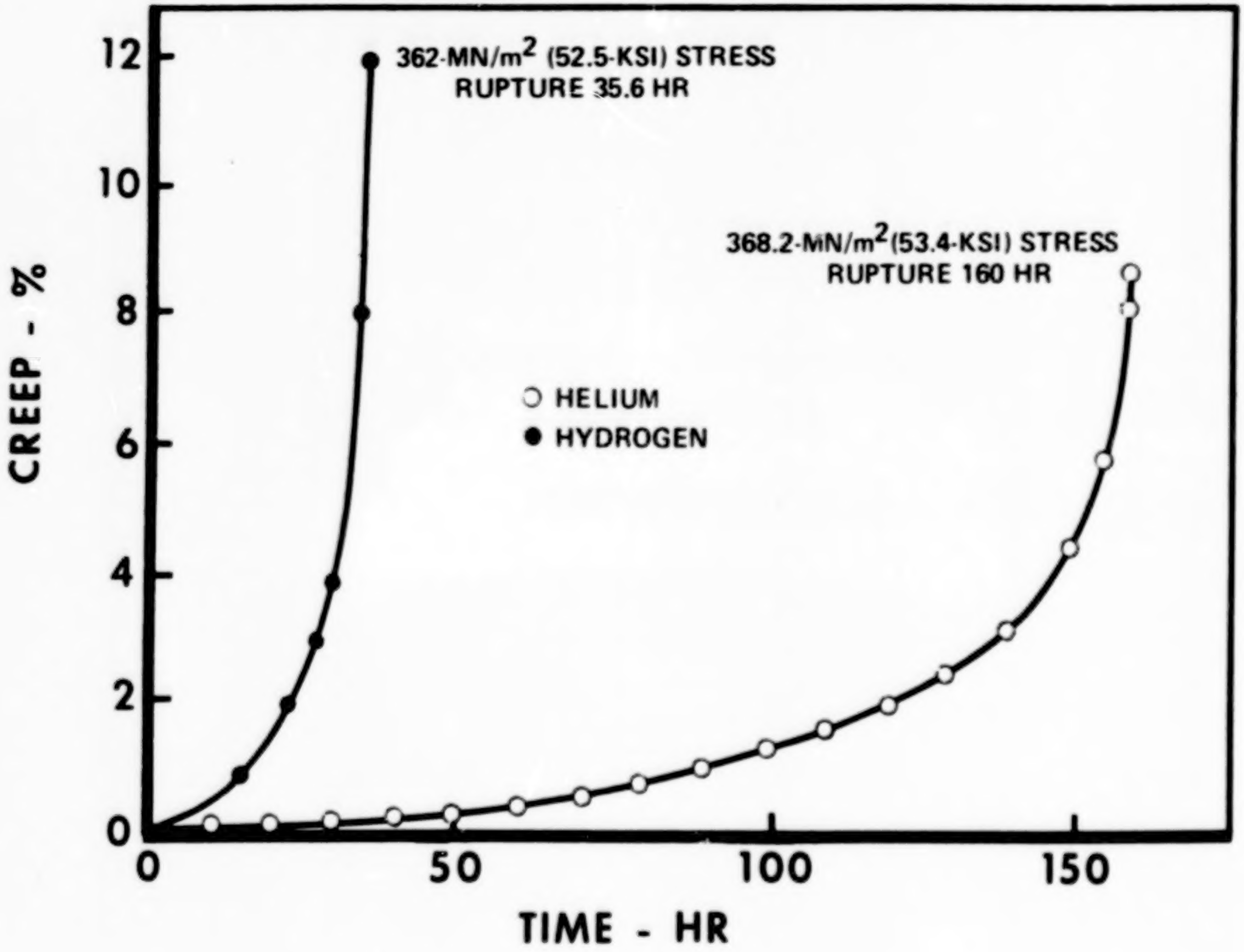

Figure 18

da/dN AS A FUNCTION OF CYCLE DURATION

(Figure 19)

The most significant effect of hydrogen environments on metals is on crack initiation and propagation. Therefore, fracture mechanics, which is the study of crack behavior, is a valuable approach to be applied, where feasible, to life verification of components of hydrogen systems. Such an analysis requires data on threshold stress intensity (K_{TH}) and cyclic-load crack growth rates (da/dN) in hydrogen under appropriate conditions. From this data, the acceptable initial crack size, i.e., the crack size that will not propagate to failure during service, can be established. Then, nondestructive inspection or proof tests are used to confirm that any cracks present are smaller than the acceptable size.

The da/dN is greatly influenced by the nature of the loading cycle applied to a metal and this is particularly true for da/dN in hydrogen for metals susceptible to hydrogen-environment embrittlement. A program was conducted at Rocketdyne to determine the effect of high-pressure hydrogen on da/dN in ASME SA-105 Grade II steel, a plain carbon steel (ref. 9). This steel was in use in a compressor used to pressurize hydrogen for rocket engine testing. As a part of the program, the effect of cycle duration on da/dN in hydrogen was determined. The results are shown in the figure for two stress intensity ranges (ΔK). It can be seen that for shorter time cycles there is a large effect of cycle duration on da/dN but the effect appears to "saturate" at longer times. Thus, da/dN in hydrogen to be used in fracture mechanics analysis must be determined with a loading cycle in hydrogen which simulates as closely as possible service loading conditions or a program must be conducted for each of the metals of interest to establish simpler, for example, shorter, cycles which adequately simulate services conditions.

da/dN AS A FUNCTION OF CYCLE DURATION

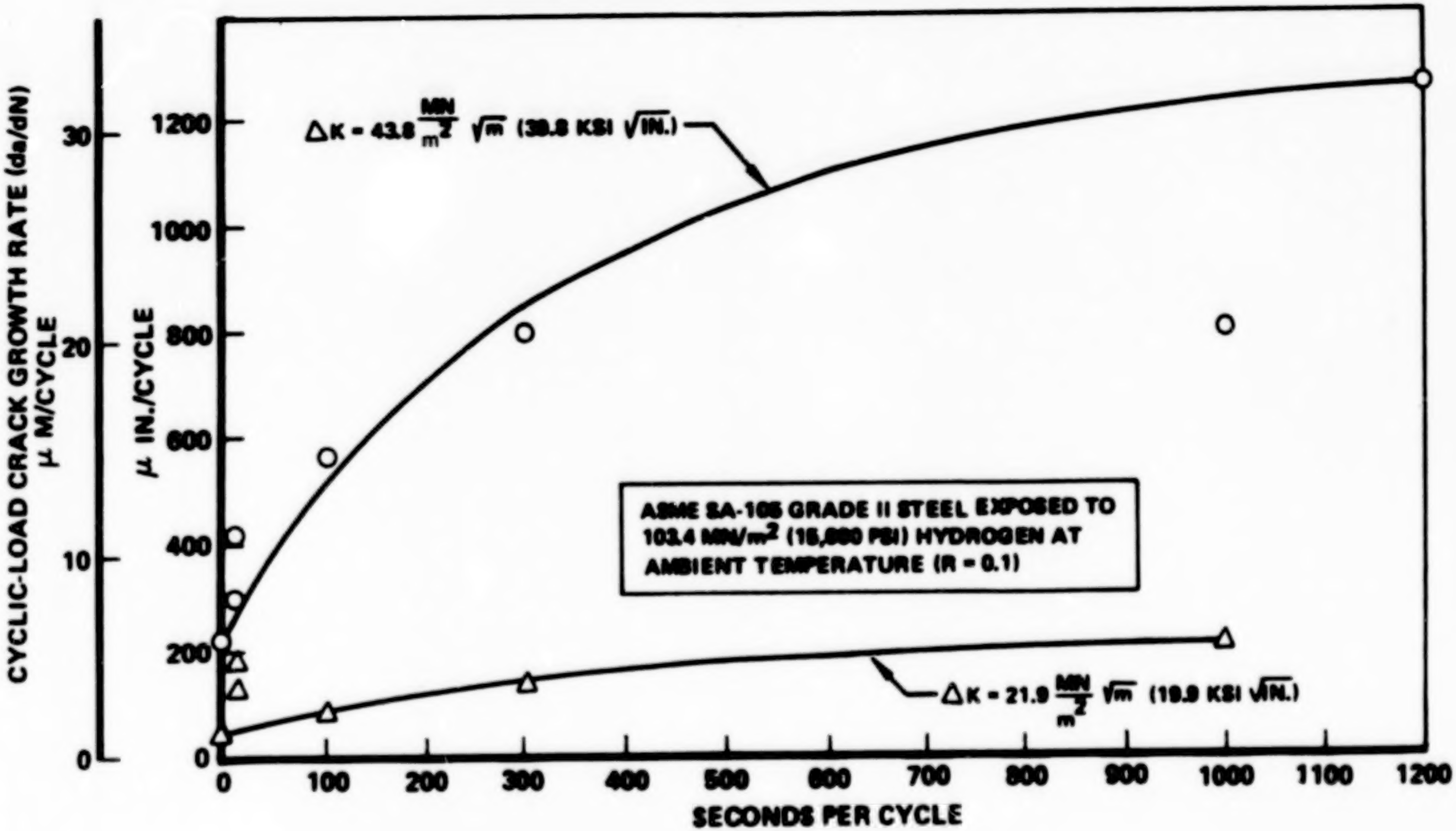

Figure 19

233

234

SIMULATED SSME LOAD-TIME CYCLE

(Figure 20)

Under the SSME program, cyclic-load crack growth rate (da/dN) tests are being conducted in support of fracture life verification analyses of all fracture critical parts, most of which are operating in contact with high-pressure hydrogen. The da/dN tests are being performed utilizing a cycle, nearly 9 minutes long, that simulates the SSME operating cycle. The load-time profile is shown in the figure. The long cycle time required to simulate the SSME engine cycle results in very long test times.

SIMULATED SSME LOAD—TIME CYCLE

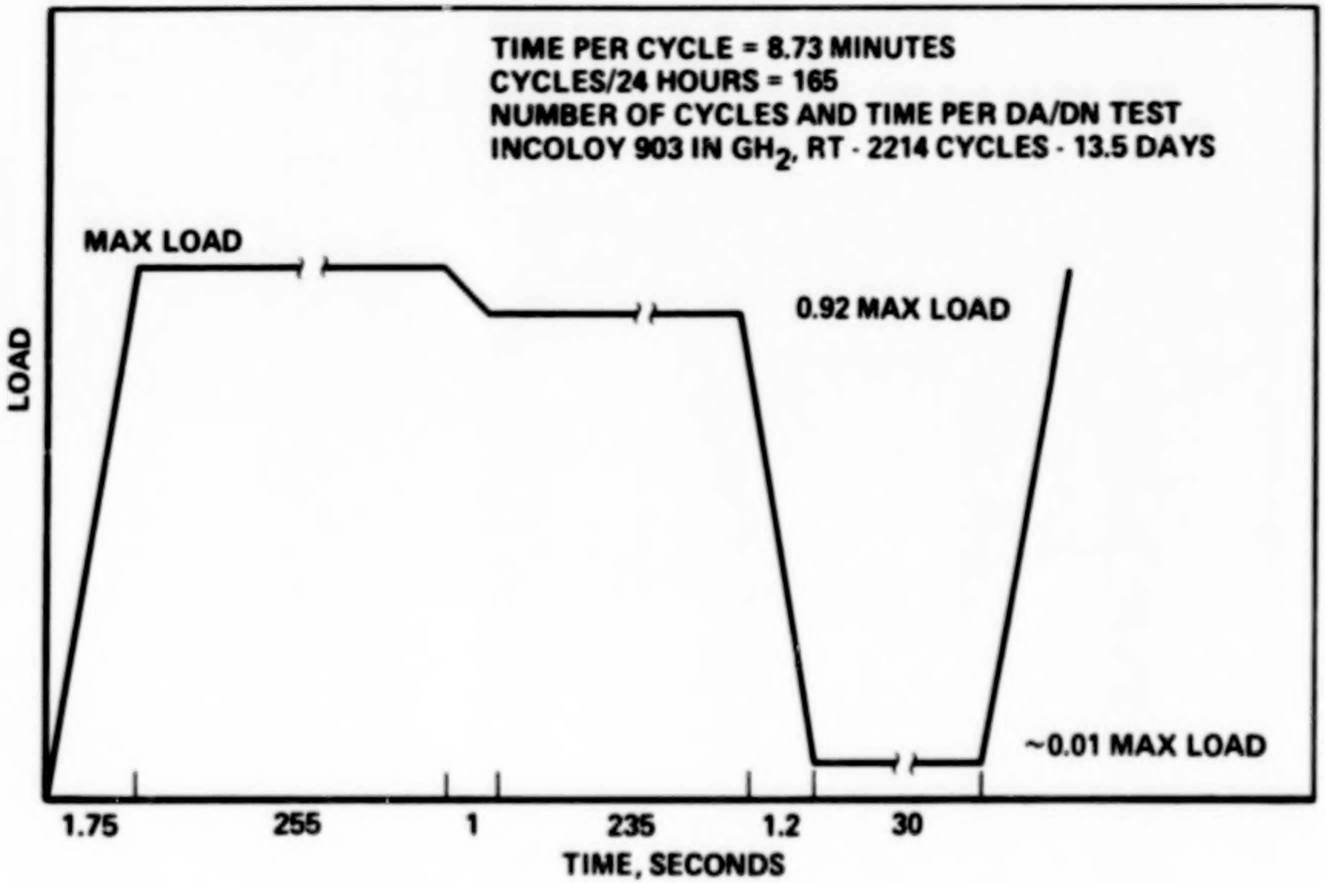

TIME PER CYCLE = 8.73 MINUTES
CYCLES/24 HOURS = 165
NUMBER OF CYCLES AND TIME PER DA/DN TEST
INCOLOY 903 IN GH_2, RT - 2214 CYCLES - 13.5 DAYS

Figure 20

EFFECT OF 34.5 MN/m^2 (5000 PSI) H_2 ON da/dN IN INCONEL 718

(Figure 21)

The most extensive investigations of da/dN in hydrogen for the SSME were conducted on Inconel 718. The da/dN in Inconel 718 was determined for forged, cast, and welded material with da/dN being determined for cracks in the weld metal and in the heat-affected zone (HAZ) for both as-welded and heat treated welds. Some of the results are presented in the figure. The weld and HAZ results are for heat-treated welds. The large effect of hydrogen on da/dN in Inconel 718 is evident. Somewhat unexpectedly, da/dN in hydrogen was slower in the weld metal and HAZ than in the forged base material.

EFFECT OF 34.5MN/m² (5000psi) H₂ ON da/dN IN INCONEL 718

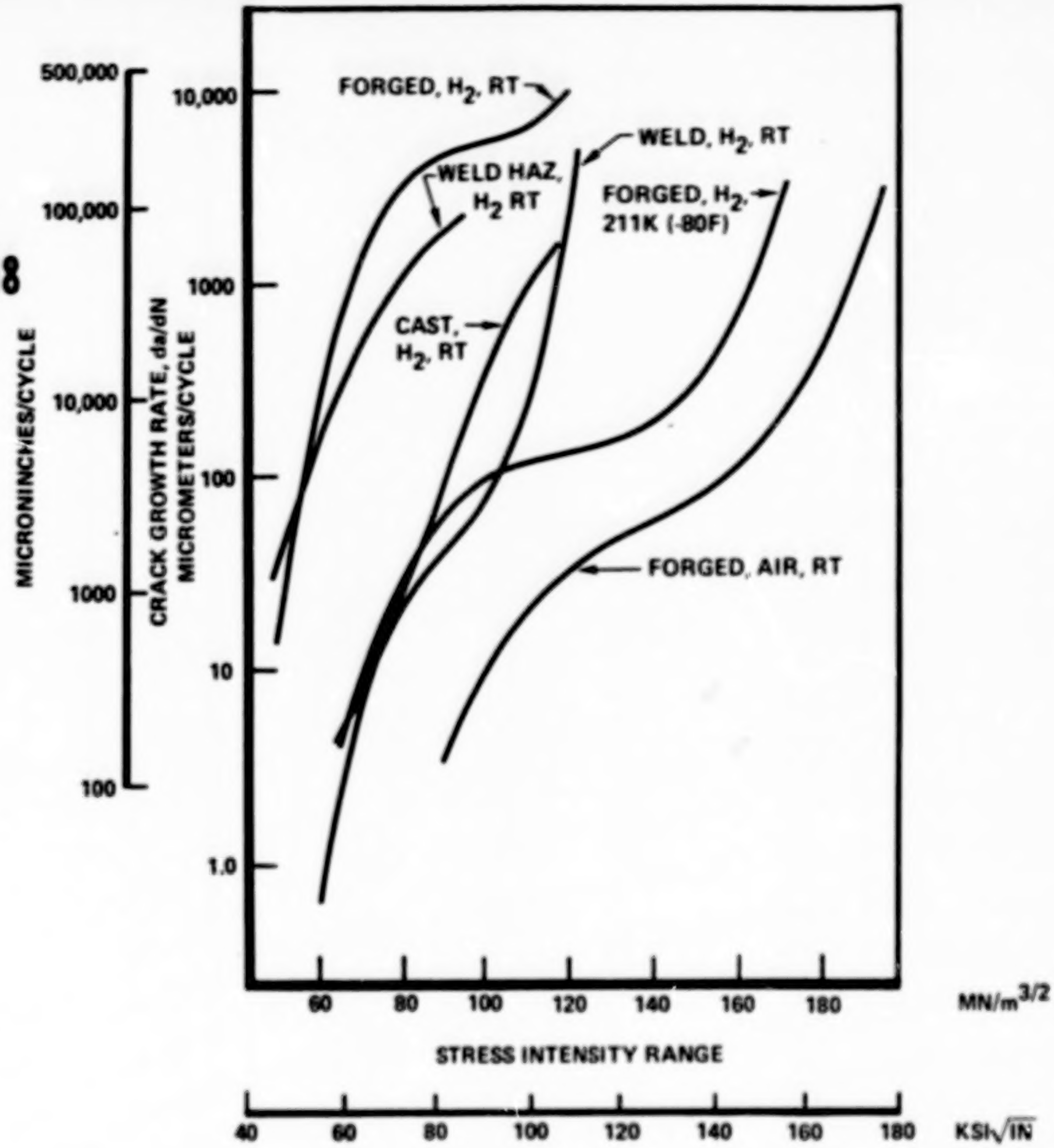

Figure 21

PREVENTION OF HEE

(Figure 22)

Situations can be expected to arise in designing hydrogen components in which a metal has such an attractive combination of properties for a certain application as to dictate its use, but it is quite susceptible to hydrogen-environment embrittlement. The most effective approach may then be to use that metal and take steps to prevent its embrittlement.

There are two basic methods by which hydrogen-environment embrittlement of susceptible metals can be prevented. One involves the use of additives to the hydrogen to inhibit its embrittling effect and the second involves the use of a barrier or coating so that the hydrogen environment cannot contact the susceptible metal. A successful technique for large, high-pressure hydrogen storage vessels has been the use of a vented liner of a nonsusceptible metal (austenitic stainless steel) to protect the load-carrying structural steel which is susceptible to hydrogen-environment embrittlement. Small holes drilled through the structural steel vent out to the atmosphere any hydrogen that diffuses through the liner. Thus, 11 large vessels made of ASTM A-533-B steel (see Figs. 5 and 12)were lined with stainless steel for the storage of hydrogen at 96.5 MN/m^2 (14,000 psi) for SSME testing at Rocketdyne.

PREVENTION OF HEE

- INHIBITION

- VENTED LINER

- COATINGS AND OVERLAYS

Figure 22

da/dN IN HP 9-4-20 STEEL IN VARIOUS ENVIRONMENTS AT ROOM TEMPERATURE

(Figure 23)

As yet, no use of inhibition to prevent hydrogen-environment embrittlement in a system has been reported. The inhibiting effects of oxygen were shown in Figure 8. Studies of the inhibiting effects of other gas species have been limited. Results from one such investigation conducted at the Rockwell International Science Center are shown in the figure (ref. 10). In these tests, the hydrogen pressure was low, 13 KN/m^2 (1.9 psi), and the partial pressure of the inhibiting gas was the same.

Liu, et al. (ref. 11) investigated the influence of inhibitors on the effect of 1 atmosphere pressure hydrogen on crack growth in SAE 4340 steel and found that the introduction of 0.5% SO_2 into the hydrogen would stop a running crack. However, in tensile tests on notched specimens of SAE 4340 steel in 48.3 MN/m^2 (7000 psi) hydrogen at Rocketdyne (ref. 12), it was found that the inhibiting effect of essentially the same concentration of SO_2 was small, the N_{H_2}/N_{He} ratio was 0.23 in hydrogen and 0.33 in the hydrogen containing SO_2. Thus, again, if one wishes to consider prevention of hydrogen-environment by inhibition, it will be necessary to conduct tests on the effect of the inhibitor using temperature, hydrogen pressure, and stressing conditions that properly simulate service conditions.

da/dN IN HP 9-4-20 STEEL IN VARIOUS ENVIRONMENTS AT ROOM TEMPERATURE

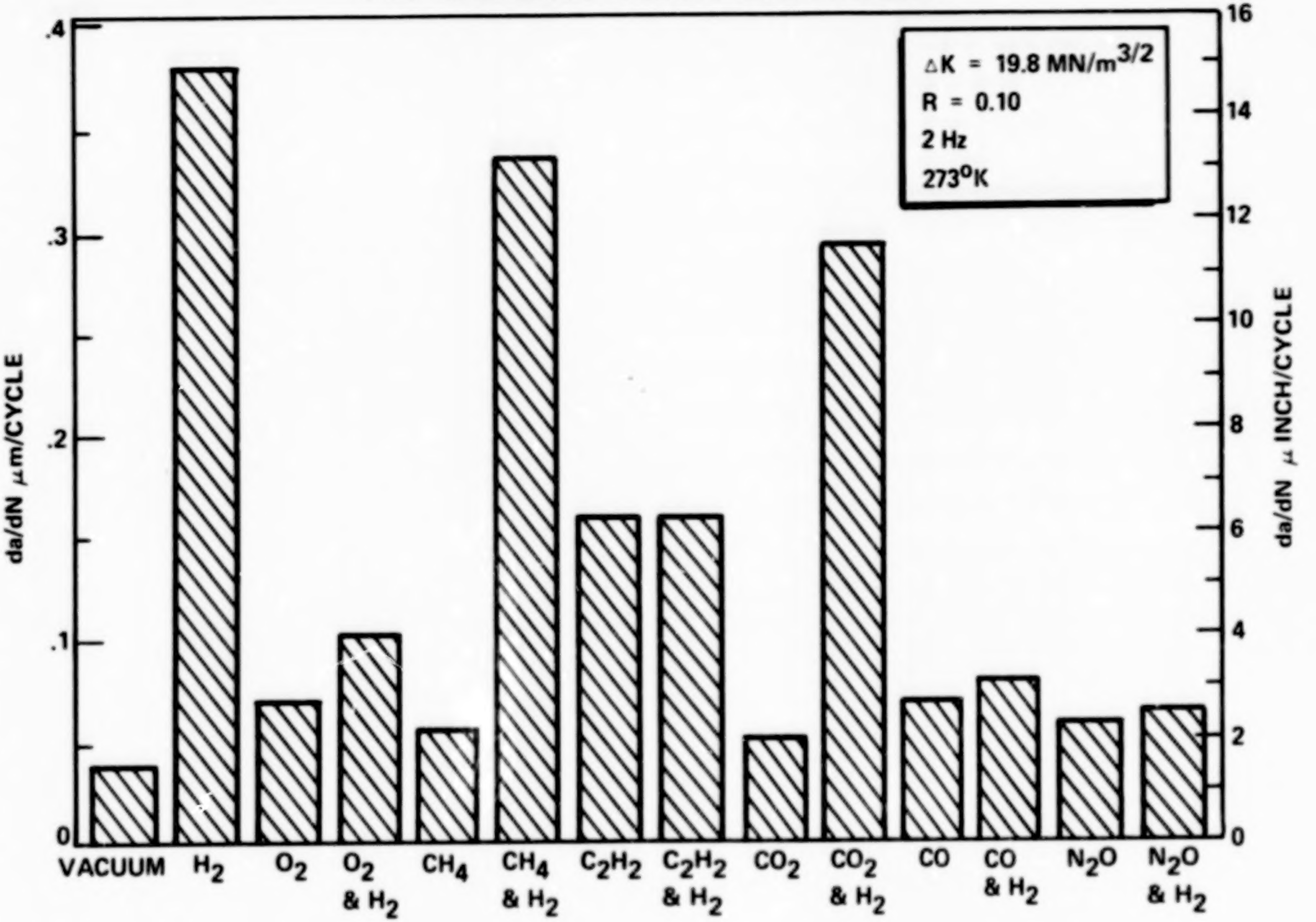

Figure 23

MACROGRAPHS OF EDNi

(Figure 24)

Extensive investigations have been conducted at Rocketdyne on the use of coatings to prevent or reduce hydrogen-environment embrittlement. It has been noted that hydrogen-environment embrittlement occurs only when the metal is plastically deformed (including that at the tip of notches or cracks) in hydrogen. It follows that any coating for the prevention of this embrittlement must be effective during plastic deformation of the metal to be protected. Investigations at Rocketdyne have shown copper and gold coatings to be effective in preventing embrittlement of susceptible metals by high-pressure hydrogen as is evident from the macrographs shown in the figure. The uncoated EDNi specimen tensile tested in hydrogen has a very brittle appearing fracture while the two specimens coated with copper and gold have the same very ductile appearance as the specimen tested in helium.

Because EDNi is considerably affected by hydrogen (see Fig. 11), the EDNi in the SSME is protected from hydrogen by a layer of electrodeposited copper (EDCu). To confirm the effectiveness of EDCu to protect EDNi, a series of burst, sustained, and cyclic pressure tests were performed on slotted specimens designed to simulate the combustion chamber coolant passages. The results of these tests have been reported elsewhere (ref. 8).

MACROGRAPHS OF EDNi

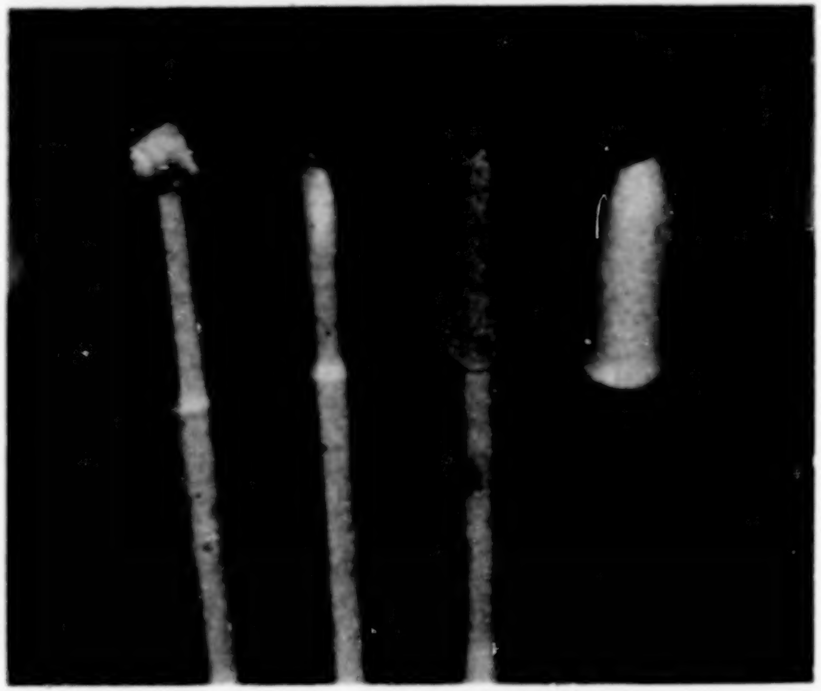

1. AS DEPOSITED, TESTED IN 8.3 MN/m^2 (1200 PSI) HYDROGEN AT AMBIENT TEMPERATURE
2. AS DEPOSITED, TESTED IN 8.3 MN/m^2 (1200 PSI) HELIUM AT AMBIENT TEMPERATURE
3. COPPER PLATED, AS DEPOSITED, TESTED IN 8.3 MN/m^2 (1200 PSI) HYDROGEN AT AMBIENT TEMPERATURE
4. GOLD PLATED, AS DEPOSITED, TESTED IN 8.3 MN/m^2 (1200 PSI) HYDROGEN AT AMBIENT TEMPERATURE

Figure 24

LCF AT RT OF EDCu AND BARE- AND Cu-COATED INCONEL 718, STA (R = -1, Hz = 0.5)

(Figure 25)

In certain locations in the SSME, Inconel 718 is protected from the hydrogen environment by EDCu. Tensile tests on unnotched specimens showed that the copper-coated Inconel 718 specimens had the same ductility in hydrogen as in helium provided that the copper was at least 38 µm (0.0015 inch) thick for specimens given the Inconel 718 STA (solution treated and aged) heat treatment after copper plating or at least 76 µm (0.003 inch) thick for specimens heat treated before plating.

However, the protection afforded Inconel 718 in low-cycle fatigue (LCF) tests was found to depend on the strain range as shown in the figure. The copper coating appears to improve low cycle fatigue life only for strain ranges above 1 percent. This is because the copper basically has poorer low cycle fatigue properties than Inconel 718 at the lower strain ranges. That is, the copper fails first because of low-cycle fatigue thus exposing the Inconel 718 to hydrogen. Fortunately, copper does afford protection at the strain ranges above 1 percent, which are the strain ranges for which protection is required in the SSME. The cycle life requirement of the SSME is 60 cycles and to provide a factor of safety it is designed to a cyclic life of 240 cycles. But again, these results show the importance of conducting tests in hydrogen which simulate service conditions.

LCF AT RT OF ED Cu AND BARE AND Cu COATED INCONEL 718, STA (R=–1,Hz=0.5)

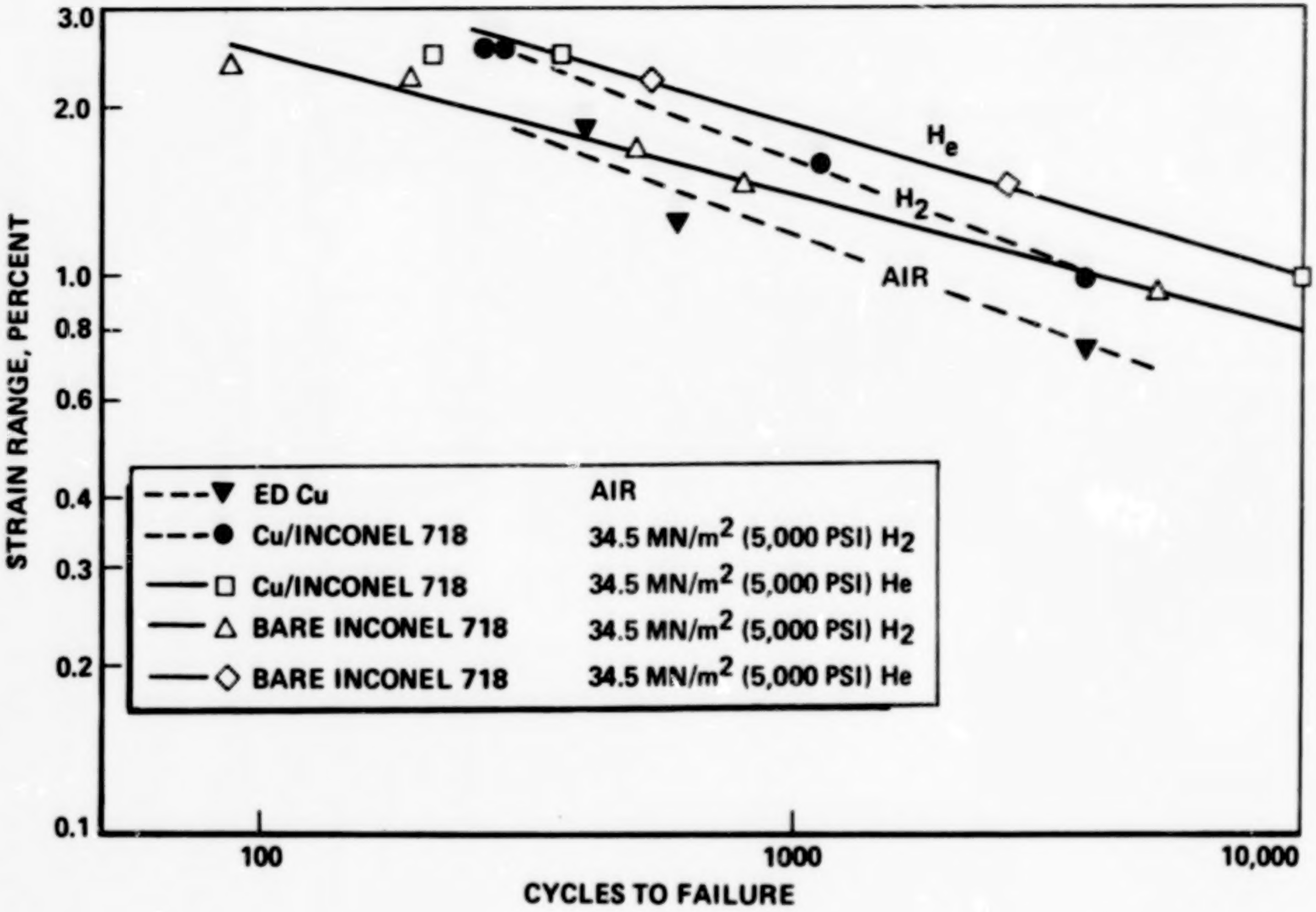

Figure 25

246

EFFECT OF H_2 ON da/dN IN INCONEL 718 WELDS AND ALLOY 903 OVERLAY AT RT

(Figure 26)

In the SSME, the Inconel 718 welds exposed to hydrogen are protected from the hydrogen. In some cases, the completed weld is copper plated but the majority of welds requiring protection are protected by using a weld overlay, with Alloy 903 (see Fig. 11) being the overlay alloy most often used. The surfaces that will be in contact with hydrogen on each of the two Inconel 718 pieces to be joined are covered with the weld overlay alloy for a distance of at least 1.27 cm (1/2 inch) from the joint surface. The overlayed pieces are then machined so that when fitted together the overlay material overlaps the Inconel 718 weld joint and the weld bottoms in the overlay material. Thus, in the weld area only the overlay material contacts the hydrogen. As required, the hydrogen exposed Inconel 718 is plated with copper up to the overlay material prior to welding.

To confirm that the weld overlay concept is effective, cyclic-load crack growth rate (da/dN) tests were conducted in hydrogen on specimens prepared to simulate the welds in Inconel 718 with the weld overlay. The results of such tests for weld overlay of Alloy 903 are shown in the figure. It can be seen that da/dN in the Alloy 903 overlay is much slower than in the Inconel 718 weld metal or heat-affected zone and approximately the same as for Inconel 718 tested in air.

EFFECT OF H_2 ON da/dn IN INCONEL 718 WELDS AND ALLOY 903 OVERLAY AT RT

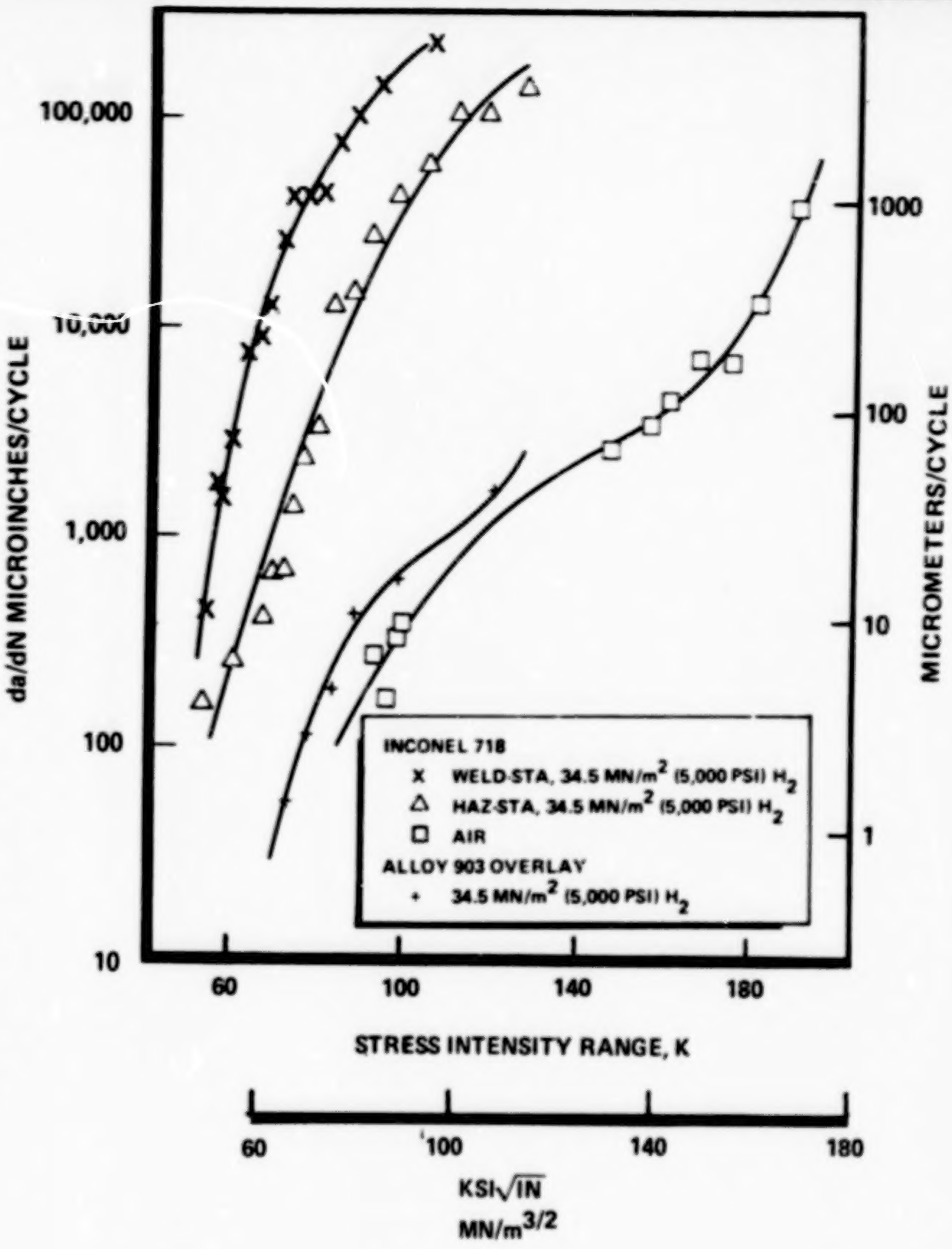

Figure 26

248

SUMMARY

To summarize, in designing components of hydrogen systems, the conditions of hydrogen exposure are analyzed to determine if hydrogen-environment embrittlement is a potential problem. If it is, then, if possible, metals not susceptible to hydrogen-environment embrittlement are used. If susceptible metals must be used, good design and production processes are especially important. Notches and stress concentrations are reduced and, if possible, eliminated and surface finishes are tightly controlled. The least susceptible condition of the metal is used. Where possible, parts are designed so that susceptible metals are not plastically deformed in hydrogen. Properties used in design are based on tests (e.g., tensile, fatigue, creep, and fracture mechanics) performed in hydrogen under conditions simulating service conditions. If required, liners or coatings are used to protect susceptible metals from the hydrogen environment.

ACKNOWLEDGMENTS

The following personnel (listed alphabetically) made major contributions to the hydrogen-environment embrittlement test programs conducted at Rocketdyne: D. A. Bowman, G. E. Dyer, R. P. Jewett, A. F. Konigsfeld, M. C. Metcalf, A. R. Murphy, R. M. Parker, D. A. Pearson, S. L. Pendleberry, R. F. Rothring, and R. J. Walter.

REFERENCES

1. Jewett, R. P., R. J. Walter, W. T. Chandler, and R. P. Frohmberg, "Hydrogen-Environment Embrittlement of Metals," A NASA Technology Survey, NASA CR-2163, March 1973.

2. Walter, R. J. and W. T. Chandler, Influence of Gaseous Hydrogen on Metals - Final Report, Rockwell International/Rocketdyne Division, Canoga Park, California. Prepared for the National Aeronautics and Space Administration, NASA CR-124410, October 1973.

3. Harris, J. A., Jr. and M. C. Van Wanderham, Properties of Materials in High-Pressure Hydrogen at Cryogenic, Room, and Elevated Temperatures, Final Report on NASA Contract NAS8-26191, Pratt & Whitney Aircraft Florida Research and Development Center, West Palm Beach, Florida, Report No. FR-5768, 31 July 1973.

4. Hofmann, W. and W. Rauls, "Ductility of Steel Under the Influence of External High-Pressure Hydrogen," Welding Journal, Vol. 44, pp 225s-230s (1965).

5. Chandler, W. T. and R. J. Walter, "Hydrogen-Environment Embrittlement Experimental Considerations," Proceedings of Symposium on Experimental Aspects of Corrosion Control, sponsored by the Southern California-Nevada Section of the Electrochemical Society and the Corrosion Panel of the North American Aerospace and Electronics Group, Rockwell International, 7 December 1973, pp 41-88.

6. Thompson, Anthony W., "Stainless Steels in High-Pressure Hydrogen," Handbook of Stainless Steels, Donald Peckner and I. M. Bernstein, Eds., McGraw Hill Book Company, 1977, pp 46, 1-8.

7. Walter, R. J. and W. T. Chandler, "Influence of Gaseous Hydrogen on Inconel 718," Hydrogen in Metals, edited by I. M. Bernstein and Anthony W. Thompson, American Society of Metals, Metals Park, Ohio, 1973, pp 515-525.

8. Chandler, W. T., R. J. Walter, C. E. Moeller, and H. W. Carpenter, "Effect of High-Pressure Hydrogen on Electrodeposited Nickel," Plating and Surface Finishing, Vol. 65, No. 5, May 1978, pp 63-70.

9. Walter, R. J. and W. T. Chandler, "Cyclic-Load Crack Growth in ASME SA-105 Grade II Steel in High Pressure Hydrogen at Ambient Temperature," Effect of Hydrogen on Behavior of Metals, Anthony W. Thompson and I. M. Bernstein, Eds., The Metallurgical Society of AIME, 1976, pp 273-286.

10. Frandsen, J. D. and H. L. Marcus, "Environmentally Assisted Fatigue Crack Propagation in Steel," Met. Trans. A, Vol. 8A, February 1977, pp 265-277.

11. Liu, H. W., Ya-Lung Hu, and P. J. Ficalora, "The Control of Catalytic Poisoning and Stress Corrosion Cracking," Journal Eng. Frac. Mech., Vol. 5, June 1973, pp 281-292.

12. Jacobs, A. J. and W. T. Chandler, "Inhibition of Hydrogen Environment Embrittlement by SO_2," Scripta Metallurgica, Vol. 9, 1975, pp 767-769.

D50

BLANK PAGE

SESSION III - COOLED AIRFRAME STRUCTURES

BLANK PAGE

CONTENTS

Part I

PREFACE . . . . iii 1/A5

WELCOME 1 1/A10
R. R. Heldenfels

SESSION I - OVERVIEWS
Chairman: A. J. Henderson

1. HYPERSONIC STRUCTURES: AN AERODYNAMICIST'S PERSPECTIVE (OR ONE MAN'S DREAM IS ANOTHER MAN'S NIGHTMARE) 5 1/B1
J. D. Watts, L. R. Jackson, and J. L. Hunt

2. STRUCTURAL REQUIREMENTS FOR MILITARY HYPERSONIC SYSTEMS (Paper not available for publication)
P. Lane

3. AIRFRAME-INTEGRATED PROPULSION SYSTEM FOR HYPERSONIC CRUISE VEHICLES 39 1/F13
Robert A. Jones and Paul W. Huber

4. RECENT ADVANCES IN CONVECTIVELY COOLED ENGINE AND AIRFRAME STRUCTURES FOR HYPERSONIC FLIGHT 47 1/G7
H. Neale Kelly, Allan R. Wieting, Charles P. Shore, and Robert J. Nowak

SESSION II - ENGINE STRUCTURES
Chairman: H. N. Kelly

5. DESIGN AND ANALYSIS OF A SCRAMJET ENGINE 65 2/A13
O. A. Buchmann

6. THERMOSTRUCTURAL ANALYSIS OF A SCRAMJET FUEL-INJECTION STRUT 119 3/B11
Allan R. Wieting and Earl A. Thornton

7. ADVANCED FABRICATION TECHNIQUES FOR COOLED ENGINE STRUCTURES 145 3/F7
O. A. Buchmann

8. HYDROGEN EMBRITTLEMENT AND ITS CONTROL IN HYDROGEN-FUELED ENGINE SYSTEMS 195 4/F11
W. T. Chandler

9. CARBON-CARBON COMPOSITE APPLICATION FOR INTEGRAL ROCKET RAMJET COMBUSTORS (Paper not available for publication)
H. A. Holman

SESSION III - COOLED AIRFRAME STRUCTURES
Chairman: C. P. Shore

10. DESIGN AND FABRICATION OF A SKIN STRINGER DISCRETE TUBE ACTIVELY COOLED STRUCTURAL PANEL 253 6/A5
Frank M. Anthony

11. DESIGN AND ANALYSIS OF A PLATE-FIN SANDWICH ACTIVELY COOLED STRUCTURAL PANEL 319 7/C13
L. M. Smith

12. FLUXLESS BRAZING AND HEAT TREATMENT OF A PLATE-FIN SANDWICH ACTIVELY COOLED PANEL 375 8/E1
Charles S. Beuyukian

13. DESIGN AND FABRICATION OF A RADIATIVE ACTIVELY COOLED HONEYCOMB SANDWICH PANEL 449 10/A13
Leland C. Koch

14. RADIATIVE, ACTIVELY COOLED PANEL TESTS RESULTS 493 11/A5
Charles P. Shore, Robert J. Nowak, and Ellsworth L. Sharpe

BLANK PAGE

DESIGN AND FABRICATION OF A SKIN STRINGER DISCRETE TUBE ACTIVELY COOLED STRUCTURAL PANEL*

Frank M. Anthony
Bell Aerospace Textron
Buffalo, N.Y.

INTRODUCTION

A number of structural concepts have been proposed and investigated for hypersonic aircraft. When such aircraft are powered by hydrogen fueled advanced airbreathing engines the heat capacity of the fuel exceeds engine cooling requirements. The excess provides an attractive heat sink for actively cooled airframe structure. Analytical studies of a hypersonic transport indicated a potentially large weight reduction if liquid cooled aluminum alloy construction could be used. Consequently, the Langley Research Center of NASA initiated several programs (Ref. 1) to investigate the design optimization and practical implementation of actively cooled structural panel concepts.

---

*This paper reviews the work performed on one particular concept by Bell Aerospace Textron under Contract NAS 1-12806. The design of the test panel resulting from this effort was derived from the optimized design of a full sized panel. The test panel will be delivered soon for experimental evaluation at the Langley Research Center.

SKIN STRINGER DISCRETE TUBE ACTIVELY COOLED STRUCTURAL PANEL

(Figure 1)

The desired actively cooled structural panel consisted of the cooled skin and a substructure whose functions are indicated. Conventional materials were used throughout. The primary load carrying components were fabricated from 2024-T3 aluminum alloy. The 3003-H14 coolant passage tubing was chosen because of its excellent corrosion resistance, workability needed to obtain the desired cross sectional shape, and strength. The Epon 951 adhesive was selected for its excellent structural properties and is the thinnest of available films, 0.064 mm (0.0025 in.). The Eccobond 58C silver filled epoxy was chosen because of its high thermal conductivity, and the alumina filled Epon 828 was chosen for structural and expansion characteristics.

SKIN STRINGER DISCRETE TUBE ACTIVELY COOLED STRUCTURAL PANEL
CONTRACT NAS 1-12806

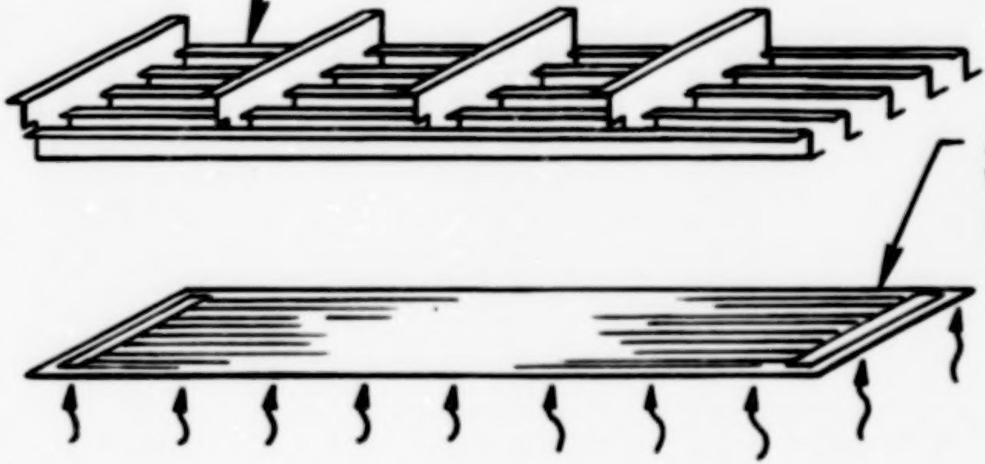

SUBSTRUCTURE
OF STRINGERS AND FRAMES

- SHARES INPLANE LOADS
- PREVENTS PREMATURE BUCKLING
- TRANSFERS SURFACE PRESSURE

2024-T3

ACTIVELY COOLED SKIN
WITH MANIFOLDED DISCRETE
PASSAGES

- ABSORBS HEAT INPUT
- RESISTS SURFACE PRESSURE
- SHARES INPLANE LOADS

2024-T3
3003-H14
EPON-951
ECCOBOND 58C
FILLED EPON 828

Figure 1

256

REDUNDANT COUNTERFLOW COOLANT CIRCUITS ARE USED

(Figure 2)

The preceding figure presented an overview of the cooled structural panel approach. This figure provides details of the coolant circuit within the skin. Two adjacent tubes of a quarter elliptical cross section form the passages through which the coolant flows in opposite directions. The two independent circuits provide redundancy. Coolant is introduced to a multiplicity of parallel paths in each circuit through manifolds at the outer edge of the panel and transverse to the coolant passages. The manifold contains two parallel coolant plenums, the supply for one coolant circuit and the return from the other. Holes through the wall of the plenums connect them to the individual coolant passages.

Concern for damage tolerance led to the investigation of crack arrestors which could be incorporated in the beads which contained the coolant passage tubing. These crack arrestors were evaluated as part of an inhouse program. Their incorporation into a panel of relatively large size posed fabrication difficulties. Therefore, they were excluded from the final test panel even though they had been used for the fatigue test specimens that will be discussed later.

REDUNDANT COUNTERFLOW COOLANT CIRCUITS ARE USED

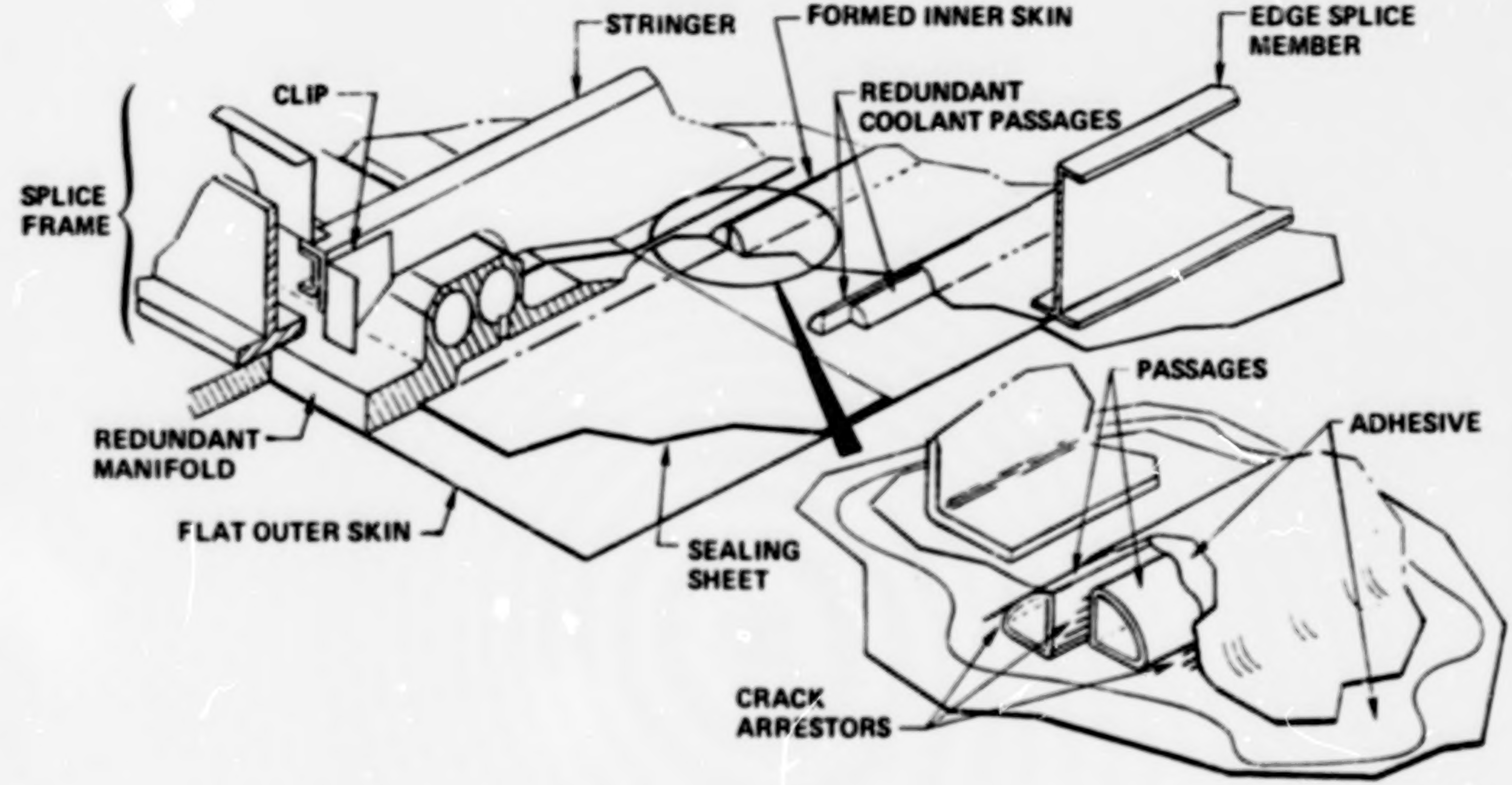
STRINGER
FORMED INNER SKIN
EDGE SPLICE MEMBER
CLIP
REDUNDANT COOLANT PASSAGES
SPLICE FRAME
REDUNDANT MANIFOLD
FLAT OUTER SKIN
SEALING SHEET
PASSAGES
ADHESIVE
CRACK ARRESTORS

Figure 2

258

DESIGN REQUIREMENTS

(Figure 3)

The requirements listed here were considered representative of the lower surface of a hypersonic transport. Local environmental conditions, factors of safety and life related considerations are included. The primary environmental conditions were defined by NASA. Supplementary requirements were introduced by Bell to further specify detailed requirements.

DESIGN REQUIREMENTS

NASA

HEAT FLUX	136 kW/m^2 (12 BTU/ft^{2}sec)
INPLANE LOADING	±210 kN/m (±1200 lb/in.)
PRESSURE LOADING	±6.89 kPa (± 1.0 psi)
DESIGN LIFE	5000 CYCLES
ALUMINUM ALLOY MATERIALS	COMPATIBLE WITH COOLANT
LENGTH AND WIDTH	6.1 x 0.61 m (20 x 2 ft)
FRAME SPACING	0.61 m (2 ft)
OUTLET PRESSURE	345 kPa (50 psi)

BELL

LIFE SCATTER FACTOR		4.0
FACTORS OF SAFETY	LOADS	1.0 LIMIT/1.5 ULTIMATE
	TEMPERATURE	1.0 LIMIT/1.0 ULTIMATE
	PRESSURE ONLY	1.5 PROOF/2.0 ULTIMATE
STRENGTH ALLOWABLES	BASED ON 10,000 HOURS OF EXPOSURE	
REDUNDANT COOLANT CIRCUITS		

Figure 3

260

MANY PARAMETERS INFLUENCE PANEL OPTIMIZATION

(Figure 4)

Optimization of an actively cooled structural panel requires consideration of a large number of parameters which may be grouped into three broad categories, thermal, structural, and environmental. By investigating the relationships among the various parameters, it is possible to define the materials and geometric configuration which result in a cooled panel of minimum mass. For this particular project the environmental conditions were defined. In the general case thermal and structural consideration may modify the environmental aspects through changes to the aircraft or its flight path which minimize total system mass.

MANY PARAMETERS INFLUENCE PANEL OPTIMIZATION

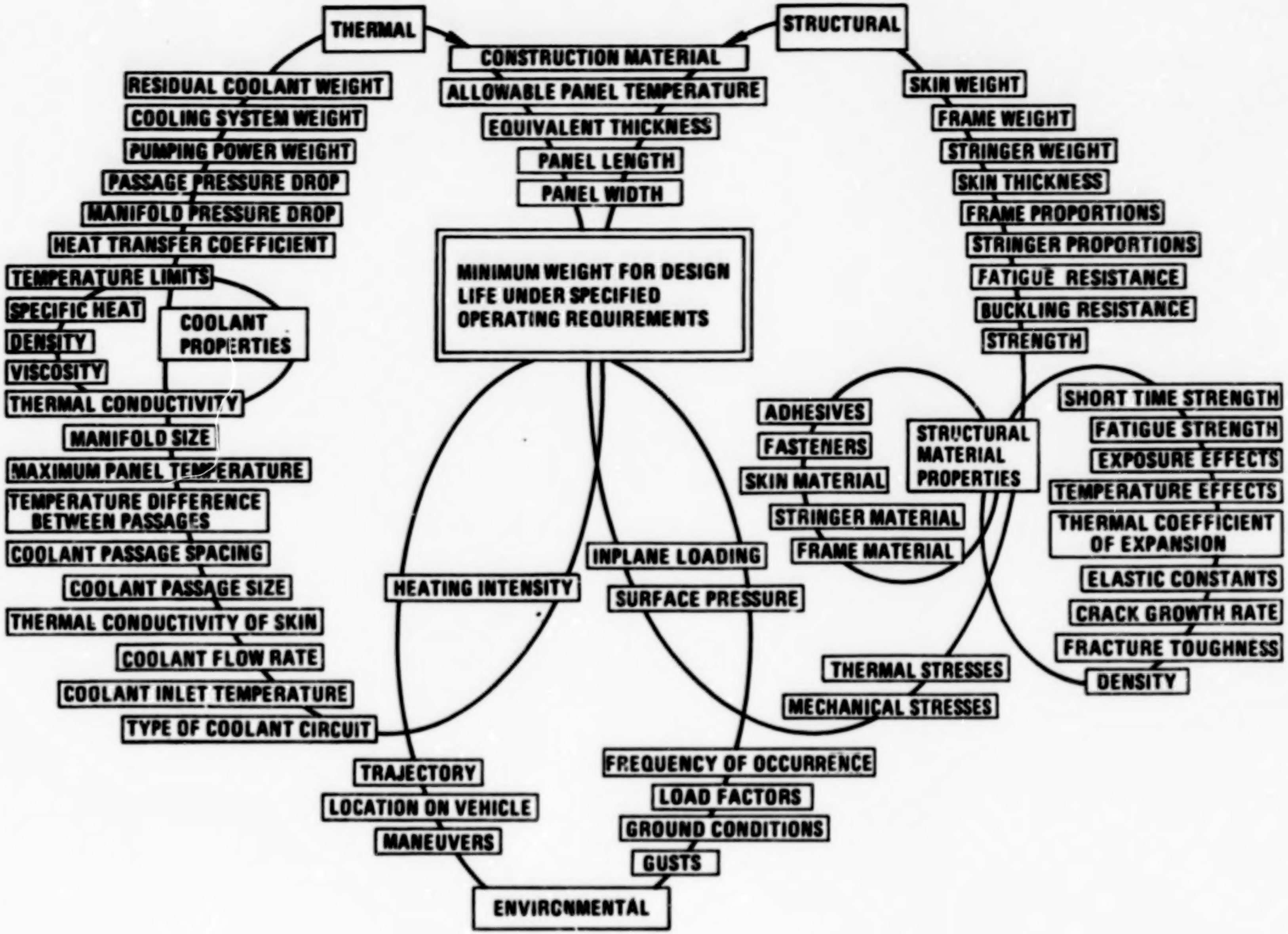
THERMAL
STRUCTURAL
CONSTRUCTION MATERIAL
ALLOWABLE PANEL TEMPERATURE
EQUIVALENT THICKNESS
PANEL LENGTH
PANEL WIDTH
MINIMUM WEIGHT FOR DESIGN LIFE UNDER SPECIFIED OPERATING REQUIREMENTS
RESIDUAL COOLANT WEIGHT
COOLING SYSTEM WEIGHT
PUMPING POWER WEIGHT
PASSAGE PRESSURE DROP
MANIFOLD PRESSURE DROP
HEAT TRANSFER COEFFICIENT
TEMPERATURE LIMITS
SPECIFIC HEAT
DENSITY
VISCOSITY
THERMAL CONDUCTIVITY
COOLANT PROPERTIES
MANIFOLD SIZE
MAXIMUM PANEL TEMPERATURE
TEMPERATURE DIFFERENCE BETWEEN PASSAGES
COOLANT PASSAGE SPACING
COOLANT PASSAGE SIZE
THERMAL CONDUCTIVITY OF SKIN
COOLANT FLOW RATE
COOLANT INLET TEMPERATURE
TYPE OF COOLANT CIRCUIT
SKIN WEIGHT
FRAME WEIGHT
STRINGER WEIGHT
SKIN THICKNESS
FRAME PROPORTIONS
STRINGER PROPORTIONS
FATIGUE RESISTANCE
BUCKLING RESISTANCE
STRENGTH
ADHESIVES
FASTENERS
SKIN MATERIAL
STRINGER MATERIAL
FRAME MATERIAL
STRUCTURAL MATERIAL PROPERTIES
SHORT TIME STRENGTH
FATIGUE STRENGTH
EXPOSURE EFFECTS
TEMPERATURE EFFECTS
THERMAL COEFFICIENT OF EXPANSION
ELASTIC CONSTANTS
CRACK GROWTH RATE
FRACTURE TOUGHNESS
DENSITY
THERMAL STRESSES
MECHANICAL STRESSES
INPLANE LOADING
SURFACE PRESSURE
HEATING INTENSITY
TRAJECTORY
LOCATION ON VEHICLE
MANEUVERS
FREQUENCY OF OCCURRENCE
LOAD FACTORS
GROUND CONDITIONS
GUSTS
ENVIRONMENTAL

Figure 4

262

REPETITION OF DESIGN PROCESS RELATES SKIN TEMPERATURE AND PANEL MASS

(Figure 5)

The iterative sequence for establishing optimum proportions for an actively cooled structural panel is illustrated here. The rectangular boxes define particular steps in the process. The oval boxes identify inputs. In essence a relationship is established between panel mass and maximum operating temperature. The panel mass reflects the material required to carry the structural loadings for the required number of cycles. This mass is distributed in such a way as to maximize the stability characteristics of the panel. The maximum temperature of the panel is controlled by the flow of coolant through passages within the panel so that the total panel weight includes contributions of coolant inventory and Auxiliary Power System mass.

Prior studies indicated that minimum mass is achieved when the equivalent skin thickness is minimized (ref. 2). Therefore, the analysis sequence begins by estimating this parameter from loading and material property data.

REPETITION OF DESIGN PROCESS RELATES SKIN TEMPERATURE AND PANEL MASS

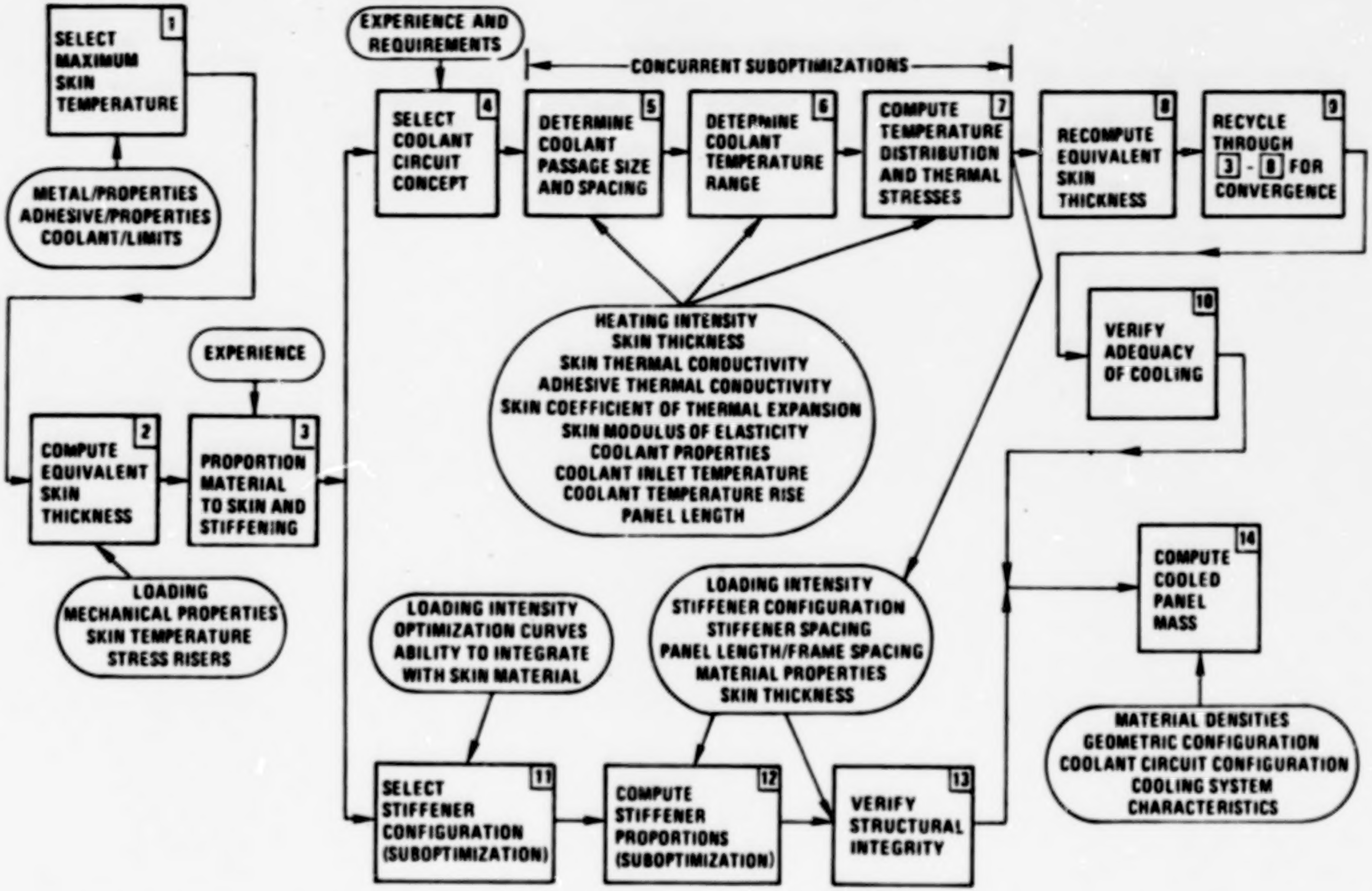
1 SELECT MAXIMUM SKIN TEMPERATURE
METAL/PROPERTIES ADHESIVE/PROPERTIES COOLANT/LIMITS
EXPERIENCE AND REQUIREMENTS
CONCURRENT SUBOPTIMIZATIONS
4 SELECT COOLANT CIRCUIT CONCEPT
5 DETERMINE COOLANT PASSAGE SIZE AND SPACING
6 DETERMINE COOLANT TEMPERATURE RANGE
7 COMPUTE TEMPERATURE DISTRIBUTION AND THERMAL STRESSES
8 RECOMPUTE EQUIVALENT SKIN THICKNESS
9 RECYCLE THROUGH 3 - 8 FOR CONVERGENCE
HEATING INTENSITY SKIN THICKNESS SKIN THERMAL CONDUCTIVITY ADHESIVE THERMAL CONDUCTIVITY SKIN COEFFICIENT OF THERMAL EXPANSION SKIN MODULUS OF ELASTICITY COOLANT PROPERTIES COOLANT INLET TEMPERATURE COOLANT TEMPERATURE RISE PANEL LENGTH
EXPERIENCE
2 COMPUTE EQUIVALENT SKIN THICKNESS
3 PROPORTION MATERIAL TO SKIN AND STIFFENING
10 VERIFY ADEQUACY OF COOLING
LOADING MECHANICAL PROPERTIES SKIN TEMPERATURE STRESS RISERS
LOADING INTENSITY OPTIMIZATION CURVES ABILITY TO INTEGRATE WITH SKIN MATERIAL
LOADING INTENSITY STIFFENER CONFIGURATION STIFFENER SPACING PANEL LENGTH/FRAME SPACING MATERIAL PROPERTIES SKIN THICKNESS
14 COMPUTE COOLED PANEL MASS
MATERIAL DENSITIES GEOMETRIC CONFIGURATION COOLANT CIRCUIT CONFIGURATION COOLING SYSTEM CHARACTERISTICS
11 SELECT STIFFENER CONFIGURATION (SUBOPTIMIZATION)
12 COMPUTE STIFFENER PROPORTIONS (SUBOPTIMIZATION)
13 VERIFY STRUCTURAL INTEGRITY

Figure 5

COOLANT CIRCUIT CONCEPTS

(Figure 6)

Coolant can be distributed through the structural panel in a number of ways. For purposes of this design, the discrete coolant passage approach was selected because of its greater ease of integration with conventional construction techniques and the potential for minimum mass as indicated by prior studies (ref. 3).

Two versions of discrete passages were considered, the single passage/single pass approach and the counterflow/dual passage redundant arrangement. The latter was chosen because of its ability to provide a more uniform temperature distribution over the panel surface and the redundancy feature which would be desirable under emergency conditions.

COOLANT CIRCUIT CONCEPTS

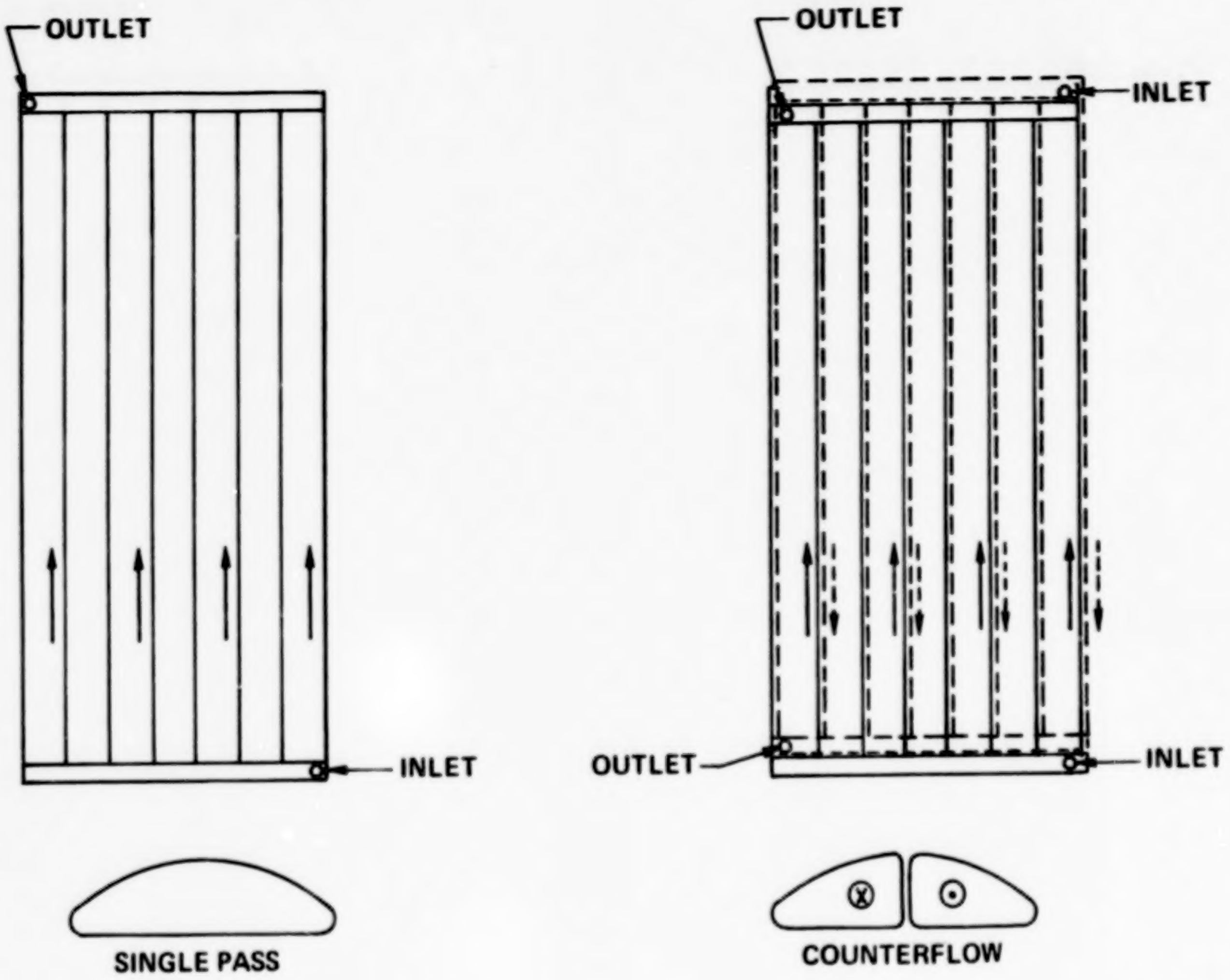
OUTLET
INLET
SINGLE PASS
OUTLET
INLET
OUTLET
INLET
COUNTERFLOW

Figure 6

COUNTERFLOW OF COOLANT MINIMIZES AXIAL TEMPERATURE DIFFERENCES

(Figure 7)

The temperature distributions in cooled panels which incorporate counterflow and single pass/single direction flow design concepts are quite different. In both cases the total coolant flow rate is the same so that the coolant temperature rise is the same. In the case of the single flow direction the very low inlet temperature results in a very low Reynolds number and heat transfer coefficient in the inlet region. The large temperature difference across the coolant film causes the maximum panel temperature to occur near the inlet rather than near the outlet as might be expected. When a counterflow arrangement is used there is very little temperature variation along the length of the panel in the direction of coolant flow. The low heat transfer coefficient near the inlet of one coolant passage is offset by the much higher heat transfer coefficient near the outlet of the adjacent coolant passage. There is relatively little difference in the temperature difference between the coolant passages. Directly over a passage the wall temperature is lower than half way between the discreet coolant passage locations.

COUNTERFLOW OF COOLANT MINIMIZES AXIAL TEMPERATURE DIFFERENCES

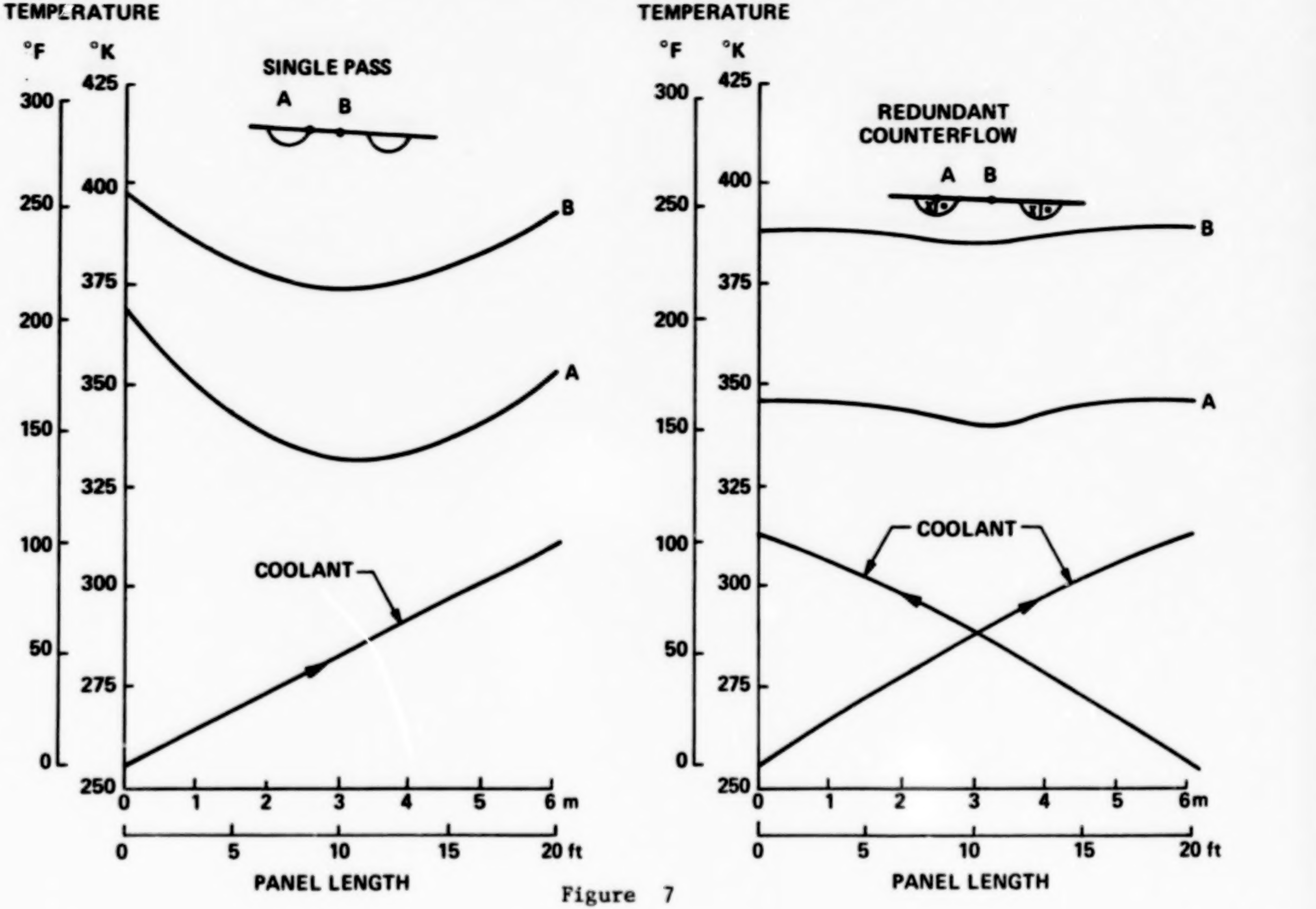

Figure 7

MAXIMUM PANEL TEMPERATURE INCREASES WITH PASSAGE SPACING

(Figure 8)

To a first approximation, the spacing of the coolant passages is related to the temperature difference between passages by various physical parameters as indicated in the following equation:

$$(s - w) = \sqrt{\frac{8\,t\,k\,\Delta T}{q}}$$

where s = passage spacing
w = passage width
t = skin thickness
k = thermal conductivity
ΔT = skin temperature difference
q = heat flux

When proper account is taken of the actual configurations and the thermal resistance of the adhesives, the relationship between maximum panel temperature and coolant passage spacing is as shown in this figure. The panel temperature is influenced by the inlet and outlet temperature of the coolant. These particular data were generated for an outer surface skin thickness of 0.8 mm (0.032 in), and inner skin thickness of 0.5 mm (0.02 in), a coolant passage wall thickness of 0.25 mm (0.01 in), and adhesive thickness of 0.064 mm (0.0025 in). Each of the data points represents an optimized combination of coolant passage and cooling system where the combined mass of the coolant inventory and the APS was minimized. Therefore, each combination represents a design with a different coolant passage width.

MAXIMUM PANEL TEMPERATURE INCREASES WITH PASSAGE SPACING

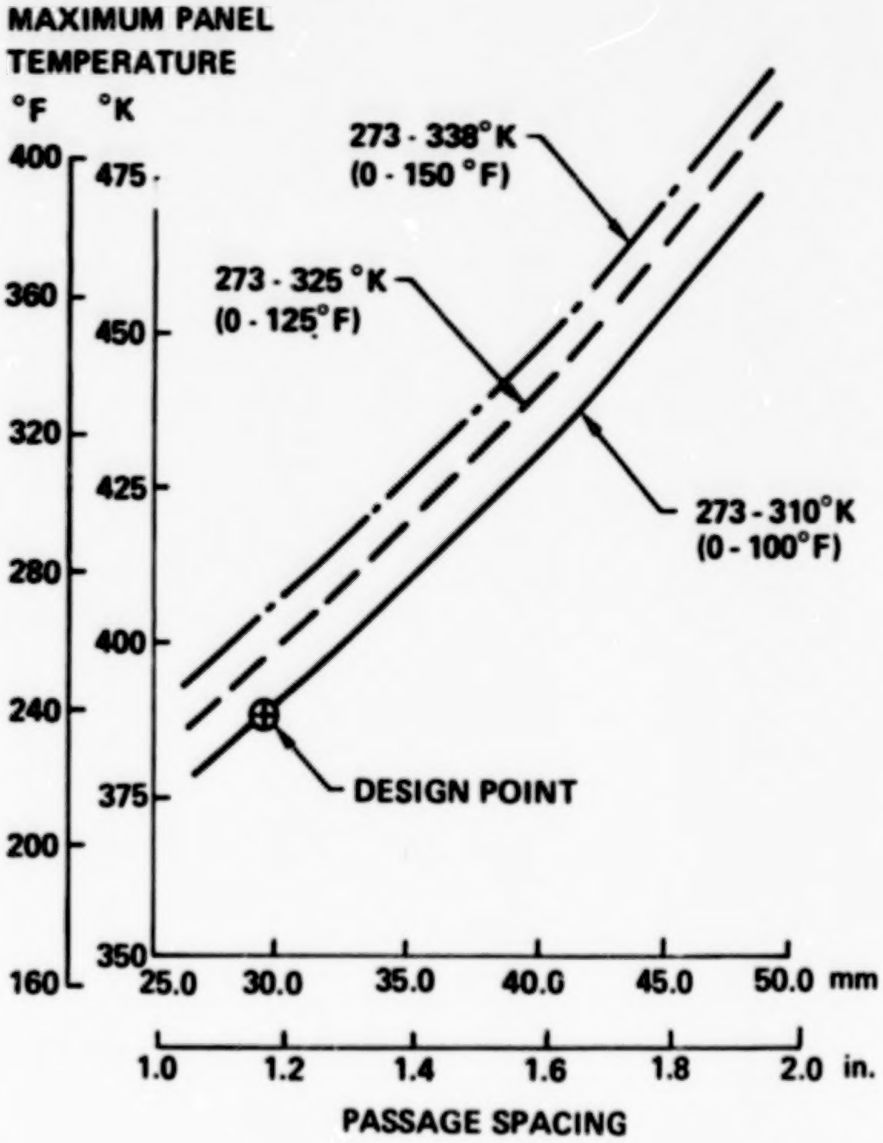

Figure 8

OPTIMUM PASSAGE WIDTH INCREASES WITH PASSAGE SPACING

(Figure 9)

As the coolant passage spacing increases, the amount of coolant which must flow through a particular passage is increased. If the coolant passage cross section is maintained constant, this flow rate increase results in an increase in pressure drop. If the coolant passage cross section is allowed to increase as the flow rate increases, a minimum mass combination of coolant passage cross section (coolant inventory) and APS weight is achieved. The widths given on this plot are the optimums which result in this minimum combined mass. Over the range of coolant passage spacing examined, the coolant passage width is a relatively weak function of spacing. Passage width is more strongly a function of the coolant temperature rise.

The design point does not fall on any of the optimum lines because the coolant ducting was sized so that it could be formed from tubing of a standard diameter, 0.76 mm (0.25 in) for the selected configuration.

OPTIMUM PASSAGE WIDTH INCREASES WITH PASSAGE SPACING

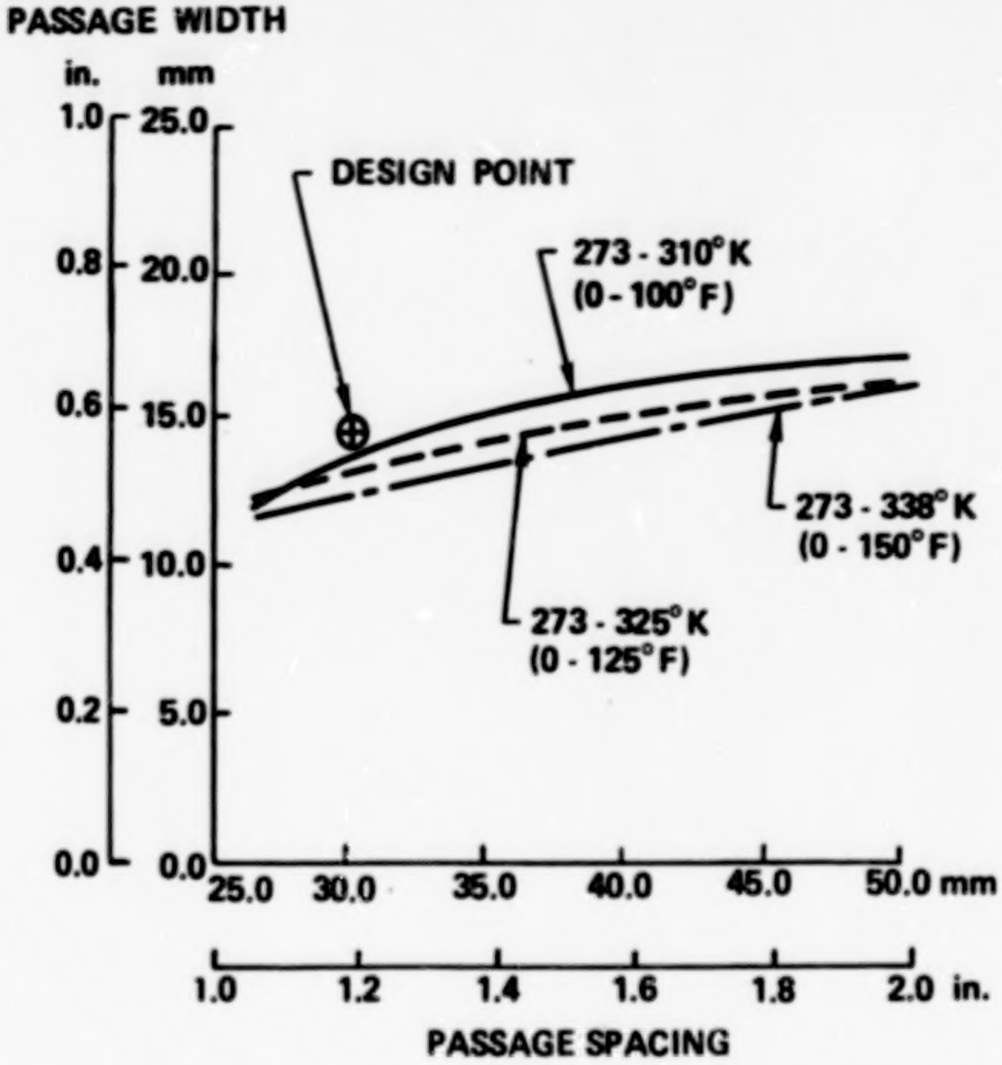

Figure 9

COOLANT TEMPERATURE HAS A GREATER INFLUENCE ON PRESSURE DROP THAN PASSAGE SPACING

(Figure 10)

The pressure drops shown on this plot are for a panel length of 6.1 m (20 ft). As the passage spacing increases, relatively more coolant flows through each passage, and as seen previously, the passage width increases. There is an increase in the coolant inventory within the passage. However, the larger cross-sectional area of the passage means a relative decrease in pressure drop for the same total flow through the panel. The net result is a decrease in pressure drop as the number of passages increases.

The pressure drop is more dependent on the coolant temperature level used for the design than on passage spacing. The temperature dependence of coolant viscosity is the dominant consideration.

COOLANT TEMPERATURE HAS A GREATER INFLUENCE ON PRESSURE DROP THAN PASSAGE SPACING

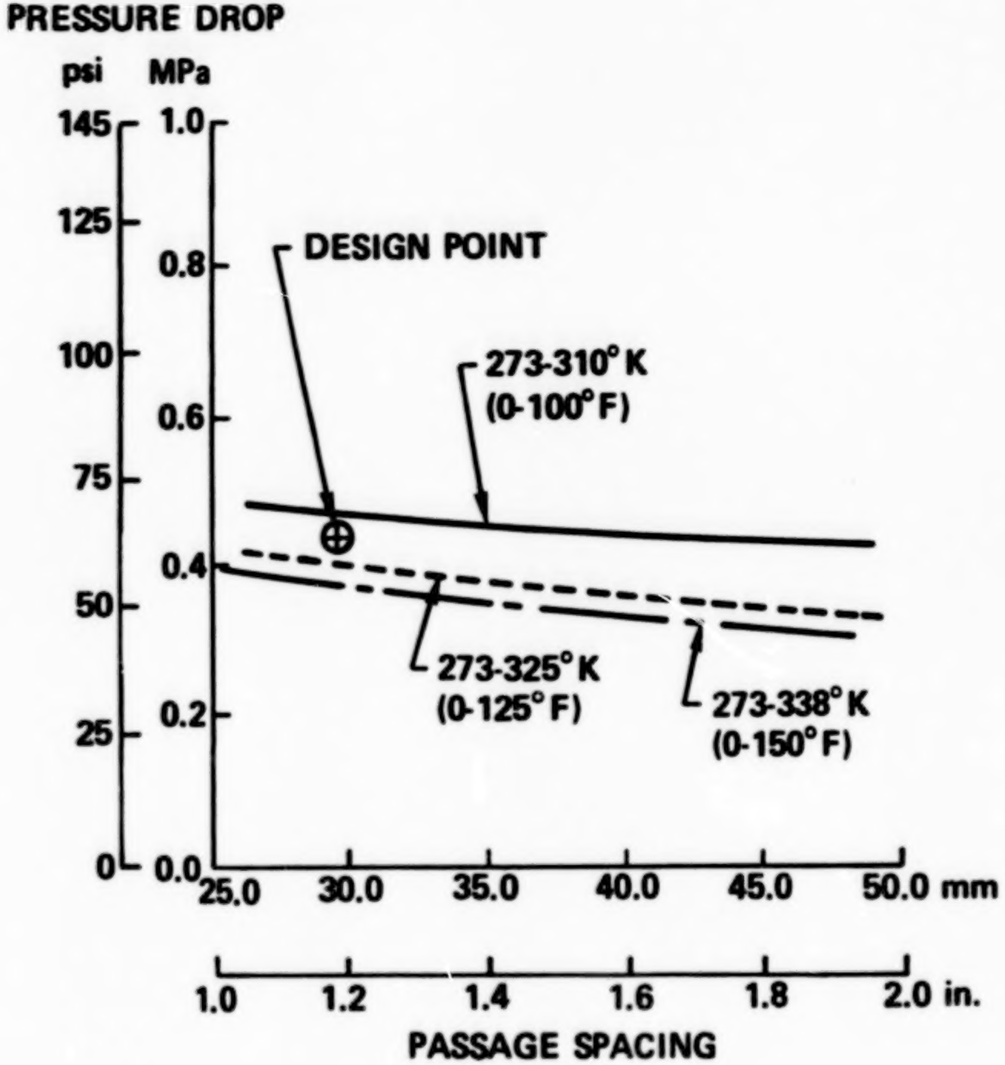

Figure 10

274

WEIGHT OF RESIDUAL COOLANT PLUS APS POWER IS INSENSITIVE TO PASSAGE SPACING

(Figure 11)

When the combined weight of the coolant inventory and APS mass is minimized the weight of these cooling system elements is a weak function of coolant passage spacing. The weight decreases slightly as coolant passage spacing increases. The coolant temperatures have a more significant influence on the mass of the cooling system elements because the coolant flow rate is directly proportional to the allowable coolant temperature rise through the panel and to the particular temperature levels as they affect coolant properties.

WEIGHT OF RESIDUAL COOLANT PLUS APS POWER IS INSENSITIVE TO PASSAGE SPACING

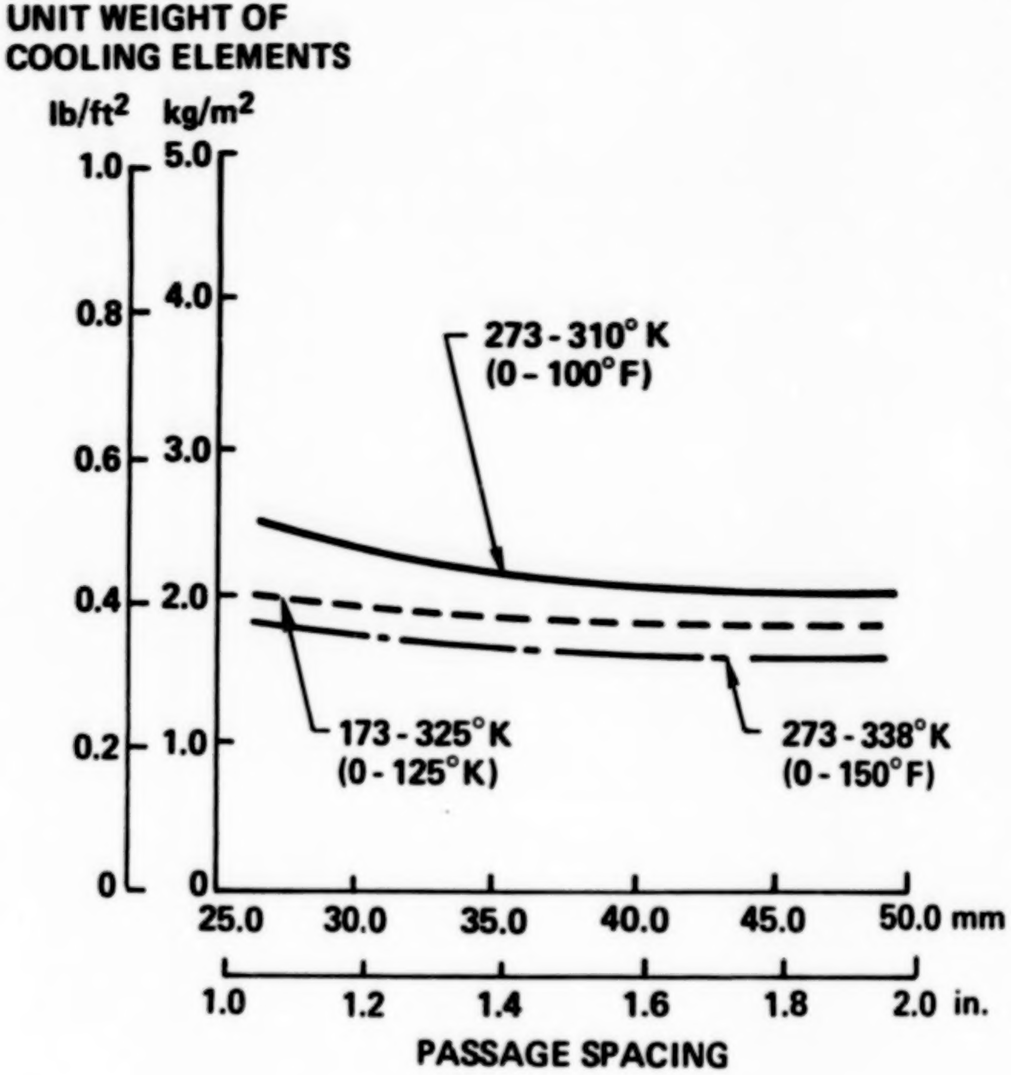

Figure 11

276

TEMPERATURE AND STRESS TRENDS

(Figure 12)

The panel temperatures and thermal stresses are related to coolant passage spacing in this figure. The temperatures influence material properties which in turn influence the thickness of material required to satisfy structural requirements. The thermal stresses add to the load stresses providing an additional impact on structural thickness requirements. Note, that as the panel temperature increases, the thermal stresses increase also so that there is a compounding of the structural weight penalties associated with increased coolant passage spacing.

TEMPERATURE AND STRESS TRENDS

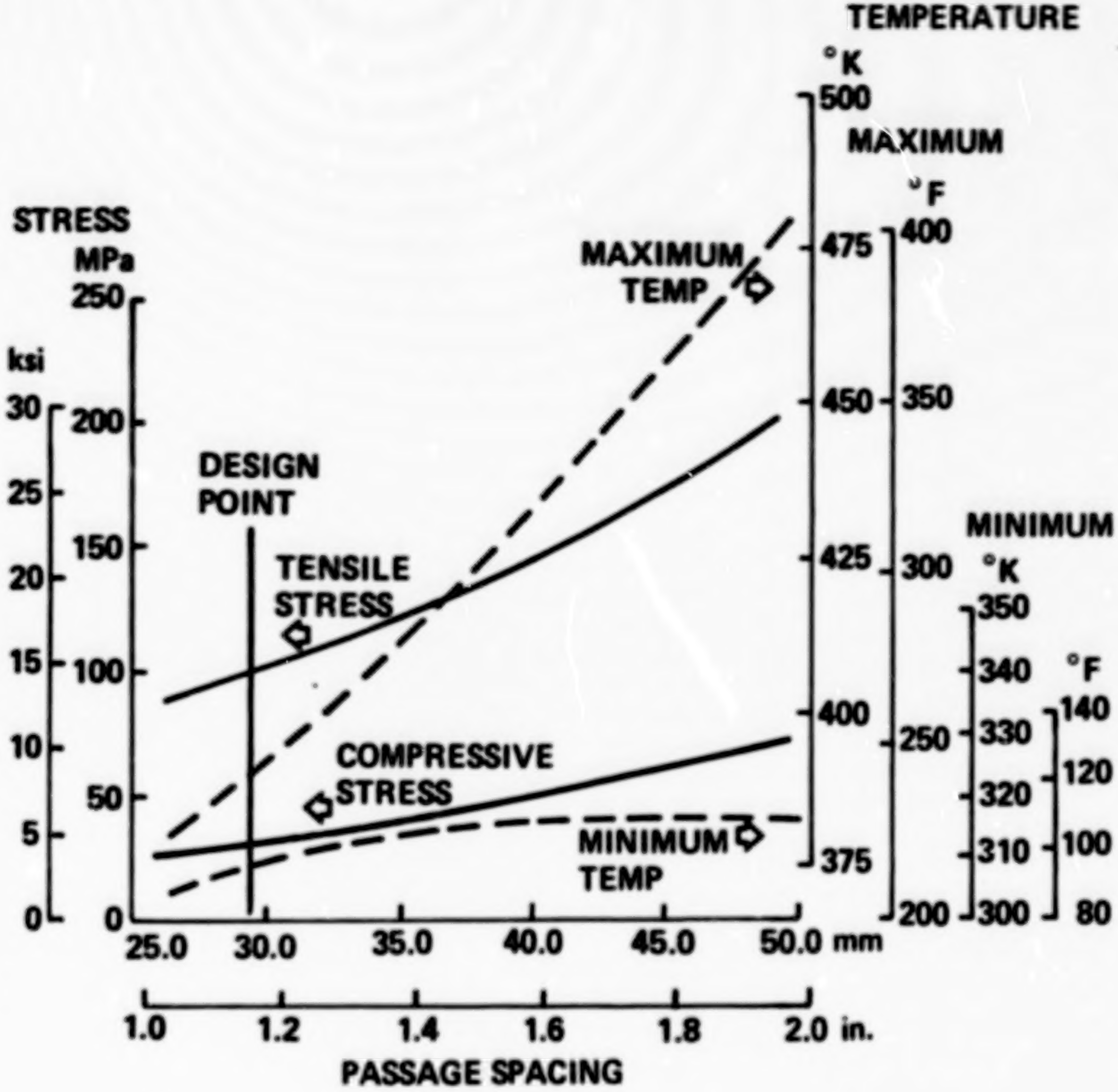

Figure 12

MINIMUM WEIGHT IS INFLUENCED BY PRACTICAL CONSIDERATIONS

(Figure 13)

As expected, the weight of the structure increases as its operating temperature is increased. The weight of the cooling system elements decreases slightly as panel temperature is increased. The combined mass of the adhesive, coolant passage tubing, and crack stoppers shows a slight decrease with temperature increase. The net result is to decrease panel mass as temperature decreases. However, with the discrete coolant passage approach, a point is reached where it is no longer possible to incorporate stringers on the portion of the skin between coolant passages. Spacers are needed to avoid interference between the stringers and the coolant passages. The point at which spacers are needed is indicated by the step in the total and structure mass curves. The design point for the panel, therefore, was established as the configuration into which the stringers could be incorporated without the use of standoff spacers.

MINIMUM WEIGHT IS INFLUENCED BY PRACTICAL CONSIDERATIONS

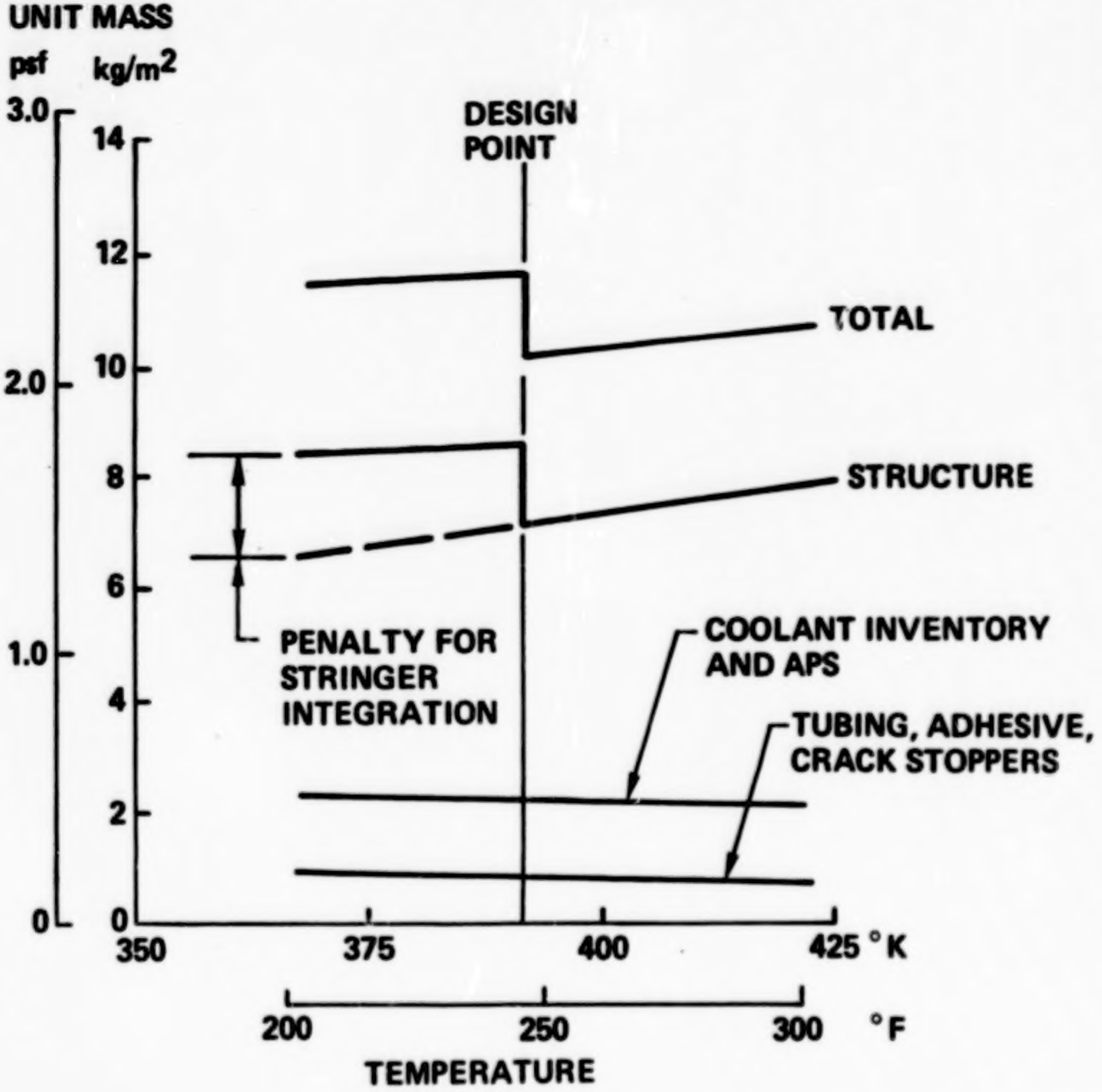

Figure 13

TEMPERATURE AT MID LENGTH

(Figure 14)

The transverse temperature distribution (perpendicular to coolant passages) is depicted here. At the coolant passage the panel temperature is lower than it is between coolant passages. The lowest temperature is adjacent to the inner beaded skin. At the mid-length location in the panel the bulk temperature of the coolant is about 286°K (55°F). The large temperature difference between the coolant bulk and the coolant passage walls indicates that while most of the heat is transferred to the coolant from the flat side of the coolant passage a significant amount of heat is conducted through the beaded skin into the curved portions of the passage.

TEMPERATURE AT MID LENGTH

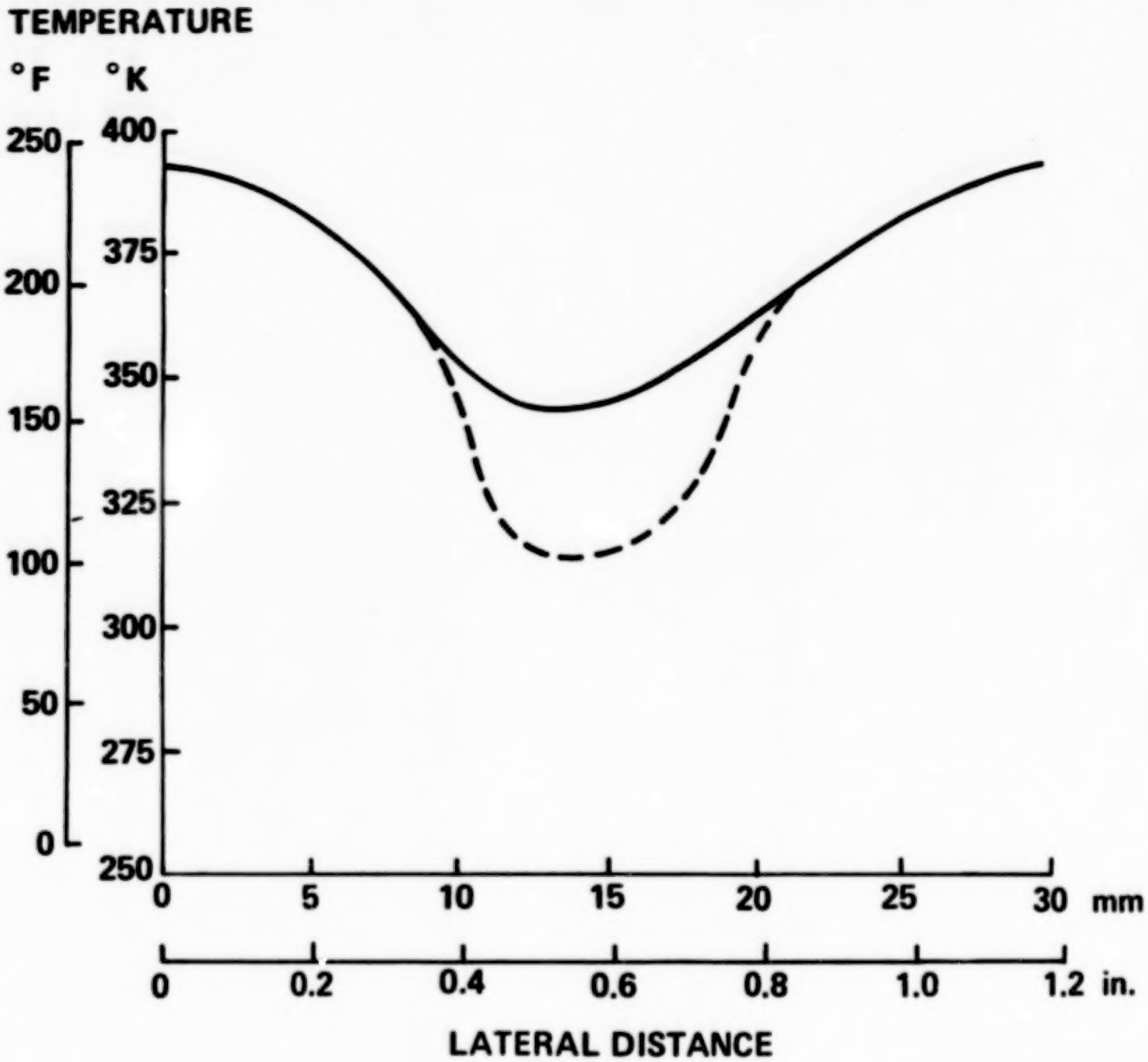

Figure 14

STRESS DISTRIBUTION AT MID LENGTH

(Figure 15)

Because of the temperature variation across the panel thermal stresses are generated. This plot shows the distribution of thermal stresses along the smooth outer surface of the skin, the beaded inner surface, and the stringer. Maximum tensile thermal stresses are generated in the vicinity of the cooled passage where temperatures are lowest. Compressive stresses are induced where the highest temperatures occur. It is in these regions of high compressive thermal stress that the mechanical fasteners for the stringers are installed. This tends to minimize the stress concentration effect of such fasteners. The stress induced by the alternating inplane loading is added to the thermal stress distribution when the design life is checked.

STRESS DISTRIBUTION AT MID LENGTH

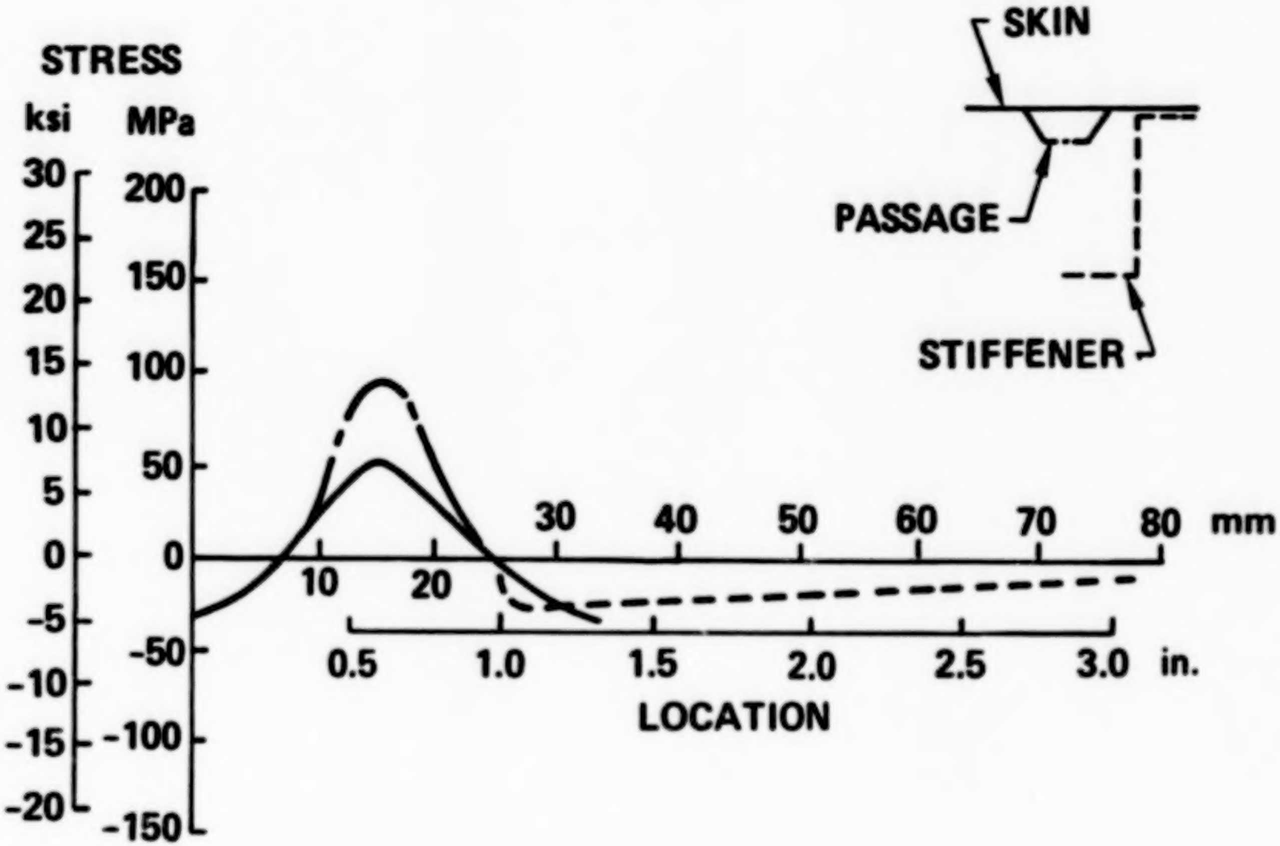

Figure 15

PANEL FATIGUE CHARACTERISTICS

(Figure 16)

During the ground-air-ground cycle, thermal stresses grow from zero to a maximum. This is equivalent to a steady stress of half the maximum thermal stress value and an alternating stress of half the maximum value. For purposes of establishing panel thickness based on fatigue considerations, the alternating portion of the thermal stress component was added to the alternating inplane load of ±210 kN/m^2 (±1200 lb/in). In using this applied stress, plots of steady versus alternating stresses were obtained from reference 4 for 2024-T3 alloy with appropriate stress concentration factors. The handbook data was corrected for 10,000 hours of exposure. The correction used to account for elevated temperature was an average between old ANC-5 data and the data of Dix (ref. 5). Stress concentration factors of 2.0 and 4.5 were applied to the region of the tubes and the attachment of the stringers respectively. The skin temperature was approximately 325°K (125°F) in the region of the tubes and 388°K (240°F) in the vicinity of the stringer attachment rivets. Because the compressive stresses enhance fatigue life, the equivalent thickness required to withstand the fatigue loading conditions was determined on the basis of the stresses induced in the region of tensile thermal stresses, the vicinity of the coolant passages.

PANEL FATIGUE CHARACTERISTICS

- $\sigma = \frac{1}{2}\sigma_{th} \pm (\frac{1}{2}\sigma_{th} + \sigma_i)$
- FATIGUE ALLOWABLE REDUCED BY:
  - FACTOR FOR 10,000 HOURS OF EXPOSURE
  - TEMPERATURE
  - STRESS CONCENTRATION OF 2.0 AND 4.5
- DESIGN LIFE OF 20,000 CYCLES (5000 x 4.0)
- EQUIVALENT THICKNESS REQUIRED = 0.51 mm (0.11 in.)

Figure 16

PANEL STABILITY CHARACTERISTICS

(Figure 17)

Having established the equivalent skin thickness to meet the life requirement, the material is proportioned to maximize panel stability. Early studies had indicated that stringer depth and thickness of about 3.8 mm (1.50 in) and 0.127 mm (0.050 in) were near optimum. The stringer pitch was dictated by the coolant passage spacing. Fabrication and efficiency considerations dictated Zee stringers. The skin thickness was dictated by convenient sheet thicknesses and a desire to apportion the equivalent thickness on an approximate 50/50 basis with the stringers. The stringer sizing was accomplished using a computer optimization code which accounted for axial loading and normal pressure loading. The computer code generated nonbuckling and buckling designs, the results of which are plotted. The thermal moment was introduced as an additional increment of normal pressure loading.

As can be seen from the figure, the particular proportions selected would permit an axial loading of approximately 470 kN/m (2700 lb/in) to be carried without inducing buckling while the axial load carried as the panel buckles would be approximately 580 kN/m (3300 lb/in). The analyses assumed a material temperature of 408°K (250°F). The panel is able to carry more than twice the design inplane loading without buckling.

PANEL STABILITY CHARACTERISTICS

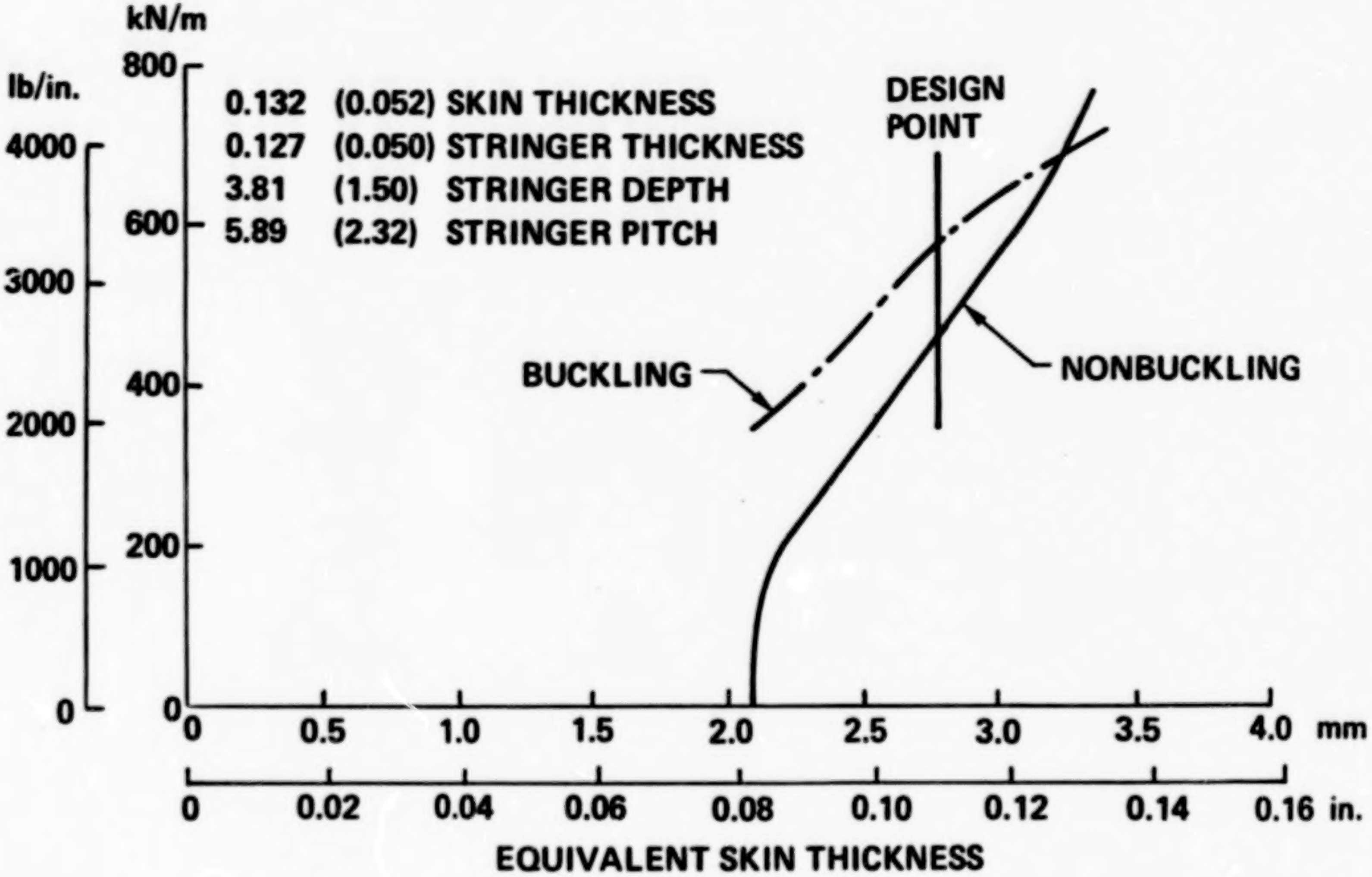

Figure 17

EXPERIMENTAL STUDIES

(Figure 18)

The initial plan envisioned validation of panel design details via a series of fatigue tests conducted at the Langley Research Center. During the fabrication of these specimens, areas in need of process refinement were identified. The NASA tests identified some areas of deficiency. Therefore, the experimental study effort was expanded to include five additional types of specimens, four of which involved aspects of adhesive utilization.

EXPERIMENTAL STUDIES

SPECIMEN TYPE	PURPOSE
• NASA FATIGUE (6)	– VALIDATE PANEL DETAILS
• MANIFOLD END PLUG (13)	– SELECT ADHESIVE
• COOLANT PASSAGE PLUG (10)	– SELECT POTTING COMPOUND
• PRESSURE PANEL (4)	– VALIDATE PRESSURE INTEGRITY
• EDGE ATTACHMENT (15)	– VALIDATE DESIGN CHANGE
• MANIFOLD REPAIR (1)	– VALIDATE REPAIR TECHNIQUE

figure 18

FATIGUE AND PRESSURE TEST SPECIMENS WERE CUT FROM A COOLED SKIN PANEL

(Figure 19)

In order to establish preliminary manufacturing procedures it was decided to fabricate a 0.61 x 1.22 m (24 x 48 in) cooled skin panel from which test specimens could be cut. The cutting plan is shown here. Leakage observed during the fatigue tests was investigated with the pressure test specimens. The fabrication procedures were those intended for use on the final test panel. Some difficulties were encountered and procedures were modified accordingly. Of particular importance were refinements in the methods for applying the silver filled Eccobond 58C adhesive.

FATIGUE AND PRESSURE TEST SPECIMENS WERE CUT FROM A COOLED SKIN PANEL

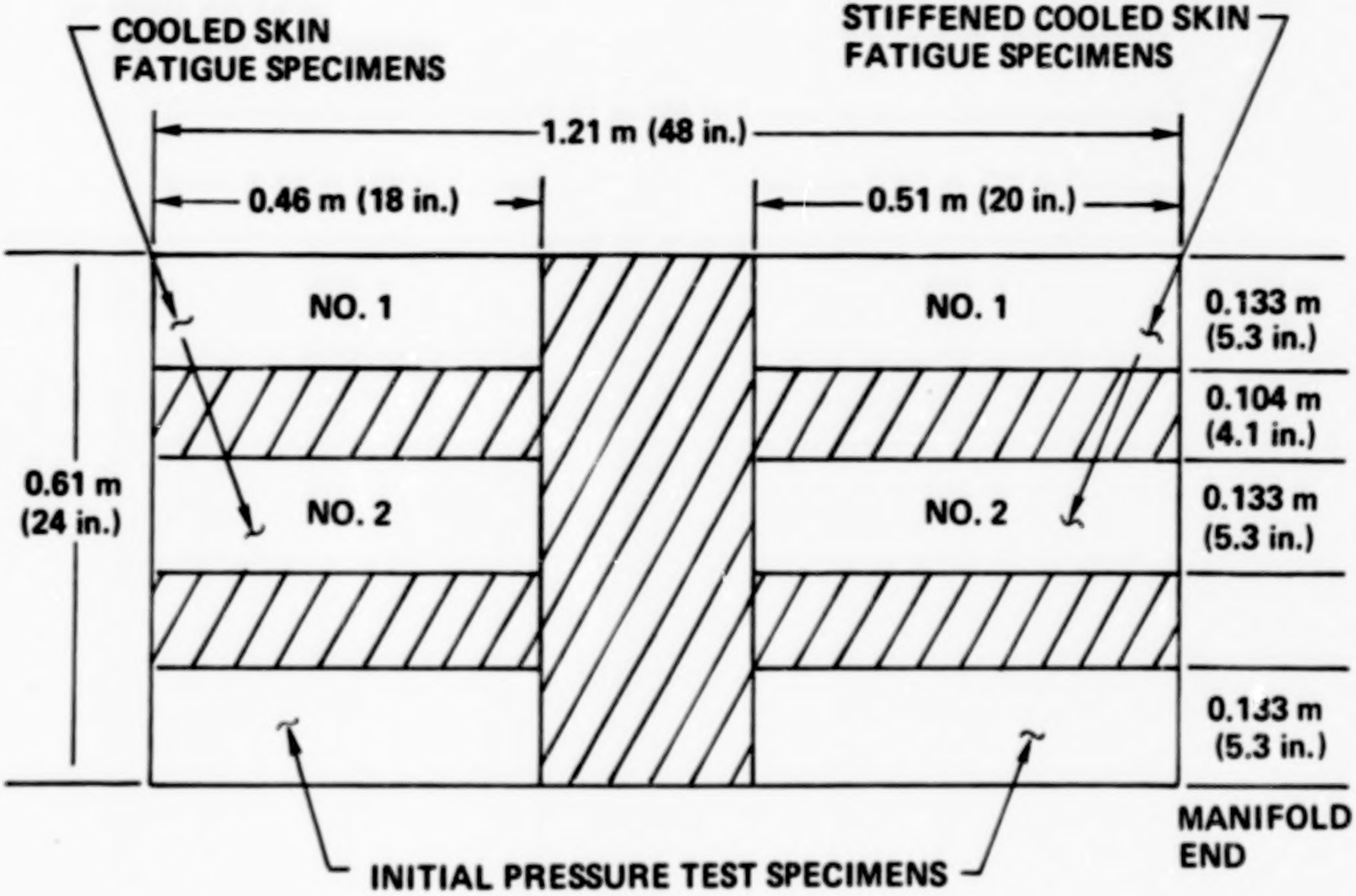
COOLED SKIN FATIGUE SPECIMENS
STIFFENED COOLED SKIN FATIGUE SPECIMENS
1.21 m (48 in.)
0.46 m (18 in.)
0.51 m (20 in.)
NO. 1
NO. 1
NO. 2
NO. 2
0.61 m (24 in.)
0.133 m (5.3 in.)
0.104 m (4.1 in.)
0.133 m (5.3 in.)
0.133 m (5.3 in.)
MANIFOLD END
INITIAL PRESSURE TEST SPECIMENS

Figure 19

291

292

UNSTIFFENED FATIGUE SPECIMENS

(Figure 20)

Two types of unstiffened fatigue specimens were fabricated for evaluation at Langley Research Center. The first type (upper photo) consisted of two flat sheets bonded together by alternating stripes of Epon 951 and Eccobond 58C. After surving 20,000 cycles at the desired load level, notches were machined into the skin and allowed to propagate until failure. When a through notch was used crack propagation proceeded in much the same manner as would be expected of aluminum alloy sheet having the total thickness of the bonded skin. When a surface notch was introduced the bond line delayed the progression of the crack from the notched skin to the other skin layer.

The lower photo illustrates the second type of unstiffened fatigue specimen which incorporated the transition between the manifold region and the inboard portion of the skin panel/tube assembly. Small squares of teflon replaced some of the adhesive film in the sloping portion of the transition. After sustaining 20,000 cycles at the design load, notches were introduced and the panel and the specimens were cycled to failure. The crack stoppers at the edges of the coolant passages appeared to delay the progress of crack growth slightly. Some leakage of the pressurized fluid within the panel was noted prior to rupture of the coolant passage tubing.

UNSTIFFENED FATIGUE SPECIMENS

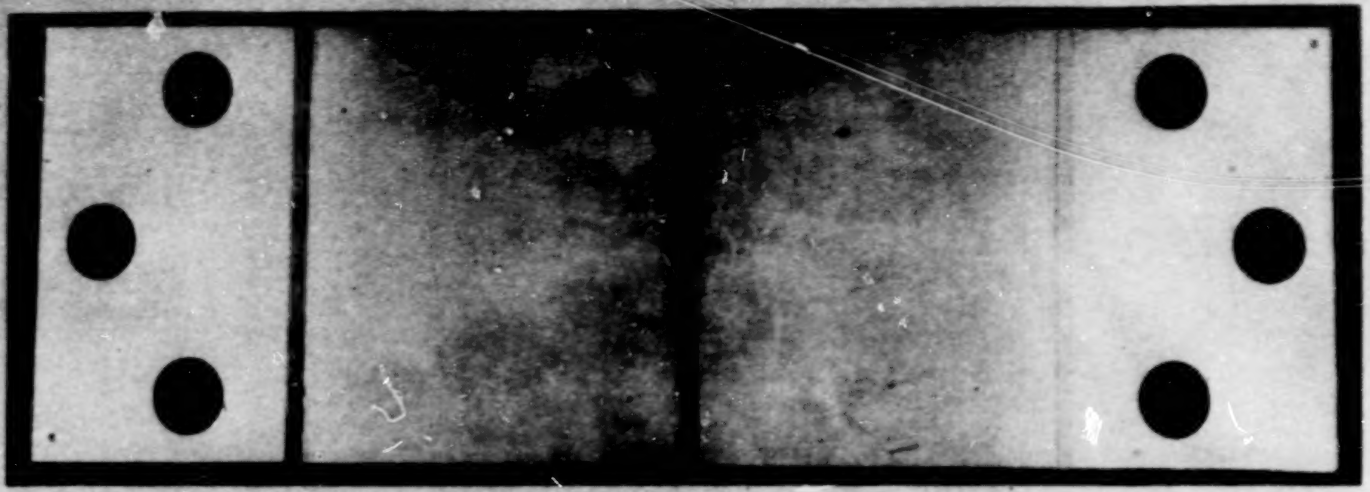

SKIN

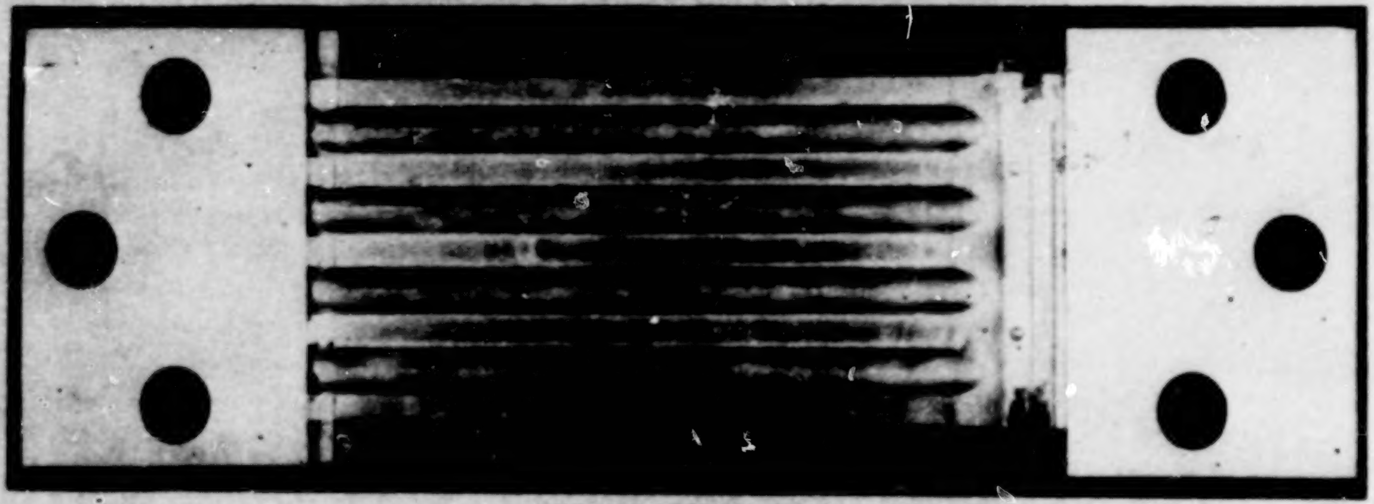

COOLANT PASSAGE/RAMP

Figure 20

STIFFENED FATIGUE SPECIMEN

(Figure 21)

The major features of the cooled panel design were incorporated in these specimens. Initial loadings indicated significant deformations at the single shear spliced joint. A double shear joint was introduced and fatigue testing was continued. Leakage of the pressurized oil within the panel was noted early in the testing. This necessitated deletion of the pressurization aspect of the fatigue tests. Both specimens failed from cracks that started at the rivets. One sustained 17,900 cycles while the other sustained 19,500 cycles. While not quite as long as the 20,000 cycle target, the results were considered adequate for verifying the design features.

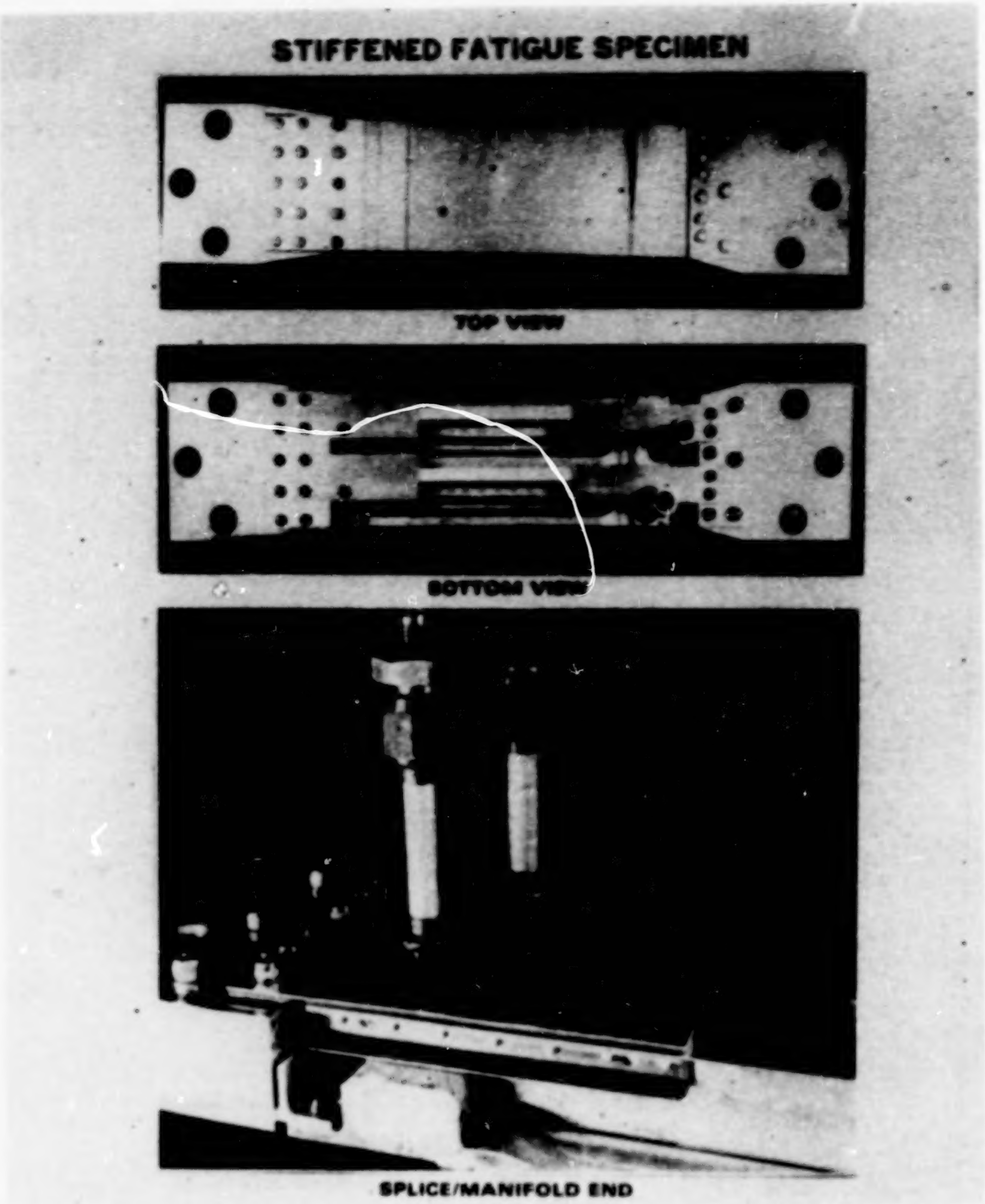
STIFFENED FATIGUE SPECIMEN
TOP VIEW
BOTTOM VIEW
SPLICE/MANIFOLD END

Figure 21

EXPERIMENTAL RESULTS

(Figure 22)

Based on the various experimental evaluations that were conducted, details of the cool panel design and the associated fabrication procedures were verified. The experimental effort required to validate manufacturing procedures was significantly greater than anticipated. As is often the case, the design concept was relatively straightforward but its successful implementation required great attention to details. The manufacturing procedures which required refinement were all associated with the use of adhesives. While it was not necessary to develop any new materials, it was necessary to compare alternate approaches before selections could be made for specific functions. The experimental results did verify that adhesive bonding could be used even when the most critical bond line thicknesses were small compared to manufacturing tolerances associated with machining and sheet metal forming.

EXPERIMENTAL RESULTS

- NASA FATIGUE
  - BONDED SKIN – SIMILAR TO SINGLE THICKNESS
  - TRANSITION – ADEQUATE FATIGUE LIFE, LEAKAGE
  - STIFFENED – INADEQUATE SPLICE DESIGN, LEAKAGE
- MANIFOLD END PLUG – ALUMINA FILLED EPON 828 SELECTED
- COOLANT PASSAGE PLUG – ALUMINA FILLED EPON 828 SELECTED
- PRESSURE PANEL – TIGHTER TOLERANCES NEEDED ON TUBING, IMPROVED MANUFACTURING TECHNIQUES DEVELOPED
- EDGE ATTACHMENT – CHERRYBUCK RIVETS USED IN DOUBLE SHEAR
- MANIFOLD REPAIR – BLIND RIVETS SEALED WITH SCOTCH WELD 1838

Figure 22

298

TEST PANEL - TOP VIEW

(Figure 23)

This figure shows the test panel and one of the two adapters which will be used for applying inplane loads. The panel configuration is no different than would be expected for a conventional skin/stringer/frame structural panel. Close examination of the actual panel with properly reflected light shows a slight undulating pattern related to the location of coolant passages. Each load adapter will introduce the inplane loading at 21 discreet locations through straps which accommodate thermal expansions. The three sets of plates at the ends of the frames will attach to the NASA test fixturing to simulate continuous frames.

TEST PANEL - TOP VIEW

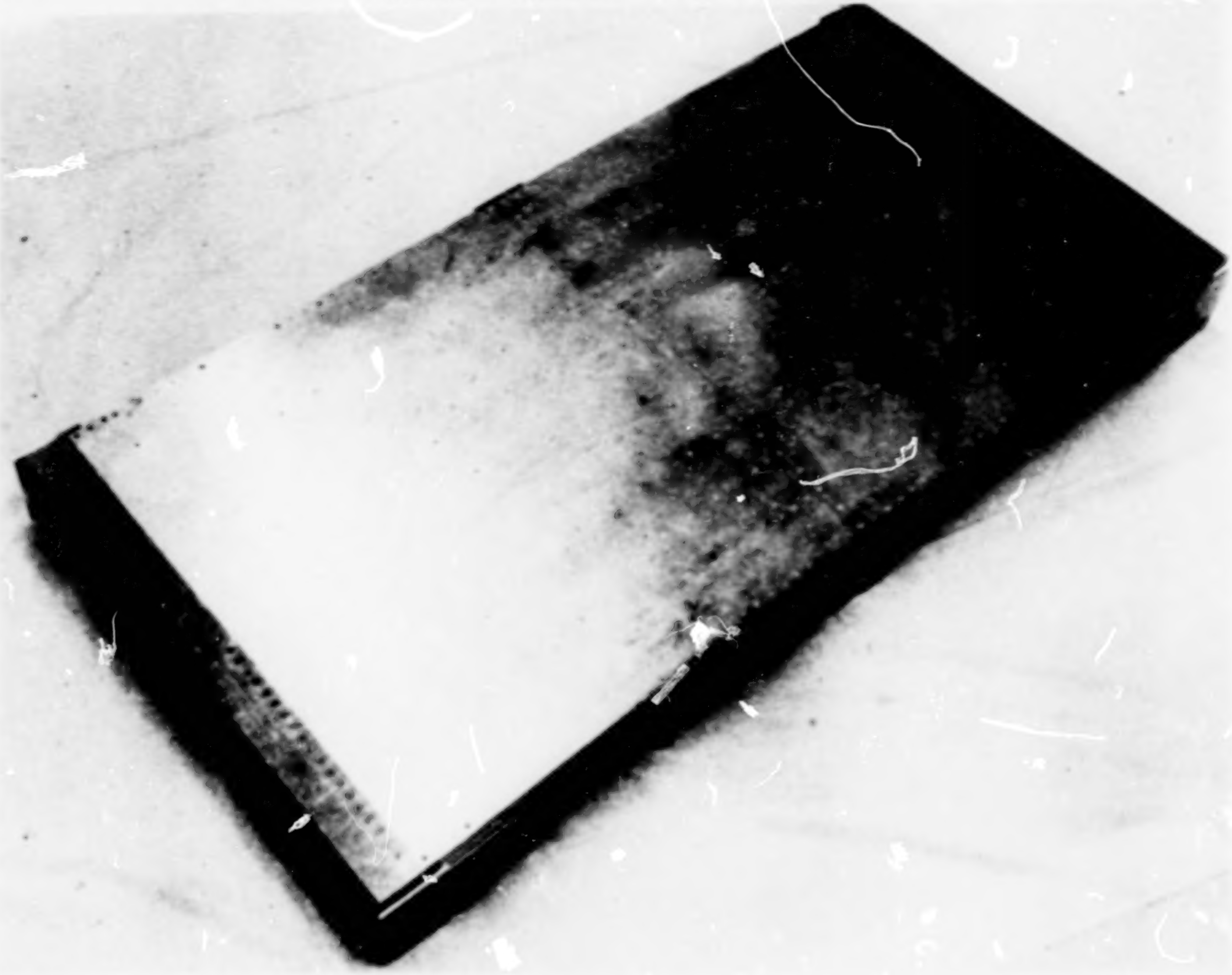

Figure 23

CONTENTS

Part I

PREFACE . . . . iii 1/A5

WELCOME 1 1/A10
R. R. Heldenfels

SESSION I - OVERVIEWS
Chairman: A. J. Henderson

1. HYPERSONIC STRUCTURES: AN AERODYNAMICIST'S PERSPECTIVE (OR ONE MAN'S DREAM IS ANOTHER MAN'S NIGHTMARE) 5 1/B1
J. D. Watts, L. R. Jackson, and J. L. Hunt

2. STRUCTURAL REQUIREMENTS FOR MILITARY HYPERSONIC SYSTEMS (Paper not available for publication)
P. Lane

3. AIRFRAME-INTEGRATED PROPULSION SYSTEM FOR HYPERSONIC CRUISE VEHICLES 39 1/F13
Robert A. Jones and Paul W. Huber

4. RECENT ADVANCES IN CONVECTIVELY COOLED ENGINE AND AIRFRAME STRUCTURES FOR HYPERSONIC FLIGHT 47 1/G7
H. Neale Kelly, Allan R. Wieting, Charles P. Shore, and Robert J. Nowak

SESSION II - ENGINE STRUCTURES
Chairman: H. N. Kelly

5. DESIGN AND ANALYSIS OF A SCRAMJET ENGINE 65 2/A13
O. A. Buchmann

6. THERMOSTRUCTURAL ANALYSIS OF A SCRAMJET FUEL-INJECTION STRUT 119 3/B11
Allan R. Wieting and Earl A. Thornton

7. ADVANCED FABRICATION TECHNIQUES FOR COOLED ENGINE STRUCTURES 145 3/F7
O. A. Buchmann

8. HYDROGEN EMBRITTLEMENT AND ITS CONTROL IN HYDROGEN-FUELED ENGINE SYSTEMS 195 4/F11
W. T. Chandler

9. CARBON-CARBON COMPOSITE APPLICATION FOR INTEGRAL ROCKET RAMJET COMBUSTORS (Paper not available for publication)
H. A. Holman

SESSION III - COOLED AIRFRAME STRUCTURES
Chairman: C. P. Shore

10. DESIGN AND FABRICATION OF A SKIN STRINGER DISCRETE TUBE ACTIVELY COOLED STRUCTURAL PANEL 253 6/A5
Frank M. Anthony

11. DESIGN AND ANALYSIS OF A PLATE-FIN SANDWICH ACTIVELY COOLED STRUCTURAL PANEL 319 7/C13
L. M. Smith

12. FLUXLESS BRAZING AND HEAT TREATMENT OF A PLATE-FIN SANDWICH ACTIVELY COOLED PANEL 375 8/E1
Charles S. Beuyukian

13. DESIGN AND FABRICATION OF A RADIATIVE ACTIVELY COOLED HONEYCOMB SANDWICH PANEL 449 10/A13
Leland C. Koch

14. RADIATIVE, ACTIVELY COOLED PANEL TESTS RESULTS 493 11/A5
Charles P. Shore, Robert J. Nowak, and Ellsworth L. Sharpe

300

COOLED SKIN – BOTTOM VIEW

(Figure 24)

The transition of the coolant circuitry from the end manifolds to the coolant passages is depicted here. Parallel adjacent plenums are machined in the manifold blocks perpendicular to the coolant passage length. The manifold block tapers at the inboard transition to the bonded skin. The outer edge of the manifold block provides for the splice which would join the cooled panels perpendicular to the primary load direction.

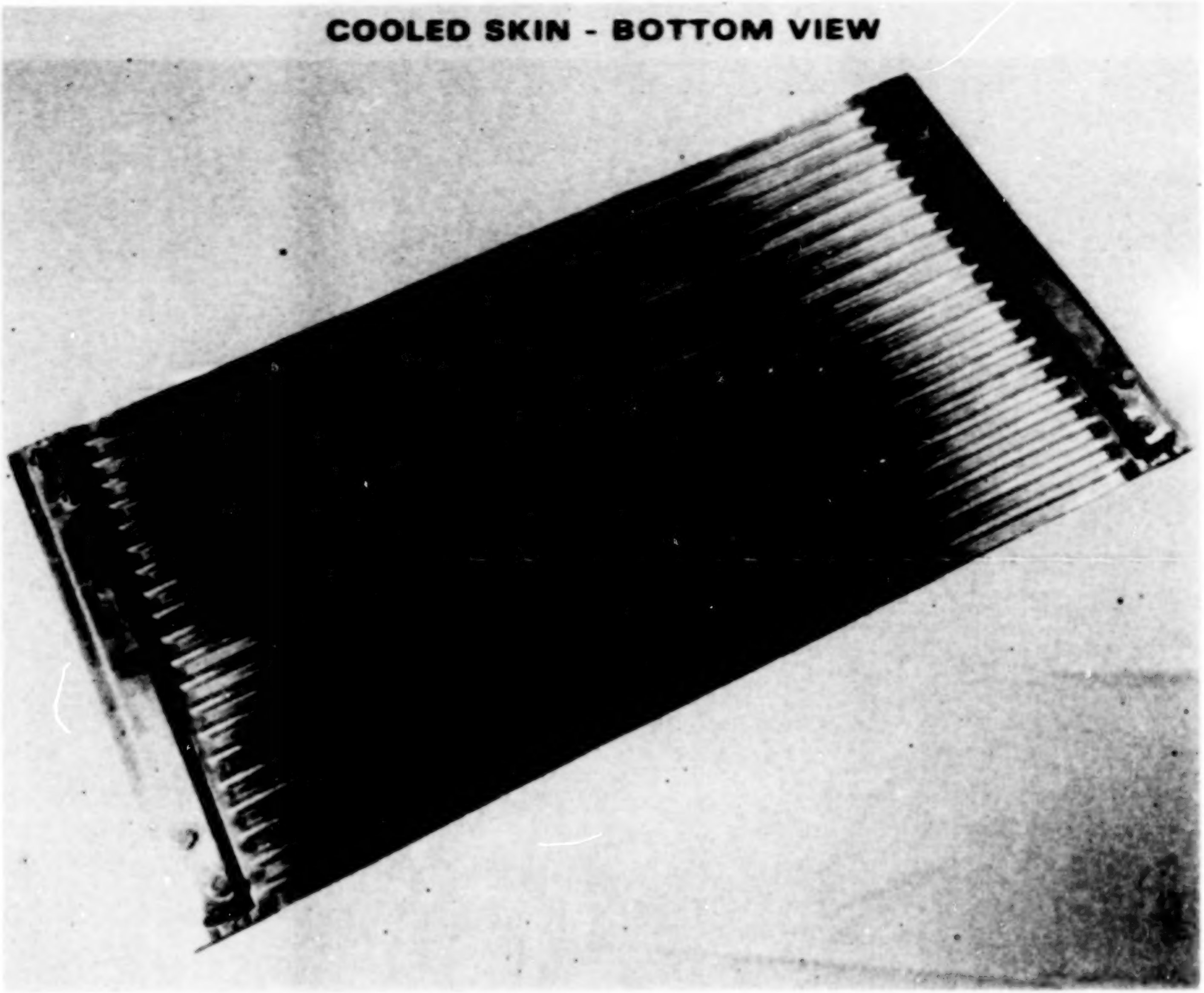

COOLED SKIN - BOTTOM VIEW

Figure 24

302

TEST PANEL – BOTTOM VIEW

(Figure 25)

When the substructure is added to the cooled skin panel it is difficult to identify the coolant passages and the manifold installation. Dominant features are the stringers and the large end attachments for the load adapters. The transitions from the load adapter to the cooled structural panel are designed conservatively so that the margins of safety are lower in the panel proper than in the test fixturing.

TEST PANEL - BOTTOM VIEW

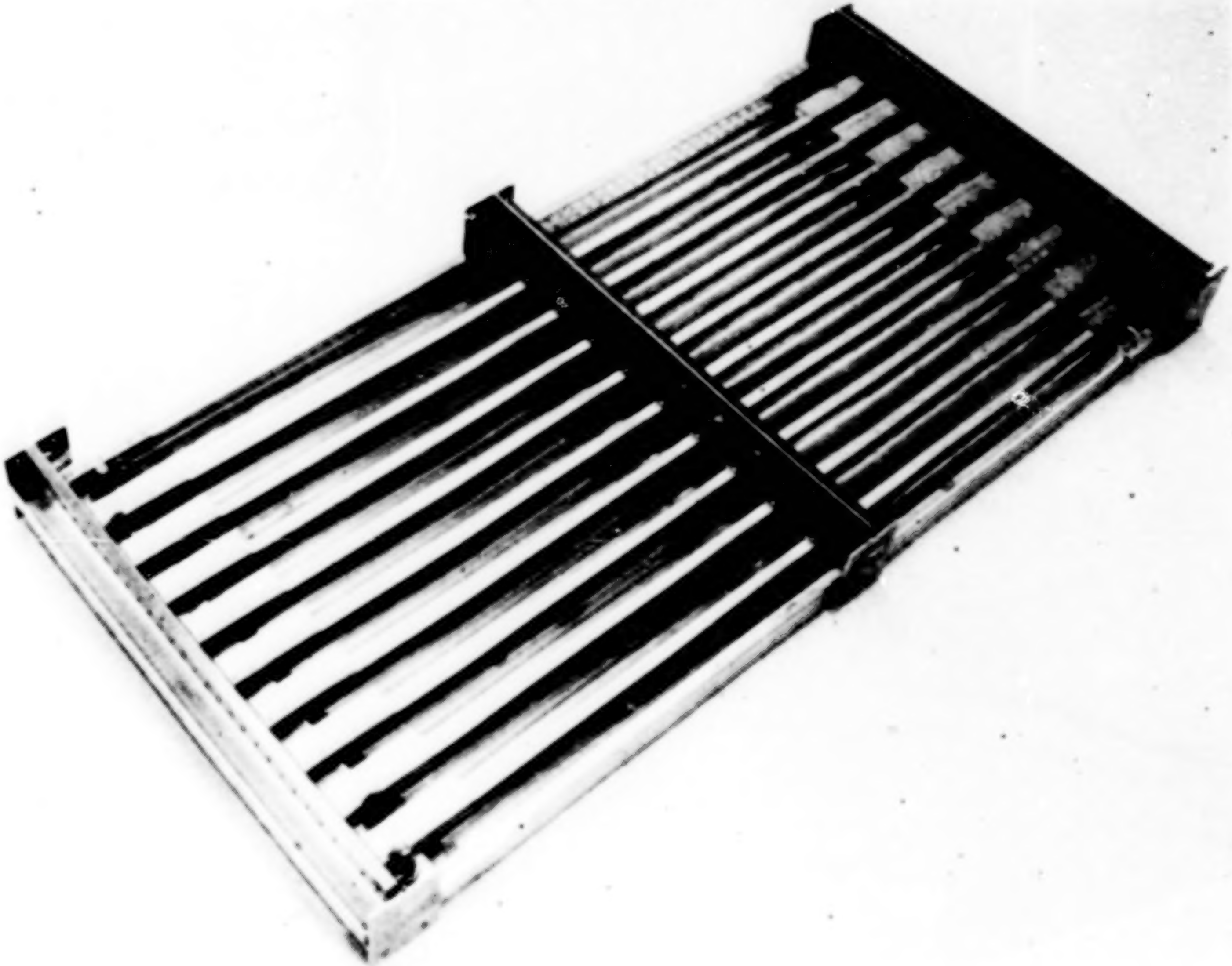

Figure 25

303

CENTER FRAME DETAILS

(Figure 26)

The details of integrating the stringers and frames with the cooled skin are illustrated here. The stringers are riveted directly to the cooled skin in the region between coolant passages. The stringers are attached to the frames by right angle clips and a right angle cap. The height of the coolant passages necessitates the use of small spacers at the skin to frame attachment. All of the riveting in this region is relatively accessible.

CENTER FRAME DETAILS

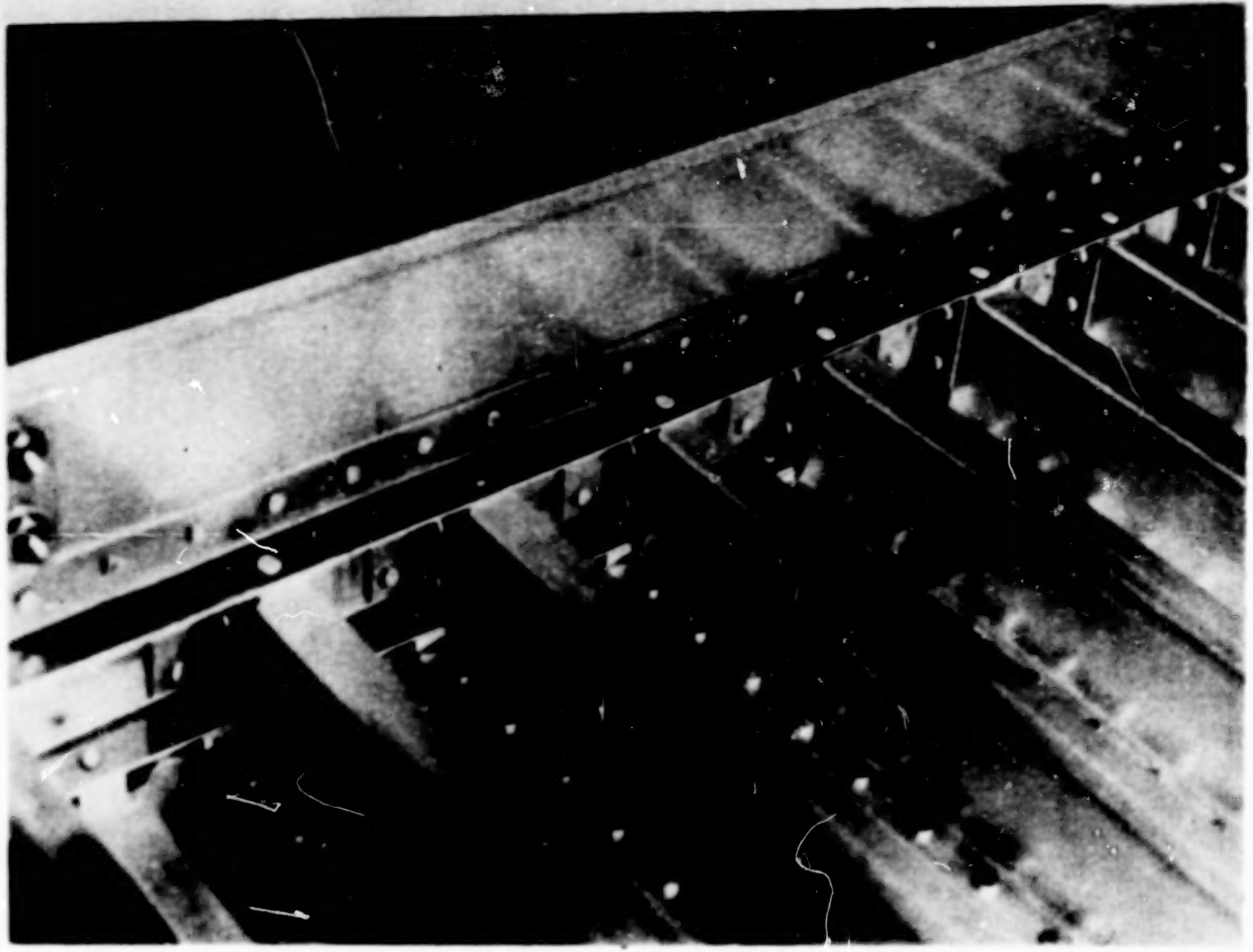

Figure 26

305

END FRAME AND STRINGER DETAILS

(Figure 27)

Installation of the details at the end frames is somewhat more complex than at the center frame. Because of the coolant manifold, it is necessary to notch each stringer and to reinforce the inner flange with a formed channel. To properly introduce the inplane load at the neutral axis of the panel, extruded T-sections were attached to the stringers. The titanium straps from the load adapter arrangement attach to the flanges of these T's as well as the double shear splice joint at the outer edge of the panel.

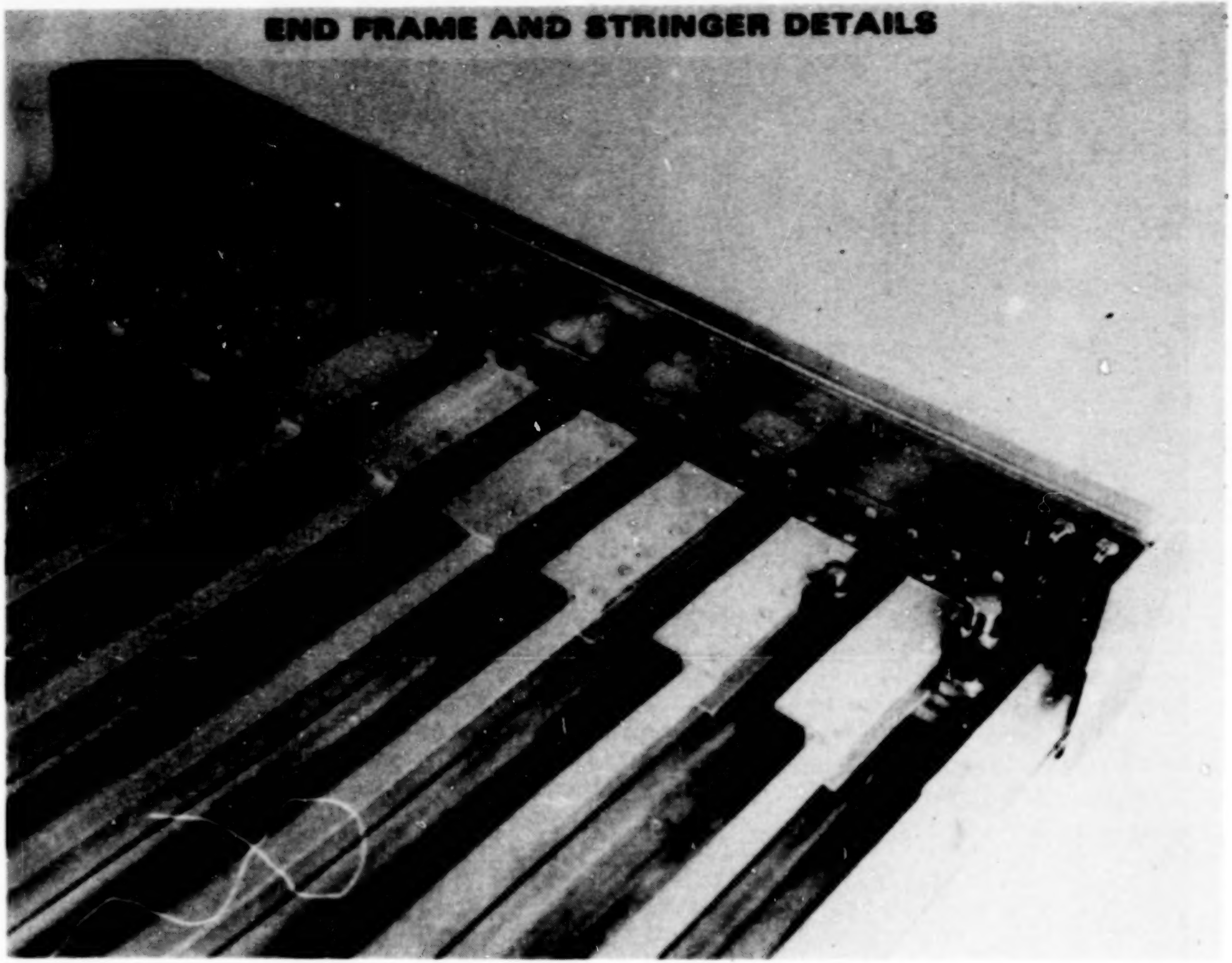

END FRAME AND STRINGER DETAILS

Figure 27

308

SPLICE AND END FRAME DETAILS

(Figure 28)

In an actual application it would be necessary to splice the cooled skins and perhaps the stringers also. The skin splice transmits about 85% of the inplane loading. This splice is made to an extruded aluminum T that forms the outer cap of the frame and a titanium splice plate along the external surface. Titanium was necessary because this external splice plate cannot be cooled down to temperatures where aluminum alloys could be considered. The extruded T's at the inner stringer flange simulate splice plates for the stringers.

SPLICE AND END FRAME DETAILS

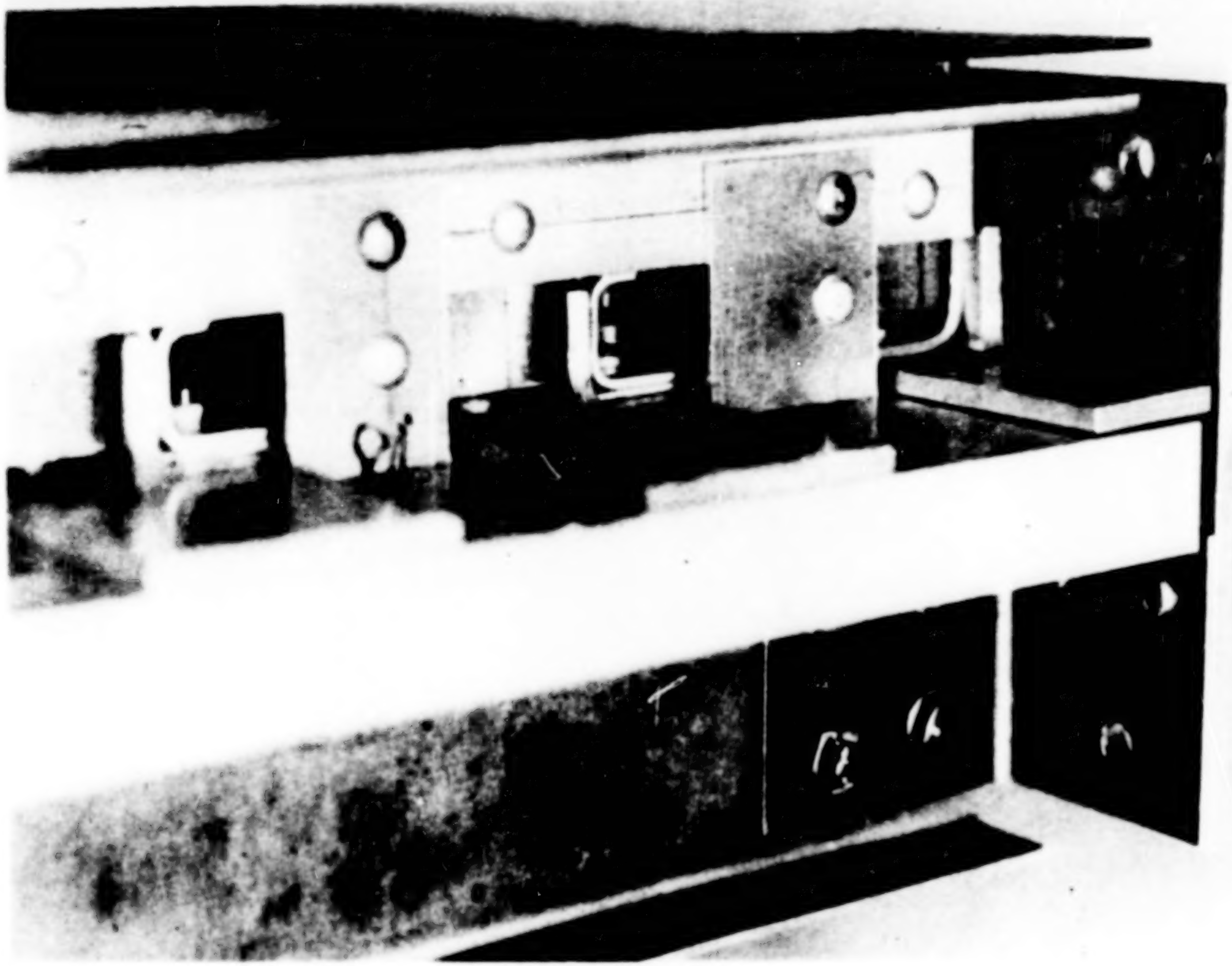

Figure 28

APPLICATION OF SILVER FILLED EPOXY

(Figure 29)

One of the most difficult fabrication operations was the application of the silver filled epoxy adhesive. This material was used between the coolant passages and the inner beaded skin, and as stripes for bonding the outer skin. The silver filled epoxy was troweled into the beads of the panel used for the fatigue specimens. Several types of spatula like devices and numerous technique variations were investigated. All were time consuming. When the final test panel was to be fabricated the need for improved techniques was recognized. A caulking gun approach seemed highly desirable. The "as received" consistency was thinned with MEK and toluene as diluents. For the relatively large beads of adhesive that were to be applied in this application thinning with between 2 and 3% of diluent was adequate for obtaining good flow of the adhesive at modest pressure. Excess adhesive was applied, the tubes were installed, and the system was debulked in two steps. Most of the excessive silver filled adhesive, which extruded from around the coolant passage tubing during the first debulking cycle, was removed prior to the second cycle. The second cycle was required because the squeeze out from the first cycle precluded obtaining a flat surface across the entire panel as the passages and skin was squeezed against the heavy caul plate.

The stripes of Eccobond 58C adhesive used in bonding the smooth outer skin to the inner subassembly were applied with a caulking gun technique as well. The small quantity of adhesive needed for each stripe required that the silver filled epoxy be thinned with about 4 to 5% diluent.

Toluene was chosen as the more desirable diluent. A minimum of 1 hour exposure in air was used before parts were mated to allow most of the diluent to evaporate.

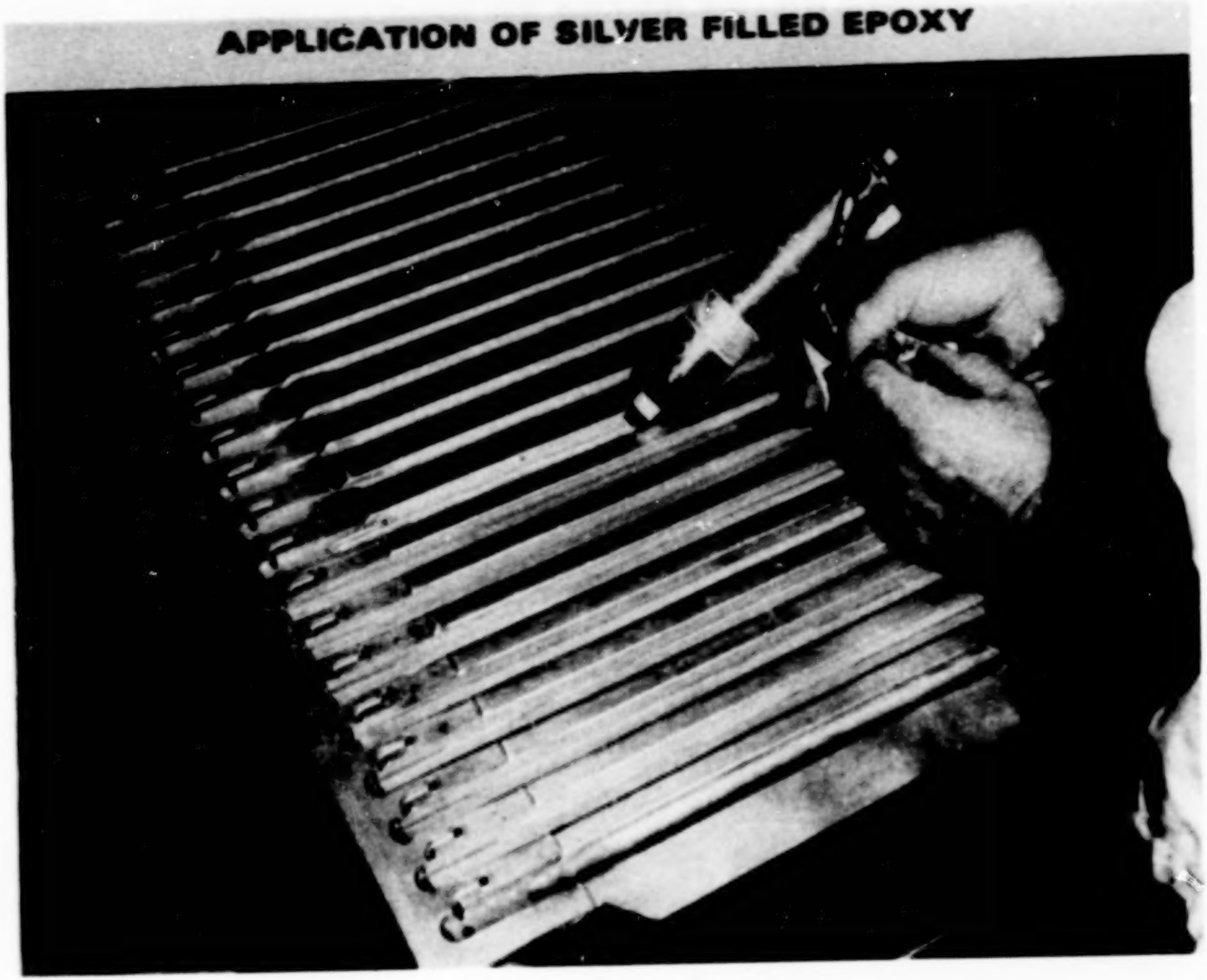

APPLICATION OF SILVER FILLED EPOXY

Figure 29

312

HOLOGRAMS OF PANEL SUBASSEMBLY, NO OUTER SKIN

(Figure 30)

A considerable effort was devoted to investigating nondestructive inspection techniques for use with bonded actively cooled panels. Radiography was used to identify the uniformity of those adhesive joints made with the silver filled epoxy. Tests with low pressure gas were used to identify leaks at various stages of the assembly fabrication. Holography was used to investigate the uniformity of bonding of the coolant passage tubing into the manifold/inner skin subassembly and to ascertain whether any of the coolant passages became plugged during bonding operations.

The holograms shown in this figure indicate the degree of uniformity achieved in the bonding operation. Careful examination of the holograms in the vicinity of the ends of the coolant passages indicates slight nonuniformity in the depth of end plug potting and apparent blockage in coolant passages.

Note in the lower photos the difference between the general pattern and those of the ninth tube from the left and the twelfth tube from the right. The former indicates an anomoly although the tube is pressurized. The latter indicates that the tube is blocked at both ends and is not pressurized.

HOLOGRAMS OF PANEL SUBASSEMBLY, NO OUTER SKIN

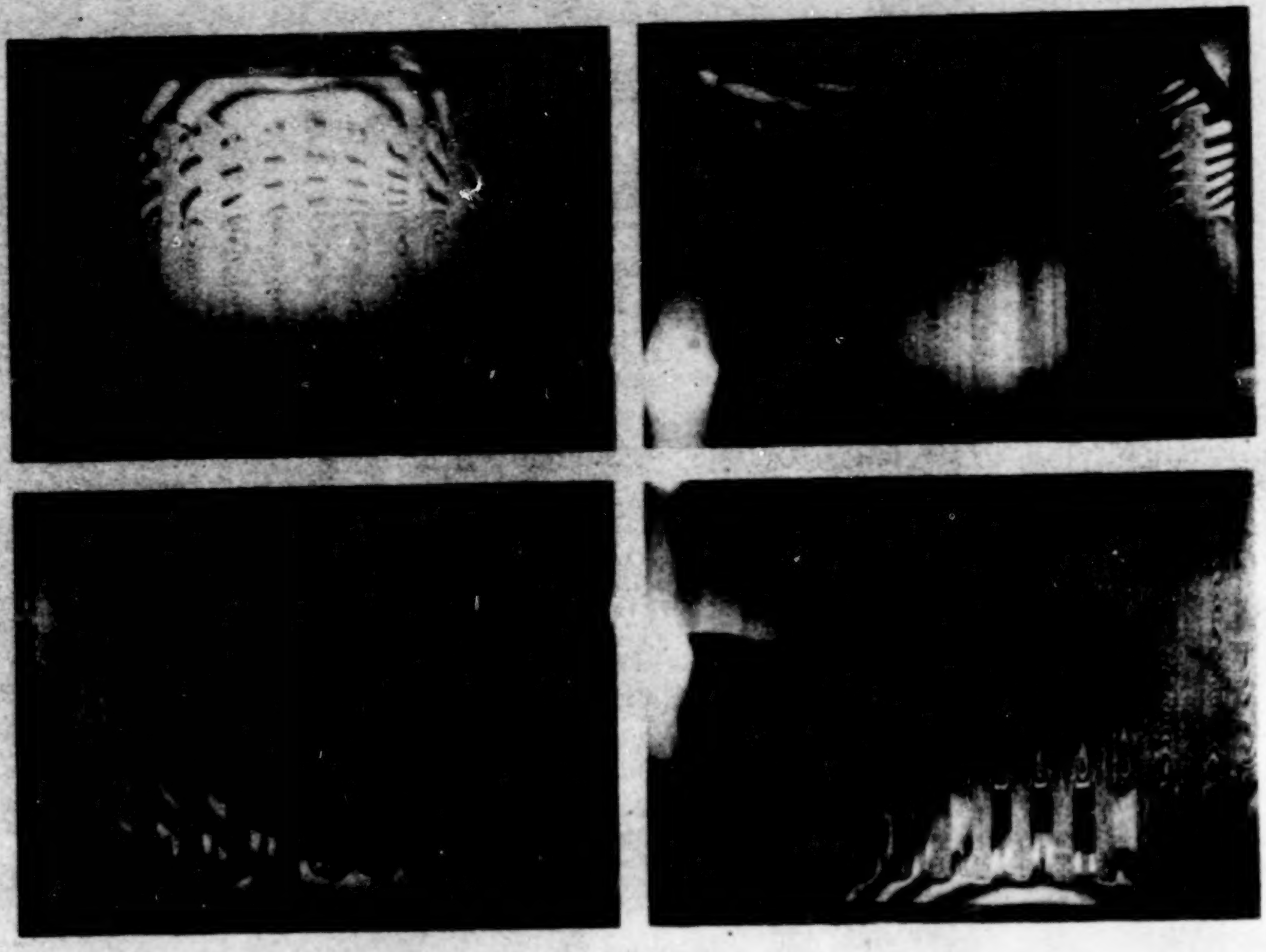

Figure 30

INFRARED SCAN RESULTS AFTER REWORK

(Figure 31)

Because of tolerances it was necessary to use thicker bondlines than anticipated between the coolant passage tubing and the manifolds. Despite the fact that the Epon 951 adhesive has low flow in thin thicknesses, the use of multiple layers increased the amount of flow. The holes between the manifolds and the coolant passages became plugged with excess adhesive. This condition was observed visually on some of the end holes, defined further through boroscopic inspection, and the severity was established by the nonuniformity of infrared scans across the panel.

After rework to open the holes between the manifold and the coolant passage tubing the infrared scans were repeated with the results shown here. The temperature of the water flowing through the panel was varied so that the scans could be made under transient conditions to maximize temperature differences. As indicated by these scans the coolant flow through the parallel passages was relatively uniform. Only one passage in each circuit lags the others to any significant degree. The flow through the end edge tubes appeared to be slightly less than average. The majority of the coolant passages did have uniform flow as evidenced by the general uniformity of temperature across the panel. Careful examination of the scans revealed the higher temperature between coolant passages and the lower temperature at the coolant passage. On casual observation these differences in temperature create the appearance of a rather wide scatter band.

INFRARED SCAN RESULTS AFTER REWORK

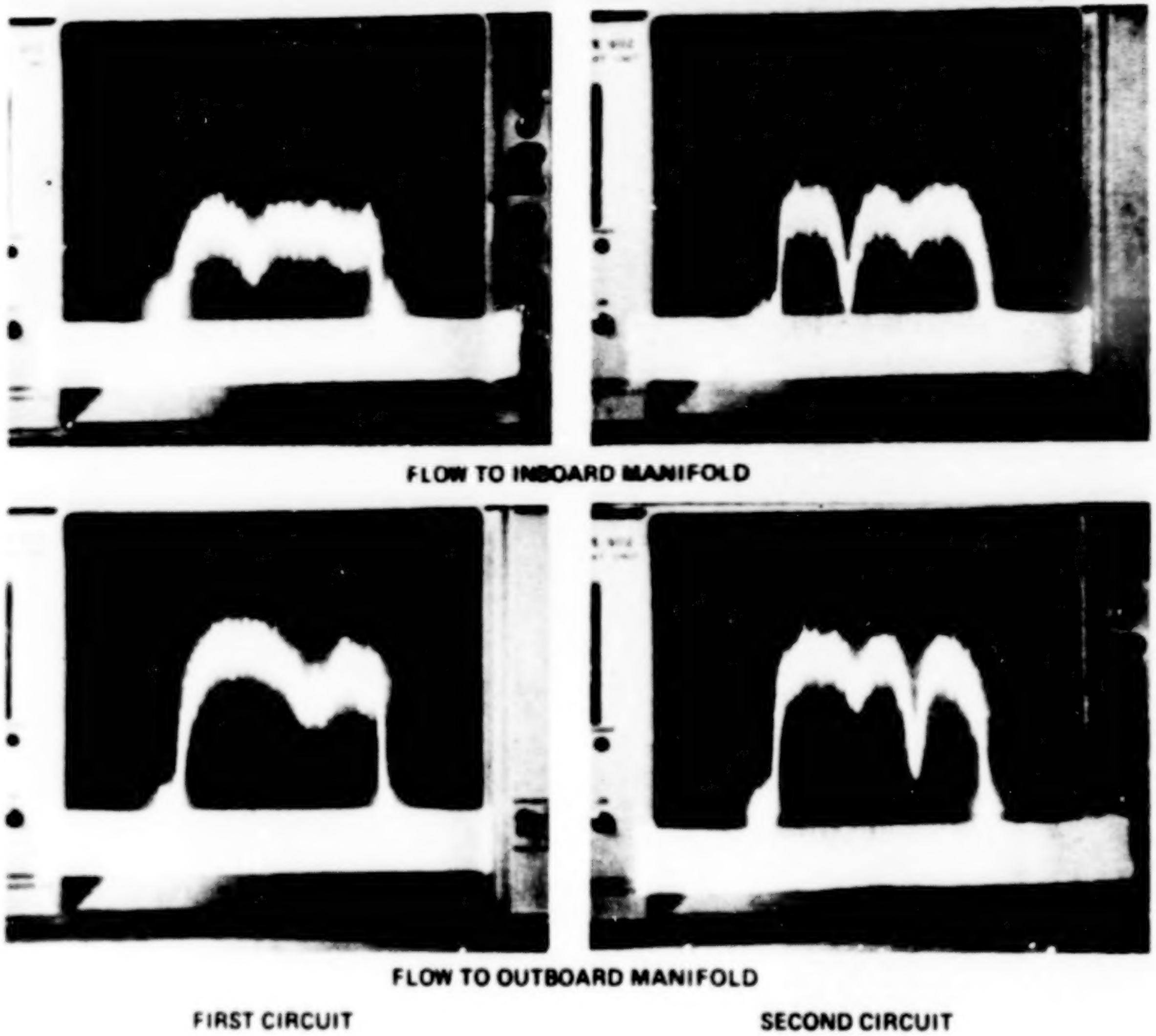

Figure 31

CONCLUDING REMARKS

(Figure 32)

Until the test panel is evaluated experimentally, it seems premature to draw conclusions. The work performed to optimize the full sized panel and to fabricate the test panel led to some observations that are presented as concluding remarks. Special attention is called to the accomplishment of the tubing fabricator who produced the unusual coolant passage shape to very stringent tolerances. Precision Tube was the only supplier willing to guarantee delivery out of twenty suppliers from whom quotes were requested.

CONCLUDING REMARKS

- STRUCTURAL CONSIDERATIONS ARE DOMINANT IN THE DESIGN OF ACTIVELY COOLED STRUCTURAL PANELS OF MINIMUM MASS
- WHEN HEAT FLUXES ARE IMPOSED DIRECTLY ONTO AN ACTIVELY COOLED STRUCTURAL PANEL THE USE OF ADHESIVE BONDING PERMITS THE USE OF OPTIMUM STRUCTURAL MATERIALS
- VARIOUS DIFFICULTIES ASSOCIATED WITH THE ACCOMMODATION OF MACHINING AND FORMED SHEET METAL TOLERANCES WITH THIN BOND LINES WERE RESOLVED
- NONDESTRUCTIVE INSPECTION TECHNIQUES WERE ADAPTED TO THE UNIQUE REQUIREMENTS OF AN ACTIVELY COOLED STRUCTURAL PANEL

Figure 32

318

REFERENCES

1. Nowak, R.J. and Kelly, H.N., "Actively Cooled Airframe Structures for High-Speed Flight," 17th Structures, Structural Dynamics, and Materials Conference Proceedings, May 1976, p. 209-217.

2. Helenbrook, R.G. and Anthony, F.M., "Design of a Convective Cooling System for a Mach 6 Hypersonic Transport Airframe," NASA CR-1918, December 1971.

3. Anthony, F.M., Dukes, W.H. and Helenbrook, R.G., "Internal Convective Cooling Systems for Hypersonic Aircraft," NASA CR-2480, February 1975.

4. Department of Defense, "Metallic Materials and Elements for Aerospace Vehicle Structures," MIL-HDBK-5A, Revised 5 January 1970.

5. Kroll, W.D., "Aerodynamic Heating and Fatigue," NASA Memo 6-4-59W, June 1959.

DESIGN AND ANALYSIS OF A PLATE-FIN SANDWICH ACTIVELY COOLED STRUCTURAL PANEL

L. M. Smith
Rockwell International
Space Systems Group

319

DESIGN & ANALYSIS OF A PLATE-FIN SANDWICH ACTIVELY COOLED STRUCTURAL PANEL*

L. M. Smith
Rockwell International

INTRODUCTION

The skin structure of hydrogen fueled hypersonic transport vehicles traveling at Mach 6 and above must be designed to withstand, for relatively long periods of time, the aerodynamic heating effects which are far more severe than those encountered by the supersonic aircraft of today. Three basic design options are available which will accommodate this aerodynamic heating. First, the use of conventional aircraft materials such as aluminum in combination with forced convection active cooling; Second, the use of radiative metallic heat shields; and Third, a combination of active cooling and radiative heat shields. This work addresses the first or active cooling option.

The basic active cooling concept, shown in Figure 1, consists of a stringer stiffened plate-fin sandwich. The sandwich surface is subjected to the aerodynamic heat flux which is transferred, via convection, to a coolant that is forced through the sandwich under pressure. The coolant, in turn, circulates in a closed loop through a hydrogen heat exchanger and back through the skin panel. The systems' aspects of the coolant loop and the hydrogen heat exchanger are not addressed in this paper.

---

*This paper summarizes a final report (Ref. 1) on a design and analysis effort conducted under contract NAS1-13382 with LaRC.

STRINGER STIFFENED PLATE-FIN SANDWICH ACTIVE COOLING CONCEPT

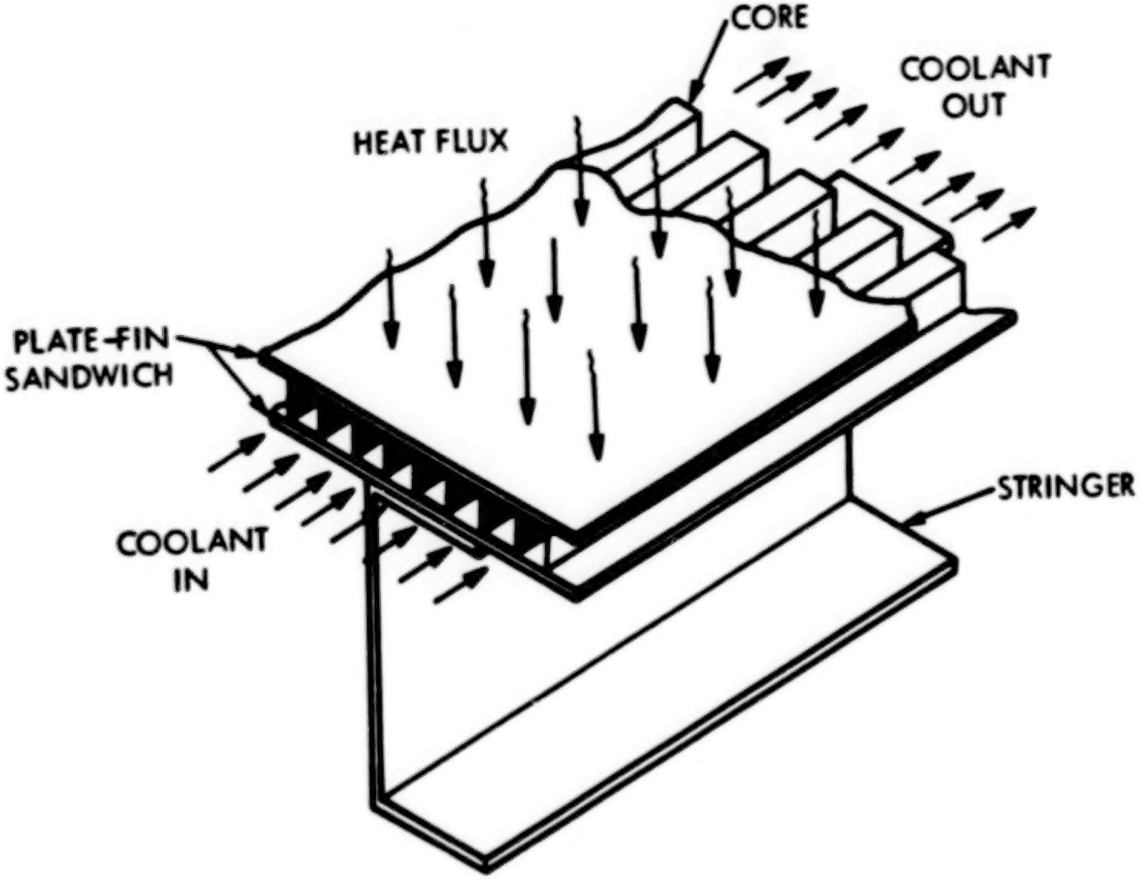
CORE
COOLANT OUT
HEAT FLUX
PLATE-FIN SANDWICH
STRINGER
COOLANT IN

Figure 1

DESIGN REQUIREMENTS & CRITERIA

(Figure 2)

Figure 2 illustrates in pictorial and tabular form the design requirements and criteria used for the design and analysis of a full scale actively cooled structural panel. The panel size, frame spacing, mechanical and thermal environment, and life requirements were established by NASA and are meant to be representative of the requirements that an actively cooled structural panel would encounter in actual application to a hypersonic aircraft. The physical loads factor of safety of 1.5 is consistent with federal standards for aircraft design and the thermal loads factor of safety of 1.0 is consistent with Rockwell requirements for elevated temperature structures such as Apollo, Shuttle and B-1.

The structure temperature limitation of 422 K (300°F) is consistent with an approximate 20 percent structural aluminum mechanical properties degradation (compared with room temperature values of ultimate tensile strength, ultimate shear strength, etc.). This temperature, 422 K (300°F), is generally considered to be the maximum temperature at which structural performance of aluminum alloys can be predicted accurately. The maximum allowable coolant temperature of 366 K (200°F) is conservative and provides an adequate margin before elevated temperature corrosion mechanisms become a serious consideration.

FULL SCALE PANEL DESIGN REQUIREMENTS

ITEM NO.	PARAMETER	REQMT/CRITERIA
1	CONSTRUCTION TYPE	STRINGER STIFFENED SANDWICH
2	PANEL MATERIAL	ALUMINUM
3	COOLANT	ETHYLENE GLYCOL/ WATER
4	COOLANT OUTLET PRESSURE	344.75 kPa (50 psi) MINIMUM
5	LOAD CYCLES	5000 WITH SCATTER FACTOR = 4 (e.g., 20,000)
6	FLIGHT LIFE	10,000 HOURS
7	FACTOR OR SAFETY PHYSICAL LOADS THERMAL LOADS	 1.5 1.0
8	STRUCTURE TEMP.	422°K (300°F) MAX
9	COOLANT TEMP.	366°K (200°F) MAX

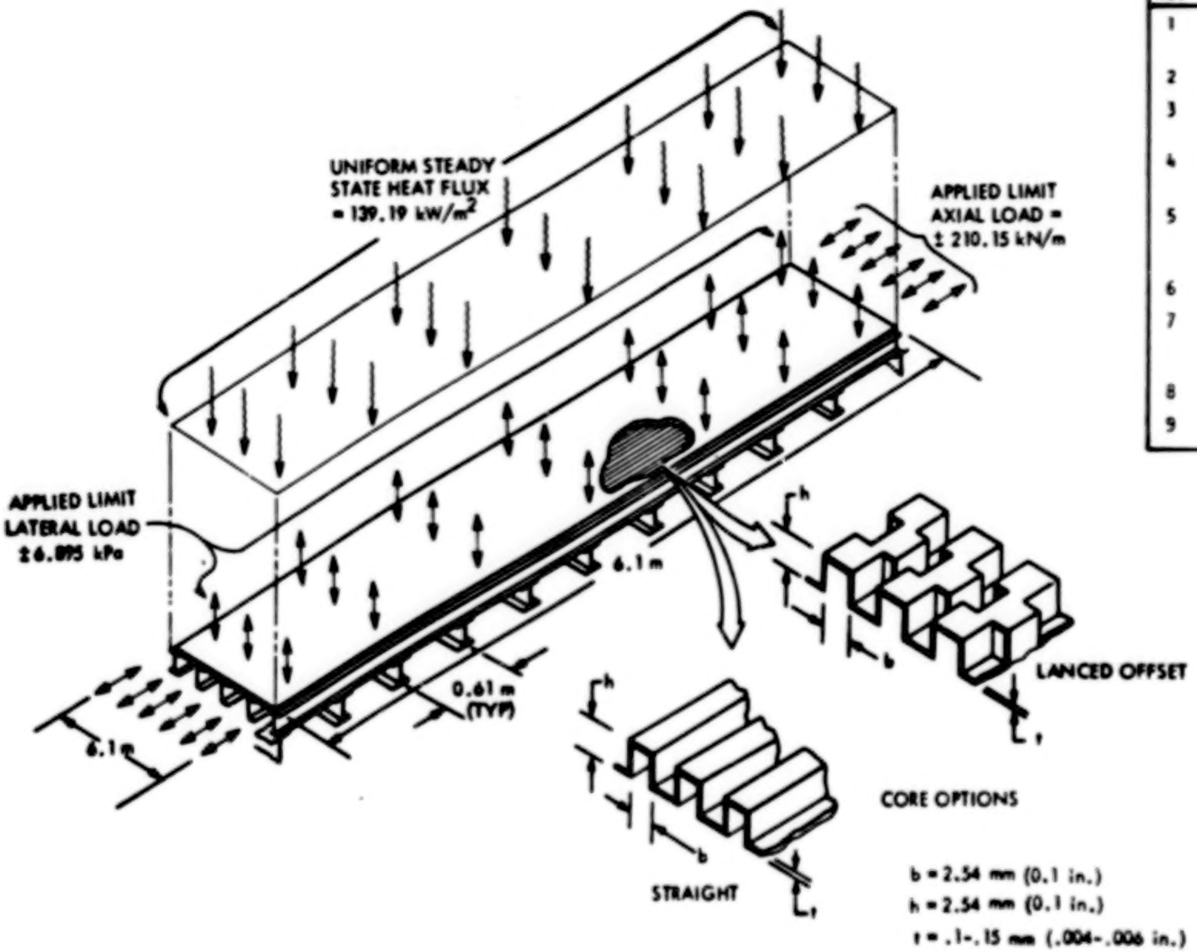
UNIFORM STEADY STATE HEAT FLUX = 139.19 kW/m²
APPLIED LIMIT AXIAL LOAD = ± 210.15 kN/m
APPLIED LIMIT LATERAL LOAD ±6.895 kPa
6.1 m
0.61 m (TYP)
6.1 m
h
b
t
LANCED OFFSET
h
b
t
STRAIGHT
CORE OPTIONS
b = 2.54 mm (0.1 in.)
h = 2.54 mm (0.1 in.)
t = .1-.15 mm (.004-.006 in.)

Figure 2

324

FULL SCALE ACTIVELY COOLED PANEL DESIGN PROCESS

(Figure 3)

The objective of this program was not only to develop the design of a full scale stringer stiffened plate-fin sandwich actively cooled panel but also to fabricate, for test by NASA/LaRC, a test panel representative of the resulting design. To develop confidence in the design and fabrication techniques and the ability of the test panel to withstand the structural and thermal test environment, the program was conducted in essentially five (5) phases as indicated on the flow chart, Figure 3. Each phase will be discussed during this presentation.

FULL SCALE ACTIVELY COOLED PANEL DESIGN PROCESS

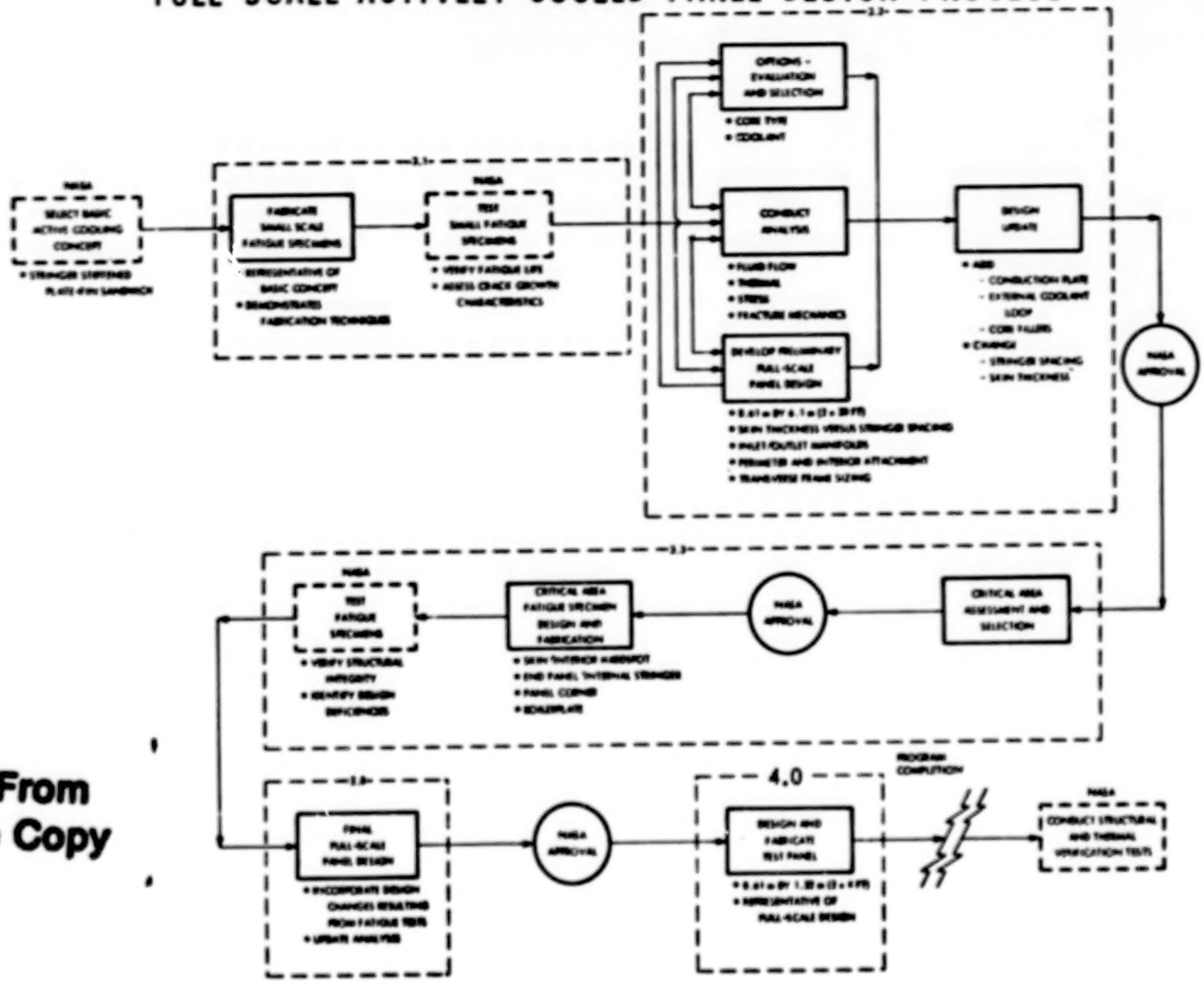
NASA
SELECT BASIC ACTIVE COOLING CONCEPT
• STRINGER STIFFENED PLATE-FIN SANDWICH
2.1
FABRICATE SMALL SCALE FATIGUE SPECIMENS
• REPRESENTATIVE OF BASIC CONCEPT
• DEMONSTRATES FABRICATION TECHNIQUES
NASA
TEST SMALL FATIGUE SPECIMENS
• VERIFY FATIGUE LIFE
• ASSESS CRACK GROWTH CHARACTERISTICS
2.2
OPTIONS - EVALUATION AND SELECTION
• CORE TYPE
• COOLANT
CONDUCT ANALYSIS
• FLUID FLOW
• THERMAL
• STRESS
• FRACTURE MECHANICS
DEVELOP PRELIMINARY FULL-SCALE PANEL DESIGN
• 0.61 m BY 6.1 m (2 × 20 FT)
• SKIN THICKNESS VERSUS STRINGER SPACING
• INLET/OUTLET MANIFOLDS
• PERIMETER AND INTERIOR ATTACHMENT
• TRANSVERSE FRAME SIZING
DESIGN UPDATE
• ADD
- CONDUCTION PLATE
- EXTERNAL COOLANT LOOP
- CORE FILLERS
• CHANGE
- STRINGER SPACING
- SKIN THICKNESS
NASA APPROVAL
2.3
CRITICAL AREA ASSESSMENT AND SELECTION
NASA APPROVAL
CRITICAL AREA FATIGUE SPECIMEN DESIGN AND FABRICATION
• SKIN INTERIOR HARDSPOT
• END PANEL INTERNAL STRINGER
• PANEL CORNER
• SCALEPLATE
NASA
TEST FATIGUE SPECIMENS
• VERIFY STRUCTURAL INTEGRITY
• IDENTIFY DESIGN DEFICIENCIES
2.4
FINAL FULL-SCALE PANEL DESIGN
• INCORPORATE DESIGN CHANGES RESULTING FROM FATIGUE TESTS
• UPDATE ANALYSES
NASA APPROVAL
4.0
DESIGN AND FABRICATE TEST PANEL
• 0.61 m BY 1.22 m (2 × 4 FT)
• REPRESENTATIVE OF FULL-SCALE DESIGN
PROGRAM COMPLETION
NASA
CONDUCT STRUCTURAL AND THERMAL VERIFICATION TESTS

Figure 3

Microfilmed From
Best Available Copy

SMALL SCALE TEST SPECIMEN

(Figure 4)

The initial phase of the program consisted of the fabrication of eight (8) small scale test specimens, whose basic configuration is a plate-fin sandwich structure terminating on either end in load adapters. Four (4) specimens were fabricated with straight core and the remainder with lanced offset core. In both cases, the core material is 0.127 mm (0.005 in.) thick 6061 aluminum formed by the supplier into a corrugated core 2.54 mm (0.10 in.) high with a pitch of 3.94 coolant channels per centimeter (10/in.). The face sheets are 0.51 mm (0.020 in.) thick ALCOA No. 21F braze sheets of 6951 aluminum alloy clad on one side with 4045 braze alloy. The specimen width is 0.13 m (5.12 in), the test section is 0.175 m (6.90 in.) long and the overall specimen length (including load adapters) is 0.39 m (15.50 in.). Each specimen has four (4) fluid access ports which are machined into the specimen after brazing and heat treatment.

The objectives of this phase of the program were: (1) to verify that acceptable fabrication results could be obtained from the Rockwell developed fluxless brazing and heat treatment processes and (2) to determine, by NASA test, if the concept, as fabricated, could survive the 20,000 cycle fatigue life requirement with and without intentionally placed cracks or flaws in the face sheets. Both objectives were met successfully.

The specimens were tested by NASA at room temperature with an internal lockup pressure of 689.5 kPa (100 psi) to a fully reversed (R = -1) alternating stress level of 124 MPa (18,000 psi). Results showed that: (1) both core configurations can meet the 20,000 cycle design requirement; (2) the straight core has a greater fatigue life than the lanced offset core; (3) even with surface flaw intentionally placed in the face sheets, the 20,000 cycle requirement was exceeded; and (4) once a flaw became a through crack, at least 1,400 additional cycles were required to produce a structural failure.

SMALL SCALE TEST SPECIMEN

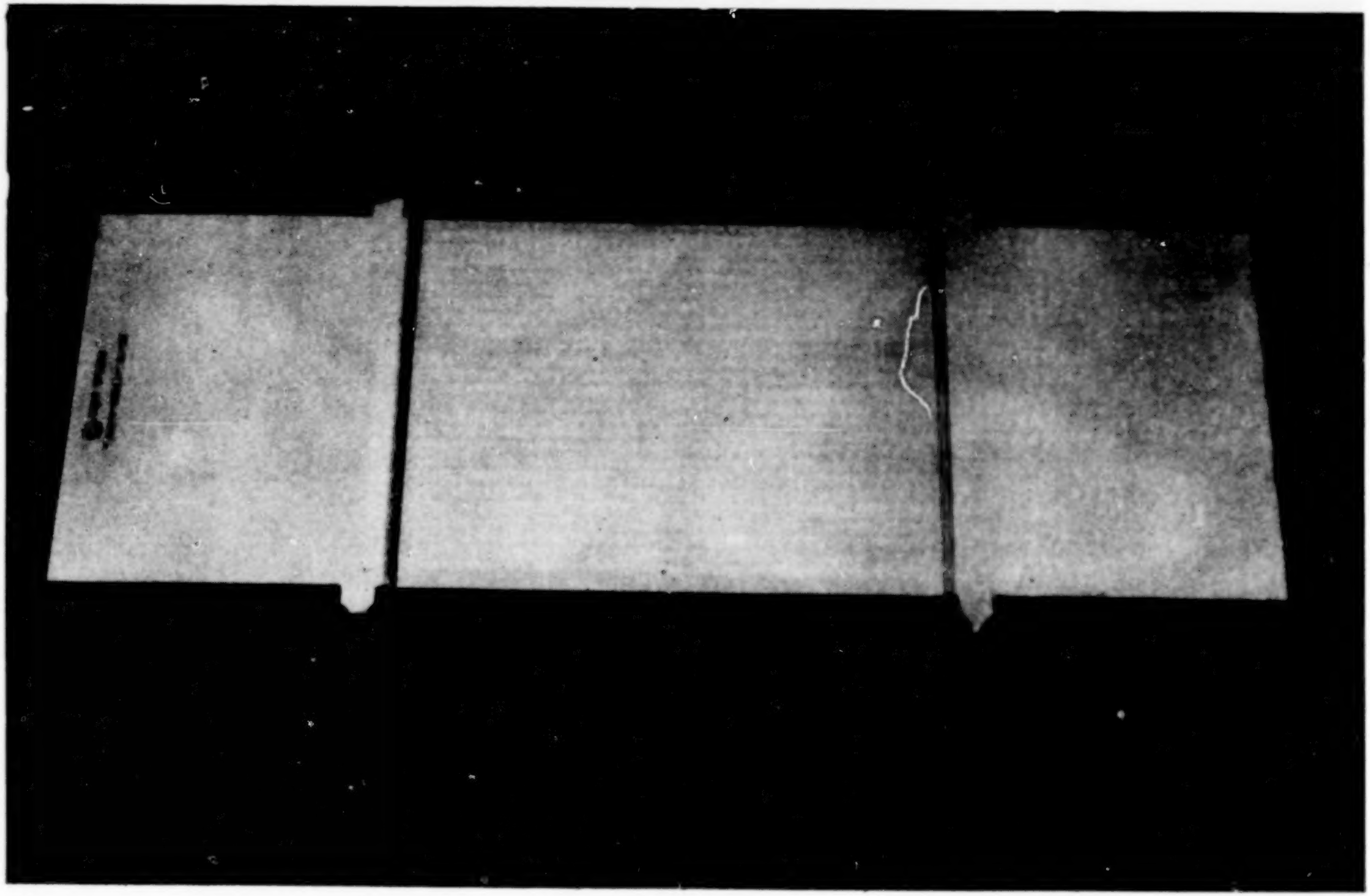

Figure 4

328

FINAL FULL SCALE ACTIVELY COOLED STRUCTURAL PANEL CONFIGURATION

(Figure 5)

Figure 5 depicts schematically the final full scale panel configuration. It consists of: (1) a 0.61 m by 6.1 m (2 by 20 ft) plate-fin brazed sandwich structure which is 4.17 mm (0.164 in.) thick except adjacent to the perimeter where the thickness is increased to 5.69 mm (0.224 in.); (2) inlet and outlet manifolds; (3) two edge stringers (I-sections); (4) three (3) internal stringers in the form of channel sections; and (5) associated bracketry and attachment hardware. It should be noted that the edge stringers provide the attachment base for adjacent panels, hence only one edge stringer is considered when panel mass is calculated.

FINAL FULL SCALE ACTIVELY COOLED STRUCTURAL PANEL CONFIGURATION

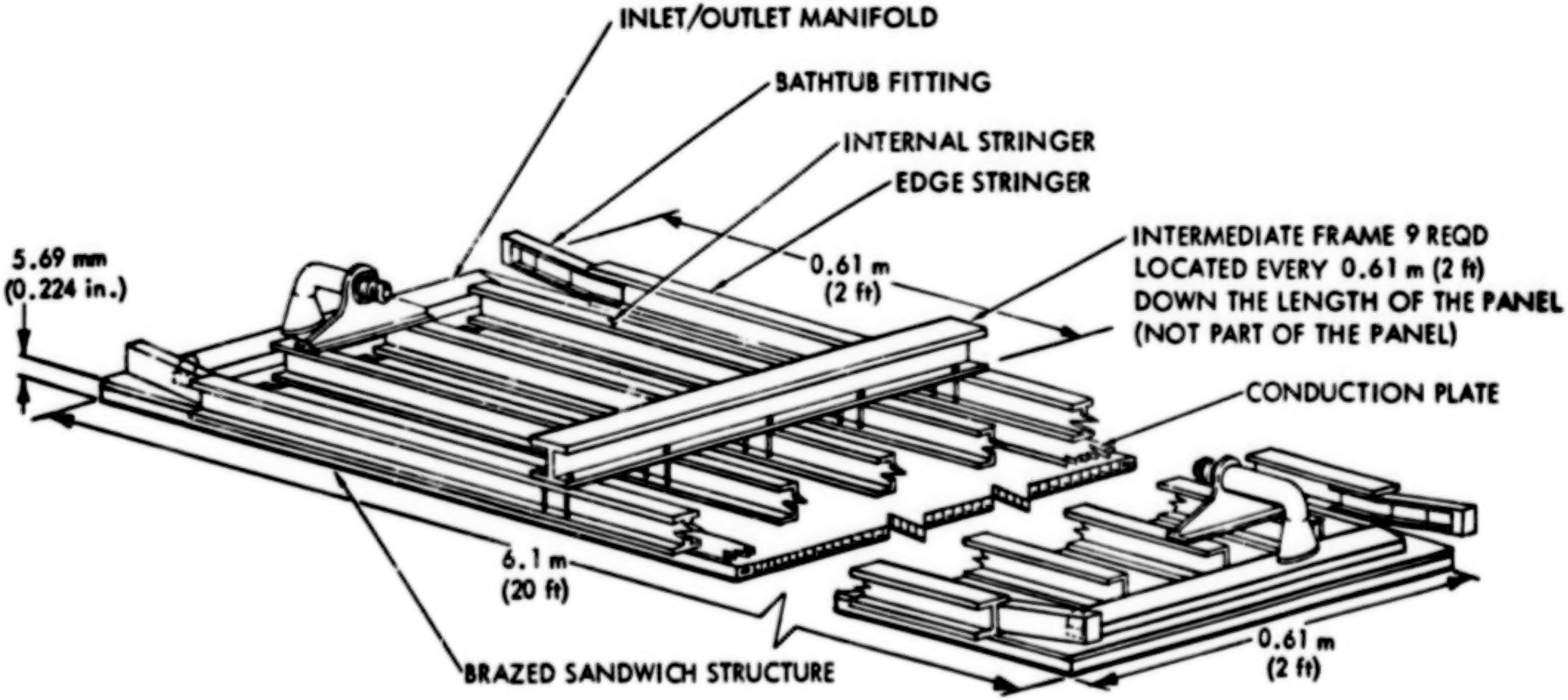
INLET/OUTLET MANIFOLD
BATHTUB FITTING
INTERNAL STRINGER
EDGE STRINGER
INTERMEDIATE FRAME 9 REQD
LOCATED EVERY 0.61 m (2 ft)
DOWN THE LENGTH OF THE PANEL
(NOT PART OF THE PANEL)
5.69 mm
(0.224 in.)
0.61 m
(2 ft)
CONDUCTION PLATE
6.1 m
(20 ft)
0.61 m
(2 ft)
BRAZED SANDWICH STRUCTURE

Figure 5

CORE CONFIGURATIONS

(Figure 6)

Two core configurations were provided by NASA for evaluation during the initial phase of the panel design phase. These cores, shown in Figure 6, are termed "lanced offset" and "straight" core. The "straight" core was selected for the actively cooled panel design for the following reasons:

1. The straight core exhibited superior fatigue life in the small scale specimen tests conducted by NASA.
2. The lanced offset core forming process produces very sharp edges between sheared surfaces which could act as local discontinuities and produce stress concentration points.
3. The lanced offset core, by virtue of its multitude of edges, would significantly increase the system drop and produce a corresponding increase in Auxiliary Power System (APS) mass penalty.

CORE CONFIGURATIONS

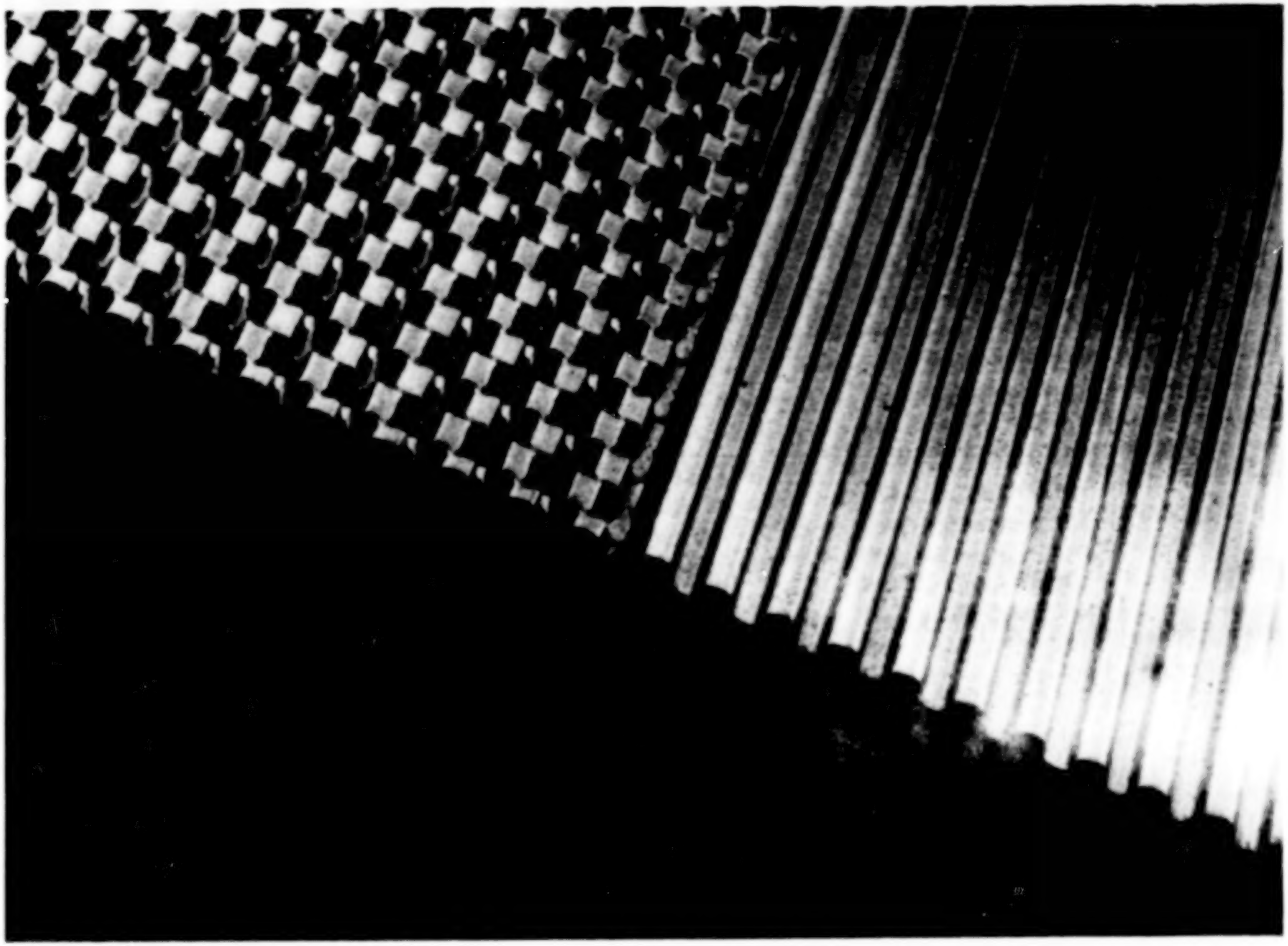

Figure 6

PLATE-FIN BRAZED SANDWICH DETAILS

(Figure 7)

The plate fin sandwich structure stack-up is shown in Figure 7. Its major components are the machined manifold bases, conduction plates, interior face sheet, core, core filler bars, end filler plates, edge filler plates, hardspots and an exterior face sheet. These components are brazed together in one operation and subsequently heat treated to the -T6 temper. The fabrication aspects will be discussed in the following presentation (Ref. 2).

The face sheets are 0.81 mm (0.032 in.) thick No. 23F braze sheets which consist of 6951 aluminum alloy clad with 4045 braze alloy.

The hardspots indicated in the figure occur at each intermediate transverse frame/internal stringer intersection. They allow a panel and stringer attachment to the intermediate frame to be made from the panel exterior via two long countersunk bolts. Twenty-seven (27) such attachments are made in the full scale panel design.

The core filler bars are solid 6061 aluminum machined to fit into a coolant passage or channel every 7.62 cm (3.0 in.) across the width of the panel. They provide rigid support and prevent core cavitation or "suck-in" during the brazing cycle.

The other components of the brazed sandwich are discussed in the following charts.

PLATE-FIN BRAZED SANDWICH DETAILS

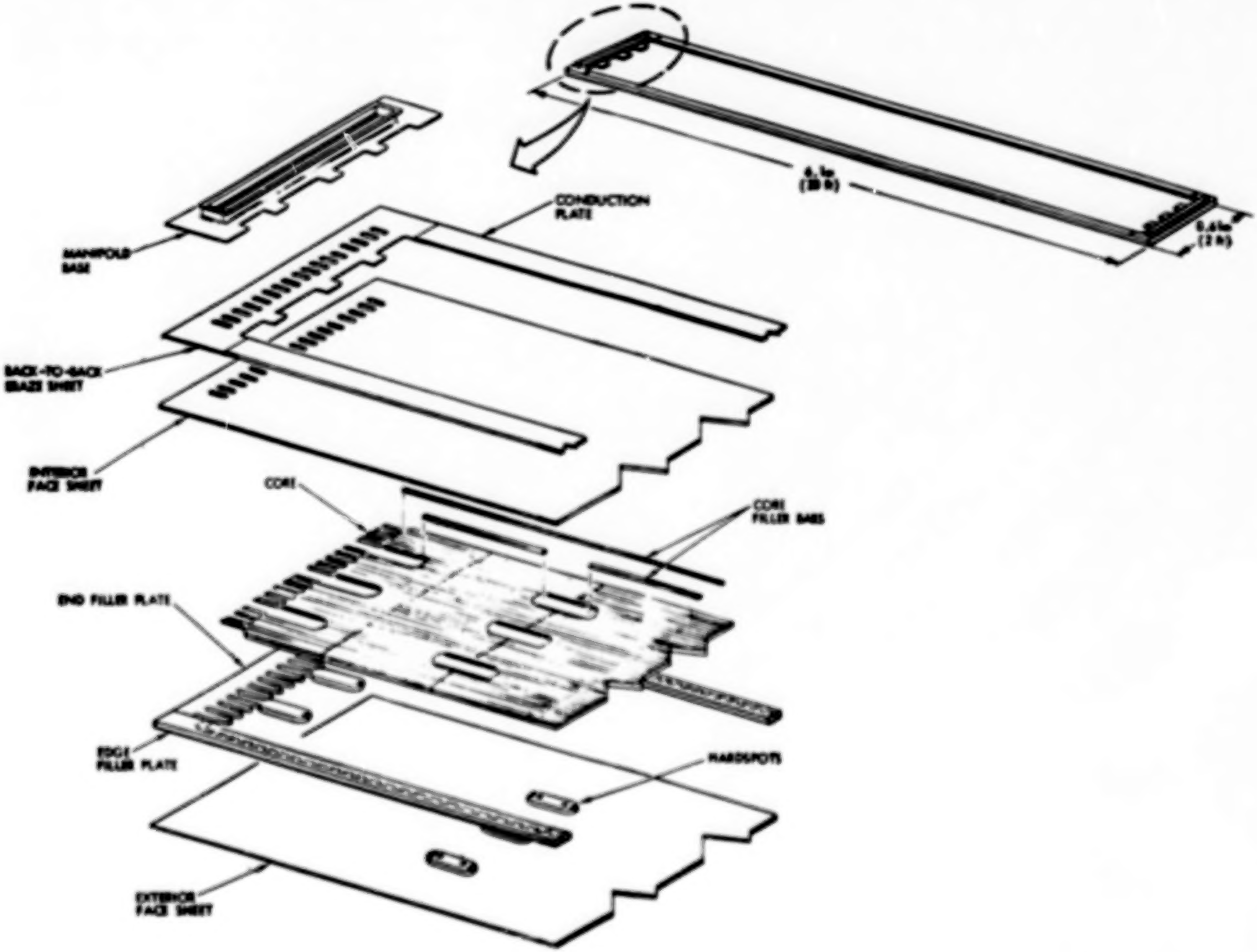
6.1m
(20 ft)
0.61m
(2 ft)
CONDUCTION PLATE
MANIFOLD BASE
BACK-TO-BACK BRAZE SHEET
INTERIOR FACE SHEET
CORE
CORE FILLER BARS
END FILLER PLATE
EDGE FILLER PLATE
HARDSPOTS
EXTERIOR FACE SHEET

Figure 7

1

END PANEL DETAILS

(Figure 8)

Figure 8 shows a closeup schematic of the end of the full scale panel. Following sandwich brazing but prior to heat treatment, the manifold dome is welded to the manifold base. Following heat treatment, the three (3) 3.86 cm (1.52 in.) deep channel shaped internal stringers are bonded to the inner face sheet with an epoxy-based, scrim reinforced, high temperature adhesive system. The sandwich structure and stringers are then mechanically attached to the edge stringers and the main frame of the aircraft. The perimeter of the sandwich structure is solid and accepts the attachment fasteners.

The blowup of the panel is presented to show the method of coolant entrance and egress to the core from the manifold. The coolant passes from the manifold thru elongated holes in the inner face sheet, between the fingers or "saw teeth" in the end panel filler plates and into the core. Also shown in phantom is the external coolant channel's exit from the manifold area. The design evolution of this coolant channel is discussed along with Figure 10.

END PANEL DETAILS

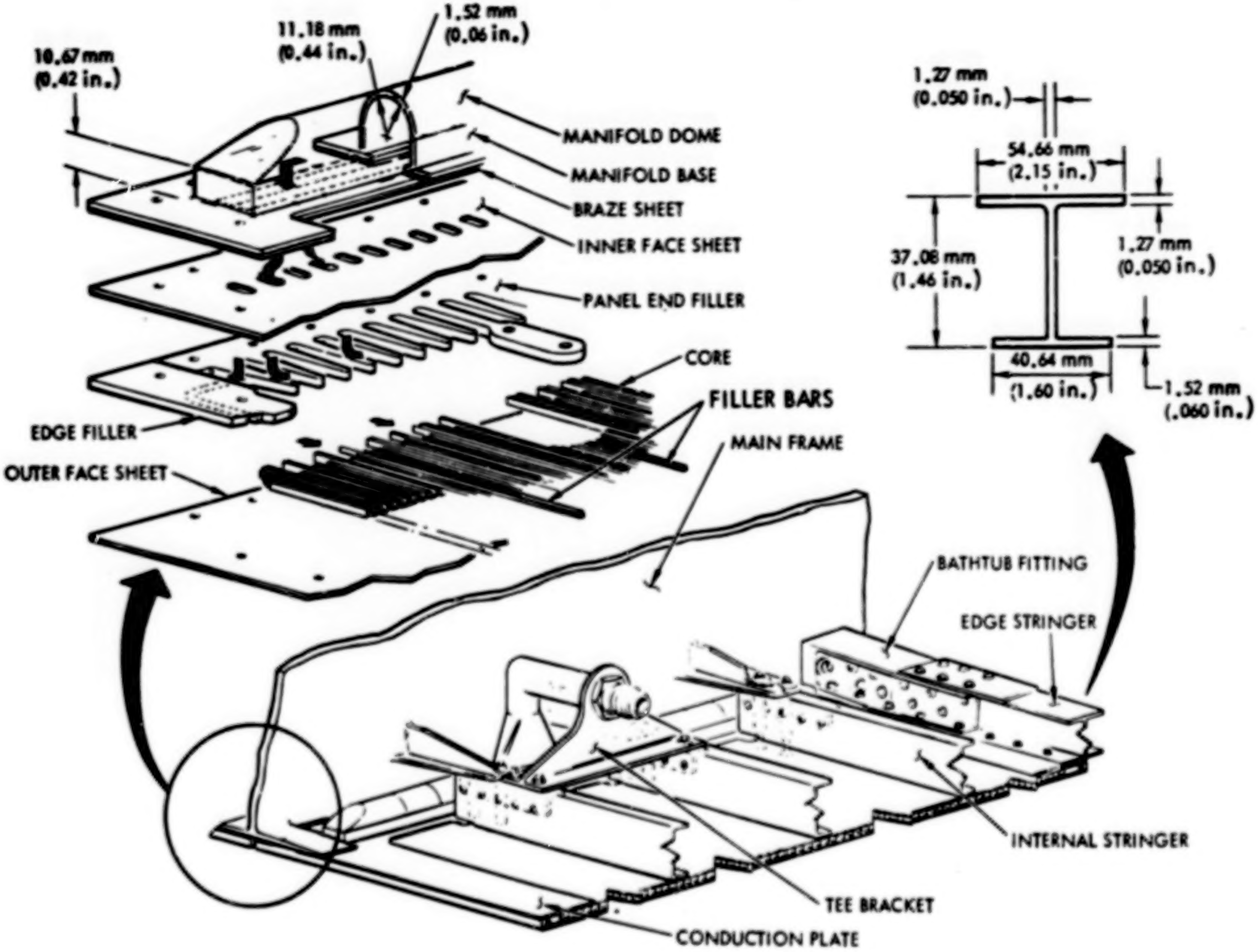
10.67 mm
(0.42 in.)
11.18 mm
(0.44 in.)
1.52 mm
(0.06 in.)
MANIFOLD DOME
MANIFOLD BASE
BRAZE SHEET
INNER FACE SHEET
PANEL END FILLER
CORE
FILLER BARS
EDGE FILLER
OUTER FACE SHEET
MAIN FRAME
1.27 mm
(0.050 in.)
54.66 mm
(2.15 in.)
37.08 mm
(1.46 in.)
1.27 mm
(0.050 in.)
40.64 mm
(1.60 in.)
1.52 mm
(.060 in.)
BATHTUB FITTING
EDGE STRINGER
INTERNAL STRINGER
TEE BRACKET
CONDUCTION PLATE

Figure 8

FULL SCALE PANEL MASS BREAKDOWN

(Figure 9)

The panel mass shown in Figure 9 is made up of three (3) elements: the dry structure mass, residual coolant mass and Auxiliary Power System (APS) mass penalty. The dry structure mass of 35.69 kg (87.50 lbm) is dominated by the 0.81 mm (0.032 in.) thick face sheets. They represent 46% of this mass. Hence, the only reasonable approach to reducing dry structure mass is by a face sheet thickness reduction. The face sheet thickness is dictated by not only compressive stability requirements, but also by internal system pressure. Structural analysis dictates a thickness of approximately 0.61 mm (0.024 in.) and the next standard size braze sheet is 0.81 mm (0.032 in.) thick. However, for actual applications, it might be economically attractive to consider chem-milling the material to an optimum thickness, which would result in a total panel mass reduction of approximately 9%.

The residual coolant mass is that fluid mass contained in the panel from the manifold inlet fitting to the outlet fitting and is based on the density of a 60/40 percent ethylene glycol/water mixture at 311 K (100°F).

The Auxiliary Power System (APS) mass penalty is a function of system flow rate ($\dot{\omega}$), pressure drop (ΔP), flight time (θ), coolant density (ρ) and an APS mass penalty conversion factor (G).

$$\mathrm{APS} = \frac{G \dot{\omega} \Delta P \theta}{\rho}$$

FULL SCALE PANEL MASS BREAKDOWN

COMPONENT	MASS kg	UNIT MASS	
		kg/m^2	lb$_m$/ft^2
DRY STRUCTURE			
BRAZED SANDWICH	(24.32)	(6.54)	1.34
FACE SHEETS	16.25		
CORE	2.31		
HARDSPOTS	0.24		
FILLER BARS	0.61		
EDGE FILLER PLATES	1.99		
END FILLER PLATES	0.33		
MANIFOLD BASES	0.42		
CONDUCTION PLATES	2.17		
MANIFOLD TOP	(0.63)	(0.17)	0.03
DOMES	0.17		
TRANSITIONS	0.03		
END FITTINGS	0.20		
BRACKETS	0.23		
INTERNAL STIFFENING	(5.08)	(1.37)	0.28
STRINGERS	4.16		
BRACKETS	0.6		
SHIMS	0.02		
ADHESIVE	0.3		
EDGE STIFFENING	(3.36)	(0.90)	0.18
STRINGERS	2.86		
BATHTUB FITTINGS	0.5		
ATTACHMENT HARDWARE	(2.3)	(0.62)	0.13
DRY STRUCTURE TOTAL	35.69	9.60	1.96
RESIDUAL COOLANT	8.27	2.22	0.45
• AUXILLARY POWER SYS PENALTY	1.99	0.54	0.11
TOTAL PANEL MASS	45.95	12.36	2.52

Figure 9

PANEL EDGE DESIGN

(Figure 10)

The attachment of the panel to the edge stringer requires that solid aluminum be placed between the face sheets in place of the core for mechanical fastener installation. As indicated in Figure 10, the initial design incorporated a 19.10 mm (0.75 in.) wide strip at the edge of the panel. Thermal analysis results indicated a peak temperature in excess of the 394 K (250°F) allowable for this area. A conduction plate which would draw heat from the edge strip and feed it via convection to the coolant was added to the design. The thermal analysis was rerun and although an improvement in peak temperature was predicted, the allowable was still exceeded. A coolant loop external to the fastener line was added to the design and a peak temperature of 388 K (235°F) was predicted at the fastener line near the outlet end of the panel adjacent to the core termination. This configuration was adopted for the full scale design.

THERMAL ANALYSIS INFLUENCE

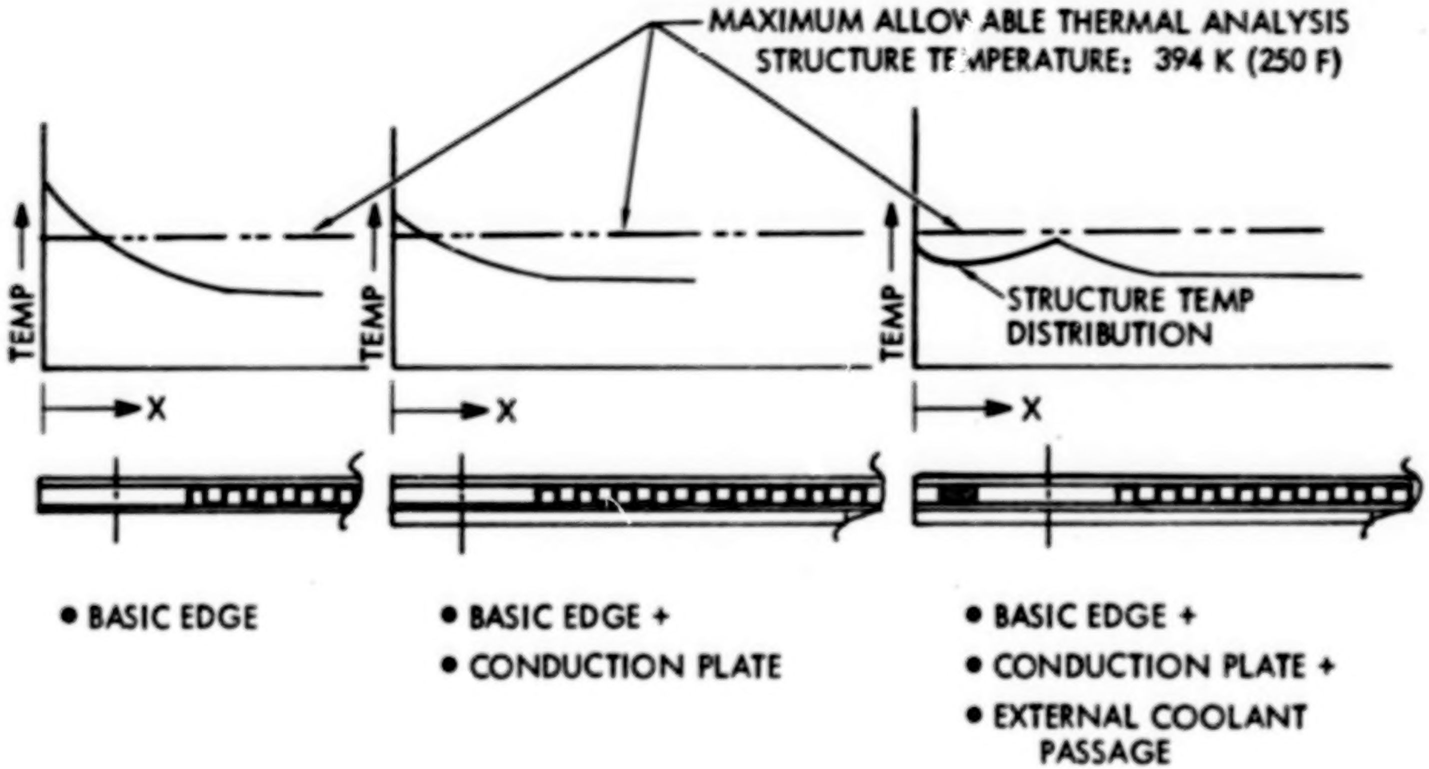
MAXIMUM ALLOWABLE THERMAL ANALYSIS STRUCTURE TEMPERATURE: 394 K (250 F)
TEMP
X
TEMP
X
TEMP
X
STRUCTURE TEMP DISTRIBUTION
• BASIC EDGE
• BASIC EDGE +
• CONDUCTION PLATE
• BASIC EDGE +
• CONDUCTION PLATE +
• EXTERNAL COOLANT PASSAGE

Figure 10

PANEL EDGE & CORE AREA TEMPERATURE DISTRIBUTION

(Figure 11)

Figure 11 plots the panel predicted temperature distribution for the indicated coolant inlet conditions of 13,608 kg/hr (30,000 lbm/hr) flow rate and 289 K (60°F) inlet temperature. This set of inlet conditions was selected for the final design based on results of a computerized parametric thermal and fluid flow analysis that varied coolant flow rate between 9,078 kg/hr (20,000 lbm/hr) and 18,156 kg/hr (40,000 lb/hr) and coolant inlet temperature between 278 K (40°F) and 311 K (100°F). The selected inlet conditions resulted in the best combination of maximum coolant temperature, maximum structure temperature and pressure drop.

The temperature plots coded ①, ②, ③, ⑤, ⑥ and ⑨ represent structure temperatures and the remainder represent coolant temperatures. The knee-in curves ⑤, ⑥ and ⑨ occur due to a change in the coolant flow regime from laminar flow to transitional flow and a corresponding significant increase in the value of coolant film conductance.

It should be noted that the thermal model and the resulting temperature predictions do not take into account localized end panel effects. This area was analyzed separately and a peak temperature of 414 K (286°F) was predicted for the corner of the panel at the outlet end.

PANEL EDGE AND CORE AREA TEMPERATURE DISTRIBUTION

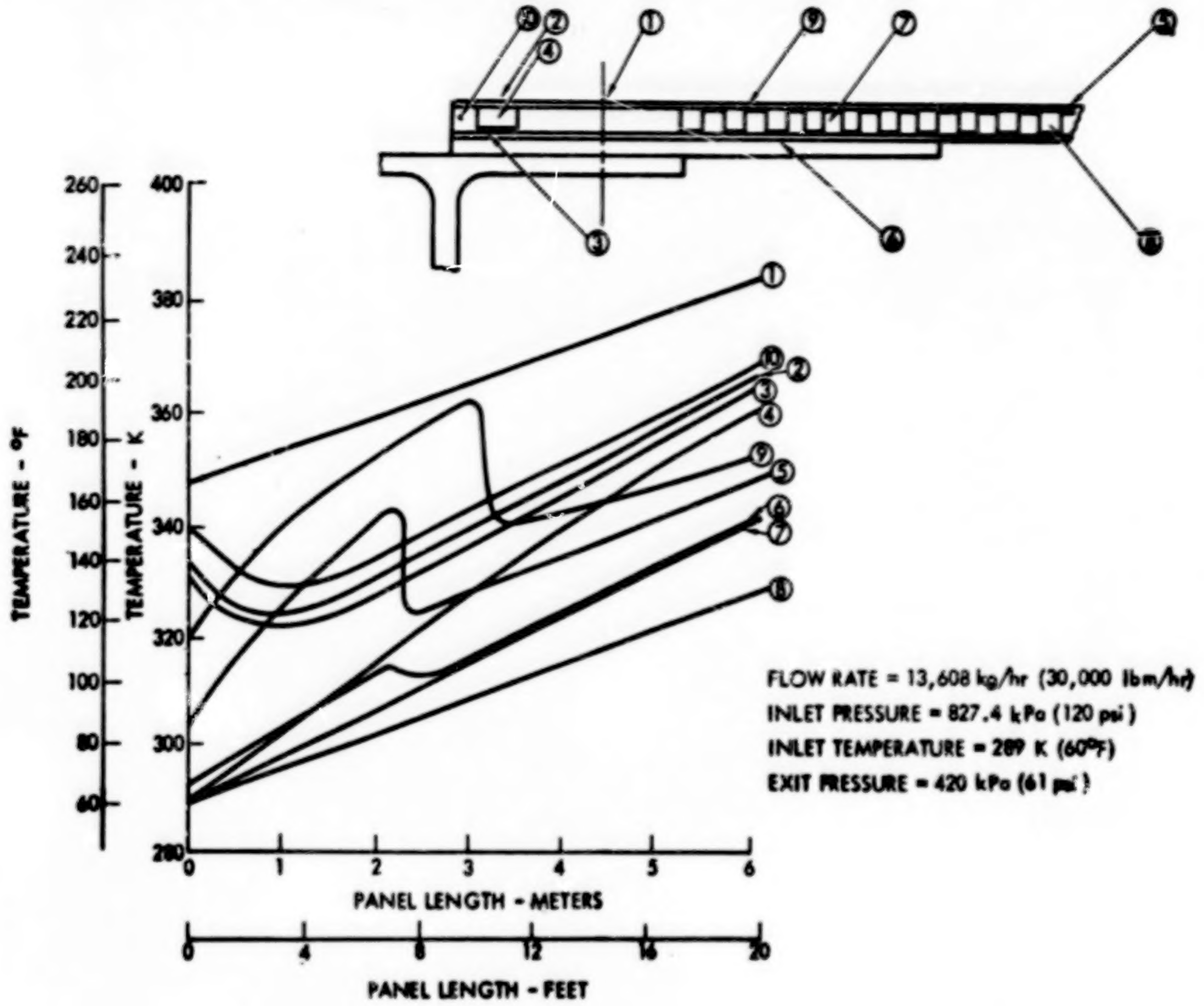

FLOW RATE = 13,608 kg/hr (30,000 lbm/hr)
INLET PRESSURE = 827.4 kPa (120 psi)
INLET TEMPERATURE = 289 K (60°F)
EXIT PRESSURE = 420 kPa (61 psi)

Figure 11

342

FULL SCALE PANEL PERFORMANCE SUMMARY

(Figure 12)

This chart tabulates the predicted performance characteristics for a full scale stringer stiffened plate-fin sandwich actively cooled panel under the influence of a hypersonic aircraft mechanical and thermal environment for the coolant inlet conditions indicated. The system pressure drop of 827.4 kPa - 362.7 kPa (120 -52.6 psi) or 464.7 kPa (67.4 psi) includes the pressure drop along the core plus the entrance/exit effects in the manifolds.

FULL SCALE PANEL PERFORMANCE CHARACTERISTICS

● COOLANT INLET CONDITIONS	
FLOW RATE	13,608 kg/hr (30,000 lbm/hr)
TEMPERATURE	289 K (60°F)
PRESSURE	827.4 kPa (120 psi)
● MAXIMUM TEMPERATURES	
COOLANT	361 K (191°F)
STRUCTURE	414 K (286°F)
● OUTLET PRESSURE	362.7 kPa (52.6 psi)
● MINIMUM STRUCTURAL MARGIN OF SAFETY	.18

Figure 12

FULL SCALE PANEL CRITICAL AREA LOCATIONS

(Figure 13)

Following completion of the full scale panel design, structurally critical areas of the panel were identified. Fatigue specimens of these areas were designed and fabricated for test by NASA.

The skin/interior hardspot area was selected to evaluate the effects of gaps between the core and hardspot and the hardspots sharp terminations on the face sheets. The end panel/internal stringer area was considered critical because the load path from the panel thru the main frame to the abutting panel joggles, and kick loads and local bending exist. The third area simulates the corner of two adjacent panels. This area was considered critical because of (1) complexity of the panel/edge stringer/bathtub fitting attachment to the main transverse frame, (2) load path from panel to panel uncertainty, and (3) the fact that the structural analysis indicates that the corner fasteners are the highest loaded fasteners in the panel.

FULL SCALE PANEL CRITICAL AREAS

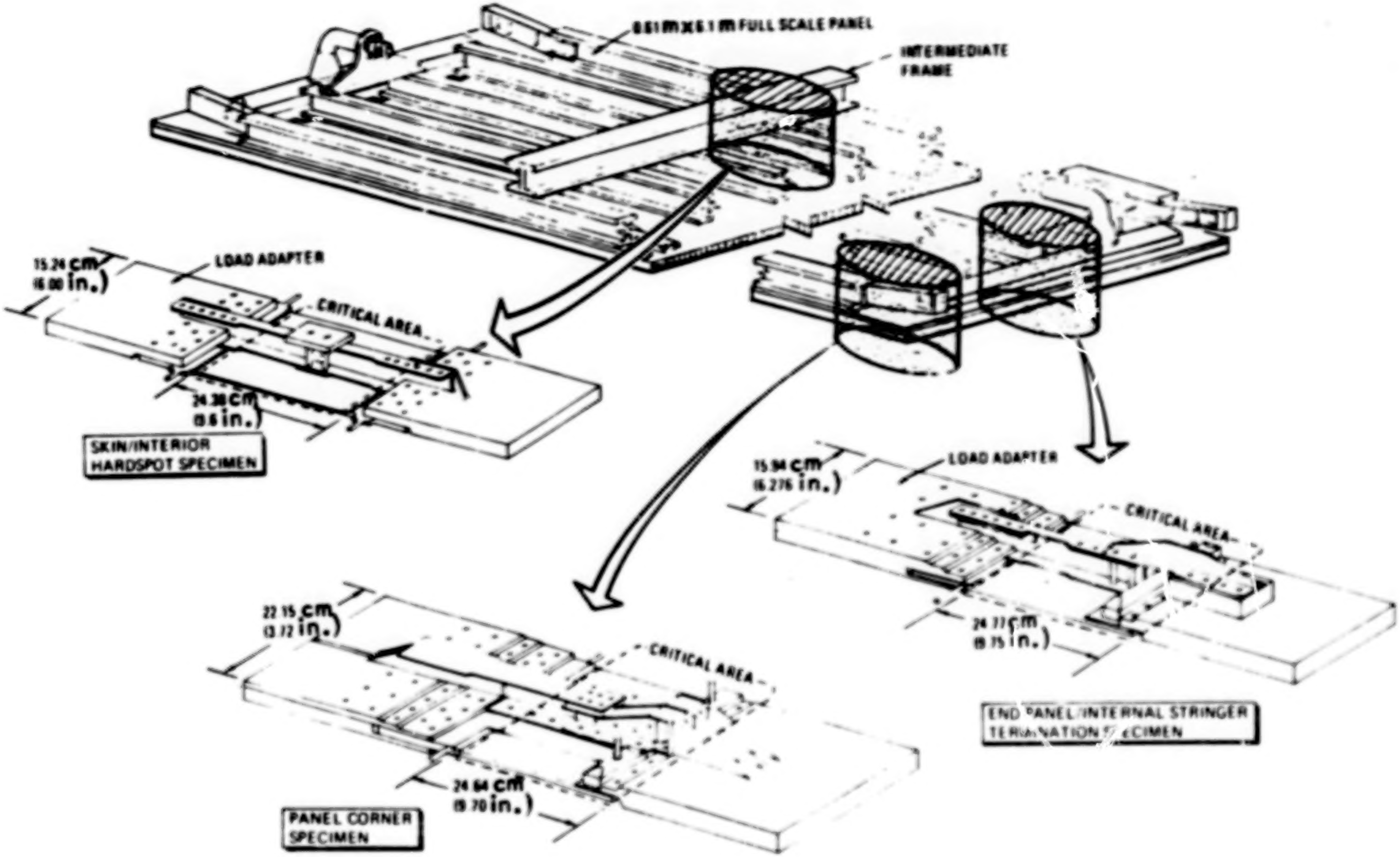
0.61 m X 6.1 m FULL SCALE PANEL
INTERMEDIATE FRAME
15.24 cm (6.00 in.)
LOAD ADAPTER
CRITICAL AREA
24.38 cm (9.6 in.)
SKIN/INTERIOR HARDSPOT SPECIMEN
15.94 cm (6.276 in.)
LOAD ADAPTER
CRITICAL AREA
24.77 cm (9.75 in.)
END PANEL/INTERNAL STRINGER TERMINATION SPECIMEN
22.15 cm (8.72 in.)
CRITICAL AREA
24.64 cm (9.70 in.)
PANEL CORNER SPECIMEN

Figure 13

Microfilmed From
Best Available Copy

SKIN/INTERIOR HARDSPOT FATIGUE SPECIMEN (SIHS)

(Figure 14)

The photograph shows the inboard side of the SIHS. The overall specimen length including load adapters is 0.67 m (26.25 in.). The specimen is 0.152 m (6.00 in.) wide. It consists of a brazed sandwich (which includes a hardspot,core and closeout strips along the edge), a section of bonded-on internal stringer and a plate which simulates the cap of an intermediate transverse frame. The sandwich and stringer are attached to the cap simulator with 6.39 mm (0.75 in.) in diameter flush head bolts. Spacers are inserted between the inboard and outboard flanges of the internal stringer. The load adapters, as is the case with all test hardware load adapters, are designed to match the neutral axis of the test section across its width to eliminate any test peculiar kick loads. Four (4) machined-in fluid access ports are provided to allow pressurization during test.

SKIN/INTERIOR HARDSPOT FATIGUE SPECIMEN (SIHS

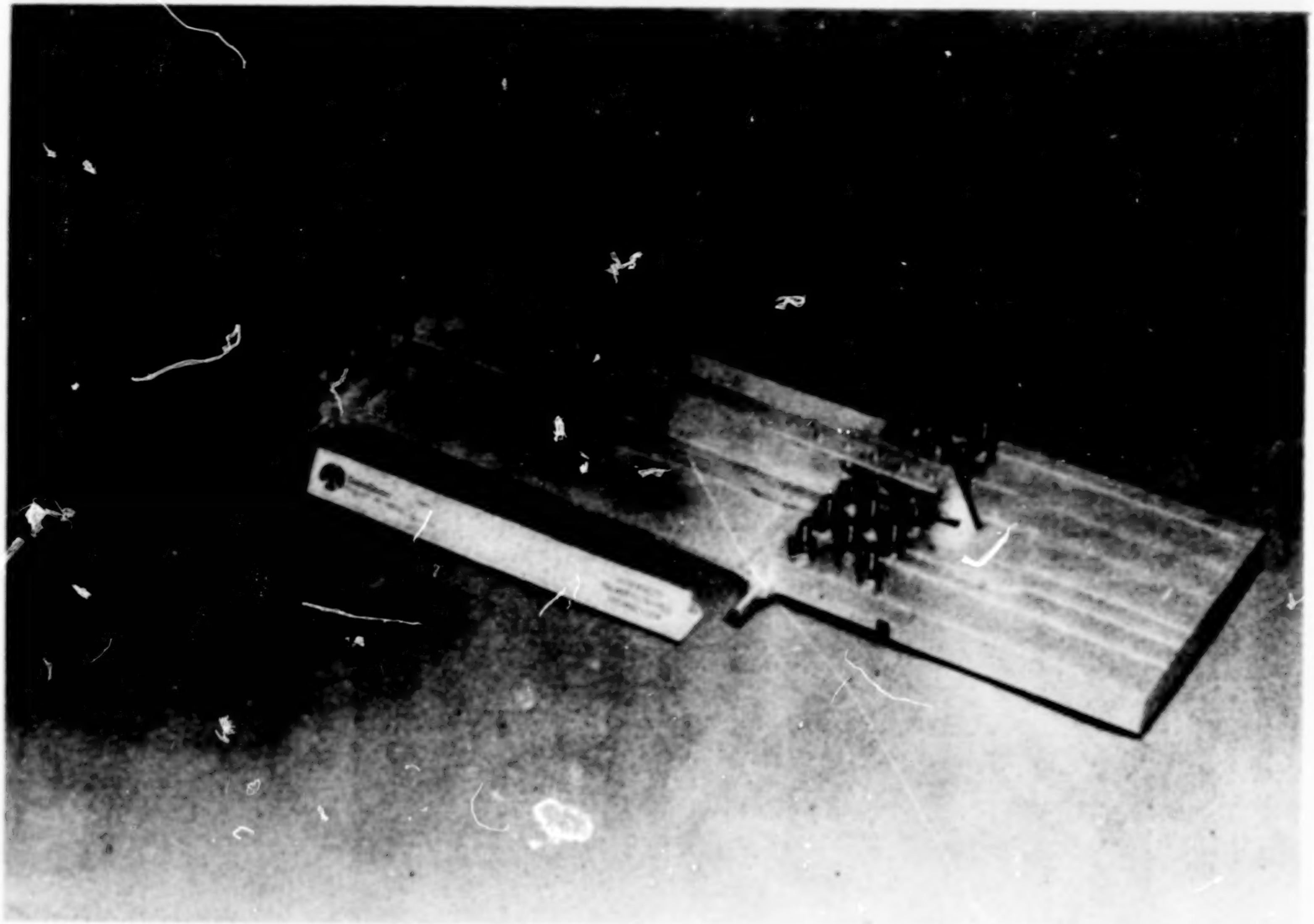

Figure 14

CONTENTS

Part I

PREFACE . . . . iii 1/A5

WELCOME 1 1/A10
R. R. Heldenfels

SESSION I - OVERVIEWS
Chairman: A. J. Henderson

1. HYPERSONIC STRUCTURES: AN AERODYNAMICIST'S PERSPECTIVE (OR ONE MAN'S DREAM IS ANOTHER MAN'S NIGHTMARE) 5 1/B1
J. D. Watts, L. R. Jackson, and J. L. Hunt

2. STRUCTURAL REQUIREMENTS FOR MILITARY HYPERSONIC SYSTEMS (Paper not available for publication)
P. Lane

3. AIRFRAME-INTEGRATED PROPULSION SYSTEM FOR HYPERSONIC CRUISE VEHICLES 39 1/F13
Robert A. Jones and Paul W. Huber

4. RECENT ADVANCES IN CONVECTIVELY COOLED ENGINE AND AIRFRAME STRUCTURES FOR HYPERSONIC FLIGHT 47 1/G7
H. Neale Kelly, Allan R. Wieting, Charles P. Shore, and Robert J. Nowak

SESSION II - ENGINE STRUCTURES
Chairman: H. N. Kelly

5. DESIGN AND ANALYSIS OF A SCRAMJET ENGINE 65 2/A13
O. A. Buchmann

6. THERMOSTRUCTURAL ANALYSIS OF A SCRAMJET FUEL-INJECTION STRUT 119 3/B11
Allan R. Wieting and Earl A. Thornton

7. ADVANCED FABRICATION TECHNIQUES FOR COOLED ENGINE STRUCTURES 145 3/F7
O. A. Buchmann

8. HYDROGEN EMBRITTLEMENT AND ITS CONTROL IN HYDROGEN-FUELED ENGINE SYSTEMS 195 4/F11
W. T. Chandler

9. CARBON-CARBON COMPOSITE APPLICATION FOR INTEGRAL ROCKET RAMJET COMBUSTORS (Paper not available for publication)
H. A. Holman

SESSION III - COOLED AIRFRAME STRUCTURES
Chairman: C. P. Shore

10. DESIGN AND FABRICATION OF A SKIN STRINGER DISCRETE TUBE ACTIVELY COOLED STRUCTURAL PANEL 253 6/A5
Frank M. Anthony

11. DESIGN AND ANALYSIS OF A PLATE-FIN SANDWICH ACTIVELY COOLED STRUCTURAL PANEL 319 7/C13
L. M. Smith

12. FLUXLESS BRAZING AND HEAT TREATMENT OF A PLATE-FIN SANDWICH ACTIVELY COOLED PANEL 375 8/E1
Charles S. Beuyukian

13. DESIGN AND FABRICATION OF A RADIATIVE ACTIVELY COOLED HONEYCOMB SANDWICH PANEL 449 10/A13
Leland C. Koch

14. RADIATIVE, ACTIVELY COOLED PANEL TESTS RESULTS 493 11/A5
Charles P. Shore, Robert J. Nowak, and Ellsworth L. Sharpe

348

END PANEL/INTERNAL STRINGER TERMINATION FATIGUE SPECIMEN (EPISTS)

(Figure 15)

This photograph shows the inboard side of the EPISTS. The specimen size including load adapters is 0.75 m (29.42 in.) long by 0.25 m (9.75 in.) wide. It consists of a brazed sandwich (which includes a section of end panel filler plate), an internal stringer and its termination attachment hardware and a section of manifold. The test section is mechanically fastened to the load adapter in a manner identical to the full scale panel design attachment to the aircraft main frame.

END PANEL/INTERNAL STRINGER TERMINATION FATIGUE SPECIMEN

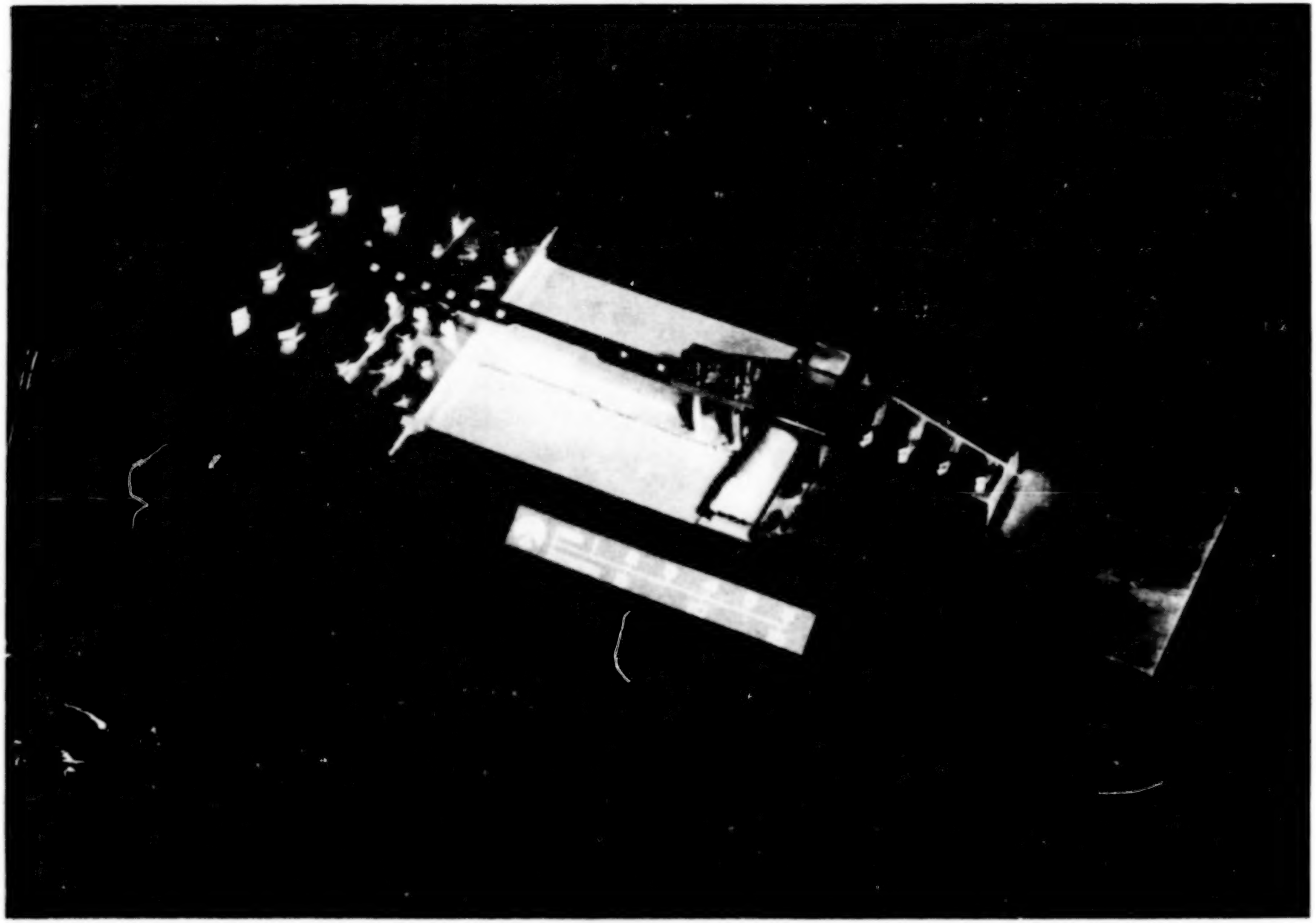

Figure 15

350

PANEL CORNER FATIGUE SPECIMEN (PCS)

(Figure 16)

This photograph shows the inboard side of the PCS. This specimen represents two (2) adjacent panel corner sections butted to the main frame. The specimen, including load adapters, is 0.77 m (30.55 in.) long and 0.22 m (8.66 in.) wide. It consists of two (2) brazed panel corner sections, two (2) manifold sections, a section of edge stringer and the back-to-back bathtub fittings that interface between the edge stringer and the main frame. The mechanical attachment of the panel and bathtub fittings to the load adapter duplicates the full scale design configuration and hardware.

PANEL CORNER FATIGUE SPECIMEN (PCS)

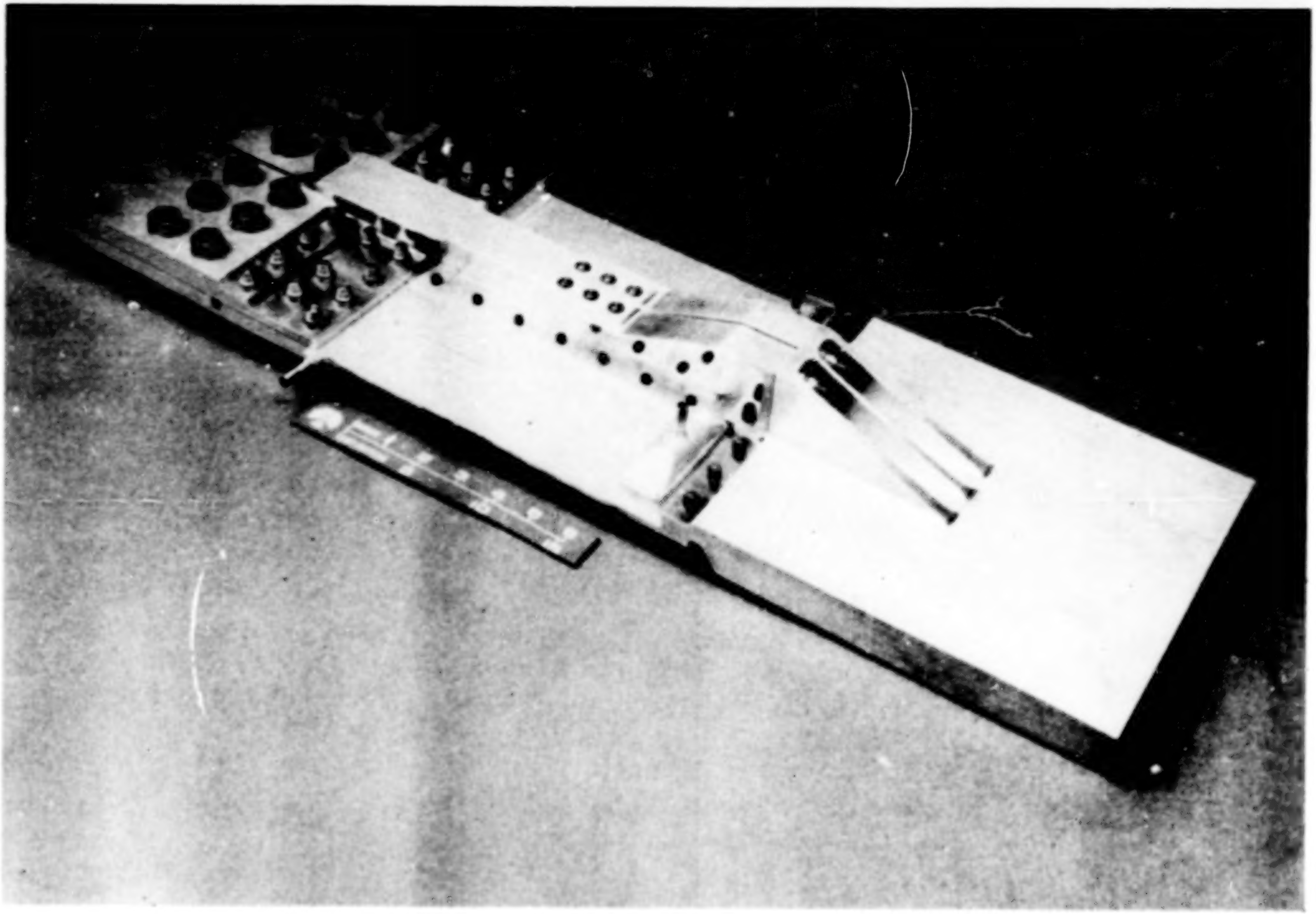

Figure 16

FATIGUE TEST PROGRAM SUMMARY

(Figure 17)

This chart summarizes the fatigue test program results. The specimens were tested by NASA at room temperature to fully reversed (R = -1) tension/compression load levels that had been corrected for the lack of an elevated temperature environment. The percentage of the design limit load of ± 210.15 KN/m (± 1,200 lbf/in.) that was allocated to each specimen based on its cross-sectional area was increased by 21.75% to compensate for the room temperature test environment. The events coded Ⓧ are described below.

Ⓐ The Skin/Interior Hardspot Specimen successfully completed the 20,000 cycle fatigue test.

Ⓑ The End Panel/Internal Stringer Specimen successfully completed 20,000 cycles without failure; however, some joint motion was observed.

Ⓒ The Bathtub Fitting inboard flange in the panel corner Specimen fractured after 3,000 cycles of test. In addition, excessive panel to load adapter joint motion was noted. The specimen was reworked incorporating a redesign bathtub fitting.

Ⓓ The inboard flange of the edge stringer fractured after 3,300 cycles of test. Again, excessive motion at the panel/load adapter riveted joint was noted.

Ⓔ A Boilerplate Panel Corner Fatigue Specimen was designed and fabricated, incorporating a new Taper-Loc Fastener system and a localized beef-up to the edge stringer inboard flange. This specimen successfully completed 20,000 cycles. No joint motion was observed.

Ⓕ The End Panel/Internal Stringer Specimen was reworked to incorporate the Taper-Loc fasteners. Three thousand (3,000) additional cycles were run. No joint motion was observed.

FATIGUE TEST PROGRAM SUMMARY

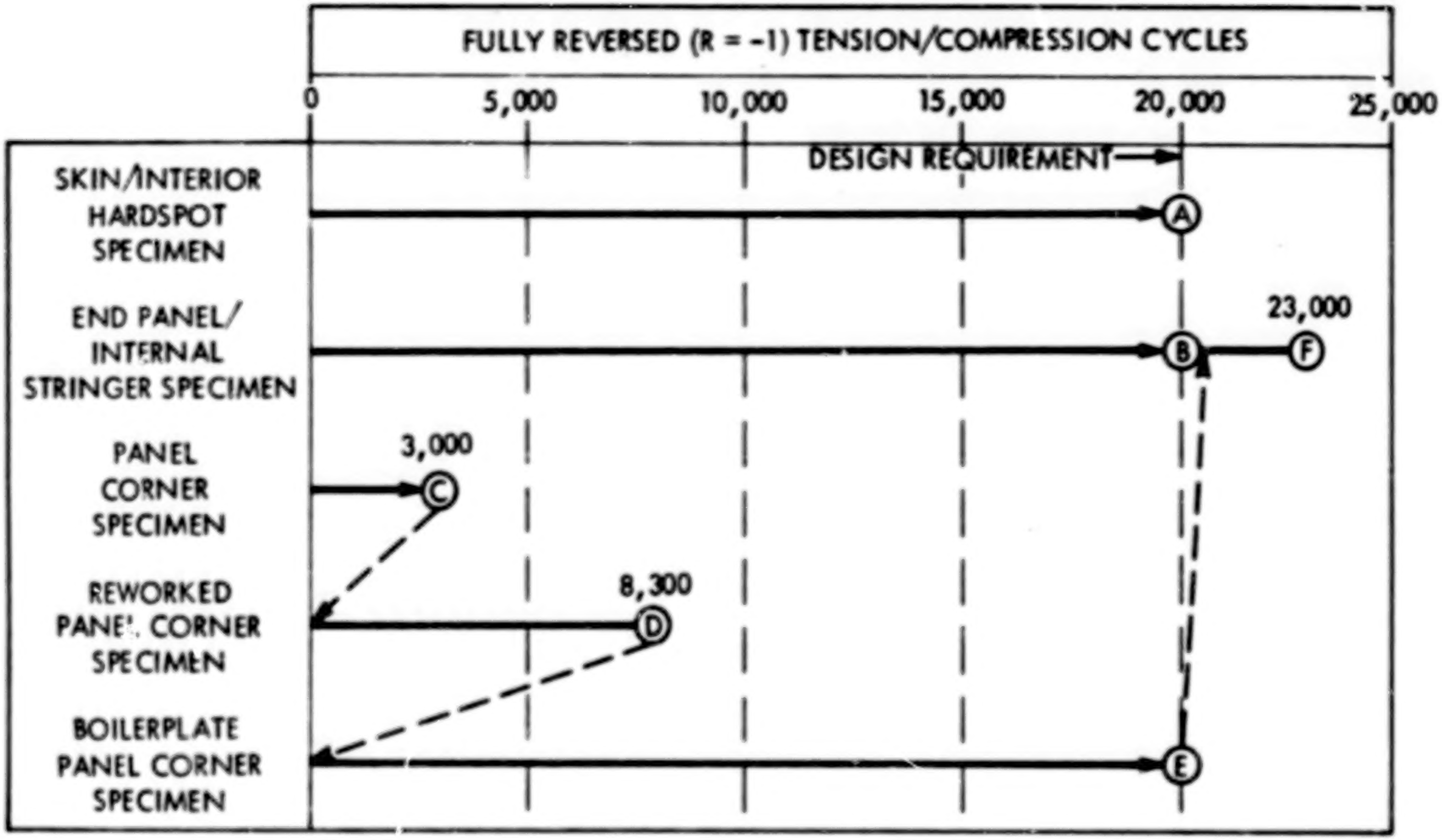

Figure 17

354

BATHTUB FITTING REDESIGN

(Figure 18)

The configuration of the initial Bathtub Fitting and the redesign are shown on this chart, along with a photograph of the reworked panel corner specimen. The joggle was essentially eliminated and the flanges thicknesses of the fitting increased.

BATHTUB FITTING REDESIGN

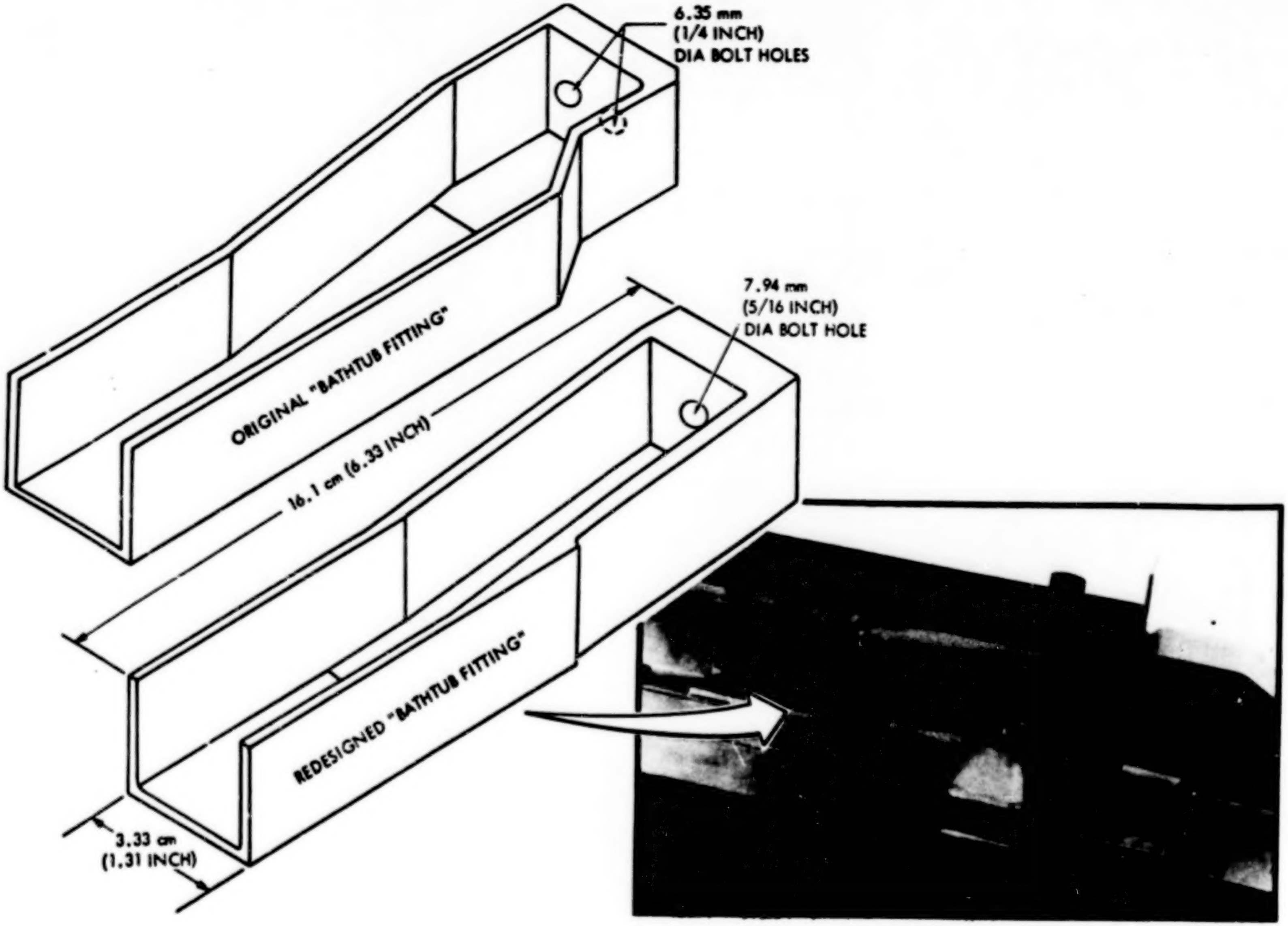
6.35 mm
(1/4 INCH)
DIA BOLT HOLES
ORIGINAL "BATHTUB FITTING"
16.1 cm (6.33 INCH)
7.94 mm
(5/16 INCH)
DIA BOLT HOLE
REDESIGNED "BATHTUB FITTING"
3.33 cm
(1.31 INCH)

Figure 18

JOINT SPECIMEN TEST SETUP

(Figure 19)

Following the second failure of the panel corner specimen, it became increasingly evident that the brazed panel to main frame (or load adapter) joint was not rigid enough to transfer its share of the axial load. As a result, the percentage of load carried through the Bathtub Fitting Flange to the inboard flange of the edge stringer was in excess of its capability. The fastener used at the panel/ load adapter interface was a blind flush head pull rivet.

A test program was initiated to evaluate a series of different types of fasteners. A series of specimens that duplicate this joint in material and thickness were fabricated and assembled with the original rivets, shear bolts, tension bolts, Jo-Bolts and Taper-Loc Bolts. Hole preparation consisted of standard structural clearances and interference fits. A total of twelve (12) specimens were tested. Testing was performed with an MTS Inc. electrohydraulic test machine. Each specimen was gripped with Amsler rigid-wedge grips capable of applying tension/compression loads to the test specimen with zero backlash when going through zero load. The specimen and test setup are shown in Figure 19.

JOINT SPECIMEN TEST SETUP

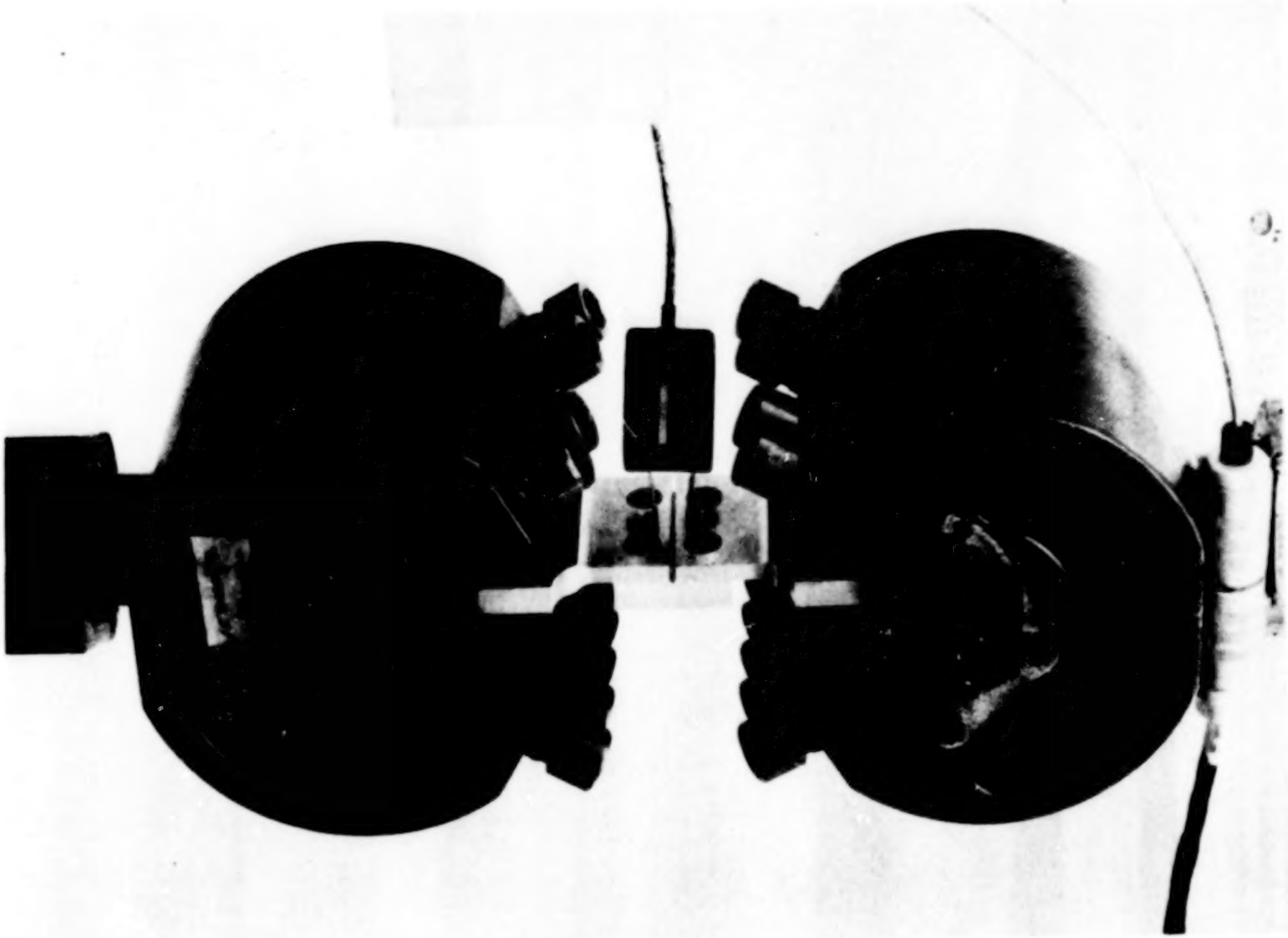

Figure 19

358

JOINT TEST SPECIMEN RESULTS COMPARISON

(Figure 20)

This chart compares the results obtained for the original blind flush head rivet and the Taper-Loc fastener. The Taper-Loc was superior to all fasteners tested. Joint motion was reduced approximately 82% with this new fastener and it was incorporated into the full scale design and was used on all future test hardware.

JOINT TEST SPECIMEN RESULTS COMPARISON

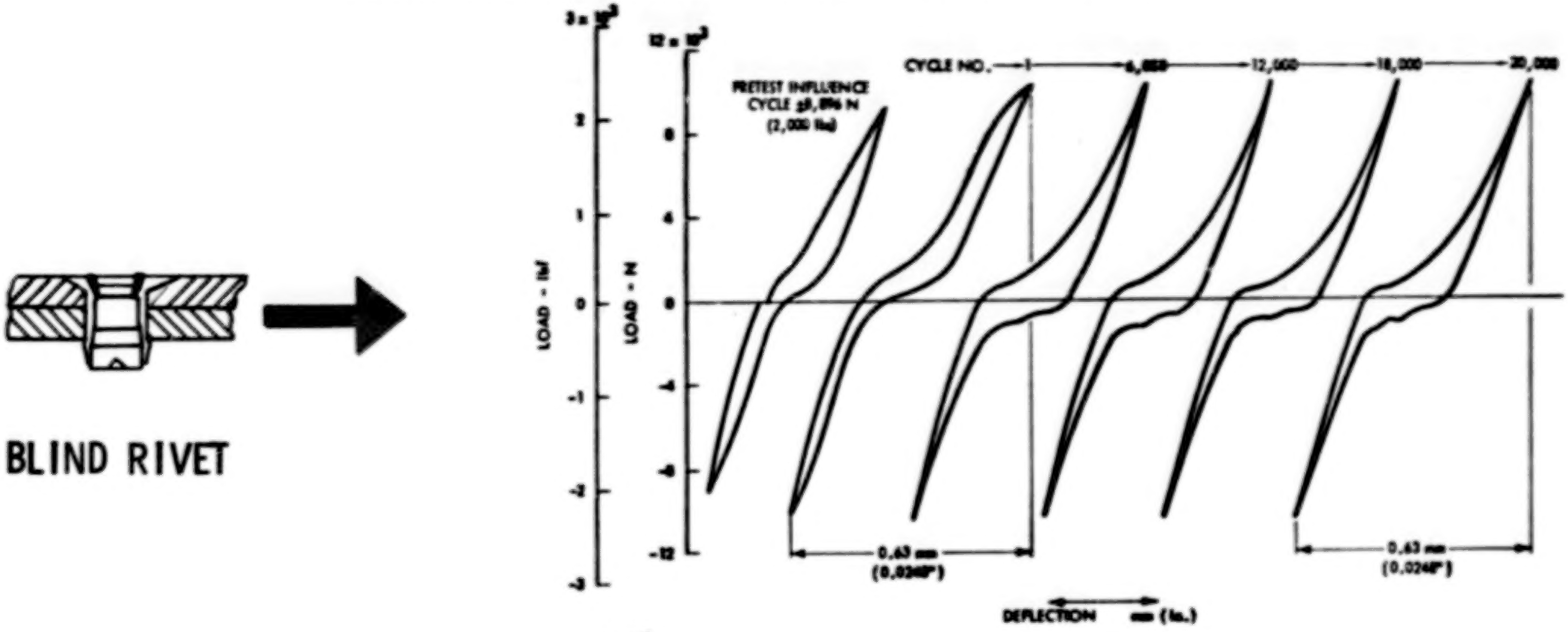

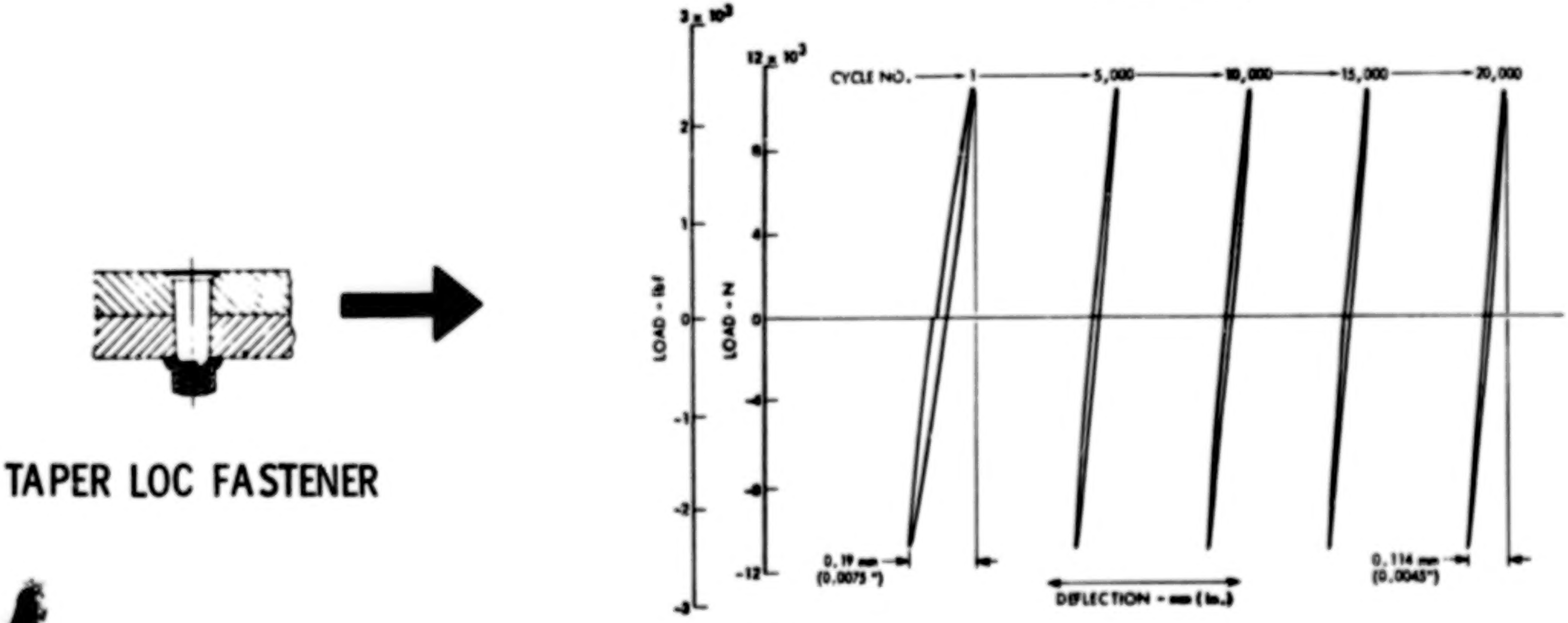

Figure 20

360

BOILERPLATE FATIGUE SPECIMEN

(Figure 21)

This photograph shows the Boilerplate Panel Corner Fatigue Specimen. The grooved plates replace the brazed sandwich structures but retained the same bending stiffness. This specimen also shows the nut side of the Taper-Loc fasteners used as replacements for the blind rivets. This specimen was successfully tested to 20,000 cycles without failure or evidence of joint motion.

BOILERPLATE FATIGUE SPECIMEN

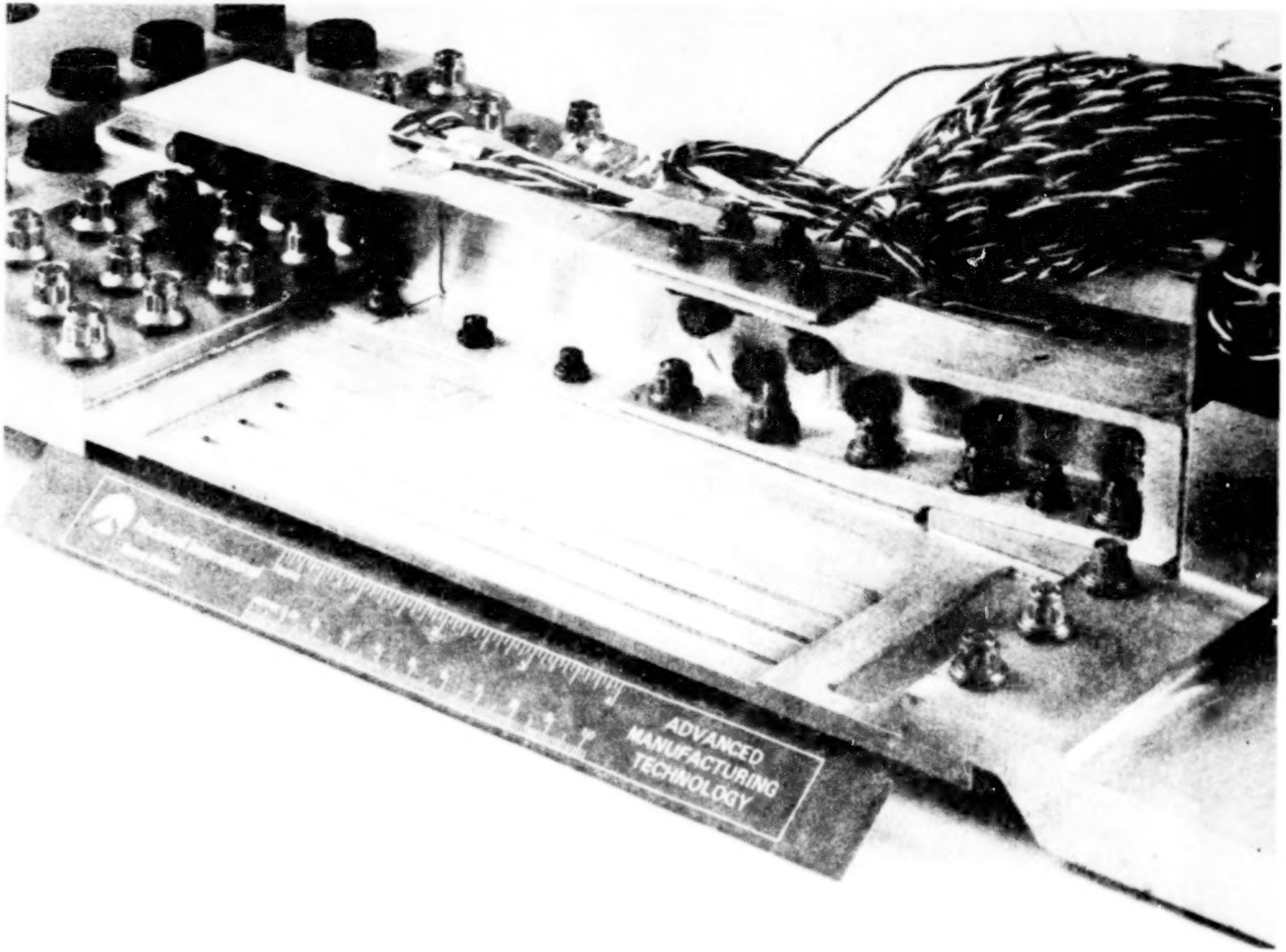
ADVANCED
MANUFACTURING
TECHNOLOGY

Figure 21

TEST PANEL SCHEMATIC

(Figure 22)

Following "successful" completion of the fatigue test program, a test panel was designed, analyzed and fabricated by Rockwell for test by NASA. The test panel is representative of the first 0.61 m (2 ft) and the last 0.61 m (2 ft) of the full scale panel design. The load adapters are designed to simulate the interface configuration and stiffness of an aircraft main frame and to distribute loads from the load grips into the test panel in the same manner as butted panels would on an aircraft. The severe sculpturing of the load adapters accomplishes these design objectives.

TEST PANEL SCHEMATIC

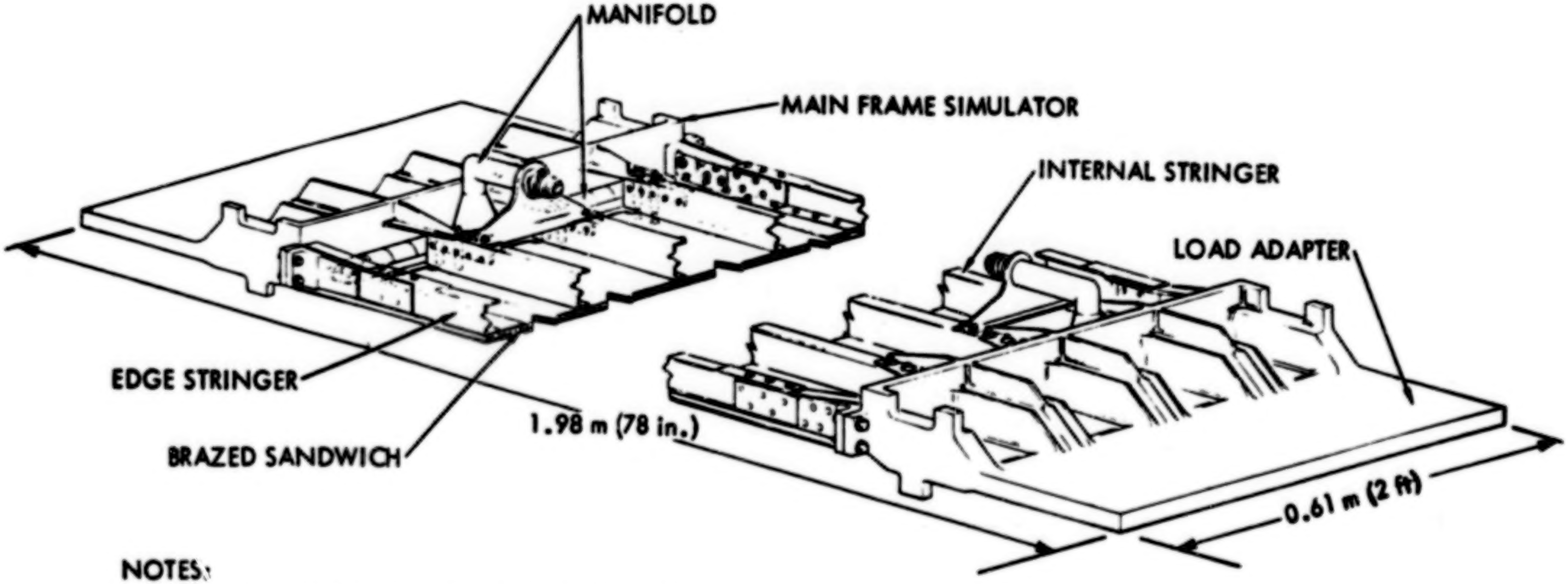
MANIFOLD
MAIN FRAME SIMULATOR
INTERNAL STRINGER
LOAD ADAPTER
EDGE STRINGER
BRAZED SANDWICH
1.98 m (78 in.)
0.61 m (2 ft)

NOTES:

(1) INTERMEDIATE TRANSVERSE FRAME NOT SHOWN

(2) HEAT STRIPS ON REVERSE SIDE OF LOAD ADAPTERS

Figure 22

TEST PANEL/LOAD ADAPTER INTERFACE OPTIONS

(Figure 23)

The full scale panel design assumes that butting panels would be installed on the aircraft structure, inlet butted to inlet and outlet to outlet. Hence, in order to simulate a flight environment during test, the heat flux applied to the test panel via a quartz lamp system should not flow, via conduction, to the load adapter and no transverse thermal stress should exist at the test panel/load adapter interface. Three (3) design options, shown in Figure 23, were considered to meet the above requirements.

Option 1 ties the test panel to the load adapter with a series of titanium links. The titanium would minimize heat flow to the load adapter and the links would allow independent transverse panel growth. This option was rejected due to concern over joint stiffness during full tension/compression load cycling.

Option 2 features slotted holes either in the test panel or the load adapter. This option was rejected because of the precision-like hole quality required and the friction restraint provided by joint clamp-up.

Option 3 utilizes a heat strip bonded to load adapter near its interface with the test panel. A control thermocouple is located on the end of the test panel and a drive thermocouple is located in close proximity on the load adapter. As panel temperature increases, the heat strips drive the load adapter at the interface to approximately the same temperature. Hence, heat flow is minimized and both the test panel and the load adapter grow together in the transverse direction so no transverse thermal stress occurs at the interface. The load adapter is insulated to prevent heat loss to the surrounding environment. This option was adopted for the test panel design.

TEST PANEL/LOAD ADAPTER INTERFACE OPTIONS

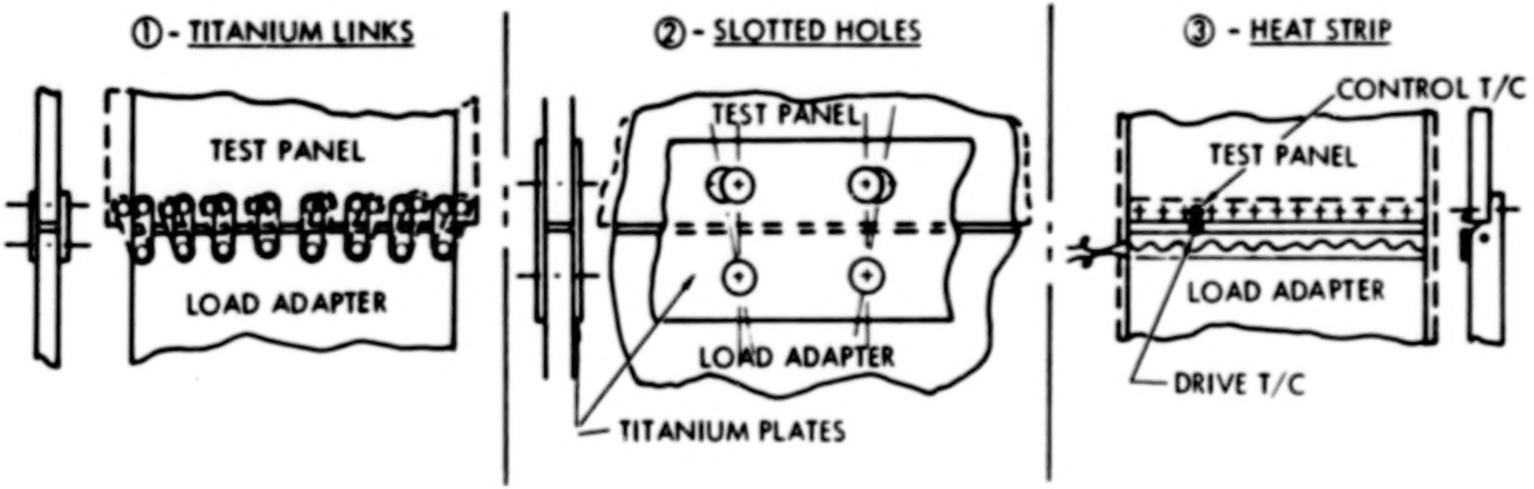

① - TITANIUM LINKS
TEST PANEL
LOAD ADAPTER
② - SLOTTED HOLES
TEST PANEL
LOAD ADAPTER
TITANIUM PLATES
③ - HEAT STRIP
CONTROL T/C
TEST PANEL
LOAD ADAPTER
DRIVE T/C

Figure 23

TEST PANEL TEMPERATURE DISTRIBUTION

(Figure 24)

Figure 24 presents a plot of predicted test panel and load adapter temperature distributions that was fed into the NASTRAN structural model. It assumes that the panel is subjected to the design heat flux of 136.2 k W/m^2 (12 Btu/ft^2.5) with a coolant inlet condition of 13,608 kg/hr (30,000 lbm/hr) at 289 K (60°F) and that the load adapters track the test panel end temperatures. This data was generated from a review of separate thermal analyses conducted on the load adapters and the test panel. The temperature gradients at the test panel/load adapter interfaces are estimated and may vary significantly during test. In retrospect, it is obvious that the thermal model elements in the vicinity of the panel ends were not sized small enough to allow a good prediction of precise temperatures in the vicinity of the manifolds and end panel filler plates. Yet the gradients as presented are considered to be severe enough to allow a conservative structural analysis to be conducted.

TEST PANEL TEMPERATURE DISTRIBUTIONS

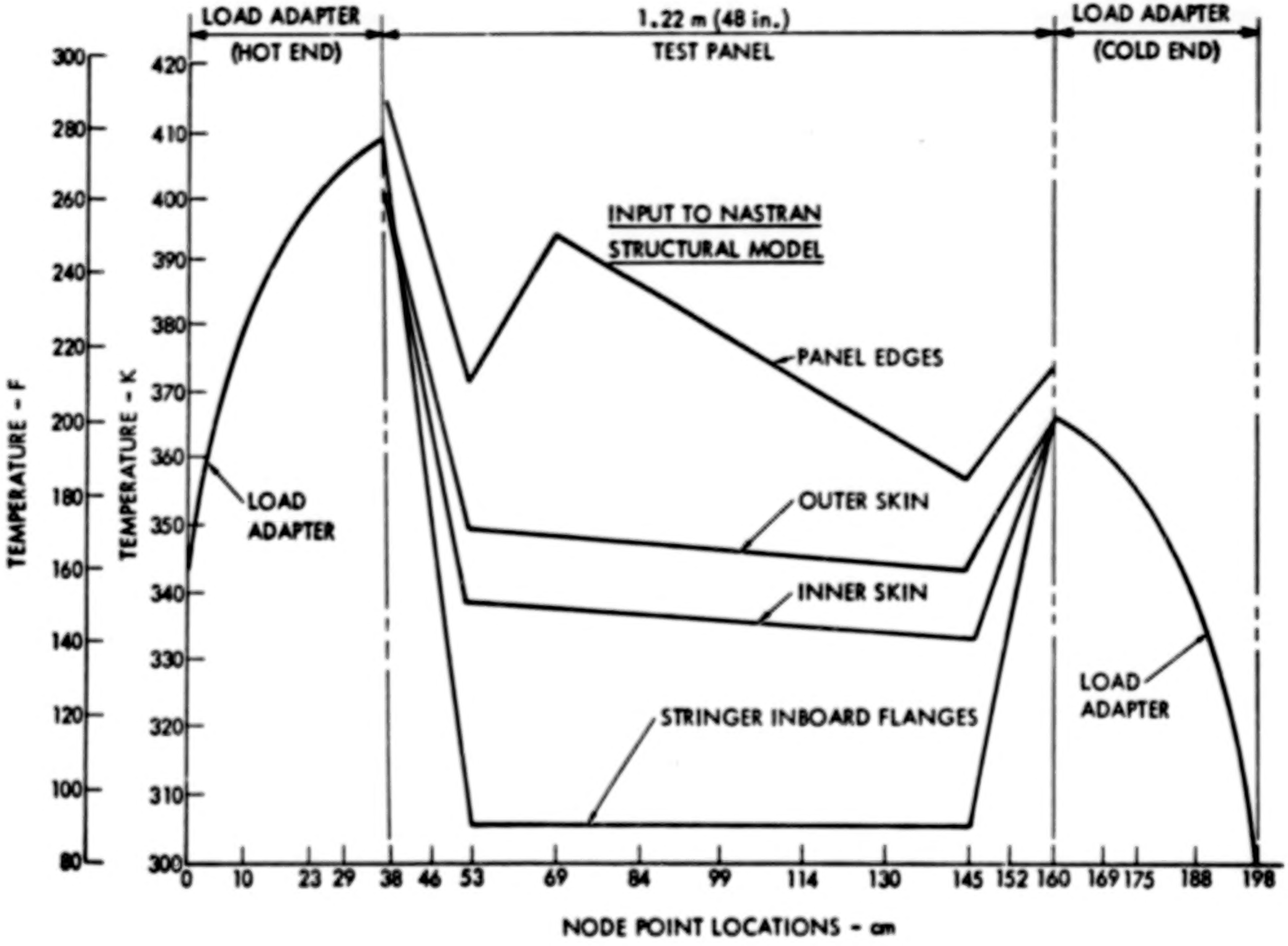

Figure 24

368

TEST PANEL STRESS DISTRIBUTIONS

(Figure 25)

This figure plots results of a NASTRAN analysis that considered mechanical loads and thermal stresses separately. The brazed sandwich will operate at stress levels essentially identical to those predicted for the outboard flanges of the stringer. A detailed review of this data will result in a calculation of a worst case combined stress level of approximately 110.3 MPa (16,000 psi) compression. This stress level occurs at a point approximately one (1) foot from the outlet end of the panel on the edge stringer outboard flange and the adjacent brazed sandwich structure.

PREDICTED TEST PANEL STRESS DISTRIBUTION

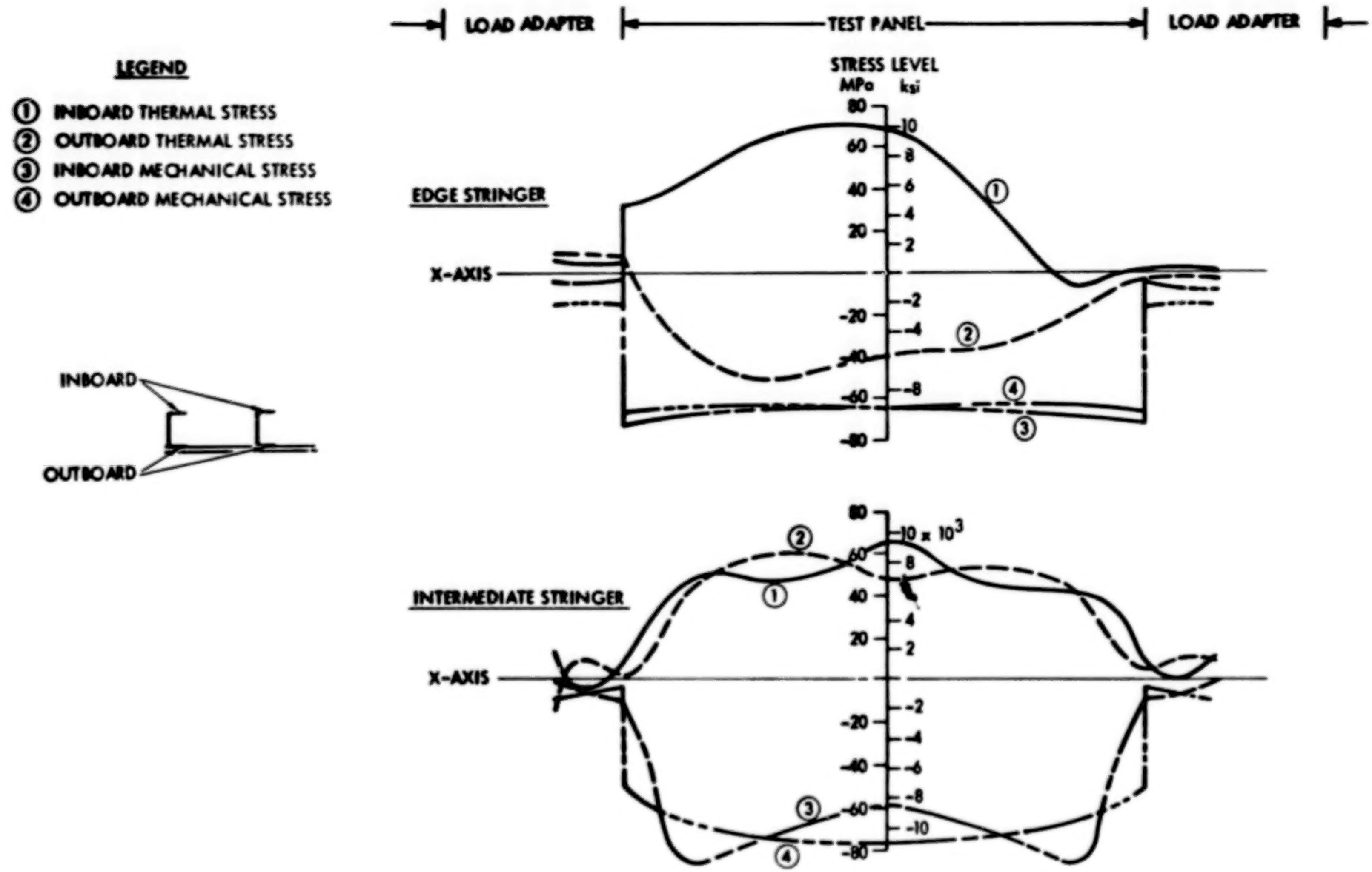

Figure 25

370

TEST PANEL

(Figure 26)

The photograph of the test panel shows some of the details not previously discussed which are test peculiar. The flight type bathtub fittings are backed up by dummy fittings so the edge stringer is attached in double shear. The test panel edge stringer is a machined channel section whereas the full scale stringer is an I-section that attaches adjacent panels together. The six (6) "pillow blocks" or dual race bearings mechanically fastened to the load adapters and the intermediate transverse frame simulator are part of the NASA test facility. These "pillow blocks" receive a hardened steel bar which is clamped to the test facility and provides lateral stiffness to the panel during test.

TEST PANEL

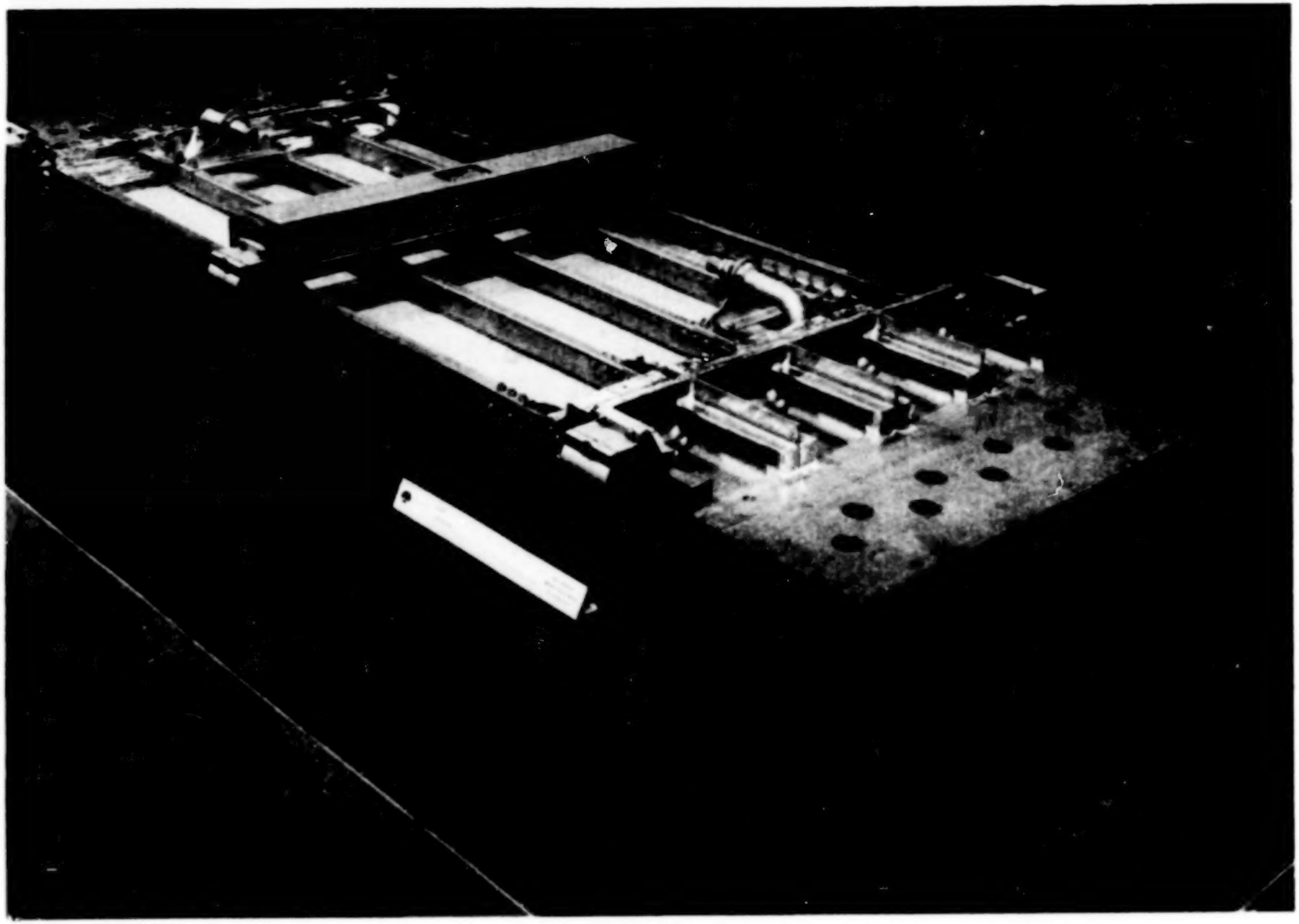

Figure 26

372

STRINGER STIFFENED PLATE-FIN SANDWICH ACTIVE COOLING CONCEPT STUDY

✓ CONCLUSIONS

- THE CONCEPT IS:
  - FEASIBLE—BASED ON ANALYSIS & LIMITED TESTING
  - VERSATILE—VARIATIONS IN COOLANT INLET CONDITIONS & CORE HEIGHT CAN ACCOMMODATE RANGE OF HEAT FLUX
- PANEL PERIMETER DESIGN FEATURES ARE CRITICAL
  - STRUCTURALLY—FASTENER SELECTION & HOLE PATTERN
  - THERMALLY—SOLID MATERIAL MUST BE MINIMIZED
- TRANSVERSE LOAD REQUIREMENTS (MECHANICAL OR THERMAL) WOULD:
  - REQUIRE CLOSER STRINGER SPACING OR
  - HONEYCOMB STIFFENING IN PLACE OF STRINGERS

  } MASS TRADE
- IF THE LUXURY OF TIME IS AVAILABLE, A PHASED PROGRAM LIKE THIS RESULTS IN MAXIMUM BENEFITS FOR $ SPENT

REFERENCES

1. Smith, L. M.; and Beuyukian, C. S.: Actively Cooled Plate-Fin Sandwich Structural Panels for Hypersonic Aircraft. Final Report, No. SD 78-AP-0074, Rockwell International, Space Systems Group, Aug. 1978.

2. Beuyukian, Charles S.: Fluxless Brazing and Heat Treatment of a Plate-Fin Sandwich Actively Cooled Panel. Recent Advances in Structures for Hypersonic Flight, NASA CP-2065, 1978. (Paper no. 12 of this compilation.)

374

BLANK PAGE

FLUXLESS BRAZING AND HEAT TREATMENT OF A PLATE-FIN SANDWICH ACTIVELY COOLED PANEL

Charles S. Beuyukian
Rockwell International, Space Systems Group

INTRODUCTION

Two processes that have a major impact on the quality of brazed plate-fin sandwich structures are the specific brazing process used and post-braze heat treatment.

Fluxless brazing of aluminum generally consists of brazing assemblies without the use of corrosive fluxes. The use of the fluxless brazing process is best suited for assemblies whose in-service inspection is not possible and/or where corrosion could result in catastrophic failure. Meanwhile, it is well known that during brazing with pre-placed alloy, application of mechanical pressure minimizes the possibility of voids in brazed joints. Thus, the application of mechanical pressure during the fluxless brazing process is highly desirable in promoting quality brazed joints.

Heat treatment of plate-fin sandwich structures having little internal support generally requires tooling fixtures to minimize distortion during quenching in water. However, some marking and surface damage to face sheets and slight local crushing of the core often occur. Heat treating without use of fixtures often increases distortion considerably. Straightening the assemblies generally requires considerable effort with resultant possible damage to the panel assembly.

This paper presents the processes and techniques used to fabricate plate-fin sandwich actively cooled panels. The materials were 6061 aluminum alloy and brazing sheet having clad brazing alloy. The panels consisted of small scale specimens, fatigue specimens and a large 0.61 m by 1.22 m (2 by 4 ft) test panel. All panels were fluxless brazed in retorts in heated platen presses while exerting external pressure to assure intimate contact of details. Distortion and damage normally associated with heat treatment were minimized by heat treating without fixtures and solution quenching in an organic polymer solution. The test panel is the largest fluxless brazed and heat treated panel of its configuration known to exist.

SMALL SCALE TEST SPECIMENS

(S.S.T.S.)

Key Elements (figures 1 to 4):

- Fluxless brazed in retort under vacuum.
- Brazed in heated platen press - exerting pressure.
- Heat treated using fixtures.
- Quenched in water.
- Successfully tested to 3.45 MPa (500 psi).
- No braze voids detected by radiographic inspection.

DETAILS FOR SMALL SCALE TEST SPECIMENS (S.S.T.S.)

(Figure 1)

Four panel details being assembled for simultaneous brazing. Cores are of straight-fin and lanced off-set types.

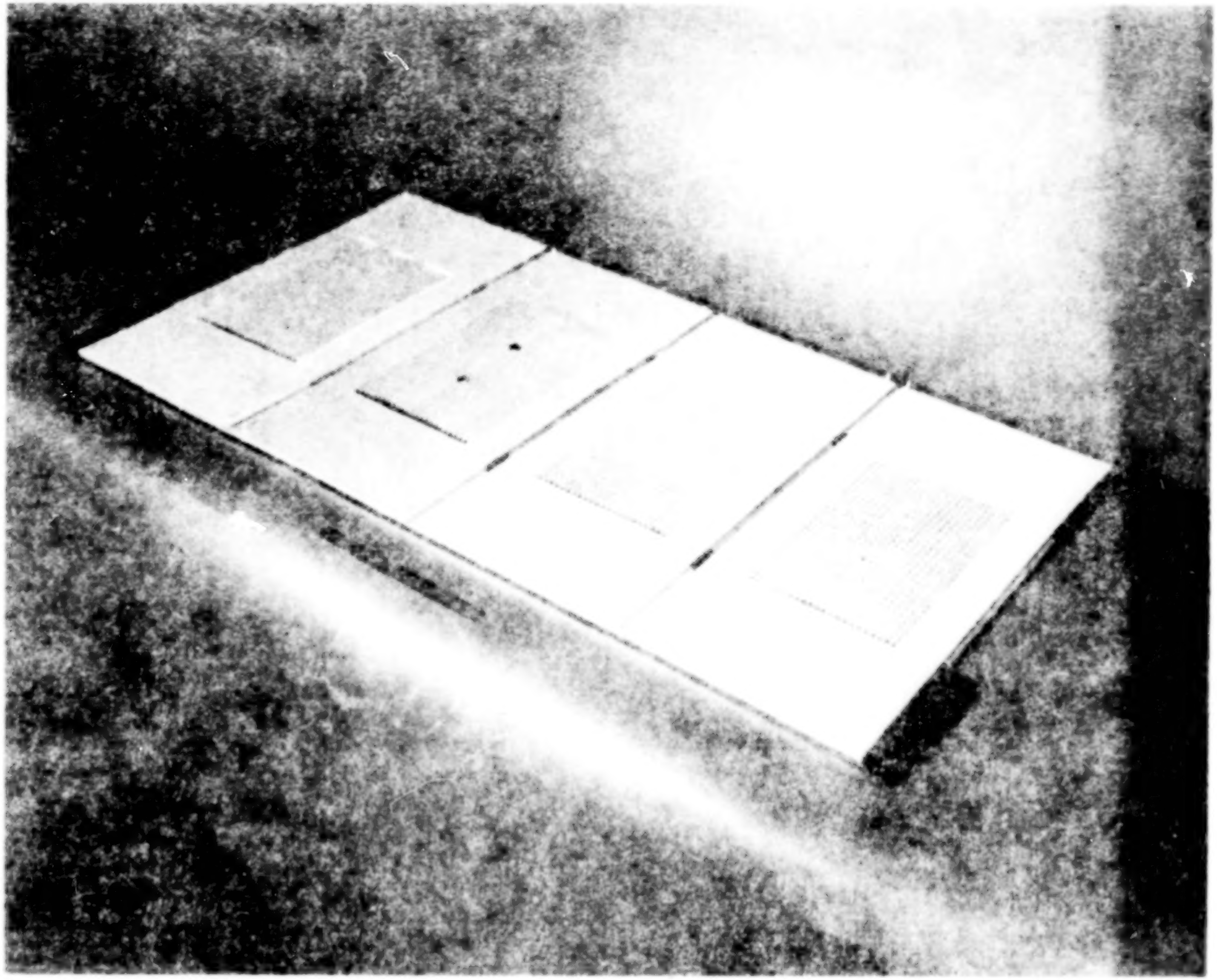

Figure 1.- Details for small scale test specimens (S.S.T.S.).

(S.S.T.S.) SIMULTANEOUSLY BRAZED PANELS

(Figure 2)

Four simultaneously brazed panels prior to removal from brazing retort. Core images are visible on face sheets.

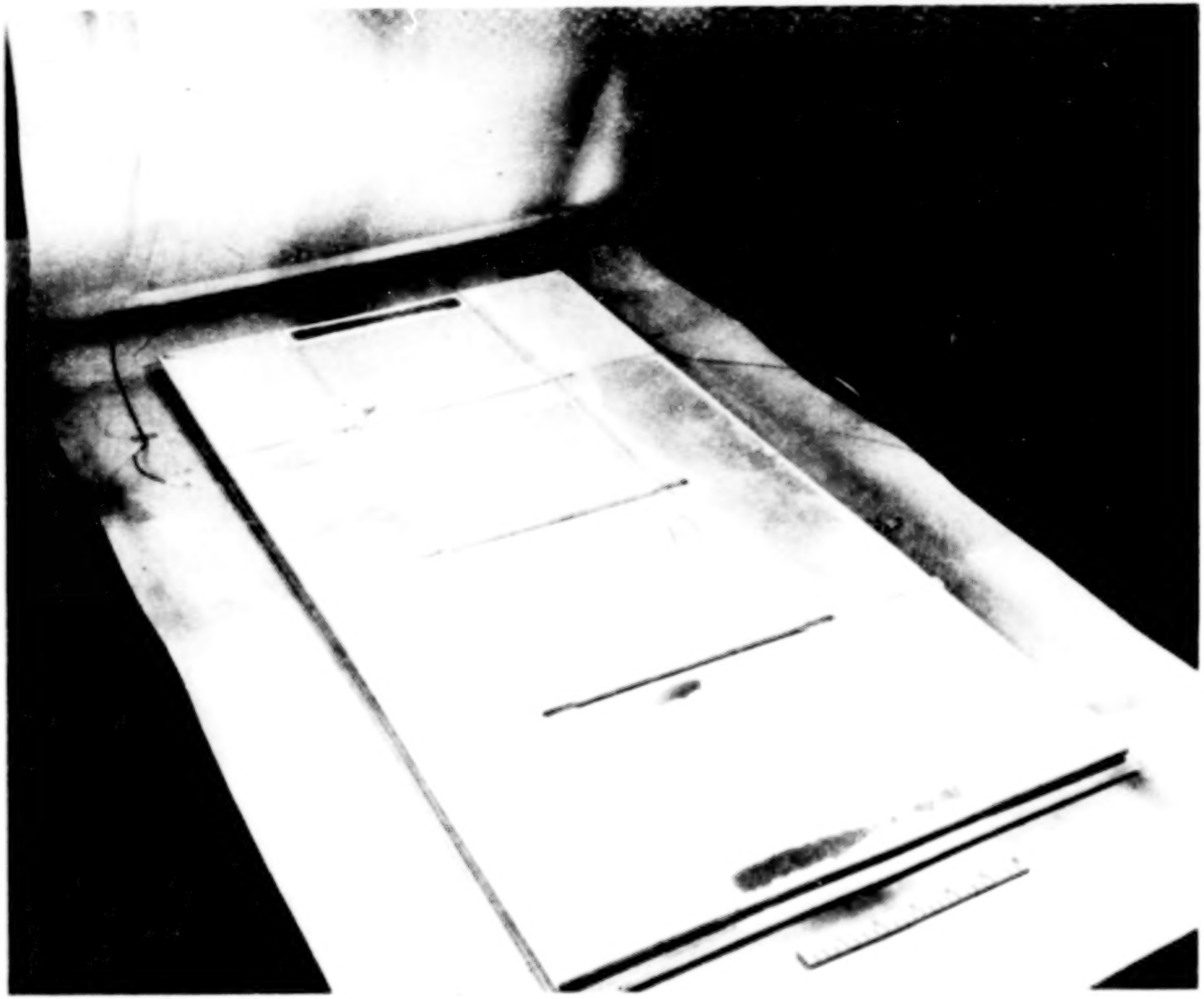

Figure 2.- (S.S.T.S.) simultaneously brazed panels.

(S.S.T.S.) BRAZED PANEL BEING INSTALLED IN HEAT TREAT FIXTURE

(Figure 3)

Brazed small scale test specimen being installed in heat treating fixture. Narrow filler strips and sheets with lightening holes compensate for differing height of panel.

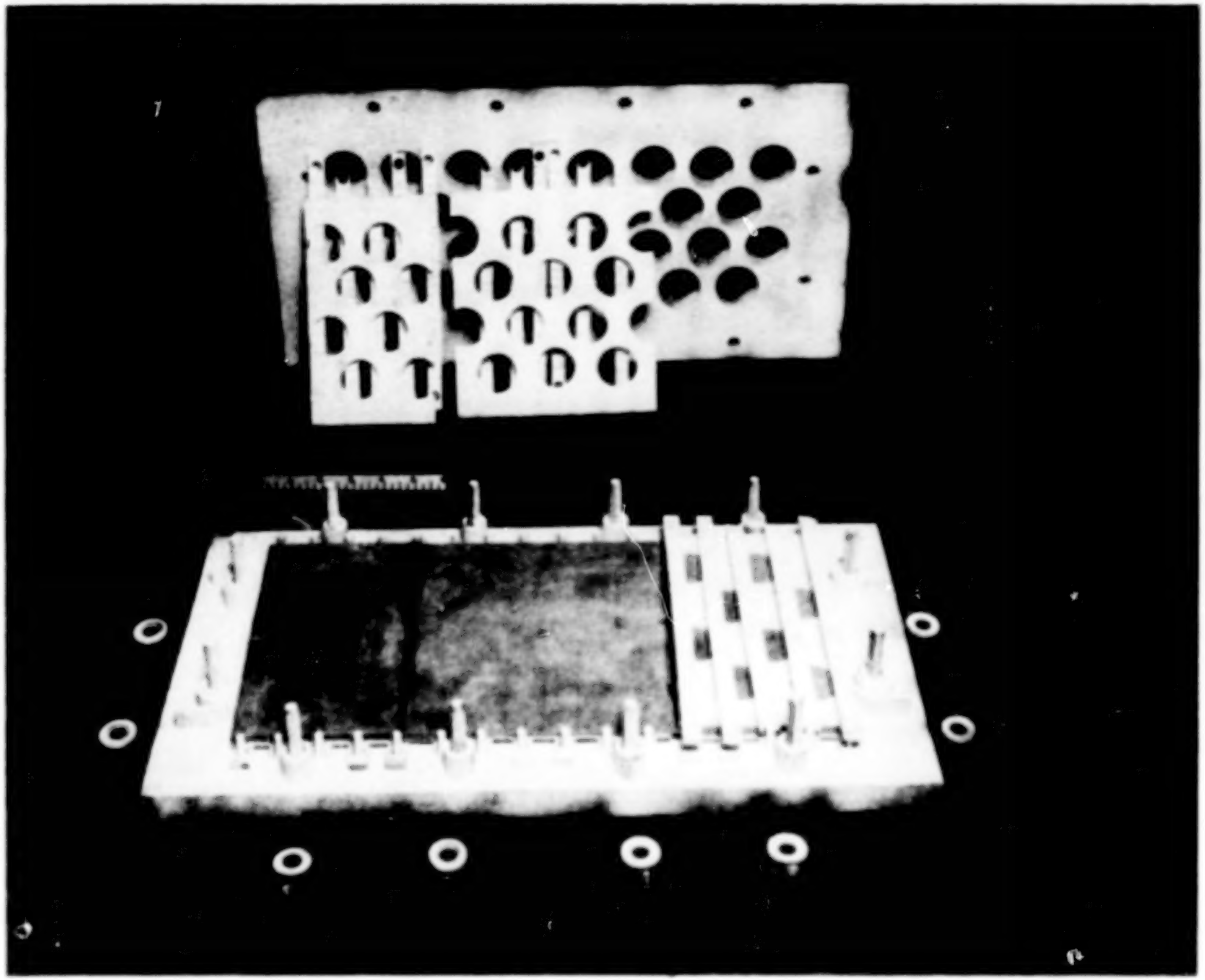

Figure 3.- (S.S.T.S.) brazed panel being installed in heat treat fixture.

382

(S.S.T.S.) BRAZED PANEL AFTER FINISH MACHINING

(Figure 4)

Brazed small scale test specimen after finish machining. Tube ports are for manifolding and attachment.

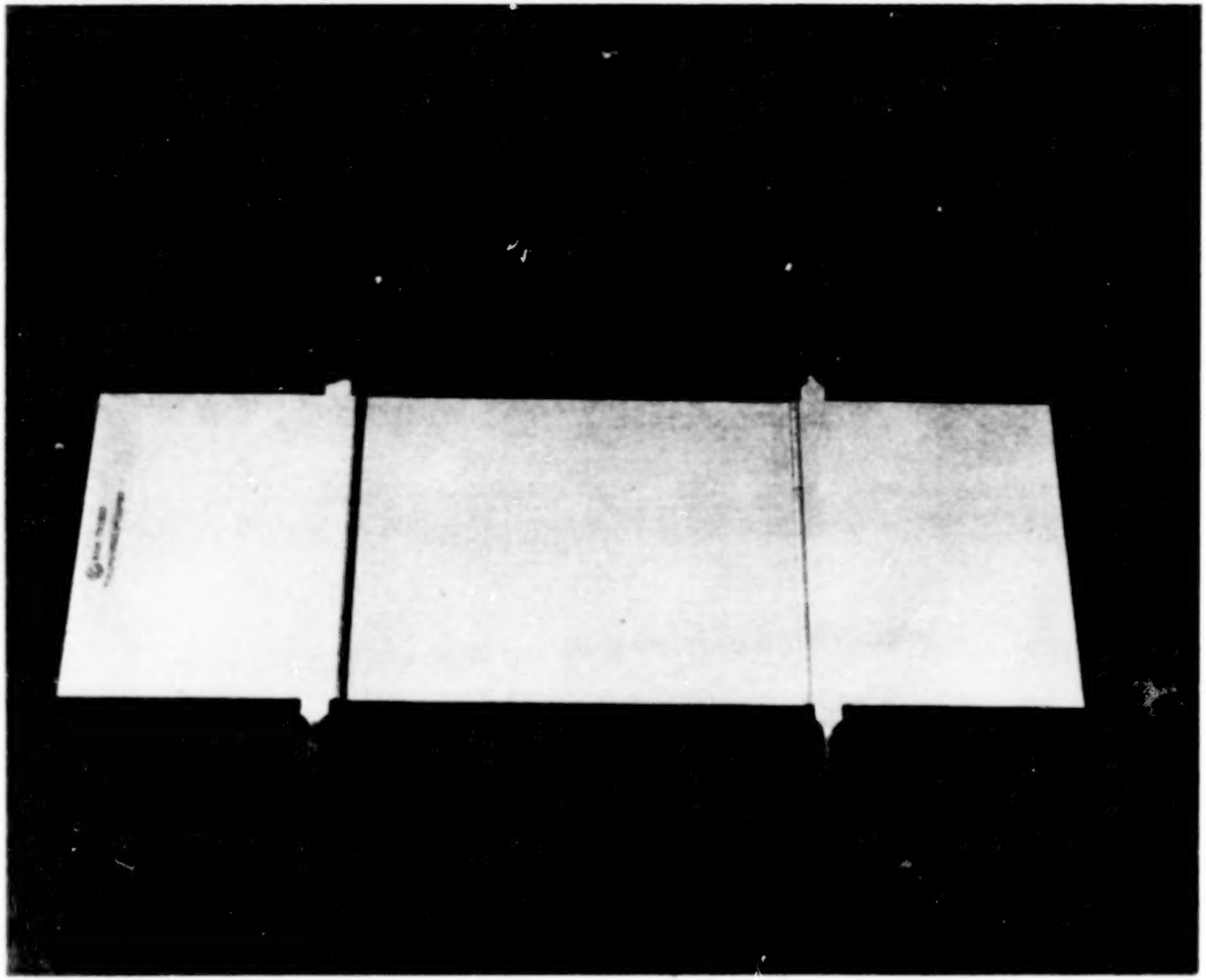

Figure 4.- (S.S.T.S.) brazed panel after finish machining.

SKIN INTERIOR HARDSPOT SPECIMEN

(S.I.H.S.)

First of Three Fatigue Specimens

Key Elements (figures 5 to 8):

- Contained integral manifolding.
- Fluxless brazed in retort under 0.10 MPa (15 psi) argon atmosphere.
- Brazed in heated platen press - exerting pressure.
- Heat treated using fixtures.
- Quenched in water.
- Successfully tested to 1.72 MPa (250 psi).
- No braze voids detected by radiographic inspection.

SKIN INTERIOR HARDSPOT SPECIMEN (S.I.H.S.) DURING ASSEMBLY

(Figure 5)

First of three fatigue specimens. Core sections and hardspot insert are located within the frame prior to brazing.

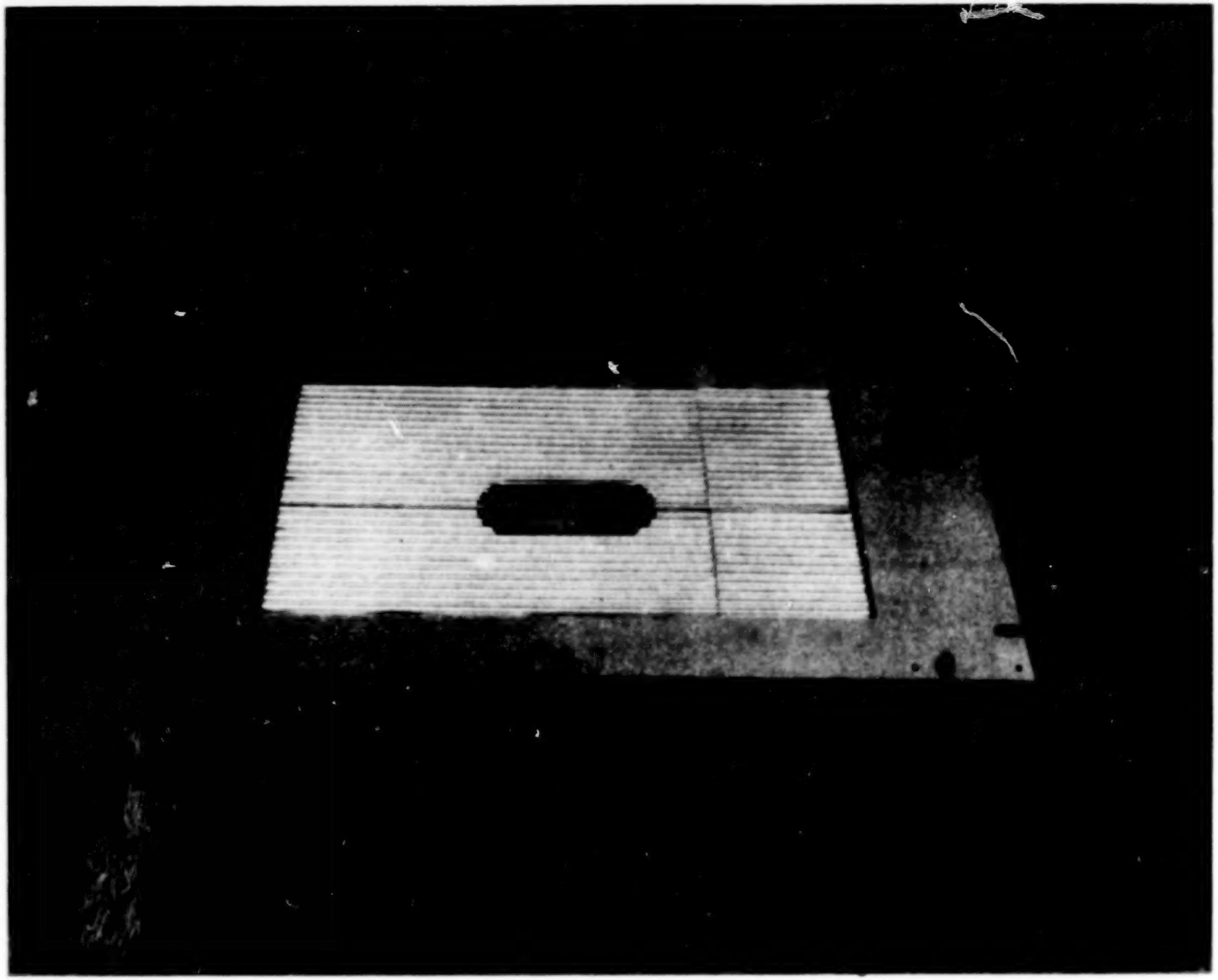

Figure 5.- Skin interior hardspot specimen (S.I.H.S.) during assembly.

(S.I.H.S.) INBOARD SIDE OF PANEL AFTER BRAZING

(Figure 6)

Inboard side of panel after brazing. Images at core convolutions and hardspot insert are visible on face sheet.

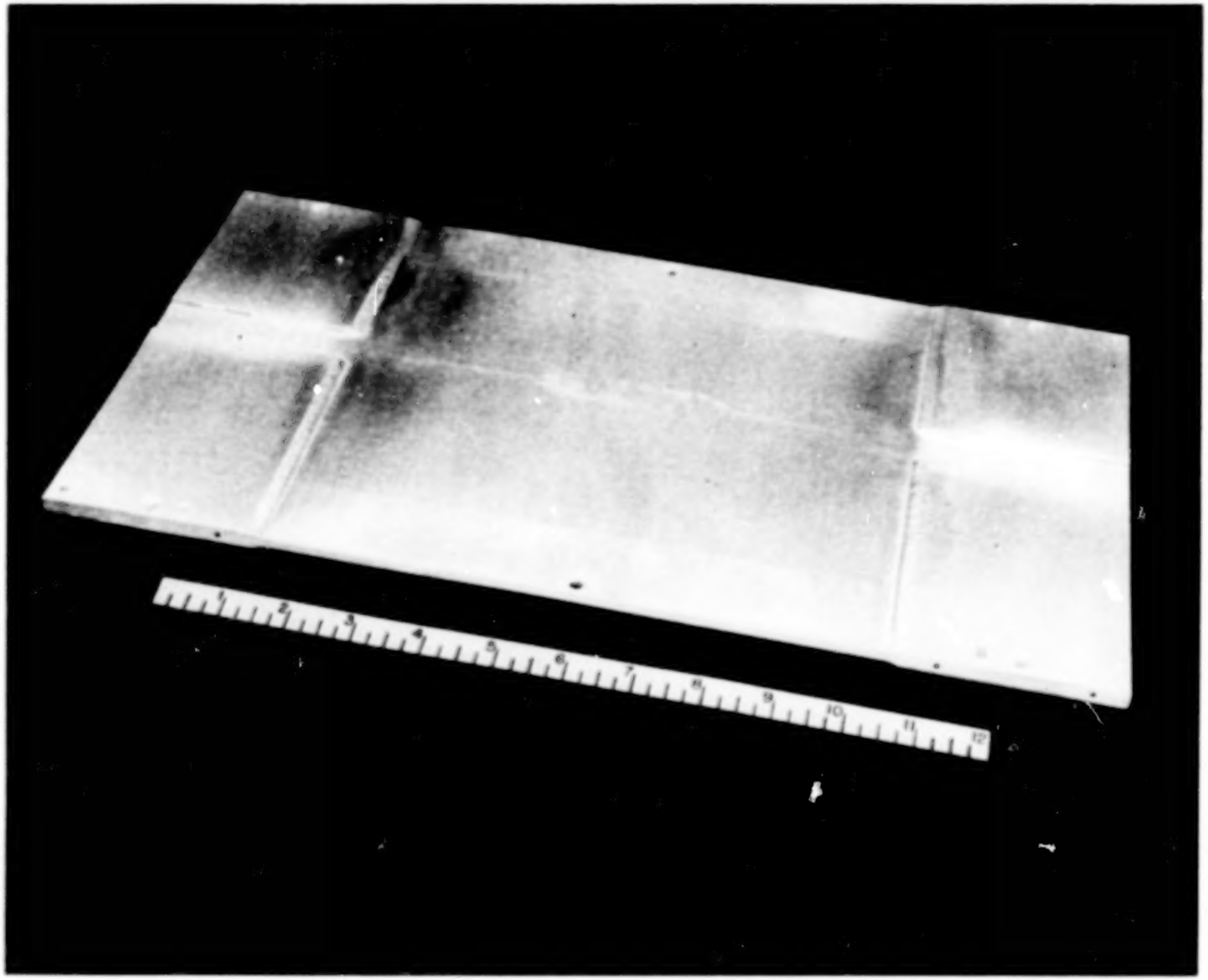
1
2
3
4
5
6
7
8
9
10
11
12

Figure 6.- (S.I.H.S.) inboard side of panel after brazing.

388

(S.I.H.S.) MOLDLINE SIDE OF BRAZED PANEL WITH LOAD ADAPTORS

(Figure 7)

Moldline side of skin interior hardspot specimen after finish machining. Tubes in edge of panel are for integral manifolds. Load adaptors are bolted to panel for testing.

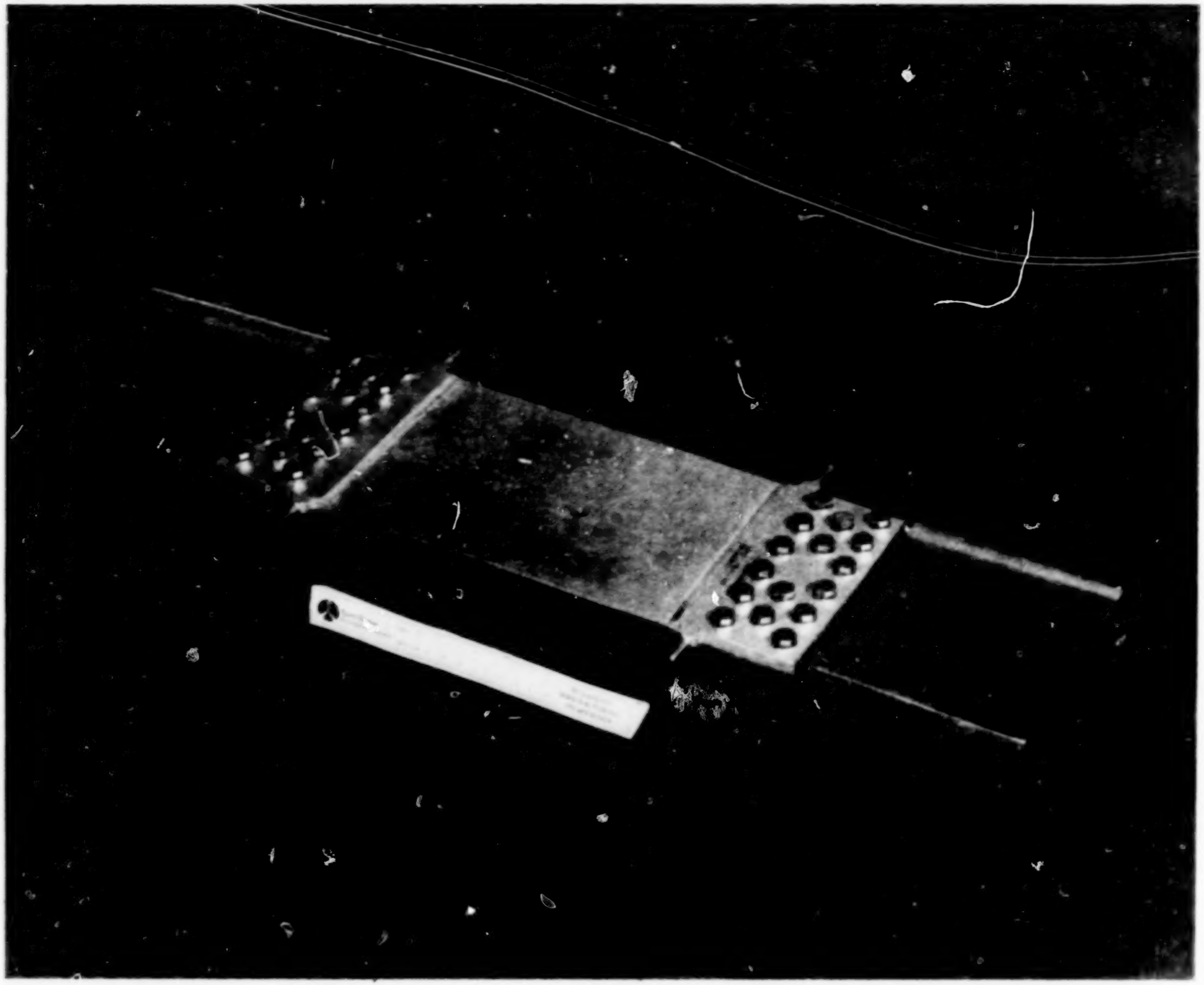

Figure 7.- (S.I.H.S.) moldline side of brazed panel with load adaptors.

390

(S.I.H.S.) INBOARD SIDE OF COMPLETED SPECIMEN

(Figure 8)

Inboard side of completed panel with center stiffener and end load adapters attached.

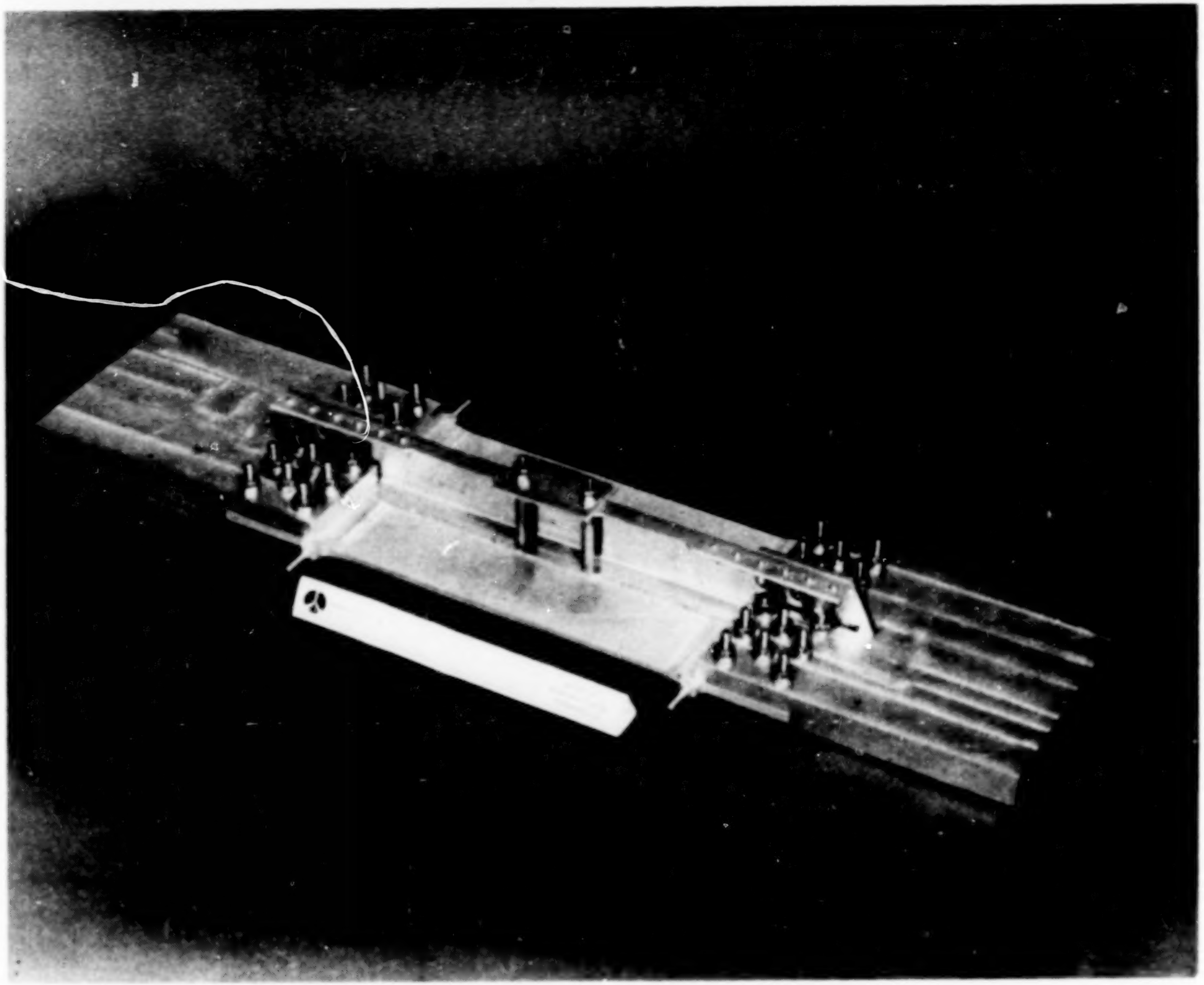

Figure 8.- (S.I.H.S.) inboard side of completed specimen.

PANEL CORNER SPECIMEN

(P.C.S.)

Second of Three Fatigue Specimens

Key Elements (figures 9 to 13):

- Contained external and integral manifolding.
- Fluxless brazed in retort under 0.10 MPa (15 psi) argon atmosphere.
- Brazed in heated platen press - exerting pressure.
- Heat treated without fixtures.
- Quenched in polymer solution.
- Fusion welded after quenching - before aging.
- Successfully tested to 1.72 MPa (250 psi).
- No braze voids detected by radiographic inspection.

PANEL CORNER SPECIMEN (P.C.S.) DETAILS DURING ASSEMBLY

(Figure 9)

Second of three fatigue specimens. Core sections are installed in frame. Channel at edge of frame is for edge cooling. Fingers in frame direct fluid flow from the manifold.

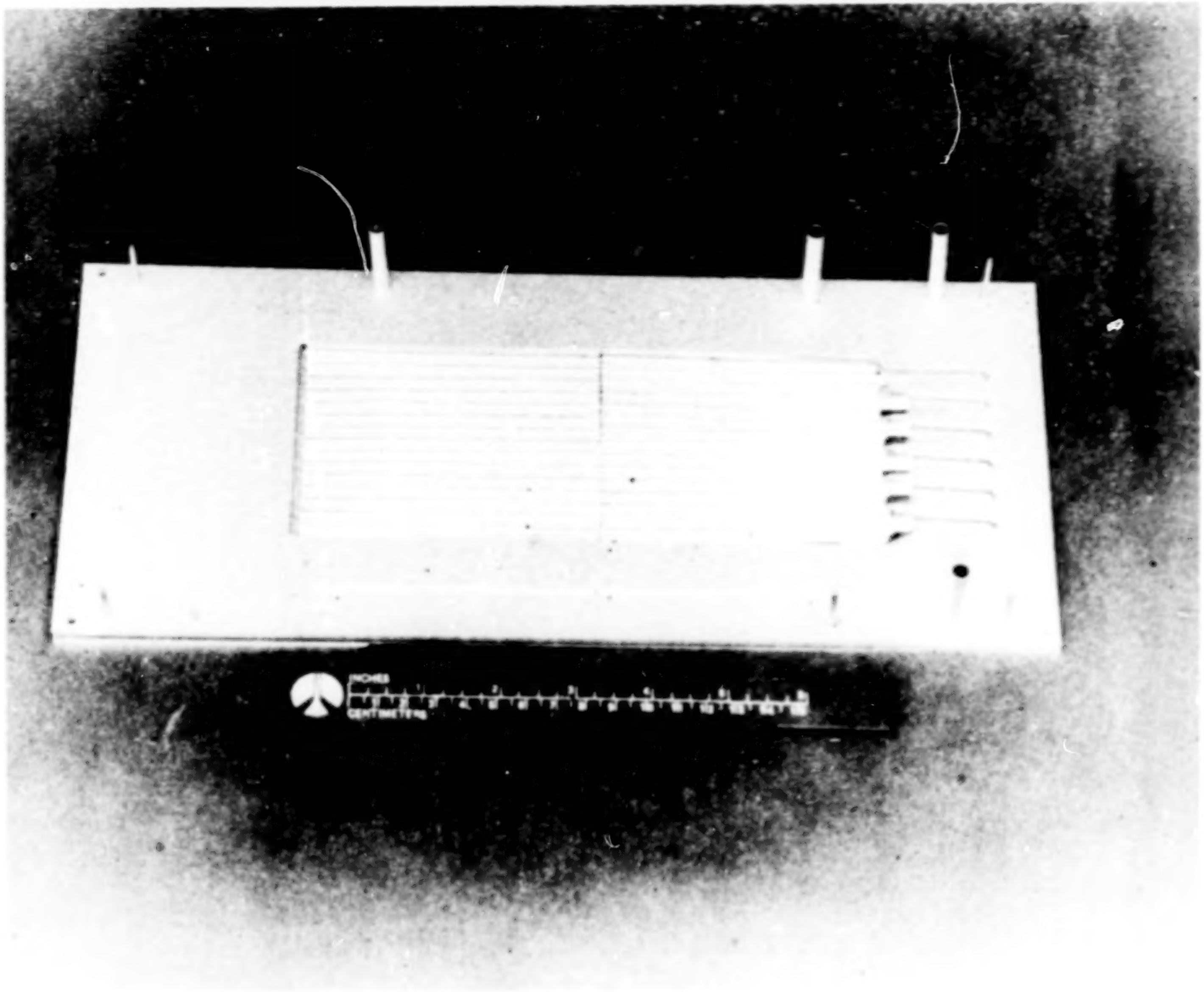
INCHES
CENTIMETERS

Figure 9.- Panel corner specimen (P.C.S.) details during assembly.

(P.C.S.) BRAZED PANEL AS REMOVED FROM RETORT

(Figure 10)

Brazed panel corner specimen after removal from retort. Note fingers in frame under the manifold prior to welding cap.

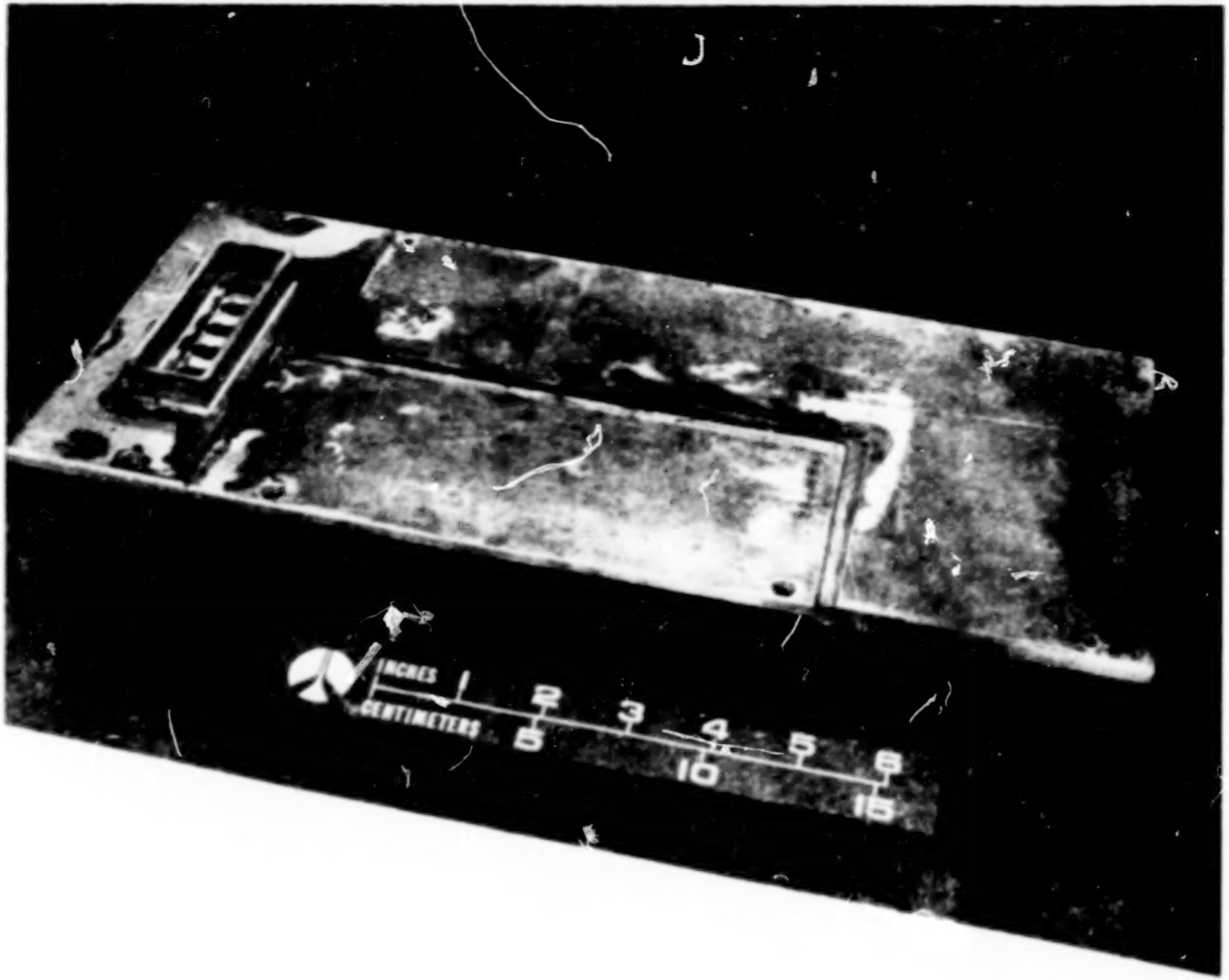
J
INCHES
CENTIMETERS
2
3
4
5
6
5
10
15

Figure 10.- (P.C.S.) brazed panel as removed from retort.

CONTENTS

Part I

PREFACE . . . . iii 1/A5

WELCOME 1 1/A10
R. R. Heldenfels

SESSION I - OVERVIEWS
Chairman: A. J. Henderson

1. HYPERSONIC STRUCTURES: AN AERODYNAMICIST'S PERSPECTIVE (OR ONE MAN'S DREAM IS ANOTHER MAN'S NIGHTMARE) 5 1/B1
J. D. Watts, L. R. Jackson, and J. L. Hunt

2. STRUCTURAL REQUIREMENTS FOR MILITARY HYPERSONIC SYSTEMS (Paper not available for publication)
P. Lane

3. AIRFRAME-INTEGRATED PROPULSION SYSTEM FOR HYPERSONIC CRUISE VEHICLES 39 1/F13
Robert A. Jones and Paul W. Huber

4. RECENT ADVANCES IN CONVECTIVELY COOLED ENGINE AND AIRFRAME STRUCTURES FOR HYPERSONIC FLIGHT 47 1/G7
H. Neale Kelly, Allan R. Wieting, Charles P. Shore, and Robert J. Nowak

SESSION II - ENGINE STRUCTURES
Chairman: H. N. Kelly

5. DESIGN AND ANALYSIS OF A SCRAMJET ENGINE 65 2/A13
O. A. Buchmann

6. THERMOSTRUCTURAL ANALYSIS OF A SCRAMJET FUEL-INJECTION STRUT 119 3/B11
Allan R. Wieting and Earl A. Thornton

7. ADVANCED FABRICATION TECHNIQUES FOR COOLED ENGINE STRUCTURES 145 3/F7
O. A. Buchmann

8. HYDROGEN EMBRITTLEMENT AND ITS CONTROL IN HYDROGEN-FUELED ENGINE SYSTEMS 195 4/F11
W. T. Chandler

9. CARBON-CARBON COMPOSITE APPLICATION FOR INTEGRAL ROCKET RAMJET COMBUSTORS (Paper not available for publication)
H. A. Holman

SESSION III - COOLED AIRFRAME STRUCTURES
Chairman: C. P. Shore

10. DESIGN AND FABRICATION OF A SKIN STRINGER DISCRETE TUBE ACTIVELY COOLED STRUCTURAL PANEL 253 6/A5
Frank M. Anthony

11. DESIGN AND ANALYSIS OF A PLATE-FIN SANDWICH ACTIVELY COOLED STRUCTURAL PANEL 319 7/C13
L. M. Smith

12. FLUXLESS BRAZING AND HEAT TREATMENT OF A PLATE-FIN SANDWICH ACTIVELY COOLED PANEL 375 8/E1
Charles S. Beuyukian

13. DESIGN AND FABRICATION OF A RADIATIVE ACTIVELY COOLED HONEYCOMB SANDWICH PANEL 449 10/A13
Leland C. Koch

14. RADIATIVE, ACTIVELY COOLED PANEL TESTS RESULTS 493 11/A5
Charles P. Shore, Robert J. Nowak, and Ellsworth L. Sharpe

(P.C.S.) PANELS AFTER FINISH MACHINING

(Figure 11)

Panel corner specimens after heat treating and welding of manifold cap. Tube at edge of panel is for outlet manifolding.

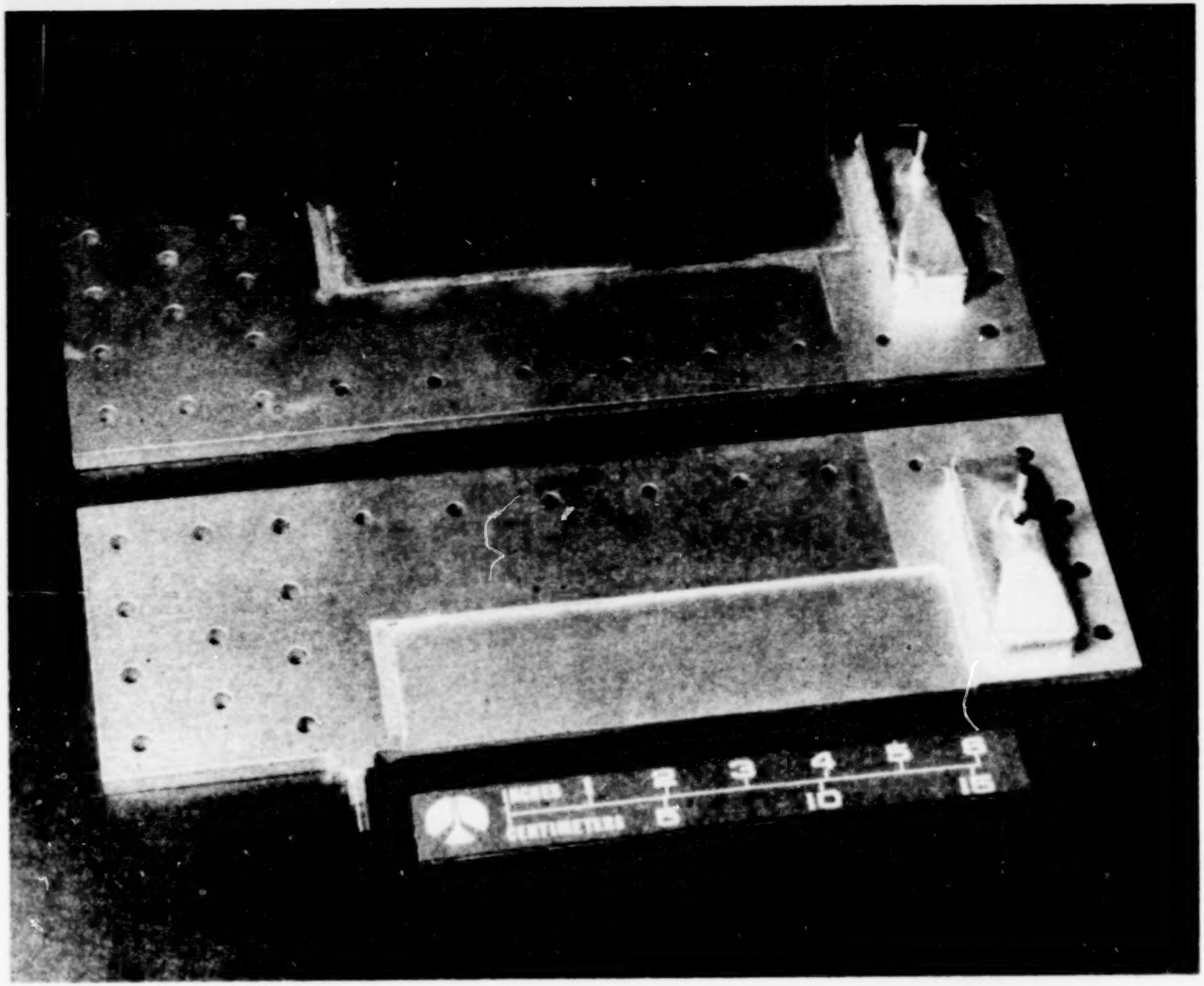
INCHES
1 2 3 4 5 6
CENTIMETERS
5 10 15

Figure 11.- (P.C.S.) panels after finish machining.

398

(P.C.S.) MOLDLINE SIDE OF COMPLETED SPECIMEN

(Figure 12)

Moldline side of panel corner specimens attached to end load adapters.

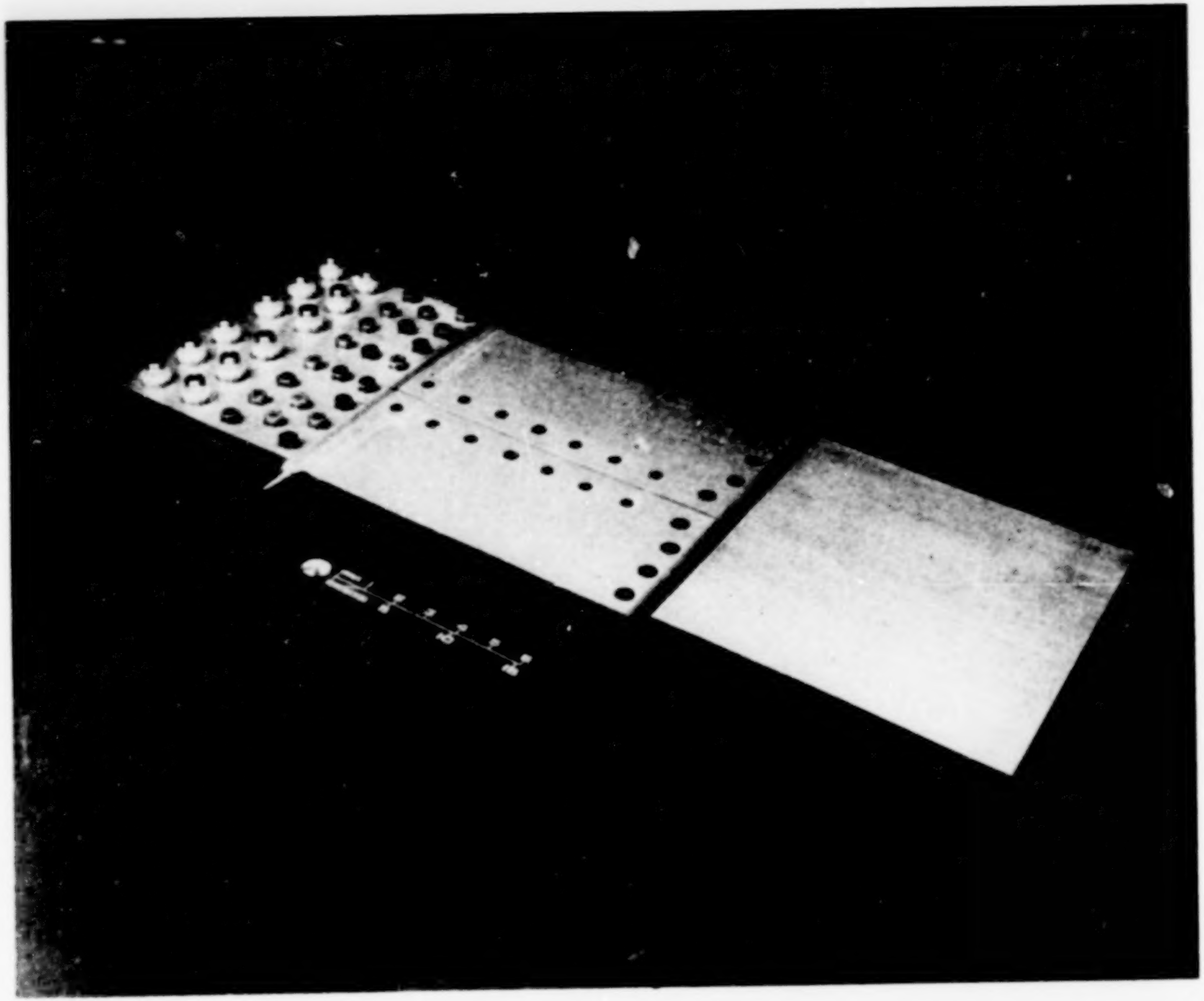

Figure 12.- (P.C.S.) moldline side of completed specimen.

9

400

(P.C.S.) INBOARD SIDE OF COMPLETED SPECIMEN

(Figure 13)

Inboard side of panel corner specimen with center stringers and end load adapters attached.

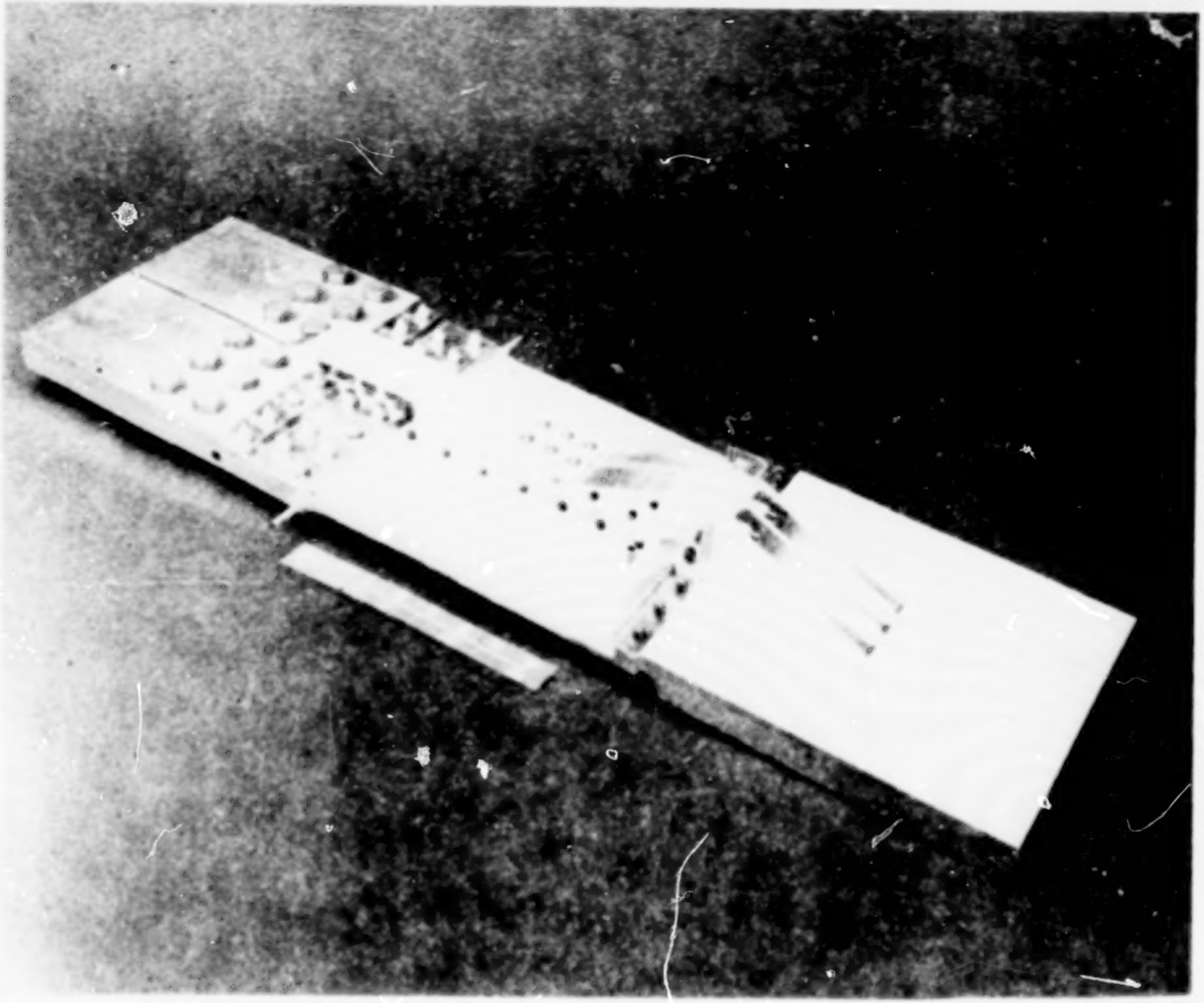

Figure 13.- (P.C.S.) inboard side of completed specimen.

END PANEL INTERIOR STRINGER TERMINATION SPECIMEN

(E.P.I.S.T.S.)

Third of Three Fatigue Specimens

Key Elements (figures 14 to 18):

- Contained external and integral manifolding.
- Fluxless brazed in retort under 0.10 MPa (15 psi) argon atmosphere.
- Brazed in heated platen press - exerting pressure.
- Heat treated without fixtures.
- Quenched in polymer solution.
- Fusion welded after quenching - before aging.
- Successfully tested to 1.72 MPa (250 psi).
- No braze voids detected by radiographic inspection.

END PANEL INTERIOR STRINGER TERMINATION SPECIMEN (E.P.I.S.T.S.) DETAILS DURING ASSEMBLY

(Figure 14)

Last of three fatigue specimens. Core sections located in frame. Note fingers and stringer hardspot machined in frame. Rod is temporarily inserted in holes in frame. Holes will later become integral manifolding ports after machining.

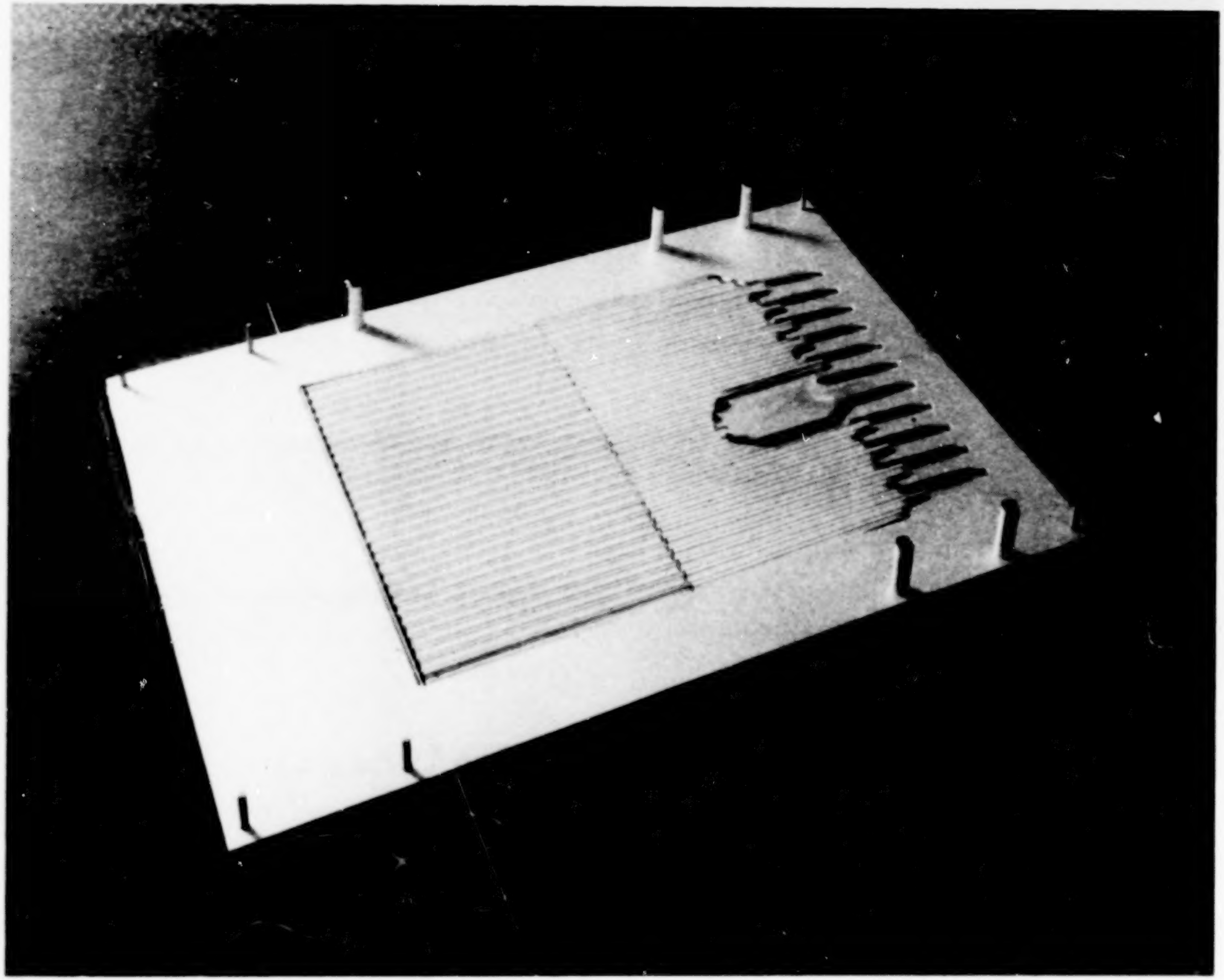

Figure 14.- End panel interior stringer termination specimen (E.P.I.S.T.S.) details during assembly.

(E.P.I.S.T.S.) BRAZED PANEL AFTER REMOVAL FROM RETORT

(Figure 15)

Brazed panel specimen before heat treating, welding, and machining. Note differing heights on surface of panel and within manifold.

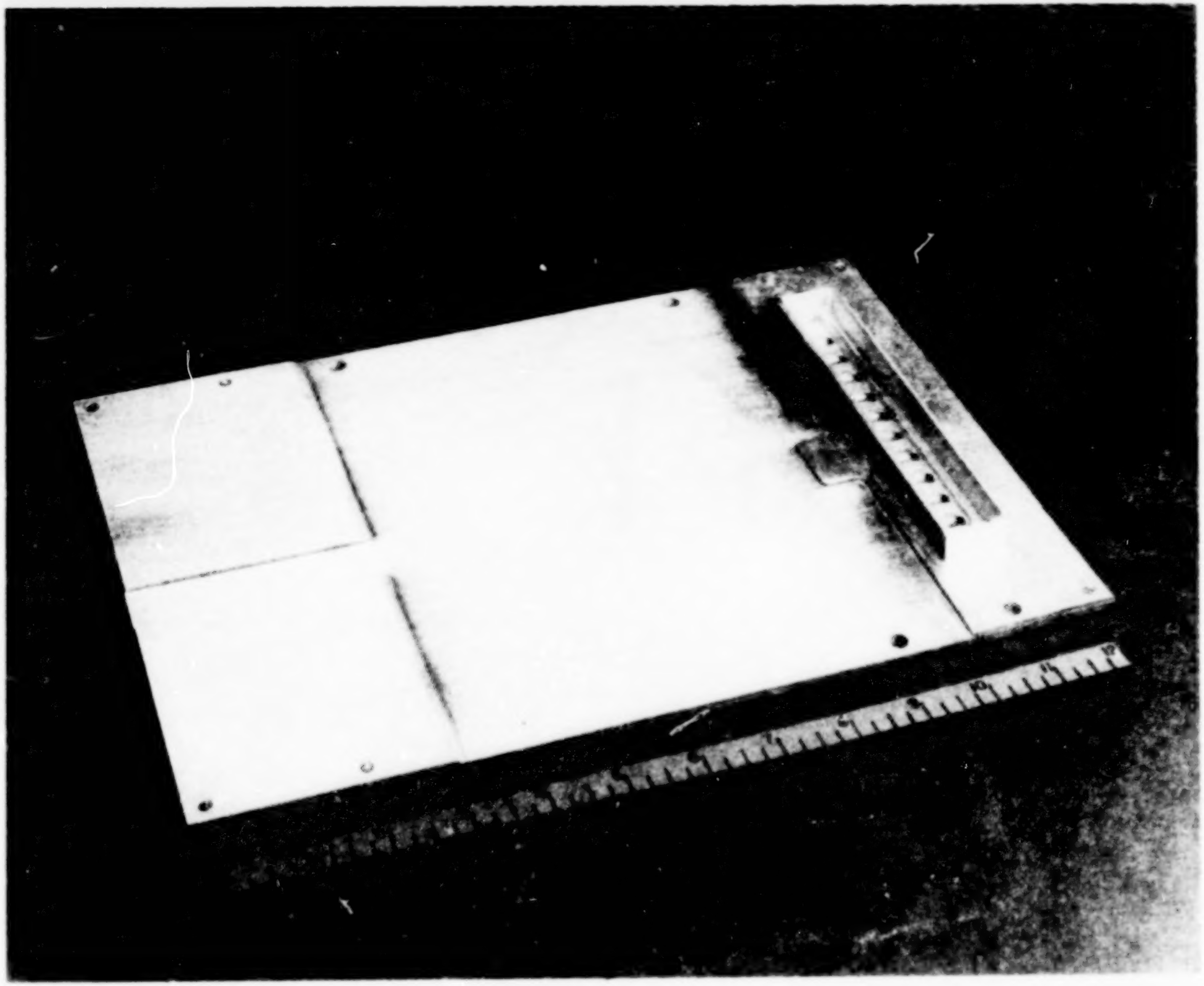

Figure 15.- (E.P.I.S.T.S.) brazed panel after removal from retort.

406

(E.P.I.S.T.S.) BRAZED PANEL COMPLETED

(Figure 16)

Panel specimen has been heat treated and cap welded to the manifold. Finish machining has left the integral manifolding ports (tubes) on the panel.

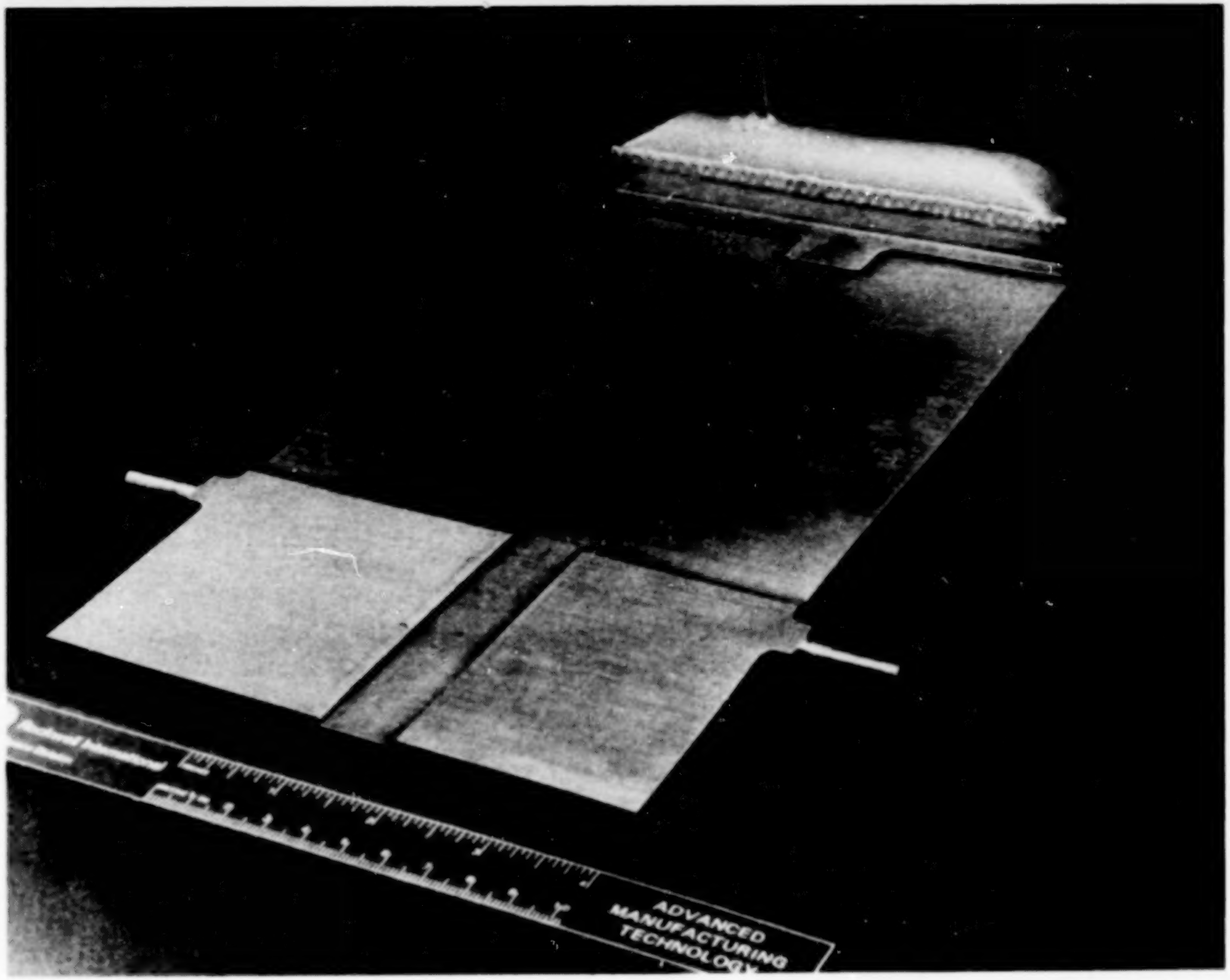
ADVANCED
MANUFACTURING
TECHNOLOGY

Figure 16.- (E.P.I.S.T.S.) brazed panel completed.

408

(E.P.I.S.T.S.) INBOARD SIDE OF COMPLETED SPECIMEN

(Figure 17)

Inboard side of completed panel specimen with center stiffener and end load adapters attached. The center stiffener has been adhesive bonded to the panel specimen.

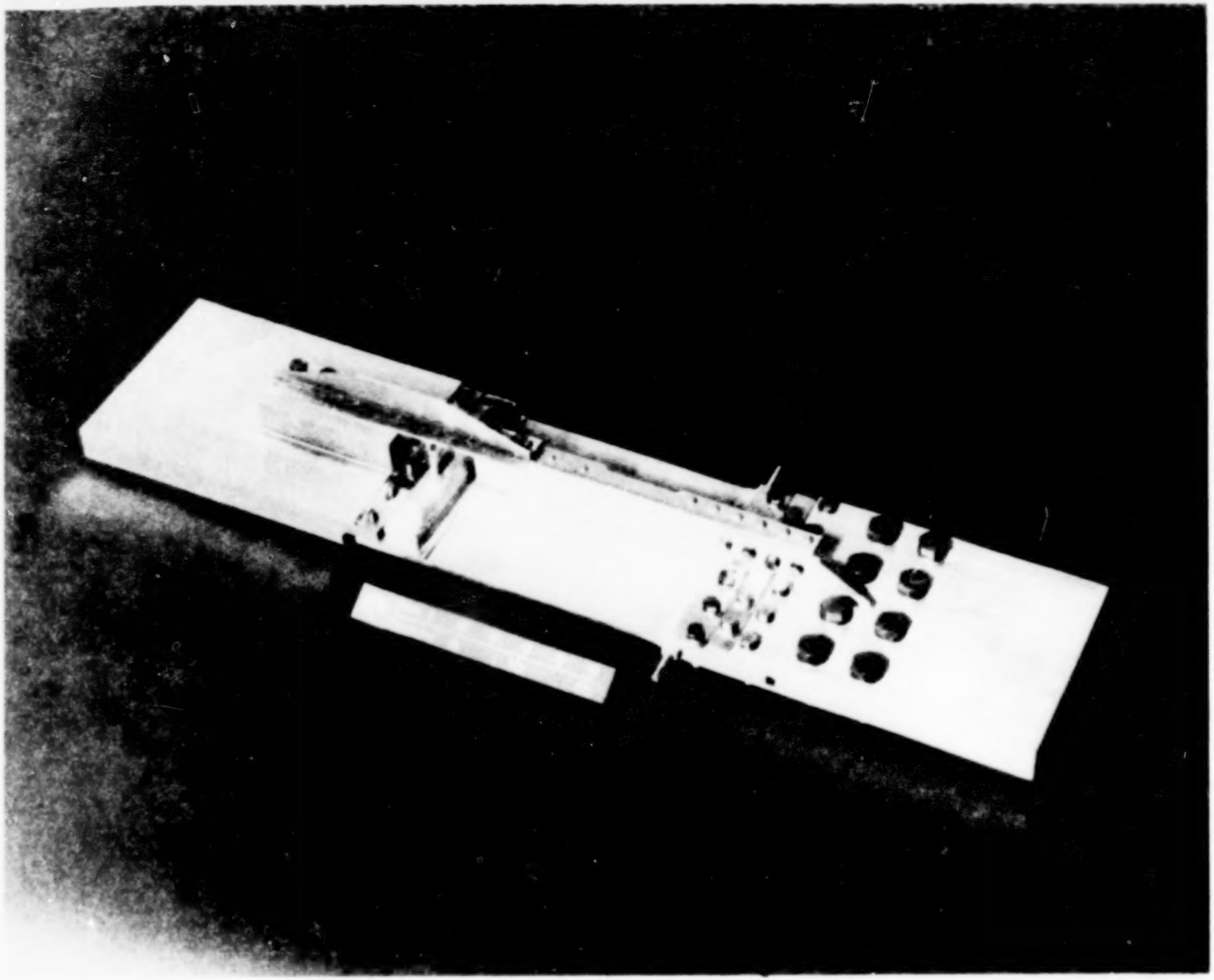

Figure 17.- (E.P.I.S.T.S.) inboard side of completed specimen.

410

(E.P.I.S.T.S.) MOLDLINE SIDE OF COMPLETED SPECIMEN

(Figure 18)

Moldline side of the completed panel ready for testing.

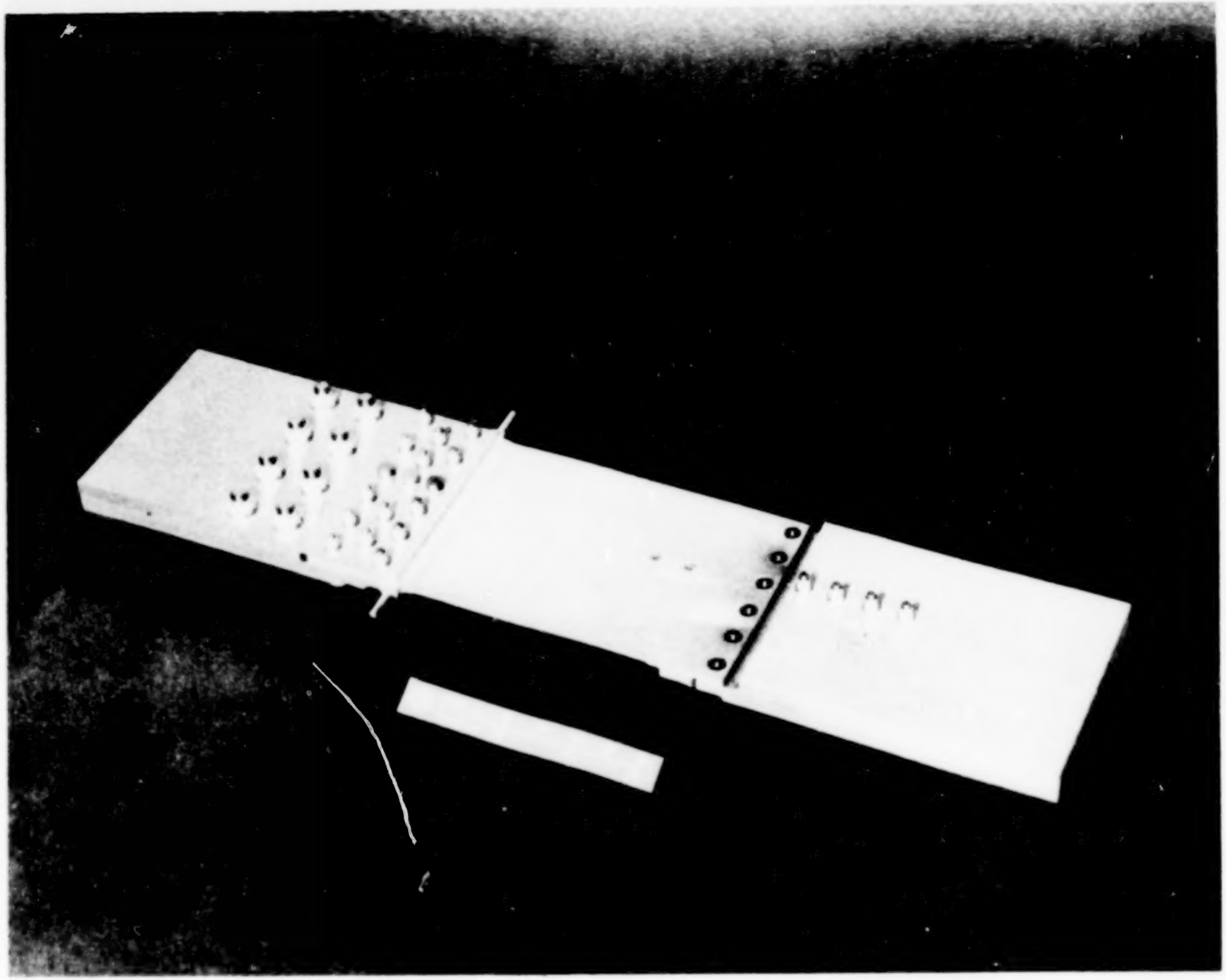

Figure 18.- (E.P.I.S.T.S) moldline side of completed specimen.

ACTIVELY COOLED TEST PANEL

(A.C.T.P.)

0.61 m by 1.22 m (2 by 4 ft)

Key Elements (figures 19 to 36):

- Largest fluxless brazed and heat treated aluminum panel of this configuration known to exist.
- Contained external inlet and outlet manifolding.
- Fluxless brazed in retort under 0.10 MPa (15 psi) argon atmosphere.
- Brazed in heated platen press - exerting pressure.
- Heat treated without fixtures.
- Quenched in polymer solution.
- Flushed with alcohol and freon.
- Fusion welded after quenching - before aging.
- Panel exterior anodized.
- Successfully tested to 1.24 MPa (180 psi).
- No braze voids detected by radiographic inspection.

ACTIVELY COOLED TEST PANEL BRAZE ASSEMBLY COMPONENTS

(Figure 19)

Composite sketch of the lay-up of all components comprising the test panel sandwich structure for brazing.

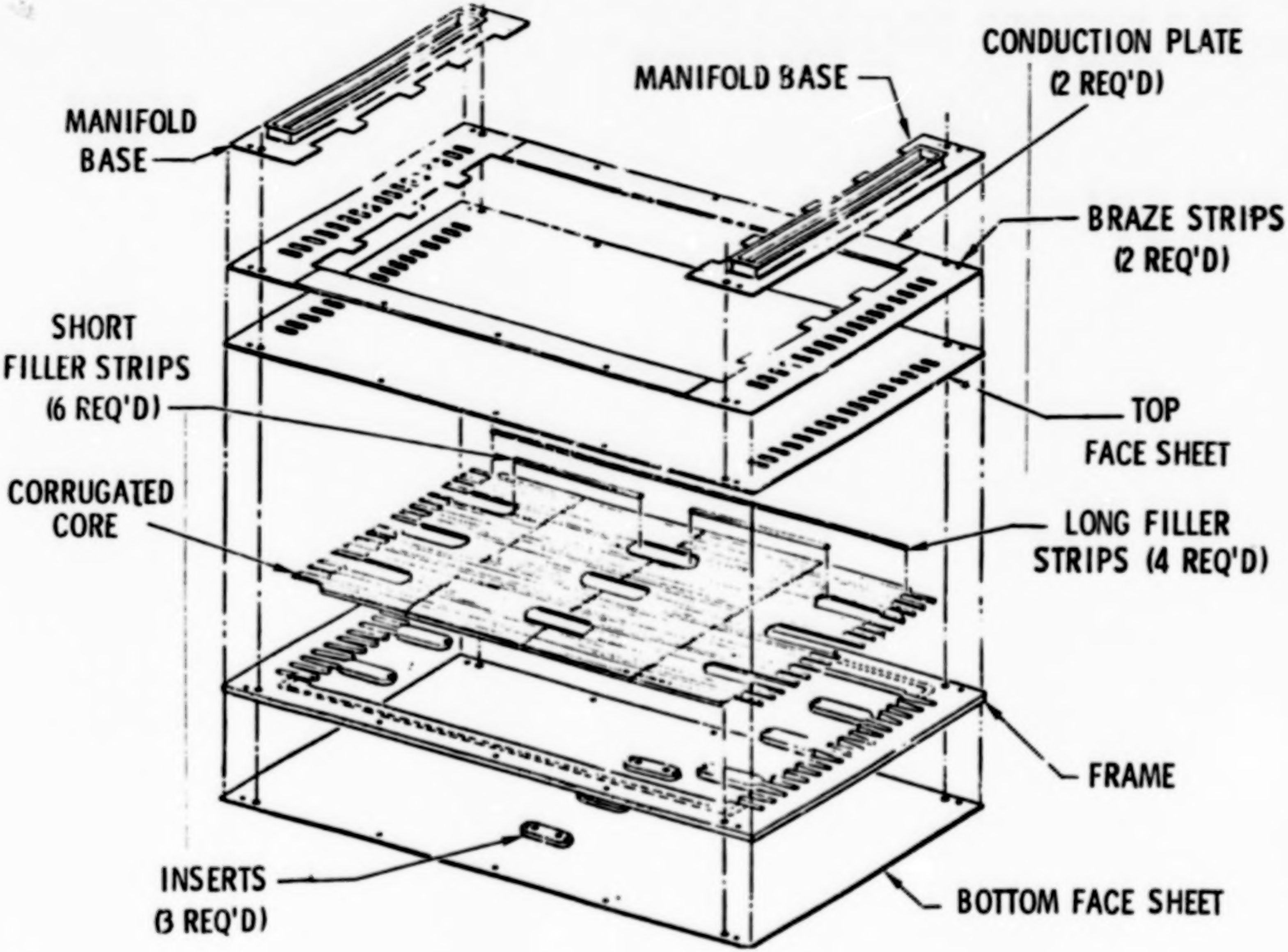
MANIFOLD BASE
MANIFOLD BASE
CONDUCTION PLATE (2 REQ'D)
BRAZE STRIPS (2 REQ'D)
SHORT FILLER STRIPS (6 REQ'D)
TOP FACE SHEET
CORRUGATED CORE
LONG FILLER STRIPS (4 REQ'D)
FRAME
INSERTS (3 REQ'D)
BOTTOM FACE SHEET

Figure 19.- Actively cooled test panel braze assembly components.

414

TOOLING LAY-UP SEQUENCE FOR BRAZING ACTIVELY COOLED TEST PANEL

(Figure 20)

Composite sketch of the tooling lay-up and test panel location in preparation to installation in retort prior to fluxless brazing.

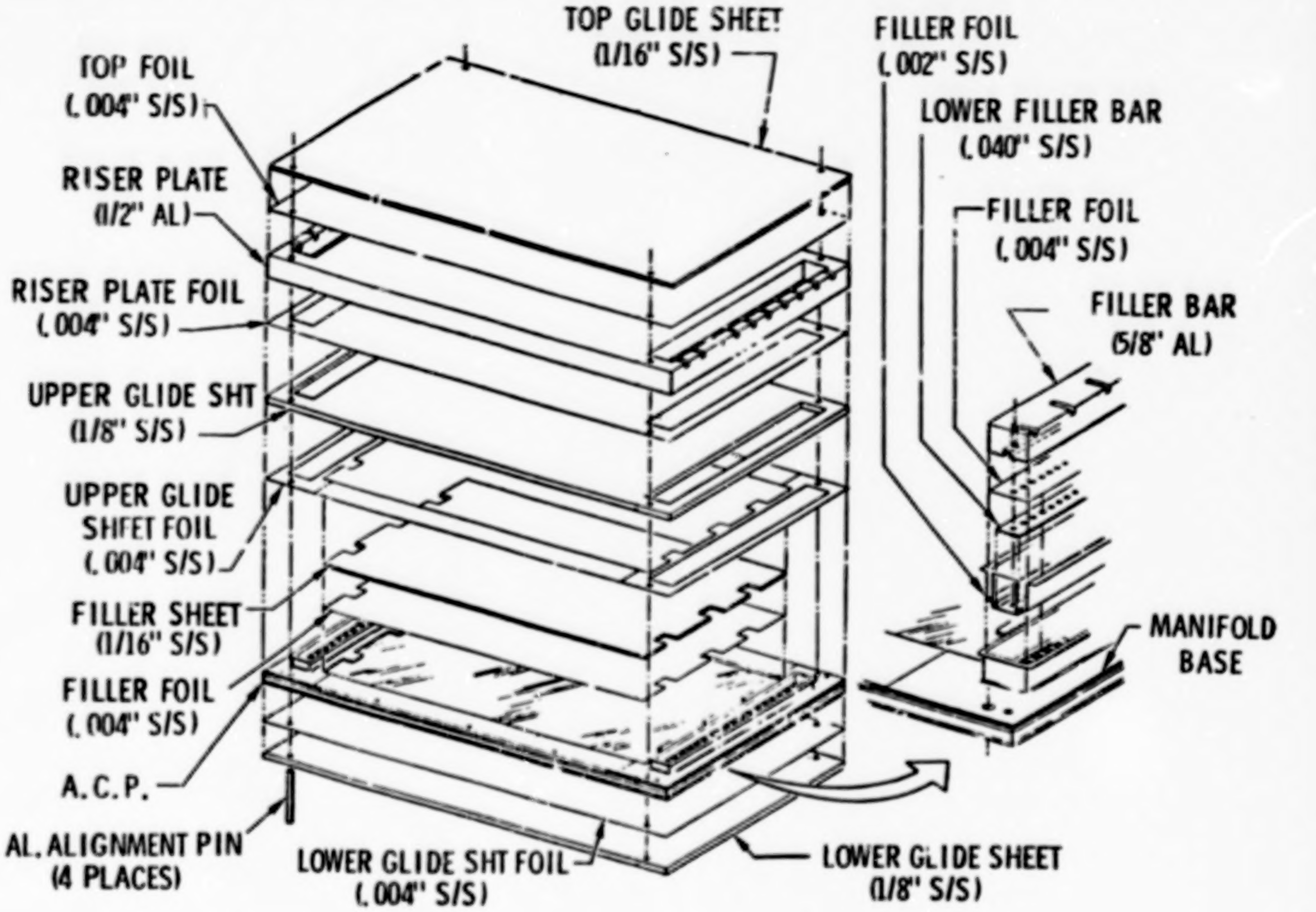
TOP FOIL
(.004" S/S)
TOP GLIDE SHEET
(1/16" S/S)
FILLER FOIL
(.002" S/S)
LOWER FILLER BAR
(.040" S/S)
RISER PLATE
(1/2" AL)
FILLER FOIL
(.004" S/S)
RISER PLATE FOIL
(.004" S/S)
FILLER BAR
(5/8" AL)
UPPER GLIDE SHT
(1/8" S/S)
UPPER GLIDE
SHEET FOIL
(.004" S/S)
FILLER SHEET
(1/16" S/S)
MANIFOLD
BASE
FILLER FOIL
(.004" S/S)
A.C.P.
AL. ALIGNMENT PIN
(4 PLACES)
LOWER GLIDE SHT FOIL
(.004" S/S)
LOWER GLIDE SHEET
(1/8" S/S)

Figure 20.- Lay-up sequence for brazing 0.61 m by 1.22 m (2 by 4 ft) actively cooled panel.

416

ACTIVELY COOLED TEST PANEL (A.C.T.P.) FRAME

(Figure 21)

The panel frame with the edge fluid channel side exposed. Fusion welds are at the four corners at ends of fingers. Hardspots are part of frame assembly.

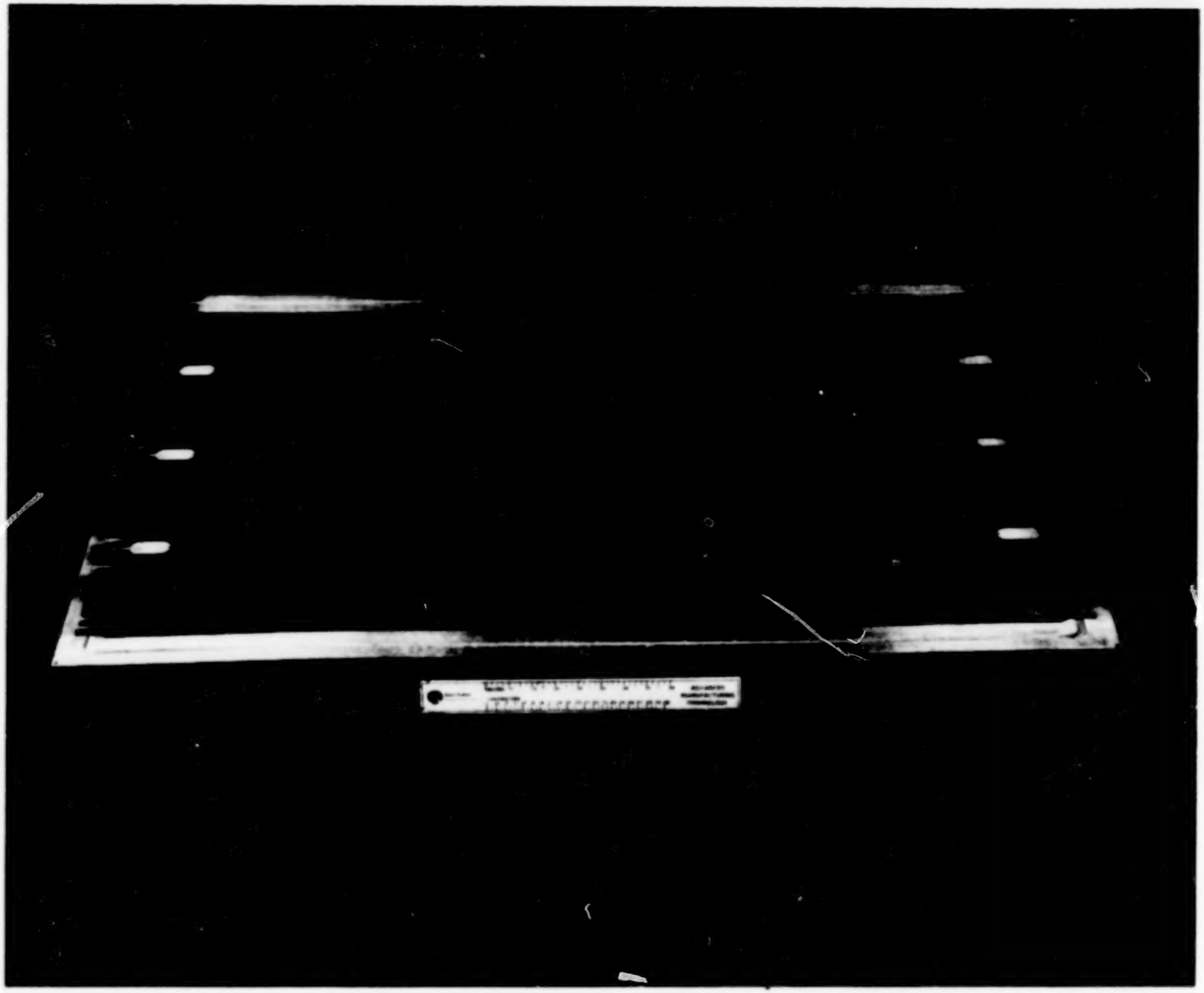

Figure 21.- Actively cooled test panel (A.C.T.P.) frame.

418

(A.C.T.P.) INTERNAL DETAILS DURING PRE-BRAZE ASSEMBLY

(Figure 22)

Internal details of test panel assembled prior to closure. Corrugated straight-fin core is in four sections. Three center hardspots are riveted to bottom face sheet.

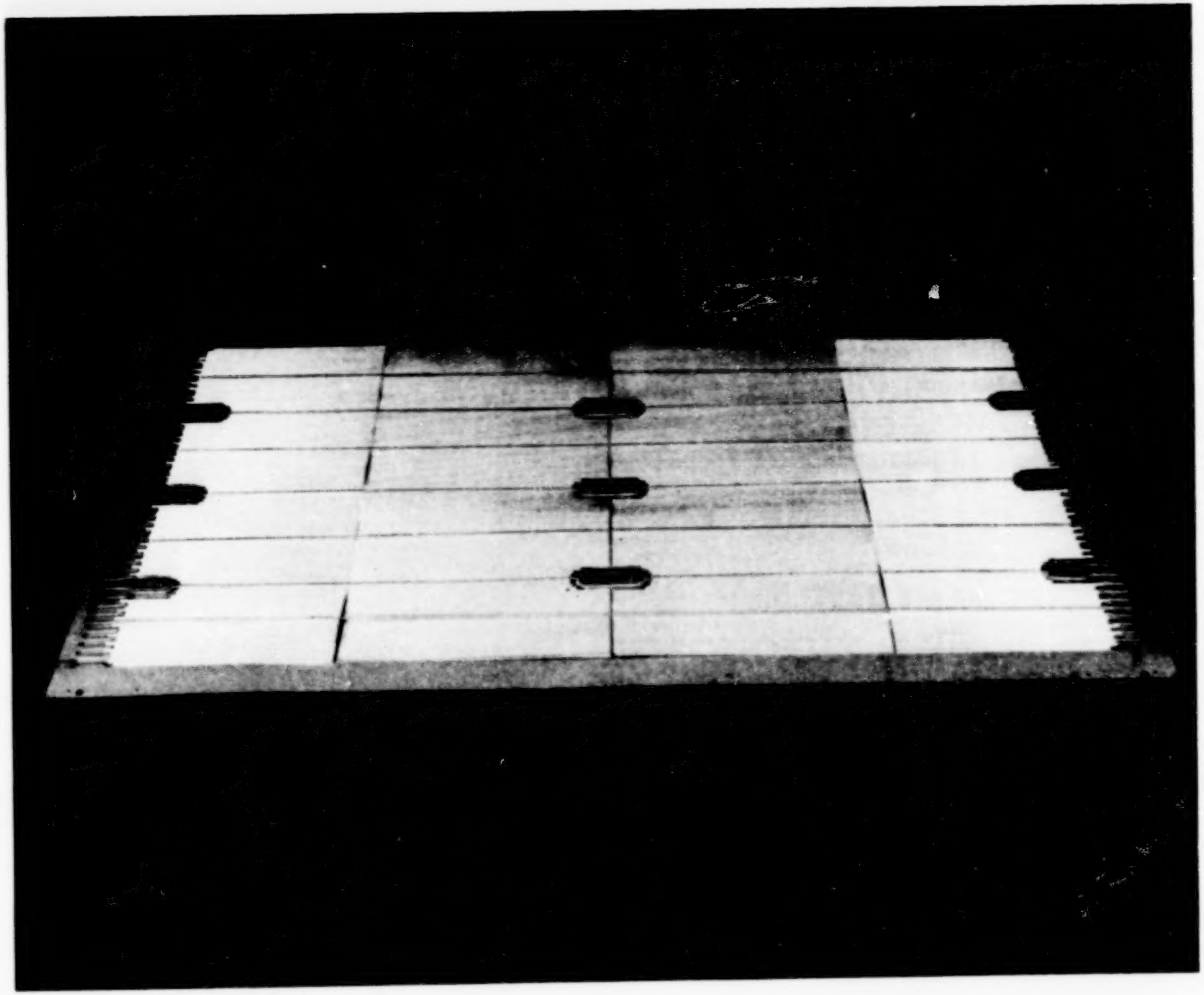

Figure 22.- (A.C.T.P.) internal details during pre-braze assembly.

420

(A.C.T.P.) PANEL DETAIL STACKED PRIOR TO BRAZING

(Figure 23)

All details of braze panel assembled and pinned together. Braze alloy is clad to inner side of each face sheet and conduction plates. Manifolds are brazed with double-sided braze sheet.

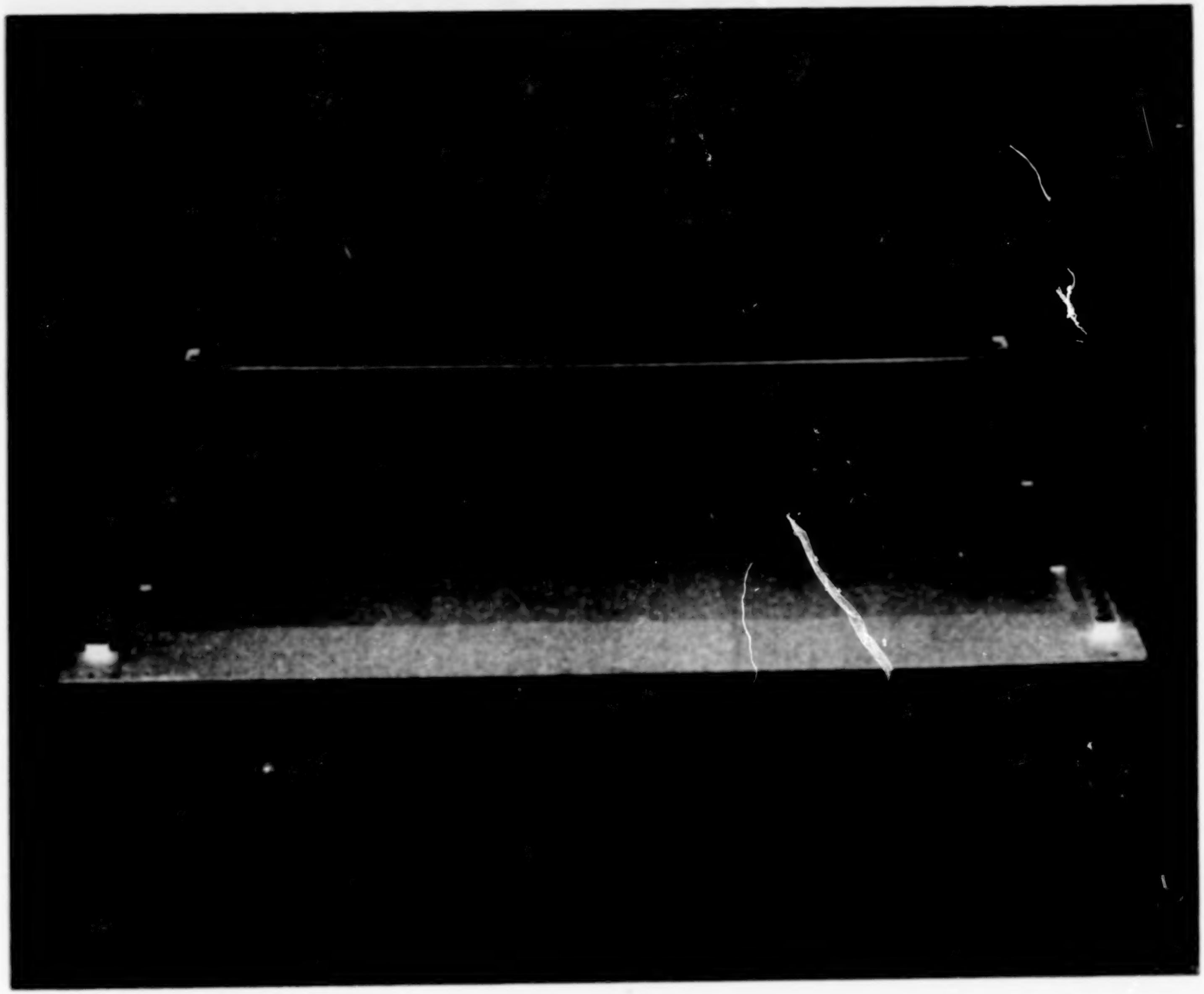

Figure 23.- (A.C.T.P.) panel detail stacked prior to brazing.

(A.C.T.P.) TOOLING RISER PLATE INSTALLED ON DETAILS

(Figure 24)

Tooling riser plate installed to bring pressure areas in one plane. This allows uniform pressure to be exerted across the panel (except in the manifold).

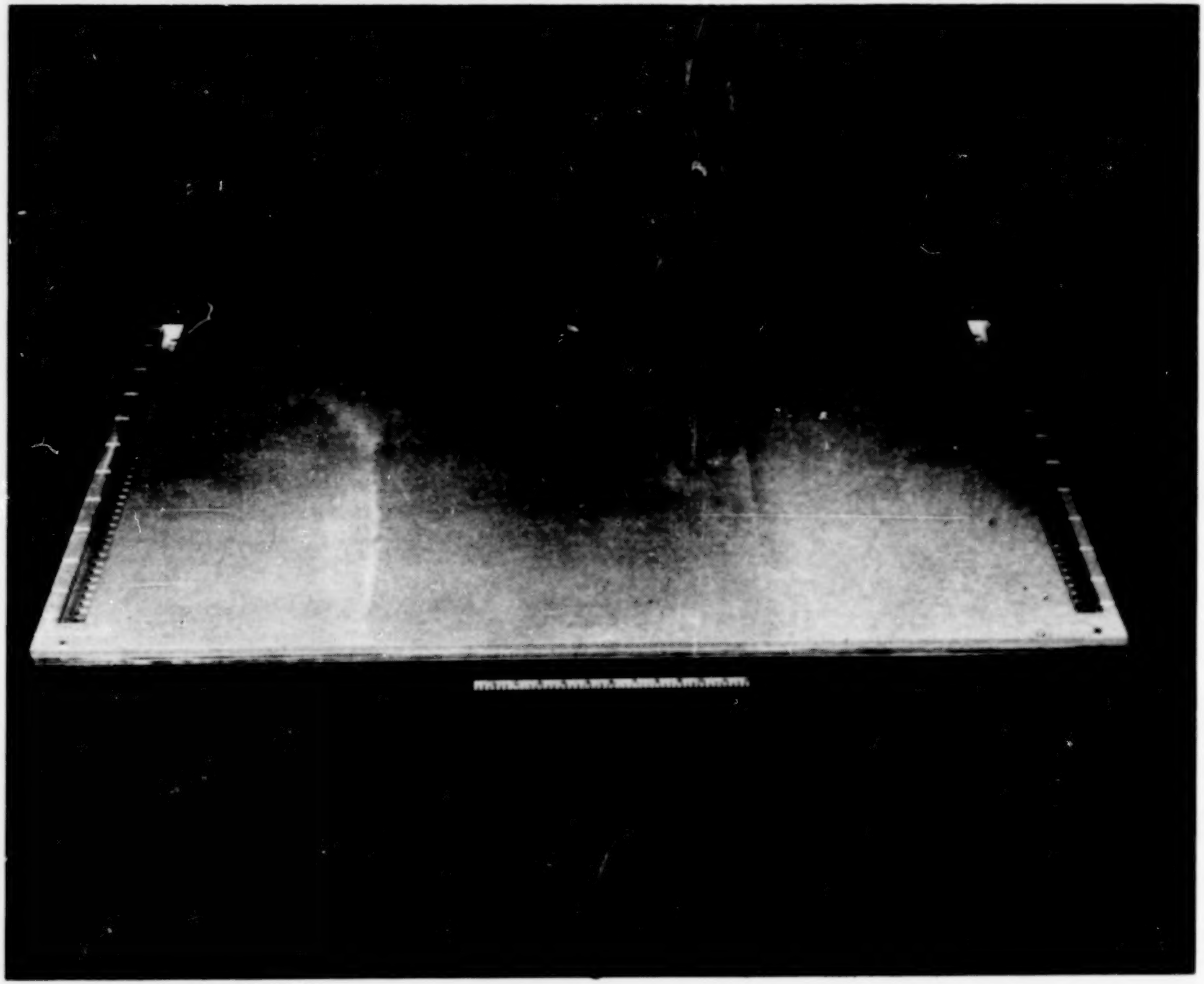

Figure 24.- (A.C.T.P.) tooling riser plate installed on details.

(A.C.T.P.) MANIFOLD FILLER BARS LOCATED OVER FINGERS

(Figure 25)

Manifold filler bars located within the manifold base. These bars permit uniform pressure exertion on the skin-to-frame finger joint areas.

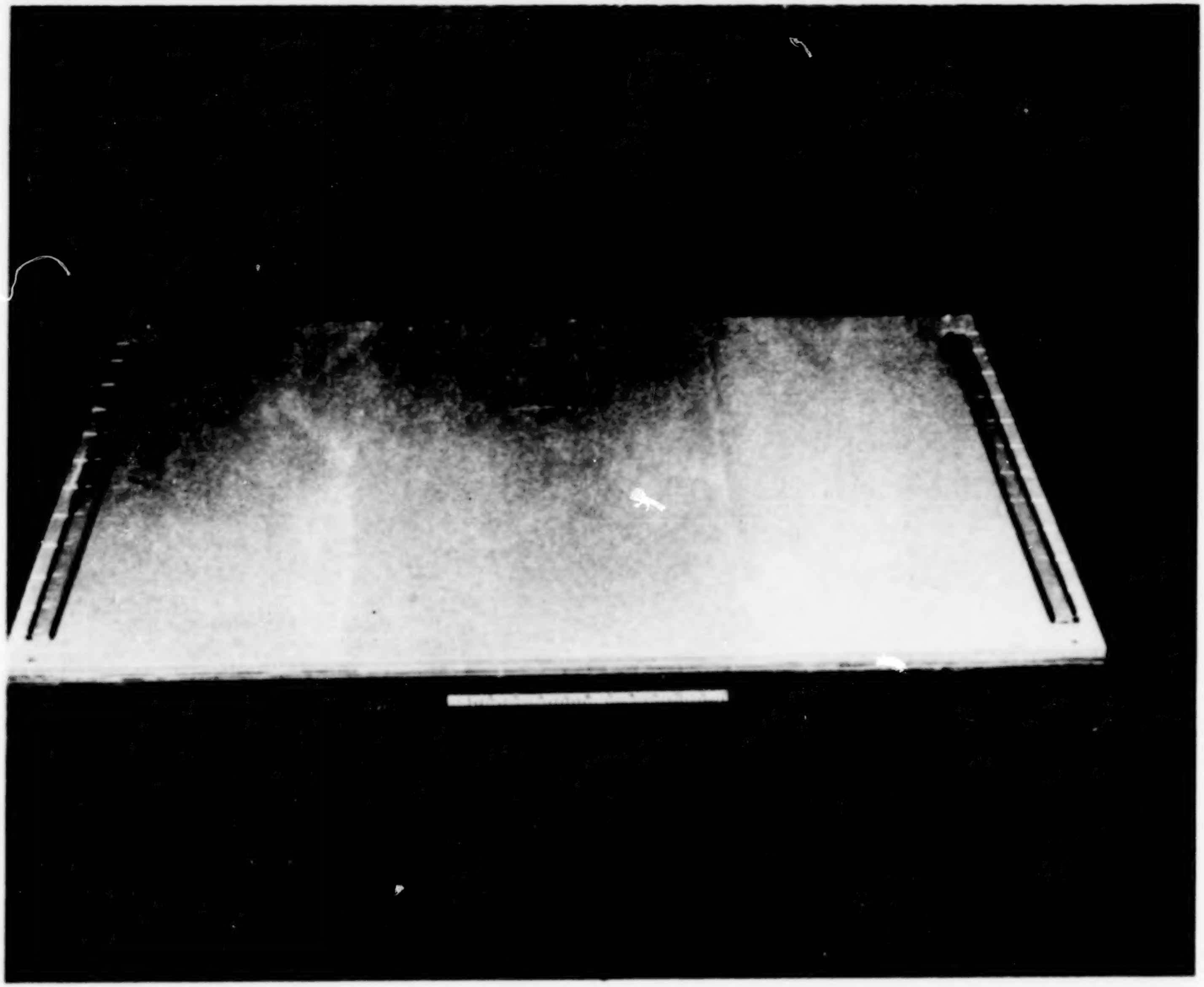

Figure 25.- (A.C.T.P.) manifold filler bars located over fingers.

426

(A.C.T.P.) DETAILS AND TOOLING IN RETORT BEFORE CLOSURE

(Figure 26)

All actively cooled test panel details and tooling positioned in stainless steel retort prior to closure and sealing. The four thermocouples attached to the A.C.T.P. monitor temperatures during brazing.

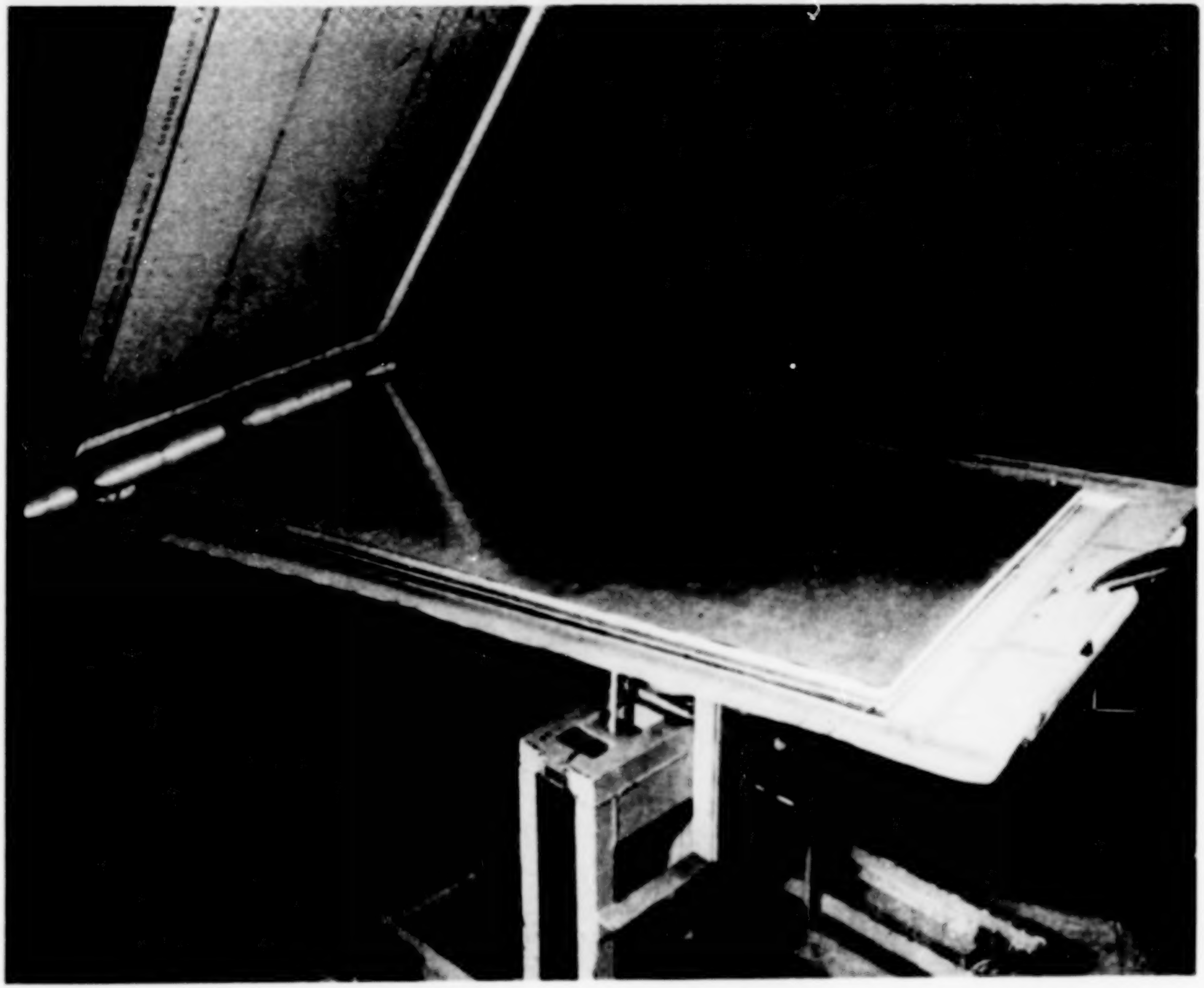

Figure 26.- (A.C.T.P.) details and tooling in retort before closure.

ACTIVELY COOLED PANEL PRESS BRAZE CYCLE

(Figure 27)

Braze cycle used on actively cooled test panel. As shown, panel is subjected to externally applied press pressure and internal argon gas pressure simultaneously during the brazing cycle. External pressure assures joint contact. Internal gas pressure minimizes cavitation.

2 BY 4 FT. ACTIVELY COOLED PANEL PRESS BRAZE CYCLE

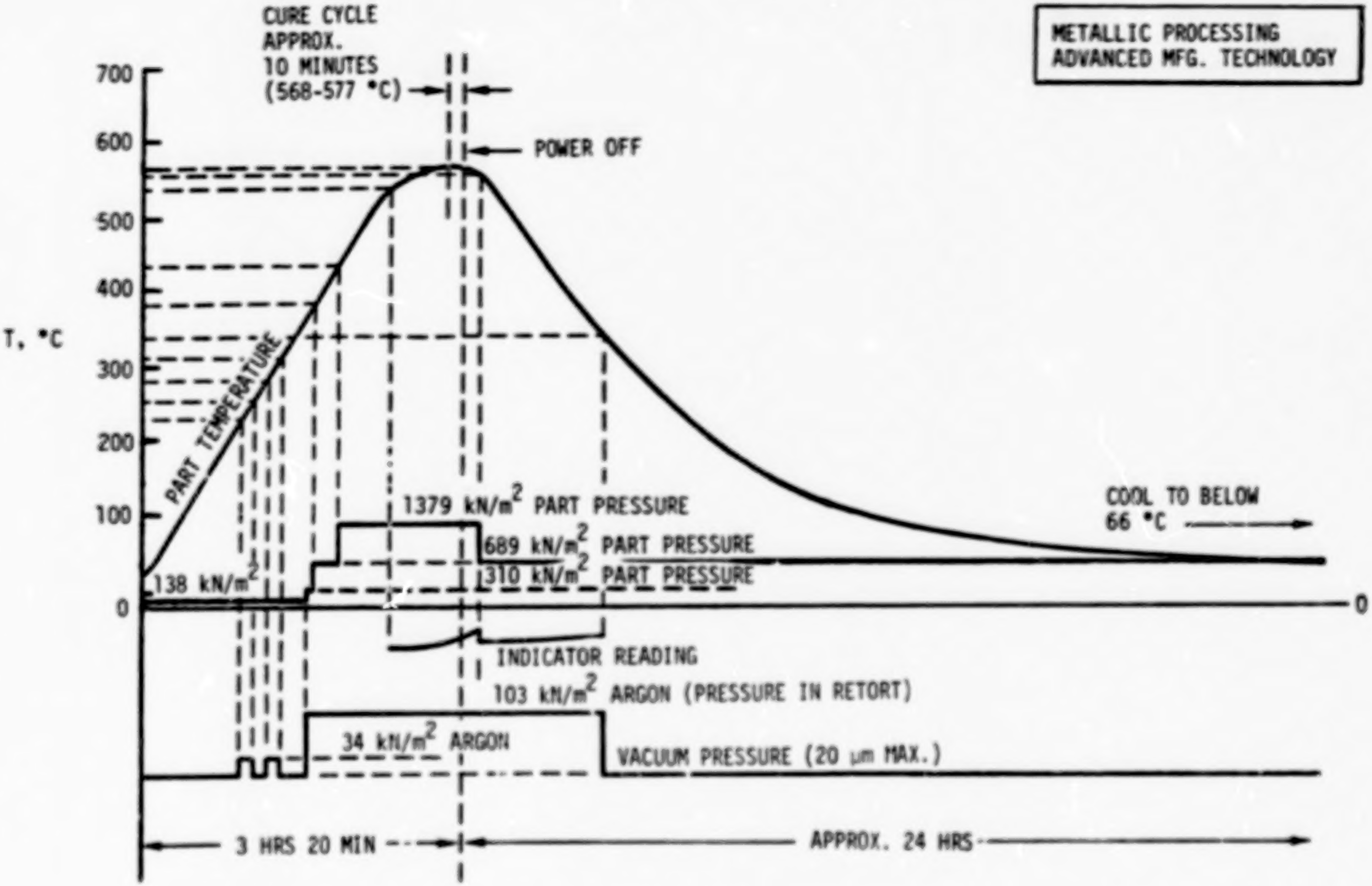

Figure 27

430

(A.C.T.P.) BRAZED PANEL AFTER REMOVAL FROM RETORT

(Figure 28)

Inboard side of brazed actively cooled test panel after removal from retort. Dark stains are from tooling separator foil. Images from support rods and hardspot inserts are visible due to press pressure applied during brazing cycle.

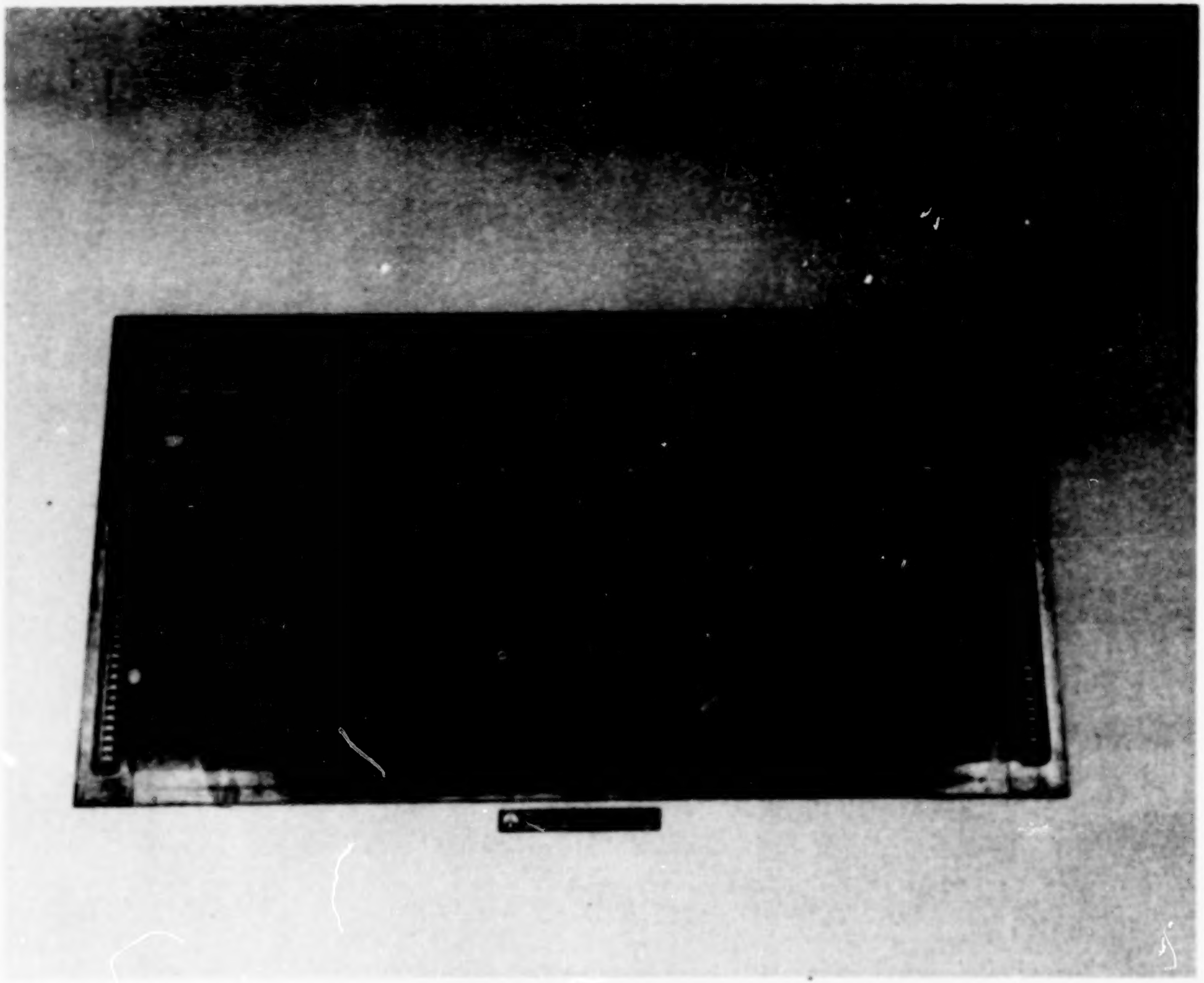

Figure 28.- (A.C.T.P.) brazed panel after removal from retort.

432

(A.C.T.P.) MOLDLINE SIDE OF TEST PANEL

(Figure 29)

Moldline side of brazed actively cooled test panel. Images of manifold fingers, center hardspot inserts, and support rods are clearly visible.

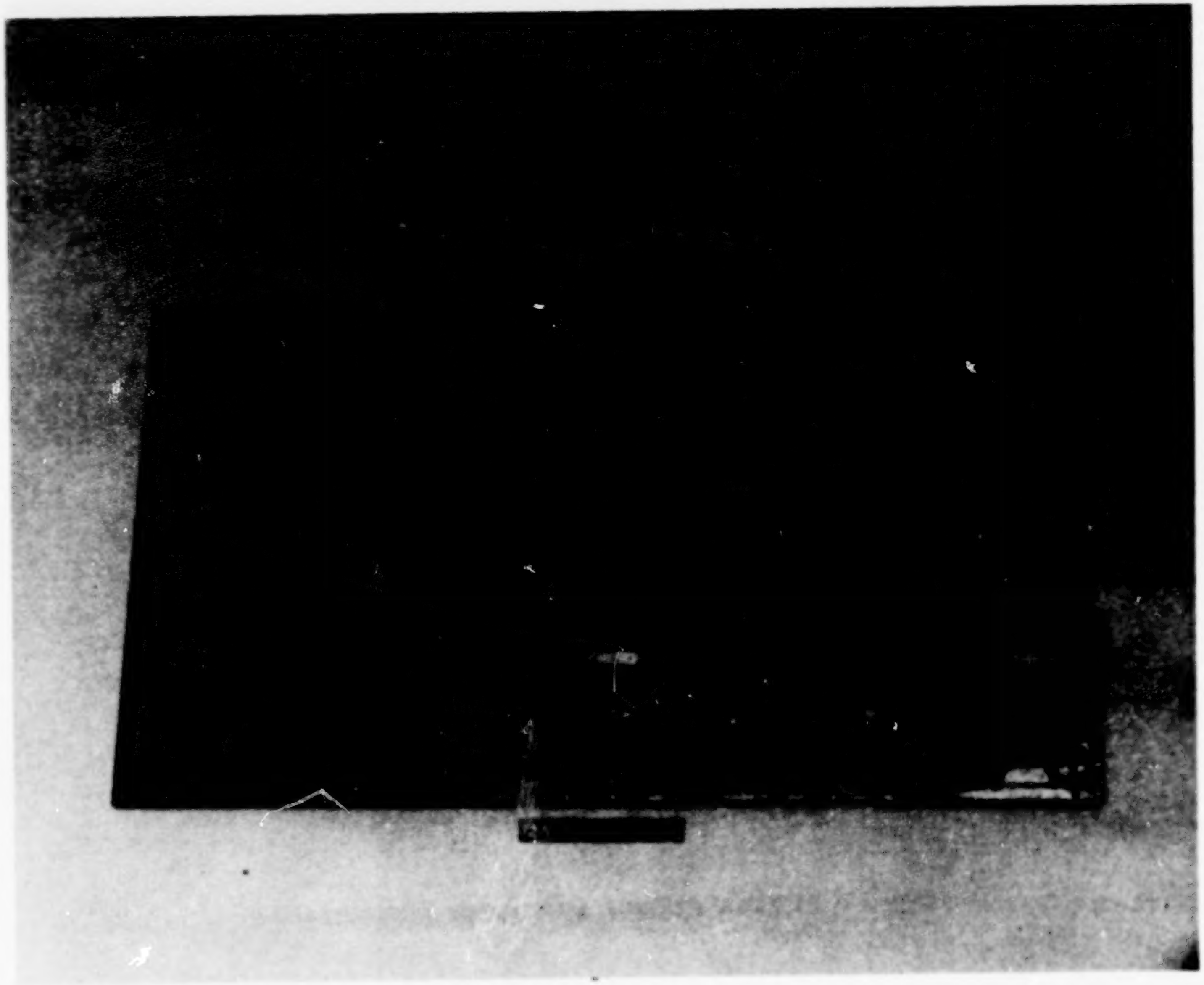

Figure 29.- (A.C.T.P.) moldline side of test panel.

434

(A.C.T.P.) HELIUM LEAK TESTING OF BRAZED TEST PANEL

(Figure 30)

Brazed actively cooled test panel being helium leak tested before heat treating or welding. Test fixtures clamp over manifold bases for complete sealing during leak and pressure testing.

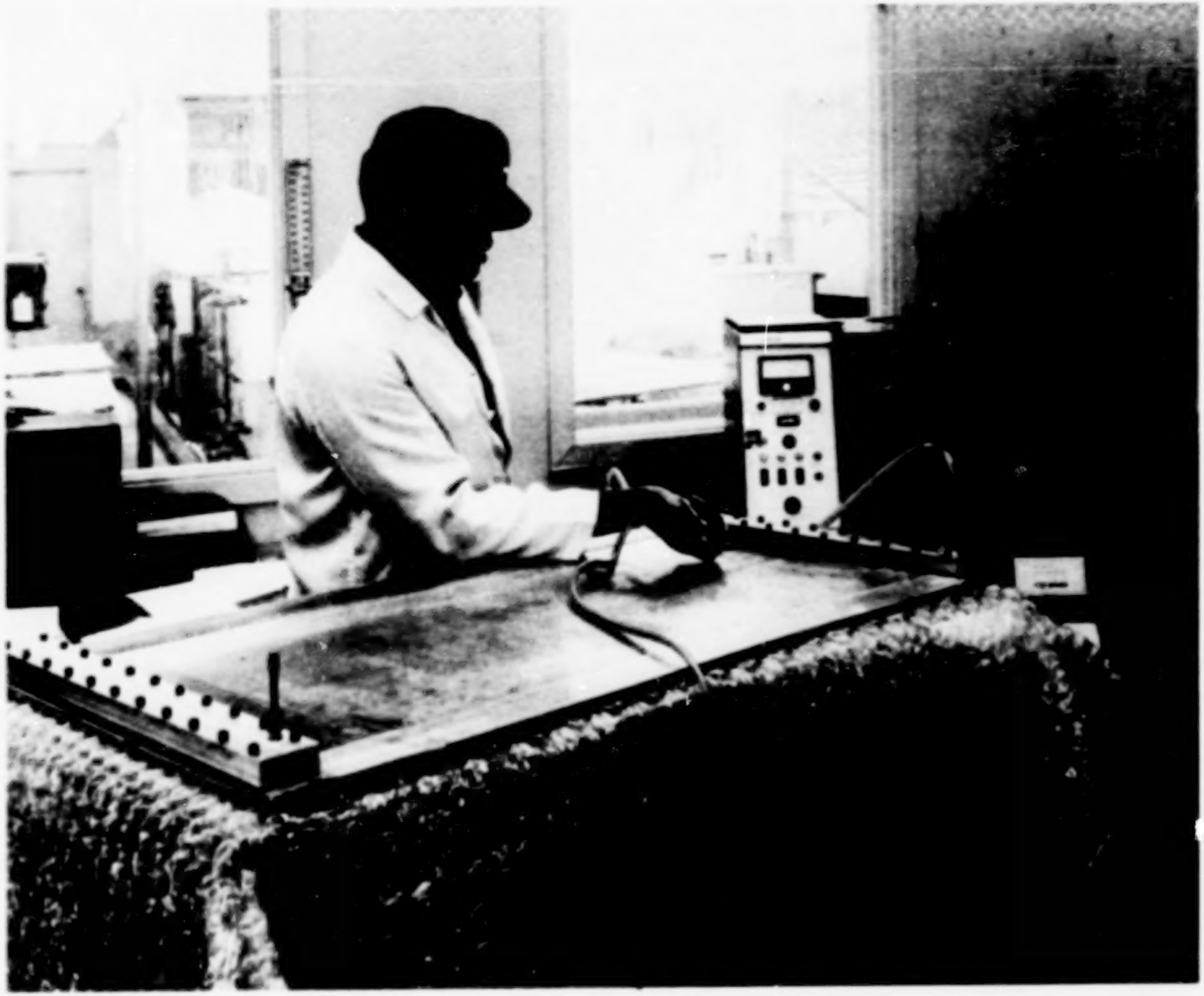

Figure 30.- (A.C.T.P.) helium leak testing of brazed test panel.

436

(A.C.T.P.) BRAZED AND WELDED TEST PANEL IN T6-TEMPER

(Figure 31)

Brazed test panel after solution heat treating, welding of manifold caps, and aging to T-6 temper. Fixtures were not used during heat treating. Panel was quenched in organic polymer solution.

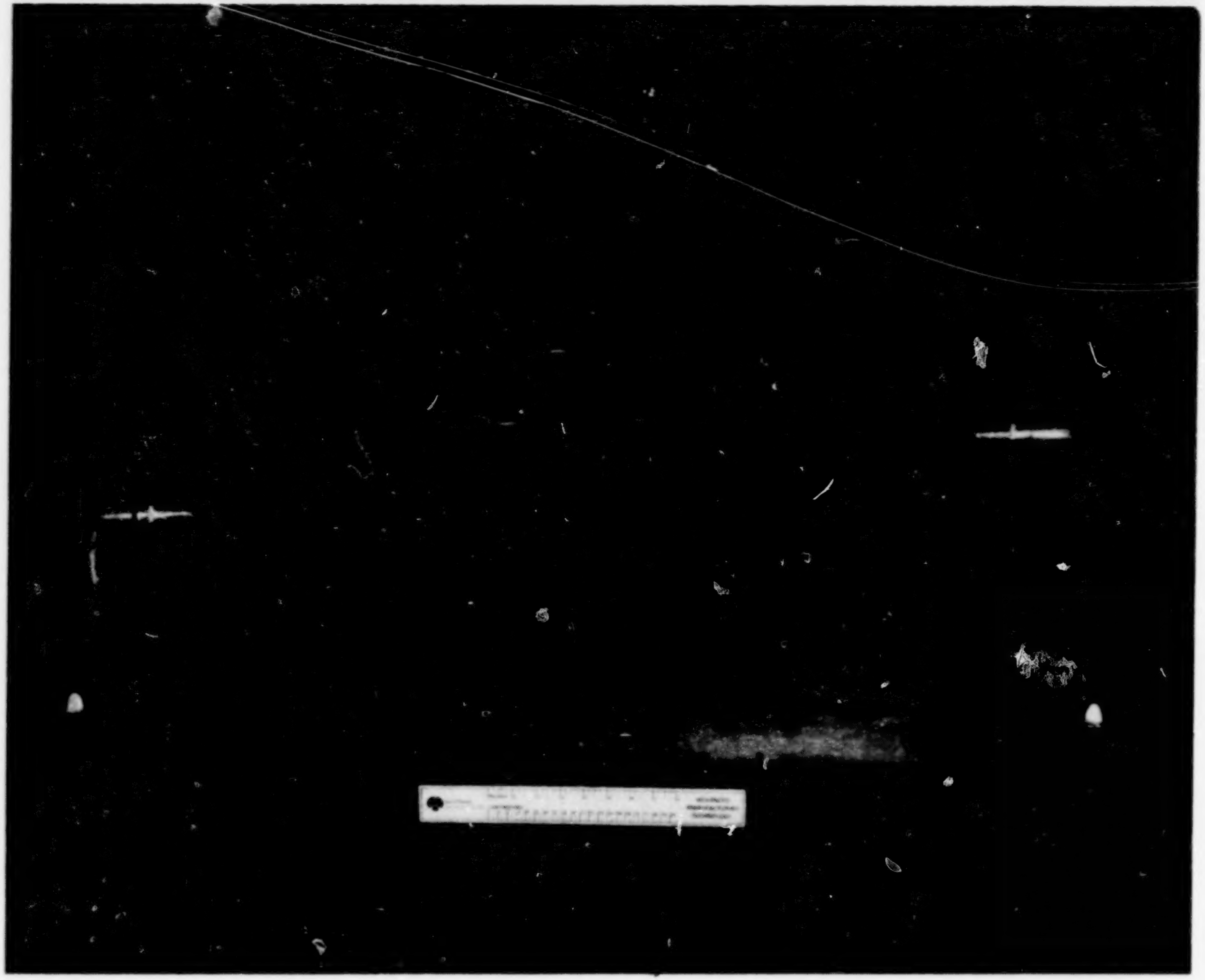

Figure 31.- (A.C.T.P.) brazed and welded test panel in T-6 temper.

(A.C.T.P.) TEST PANEL WITH ADHESIVE BONDED STRINGERS

(Figure 32)

Inboard side of test panel after adhesive bonding three center stringers. Panel had been chromic-acid anodized prior to bonding.

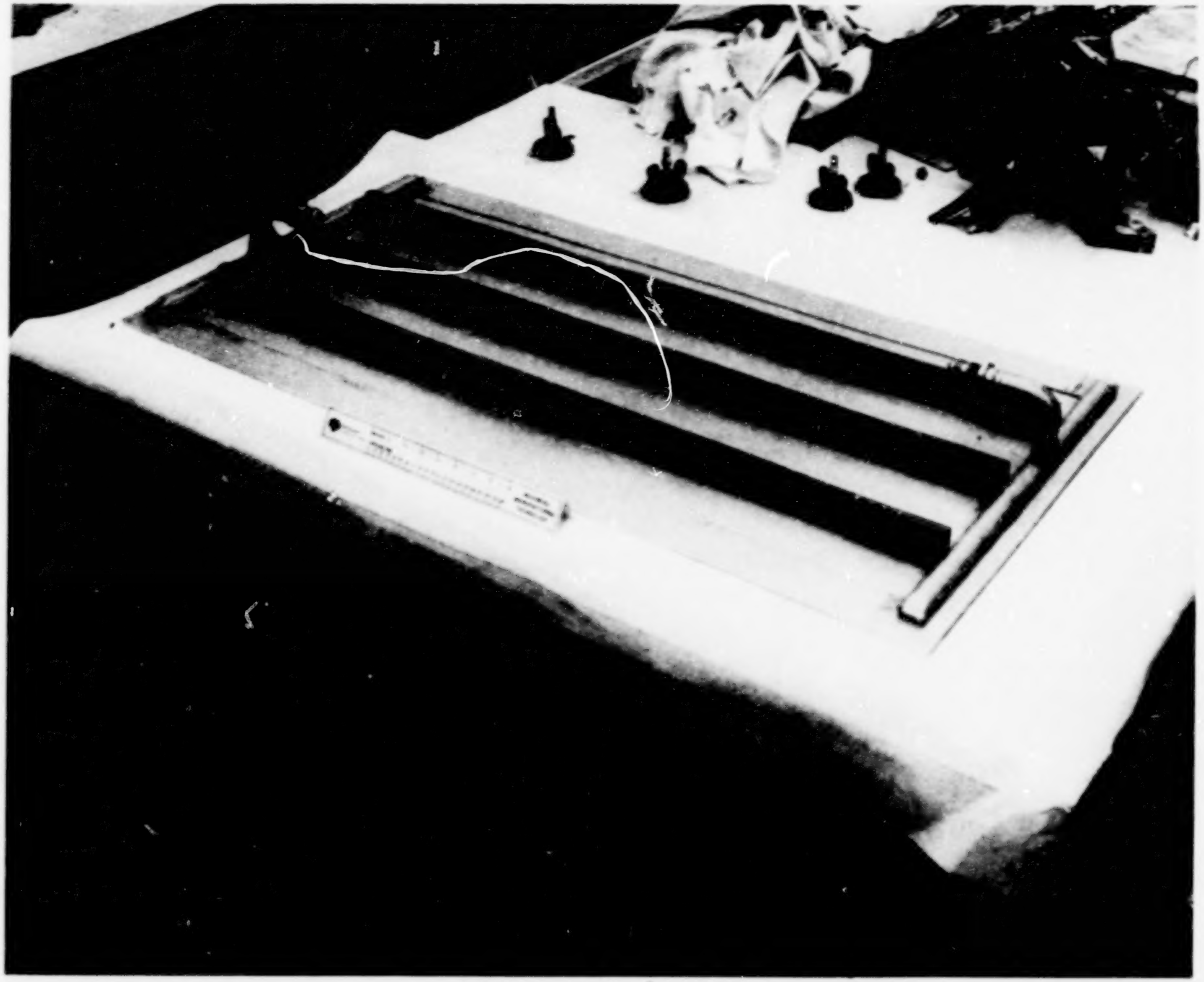

Figure 32.- (A.C.T.P.) test panel with adhesive bonded stringers.

440

(A.C.T.P.) INBOARD SIDE OF TEST ARTICLE SHOWING ALL MEMBERS

(Figure 33)

Inboard side of test article showing the panel, end load adapters, frame assembly, center structure beam, pillow blocks, manifold plumbing and all fasteners.

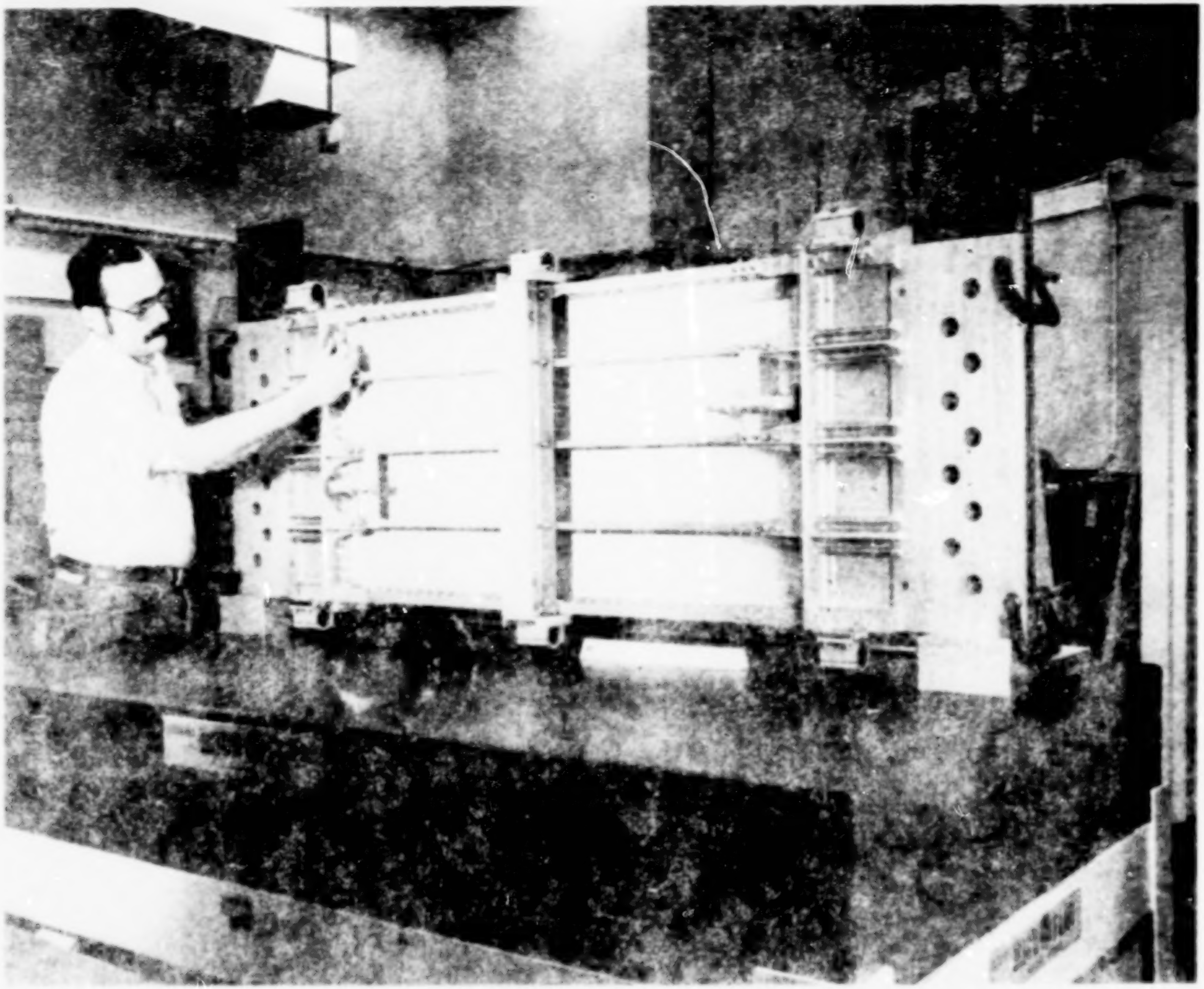

Figure 33.- (A.C.T.P.) inboard side of test article showing all members.

442

(A.C.T.P.) MOLDLINE SIDE OF TEST ARTICLE

(Figure 34)

Moldline side of test article with heater strips bonded to the end load adaptors.

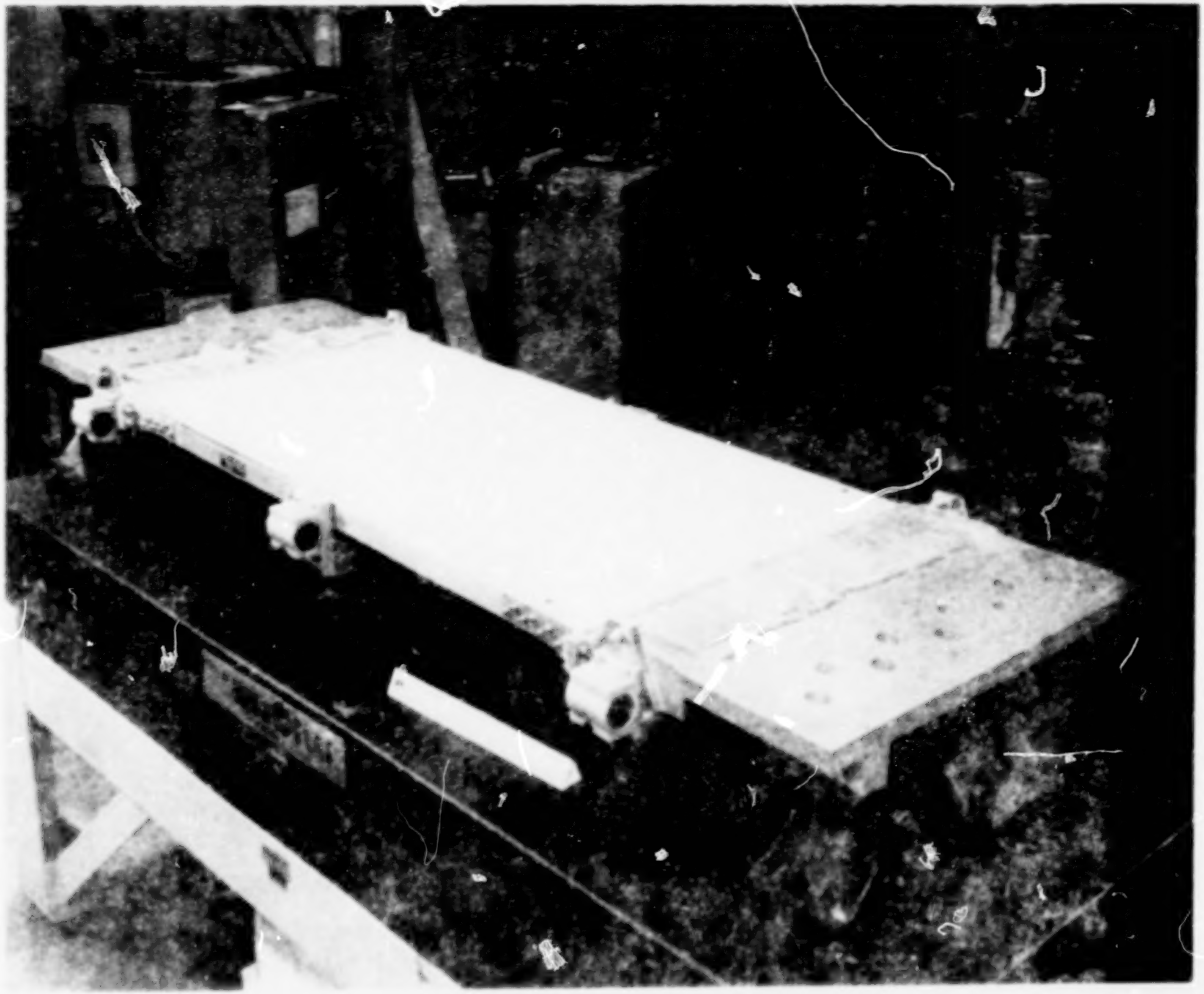

Figure 34.- (A.C.T.F.) moldline side of test article.

81

1143

CONTENTS

Part I

PREFACE . . . . iii 1/A5

WELCOME 1 1/A10
R. R. Heldenfels

SESSION I - OVERVIEWS
Chairman: A. J. Henderson

1. HYPERSONIC STRUCTURES: AN AERODYNAMICIST'S PERSPECTIVE (OR ONE MAN'S DREAM IS ANOTHER MAN'S NIGHTMARE) 5 1/B1
J. D. Watts, L. R. Jackson, and J. L. Hunt

2. STRUCTURAL REQUIREMENTS FOR MILITARY HYPERSONIC SYSTEMS (Paper not available for publication)
P. Lane

3. AIRFRAME-INTEGRATED PROPULSION SYSTEM FOR HYPERSONIC CRUISE VEHICLES 39 1/F13
Robert A. Jones and Paul W. Huber

4. RECENT ADVANCES IN CONVECTIVELY COOLED ENGINE AND AIRFRAME STRUCTURES FOR HYPERSONIC FLIGHT 47 1/G7
H. Neale Kelly, Allan R. Wieting, Charles P. Shore, and Robert J. Nowak

SESSION II - ENGINE STRUCTURES
Chairman: H. N. Kelly

5. DESIGN AND ANALYSIS OF A SCRAMJET ENGINE 65 2/A13
O. A. Buchmann

6. THERMOSTRUCTURAL ANALYSIS OF A SCRAMJET FUEL-INJECTION STRUT 119 3/B11
Allan R. Wieting and Earl A. Thornton

7. ADVANCED FABRICATION TECHNIQUES FOR COOLED ENGINE STRUCTURES 145 3/F7
O. A. Buchmann

8. HYDROGEN EMBRITTLEMENT AND ITS CONTROL IN HYDROGEN-FUELED ENGINE SYSTEMS 195 4/F11
W. T. Chandler

9. CARBON-CARBON COMPOSITE APPLICATION FOR INTEGRAL ROCKET RAMJET COMBUSTORS (Paper not available for publication)
H. A. Holman

SESSION III - COOLED AIRFRAME STRUCTURES
Chairman: C. P. Shore

10. DESIGN AND FABRICATION OF A SKIN STRINGER DISCRETE TUBE ACTIVELY COOLED STRUCTURAL PANEL 253 6/A5
Frank M. Anthony

11. DESIGN AND ANALYSIS OF A PLATE-FIN SANDWICH ACTIVELY COOLED STRUCTURAL PANEL 319 7/C13
L. M. Smith

12. FLUXLESS BRAZING AND HEAT TREATMENT OF A PLATE-FIN SANDWICH ACTIVELY COOLED PANEL 375 8/E1
Charles S. Beuyukian

13. DESIGN AND FABRICATION OF A RADIATIVE ACTIVELY COOLED HONEYCOMB SANDWICH PANEL 449 10/A13
Leland C. Koch

14. RADIATIVE, ACTIVELY COOLED PANEL TESTS RESULTS 493 11/A5
Charles P. Shore, Robert J. Nowak, and Ellsworth L. Sharpe

444

(A.C.T.P.) INBOARD SIDE OF COMPLETED TEST ARTICLE

(Figure 35)

Inboard side of completed test article prior to delivery with foam insulation blocks covering end load adapter fins. Aluminum tape covers foam.

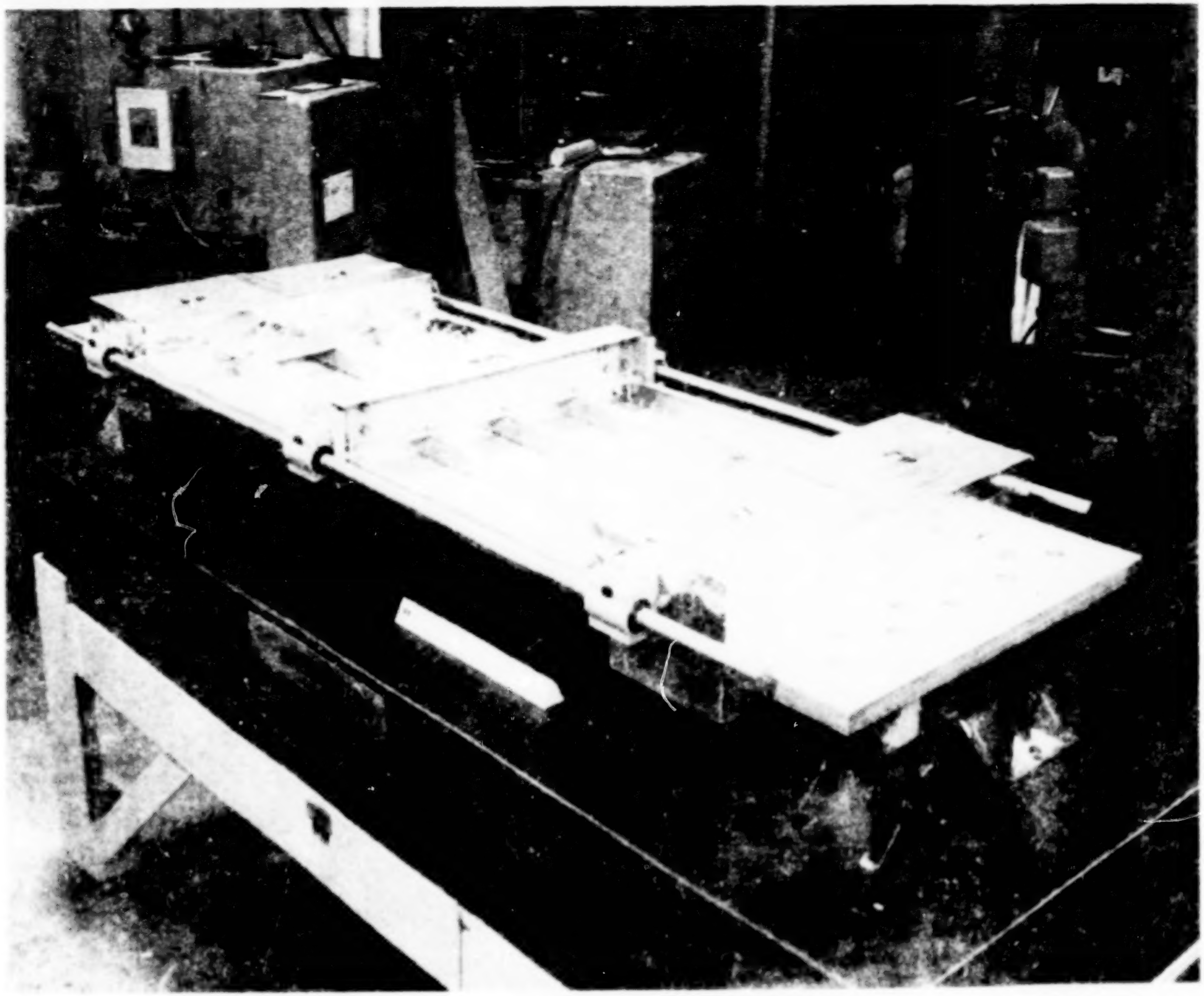

Figure 35.- (A.C.T.P.) inboard side of completed test article.

446

(A.C.T.P.) MOLDLINE SIDE OF COMPLETED TEST ARTICLE

(Figure 36)

Moldline side of completed test article prior to delivery. Aluminum tape covered foam insulation blocks are located over heater strips.

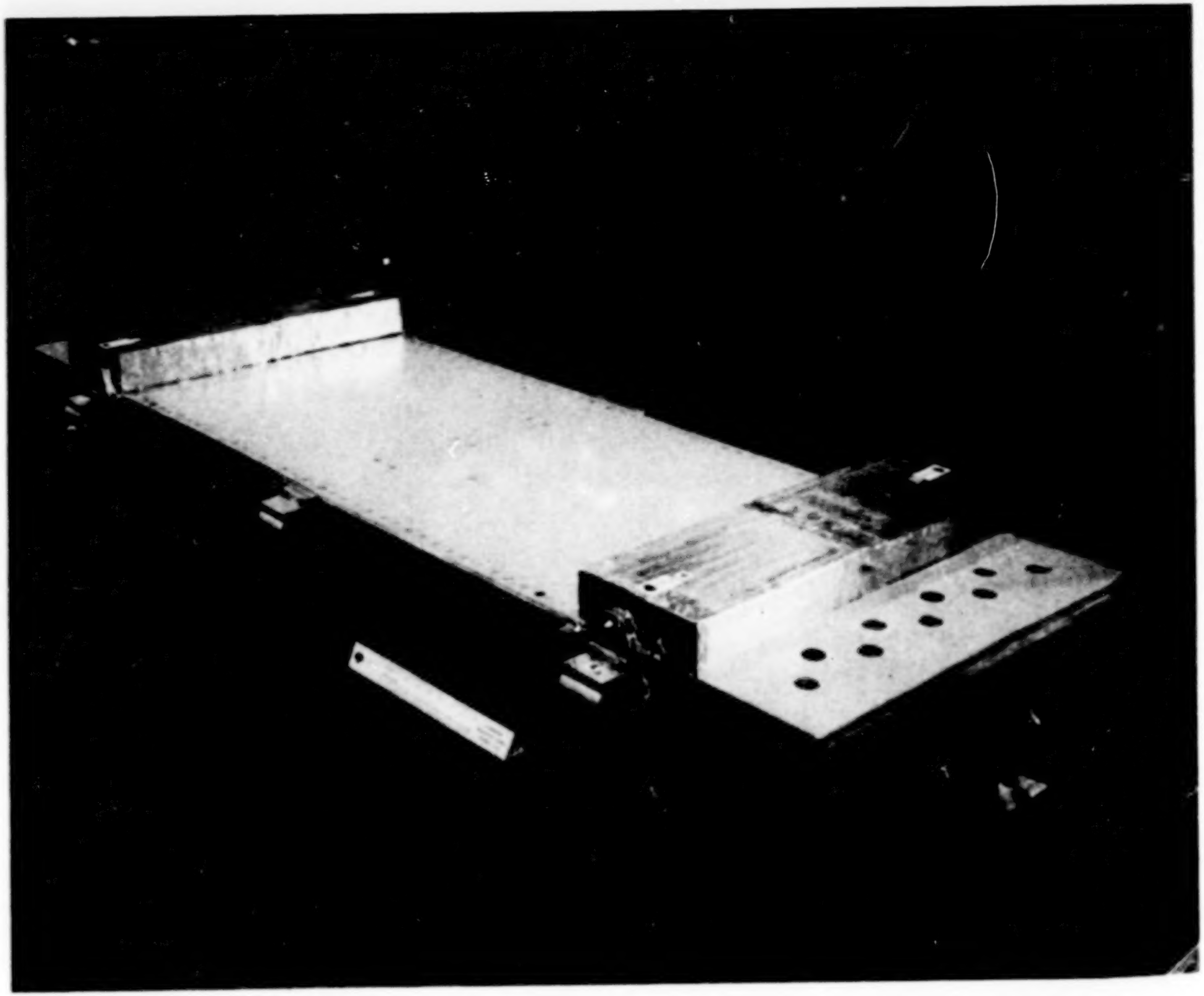

Figure 36.- (A.C.T.P.) moldline side of completed test article.

448

BLANK PAGE

DESIGN AND FABRICATION OF A RADIATIVE ACTIVELY COOLED HONEYCOMB SANDWICH PANEL

by Leland C. Koch

McDonnell Aircraft Company, St. Louis, Mo.

INTRODUCTION

Design of structures to operate efficiently for long periods in the severe thermal environment encountered by hypersonic cruise aircraft requires careful selection of materials and structural concepts. In Reference 1 an actively cooled aluminum panel which absorbs all of the incident heat load was designed for hypersonic aircraft application. Hydrogen fuel was used as the heat sink to cool the structure to relatively low temperatures so that long life could be achieved. However, since cooling of the engines and the inlets requires a high percentage of the available heat sink it was doubtful that the remaining heat sink would be sufficient for airframe cooling. A solution to this problem is a radiative actively cooled panel which uses heat shields and insulation on the outer surface of the actively cooled structural panel. With this system, the outer surface operates at high temperatures which radiates an appreciable amount of the incident heat load back to the atmosphere and reduces the heat load that must be absorbed by the fuel. The program described here uses the honeycomb-sandwich actively cooled panel concept from Reference 1 with coolant passages in contact with the outer skin. However, the panel was optimized to be compatible with a radiative thermal protection system and the heat sink available for a representative hypersonic vehicle.

A primary purpose of the program was to compare the mass of a radiative actively cooled panel to the mass of a bare actively cooled panel designed to the same conditions and constraints. The approach was to design and optimize a 0.61 x 6.1-m (2 x 20 ft) full-scale panel which combines radiative and active cooling to control structural temperatures to levels compatible with use of lightweight materials and to fabricate a 0.61 x 1.22-m (2 x 4 ft) panel for performance testing by NASA.

Results of the design and optimization of the full-scale radiative actively cooled structural panel, including radiative concept selection, final configuration details, test panel description, and conclusions of the study are summarized herein.

RADIATIVE ACTIVELY COOLED PANEL (RACP) PROGRAM
(Figure 1)

Design of efficient structures for long time operation in the severe thermal environment experienced by hypersonic cruise aircraft is a difficult problem. Actively cooled structural panels have been proposed as one approach with high potential for structural mass reduction and cost savings. This concept uses a coolant circulating in a closed loop through the structure and then through a heat exchanger where the absorbed heat is transferred to hydrogen fuel enroute to the engines.

The problem is that cooling of the engines and inlets requires a high percentage of the available heat sink and there is not enough left to cool the structure. A solution to this problem is to use insulation and heat shields on the actively cooled panel (ACP) external surfaces to radiate most of the heat load back to the atmosphere.

The objectives of the program described herein were to demonstrate feasibility of the radiative actively cooled system by designing and fabricating a hypersonic aircraft panel and to compare the mass of this system with that of a base panel designed for the same conditions.

RADIATIVE ACTIVELY COOLED PANEL (RACP) PROGRAM

PROBLEM:

ACTIVE COOLING WOULD BE VIABLE EXCEPT HEAT LOAD >> HEAT SINK

SOLUTION:

REDUCE HEAT LOAD VIA RADIATION

APPROACH:

HEAT SHIELD AND INSULATION ON ACTIVELY COOLED PANEL SURFACE

OBJECTIVE:

DEMONSTRATE RACP FEASIBILITY AND COMPARE WITH BARE ACP

Figure 1

452

PANEL DESIGN CONDITIONS
(Figure 2)

This figure shows design conditions of greatest significance to the .61-m (2.0 ft) wide and 6.1-m (20.0 ft) long radiative actively cooled panel that was developed in this program. The design limit in-plane running loads and normal pressures are about the same magnitude as those experienced in the highly loaded areas of a hypersonic transport aircraft fuselage. The structure was designed to sustain ultimate load (1.5 times design limit load) combined with thermal loads without failure. In addition, the structure was designed to sustain, without failure or coolant leakage, 20 000 cycles of fully reversed design limit loads combined with thermal loads.

The design incident heat flux was equivalent to 136 kW/m^2 (12 Btu/ft^2sec) to a 422 K ($300^{\circ}F$) surface temperature.

To assure realism, the panel edges and attachments to support frames were designed as in an airplane.

PANEL DESIGN CONDITIONS

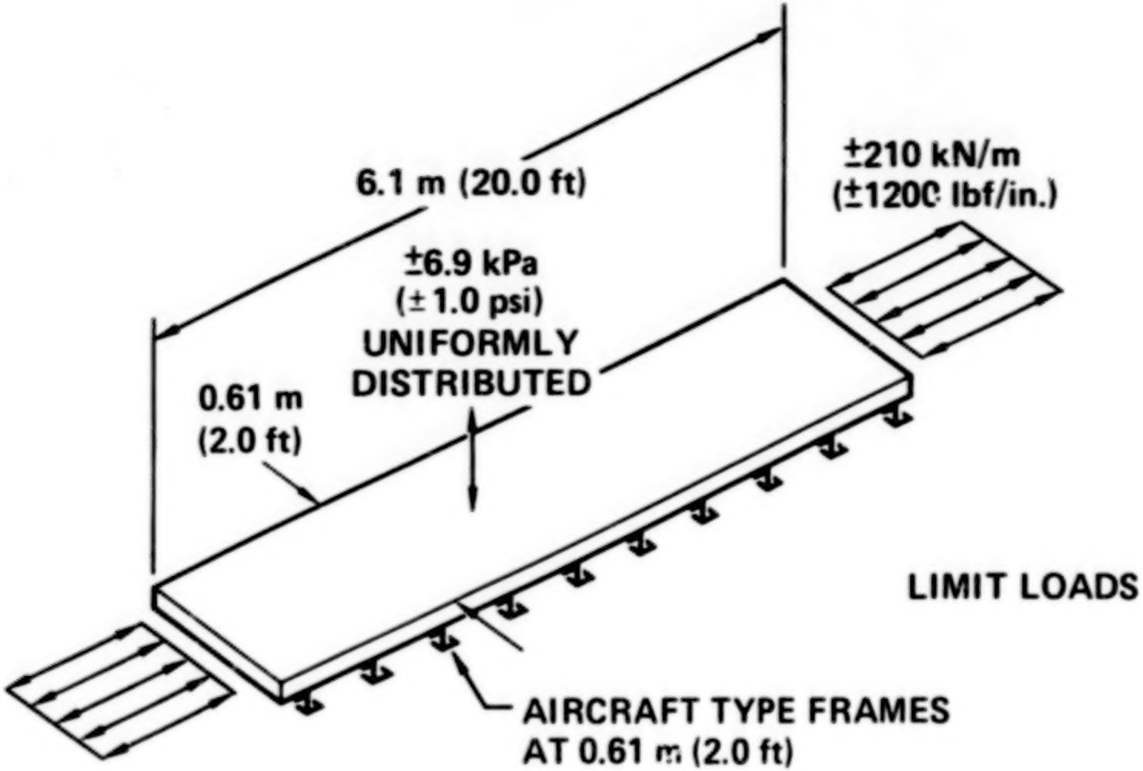
6.1 m (20.0 ft)
±210 kN/m
(±1200 lbf/in.)
±6.9 kPa
(± 1.0 psi)
UNIFORMLY
DISTRIBUTED
0.61 m
(2.0 ft)
LIMIT LOADS
AIRCRAFT TYPE FRAMES
AT 0.61 m (2.0 ft)

DESIGN LIFE - 20000 CYCLES

REFERENCE HEAT FLUX - 136 kW/m^2 (12 Btu/ft^2 sec) AT 422K (300°F) SURFACE TEMPERATURE

Figure 2

DESIGN AND OPTIMIZATION APPROACH
(Figure 3)

This figure outlines the approach to design and optimization of the radiative actively cooled panel (RACP). Some of these activities were ongoing at the same time because several iterations, involving various engineering disciplines, were required to get the minimum weight solution. Each of these activities will be discussed in the presentation that follows.

Selection of actively cooled panel concept and structural materials was based on the results of the Reference 1 bare actively cooled panel program and the desire, in this program, to make a direct comparison between radiative and bare actively cooled panels.

A 60/40 mass solution of ethylene glycol/water was selected as the RACP coolant to assure compatibility with the NASA Langley Research Center test facility which was to be used for RACP panel testing. Reference 1 studies indicated lower system mass using a 60/40 mass solution of methanol/water coolant.

Trade studies and analyses were planned to select insulation materials and heat-shield concepts.

To determine minimum system mass, the minimum mass of each RACP component was determined as a function of cooling-system absorbed heat flux. By summing these masses vs absorbed heat flux, the minimum total mass and corresponding absorbed heat flux was determined and the details of the component parts were known.

Concurrent with the above activities, the joints and edges of all components were being designed and analyzed to minimize their mass.

DESIGN AND OPTIMIZATION APPROACH

- SELECT PANEL CONCEPT AND MATERIALS
- SELECT COOLANT AND INSULATION MATERIALS
- SELECT HEAT-SHIELD CONCEPT
- DETERMINE MINIMUM MASS vs ABSORBED HEAT FLUX
- DESIGN JOINTS AND EDGES FOR MINIMUM MASS

Figure 3

RADIATIVE ACTIVELY COOLED PANEL CONCEPT

(Figure 4)

This figure illustrates the radiative actively cooled panel concept as it was envisioned at the beginning of the program. It consisted of an actively cooled honeycomb-sandwich structure, an external heat shield (the concept was not yet decided on), and a layer of insulation.

The actively cooled panel concept is an all-aluminum, adhesive bonded, honeycomb sandwich with D-shaped coolant tubes (Dee tubes) nested in the honeycomb core against the outer skin. The coolant tubes are attached to manifolds which are located at the ends of the panel. These manifolds also incorporate provisions for attachment to adjacent panels. To provide adequate cooling in the area of the manifold, a split coolant passage was provided, as indicated in the figure. The coolant flows out to the manifold edges and then to the individual tubes. At the exit manifold the process is reversed.

Interface conductance of the adhesive joint between the panel outer skin and cooling passages was our primary concern. In the Reference 1 program, it was found that a bare panel subjected to 136 kW/m^2 (12 Btu/ft^2sec) needed high interface conductance, such as provided by solder, to avoid excessive temperature gradients and large mass penalties. With a much reduced heat flux resulting from addition of the heat shield and insulation, this panel performed well using the adhesive joint which has interface conductance of 1.65 kW/m^2K (290 $Btu/hr\ ft^2{}^\circ F$).

As indicated in section B-B, the insulation, heat shield and actively cooled panel are snugged up against each other. The primary reason for this is to minimize flow of boundary-layer air under the heat shield and insulation. Influx of boundary-layer air, if not planned for, could overheat the panel and overload the cooling system.

Several insulations were evaluated for this application. A fibrous, flexible, blanket-type insulation with a density of 256 kg/m^3 (16 lbm/ft^3) was selected because it was very efficient, flexible, and easily shaped to fuselage contour.

It will be noted that the heat shield is shown as a flat sheet in section B-B. Initially, the choice of heat shield concept was left open. Heat shield concept selection and optimization will be described later.

RADIATIVE ACTIVELY COOLED PANEL CONCEPT

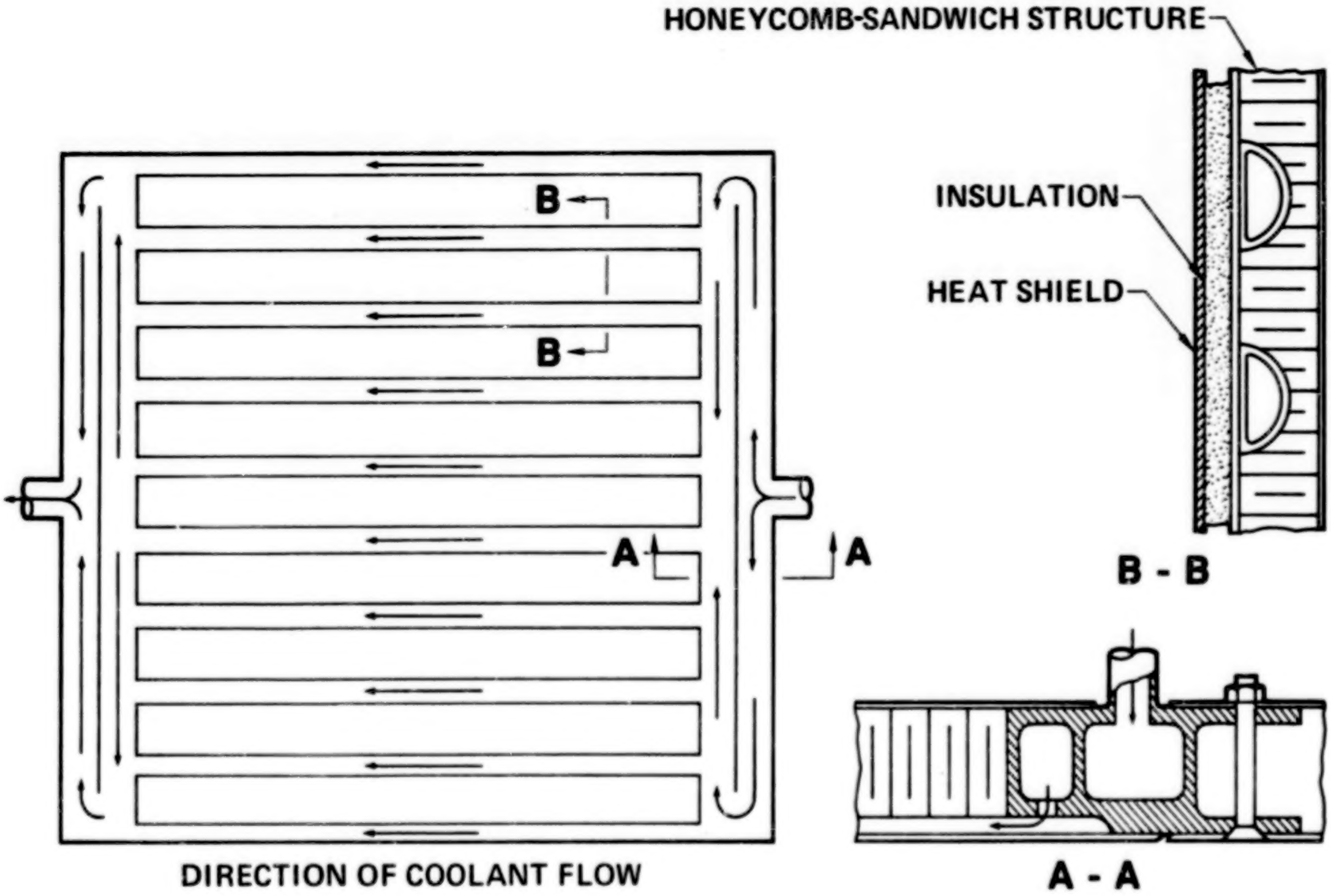
HONEYCOMB-SANDWICH STRUCTURE
INSULATION
HEAT SHIELD
B
B
A
A
B - B
A - A
DIRECTION OF COOLANT FLOW

Figure 4

COOLING-SYSTEM AND INSULATION MASS VS ABSORBED HEAT FLUX
(Figure 5)

This figure shows how active-cooling-system (ACS) absorbed heat flux affects active-cooling-system and insulation mass. Also shown is the variation of heat-shield temperature as a function of absorbed heat flux. With the heat-shield temperatures indicated here, it is evident that superalloys are required.

As the mass of the insulation is reduced, less of the aerodynamic heat load is radiated to space and more is absorbed by the active cooling system. As shown, the active-cooling-system mass, which includes all elements external to the panel as well as propellant for the pumps, is highly sensitive to increased heat flux. The lowest combined mass of active cooling system and insulation is obtained at an absorbed heat flux of 9.1 kW/m^2 (0.8 Btu/ft^{2}sec). The RACP system was optimized using a 60/40 mass solution of ethylene glycol and water as the coolant with an inlet temperature of 283 K (50°F).

Of course, the effects of coolant temperatures and pressures and the variation of actively cooled panel and heat-shield mass with absorbed heat flux had to be determined before total system optimization was complete.

COOLING-SYSTEM AND INSULATION MASS vs ABSORBED HEAT FLUX

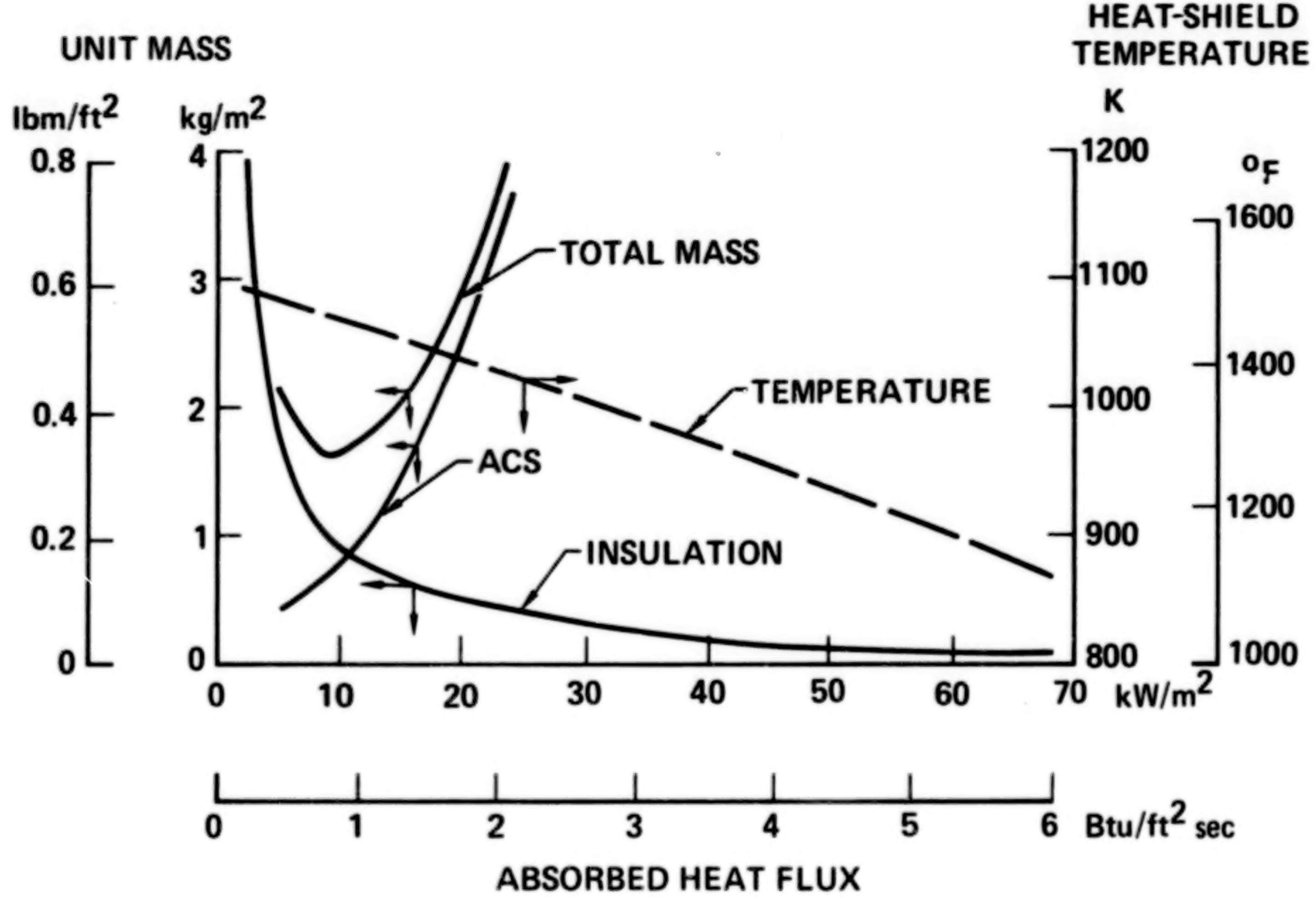

Figure 5

INCREASING PRESSURE REDUCES COOLING-SYSTEM MASS
(Figure 6)

As shown in the figure, a significant reduction (25%) in active cooling system mass was achieved by increasing the system pressure from 0.7 MPa (100 lbf/in^2) to 1.4 MPa (210 lbf/in^2). The figure also shows mass of individual components and identifies the reduction in residual coolant mass (as a result of smaller line sizes) as the driving element. At pressures above the design value of 1.4 MPa (210 lbf/in^2), no additional benefits are realized as the reduction in residual coolant mass is negated by a comparable increase in the mass of the pumps and auxiliary power system (APS) propellant, due to the increase in system pressure drop.

The data presented on this figure are for a 60/40 mass solution ethylene glycol/water coolant with inlet/outlet temperatures of 283 K/322 K (50°F/120°F). Varying inlet/outlet temperatures within practical limits, did not alter the conclusions presented here. Cooling-system masses were calculated using equations developed in this program and by other investigators in previous programs. A complete discussion of these equations is given in the program final report, Reference 2.

INCREASING PRESSURE REDUCES COOLING-SYSTEM MASS

60/40 MASS SOLUTION OF ETHYLENE GLYCOL AND WATER
COOLANT INLET/OUTLET TEMPERATURE = 283 K/322 K (50°F/120°F)

$P_s = \Delta P_{lines} + 414$ kPa (60 lbf/in.^{2})

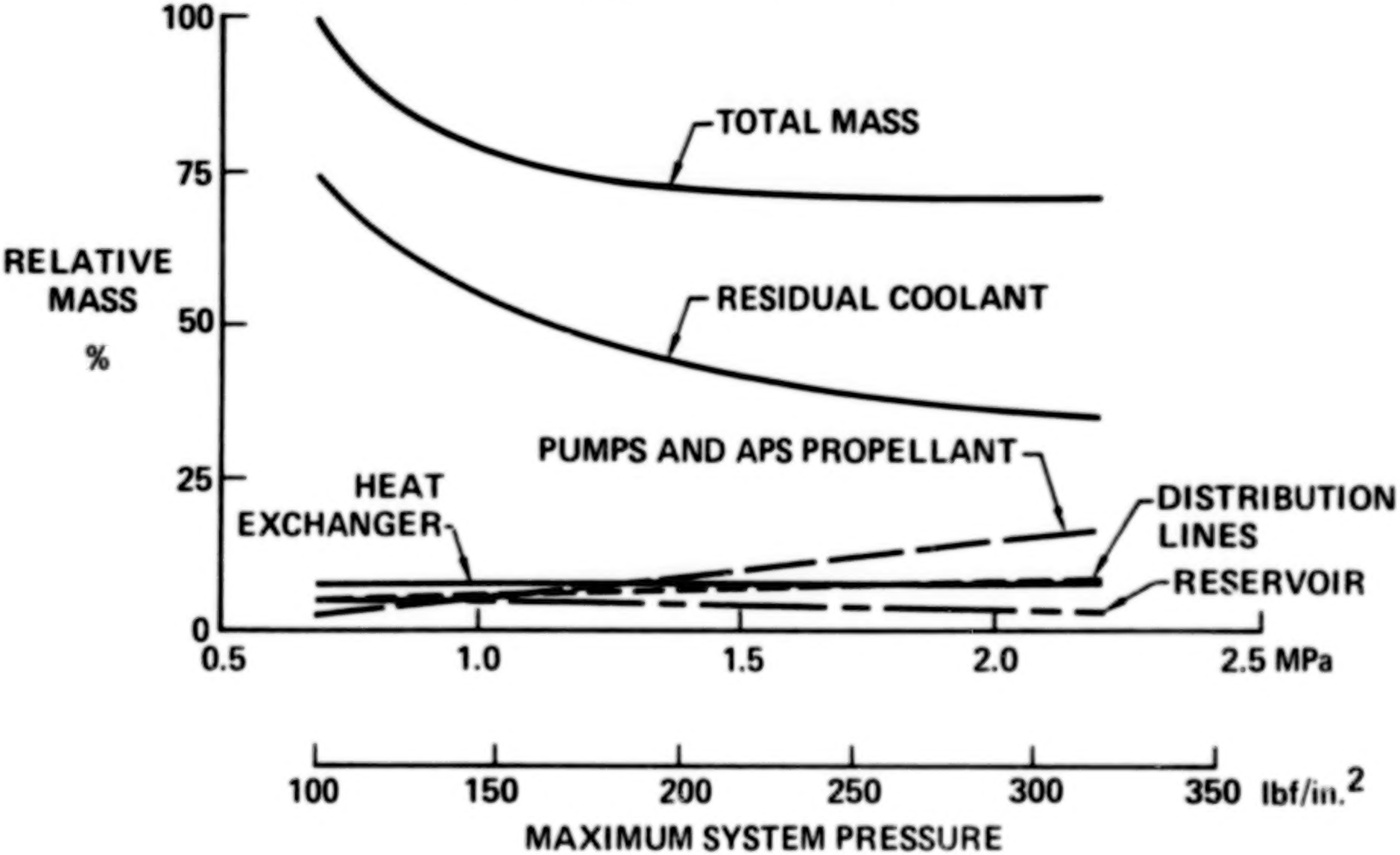

Figure 6

462

OUTER SKIN/TUBE/HEAT FLUX PARAMETRIC
(Figure 7)

Outer skin thickness as a function of tube diameter (with absorbed heat flux and tube pitch as parameters) is presented in the figure for a 422 K (300°F) maximum skin temperature. Analysis results were obtained assuming a uniform heat flux is absorbed by the outer skin and transferred via conduction in the outer skin, across the bond joint, and through the tube wall where it is then transferred via convection to the coolant.

The data presented here are for a 60/40 mass solution of ethylene glycol/water coolant, a maximum outer surface skin temperature (T_{MAX}) of 422 K (300°F), and a Dee-tube wall thickness of 0.089 cm (0.035 in). Similar data were developed for other combinations of skin thickness, T_{MAX}, and tube wall thickness and were used in the optimization process.

As indicated, the thermodynamic requirements for heat transfer can be satisfied with various combinations of skin thickness and tube diameter. This benefits the strength analyst because he can now determine, for each of these combinations, the minimum-mass honeycomb core and inner skin that will satisfy the strength requirement. When that is done, he will know the minimum actively cooled panel mass for any absorbed heat flux. This is illustrated in the next figure.

OUTER SKIN/TUBE/HEAT FLUX PARAMETRIC

60/40 MASS SOLUTION OF ETHYLENE GLYCOL/WATER

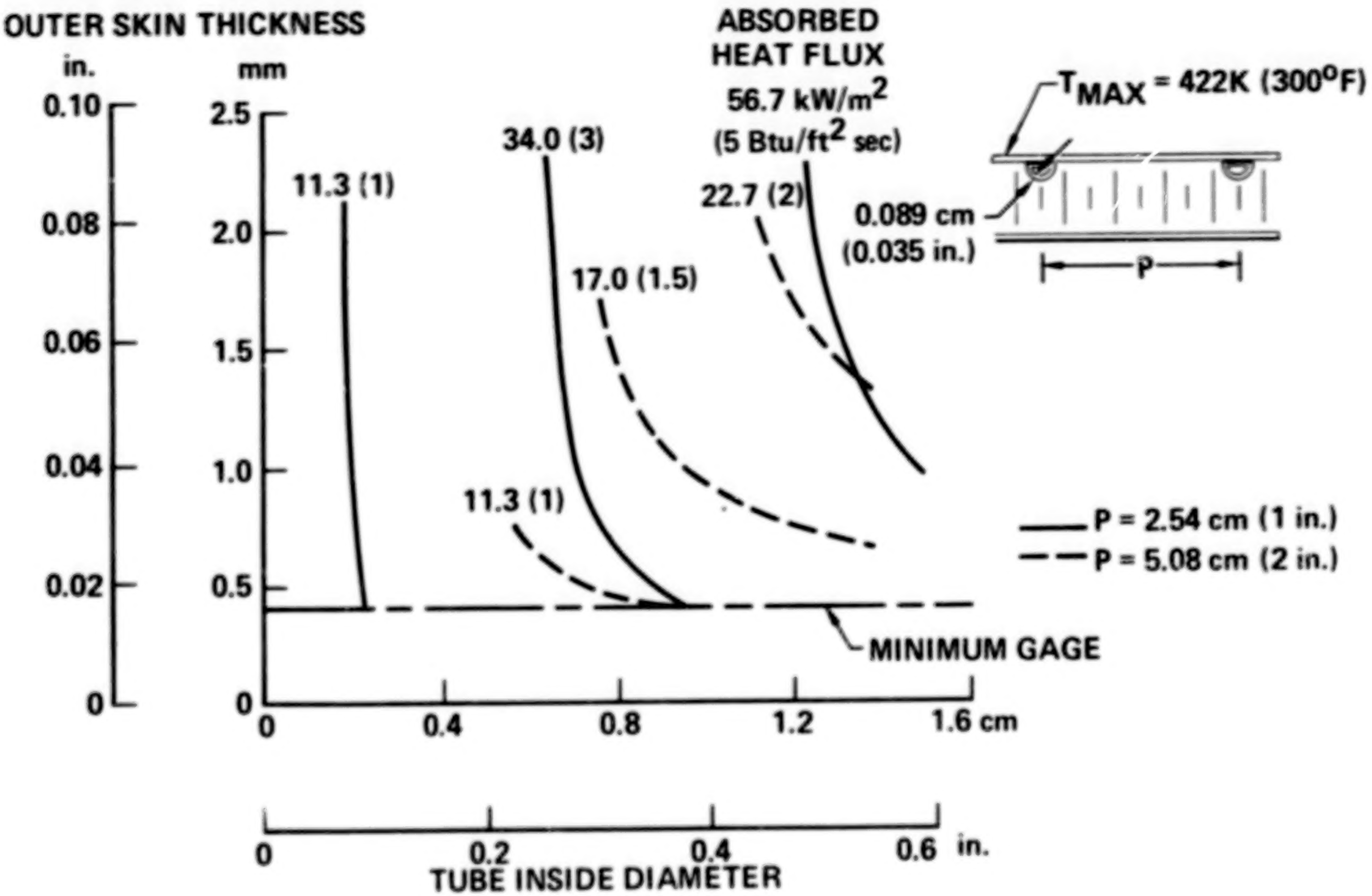

Figure 7

463

ACTIVELY COOLED PANEL MASS VERSUS ABSORBED HEAT FLUX
(Figure 8)

This figure shows how the optimized actively cooled panel plus residual coolant mass varies with absorbed heat flux for three different values of tube pitch. Each point on these curves represents a unique combination of inner and outer skin thicknesses, honeycomb core height and tube diameter that results in minimum mass for the specified materials, maximum outer skin temperature (T_{MAX}), and coolant temperature change (ΔT_c), and tube wall thickness (t_t). Similar plots, not shown, were developed for other combinations of T_{MAX}, ΔT_c and t_t. They showed that panel mass was not sensitive to significant variations of these parameters; except when T_{MAX} exceeded approximately 436 K (325°F).

These curves indicate that panel plus residual coolant mass approaches a minimum at low absorbed heat flux levels. The same trend was observed earlier for the insulation and active cooling system. They also show that mass is reduced by using smaller diameter coolant tubes. However, the minimum mass at an absorbed heat flux of 9.1 kW/m^2 (0.8 Btu/ft^{2}sec) is virtually the same for tube pitches ranging from 2.54 cm to 5.08 cm (1.0 in to 2.0 in). Based on this parametric study, the optimum coolant parameters, and basic actively cooled panel materials and dimensions were determined.

In order to size the structure for the specified design conditions (Figure 2), allowable operating stresses had to be determined for all of the panel structural elements. Following is a discussion of the approach to establishing these allowables.

ACTIVELY COOLED PANEL MASS vs ABSORBED HEAT FLUX

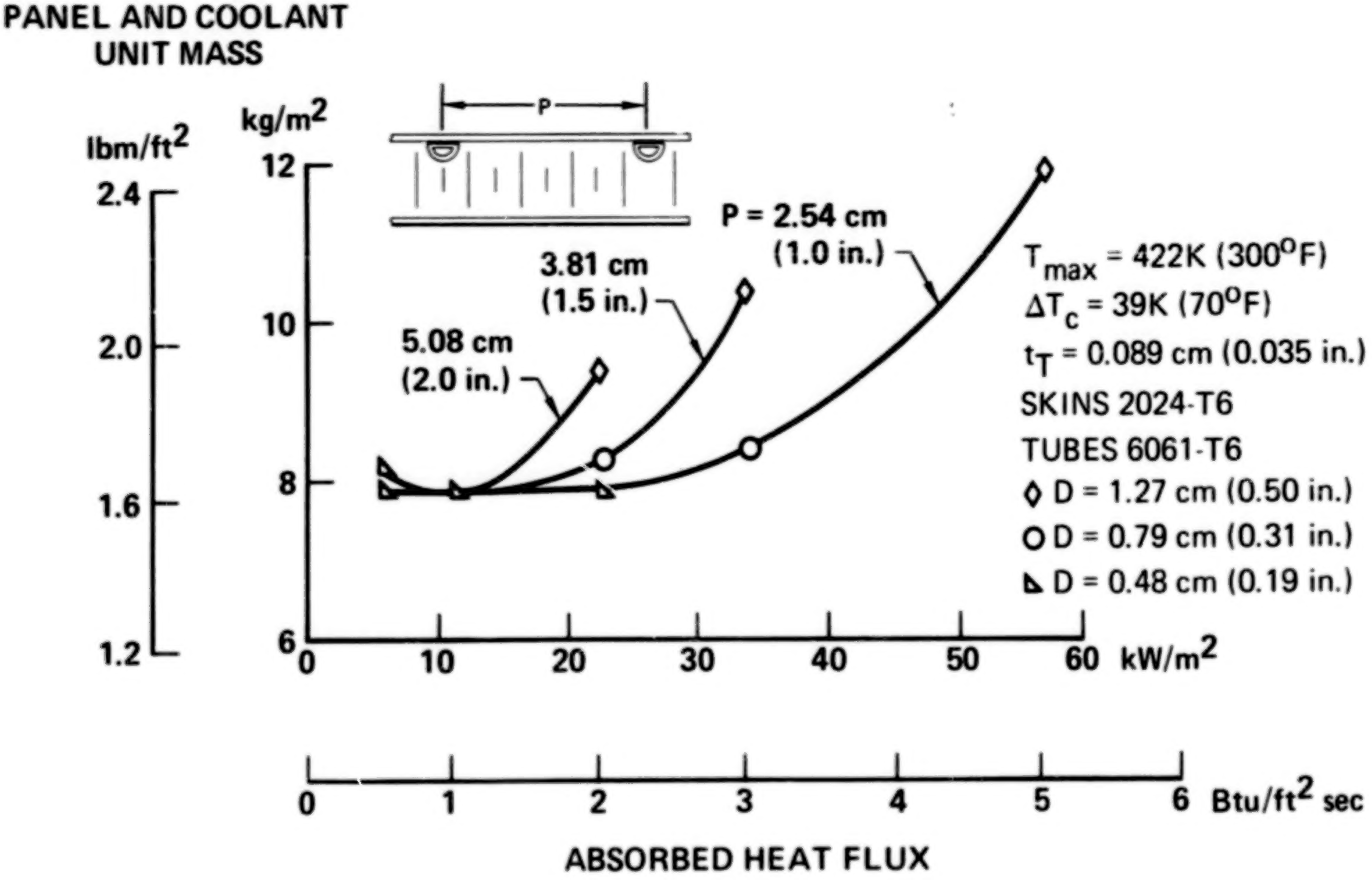

Figure 8

466

DEE-TUBE CRACK GROWTH
(Figure 9)

The actively cooled panel was designed to sustain a fully reversed mechanical loading, which was specified, combined with thermal loading, which could only be calculated after panel element temperatures and sizes were determined. Thus, establishment of allowable stress levels and sizing of the elements was an iterative process. Initially, allowable tension stresses were based on fatigue analysis and crack propagation analysis assuming fully reversed loading. Allowable compression stresses were set equal to the material's compression yield strength. Later iterations showed the compression allowables were O.K., but that the tension stresses needed revision to account for the change in stress ratio due to combining the fully reversed mechanical loads (Stress ratio = minimum stress/maximum stress = -1.0) with thermal stresses, which sometimes added and sometimes subtracted.

This figure shows fatigue crack propagation in a 6061-T6 Dee-tube with an initial flaw of the largest size that McDonnell Aircraft felt would escape detection during nondestructive inspection. The assumed flaw was a surface crack 0.46 mm (0.018 in) long and 0.23 mm (0.009 in) deep. It was determined that the crack would grow to the tube wall thickness in 23 000 cycles with a stress ratio of -0.09 and a maximum tension stress in each cycle of 163.27 MPa (23 680 lbf/in^2). This analysis was the basis for establishing the 6061-T6 Dee-tube wall thickness and allowable tension stress.

DEE-TUBE CRACK GROWTH

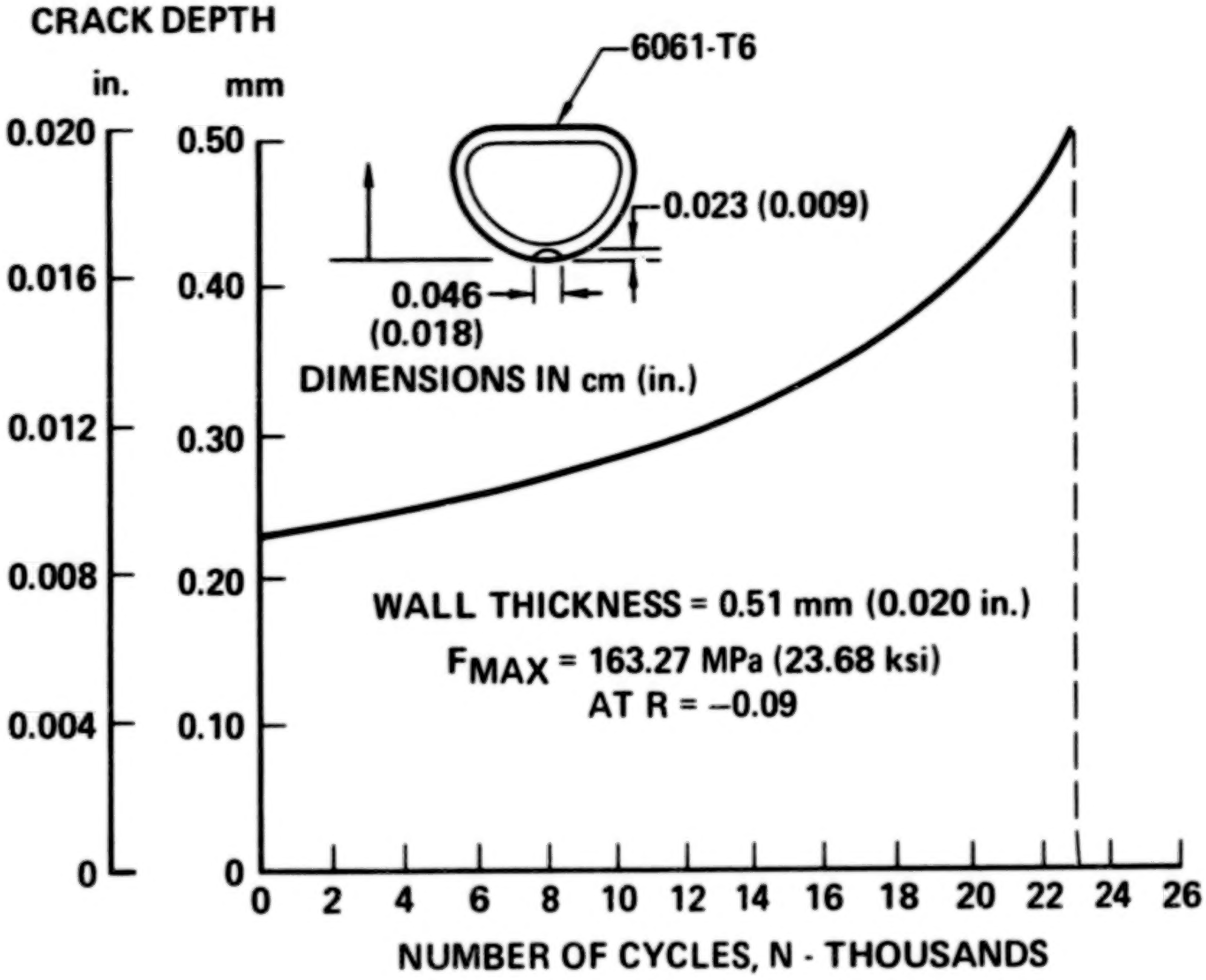

Figure 9

OPTIMIZED PANEL DETAILS AND COOLANT PARAMETERS
(Figure 10)

This figure identifies the optimized, actively cooled honeycomb-sandwich panel structural materials, geometry and coolant parameters. Both face skins are 0.101 cm (0.040 in) 2024-T81 aluminum. A low density 5056-H39 nonperforated core is used. Total depth of the sandwich is 3.01 cm (1.185 in).

The 6061-T6 Dee-tube illustrated here is the configuration selected for the test panel. It is fabricated by flattening a round tube against an internal, removable mandrel. For production application, a drawn extrusion with a wider flat, hence more area for conduction, would be selected.

The skins, tubes and honeycomb were designed to be joined by adhesive bonding. An aluminum-filled, film-type adhesive was selected for use in the skin/tube joints and the skin/honeycomb joints. The aluminum-filled adhesives have better thermal conductivity than the nonfilled types and the system selected for this application can be used up to 491 K (425°F). To assure adequate heat transfer a maximum skin/tube bondline thickness of 0.25 mm (0.010 in) was selected. This was assured by using only one layer of adhesive in this joint. A foaming adhesive, capable of expanding to fill gaps, was used in the tube/honeycomb joint as the fit was not expected to be good enough for film-type adhesives.

The actively cooled panel was designed for a maximum operating temperature (midway between tubes near the exit manifold) of 422 K (300°F). The panel is cooled by pumping a 60/40 mass solution of ethylene glycol and water through the coolant passages at a mass flow rate of 62 g/sm^2 (46 lbm/hr ft^2) with an inlet coolant temperature of 283 K (50°F). The use of ethylene glycol/water as the coolant and the 283 K (50°F) inlet temperature was based on results from Reference 1. Including losses in the inlet and exit manifold, a pressure drop of 110 kPa (16 lbf/in^2) is experienced across the panel. The panel was designed for a maximum inlet pressure of 862 kPa (125 lbf/in^2) and a minimum exit pressure of 345 kPa (50 lbf/in^2).

OPTIMIZED PANEL DETAILS AND COOLANT PARAMETERS

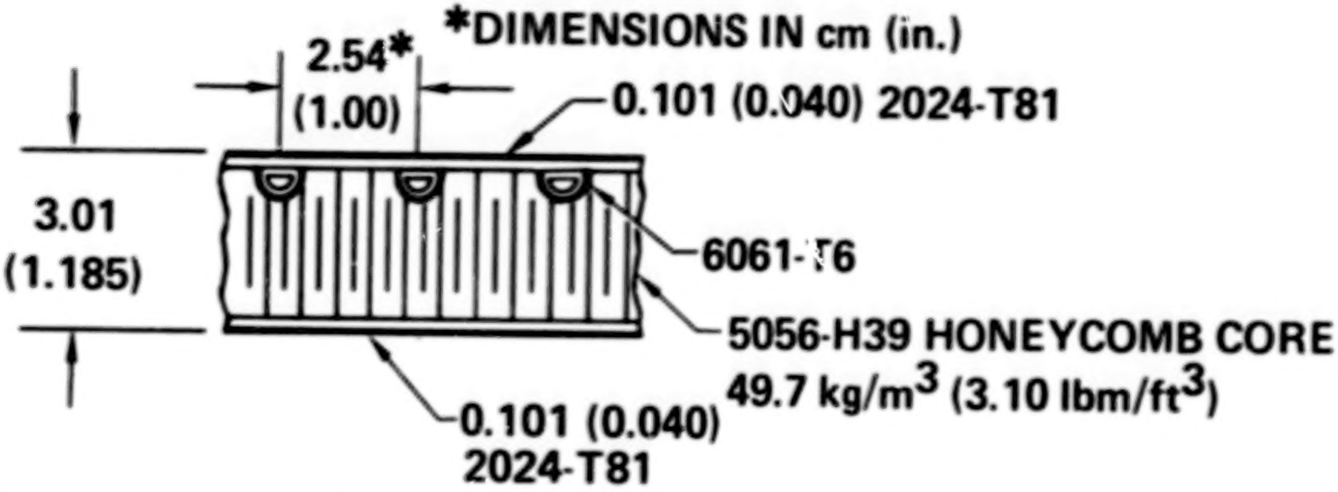
*DIMENSIONS IN cm (in.)
2.54*
(1.00)
0.101 (0.040) 2024-T81
3.01
(1.185)
6061-T6
5056-H39 HONEYCOMB CORE
49.7 kg/m³ (3.10 lbm/ft³)
0.101 (0.040)
2024-T81

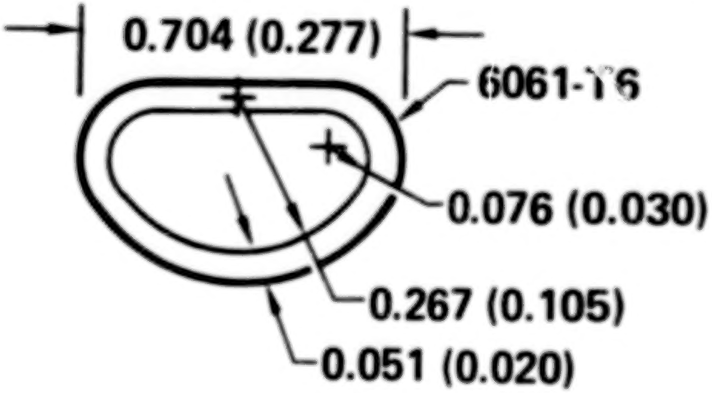
0.704 (0.277)
6061-T6
0.076 (0.030)
0.267 (0.105)
0.051 (0.020)

T_{max} = 422K (300°F)
T_{ci} = 283K (50° F)
T_{co} = 329K (133°F)
P_i = 456 kPa (66 lbf/in.^{2})
P_o = 345 kPa (50 lbf/in.^{2})

Figure 10

ATTACHMENT OF DEE TUBE TO MANIFOLD
(Figure 11)

This figure shows the method of attaching the Dee tubes to the manifold. Initially, the plan was to dip braze the 6061-0 Dee tubes to individual sockets in the 6061-0 manifold and then to solution treat this subassembly to the W condition before it is straightened, aged to T6 and bonded to the outer skin. Manufacturing felt that straightening and heat treatment of these large assemblies would require considerable development and would be expensive. Therefore, the approach shown here was adopted. It allows the tubes and manifold to be straightened and heat treated separately. Then they are joined together and to the outer skin by adhesive bonding.

The 6061-0 Dee tubes are cut approximately 2.5 percent shorter than ultimately required, and the ends are crimped and spot welded shut. The ends are then torch brazed to the recess of the machined 6061-0 aluminum tabs. After the coolant passage is electrical-discharge machined (EDM) as indicated in the inset, the tube/tab assembly is solution treated to the W condition, stretch straightened to final length, and aged to the T6 condition.

The manifolds were designed as machined 6061-T6 aluminum extrusions with welded-on end caps and inlet port. For the test panel, they were welded-up of several machinings. Holes were drilled in the tube/tab recesses to allow coolant flow.

An adhesive film between the manifold and the tab provides for load transfer and seals the joint against leakage. To prevent the adhesive from flowing into and blocking the passages during the bonding operation, rubber rods were inserted through small access holes drilled in the manifold surface opposite each coolant tube passage. After bonding, rods were removed and the access holes were plugged with Lee plugs.

ATTACHMENT OF DEE TUBE TO MANIFOLD

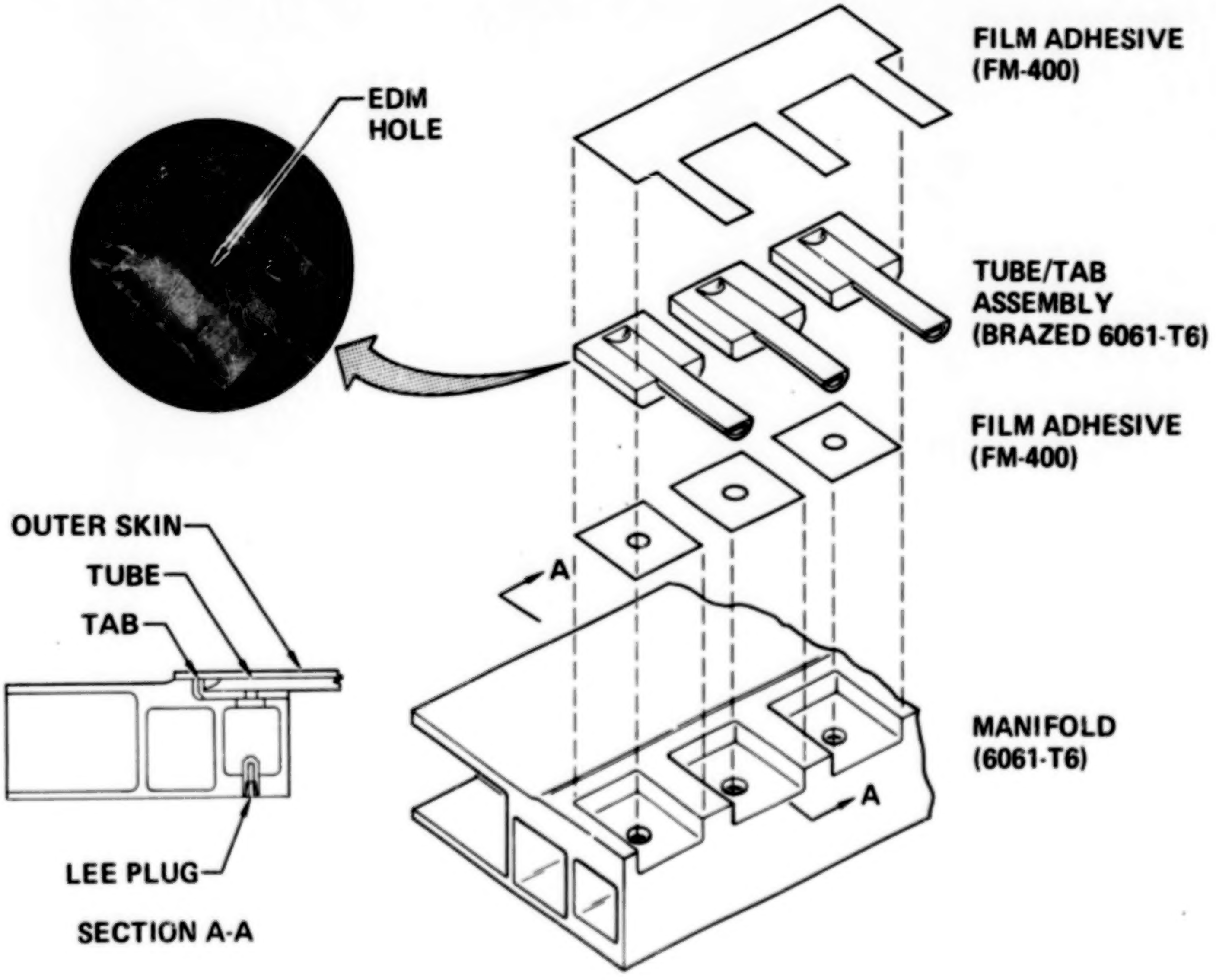
EDM HOLE
FILM ADHESIVE (FM-400)
TUBE/TAB ASSEMBLY (BRAZED 6061-T6)
FILM ADHESIVE (FM-400)
MANIFOLD (6061-T6)
A
A
OUTER SKIN
TUBE
TAB
LEE PLUG
SECTION A-A

Figure 11

472

ACTIVELY COOLED PANEL JOINT DETAILS
(Figure 12)

Some of the actively cooled panel joint and edging details are illustrated in this figure. The longitudinal and transverse splices, with help from the frames and bulkheads, can handle any type of loading. This is one of the reasons the actively cooled panel, which was designed for a unidirectional longitudinal loading, can sustain an additional tranverse loading equal to 50 percent of the longitudinal loading with no mass increase.

The longitudinal splice plates are 0.082-cm (0.032 in) thick 2024-T81 aluminum. They are attached with permanent fasteners that pass through the panel. A potting compound in the honeycomb core prevents crushing during fastener installation.

The transverse splice is accomplished by the bulkhead and a 0.254-cm (0.10 in) thick outer splice plate. A double row of bolts through the splice plate, a solid pad in the manifold, and the bulkhead flanges complete the joint.

A RTV 560 adhesive is used in attaching the outer splice plates to the panel. This was necessary to improve heat transfer to the panel and, thus, avoid excessive splice plate temperatures.

Intermediate frames are attached to the panel by bolts that pass through the panel and between coolant tubes. Aluminum bushings are used in the panel to prevent core crushing when the bolts are torqued up. These are removable bolts because, as will be shown later, they are also used for heat shield attachment. The abestos phenolic washer under the platenut reduced heat transfer from the bolt to the panel and frame.

ACTIVELY COOLED PANEL JOINT DETAILS

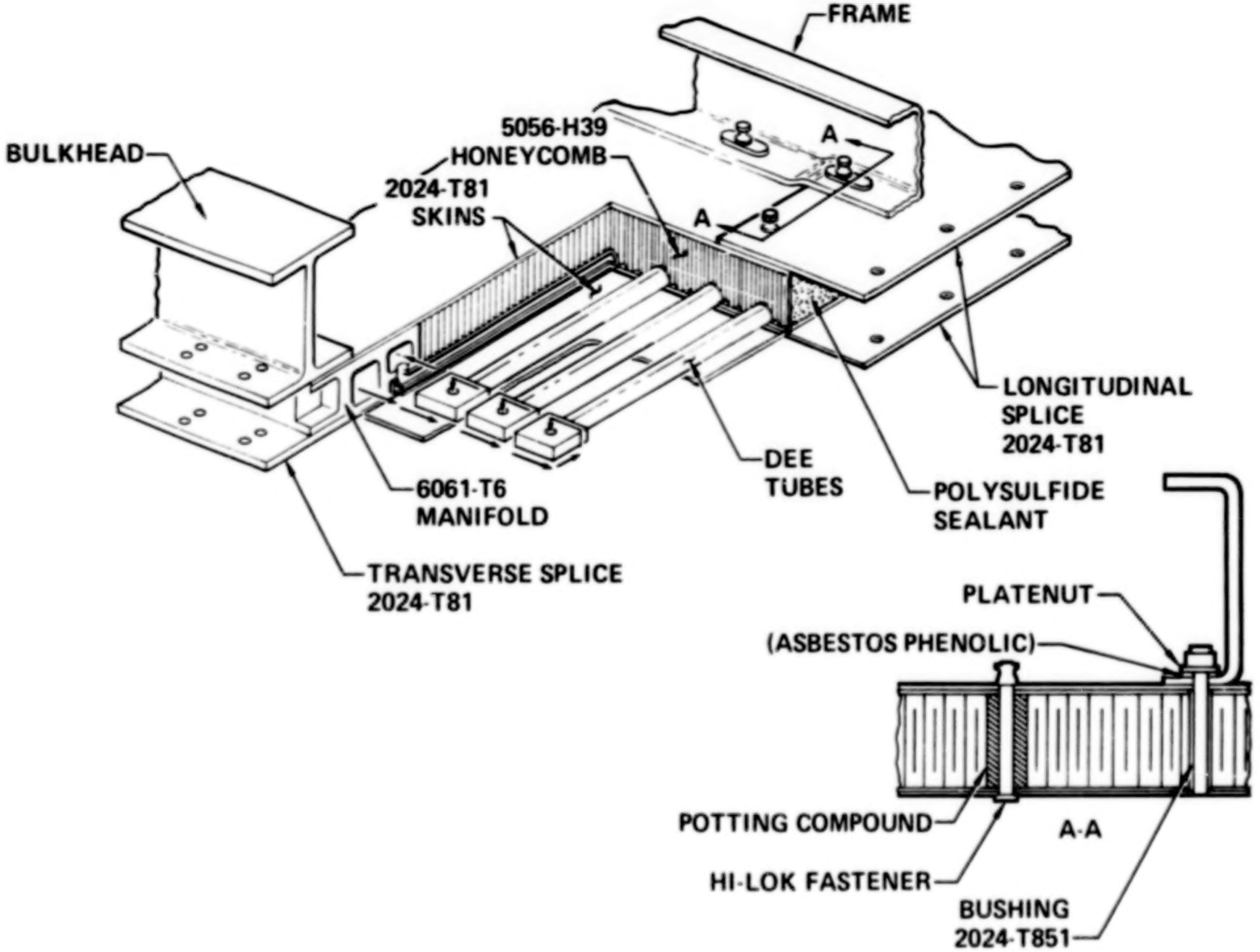
FRAME
BULKHEAD
5056-H39
HONEYCOMB
2024-T81
SKINS
A
A
LONGITUDINAL
SPLICE
2024-T81
DEE
TUBES
POLYSULFIDE
SEALANT
6061-T6
MANIFOLD
TRANSVERSE SPLICE
2024-T81
PLATENUT
(ASBESTOS PHENOLIC)
POTTING COMPOUND
A-A
HI-LOK FASTENER
BUSHING
2024-T851

Figure 12

HEAT-SHIELD CONCEPT RANKING
(Figure 13)

Nine different radiation system concepts were evaluated to identify the concept to be used on the radiative actively cooled panel. This figure shows the four highest ranked concepts, based on consideration of mass, cost, producibility, inspectibility, maintainability, durability, volmetric efficiency, thermal/structural performance and integrity, advanced development needs, resistance to hot gas influx, and tolerance to overheating.

The screen-sandwich concept consisted of a layer of insulation encased in a very fine mesh screen and bonded directly to the structure. It ranked first but was not selected because it required manufacturing development, which was beyond the scope of the contract, and there was a good deal of uncertainty about its durability and maintenance requirements.

The corrugation stiffened beaded-skin concept ranked number two and was selected for use on the radiative actively cooled panel. Rene' 41 was selected in consideration of the 1080 K (1485°F) temperature experienced on the outer surface. The metallic heat shield seems to inspire greater confidence because of the amount of experience with it. The design adapted in this program has open beads and corrugations, which overlap those of adjacent heat shields, and has attachments to the panel at each flat. The beaded and corrugated skins are joined by spot welding and the Rene' 41 is oxidized to increase emissivity.

The preloaded dome is a Rene' 41 square plate which is formed to a spherical shape. This dome is then preloaded by means of a bolt at the center of the plate attached to the actively cooled panel. The optimized, domed heat shield was 20.3 cm (8.0 in.) square. An attractive feature of the design is that one heat shield would fit almost anywhere on the aircraft's surface. However, aerodynamic drag was the undoing of this design. It was estimated that the increase in fuel volume, aircraft size and engine performance required to maintain equal performance with this high drag, was equivalent to zero-drag domed heat shields that weighed 38.5 kg/m^2 (7.9 lbm/ft^2). The heat shield itself had quite low mass.

The Rene' 41 beaded skin concept ranked fourth. It is a very simple design. However, it was designed by stiffness requirements to prevent flutter and had significantly higher mass than the selected concept.

HEAT-SHIELD CONCEPT RANKING

1. SCREEN SANDWICH

16.5 kg/m^2 (3.38 lbm/ft^2)

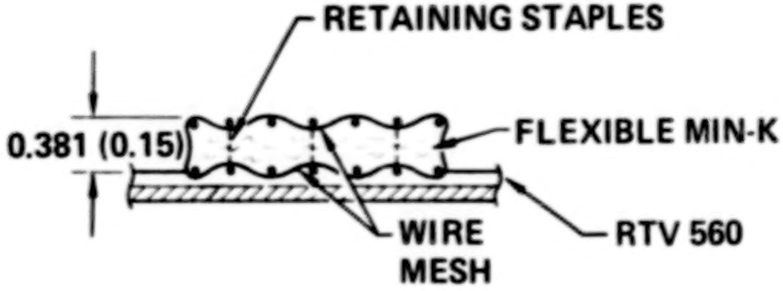
RETAINING STAPLES
0.381 (0.15)
FLEXIBLE MIN-K
WIRE MESH
RTV 560

2. CORRUGATION STIFFENED BEADED SKIN

19.8 kg/m^2 (4.07 lbm/ft^2)

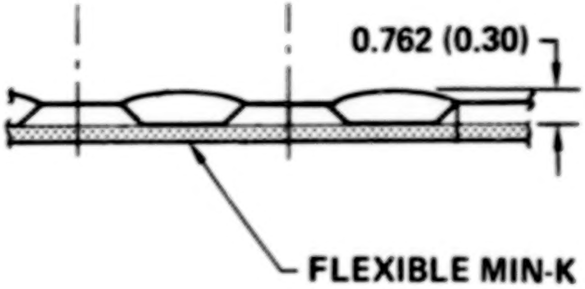
0.762 (0.30)
FLEXIBLE MIN-K

3. PRELOADED DOME

38.5 kg/m^2 (7.9 lbm/ft^2)

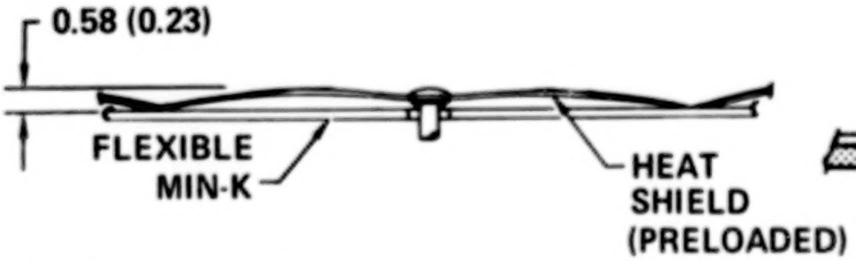
0.58 (0.23)
FLEXIBLE MIN-K
HEAT SHIELD (PRELOADED)

4. BEADED SKIN

23.8 kg/m^2 (4.89 lbm/ft^2)

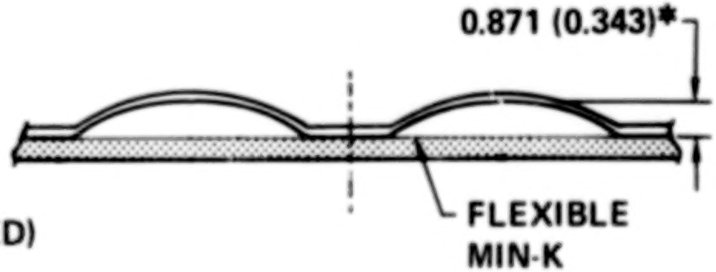
0.871 (0.343)*
FLEXIBLE MIN-K

*DIMENSIONS IN cm (in.)

Figure 13

RENE' 41 HEAT-SHIELD MASS VS SUPPORT SPACING
(Figure 14)

All elements of the heat shield were optimized for minimum mass, except that skin thickness was not allowed to be less than indicated on this figure. The heat shield was designed to be restrained against lateral thermal expansion but not against longitudinal expansion.

Lateral expansion had to be accommodated by bending of the beads and corrugations. This sized the beaded skin but was not significant to the corrugations which were much less stiff. Minimum-mass outer skin was achieved with a 5.08-cm (2.0 in) bead pitch, 0.025-cm (0.010 in) skin thickness and 0.318-cm (0.125 in) crown on the corrugation.

With the minimum-mass beaded skin described above, the height of a minimum gage corrugation was varied as required to provide adequate bending strength for various heat-shield support spacings. Thus, the effect of support spacing on heat-shield mass could be determined. The results are shown on this figure. The heat-shield attachment mass is included in all cases.

It will be noted that significant mass reduction is achieved with support spacings of 30.4, 40.6, 45.8, and 50.8 cm (12, 16, 18 and 20 in). This is due to the fact that some of the frame attachments can also be used as heat-shield attachments.

Based on the above trade study, the selected heat-shield support spacing was 30.4 cm (12.0 in). The size of the heat shield was also studied, and it was determined that they could be 61.0 cm (24.0 in) long with a row of supports at each end and a row in the middle. Heat-shield width was set, somewhat arbitrarily, at 61.0 cm (24.0 in) because that was the width of the actively cooled panel. They could well be made wider.

RENE' 41 HEAT-SHIELD MASS vs SUPPORT SPACING

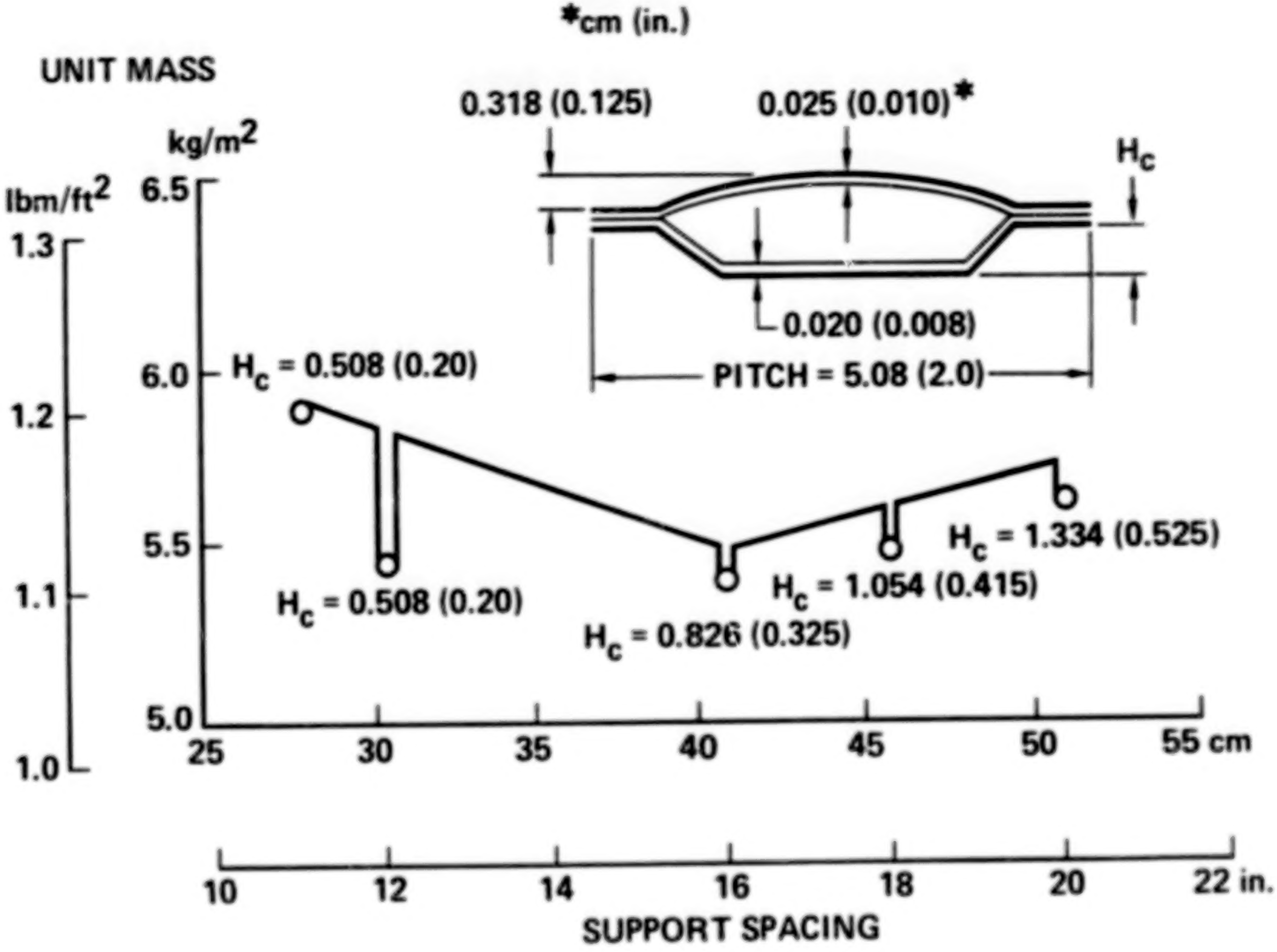

Figure 14

HEAT-SHIELD MASS VS ABSORBED HEAT FLUX
(Figure 15)

This figure shows how heat-shield mass varies with absorbed heat flux. It also shows that increasing bead/corrugation pitch increases mass.

The increase in heat-shield mass at low absorbed heat flux results from reduced material properties at higher temperatures. The Rene' 41 properties drop rapidly at temperatures above 1060 K (1450°F) which is experienced when the absorbed heat flux is less than 11 kW/m^2 (1.0 Btu/ft^{2}sec). At lower temperatures, the change in material properties is much less dramatic.

HEAT-SHIELD MASS vs ABSORBED HEAT FLUX

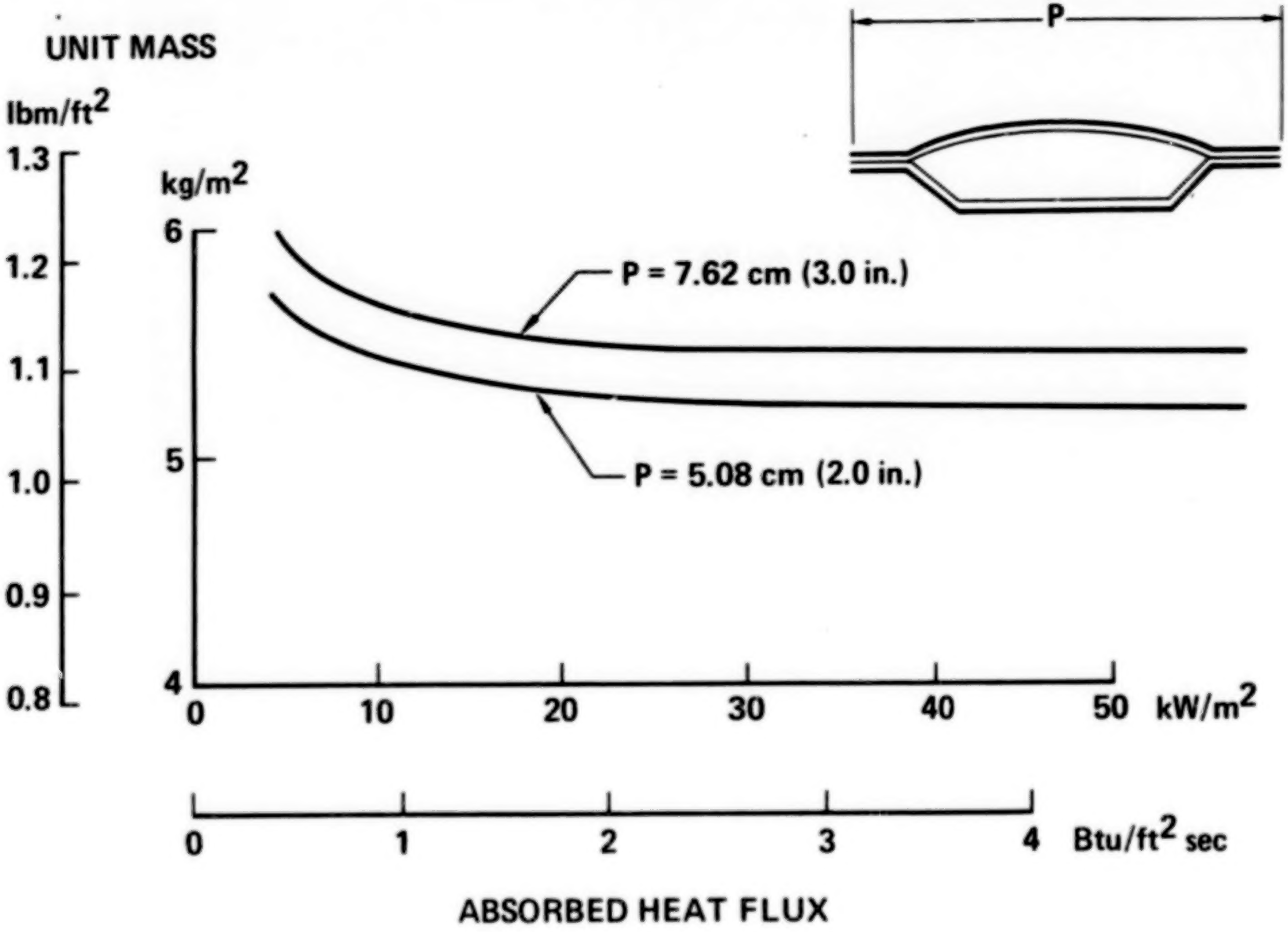

Figure 15

HEAT-SHIELD AND INSULATION DETAILS
(Figure 16)

This figure shows additional heat-shield and insulation details and the provisions for attaching them to the actively cooled panel. The method of determining the optimized heat-shield geometry, shown here, was discussed previously.

Heat-shield end details are illustrated on the right. The corrugations on the heat-shield trailing edges, and the beads on the leading edges, are trimmed back to allow adjacent panels to overlap and expand longitudinally without binding. Slotted holes at the overlays are also required at the attachment bolts to provide for thermal expansion.

The insulation is only 0.381 cm (0.15 in) thick. It is packaged in a stainless steel foil.

The heat-shield stand-off posts are an integral part of the insulation package. The heat-shield attachments pass through the stand-off posts and the actively cooled panel as the next figure illustrates.

HEAT-SHIELD AND INSULATION DETAILS

*DIMENSIONS IN cm (in.)

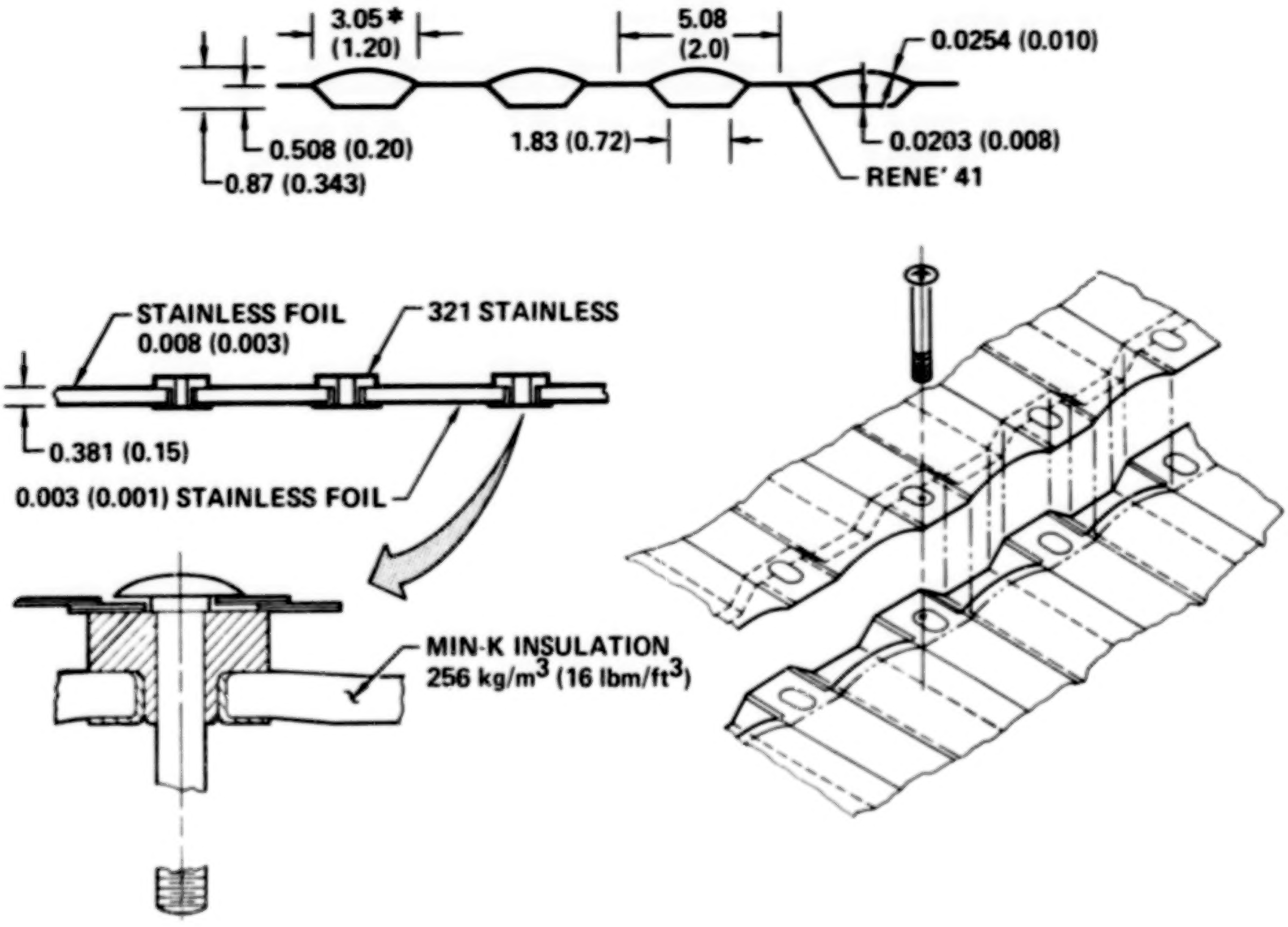
3.05*
(1.20)
5.08
(2.0)
0.0254 (0.010)
0.508 (0.20)
0.87 (0.343)
1.83 (0.72)
0.0203 (0.008)
RENE' 41
STAINLESS FOIL
0.008 (0.003)
321 STAINLESS
0.381 (0.15)
0.003 (0.001) STAINLESS FOIL
MIN-K INSULATION
256 kg/m3 (16 lbm/ft3)

Figure 16

482

MAXIMUM TEMPERATURES AT LONGITUDINAL SPLICE
(Figure 17)

This figure shows the temperatures that exist in one of the hottest spots on the panel, which is at the edge of the panel near the exit manifold. The figure also shows more of the heat-shield attachment detail and the coolant tube that is located outside the longitudinal-splice attachment line to provide better cooling.

Maximum panel temperature is on the outer splice plate at the panel edge. Maximum heat-shield temperature is on the top of the bead.

The heat-shield stand-off post and the bolt act almost like direct heat shorts to the panel. This was accounted for by slightly increasing insulation thickness so that the absorbed heat flux accounts for heat shorts as well as heat passing through the insulation.

MAXIMUM TEMPERATURES AT LONGITUDINAL SPLICE

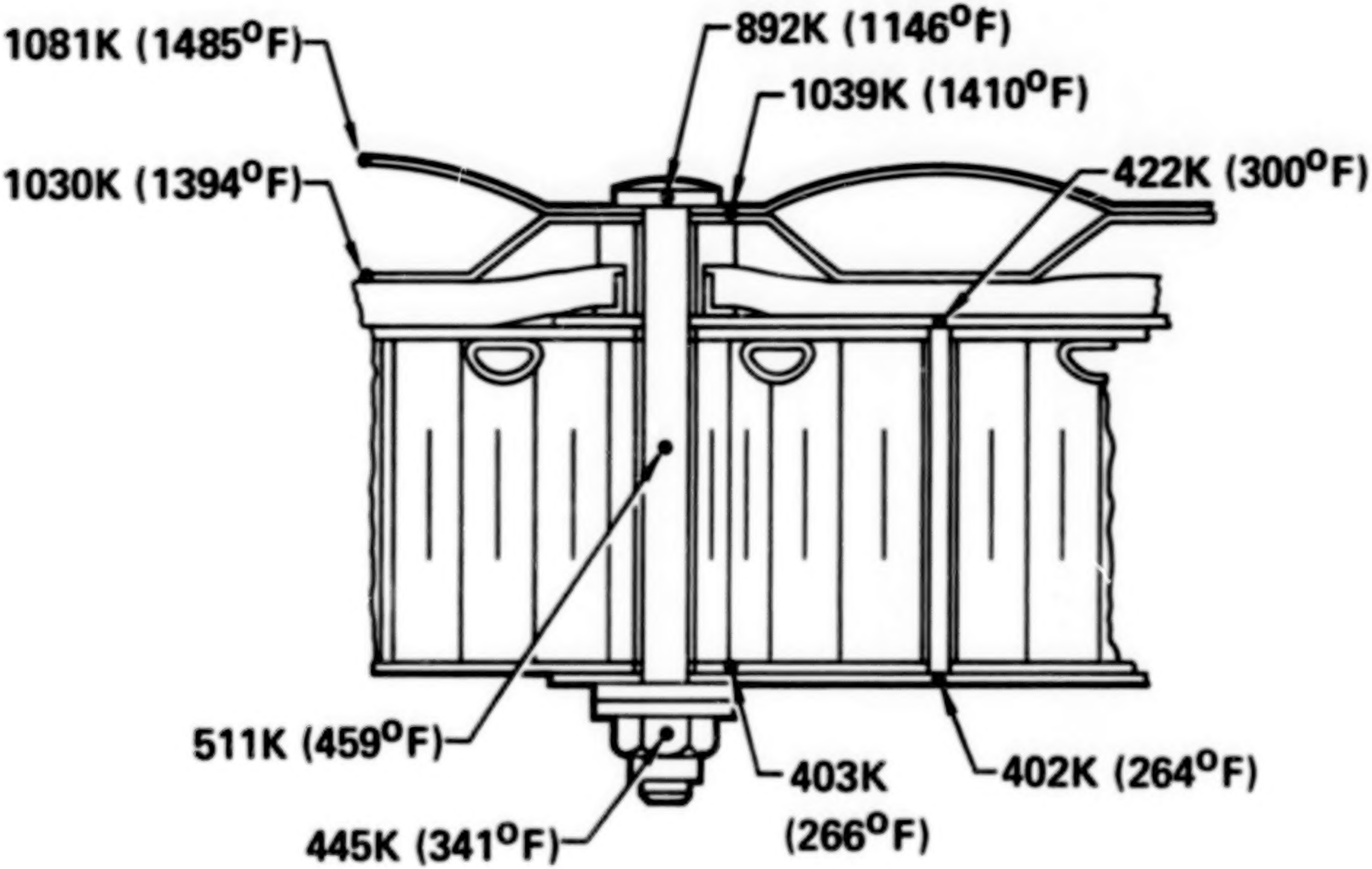
1081K (1485°F)
892K (1146°F)
1039K (1410°F)
1030K (1394°F)
422K (300°F)
511K (459°F)
403K (266°F)
402K (264°F)
445K (341°F)

Figure 17

RACP SYSTEM MASS IS LESS THAN FOR BARE ACP
(Figure 18)

This figure shows that the total mass of a radiative actively cooled structural system is less than that of a bare actively cooled system designed for the same conditions.

There is not much difference in actively cooled panel mass for the two systems. This is not due to an insensitivity of panel mass to absorbed heat flux. It is more likely due to a difference in methods of attaching the Dee tubes to the outer skin. The bare panel, with absorbed heat flux of 136 kW/m^2 (12 Btu/ft^{2}sec), had tubes soldered to the skin. The radiative actively cooled panel (RACP), with an absorbed heat flux of 9.1 kW/m^2 (0.8 Btu/ft^{2}sec), had tubes adhesively bonded to the skin. With bonded joints, the RACP could not absorb 136 kW/m^2 regardless of tube spacing and coolant mass flow.

The combined mass of the radiation and cooling system of the RACP is slightly less than the mass of the cooling system for the bare panel.

RACP SYSTEM MASS IS LESS THAN FOR BARE ACP

COMPONENTS	RACP		ACP	
	kg/m^2	lbm/ft^2	kg/m^2	lbm/ft^2
ACTIVELY COOLED PANEL				
SKINS	5.86	1.20	3.76	0.77
COOLING PASSAGES	0.78	0.16	2.73	0.56
HONEYCOMB	1.42	0.29	1.32	0.27
MANIFOLDS	0.78	0.16	0.64	0.13
CLOSEOUTS	0.63	0.13	1.76	0.36
ADHESIVES	1.95	0.40	2.10	0.43
FASTENERS, ETC.	1.02	0.21	0.49	0.10
PANEL MASS	12.44	2.55	12.80	2.62
RADIATION SYSTEM				
HEAT SHIELDS	4.34	0.89	–	–
INSULATION PACKAGES	1.86	0.38	–	–
FASTENERS, ETC.	1.07	0.22	–	–
RADIATION SYSTEM MASS	7.27	1.49		
COOLING SYSTEM				
COOLING INVENTORY	0.59	0.12	1.86	0.38
PUMPING PENALTY	0.01	–	0.34	0.07
DISTRIBUTION SYSTEM	1.76	0.36	8.64	1.77
COOLING SYSTEM MASS	2.36	0.48	10.84	2.22
TOTAL MASS	22.07	4.52	23.64	4.84

Figure 18

BONDED OUTER SKIN AND DEE-TUBE ASSEMBLY
(Figure 19)

A 0.61m (2 ft) x 1.22m (4 ft) radiative actively cooled test panel has been fabricated and delivered to NASA Langley Research Center for tests. This figure shows the partially completed actively cooled panel after the outer skin, tubes and manifolds had been bonded together. This was accomplished in one bonding operation.

After bonding, the cooling system was pressure checked to locate leaks and a Thermovision (IR scanning system) check was run to be sure all of the coolant passages were clear. Thermovision indicated one tube was blocked. The Lee plugs (see Figure 11) were removed and the adhesive blocking the coolant was removed. The panel was replugged, and Thermovision confirmed that all passages were clear and flow was uniform across the panel.

After that, the honeycomb core, with machined recesses for the tubes, and the inner skin were bonded in place. Foaming adhesive was used between the tube and core and between the manifold and core.

BONDED OUTER SKIN AND TUBE/MANIFOLD ASSEMBLY

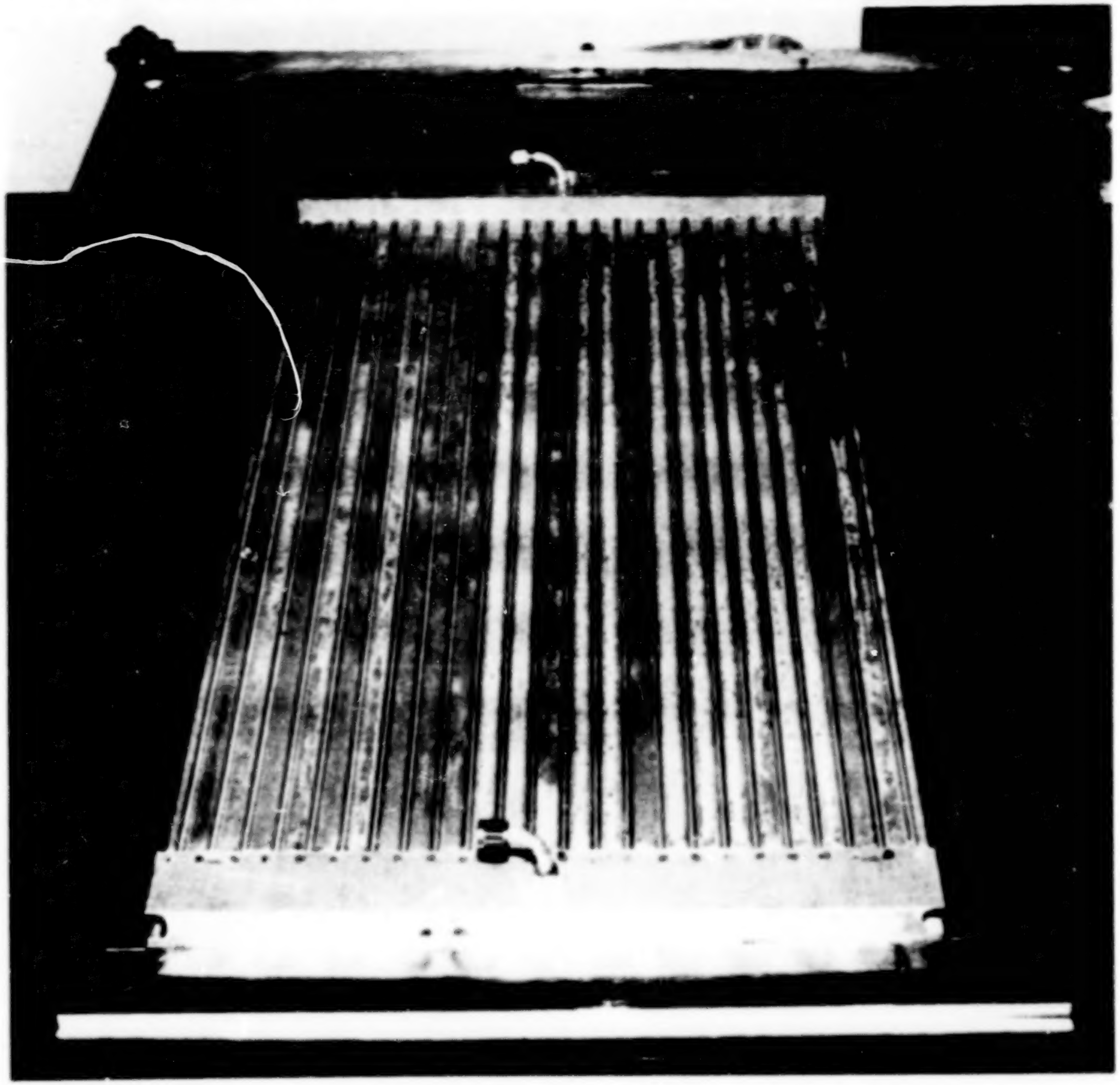

Figure 19

BONDED ACTIVELY COOLED PANEL
(Figure 20)

This figure shows the actively cooled panel after bonding. A drilling fixture was used to locate all fastener holes in the panel. The same fixture was then used to locate the mating holes in the heat shields and insulation packages. This was done to make sure the holes lines up properly.

BONDED ACTIVELY COOLED PANEL

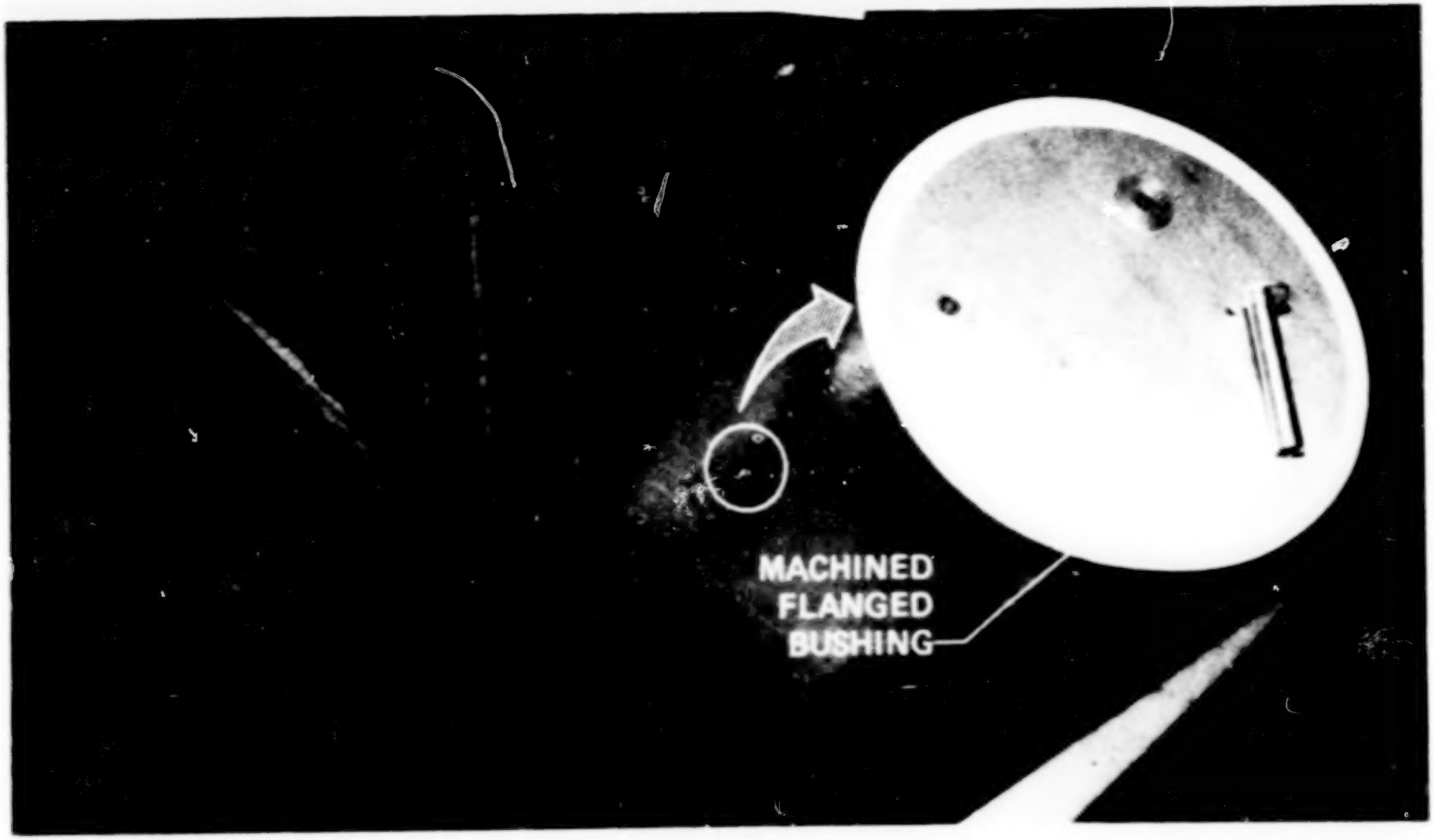

MACHINED
FLANGED
BUSHING

Figure 20

CONCLUSIONS
(Figure 21)

The primary objectives of the RACP program were achieved. Specific conclusions regarding sensitivity of component masses to geometric and coolant parameters were described earlier. General conclusions, which could significantly affect future systems design and R and D plans are summarized on this figure.

This program proved the feasibility of the radiative actively cooled structure approach for hypersonic cruise aircraft. It permits matching of the heat load to the available heat sink. Further, this match can probably be achieved by applying radiative active cooling to just part of the airframe surface.

The RACP designed in this program is seven percent lighter than a bare ACP designed for the same conditions. It is reasonable to expect that a similar conclusion would be reached using other actively cooled panel concepts.

The honeycomb-sandwich actively cooled panel is more difficult (complex) to fabricate than a conventional honeycomb panel. This is due to integration of the manifolds and cooling tubes. This was expected. A comparison of the fabricability of this RACP concept with alternate concepts for hypersonic cruise aircraft would be more meaningful.

CONCLUSIONS

- RACP PERMITS MATCHING HEAT LOAD AND AVAILABLE HEAT SINK
- RACP IS 7% LIGHTER THAN ACP
- RACP FABRICATION MORE DIFFICULT THAN CONVENTIONAL HONEYCOMB SANDWICH

Figure 21

CONTENTS

Part I

PREFACE . . . . iii 1/A5

WELCOME 1 1/A10
R. R. Heldenfels

SESSION I - OVERVIEWS
Chairman: A. J. Henderson

1. HYPERSONIC STRUCTURES: AN AERODYNAMICIST'S PERSPECTIVE (OR ONE MAN'S DREAM IS ANOTHER MAN'S NIGHTMARE) 5 1/B1
J. D. Watts, L. R. Jackson, and J. L. Hunt

2. STRUCTURAL REQUIREMENTS FOR MILITARY HYPERSONIC SYSTEMS (Paper not available for publication)
P. Lane

3. AIRFRAME-INTEGRATED PROPULSION SYSTEM FOR HYPERSONIC CRUISE VEHICLES 39 1/F13
Robert A. Jones and Paul W. Huber

4. RECENT ADVANCES IN CONVECTIVELY COOLED ENGINE AND AIRFRAME STRUCTURES FOR HYPERSONIC FLIGHT 47 1/G7
H. Neale Kelly, Allan R. Wieting, Charles P. Shore, and Robert J. Nowak

SESSION II - ENGINE STRUCTURES
Chairman: H. N. Kelly

5. DESIGN AND ANALYSIS OF A SCRAMJET ENGINE 65 2/A13
O. A. Buchmann

6. THERMOSTRUCTURAL ANALYSIS OF A SCRAMJET FUEL-INJECTION STRUT 119 3/B11
Allan R. Wieting and Earl A. Thornton

7. ADVANCED FABRICATION TECHNIQUES FOR COOLED ENGINE STRUCTURES 145 3/F7
O. A. Buchmann

8. HYDROGEN EMBRITTLEMENT AND ITS CONTROL IN HYDROGEN-FUELED ENGINE SYSTEMS 195 4/F11
W. T. Chandler

9. CARBON-CARBON COMPOSITE APPLICATION FOR INTEGRAL ROCKET RAMJET COMBUSTORS (Paper not available for publication)
H. A. Holman

SESSION III - COOLED AIRFRAME STRUCTURES
Chairman: C. P. Shore

10. DESIGN AND FABRICATION OF A SKIN STRINGER DISCRETE TUBE ACTIVELY COOLED STRUCTURAL PANEL 253 6/A5
Frank M. Anthony

11. DESIGN AND ANALYSIS OF A PLATE-FIN SANDWICH ACTIVELY COOLED STRUCTURAL PANEL 319 7/C13
L. M. Smith

12. FLUXLESS BRAZING AND HEAT TREATMENT OF A PLATE-FIN SANDWICH ACTIVELY COOLED PANEL 375 8/E1
Charles S. Beuyukian

13. DESIGN AND FABRICATION OF A RADIATIVE ACTIVELY COOLED HONEYCOMB SANDWICH PANEL 449 10/A13
Leland C. Koch

14. RADIATIVE, ACTIVELY COOLED PANEL TESTS RESULTS 493 11/A5
Charles P. Shore, Robert J. Nowak, and Ellsworth L. Sharpe

REFERENCES

1. Koch, L. C.; and Pagel, L. L.: High Heat Flux Actively Cooled Honeycomb Sandwich Structural Panel for a Hypersonic Aircraft. NASA CR-2959, 1978.

2. Ellis, D. A.; Pagel, L. L.; Schaeffer, D. M.: Design and Fabrication of a Radiative Actively Cooled Honeycomb Sandwich Structural Panel for a Hypersonic Aircraft. NASA CR-2957, 1978

RADIATIVE, ACTIVELY COOLED PANEL TESTS RESULTS

Charles P. Shore, Robert J. Nowak, and Ellsworth L. Sharpe
NASA Langley Research Center, Hampton, Va.

INTRODUCTION

This paper describes a test program and some preliminary test results on a 0.61 m (2 ft.) by 1.22 m (4 ft.) radiative, actively cooled panel (RACP). The RACP (described in references 1 and 2) incorporates all of the essential features of a full scale 0.61 m (2 ft.) by 6.1 m (20 ft.) panel designed to withstand a uniform incident heat flux of 136 kW/m^2 (12 Btu/ft^2-sec) to a 422 K (300°F) surface temperature. The structure was designed to carry a uniform inplane limit load of ±210 kN/m (±1200 lb/in) and a uniform normal pressure of ±6.89 kPa (+1.0 psi). Additionally, the panel was designed to sustain, without failure or coolant leakage, 20 000 cycles of fully reversed load.

494

RADIATIVE AND ACTIVELY COOLED PANEL (RACP)

(Figure 1)

The RACP features corrugation-stiffened beaded-skin René 41 shields backed by a thin layer of high temperature insulation contained within a stainless steel foil package, and an adhesively bonded aluminum honeycomb sandwich structure with half round coolant tubes next to the outer skin. Frames representative of typical transport construction support the panel at 0.61 m (2 ft.) intervals. The aluminum panel duplicates the essential features of the full scale design except that the coolant inlet and outlet manifolds located at the panel ends are only 1.22 m (4 ft.) apart rather than 6.1 m (20 ft.). The heat shield has a longitudinal row of fasteners to simulate a splice and transverse joints which allow thermal growth. The longitudinal splice was not necessary for this panel but was included since the heat shield design does require a limited number of such splices. Performance evaluation of the RACP consisted of preliminary static thermal/mechanical loading and aerothermal flow tests in the facilities indicated on figure 2.

RADIATIVE AND ACTIVELY COOLED PANEL (RACP)

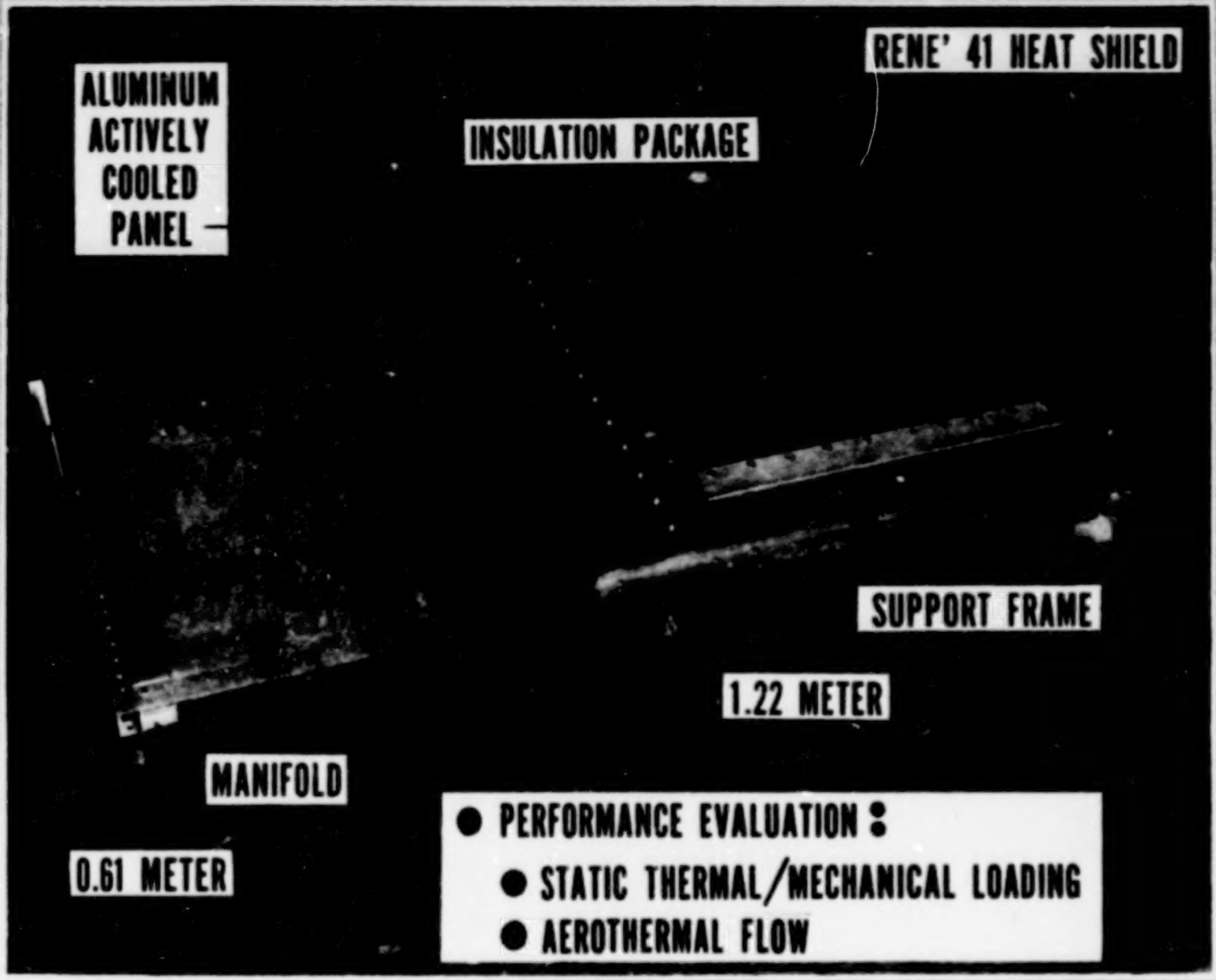
RENE' 41 HEAT SHIELD
ALUMINUM ACTIVELY COOLED PANEL
INSULATION PACKAGE
SUPPORT FRAME
1.22 METER
MANIFOLD
0.61 METER

- PERFORMANCE EVALUATION:
  - STATIC THERMAL/MECHANICAL LOADING
  - AEROTHERMAL FLOW

Figure 1

PANEL TESTS

(Figure 2)

Two Langley facilities were used to evaluate the RACP performance. The active cooling test stand (ACTS) employs a bank of air cooled radiant heaters to provide long term heating of test articles of up to 284 kW/m^2 (25 Btu/ft^2-sec). At the same time a uniaxial fatigue testing machine can be used to impose cyclic loading of up to ±489 kN (±110 000 lb.). The Langley 8-foot high-temperature structures tunnel (8-foot HTST) is a $M=7$ blowdown facility which simulates aerodynamic heating conditions at altitudes ranging from 24 km (80 000 ft.) to 40 km (132 000 ft.) and imposes realistic pressure loading on test specimens. Details of the 8-foot HTST and appropriate test techniques for flight weight test articles are discussed in reference 3. Coolant flow to the RACP for tests in either facility was provided by the cooling system shown in figure 3.

PANEL TESTS

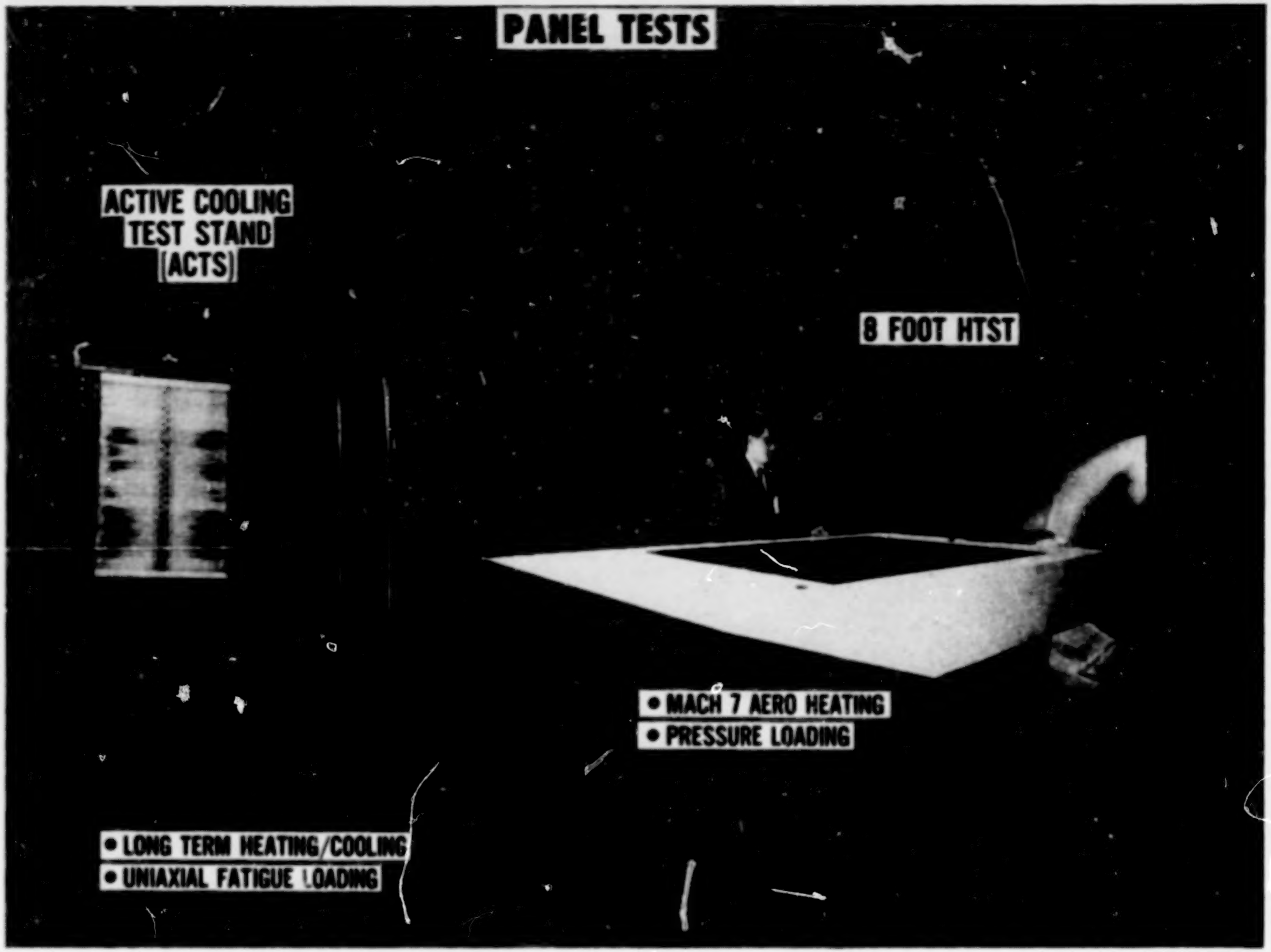
ACTIVE COOLING TEST STAND (ACTS)
8 FOOT HTST
• MACH 7 AERO HEATING
• PRESSURE LOADING
• LONG TERM HEATING/COOLING
• UNIAXIAL FATIGUE LOADING

Figure 2

ACTS COOLING SYSTEM

(Figure 3)

A chilled (244 K (-20°F)) 60/40 mass solution of ethylene glycol/water was used to cool the RACP. The cooling system consists of a 19 kiloliters (5000 gal.) storage tank, circulating pumps, flow control valves and a 47 kW (13.5 ton) refrigeration unit. As shown on the figure inset, independent pumping systems circulate the coolant from the storage tank through the panel and the refrigeration unit. Coolant mass flow rate and the coolant pressure and temperature at the RACP inlet were controlled by the flow system and the coolant pressure and temperature at the RACP outlet were monitored during the tests. Heated coolant from the RACP was mixed with chilled coolant from the storage tank to maintain the desired inlet temperature.

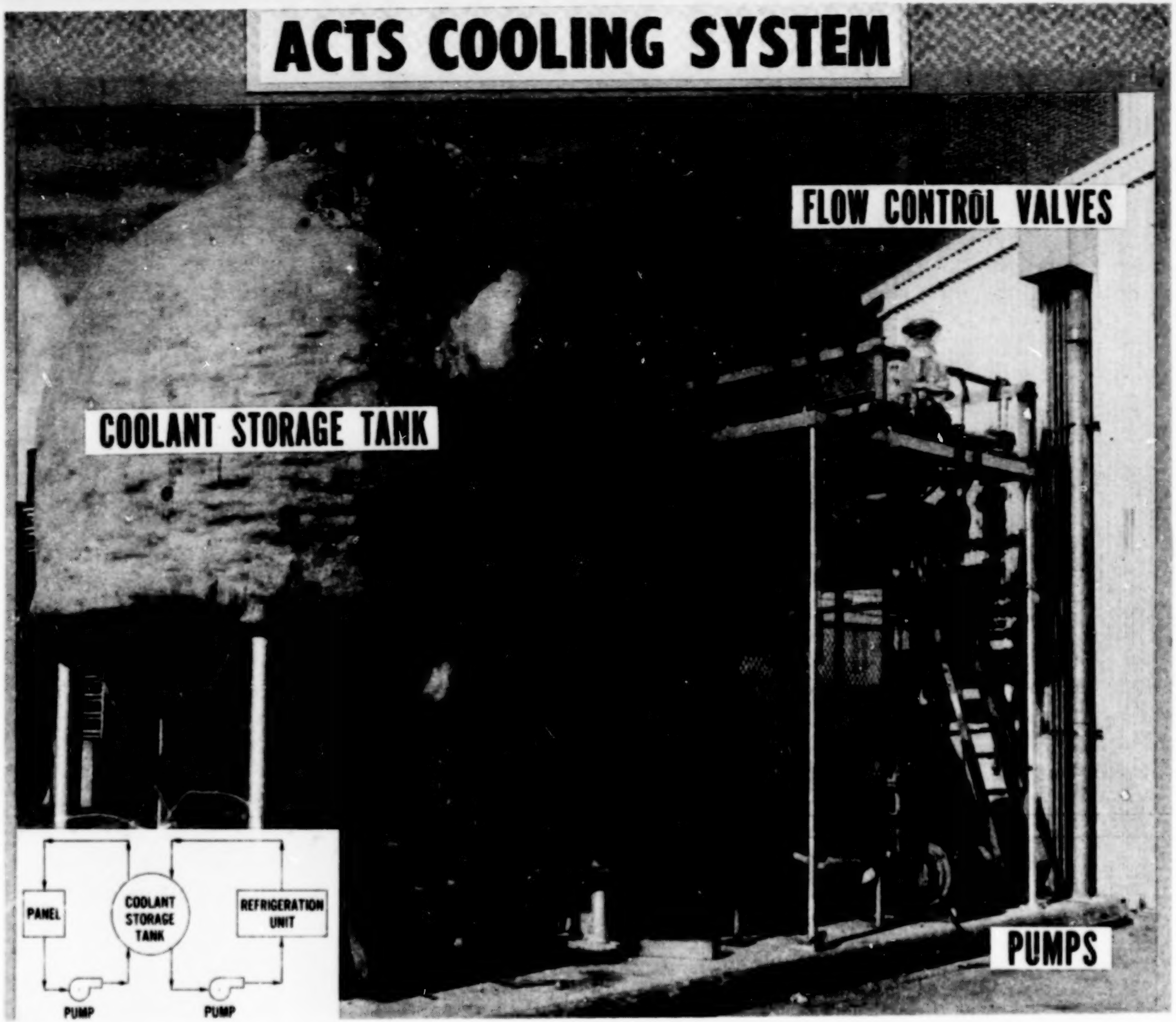
ACTS COOLING SYSTEM
FLOW CONTROL VALVES
COOLANT STORAGE TANK
PUMPS
PANEL
COOLANT STORAGE TANK
REFRIGERATION UNIT
PUMP
PUMP

4

Figure 3

500

TEST PROGRAM FOR RADIATIVE AND ACTIVELY COOLED PANEL

(Figure 4)

The test program for the RACP consists of four types of tests. (1) Preliminary static thermal/structural check-out tests were conducted in ACTS. In these tests the RACP was exposed to the design incident heat flux of 136 kW/m^2 (12 Btu/ft^2-sec), and design limit load of ±210 kN/m (±1200 lb/in.). The coolant flow rate was maintained at the design value of 13 liters/min (3.4 gal./min) and the coolant inlet temperature varied between 272 and 320 K (20 to 120°F). Variation of the coolant inlet temperature allows the 1.22 m (4 ft.) test panel to simulate various regions of the full scale 6.1 m (20 ft.) panel.

(2) Aerothermal performance tests were then conducted in the 8-foot HTST at a nominal Mach number of 7. In these tests the RACP was exposed to the design incident heat flux by aerodynamic heating for various coolant inlet temperatures. An important objective of these tests was to check for hot gas ingress to the cooled aluminum panel which could seriously degrade the performance of the RACP. Other objectives were to look for hot spots on the panel and fasteners and to evaluate heat shield joint motion.

(3) As a part of the ongoing RACP evaluation program the RACP will be reinstalled in the ACTS for some detailed thermal/structural tests including some cyclic loading tests to provide fatigue data for the cooled panel.

(4) Thermal fatigue tests will be conducted on a seperate heat shield specimen to provide life data on such structures which have previously been designed for hundreds of cycles rather than the thousands of cycles required for the RACP.

TEST PROGRAM FOR RADIATIVE AND ACTIVELY COOLED PANEL

- COMPLETED
  - PRELIMINARY STATIC THERMAL/STRUCTURAL CHECK-OUT IN ACTS
    - DESIGN INCIDENT COLD WALL HEAT FLUX: 136 kW/m^2
    - VARIOUS COOLANT INLET TEMPERATURES: 272 TO 320 K
    - DESIGN LIMIT LOAD: ± 210 kN/m
  - AEROTHERMAL PERFORMANCE IN MACH 7 8-ft HTST
    - DESIGN INCIDENT HEAT FLUX
    - VARIOUS COOLANT INLET TEMPERATURES
    - CHECK FOR HOT GAS INGRESS

- FUTURE
  - DETAILED THERMAL/STRUCTURAL TESTS IN ACTS
  - THERMAL FATIGUE TESTS ON SEPARATE HEAT SHIELD SPECIMEN

Figure 4

502

RENÉ 41 HEAT SHIELD

(Figure 5)

To monitor temperatures over the heat shields, 32 thermocouples were spot welded to the back side of the corrugation stiffening sheet in the locations shown on the figure. The photo also shows the condition of the surface after preliminary tests in ACTS.

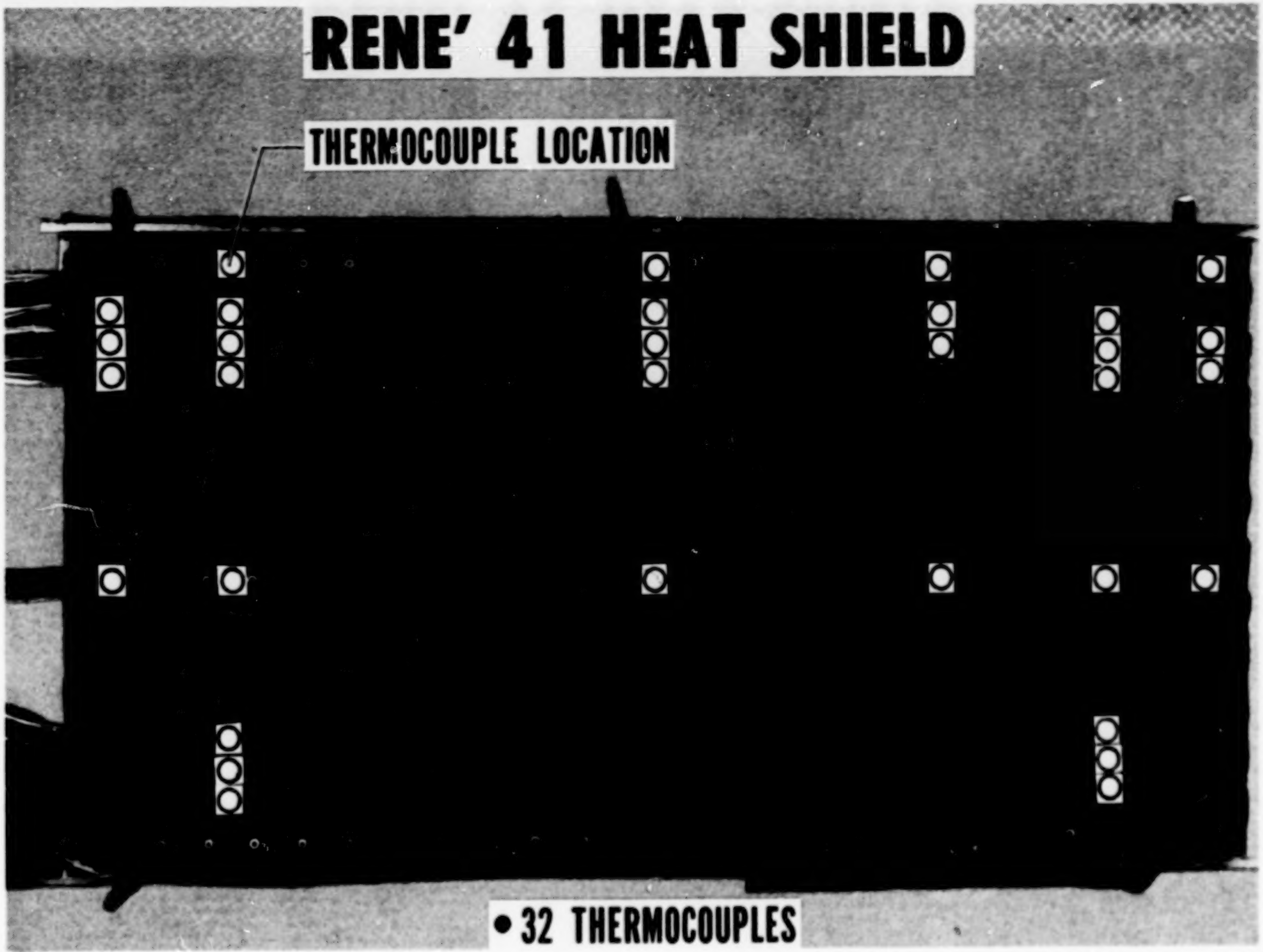
RENE' 41 HEAT SHIELD
THERMOCOUPLE LOCATION
• 32 THERMOCOUPLES

Figure 5

504

HIGH TEMPERATURE INSULATION BLANKET

(Figure 6)

A total of 19 thermocouples spot welded to small stainless steel tabs which were then spot welded to the insulation package were used to monitor the insulation package temperatures: seven on the hot side and 12 on the cool side. This photo, which was taken after the preliminary tests in ACTS, also shows the condition of the insulation package after several exposures to design operating conditions. The most noticeable effects of the heating are the darkening of the surface from oxidation and the large number of wrinkles induced by thermal expansion of the stainless steel foil package and interference with the heat shield.

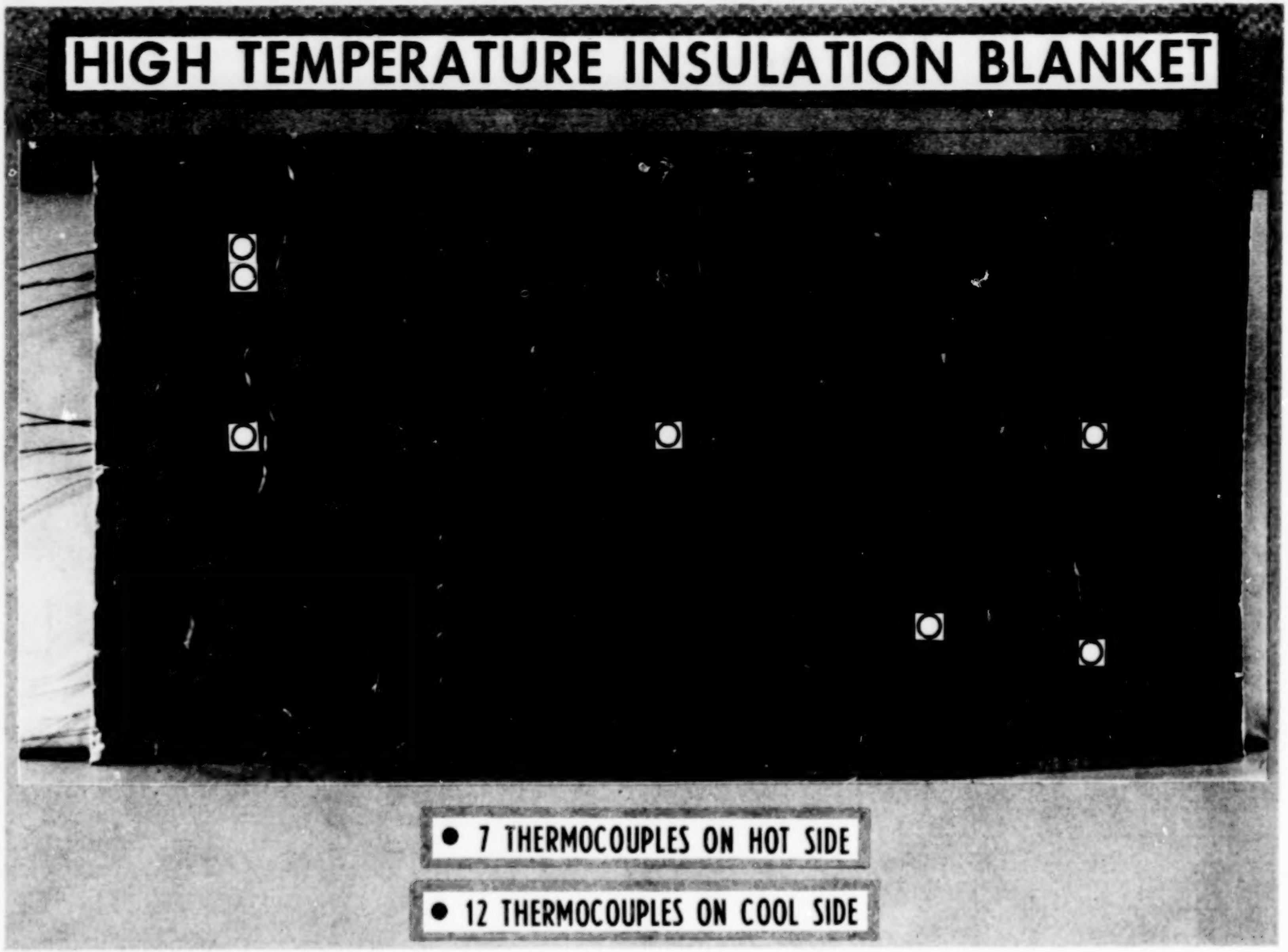
HIGH TEMPERATURE INSULATION BLANKET
● 7 THERMOCOUPLES ON HOT SIDE
● 12 THERMOCOUPLES ON COOL SIDE

Figure 6

506

COOLED ALUMINUM HONEYCOMB PANEL

(Figure 7)

A total of 120 thermocouples were used to monitor temperatures over the surface of the cooled panel. The thermocouples were bonded to the aluminum surfaces to avoid possible crack starters from welding or peening. To monitor both thermal and mechanical stresses, longitudinal and transverse strain gage pairs were bonded to the panel surfaces at the eleven locations denoted by the white spots on the figure. Before testing, the panel was heated in an oven to 422 K (300°F) to calibrate the temperature sensitivity of the strain gages.

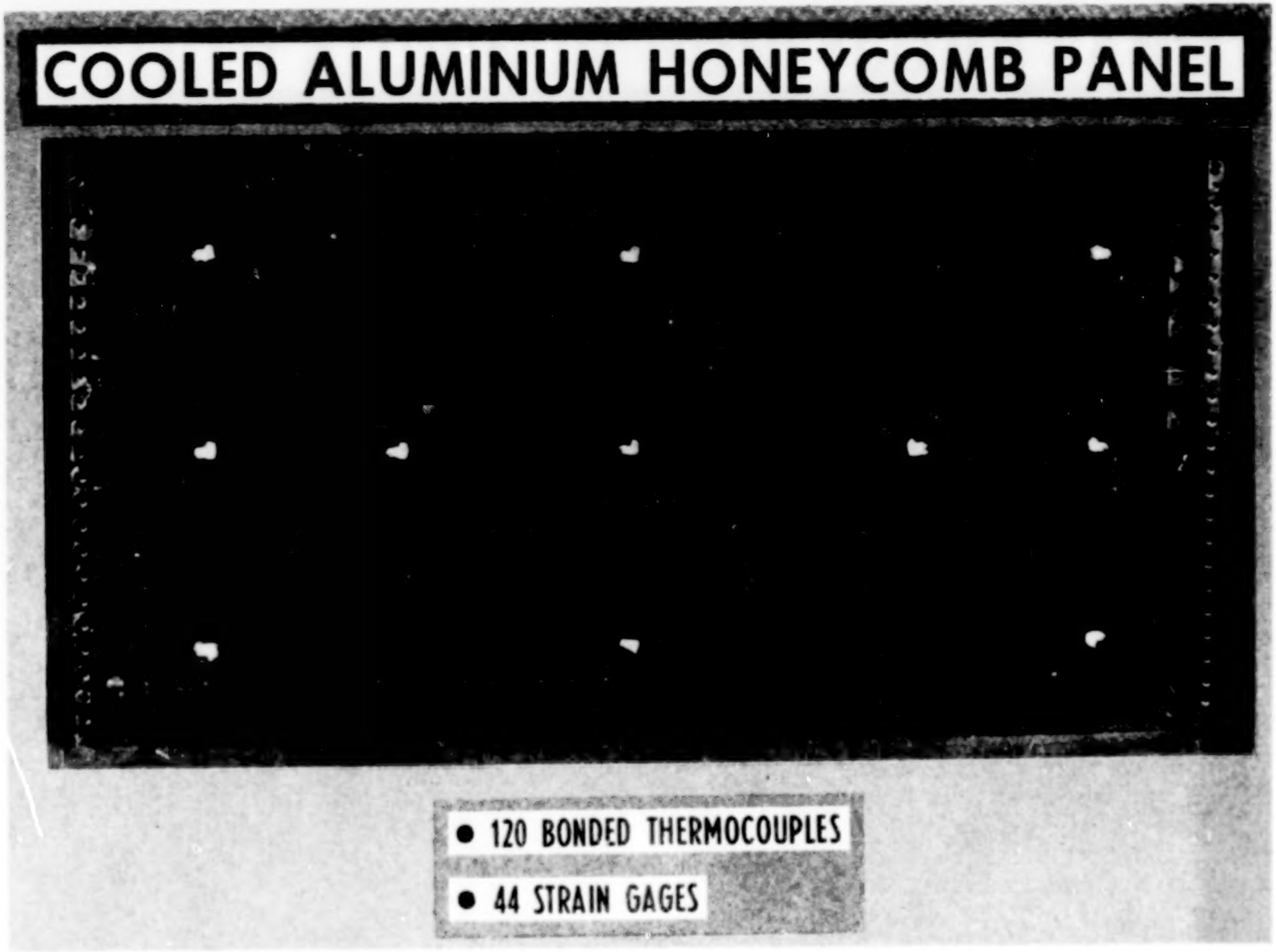

COOLED ALUMINUM HONEYCOMB PANEL

- 120 BONDED THERMOCOUPLES
- 44 STRAIN GAGES

Figure 7

ACTS HEATER SYSTEM

(Figure 8)

This figure shows the ACTS heater in place over the RACP during a hot test. Heater coolant air enters the manifolds on either side of the heater from the supply lines near the bottom of the heaters and is collected by the center manifold and subsequently vented by the large diameter hose at the top of the heaters. Other lines visible in the picture are supply and return lines for the water cooled reflector which encases the heaters. Calibration of the heaters indicated the heat flux variation over the test panel surface was about 10 percent.

ACTS HEATER SYSTEM

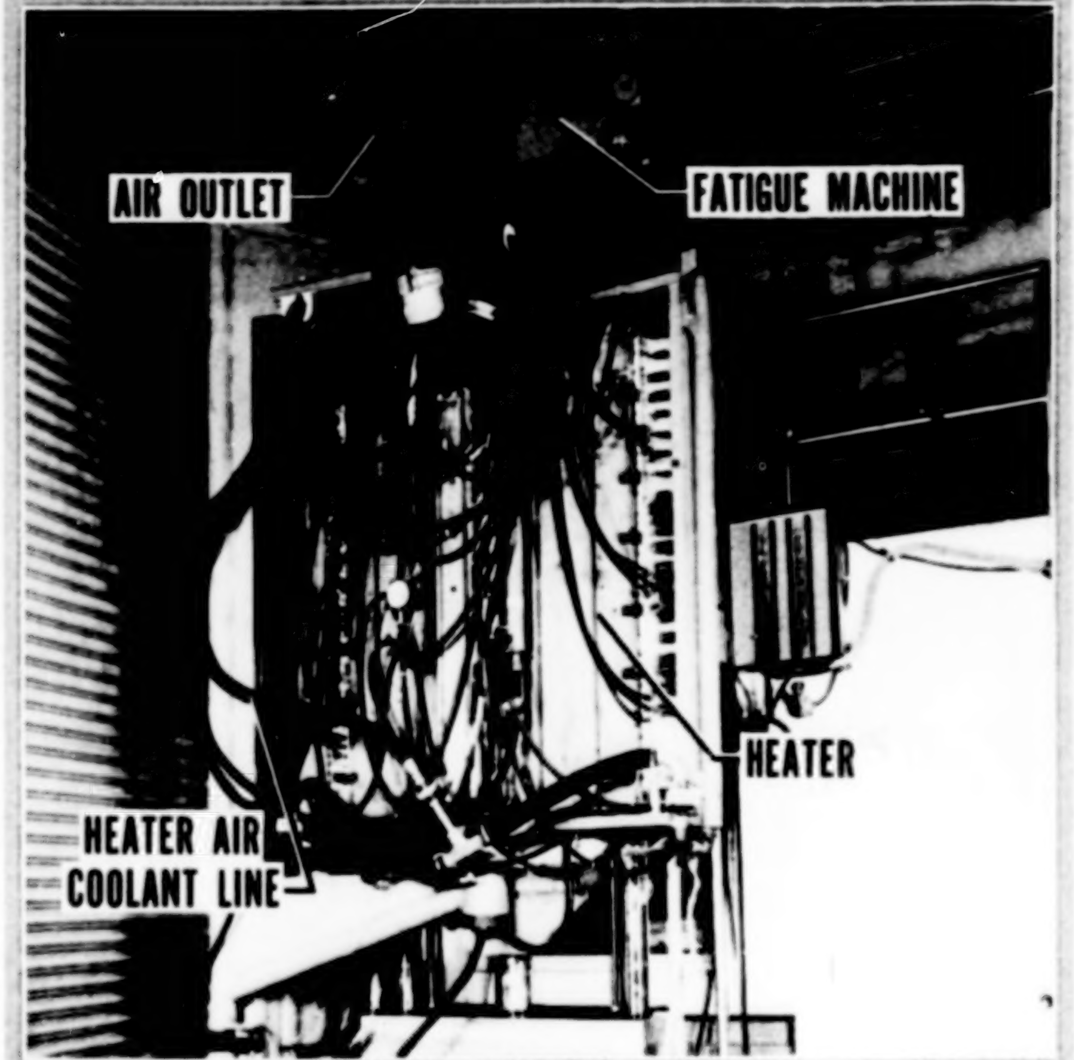
AIR OUTLET
FATIGUE MACHINE
HEATER
HEATER AIR COOLANT LINE

- HEAT FLUX UNIFORM WITHIN 10%

Figure 8

510

ACTS PANEL LOADING SYSTEM

(Figure 9)

This figure shows the rear of the RACP during a hot test and illustrates some additional features of the test set-up. The glycol/water coolant supply and return lines are shown on the right side of the figure. The loading heads of the fatigue testing machine are visible at the center top and bottom of the figure. Additional support of the test panel is provided by the linear bearings (denoted frame supports) which are attached to the panel frames. These bearings prevent out-of-plane motion of the frames but permit unrestrained longitudinal thermal expansion of the panel since the bearings are free to move along the vertical rods on either side of the test fixture. Transverse thermal growth is accommodated by slots in the vertical rod supports.

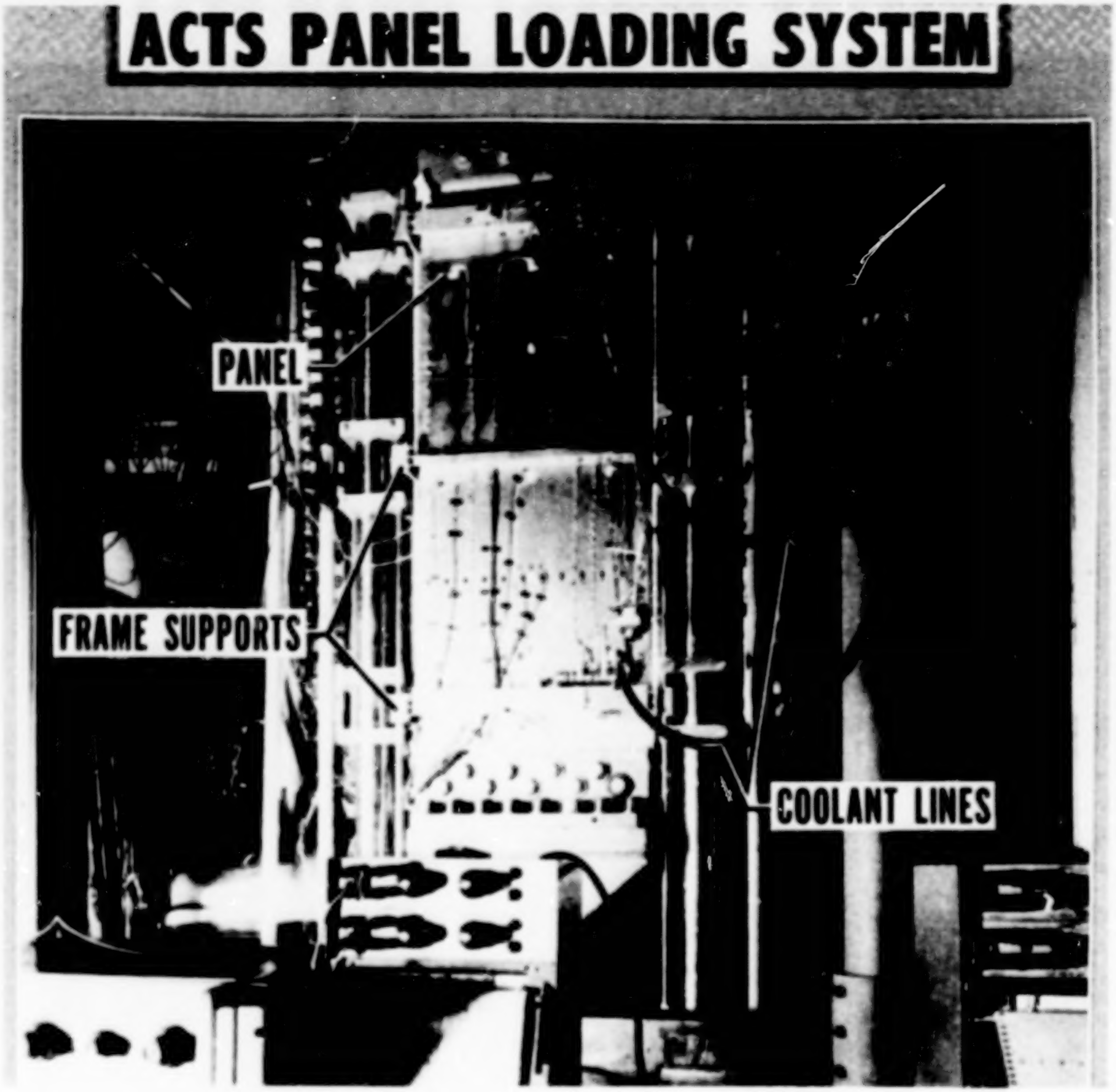
ACTS PANEL LOADING SYSTEM
PANEL
FRAME SUPPORTS
COOLANT LINES

Figure 9

SUMMARY OF RACP TESTS IN ACTS

(Figure 10)

During the preliminary static thermal/structural check-out tests six thermal cycles and 17 limit load cycles (±210 kN/m (±1200 lb/in.)) were imposed on the RACP for a total of 4.8 hours at operating temperature. The performance of the RACP was within 90 percent of predicted values for heat shield temperatures, cooled panel temperatures, heat flux absorbed by the cooled panel and mechanical stresses in the aluminum panel skins. Although strain measurements were taken under heated conditions, time constraints have prevented analysis of these data to determine thermal stresses in the cooled panel. Post test examination of the RACP components revealed no apparent structural degradation and the tests revealed no test-to-test degradation of thermal performance. Additionally, no evidence of coolant leakage was found during the 4.8 hours of operation.

SUMMARY OF RACP TESTS IN ACTS

- 6 THERMAL CYCLES
- 17 LOAD CYCLES
- 4.8 HOURS AT OPERATING TEMPERATURE
- PERFORMANCE WITHIN 90% OF PREDICTED VALUES
  - HEAT SHIELD TEMPERATURE: 978 VERSUS 1081 K
  - COOLED PANEL TEMPERATURE: 326 VERSUS 340 K
  - ABSORBED HEAT FLUX: 8.2 VERSUS 9.1 kW/m^2
  - MECHANICAL STRESS: 81.7 VERSUS 86.0 MPa
- NO APPARENT THERMAL/STRUCTURAL DEGRADATION
- NO COOLANT LEAKAGE

Figure 10

PANEL TEMPERATURES

(Figure 11)

Typical RACP test temperatures are shown as a function of distance from the coolant inlet. Temperatures are shown for the heat shields and cooled panel and at the coolant inlet and outlet. The bars connecting the symbols for the heat shields indicate the lateral variation in heat shield temperatures. Center line temperatures only are shown for the cooled panel. Although there is some scatter in the measured heat shield temperatures the overall level agrees well with predicted values. The cooled panel temperatures are in good agreement with predicted values. The measured coolant temperature rise of 8.9 K (16°F) along with the measured mass flow gave a calculated average absorbed heat flux of 8.2 kW/m^2 (0.72 Btu/ft^2-sec) compared to the design flux of 9.1 kW/m^2 (0.8 Btu/ft^2-sec). The predicted temperatures on figure 11 are calculated values based on the measured absorbed heat flux.

The figure inset shows a temperature distribution through the thickness of the RACP and indicates that although the heat shields are operating at 985 K (1313°F), the cooled panel, less than 1.27 cm (0.5 in.) away, is operating at about 331 K (136°F) and that the majority of this temperature drop occurs through the 0.32 cm (0.125 in.) thick insulation package.

After the preliminary static thermal/structural check-out tests in ACTS the RACP was tested in the Langley 8-foot high-temperature structures tunnel. A schematic of the tunnel is shown in figure 12.

PANEL TEMPERATURES

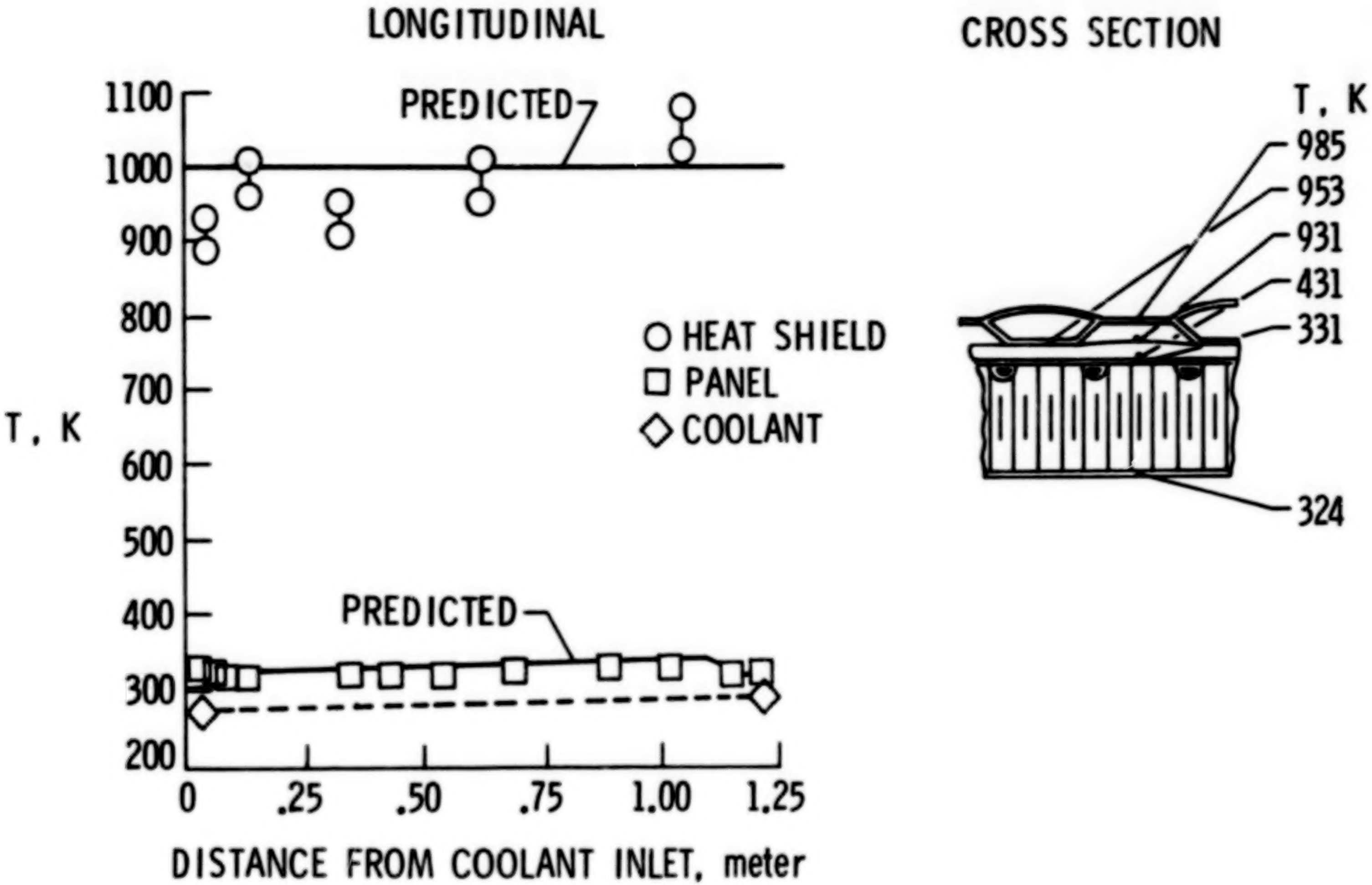

Figure 11

516

LANGLEY 8-FOOT HIGH-TEMPERATURE STRUCTURES TUNNEL

(Figure 12)

The tunnel is a blowdown facility which uses products of combustion as a test medium. Fuel and air are burned in the combustor and the combustion products are expanded in the nozzle to a nominal free stream Mach number of 7; flow continues through the test section and diffuser sections and into the ambient atmosphere. The air ejector is used to lower the pressure in the test section and thereby reduce starting loads on the test article which is stored in the pod beneath the test section while the tunnel is started. The test article is then injected into the stream once flow is established. Since the tunnel is a blowdown facility with limited run time, radiant preheaters are used to bring test articles to thermal equilibrium before exposure to the test stream. Some details of the heater apparatus are shown in figure 13.

LANGLEY 8-FOOT HIGH-TEMPERATURE STRUCTURES TUNNEL

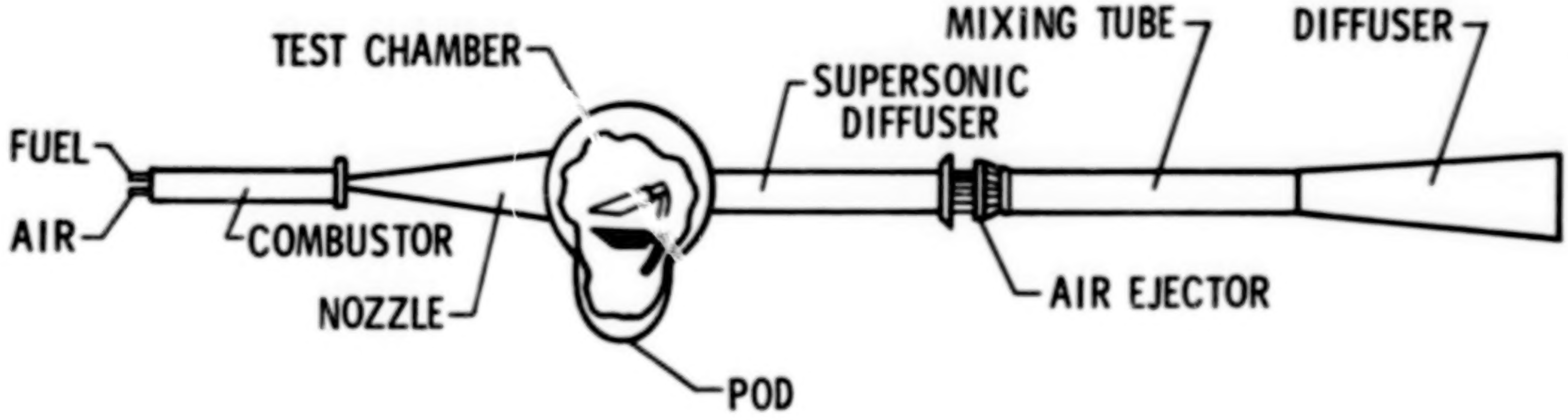
TEST CHAMBER
MIXING TUBE
DIFFUSER
SUPERSONIC DIFFUSER
FUEL
AIR
COMBUSTOR
NOZZLE
AIR EJECTOR
POD

Figure 12

8-FT HTST RADIANT PREHEATING APPARATUS

(Figure 13)

Before the tunnel test begins the test article is located in the pod beneath the test section. The inset on the right shows the radiant preheaters in place over the test article. After desired thermal equilibrium is reached the tunnel is started. Once flow is established the heaters are retracted (lower left inset) and the test article is raised to the test position (upper left inset). At the end of the test the procedure is reversed and the heaters may be used to follow a preselected cool-down rate for the test article.

8-FT HTST RADIANT PREHEATING APPARATUS

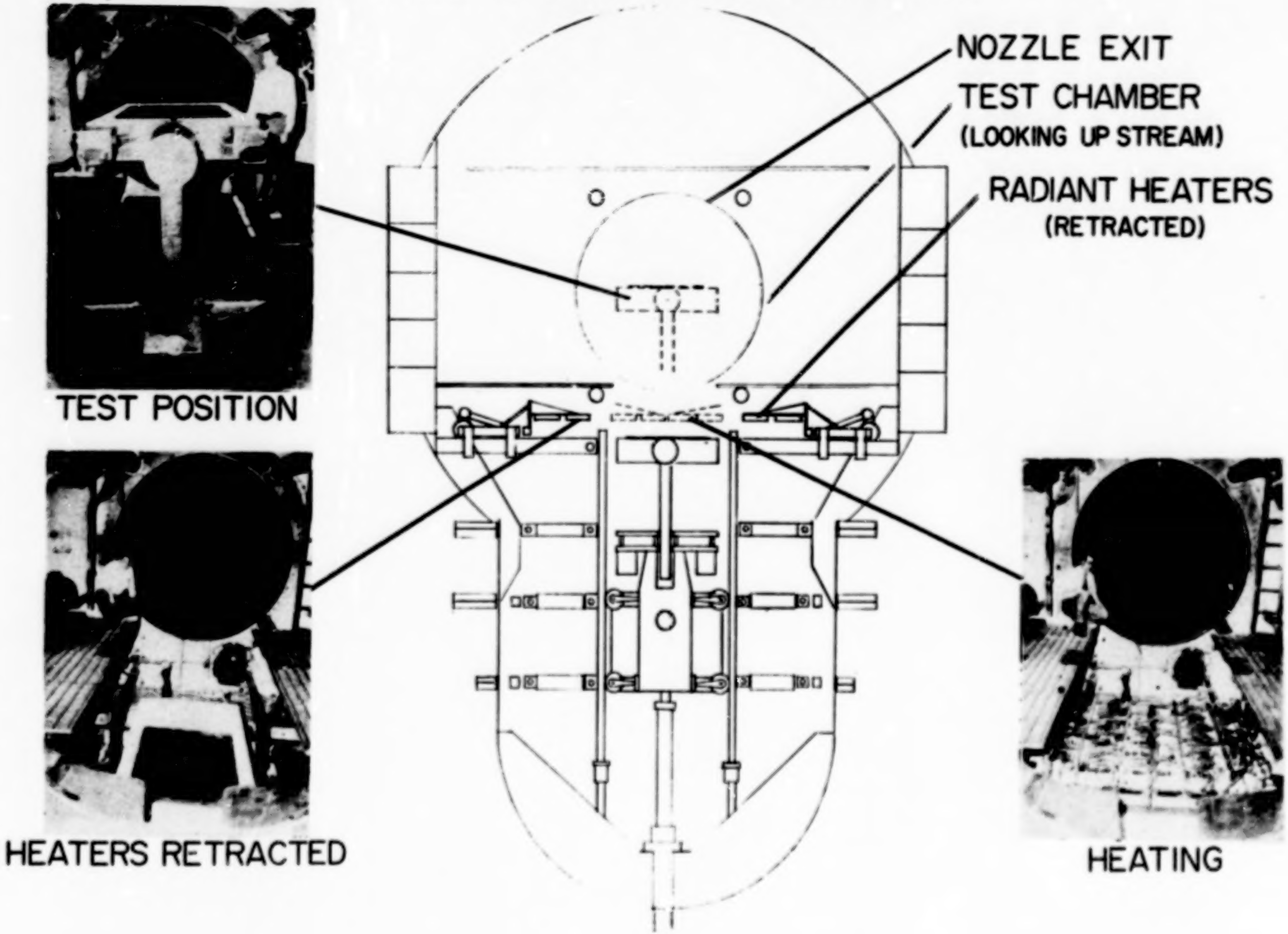
NOZZLE EXIT
TEST CHAMBER
(LOOKING UP STREAM)
RADIANT HEATERS
(RETRACTED)
TEST POSITION
HEATERS RETRACTED
HEATING

Figure 13

RACP MOUNTED IN WIND TUNNEL

(Figure 14)

For tests in the 8-foot high-temperature structures tunnel the RACP was mounted in a fixture known as the 2-D test sled. The RACP is located in a test cavity near the center of the fixture. Aerodynamic fences along either side of the test sled maintained nominally two-dimensional flow over the test cavity. A row of small metal spheres near the leading edge of the test sled tripped the flow boundary layer to insure turbulent flow over the test panel. The heating rate was controlled by preselected values of the tunnel total pressure (17 MPa, (2500 psia)), stagnation temperature (1920 K (3000°F)) and test sled angle of attack. For these tests the sled was pitched down approximately 8°.

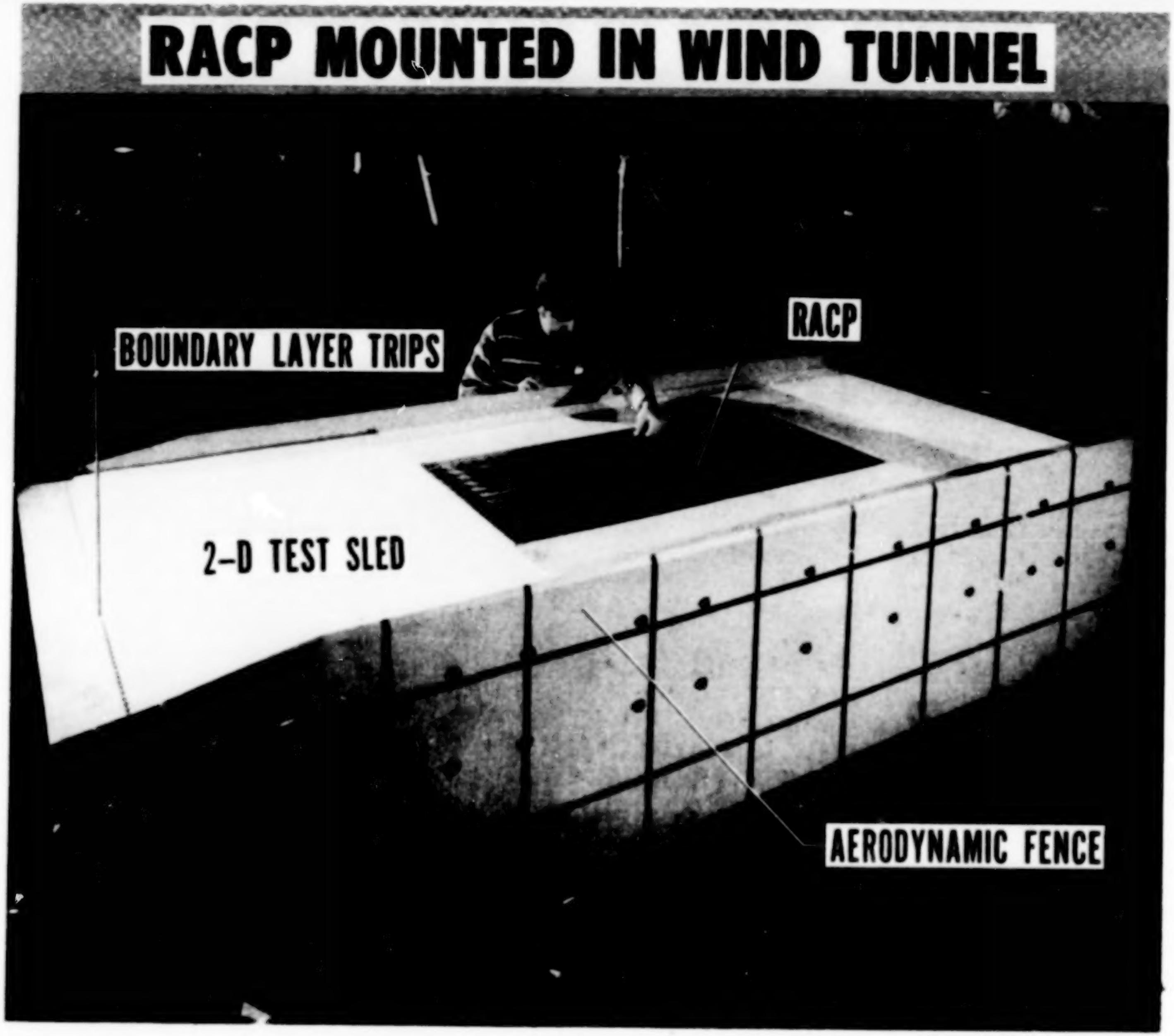
RACP MOUNTED IN WIND TUNNEL
BOUNDARY LAYER TRIPS
RACP
2-D TEST SLED
AERODYNAMIC FENCE

Figure 14

TEMPERATURE PROFILE FOR TYPICAL TUNNEL RUN

(Figure 15)

This figure illustrates the RACP temperature response for a typical tunnel run. While the RACP was located in the tunnel pod, the desired coolant inlet temperature and pressure and flow rate through the cooled panel were established. The RACP was then radiantly heated at 2.8 K/sec (5°F/sec) until the heat shields reached 1061 K (1450°F). The RACP was then allowed to come to thermal equilibrium. After the RACP reached equilibrium the tunnel starting process was begun and after flow was established (note change in time scale) the heaters were retracted and the RACP injected into the stream. During this process the heat shields cooled to about 950 K (1250°F). The aerodynamic heating provided by the stream rapidly reheated the heat shields to a near equilibrium temperature of about 1090 K (1500°F). However, because of the short run time and lag in thermal response of the cooled panel provided by the insulation, the cooled panel did not begin to recover to its initial equilibrium temperature. At the end of the run the RACP was retracted from the stream, the tunnel shut down, and the preheaters used to control the RACP cool-down rate. During the time in the stream an infrared scanner was used to monitor temperatures on the heat shield surface. Some typical data from these scans are shown in figure 16.

TEMPERATURE PROFILE FOR TYPICAL TUNNEL RUN

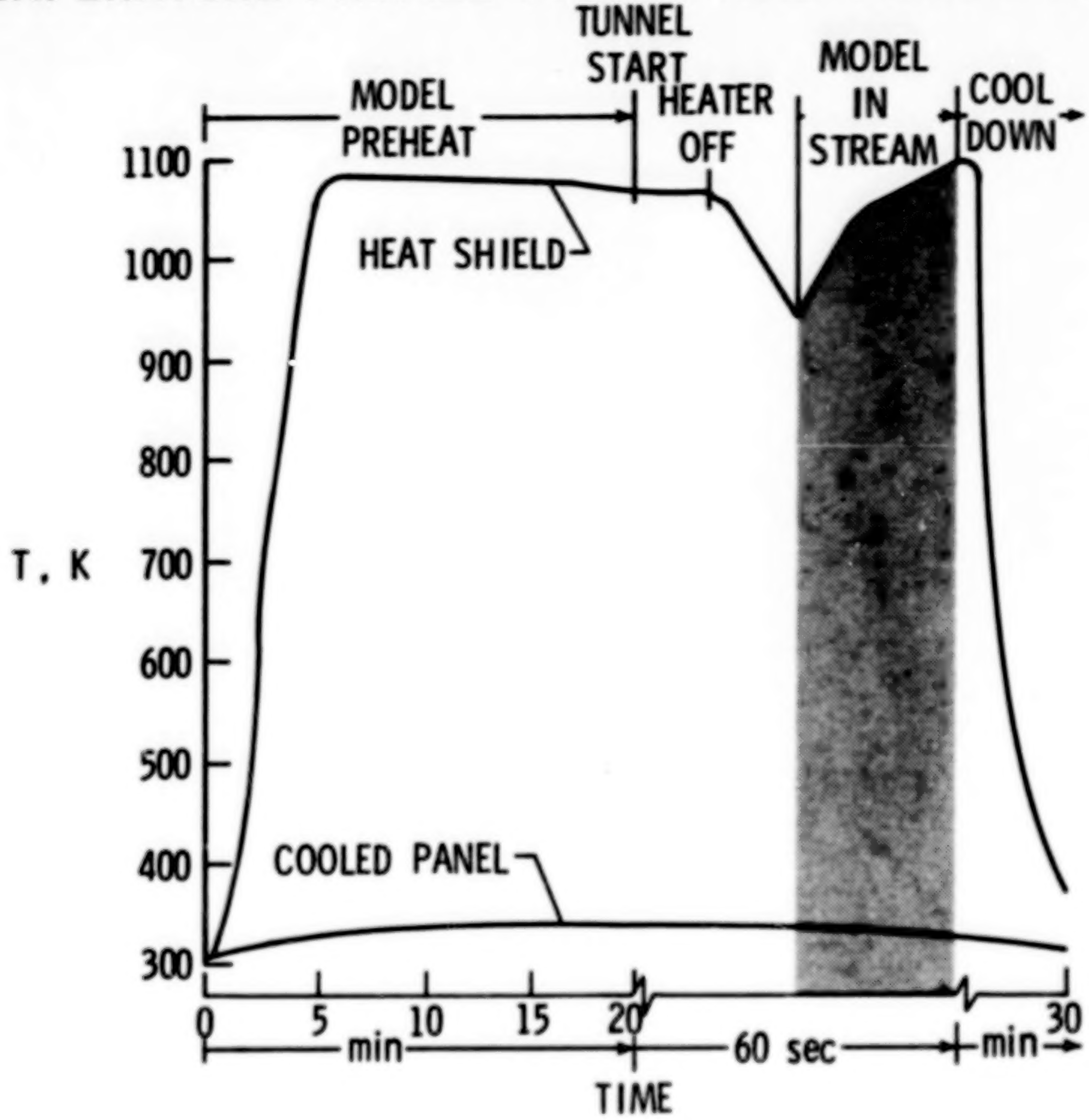

Figure 15

a

INFRARED TEMPERATURE DATA FROM HEAT SHIELD

(Figure 16)

The infrared system provides immediate pictorial temperature data which can later be electronically digitized to yield quantitative temperature data. Three different types of output are indicated on the figure. The contour plot shows the overall temperature level attained by the heat shields and also indicates hot spots caused by fastener heads which protrude into the stream. The temperature relief map shows the transition from the cooler regions of the test sled to the hotter heat shield and clearly shows the variation of heating across the shields caused by the beaded heat shield surface. The single temperature profile corresponds to a slice across the heat shields at a row of fasteners and indicates that the fastener heads are about 28 K (50°F) hotter than the surrounding surface.

INFRARED TEMPERATURE DATA FROM HEAT SHIELD

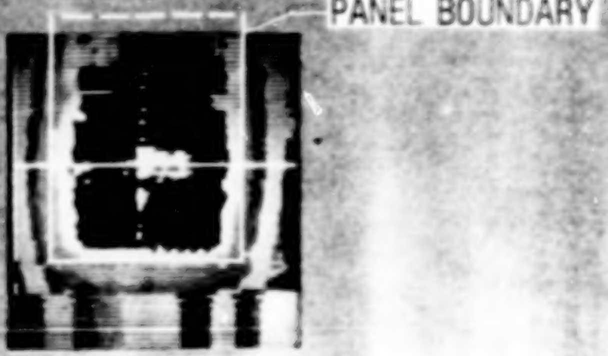

CONTOUR PLOT

- IMMEDIATE PICTORIAL TEMPERATURE DATA
- DIGITIZED DATA

RENÉ 41 SHIELD AFTER WIND TUNNEL TESTS

(Figure 17)

The photos show the post test condition of the heat shields and indicate that there was no structural degradation to the heat shields as a result of the preliminary static tests in ACTS or the aerodynamic tests in the wind tunnel. Scratch marks at the heat shield joints indicate 0.6 cm (0.25 in.) movement which is consistent with the 790 K (1420°F) temperature change from ambient conditions. Additionally, there was no evidence of binding at the joints or of buckling or wrinkling of the heat shield skins.

RENE' 41 SHIELD AFTER WIND TUNNEL TESTS

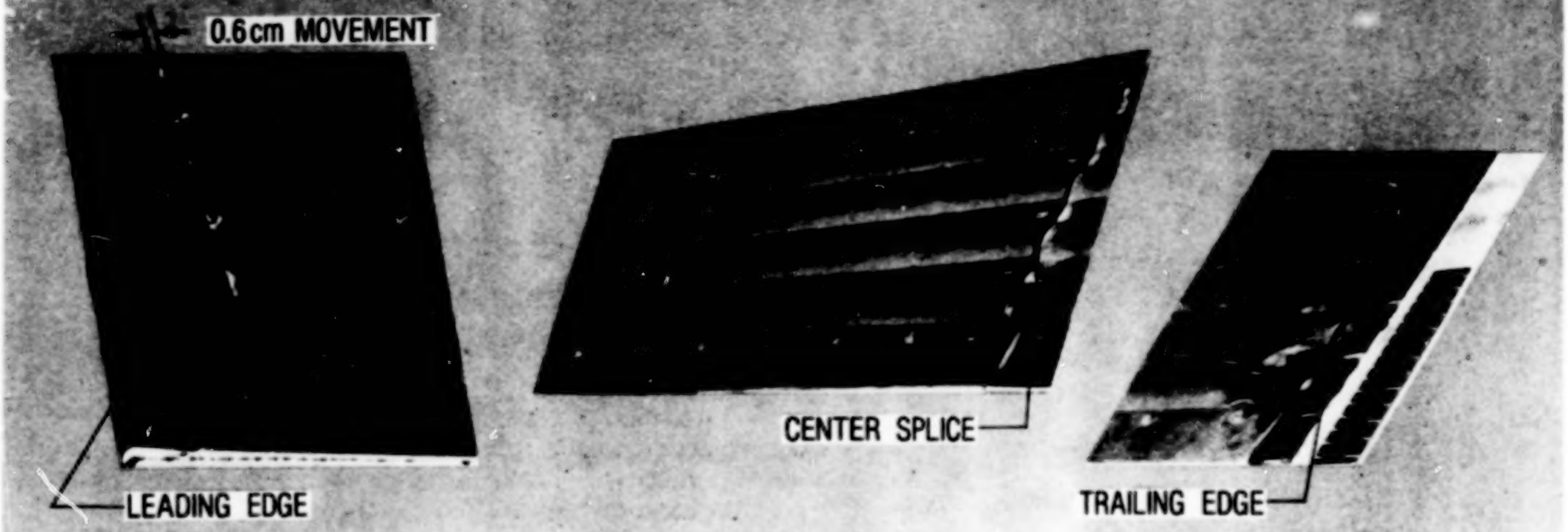
0.6cm MOVEMENT
CENTER SPLICE
LEADING EDGE
TRAILING EDGE

- NO DEGRADATION OF HEAT SHIELD

Figure 17

528

SUMMARY OF RACP TESTS IN 8-FT. HTST

(Figure 18)

The tunnel tests imposed an additional 15 thermal cycles, 3.5 hours at operating temperatures and 2.2 minutes exposure to M=7 flow on the RACP. The panel responded to aerodynamic heating as predicted: the heat shields reached 1090 K (1500°F), the cooled panel reached a maximum temperature of 367 K (200°F) and the cooled panel absorbed heat flux was 11.1 kW/m^2 (0.98 Btu/ft^2-sec). There were no unexpected hot spots and no evidence of hot gas ingress to the cooled panel. Additionally, there was no evidence of coolant leakage.

SUMMARY OF RACP TESTS IN 8–FT HTST

- 15 THERMAL CYCLES
- 3.5 HOURS AT OPERATING TEMPERATURES
- 2.2 MINUTES EXPOSURE TO MACH 7 FLOW
- PANEL RESPONSE TO AERO CONDITIONS AS PREDICTED
  - MAX HEAT SHIELD TEMPERATURE: 1089 K
  - MAX PANEL TEMPERATURE: 367 K
  - ABSORBED HEAT FLUX: 11.1 kW/m^2
- NO UNEXPECTED HOT SPOTS
- NO HOT GAS INGRESS TO COOLED PANEL

Figure 18

FUTURE TESTS FOR RACP

(Figure 19)

The RACP will be reinstalled in ACTS for some detailed thermal/structural tests including simulated inlet and outlet conditions for the full scale panel, simulated coolant system failure, simulated flight maneuvers and cyclic mechanical loading at temperature. The panel will not be tested to failure since it may be used as a test bed for alternate heat shield concepts. Thermal fatigue tests will be conducted on a seperate heat shield specimen. These tests are described in figure 20.

FUTURE TESTS FOR RACP

- DETAILED THERMAL/STRUCTURAL TESTS IN ACTS
  - FULL SCALE PANEL SIMULATION
    - INLET CONDITIONS
    - OUTLET CONDITIONS
  - COOLANT SYSTEM FAILURE SIMULATION
    - ABORT HEATING TRAJECTORY
    - ONE-HALF COOLANT FLOW RATE
  - SIMULATED FLIGHT MANEUVER
  - CYCLIC MECHANICAL LOADING AT TEMPERATURE
- THERMAL FATIGUE TESTS ON SEPARATE HEAT SHIELD SPECIMEN

Figure 19

HEAT SHIELD THERMAL FATIGUE TESTS

(Figure 20)

Most heat shields have been designed for hundreds of thermal cycles rather than the thousands of cycles required for hypersonic transport vehicles. Since little thermal fatigue data exist beyond about a hundred cycles, the specimen shown on the left in figure 20 will be thermally cycled to determine its thermal fatigue characteristics. The specimen will be heated at 2.8 K/sec (5°F/sec) to 1090 K (1500°F), allowed to come to equilibrium and then cooled as indicated by the curve on the left of figure 20. Tests will be run until the specimen fails or accrues 5000 thermal cycles.

HEAT SHIELD THERMAL FATIGUE TESTS

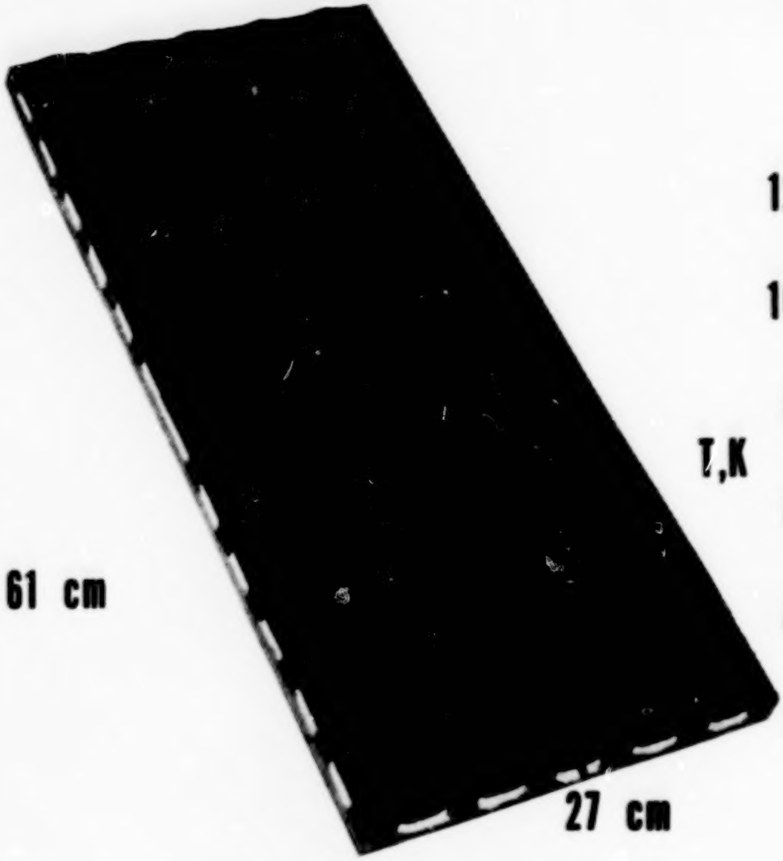

TEST SPECIMEN

- GOAL = 5000 CYCLES

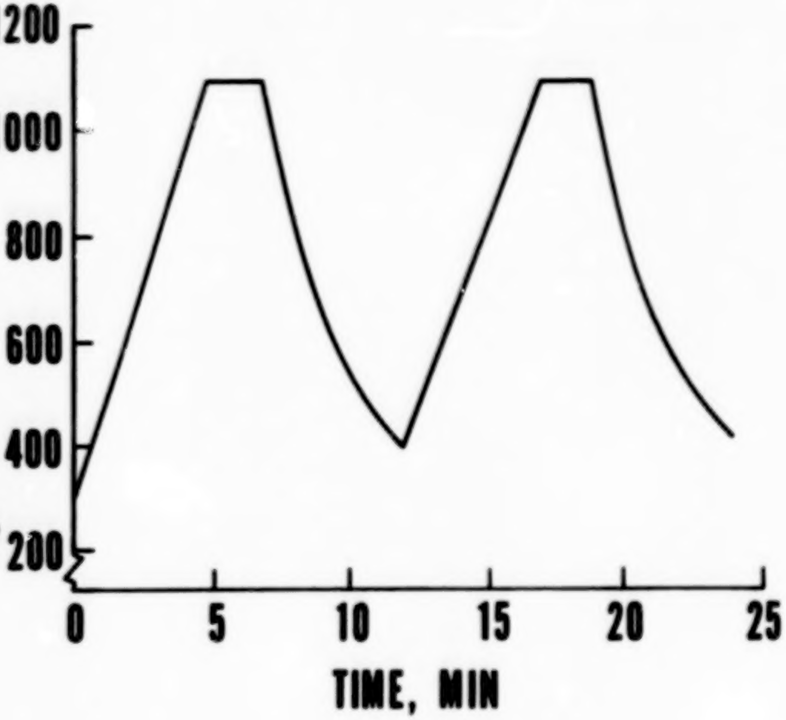

CYCLIC TEMPERATURE

Figure 20

CONCLUSIONS

(Figure 21)

The preliminary tests of the RACP were successful in that the mechanical loading gave predicted mechanical stresses, the panel responded thermally as predicted, the overall panel behavior was acceptable and the tests revealed no surprises. Future tests will check the detailed thermal/structural response of the panel and will address the life characteristics of both the cooled panel and the heat shields.

CONCLUSIONS

- PRELIMINARY TESTS WERE SUCCESSFUL
    - MECHANICAL LOADING GAVE PREDICTED STRESSES
    - THERMAL RESPONSE AS PREDICTED
    - PANEL BEHAVIOR GOOD
    - AEROTHERMAL TESTS GAVE NO SURPRISES

- FUTURE TESTS WILL CHECK DETAILS
    - THERMAL/ STRUCTURAL
    - FATIGUE OF PANEL
    - HEAT SHIELD FATIGUE

Figure 21

REFERENCES

1. Ellis, D.A.; Pagel, L.L.; Schaeffer, D.M.: Design and Fabrication of a Radiative Actively Cooled Honeycomb Sandwich Structural Panel for a Hypersonic Aircraft. NASA CR-2957, 1978.

2. Koch, Leland C.: Design and Fabrication of a Radiative Actively Cooled Honeycomb Sandwich Panel. Recent Advances in Structures for Hypersonic Flight, NASA CP-2065, 1978. (Paper no. 13 in this compilation.)

3. Deveikis, William D.; Bruce, Walter E., Jr.; and Karns, John R.: Techniques for Aerothermal Tests of Large, Flightweight Thermal Protection Panels in a Mach 7 Wind Tunnel. NASA TM X-71983, 1974.

*U.S. GOVERNMENT PRINTING OFFICE: 1979 - 636-008

537

1. Report No. NASA CP-2065, Part I	2. Government Accession No.	3. Recipient's Catalog No.
4. Title and Subtitle RECENT ADVANCES IN STRUCTURES FOR HYPERSONIC FLIGHT		5. Report Date December 1978
		6. Performing Organization Code
7. Author(s)		8. Performing Organization Report No. L-12653
		10. Work Unit No. 505-02-53-01-00
9. Performing Organization Name and Address NASA Langley Research Center Hampton, VA 23665		11. Contract or Grant No.
		13. Type of Report and Period Covered Conference Publication
12. Sponsoring Agency Name and Address National Aeronautics and Space Administration Washington, DC 20546		14. Sponsoring Agency Code

15. Supplementary Notes

16. Abstract

The proceedings of the NASA Symposium - Recent Advances in Structures for Hypersonic Flight held at Langley Research Center on September 6-8, 1978, are reported in this NASA Conference Proceedings. The papers at this Symposium were presented by 24 speakers representing airframe, missile, and engine manufacturers, the U.S. Air Force, and two NASA Research Centers. The papers cover a variety of topics including engine structures, cooled airframe structures, hot structures, thermal protection systems, cryogenic tankage structures, cryogenic insulations, and analysis methods for thermal/structures.

17. Key Words (Suggested by Author(s)) Hypersonic aircraft Actively cooled structure Thermal/Structures analysis methods Thermal protection Cryogenic tankage Cryogenic insulation	18. Distribution Statement Unclassified - Unlimited Subject Category 39

19. Security Classif. (of this report) Unclassified	20. Security Classif. (of this page) Unclassified	21. No. of Pages 542	22. Price* $15.50

* For sale by the National Technical Information Service, Springfield, Virginia 22161

END

July 2, 1981